Metamorphic and Structural Evolution and Provenance

of the Blue Ridge Area, Fremont County, Colorado

By

Tyson Richard Berndt

Submitted to the graduate degree program in Geology and the Graduate Faculty of the University of Kansas in partial fulfillment of the requirements for the degree of Master of Art

_____

Chairperson Andreas Möller

_____

J. Douglas Walker

_____

Leigh Stearns

Date Defended: 11/16/2015

The thesis committee for Tyson Richard Berndt

certifies that this is the approved version of the following thesis:

Metamorphic and Structural Evolution and Provenance

of the Blue Ridge Area, Fremont County, Colorado

_____

Chairperson Andreas Möller

Date approved: 11/16/2015

Abstract

New field studies combined with U-Pb zircon/apatite geochronology, thermodynamic equilibrium modeling, whole-rock/rare earth element geochemistry, heavy mineral comparison, and petrographic analysis yield new insights into the age and timing of deposition, deformation, metamorphism, and the provenance and boundary relationships of exposed Precambrian metasedimentary and associated granitic and pegmatitic rock in the Blue Ridge area, Fremont County, Colorado. The Blue Ridge area is comprised of alternating layers of quartzite, schist, and quartzitic-gneiss, and is in contact with ~ 1.7 Ga granitic basement at both its northern and southern boundary, with ~1.4 Ga concordant and discordant pegmatite dikes exposed throughout. Previous research has used the boundary relationships and U-Pb crystallization and detrital zircon ages to propose two hypotheses: 1) The northern boundary is depositional in nature and represents original sedimentation of quartz-rich sediment sourced from the adjacent granitic basement onto a weathered granitic surface after a period of very efficient and rapid weathering at 1.7 Ga due to altered ocean chemistry (Jones et al. 2009, Medaris et al. 2003, Cox et al. 2002); and; 2) The major deformational and tectonic events that are responsible for the present configuration at Blue Ridge occurred during emplacement of granitic basement at 1.7 Ga (Mai 2002) and/or during inboard deformation associated with the ca. 1.66 – 1.60 Ga Mazatzal orogeny (Jones et al. 2009). My field observations coupled with geochronologic and geochemical data acquired from previously undocumented structural marker units infer that an episode of deformation occurred at ~1.4 Ga during pegmatite emplacement, and that an additional pulse of igneous activity occurred at ~1.1 Ga associated with emplacement of the Pike's Peak batholith. The newly identified structural marker units include syndeformational pegmatite dikes located at both the northern and southern boundary, an amphibole-bearing

leucosome infiltrating quartzite and augen-gneiss along the southern boundary, and the identification of granodiorite and an associated cross-cutting diabase dike that appear to cross-cut existing metasedimentary units.

The presence of attenuated and ductiley deformed pegmatite dikes found at both boundaries, combined with published U-Pb zircon ages ca. 1436 – 1431 Ma from pegmatites at Blue Ridge (Jones et al., 2009), show that movement and deformation occurred at this time. U-Pb geochronologic data from the amphibole-bearing leucosome define discordia arrays with lower intercept ages of 1097 ± 93 Ma and 1109 ± 43 Ma for zircon and 1185 ± 39 Ma for apatite. The granodiorite yielded little to no zircon, but had a U-Pb apatite lower intercept age of 1016 ± 65 Ma. Sm/Nd isotopic data of the diabase dike revealed a depleted mantle model age of 1.2 Ga. Field observations coupled with geochemical and petrographic analyses from the northern boundary show that the contact of granite with metasedimentary rocks was initially depositional in nature, but subsequently deformed as a shear zone ca. 1.4 Ga. Rare earth element (REE) patterns from the northern granite and adjacent metasedimentary rocks are very similar, leading to the interpretation of the granite being the source for the metasediments. Heavy mineral comparisons across the northern boundary are less clear, but apatite/zircon ratios within the granite and basal quartz pebble conglomerate (QPC) of the metasedimentary package display moderate similarities. Additionally, new pressure-temperature (P-T) thermodynamic modeling based on schists and quartz-schists combined with garnet-biotite thermometry was used to quantify that amphibolite-grade metamorphism reached a maximum pressure of 5.2 kb and a maximum temperature of 635 ^{o}C.

Acknowledgements

I would like to thank my advisor, Andreas Möller, for introducing me to this project and for his guidance and support over the course of this study. I would also like to thank my committee members, J. Douglas Walker and Leigh Stearns for their time and efforts in providing helpful comments and discussion for this project. Many colleagues at The University of Kansas were willing to provide me with additional support, both in and out of the laboratory, including Jeff Oalmann, Ty Tenpenny, Noah McClean, Josh Feldman, Brian Sitek, Maggie Graham, Wayne Dickerson, Joe Andrew, and Jake Clayton. I would like to again thank Brian Sitek and Jake Clayton for taking part in individual undergraduate research projects that directly aided this study. Brian performed insightful petrographic analysis on rock units at Blue Ridge and Jake Clayton prepared and analyzed samples for QEMSCAN® analysis. Special thanks are also due to Debra Giffords who allowed access to her private land in the Blue Ridge area. I also credit my brother Kenneth for accompanying me on a regrettably cold field excursion to Blue Ridge during the winter months.

Funding for this study was provided by grants from the Geological Society of America and the Colorado Scientific Society. Additional funds were provided courtesy of Andreas Möller and the Isotope Geochemical Laboratory as well as The University of Kansas Dept. of Geology.

Thanks are also due to my undergraduate colleagues at Montana State University, who simply put, made studying geology fun. Dan, Dave and Nate, I'm proud of you.

Finally, I would like to thank my wife Molly and daughter Evelyn for agreeing to join me on this geologic journey and providing the countless hours of support needed to accomplish this goal.

Table of Contents

List of Figures

Chapter 1. Introduction

Exposures of Precambrian metasedimentary sequences stretch from Wisconsin to Arizona. The rocks are used to interpret the age and timing of deposition and tectonic events associated with the growth of southern Laurentia (Jones and Thrane, 2012). Current tectonic models for the evolution of southern Laurentia during Paleo- and Mesoproterozoic time involve multiple phases beginning with crust formation and orogenesis between ca. 1.8 and 1.6 Ga, 200 m.y. of tectonic quiescence from ca. 1.6 to 1.4 Ga, a widespread tectonothermal event at ~1.4 Ga, and additional orogenic and magmatic activity at ~1.1 Ga (e.g. Hedge, 1967; Bickford et al., 1986; Selverstone et al., 1997; Anderson and Cullers, 1999; Read et al., 1999; Williams et al., 1999; McCoy et al., 2005; Jones et al., 2010; Jones et al., 2012). Whitmeyer and Karlstrom (2007) provide the most comprehensive plate-scale model for the growth and evolution of the Laurentian continent and identify four major northeast trending accretionary provinces in the continental United States based on geologic and geochronologic data acquired from Proterozoic outcrops as well as drill core and aeromagnetic data acquired from the mid-continent. These provinces, from north to south, include the Yavapai (1.80 – 1.70 Ga), Mazatzal (1.70 – 1.65 Ga), Granite-Rhyolite province (1.50 – 1.30 Ga), and Llano-Grenville province (1.30 – 1.00 Ga) (Figure 1). Common in many of these Precambrian rocks are abundant and exceptionally mature quartzite and quartz-pebble conglomerate (QPC) units. They occur in the Baraboo quartzite of the Great Lakes region (Medaris et al., 2003) and in multiple exposures across the southwestern United States as reported by Jones et al. (2009) and Jones and Thrane (2012) (Figure 2). QPC typically constitutes the basal unit in the metasedimentary sequences and is overlain by exceptionally pure quartzite. The QPC deposits are dominated by polycrystalline quartz grains and white mica, but feldspars, granite clasts, and iron-oxides (Reuss, 1974; Jones et al., 2009) are

present as minor accessory minerals. The circumstances surrounding the preferential accumulation of quartz-rich protoliths in Precambrian time is not fully understood, and the age and timing of deposition, deformation, and metamorphism for some of the metasedimentary packages are not well constrained, warranting further study.

The research herein focuses on the metasedimentary sequence in the Blue Ridge area, Fremont County, Colorado (Figure 3). The Blue Ridge area has been the topic of multiple studies since the late 19th century, beginning with the Hayden Survey, which published a geologic map of the area in 1877 and referred to the Precambrian rocks as "metamorphic granites" (Reuss 1970). Whitman Cross performed a regional study of the Pike's Peak area in 1894 and interpreted the metasedimentary rocks as inclusions in granite, and recognized them as the oldest sedimentary protoliths in the area (Knepper 1972). Reuss (1970) and Knepper (1972) focused on the stratigraphy and structure of the area and more recent studies by Jones et al. (2009) have further enhanced the geologic understanding of Blue Ridge through the use of U-Pb zircon age data and field relationships.

The Blue Ridge metasedimentary exposure is in direct contact with granitic basement at both its northern and southern boundary (Figure 4). Previous research has used this relationship and U-Pb zircon ages to propose the following hypotheses: the northern boundary is depositional in nature; the quartz-rich rocks were sourced from the adjacent granitic basement during a period of very efficient and rapid weathering at 1.7 Ga due to acidic ocean chemistry and/or enhanced diagenetic alteration (Jones et al. 2009; Medaris et al. 2003; Cox et al., 2002; Canfield, 1998; Canfield and Teske, 1996); the primary deformational and tectonic events at Blue Ridge occurred at ~ 1.7 Ga during emplacement of granitic basement (Mai 2002), and/or during the culmination of the ca. 1.66 – 1.60 Mazatzal orogeny (Jones et al., 2009). The hypotheses posited

by Jones et al. (2009) that the sediment source of the basal conglomerate and quartzite layers was the underlying granitic basement and that these rocks have a nonconformable depositional contact has important implications for both the local and regional depositional, structural, and metamorphic models. Recent field observations from this study at both boundaries, coupled with work from prior studies at Blue Ridge and the surrounding region, do not directly support all of these interpretations. Initial field reconnaissance performed during the 2013 field season at the northern granite/QPC contact did not present direct evidence for a depositional contact. Field reconnaissance from additional locations along the northern and southern boundaries revealed geologic relationships suggesting additional stages of deformation and igneous activity that have not been previously documented. These field studies provided the impetus for the detailed and multi-method analyses for this research, with the aim of further constraining the nature and timing of geological events in the Blue Ridge area.

This study utilizes field observations, petrography, geochronology, geochemistry, and thermodynamic modeling to focus on the following goals: 1) testing the hypothesis that the basal conglomerate and overlying quartzite units are the result of erosion and first-cycle deposition from the northern granitic basement, 2) verifying the timing constraints on sediment deposition, 3) quantitatively determining the pressure/temperature conditions and trajectory during metamorphism, 4) constraining the timing of deformation, metamorphism, and igneous activity.

The first-cycle sedimentation and deposition hypothesis presented by Jones et al. (2009) was tested by analyzing micro-textures in thin-section, analyzing geochemical signatures of selected samples, and by comparing the heavy mineral abundance of northern granitoids and adjacent metasediments through the use of **Q**uantitative **E**valuation of **M**inerals by **SCAN**ning electron microscopy (QEMSCAN®). Whole rock compositions obtained from a representative

suite of metapelitic samples were processed at the Texas Tech University GeoAnalytical Laboratory and used for thermodynamic modeling using the Theriak/Domino software (Capitani and Petrakakis, 2010) in order to quantify the P-T conditions of metamorphism. Electron microprobe analyses of garnet and biotite from metasedimentary samples were performed at the University of Kiel and subsequently used to model temperature conditions of garnet growth. U-Pb zircon and apatite grains obtained from both metasedimentary and igneous samples were analyzed using Laser Ablation Inductively Coupled Mass Spectrometry (LA-ICP-MS) at The University of Kansas Isotope Geochemical Laboratories in order to further constrain the timing of depositional and magmatic events. Zircon grains from known and suspected shear zones were also analyzed for metamorphic overgrowths using cathodoluminescence imaging (CL) with the aim of identifying additional episodes of metamorphism (Nasdala et al., 2003).

Chapter 2. Geologic Setting and Geology of Blue Ridge

Precambrian Regional Setting

Precambrian exposures located in the south-central Colorado Front Range are comprised of assemblages of metavolcanic and metasedimentary rocks in addition to mafic and felsic plutons. These assemblages were formed and subsequently accreted to the southern margin of Laurentia ca. 1.8 – 1.6 Ga (Condie, 1982; Karlstrom and Bowring, 1988; Anderson and Cullers, 1999; Whitmeyer and Karlstrom, 2007). Additional granitic plutonism occurred ca. 1.44 – 1.36 Ga, emplacing A-type granite batholiths and numerous smaller-scale intrusions, and again at ca. 1.30 – 0.95 Ga during and after the culmination of the Llano-Grenville orogeny (Anderson and Cullers, 1999; Smith et al., 1999; Bright et al., 2014). The greater extent of the Precambrian rocks exposed throughout the southwestern United States have been divided into orogenic provinces based on age data and isotopic characteristics, with a noticeable decrease in age to the south (Figure 1, Whitmeyer and Karlstrom, 2007; also see DePaolo, 1981; Bennett and DePaolo, 1987; Shaw and Karlstrom, 1999). The exposures at Blue Ridge fall within the greater Yavapai crustal province and sit near the northern extent of the Mazatzal deformation front (Jones et al., 2009; see Figure 2). The Yavapai province was accreted to southern Laurentia during the 1.71 – 1.68 Ga Yavapai orogeny, and inboard deformation associated with the Mazatzal orogeny occurred ca. 1.65 – 1.60 Ga (Whitmeyer and Karlstrom, 2007). The exposed granitic plutons at the northern and southern boundary of Blue Ridge are part of the Twin Mountain batholith, which has been dated by Jones et al. (2009) at 1706 ± 5 Ma (Figure 4, inset). Pegmatite from Blue Ridge has also been dated by Jones et al. (2009) at 1436 – 1431 Ma. Additional ~1.7 Ga and ~1.4 Ga plutons are found within close proximity to the Blue Ridge area and the ~1.1 Ga Pike's Peak pluton is located 35km to the northeast (Anderson and Cullers, 1999) (Figure 5).

Smith et al. (1999) has dated zircon from syenite associated with the Pike's Peak event at 1085.6 ± 2.5 Ma. Prior to this study, Pike's Peak ages have not been reported for the Blue Ridge area.

Present Day Setting

The Blue Ridge area is a 1.3km wide by 7.5km long exposure of Precambrian metasedimentary rocks that consist of alternating packages of quartzite, schist, and quartz-gneiss (Figure 4). Compositional layering strikes NE (~050^o – 070^o) and is locally isoclinally folded. These rocks are in contact with granitic basement at both their northern and southern boundary. Relict ripple marks in quartzite show that the sedimentary protoliths were deposited in a shallow marine environment and cross-beds seen within quartzite indicate a facing direction to the south (Reuss, 1970, 1974). En echelon folds on the scale of 150-200 meters are visible in the more competent quartzite layers and display a sinistral sense of shear. The exposure is interpreted as the northern limb of a slightly overturned NE plunging syncline or synform, with the southern limb being removed during emplacement of the adjacent southern granitic basement (Reuss, 1970; Knepper, 1972; Mai, 2002). Concordant and discordant pegmatite dikes, from meter to kilometer scale in length, are pervasive and are found to follow the general trend of strike as well as cross-cut both granite and metasedimentary units. Two major faults flank the study area and bring Paleozoic and Mesozoic strata into direct contact with Precambrian rocks, the Twin Mountain fault to the east and the Twelve Mile fault to the south (Figure 4). The present structural configuration at Blue Ridge was formed during the late Cretaceous to Miocene during the Laramide orogeny (Knepper, 1972).

The quartzite units at Blue Ridge are exceptionally mature and composed of ~95% quartz, with minor feldspar and oxides. These units are highly competent and form prominent

ridges. Locally the quartzite grades into quartz-gneiss or quartz-schist. Large boudinaged sections of quartzite can be found at the meter to tens-of-meter scale in well-exposed areas. The schist and quartz-schist units at Blue Ridge contain quartz – muscovite – biotite – iron oxides ± andalusite ± chlorite ± cordierite ± garnet ± staurolite ± sillimanite. These units have a well-defined foliation with localized crenulation cleavage in many exposures. Contact with quartzite can be sharp or gradational, with lenticular bodies of quartzite typically present within the schist. Petrographic studies by Reuss (1970, 1974) and Mai (2002) indicate amphibolite-grade metamorphic conditions at Blue Ridge. However, the age and conditions of the main metamorphic event within the metasedimentary package has never been quantitatively investigated and current P-T estimates are based solely on observed mineral assemblages.

Newly Identified Field Relations and Motivation of Current Study

The presence of newly identified ductiley deformed pegmatite and an undeformed amphibole-bearing leucosome show that additional episodes of deformation and igneous activity have occurred at Blue Ridge. The ductiley deformed pegmatite is interpreted to be synkinematic with emplacement. The amphibole-bearing leucosome, which is in close proximity to attenuated pegmatite at the southern boundary, contains randomly oriented amphiboles, lacks a mineral orientation or deformation fabric, and infiltrates the sheared granitic basement and adjacent quartzite. This suggests emplacement that post-dates pegmatite intrusion. Additional marker units at Blue Ridge include a granodioritic grus and diabase dike located along a road cut in the southeastern exposure of the area. These bodies appear to truncate the overlying metasediments and cannot be directly correlated to other igneous bodies in the area.

Chapter 3. Methods

Field Sampling

Field work and sample collection was carried out during four field sessions (June 2013, January 2014, November 2014, July 2015). Approximately 70 samples were collected at Blue Ridge from both igneous and metasedimentary rocks for the purpose of hand sample analysis, petrography, metamorphic petrology, geochemistry, and geochronology (Figure 6). Rock type, location, and analysis performed for each sample are listed in Appendix A. Three to four kilograms were collected for each sample, unless the sample was being used explicitly for hand sample analysis or petrography. Samples were reduced to small chips in the field or under clean lab conditions. All samples intended for heavy mineral separation were scrubbed, rinsed, and dried with compressed air under clean conditions.

Thin-section Preparation

Approximately 60 samples were selected for petrographic analysis and made into polished thin sections. Oriented and non-oriented samples were cut into billets using a wet saw at The University of Kansas rock crushing facility. Billets were then processed in house at The University of Kansas optical laboratory and/or sent to Spectrum Petrographics® in Vancouver, Washington. Thin sections were used for mineral identification, Electron Probe Micro-Analysis (EPMA), and Laser Ablation Inductively Coupled Mass Spectrometry (LA-ICP-MS).

Heavy Mineral Separation

All sample processing performed for geochronology and heavy mineral comparison was performed at The University of Kansas rock crushing and mineral separation facilities. Bulk rock

samples were crushed using a jaw crusher, cone crusher, and then reduced to a coarse powder with a steel disc mill. The jaw crusher was cleaned and self-contaminated before each use. An analytical split was isolated for select samples following the use of the jaw crusher. Initial heavy mineral separation was performed on a Gemini® water table. This was followed by heavy liquid separation using Bromoform (specific gravity (s.g.) 2.85 g/cm^3), Lithium Metatungstate (LMT) (s.g. 2.85 g/cm^3), or Methylene Iodide (MEI) (s.g. 3.3 g/cm^3), depending on the requirements of the analysis. Magnetic separation was then utilized using a Frantz® magnetic separator with settings of 0.2, 0.4, 0.6, and 1.0 Amps at 10º sideways and 10º forward tilt. Individual zircon and apatite grains intended for U-Pb analysis were hand-picked from the zircon heavy mineral fraction using a binocular stereo microscope, set in epoxy resin discs, and then polished to expose the approximate centers of each grain.

***Q**uantitiative **E**valuation of **M**inerals by **SCAN**ning electron microscopy (QEMSCAN®)*

Heavy mineral fractions used for modal abundance comparison followed the methods of heavy mineral separation mentioned above. After separation, representative mineral fractions were obtained using a micro-splitter, set in epoxy resin discs and polished to expose the center of the grains. Due to the randomness of size and shape, not all grains were exposed at the polished surface. The polished discs were sent to the Advanced Mineralogy Research Center at the Colorado School of Mines and analyzed using the **Q**uantitiative **E**valuation of **M**inerals by **SCAN**ning electron microscopy (QEMSCAN®). The QEMSCAN® is an automated Carl Zeiss EVO50 scanning electron microscope (SEM) that employs four Bruker X275HR energy dispersive x-ray spectrometers (EDS) and a backscatter electron (BSE) detector to assign mineral identity to mapped pixels (Barnhardt et al., 2012). After the minerals are identified, they are color coded and then quantified, resulting in a modal abundance for a selected sample (Figure 7).

The color coded images were also used to locate zircon grains for U-Pb zircon analysis using LA-ICP-MS.

Laser Ablation Inductively Coupled Mass Spectrometry (LA-ICP-MS)

LA-ICP-MS was utilized on zircon, apatite, and sphene mineral fractions at The University of Kansas Isotope Geochemistry Laboratories to measure U/Pb ratios in selected grains. Zircon and apatite grains were separated and isolated using heavy mineral separation techniques described above. Additional apatite grains were identified and ablated in polished thin section. Zircons identified in grain mounts by QEMSCAN® were also analyzed using LA-ICP-MS. Zircon fractions from an amphibole-bearing leucosome (BR072815-01), pegmatite (BR072815-02), and foliated granite (BR073015-01) were annealed in quartz beakers at 900 ^{o}C for 60 hours following protocols of Mattinson (2005). Cathodoluminescence (CL) imaging of zircon grains was performed prior to ablation at The University of Kansas Microscopy and Analytical Imaging Laboratory (MAI Lab) to identify growth zonation and possible metamorphic rims. The MAI facility employs a FEI Versa 3D Dual Beam scanning electron microscope and associated Gatan CL detector. The LA-ICP-MS laboratory at The University of Kansas consists of a Thermo Scientific Element 2® high resolution sector-field ICP-MS and a Photon Machines ANALYTE.G2® excimer laser with 193nm wavelength and 5ns pulse width. A laser spot size of 20 μm was used with a laser fluency of 2.0 J/cm^2 at 10 Hz laser repetition rate. Ablated material was transferred to the ICP-MS in He gas. Elemental fractionation, downhole fractionation, and calibration drift were corrected by bracketing measurements of unknowns with measurements of the GJ-1 reference material (Jackson et al., 2004). Two secondary standards were used for selected analyses including Plešovice (Sláma et al., 2008) and the Duluth Gabbro (Paces and Miller, 1993). In this study, Plešovice (Sláma et al., 2008) yielded

a weighted mean $^{206}Pb/^{238}U$ date of 339.1 ± 1.5 (2σ) (n=25; MSWD=1.5), which is within 1% of the 337.13 ± 0.37 Ma age determined by TIMS (Sláma et al., 2008). The Duluth Gabbro (Paces and Miller, 1993) yielded a weighted mean $^{206}Pb/^{238}U$ date of 1108.1 ± 3.6 Ma (2σ) (n=25; MSWD=0.55), which is within 1% of the 1099 ± 0.5 Ma age determined by TIMS (Paces and Miller, 1993). U-Pb LA-ICP-MS data from zircon and apatite were processed using the Iolite® 2.5 (Paton et al. 2010; 2011) and VizualAge (Petrus and Kamber 2011) software packages and the Isoplot/Ex (Ludwig, 2003) excel add-on program.

Electron Probe Micro Analysis (EPMA) and Mineral Equilibrium Thermometry

Electron microprobe analysis (EPMA) of garnet and biotite from select metasedimentary samples was performed at The University of Kiel, Germany. Garnet and biotite grains were isolated in polished thin section and analyzed using a JEOL Superprobe JXA-8900R electron microprobe. The mineral composition data was used to create garnet composition transects and to calculate equilibrium temperature conditions at varying pressure for garnet porphyroblasts using a garnet-biotite thermometer. Thermodynamic modeling was performed using the Garnet Pressure Temperature (GPT) Reche and Martinez (1996) Excel Spreadsheet for thermobarometric calculations in metapelitic rocks. The GPT spreadsheet contains garnet-biotite thermometers for 14 published methods. The preferred reduction method for the Blue Ridge analyses was that of Perchuk and Lavrent'Eva (1983) following the guidelines of Kleemann and Reinhardt (1994).

Bulk Rock and Rare Earth Element Analysis

Twenty one samples (5 igneous, 16 metasedimentary) were collected for bulk rock and rare earth element analysis. Fist-sized samples of whole-rock were sent to the GeoAnalytical Laboratory at Texas Tech University for processing. Rock samples were crushed with steel jaw crushers, then coned and quartered. A split of the crushed sample was powdered in a ceramic shatterbox for 6 minutes. The shatterbox was cleaned by running with silica sand and rinsing with deionized water and acetone between every sample. The powdered samples were fused in a Claisse M4 Fluxer with a sample-to-flux ratio of 1:5 (1.2g sample mixed with 4.8g of flux, whose composition was 49.75% lithium metaborate, 49.75% lithium tetraborate, and 0.50% lithium bromide). Major oxide, minor oxide and trace element (Ba, Cr, Cu, Ni, Sr, V, Zn, Zr) concentrations were measured on fused discs in an ARL Perform'X 4200 X-ray fluorescence spectrometer. In order to monitor accuracy and precision during the analysis, duplicates of five unknown samples were analyzed and USGS standards BHVO, ABA, STM and PCC were analyzed as unknowns. On the basis of repeated analysis of USGS standard BHVO-1, precision of the major and minor oxides was better than ~0.3% and accuracy was better than 2% except for P2O5 (~3%) and Na2O (~7%). Precision for the trace elements was better than 2% except for Ba (~7%). Accuracy for Zr, Zn, V Ni and Cr was better than 5% accuracy, for Cu and Sr better than 10%, and for Ba ~11%. Bulk rock concentrations of the rare earth elements La, Ce, Pr, Nd, Sm, Eu, Gd, Tb, Dy, Er, Yb, and Lu and Na, Mg, Al, Si, Ca, Sc, Ti, V, Ga, Rb, Sr, Y, Zr, Nb, Ba, Hf, Ta, Pb, Th, and U were determined by LA-ICP-MS on the fused glass discs used for XRF analysis. Data were collected on an Agilent 7500cs ICPMS coupled with a New Wave 213 Nd:YAG laser using a 80 um diameter spot size, 10 Hz laser pulse rate, and 10-13 Jcm-2 fluence. The USGS glass standard BHVO-2G and fused powders of USGS standards BHVO, G2, PCC,

RGM and STM (using the same fusion method as for XRF analysis) were run as unknowns during each run, and duplicates of several of the samples were also analyzed. Data were reduced using the SiO_2 concentrations as an internal standard determined from XRF analysis.

Bulk Rock Thermodynamic Modeling

Bulk rock geochemical analyses produced at Texas Tech University were used for pressure-temperature (P-T) modeling using the Theriak/Domino software of Capitani and Petrakakis, (2010). Equilibrium phase diagrams were created from 13 metasedimentary samples in order to constrain the maximum P-T conditions for a given bulk rock composition. Equilibrium P-T phase diagrams were calculated using a pressure range of 1 – 7 kbar and a temperature range of 350-800^{o}C. Garnet composition isopleths and garnet reaction lines were calculated as needed to help constrain the P-T conditions of garnet formation.

Neodymium Isotope Analysis

Six samples were selected for Neodymium (Nd) isotope analysis. These include northern granite (BR060913-04A), northern syenite (BR060913-04B), southern granite (BR061113-01), southern granodiorite (BR061113-02), amphibole-bearing leucosome (BR060913-01), and diabase dike (BR060314-01). Samples were first crushed in a jaw crusher, pulverized in a steel disc mill, and turned into a homogeneous powder using a ceramic ball mill. Whole rock Nd isotope analyses were performed by thermal ionization mass spectrometry (TIMS) at the University of Kansas Isotope Geochemistry Laboratory. Analyses for Nd and Sm were done on a VG Sector 54 mass spectrometer (both run as metal), with typical internal and external precisions of ± 20 ppm (2σ). Nd ratios were corrected using a KU internal standard (using a value of 0.511905) that is tied to LaJolla Nd by using a value of 0.511860 for the $^{143}Nd/^{144}Nd$ of

LaJolla. Adjustment was minimal and was done after fractionation was corrected using $^{146}Nd/^{144}Nd=0.7219$. The measured laboratory value was 0.511905 on the KU standard based on 5 standard runs with these samples and more than 20 over the last 2 years. Samples were prepared for analysis by using standard HF-HNO_3 and HCl dissolution techniques. Elemental separation was done using cation exchange columns with Biorad® resin. Nd and Sm were purified using Eichrome LN-spec® resin columns.

Chapter 4. Results of Field Research

Field work at Blue Ridge focused on boundary relationships and structural marker units at the northern and southern contacts of the metasedimentary units with the granitic basement as well as additional structural marker units exposed in road cuts along Forest Service Road 69 (Figure 8). Field research at the northern boundary concentrated on the identification of geologic relationships used to test the hypothesis posited by Jones et al. (2009) that the QPC/granite contact is depositional in nature and that sediment was derived directly from this granite. Field research along the southern boundary centered on the identification of geologic evidence for potential additional stages of deformation occurring post-1.7 Ga. Figure 8 shows the location of important field relationships for this study.

Field Relationships at the Northern Boundary

The northern boundary consists of QPC that is in direct contact with a 1706 ± 5 Ma granitic pluton (Jones et al., 2009). The granite is compositionally variable, ranging from fine and medium-grained weakly foliated quartz monzonite to medium and coarse-grained foliated biotite granodiorite (Wobus et al., 1979) The QPC consists of mono- and polycrystalline quartz

grains up to 3cm with abundant intergranular white mica that appears to concordantly surround the larger pebbles. Large grains of potassium-feldspar up to 5 cm are locally present within the QPC (Figure 9). The QPC displays a distinct foliation that is defined by the alignment of quartz pebbles and mica. Foliation in the biotite granodiorite generally parallels that of the metasedimentary rock, but local variations persist.

The QPC/granite contact is not well exposed and is commonly weathered and eroded or covered with thick accumulations of vegetative duff (Figure 10). Outcrops of QPC and granite with inferred contacts were found within Gooseberry, Spoon, and Devil's gulch, and a sharp contact was located in Maverick Gulch (see Figure 8 for location). QPC exposed in Spoon and Devil's Gulch was relatively homogeneous and showed no variation in grain size. The QPC in Gooseberry and Maverick Gulch displayed variation in grain size, with an overall reduction in size closer to the contact. Pegmatite dikes were also present at or near the contact in both Maverick Gulch (Figure 11) and Gooseberry Gulch (Figure 12).

Figure 11 displays the sharp, but irregular contact between the granite and QPC in Maverick Gulch. The exposure is highly weathered and partially obscured by lichen, but the differences in mineralogy between the two units help distinguish the contact. The QPC lacks biotite in all exposures while the granite in Maverick Gulch is biotite-rich. Additionally, the strike and dip of foliation in the QPC and granite do not align. The strike and dip of foliation (by right-hand-rule, RHR) in the granite is 315/24 while the strike and dip of foliation in the QPC is 270/28. As noted above, the size of quartz pebbles within the QPC is gradational and pebbles become noticeably smaller closer to the contact. Quartz pebbles located >1m from the contact are found at the centimeter-scale while grains <1m from the contact range from the centimeter to

millimeter scale. A pegmatite dike is also visible at the contact and cross-cuts both units (Figure 11A & B).

Geologic relationships in Gooseberry Gulch (Figure 12) are similar to those in Maverick Gulch; however, the QPC/granite contact is not exposed. Mineralogy and strike and dip of foliation were again used to delineate the contact, but unlike Maverick Gulch, the foliated granite (BR061613-03, BR073015-01) closest to the contact in Gooseberry Gulch lacks biotite and the mineral foliations in both units are almost identical. Variations in grain size within the QPC are clearly evident and a marked decrease in quartz pebble size is visible towards the contact (Figure 13). QPC located ~10m south of the contact contain grains ~2.5cm in diameter while QPC within ~1-2m of the contact contain grains are ~0.5cm to 1.0mm. At a distance of ~5m from the contact a pegmatite dike has intruded the QPC and both units are visibly deformed. The pegmatite appears to be boudinaged and the less competent, mica-rich QPC appears to flow around the segmented pegmatite.

Field Relationships at the Southern Boundary

The southern boundary is a sheared contact and juxtaposes 1698 ± 4 Ma (Jones et al., 2009) granodiorite with quartzite and/or quartz gneiss and schist (see Figure 8 for study location). The main granitoid rock unit south of the boundary is a medium to coarse-grained biotite granodiorite (Wobus et al., 1979) that contains large phenocrysts of potassium-feldspar and quartz. Meter-scale blebs of fine-grained granite are locally distributed and metasedimentary xenoliths up to 3m long are also present. The coarse granodiorite becomes increasingly foliated towards the contact and grades into augen gneiss and mylonite. The quartzite is exceptionally

pure and is comprised almost entirely of quartz and a small percentage of iron oxides. A ductiley deformed pegmatite dike intrudes the augen gneiss and adjacent quartzite and parallels the deformation fabric within the augen gneiss, showing a sinistral sense of shear (Figure 14, 15). The pegmatite (BR072815-02) is megacrystic and contains abundant quartz and alkali-feldspar. An amphibole-bearing leucosome (BR060913-01, BR072815-01) is also present at the contact and intrudes both quartzite and augen gneiss along strike (Figure 14B). The amphibole-bearing leucosome contains randomly oriented hornblende phenocrysts and has no apparent foliation or mineral orientation. This unit is apparently a minor component of the outcrop, and was only found in situ at one locale along the southern boundary within an unnamed gulch shown in Figure 14 and 15 (see Figure 8 for location). Figure 15 shows the relationship of the pegmatite and amphibole-bearing leucosome with the surrounding units.

Additional Structural Marker Units: A Granodioritic Grus and Diabase Dike

A granodioritic grus (BR061713-01) and diabase dike (BR060314-01) are exposed in a roadcut along FS Road 69 in the southeastern extant of the field area (Figure 16, see Figure 8 for location). These units are located approximately 1.0 km from the boundary with the northern granitic basement and 0.2 km from the boundary with the southern granitic basement and appear to have no direct correlation to either basement units. The granodioritic grus is exposed for ~80m and ~175m in two locations along FS Road 69 and appears to truncate and intrude a quartz-schist unit within the metasedimentary package at Blue Ridge. Due to the topography in the area and amount of talus covering the hillside it was unclear whether this unit was sheeted or bulbous in its outcrop pattern. The mineralogy of the granodioritic grus, as seen in thin-section, is composed of plagioclase feldspar, oxides, biotite, possibly orthopyroxene and minimal quartz. Accessory minerals included apatite and sphene. The top few centimeters of the grus exposure is loose and

friable, but becomes competent with increased depth. The contact with the adjacent metasedimentary rock is highly weathered and it is difficult to determine if the metasedimentary body shows any signs of contact metamorphism. The diabase dike contains phenocrysts of plagioclase up to 3mm and intrudes along the granodiorite-metasediment contact, displaying a chilled margin. Diabase float has also been identified in Devil's and Maverick Gulch.

Chapter 5. Results of U-Pb Zircon and Apatite Geochronology

Fifteen samples were collected for U-Pb zircon and apatite study utilizing LA-ICP-MS to constrain the age and timing of geologic events at Blue Ridge. Four metasedimentary samples were collected for detrital zircon analysis and include QPC-07 (BR060913-07), QPC-08 (BR060913-08), a quartzite (BR061013-01) located approximately 700m structurally above the QPC and one mica-quartz schist (BR061213-01) located approximately 400m structurally above the quartzite. Eight igneous samples were collected to verify geochronologic data reported by Jones et al. (2009) and to obtain data on newly identified structural marker units. The samples collected similar to those of Jones et al. (2009) include a granite (BR060913-04A) and a foliated granite (BR060913-05) from the northern granitic basement collected along FS Road 69, one sample of southern granodiorite (BR061113-02) collected ~15m south of the southern quartzite/granodiorite contact, and two pegmatite samples (BR061113-05, BR072815-02) that intrude and cross-cut both quartzite and augen-gneiss at the southern contact. Samples collected on new structural marker units include one sample of granodiorite (BR061713-03) obtained from a road cut along FS Road 69 and two samples of amphibole-bearing leucosome (BR060913-01, BR072815-01) obtained from the southern boundary in an unnamed gulch. The remaining three

samples were collected from near the northern and southern boundaries with the intent of dating metamorphic overgrowths in known and presumed shear zones. These rocks include one sample of augen gneiss (BR061113-04) collected from the southern contact and two samples of foliated granite (BR061613-03, BR073015-01) collected from the northern contact in Gooseberry Gulch. Figure 17 displays the location of all zircon/apatite geochronology samples collected for this study and Figure 18 displays all samples collected by Jones et al. (2009). LA-ICP-MS U-Pb data of zircon and apatite can be found in Appendix B.

Many of the analyses from both the detrital and igneous zircon fractions were highly discordant and displayed signs of Pb-loss and/or the effects of common-Pb. An analysis is considered to be concordant when the $^{207}Pb/^{235}U$ age and $^{206}Pb/^{238}U$ age are equal and discordant when these ages are unequal (Wetherill, 1956). Discordance, as described by Wetherill (1956) is related to gains or losses of uranium and lead since the formation time for a given system. All samples that have remained a closed system since the time of formation fall on a "Concordia" line and those that are discordant and assumed to be part of an open system fall on a "Discordia" line (Schoene et al., 2014). Schoene et al. (2014) also states that discordance can arise from the mixture of different-aged material. Many of the grains collected for U-Pb zircon work in this study were 50 µm or less in size, making it difficult to isolate and analyze distinct growth zones with a 20 µm spot size, the size used for this study. Analyses from pegmatite 2 (BR072815-02) displays both concordant and discordant analyses and accurately depict the effect of Pb-loss described by Wetherill (1956). In some instances, grains determined to be concordant yield a wide range of ages that fall along Concordia, as seen in sample HBL-QEM1. These analyses are either concordant or have experienced mixing or Pb-loss, producing a false concordia age. Selected samples in this study that yield clustered but relatively broad ranges of concordant

analyses were checked for trends indicative of mixing and/or Pb-loss by reviewing data plots calculated from Th/U vs. $^{207}Pb/^{206}Pb$ age diagrams and date-effective uranium (eU) vs $^{206}Pb/^{238}U$ age diagrams. Younger grains will typically have higher Th/U ratios, which are interpreted on a Th/U vs. $^{207}Pb/^{206}Pb$ age diagram. The date-effective uranium (eU) vs $^{206}Pb/^{238}U$ age diagram is used to interpret trends toward Pb-loss, with definitively positive or definitively negative eU trends indicating significant radiation damage and subsequent Pb-loss (Guenther et al., 2013) (eU = [(U ppm) + (.235*Th ppm)]).

CL imagery is also useful for identifying zones of potential radiation damage and Pb-loss in zircon grains. CL intensity is linked to the crystallinity and structural perfection of the lattice for a given grain, with high intensity CL imagery indicating undamaged grains and low intensity CL imagery indicating damaged grains (Nasdala et al., 2003). Thus, if the CL intensity is relatively low it indicates that parts of the grain have been damaged, either by radiation or diagenetic alteration. CL imagery was utilized in this study to identify damaged zones and zones of potential recrystallization. CL imagery for select analyses is located in Appendix C.

Results of Metasedimentary Detrital Zircon Geochronology: QPC, Quartzite, and Schist

U-Pb detrital zircon ages have been reported at Blue Ridge for the basal conglomerate and an overlying quartzite by Jones et al. (2009). Jones et al. (2009) reported basal conglomerate to display a Paleoproterozoic detrital age population ranging from 1681-1815 Ma with a peak population at 1722 Ma and a reported minimum age of 1701±16 Ma. The quartzite display a Paleoproterozoic age range from 1696-3079 Ma with a peak population at 1734 Ma and a reported minimum age of 1707±18 Ma.

Detrital zircon samples for the study reported in this thesis were selected for two purposes: 1) to verify the QPC detrital signature reported by Jones et al. (2009), and 2) to analyze units structurally higher (further away from the contact with the basement) in order to determine if the detrital zircon signature changes significantly over the course of deposition. Zircon fractions from QPC-07 (BR060913-07), QPC-08 (BR060913-08), and quartzite (BR061013-01) were identified and selected from grain mounts analyzed by QEMSCAN®. Zircon fractions for the mica-quartz schist (BR061213-01) were hand-picked from heavy-mineral separates.

QPC samples

Zircon morphology in the detrital samples varied from acicular and prismatic to subhedral and subrounded, with the majority of grains falling into the latter category. Some grains appeared frosted and pitted while others did not. Color was heterogeneous and ranged from clear to slightly pink or yellow. The detrital zircon $^{207}Pb/^{206}Pb$ age range in the two basal QPC samples based on analyses <3% discordant is 1681 – 1811 Ma (Figure 19C and 20C). Concordia ages calculated for grains established to be <3% discordant produced peak ages of 1720.1 ±4.8 Ma for QPC-07 (BR060913-07) (Figure 19B) and 1707.7 ±4.7 Ma for QPC-08 (BR060913-08) (Figure 20B). These results are consistent with those of Jones et al. (2009). Concordant Archean-aged analyses were not obtained from the QPC samples. CL imagery for zircon grains in the QPC commonly displayed high- to medium- intensity cores and relatively dark rims. Many of the grains showed well-developed oscillatory zoning patterns with distinct rims and cores. Some grains were completely dark, indicating pervasive crystal lattice damage. A small percentage of grains displayed a granular texture, with no zoning and low-intensity imagery (see Appendix B for U-Th-Pb data and Appendix C for CL imagery).

Quartzite sample

The detrital zircon $^{207}Pb/^{206}Pb$ age range in the quartzite (BR061013-01) located ~700m south of the QPC was 1682-2976 Ma for analyses <3% discordant (Figure 21A and 21B and 21D). This sample is characterized by Proterozoic-aged grains and very little Archean input (<6% of analyzed grains). The majority of analyses were between 1682 and 1820 Ma (Figure 21B). The minimum calculated age on the three youngest grains <3% discordant for the quartzite is 1696.6 ± 7.5 Ma (n = 3) (Figure 21C). A Th/U vs. $^{207}Pb/^{206}Pb$ age diagram and effective uranium (eU) vs $^{206}Pb/^{238}U$ age diagram were calculated on grains <3% discordant to check for unique data populations and trends indicative of Pb-loss (Figure 21E and 21F). Th/U ratios are variable for all analyses, ranging from 0.1 to 0.8, with no unique clusters or populations. The eU concentrations are mostly restricted to values below 400, with two outliers close to 800, with no clear trend towards Pb-loss. CL imagery for zircon grains in the quartzite is similar to that of the QPC, displaying distinct zoning patterns with generally light cores and dark rims. Some grains appeared relatively homogeneous with no apparent zoning pattern and a medium-intensity CL signature. Completely dark and metamict grains were also present but accounted for a only a small percentage of all imaged grains. The youngest (1682 Ma) and oldest (2976 Ma) concordant grains had similar CL signatures, with relatively light cores and darker rims. (See Appendix B for U-Th-Pb data and Appendix C for CL imagery).

Schist sample

The detrital zircon $^{207}Pb/^{206}Pb$ age range for the schist (BR061213-01), which is ~400m across strike from the quartzite, was 30-2564 Ma (Figure 22), with anomalously young concordant ages at 30 Ma and 421 Ma on single grains, and 1163-1463 Ma on four grains. The

Oligocene aged analysis can only be explained by surface contamination from the ca. 28 Ma Fish Canyon Tuff (Schmitz et al., 2001, Gleadow et al. 2015) or from contamination during mineral separation. The Silurian-aged analysis may be related to grain recycling and sediment influx from eastern sources. Charnock et al. (2014) report Silurian dates for zircon in the Merrimack Belt of eastern Massachusetts and Talavera-Mendoza et al., (2007) report Silurian-aged zircon fractions in the Guerrero Terrane of southern Mexico, which they state as being sourced from areas in both North and South America. The Mesoproterozoic aged analyses are known from events in the region and can be correlated to igneous activity related to both the Mazatzal and Grenville orogenic events. However, due to the presence of younger contamination these ages have to be disregarded and only Proterozoic analyses can be reported with any degree of certainty. The Proterozoic $^{207}Pb/^{206}Pb$ age range for the schist based on analyses <3% discordant is 1681-1821Ma, which is almost identical to the basal QPC. A concordia age was calculated on grains <1.5% discordant producing an age of 1710.4 ±3.4 Ma on n = 45 analyses (Figure 22B). The minimum calculated age on the three youngest grains <1.5% discordant for this sample overlapped the calculated concordia age. CL imagery for zircon grains in the schist is similar to the other detrital samples, displaying high- to medium-intensity cores and dark rims. Grains interpreted to be young contaminants had a more intense CL signature and lacked dark rims. (See Appendix B for U-Th-Pb data and Appendix C for CL imagery).

Results of U-Pb Zircon and Apatite Geochronology of Igneous Samples

U-Pb zircon crystallization ages have been reported for the Blue Ridge area by Jones et al. (2009) and include a foliated granodiorite from the northern basement, a sheared granodiorite from the southern contact, and two cross-cutting pegmatite dikes, also from the southern boundary. For the northern granite Jones et al. (2009) report an upper intercept age of 1706 ± 5

Ma, for the southern granite an upper intercept age of 1698 ±4 Ma, and for the pegmatite a reported crystallization age of ca. 1436 Ma based on a concordant zircon fraction that is interpreted to be coeval with a well-documented regional suite of granites and pegmatite dikes emplaced ca. 1440 – 1430 as reported by Reed et al., (1993) and Karlstrom et al., (2004).

The igneous samples collected for this study were used to verify the existing age constraints and to better understand the geologic evolution of the newly identified structural marker units. Zircon fractions from the northern granites (BR060913-04A, BR060913-05), southern granite (BR061113-02), southern augen-gneiss (BR061113-04) and amphibole-bearing leucosome (BR060913-01) were selected from grain mounts analyzed by QEMSCAN®. All other zircon fractions were hand-picked from heavy-mineral separates, including additional grains from the amphibole-bearing leucosome (BR060913-01, BR072815-01). Apatite fractions for the granodiorite (BR061713-03) were hand-picked from heavy mineral separates. Apatite fractions for the amphibole-bearing leucosome (BR060913-01) were identified and analyzed from polished thin-sections. The LA-ICP-MS analyses performed on apatite were done so using zircon GJ1, a non-apatite standard, which can introduce a U-Pb error of 10-12% (Andreas Möller, personal communication, July 12, 2015). Single apatite grains from the granodioritic grus sample were analyzed using Thermal Ionization Mass Spectrometry (TIMS), but the resultant data set was very poor due to low U contents and high common Pb content and not used for this study. Data points from many of the U-Pb zircon igneous samples were discordant to highly discordant (3-97%), likely the result of Pb-loss and/or common Pb. These highly discordant data points were subsequently not included in the age calculations.

Northern Granitoid samples

Two granitoid samples were collected from exposures north of the QPC/granite contact along FS Road 69. The first sample is foliated granite (BR060913-05) located ~1.5 km from the northern contact and the second sample is a weakly foliated biotite-poor granite (BR060913-04A) ~1.1 km from the northern contact. Zircon morphology from both samples consisted of euhedral to subhedral, relatively equant grains with an average aspect ratio of ~1:2.5. Large acicular and small stubby grains were also present, but in limited abundance. Zircon fractions from foliated granite (BR060913-05) define a line with an upper intercept age of 1702 ± 6 Ma and a concordia age of 1708 ± 10 Ma (MSWD of 1.7 for n = 3) (Figure 23B and 23D). A Th/U vs. $^{207}Pb/^{206}Pb$ age diagram and effective uranium (eU) vs $^{206}Pb/^{238}U$ age diagram were calculated on grains <3% discordant to check for unique data populations and trends indicative of Pb-loss (Figure 23E and 23F). Th/U ratios have a range of 0.1 – 0.5, with the three youngest analyses forming a small cluster at ~0.3. The eU concentrations appear to decrease with increasing age, which may indicate a trend towards Pb-loss. The zircon fraction from the granite (BR060913-04A) poorly defines a line with an upper intercept of 1699.7 ± 8.4 Ma (MSWD of 2.3 for n = 24) (Figure 24). A concordia age could not be calculated. CL imagery of zircon grains from both granitoid samples are similar, with high- to medium-intensity signatures and well-defined oscillatory zoning. A few grains display dark rims and/or dark cores, but entirely metamict grains are not present. (See Appendix B for U-Th-Pb data and Appendix C for CL imagery).

Southern granodiorite sample

A sample of coarse-grained biotite granodiorite (BR061113-02A) was collected ~15m from the southern contact and yielded both prismatic, euhedral to subhedral zircon grains and highly fractured and damaged anhedral to subhedral grains and grain fragments. The zircon

fraction in this sample defines a line with an upper intercept of 1698.8 ± 7.5 with an MSWD of 2.0 for n = 38 and a concordia age of 1702.5 ± 4.3 Ma with an MSWD of 1.3 for n=10 analyses (Figure 25A-25C). Jones et al. (2009) report an upper intercept age of 1698 ± 4 Ma for this unit, which falls within error of the age determined in this study. Analyses <3% discordant show a wide spread of results along concordia (Figure 25B). A Th/U vs. $^{207}Pb/^{206}Pb$ age diagram and effective uranium (eU) vs $^{206}Pb/^{238}U$ age diagram were calculated on grains <3% discordant to check for unique data populations and trends indicative of Pb-loss (Figure 25D and 25E). Th/U ratios are similar for all except one young analysis (~1680 Ma), which has a Th/U ratio of 0.6; two times the rest of the data set. The eU concentrations are scattered, with no clear trend inferring Pb-loss. CL imagery of zircons for this sample shows that most grains are fractured, with low-intensity signatures associated with the most-fractured grains. Oscillatory zoning is still discernable, displaying both dark/light cores and rims. Some grains are entirely metamict, but have apparent zircon inclusions that display a high-intensity signature. (See Appendix B for U-Th-Pb data and Appendix C for CL imagery).

Pegmatite Dike samples

Two pegmatite samples were collected along the southern boundary. The first sample was collected from a pegmatite dike intruded into quartzite (pegmatite 1, BR061113-05) and the second was taken from an attenuated pegmatite dike that had intruded augen gneiss (pegmatite 2, BR072815-02). Both pegmatite samples are megacrystic and composed almost entirely of alkali-feldspar and quartz, giving them a distinct pink color. The dikes are <0.4m in thickness and are oriented discordant to the local strike. Extracted zircon show a wide range of morphologies including acicular and prismatic grains with aspect ratios of 5:1 and much smaller euhedral to subhedral prismatic grains with aspect ratios closer to 3:1 and 2:1. Zircons are colorless to pink

and also dark red. Zircon fractions from pegmatite 1 (BR061113-05) are variably concordant and discordant and show signs of Pb-loss (Figure 26A), but selected analyses define a discordia line with an upper intercept of 1714.7 ± 5.1 Ma with a MSWD of 1.3 for n = 42 analyses, and a concordia age of 1716.6 ± 5.1 Ma for n = 20 analyses (Figure 26B and 26C). The zircon fraction from pegmatite 2 (BR072815-02), which has intruded augen gneiss (BR01113-04), also display signs of Pb-loss (Figure 27A), but selected analyses define a discordia line with an upper intercept age of 1713 ± 23 Ma with an MSWD of 0.45 for n = 10 analyses and a concordia age of 1724.1 ± 7.9 Ma with an MSWD of 1.4 for n = 8 analyses (Figure 27B and 27C). The TIMS U-Pb age of pegmatites reported by Jones et al. (2009) is ca. 1436 Ma, but no concordant fraction of that age was found in this study. Analyses <3% discordant yield a range of ages along concordia (Figure 27C). A Th/U vs. $^{207}Pb/^{206}Pb$ age diagram and effective uranium (eU) vs $^{206}Pb/^{238}U$ age diagram were calculated on grains <3% discordant to check for unique data populations and trends indicative of Pb-loss (Figure 27D and 27E). Th/U ratios reveal no significant outliers and eU concentrations are relatively flat for most analyses which do not indicate a trend toward Pb-loss. CL imagery of zircons from both samples is varied. Pegmatite 1 displays grains with well-defined oscillatory zoning and grains that are completely homogeneous, with medium- to high- intensity signatures. Dark, metamict cores are present in some grains, but most display bright cores and low-intensity to dark rims. Pegmatite 2, which was annealed at 900 ^{o}C for 60 hours prior to CL imaging, has a bimodal distribution of grains, with half appearing granular and relatively dark, and the other half appearing prismatic with a bright signature. Oscillatory zoning is visible in the prismatic grains but not present in the metamict granular grains. (See Appendix B for U-Th-Pb data and Appendix C for CL imagery).

Amphibole-bearing Leucosome samples

Two amphibole-bearing leucosome samples were collected from the southern boundary outcrop in an unnamed gulch shown in Figures 14 and 15. The first sample was collected during the field season of 2013 (BR060913-01) and the second during the field season of 2015 (BR072815-01). The leucosome consists of prismatic and bladed hornblende phenocrysts up to 4 cm long in a matrix of quartz and alkali-feldspar. Splits from the sample collected in 2013 were analyzed for U-Pb in zircon four times and for U-Pb in apatite one time using LA-ICP-MS. Zircon analyses were performed twice on grains identified and selected in a grain mount analyzed by QEMSCAN®, and two times on grains handpicked from heavy mineral separates. Analyses from the 2013 samples had various contamination issues that will be discussed below. The sample collected in 2015 was analyzed once from grains hand-picked from heavy mineral separates. LA-ICP-MS analyses performed on QEMSCAN® analyzed grain mounts will be referred to as HBL-QEM1 and HBL-QEM2. Analyses performed on epoxy grain mounts will be referred to as HBL-GM1, HBL-GM2, and on epoxy surface mounts as HBL-TM. The apatite analysis will be referred to as HBL-AP. Most zircons obtained are euhedral to subhedral grains with an average aspect ratio of 2:1. Many grains appeared pock-marked and/or pitted. Color varied from colorless to light pink or pink. A fair amount of grains were fractured or present as fragments of once larger grains.

The zircon fraction from HBL-QEM1 (BR060913-01) yields a poor discordia line with an upper intercept of 1699.4 ± 9.3 Ma with a MSWD of 3.2 on n = 54 analyses (Figure 28A) This same fraction defines a discordia line with an upper intercept age of 1695 ± 17 Ma and a lower intercept age of 1097 ± 93 Ma on 33 analyses <3% discordant (Figure 28B). The lower intercept age is defined by a concordant analysis of a single zircon rim with a $^{207}Pb/^{206}Pb$ concordia age of 1120 ± 20 Ma and a calculated discordance of 1.5% (within error of the

analysis, this is concordant). The core of this grain has a $^{207}Pb/^{206}Pb$ age of 1051 ± 45 Ma and a discordance of -13.4%. When the single concordant ca. 1120 Ma data point is removed from the age calculations the zircon fraction defines a line with an upper intercept age of 1695 ± 19 Ma and a lower intercept age of 1125 ± 330 Ma, similar to the result including the young analyses (Figure 28C and 28D). The upper intercept age is interpreted to represent inheritance of older grains and the lower intercept age is interpreted as a crystallization age of a new zircon rim. A Th/U vs. $^{207}Pb/^{206}Pb$ age diagram and a eU vs $^{206}Pb/^{238}U$ age diagram were calculated on grains <3% discordant to check for unique data populations and trends indicative of Pb-loss (Figure 28E and 28F). The single ca. 1120 Ma data point has a higher Th/U ratio than all but one of the older analyses, which form a relatively uniform cluster. The eU concentration of the young analysis is similar to many of the older analyses, indicating no trend toward Pb-loss. This indicates that the young data point is unique and represents a different stage of zircon crystallization separate from the older analyses. CL imagery of zircon for this sample shows a distribution similar to pegmatite 2, with a relatively even mixture of prismatic grains with high- to medium-intensity signatures and granular grains with medium to low and even dark signatures. The ca. 1120 Ma analysis is from the rim of a prismatic crystal, with a bright CL signature. (See Appendix B for U-Th-Pb data and Appendix C for CL imagery).

Analyses of the zircon fraction from HBL-QEM2 (BR060913-01) are variable and do not yield intercept ages (Figure 29A). Even analyses <3% discordant show a very wide spread of results along concordia, ranging from ~1400-1800 Ma (Figure 29B), making it difficult to assign an age. The highest density cluster of data points exist at 1700 Ma. A Th/U vs. $^{207}Pb/^{206}Pb$ age diagram and a eU vs $^{206}Pb/^{238}U$ age diagram were calculated on grains <3% discordant to check for unique data populations and trends indicative of Pb-loss (Figure 29C and 29D). The Th/U

ratio was shown to decrease with decreasing age and eU concentration was shown to increase with decreasing age. These trends are likely the result of radiation damage and Pb-loss as described by Geunther et al. (2013) and Schoene et al. (2014). This analysis contained one anomalously young grain with a $^{206}Pb/^{238}U$ age at ca. 300 Ma. This age may be attributed to surface contamination from grains sourced from Appalachian age populations. Dickinson (2009) reports detrital U-Pb zircon ages of this range in the Colorado Plateau and High Plains, with Alleghenian plutons to the east as potential sources. CL images were not acquired for this split. (See Appendix B for U-Th-Pb data).

The zircon fraction from HBL-GM1 (BR060913-01) loosely defines a discordia line with an upper intercept age of 1687.1 ± 7 Ma with a MSWD of 3.0 on n = 77 analyses (Figure 30A and 30B), after some outlier removal. Forty-nine analyses <3% discordant define a discordia line with an upper intercept age of 1667 ± 34 Ma with a MSWD of 2 (Figure 30C). These analyses display an age range of ~1600-1750 Ma and the three youngest concordant analyses have a calculated concordia age of 1616 ± 8.9 Ma (Figure 30D). A Th/U vs. $^{207}Pb/^{206}Pb$ age diagram and a eU vs $^{206}Pb/^{238}U$ age diagram were calculated on grains <3% discordant to check for unique data populations and trends indicative of Pb-loss (Figure 30E and 30F). The three youngest grains have Th/U ratios consistent with the rest of the population. The same was true for eU concentrations, indicating no apparent trends toward Pb-loss. CL imagery for this split show a greater amount of medium- to high- intensity signatures of relatively prismatic grains and fewer metamict granular grains. Grains are evenly distributed with both light and dark cores and rims. (See Appendix B for U-Th-Pb data and Appendix C for CL imagery).

The zircon fraction from HBL-GM2 (BR072815-01), with select outliers removed, defines a line with an upper intercept age of 1681.3 ± 8 Ma with a MSWD of 1.8 on n = 53

analyses (Figure 31A). This same fraction defines a line with an upper intercept of 1679 ± 19 Ma and a lower intercept age of 1109 ± 61 Ma (Figure 31B) on analyses <3% discordant. The lower intercept age is defined by four concordant analyses from two grains. Concordia ages calculated on analyses from each grain have an age of 1143 ± 16 Ma on n = 1 analysis and 1073.8 ± 9.2 Ma on n = 3 analyses (Figure 31c and 31D). A Th/U vs. $^{207}Pb/^{206}Pb$ age diagram and a eU vs $^{206}Pb/^{238}U$ age diagram were calculated on the young grains to check for unique data populations and trends indicative of Pb-loss (Figure 31E and 31F). Th/U ratios for the young grains were elevated compared to older Paleoproterozoic grains, and eU concentrations showed no significant trends, indicating that these grains likely crystallized at the calculated time. This split was annealed at 900 ^{o}C for 60 hours prior to CL imaging. CL imagery show medium- to high-intensity signatures for all but a few grains. Approximately half of the grains appear granular and fractured, with no oscillatory zoning. The remainder display well-defined zoning patterns. (See Appendix B for U-Th-Pb data and Appendix C for CL imagery).

Thirty one analyses from the zircon fraction HBL-TM (BR060913-01) defines a line with an upper intercept age of 1704.9 ± 7.8 Ma with a MSWD of 1.7 and a near zero age lower intercept (Figure 32A). Grains determined to be <3% discordant define a line with an upper intercept age of 1693 ± 10 Ma with a MSWD of 1.5 on n = 11 analyses (Figure 32B). A concordia age could not be calculated for this sample. This sample contained two anomalously young grains with $^{206}Pb/^{238}U$ ages of 149 Ma and 37 Ma (Figure 32A). As mentioned previously, these ages may be the result of grain recycling and surface contamination in the field. Dickinson et al. (2009) has reported detrital zircon ages similar to the 149 Ma analysis. The 37 Ma analysis is older than the ca. 28 Ma Fish Canyon Tuff (Schmitz et al., 2001, Gleadow et al. 2015) reported for this area and cannot be directly rectified.

The data obtained from HBL-AP (BR060913-01) yielded no concordant results, as expected from apatite, which typically contains high amounts of common Pb (e.g. Thomson et al. 2012). The data points did, however, define a discordia line with a lower intercept age of 1248 ± 42 Ma (Figure 33A). When only young age analyses are considered, the data points define a discordia line with a lower intercept age of 1185 ± 39 Ma and a MSWD of 2.6 for n = 10 analyses (Figure 33B).

Granodioritic Grus

Heavy mineral separation yielded little to no zircon but abundant apatite. Due to the lack of zircon, apatite was analyzed using LA-ICP-MS. Apatite grains were euhedral, elongate and prismatic and mostly clear in color. Some grains were fractured and broken, likely the result of mineral separation techniques. The apatite fraction was relatively homogeneous and defined a discordia line with a lower intercept of 1016 ± 65 Ma with a MSWD of 1.3 for all 30 analyses (Figure 34A and 34B).

Northern and Southern Boundary Deformation Zones

Three samples were collected from the northern and southern boundary with the intent of constraining the age and timing of deformation at Blue Ridge. The northern contact has been interpreted as depositional by Jones et al. (2009), but deformation fabrics discovered during field research for this study suggest the contact may be a shear zone. The southern contact is a documented shear zone (Knepper, 1972; Reus, 1970, 1974; Mai, 2002; Jones et al., 2009) and samples collected for this study were aimed at identifying metamorphic overgrowths on zircon crystals at both contacts to possibly date the timing of these deformation events.

Northern Foliated Granite

Two samples of foliated granite were collected from the northern boundary in Gooseberry Gulch. One sample was collected during the 2013 field season (BR061613-03) and the second was collected during the 2015 field season (BR073015-01). The foliated granite is leucocratic, fine to medium grained, containing muscovite, quartz, and alkali feldspar. Biotite was notably absent in this sample, but biotite-bearing granite was exposed in a small outcrop <1m away. Zircon morphology was variable, ranging from euhedral prismatic grains to rounded and subrounded subhedral grains. Grains were colorless to pink or light pink. The sample collected in 2013 was analyzed for U-Pb in zircon by LA-ICP-MS three times and the 2015 sample one time. All analyses were performed on grain mounts with zircon selected from heavy mineral separates. Samples will be referred to as NFG13-GM1 (BR061613-03), NFG13-GM2 (BR061613-03), and NFG15-GM1 (BR073015-01). Samples NFG13-GM1 (BR061613-03) and NFG15-GM1 (BR073015-01) contain zircon grains that are interpreted as contaminants, which will be discussed below.

The zircon analyses from NFG13-GM1 (BR061613-03), with selected outliers removed, define a discordia line with an upper intercept age of 1703.3 ± 7 Ma with a MSWD of 1.8 on n = 21 analyses (Figure 35A). Analyses <3% discordant produce a cluster of ages centered around 1710 Ma and one age centered at 1450 Ma (Figure 35B). Grains <1% discordant define a concordia age of 1710.8 ± 3.9 Ma with a MSWD of 1.01 for n = 13 analyses (Figure 35C). This sample contained one concordant analysis on a zircon core with a concordia age of 1447 ± 13 Ma (grain 45c, Appendix C). A Th/U vs. $^{207}Pb/^{206}Pb$ age diagram and an eU vs $^{206}Pb/^{238}U$ age diagram were calculated on analyses <3% discordant to check for unique data populations and trends indicative of Pb-loss (Figure 35E and 35F). The analyses at ca. 1450 Ma shows increased Th/U content compared to the older cluster of ~ 1710 Ma analyses. The eU concentration of all

grains is similar and does not indicate a trend toward Pb-loss. This analysis also contained three analyses with anomalously young ages, one with a $^{206}Pb/^{238}U$ age of ~30 Ma, and two with $^{206}Pb/^{238}U$ ages of ~150 Ma. The age and possible source of these grains are similar to inferred contaminants mentioned above. Because of the presence of these potential contaminants, the ca. 1450 Ma grain cannot be interpreted as a reliable age. CL imagery for this split revealed that many grains have metamict anhedral or granular rims that surround high-intensity signature cores. Analyses on the metamict rims resulted in highly discordant data points. Additional grains are entirely dark, with faint traces of primary oscillatory zoning. (See Appendix B for U-Th-Pb data and Appendix C for CL imagery).

The zircon analyses from NFG13-GM2 (BR061613-03), after removal of outliers influenced by common Pb, define a discordia line with an upper intercept of 1714 ± 11 Ma with a MSWD = 1.2 for n = 13 analyses (Figure 36A) and a concordia age of 1713.6 ± 7.2 Ma on 8 analyses <3% discordant (Figure 36B). (See Appendix B for U-Th-Pb data and Appendix C for CL imagery).

The zircon analyses from NDG15-GM1 (BR073015-01) (Figure 37A) are scattered along a discordia line that does not define an accurate intercept. A concordia age of 1718.3 ± 7.2 Ma with a MSWD of 0.66 was determined on 9 analyses <3% discordant (Figure 37B). Inheritance of an older component is indicated by an analysis at 1841 Ma. This zircon separate contained four analyses with anomalously young $^{206}Pb/^{238}U$ ages at 86 Ma, 149 Ma, ca. 250 Ma, and 558 Ma. The 149 Ma age grain is similar to contaminants present in samples HBL-TM and NFG13-GM1. The additional young ages are similar to detrital zircon ages reported by Dickinson et al. (2009) in the Colorado Plateau and High Plains are likely the result of surface contamination. This split was annealed at 900 ^{o}C for 60 hours prior to CL imaging. CL imagery acquired for this

split is similar to that described in NFG13-GM1, but has a greater abundance of completely metamict grains. (See Appendix B for U-Th-Pb data and Appendix C for CL imagery).

Southern Augen Gneiss

One sample was collected from the southern augen gneiss (BR061113-04). Zircon from this sample was analyzed twice using LA-ICP-MS, one on a hand-picked polished grain mount SAG-GM (BR061113-04) and one from grains on a hand-picked surface mount SAG-TM (BR061113-04). The augen gneiss is heavily foliated and coarse grained, containing large phenocrysts of alkali-feldspar and quartz. The separated zircons have different morphologies and grain sizes, ranging from 50 – 200 μm. Most grains were euhedral to subhedral and range from colorless to light pink. Approximately half of the grains showed heavy fracturing and/or pitting.

Forty-seven zircon analyses from SAG-GM (BR061113-04) define a discordia with an upper intercept age of 1717 ± 5.4 Ma with an MSWD of 2.0, after removal of some outliers (Figure 38A). A concordia age of 1712.4 ± 6.3 Ma with an MSWD of 1.9 was obtained from 13 analyses <3% discordant (Figure 38B).

Forty-seven analyses were carried out on SAG-TM (BR061113-04) (Figure 39A), but these were scattered along discordia and an accurate upper intercept could not be calculated. Analyses <3% yielded a range of ages along concordia, which also prevented the calculation of an intercept age (Figure 39B). A concordia age on 11 analyses <2% discordant yields a more reliable age estimate of 1717.4 ± 8.3 Ma with a MSWD of 2.0 (Figure 39C). A Th/U vs. $^{207}Pb/^{206}Pb$ age diagram and a eU vs $^{206}Pb/^{238}U$ age diagram were calculated on analyses <3% discordant to check for unique data populations and trends indicative of Pb-loss (Figure 39D and 39E). The resultant data did not identify any unique populations and showed no trends toward

Pb-loss. CL imagery for this sample reveals grains with moderate- to high-intensity signatures with little to no metamict rims or cores. Oscillatory zoning is well defined in the majority of grains. (See Appendix B for U-Th-Pb data and Appendix C for CL imagery).

Chapter 6. Results of Neodymium Isotope Analysis

Six samples were selected for neodymium isotope analysis to determine crustal residence ages for igneous bodies at Blue Ridge and to correlate the newly identified structural marker units with granitic plutons at the northern and southern boundary of the Blue Ridge metasedimentary units and with plutons exposed in the greater mid-central Front Range. Plutons associated with the Boulder Creek (~1.7 Ga), Silver Plume (~1.4 Ga), and Pike's Peak event (~1.1 Ga) are all present within a short distance of Blue Ridge (Anderson and Cullers, 1999). The samples selected for this study include northern granite (BR060913-04A), northern syenite (BR060913-04B), southern granite (BR061113-01), southern granodiorite (BR061113-02), amphibole-bearing leucosome (BR060913-01), and a diabase dike (BR060314-01). The granodioritic grus was highly weathered and not analyzed due to possible contamination from surrounding units. Data for all neodymium analyses is in Appendix D.

Figure 40 displays Nd isotopic evolution paths for all samples as well as the εNd evolution path for typical 1800 Myr Colorado crust as determined by DePaolo (1981). Results show that the northern granite (BR060913-04A), northern syenite (BR060913-04B), southern granodiorite (BR061113-02), and amphibole-bearing leucosome (BR060913-01) follow very similar εNd evolution lines, with εNd(0) values ranging from -12.00 to -16.00 and depleted mantle model (T_{DM}) ages ranging between 1680 and 1914 Ma. The southern granite (BR061113-01) has a very low εNd(0) value of -23.16, but corrects back to the DePaolo depleted mantle line

at a T_{DM} age of 1766 Ma, due to its low Sm/Nd ratio. The four samples with similar evolution paths also directly parallel the εNd path of typical 1800 Myr Colorado crust, indicating that the granitic bodies at Blue Ridge were formed from the same homogeneous mantle material during the 1,800 Myr crustal formation event and/or that their Sm/Nd ratio was not fractionated at a later time. The diabase dike is very different from the other samples and follows a distinctive Nd isotope evolution line with an εNd(0) value of -6.10 and a T_{DM} age of 1182 Ma. This may indicate a mantle-derived basaltic melt associated with Grenville-aged igneous activity, possibly the Pike's Peak event which has a reported U-Pb zircon age of 1085.6 ± 2.5 Ma (Smith et al., 1999).

Chapter 7. Results of Major and Trace Element Geochemistry of Select Igneous and Metasedimentary Rocks at Blue Ridge

Twenty-one samples (5 igneous, 16 metasedimentary) were collected for whole rock major and trace element analyses, which were used for pressure-temperature (P-T) modeling of select metasedimentary units (discussed in chapter 8) and for elemental comparison of select igneous and metasedimentary signatures. Multi-element and rare earth element (REE) signatures of the northern and southern granites were compared with those of the amphibole-bearing leucosome in order to determine if these units evolved from similar source regions. Multi-element and REE patterns from the northern granitic basement were compared with patterns from select metasedimentary units in order to determine if the northern granitic basement was a potential source for the original Blue Ridge metasedimentary protoliths. Multi-element data was normalized using the chondrite values of Sun and McDonough (1989) and REE data was normalized using the chondrite values of Anders and Grevesse (1989). Additionally, whole-rock data was used to model the degree of weathering in the northern granitic basement based on the

chemical index of alteration (CIA) calculation of Nesbitt and Young (1982, 1984, 1989). Select plutonic rocks were classified using the total alkali versus silica (TAS) diagram of Wilson (1989). The location of all geochemistry samples is shown in Figure 41 and whole rock and REE data can be found in Appendix E, Table E-1.

Comparison of Elemental Signatures of Select Igneous Rocks

Elemental signatures of two northern granitoids (BR060913-04A, BR060913-04B) and two southern granitoids (BR061113-01, BR061113-02) are compared with those of an amphibole-bearing leucosome (BR060913-01). The northern granitic basement includes biotite-rich (BR060913-04B) and biotite-poor (BR060913-04A) granitoids and the southern granitic basement includes fine-grained (BR061113-01) and coarse-grained (BR061113-02) granitoid samples. Whole-rock data from each sample are plotted on the TAS diagram of Wilson (1989) in order to determine their rock type (Figure 42, [SiO_2 vs. $Na_2O + K_2O$]; based on data in Appendix E, Table E-1). The samples from the northern granitic basement are classified as granite (BR060913-04A) and syenite (BR060913-04B). Samples from the southern granitic basement are classified as granite (BR061113-01) and granodiorite (BR061113-02). The amphibole-bearing leucosome (BR060913-01) is classified as a granodiorite.

Multi-element and REE concentrations were normalized to chondrite meteorite compositions and plotted in Figure 43 (data listed in Appendix E, Table E-3 and E-4). The Average Upper Crust (AUC) values of Taylor and McLennan (1981) were added to both diagrams for comparison, and the North American Shale Composite (NASC) values of Gromet et al. (1984) were included in the REE plot. The AUC and NASC are representative of average crustal material and deviations from these values can be used to infer source heterogeneity.

Multi-element patterns for the samples from the northern and southern granitoid basement rocks follow the same general trends, with marked variations in K, Ta and Nb (Figure 43A). The northern syenite (BR060913-04B) has higher K (as expected for this tock type) than all other granitoids and increased Ta and Nb concentrations. This syenite also displays a pronounced negative slope from Ta to Nb, while all other granitoids display a slightly negative or slightly positive slope. Ta/Nb for the syenite is 2.8, while all other granitoids show Ta/Nb between 0.93 and 1.21. Additionally, both of the northern granitoids (BR060913-04A and 04B) appear to be depleted in Sr compared to the southern granitoids (BR061113-01 and -02). The amphibole-bearing leucosome (BR060913-01) shows a negative Nb anomaly and displays an overall negative trend towards Y. The average upper crust (AUC) generally follows the enrichment patterns of the granitoids but drops off significantly toward Y, similar to the amphibole-leucosome. REE patterns for the northern and southern granitoid basement samples have similar trends, showing a gradual depletion from La to Eu, very minor Eu anomalies, and relatively flat HREE patterns with Gd/Lu between 1.966 and 2.152 (Figure 43B). When compared to the AUC and NASC, the granitoids follow the same general pattern, but have higher concentration values for almost all elements listed. The amphibole-bearing leucosome displays a pronounced negative slope, showing depletion in heavy REE, with Gd/Lu at 3.348, and a marked deviation from both the AUC and NASC. The La/Yb ratio is also very high (60:1) compared to the granitoid samples (8:1).

Comparison of Northern Granite and Metasedimentary Elemental Signatures

Multi-element and REE concentrations from two samples of northern granitoid (BR060913-04A and -04B, described above) and sixteen metasediments are plotted in Figure 44. Figure 45 shows multi-element concentrations for the sixteen metasediments as compared to the

NASC. The metasediments include mica-quartz schist (BR011314-01, BR061313-01), cordierite-mica-quartz schist (BR061513-06, BR061613-08), cordierite-garnet-mica-quartz schist (BR061513-03), garnet-mica-quartz schist (BR061213-04, BR061413-02, BR061513-01, BR061713-01, BR011314-03, BR011414-04), garnet-biotite-quartz schist (BR061313-03, BR011414-03), sillimanite-garnet-mica-quartz schist (BR061213-01, BR061213-05), and staurolite-garnet-mica-quartz schist (BR060912-02). As noted above multi-element variability exists between the two northern granitoid samples (BR060913-04a and -04B), with marked differences in Ta/Nb. The metasediments display very similar multi-element patterns, with more variability in the mobile elements Ba, Th, and K. Zr concentrations are also variable, with marked positive and negative anomalies, probably controlled by minor variations in heavy mineral content. Compared to the granitoid patterns, the metasediments follow the trend of the northern granite (BR060913-04A) more closely than that of the northern syenite (BR060913-04B). The northern syenite has higher concentrations of Rb, Ba, K, Ta, and Nb, than the metasediments, but follows the same general pattern from La to Y. The northern granite has slightly higher values of Ba and Th, but otherwise follows the same trend as the metasediments. The metasediments do display a more pronounced negative Sr anomaly than either granitoid.

The REE patterns for the metasediments are relatively homogeneous in LREE concentrations, but more variable in HREE concentrations. Some HREE trends have a flat or even slightly positive slope, while others maintain an overall negative slope, with a noticeable range in concentrations between samples. The samples with flat and/or positive HREE trends include cordierite-mica-quartz schist (BR061613-08), garnet-mica-quartz schist (BR061213-04, BR061513-01, BR011314-03, BR011414-04), garnet-biotite-quartz schist (BR061313-03) and staurolite-garnet-mica-quartz schist (BR060912-02). The remaining samples have negative

HREE patterns and include mica-quartz schist (BR011314-01, BR061313-01), cordierite-mica-quartz schist (BR061513-06), cordierite-garnet-mica-quartz schist (BR061513-03), garnet-mica-quartz schist (BR061413-02, BR061713-01), garnet-biotite-quartz schist (BR011414-03), and sillimanite-garnet-mica-quartz schist (BR061213-01, BR061213-05). A minor Eu anomaly is present in all metasediment samples, as in the granitoid samples. Overall, the REE concentrations in the metasediments follow the same general trend of the northern granitoids, with noted variability in HREE trends. Comparing multi-element concentrations of the metasediments with those of the NASC (Figure 45) revealed a relative depletion in Ti and enrichment in Zr and Y. The metasediments also show greater depletion in Sr as compared to the NASC. REE concentrations follow the same general trend of the NASC, with most metasediments showing elevated values higher than the NASC. Flat, negative, and positive HREE trends are seen in all metasediment samples and cannot be correlated to a single rock type and mineral assemblage.

Chemical Index of Alteration (CIA) Calculations

Whole-rock data was used to calculate the CIA of metasediments in order to quantify the degree of weathering experienced prior to burial and metamorphism. The $(Na_2O + CaO) – Al_2O_3 – K_2O$ ternary diagram of Nesbitt and Young (1984, 1989) was also used to model the weathering trend of the metasediments. The interpretation of weathering trends is based on the hypothesis by Jones et al. (2009) that the northern granites are the source of material for the metasedimentary units at Blue Ridge. In the ternary, average granite is plotted with muscovite, illite, kaolinite, and K-feldspar. Typical granite displays a weathering pattern towards the composition of illite, and an advanced weathering pattern toward the composition of kaolinite (Deer, 1992, after Nesbitt and Young, 1984 and 1989). The northern granite (BR060913-04A),

northern syenite (BR060913-04B), and all metasediments (see sample numbers above) are plotted on the $(Na_2O + CaO) – Al_2O_3 – K_2O$ ternary to establish their comparative compositional relationship to typical granite and the inferred weathering by-products of illite and kaolinite. CIA is calculated using the following equation (oxide molar proportions) from Nesbitt and Young (1982) and is expressed as a percent:

$$CIA = [Al_2O_3/(Al_2O_3 + CaO + Na_2O + K_2O)]*100$$

The range of CIA values calculated for 16 metasediments [mica-quartz schist (BR011314-01, BR061313-01), cordierite-mica-quartz schist (BR061513-06, BR061613-08), cordierite-garnet-mica-quartz schist (BR061513-03), garnet-mica-quartz schist (BR061213-04, BR061413-02, BR061513-01, BR061713-01, BR011314-03, BR011414-04), garnet-biotite-quartz schist (BR061313-03, BR011414-03), sillimanite-garnet-mica-quartz schist (BR061213-01, BR061213-05), and staurolite-garnet-mica-quartz schist (BR060912-02)], is 68 – 84%, with an average of 74% (see Appendix E, Table E-5). The northern granitoid samples (BR060913-04A and -04B) from this study have CIA values between 45 – 55%. Average shales range from 70 – 75% (Nesbitt and Young, 1982). Low values are typically associated with fresh rock and high values are associated with more altered material. The overall change in CIA is interpreted to be related to changes in the proportion of feldspar to clay minerals (Nesbitt and Young, 1982). Results from this study infer that the 16 metasediments fall within the range of an average shale as described above by Nesbitt and Young (1982). The $(Na_2O + CaO) – Al_2O_3 – K_2O$ ternary diagram in Figure 46 shows the weathering pattern of a typical granite compared to the weathering pattern of the northern granite and syenite at Blue Ridge. The weathering pattern at Blue Ridge is inferred by comparing the plotted location of the northern granite and syenite (source) with the plotted location of the metasediments (sink). Any deviation from the

weathering pattern of typical granite infers that chemical changes have occurred possibly as a result of diagenesis or metasomatism (Deer, 1992, after Nesbitt and Young, 1989). The northern granite (BR060913-04A) plots concordantly with the typical granite on the ternary diagram. The northern syenite (BR060913-05) plots closer to the average composition of K-feldspar, which is expected for this rock type. The majority of metasediments plot above both granite and syenite, with a general trend towards the compositions of muscovite and illite; however, there is noticeable scatter, with small populations visibly deviating from assumed trends. Some metasediments appear to have higher (Na_2O + CaO) values, and others show higher K_2O values. Nesbitt and Young (1989) indicate that early and late diagenetic reactions can occur in which groundwater, basin water, seawater, or brines react with secondary weathering products resulting in high accumulations of Si, CO_2, Ca, and Mg. These authors also note that metosomatic effects can reconstitute partially degraded feldspars to form potash feldspar and albite at the expense of kaolinite. The trends displayed for the Blue Ridge metasediments may be the result of both of these factors. Mclennan et al. (1995) reports that Paleoproterozoic metasedimentary rocks of the Hondo Group and Uncompahgre Formation in northern New Mexico and southern Colorado have high CIA values that plot close to illite, which is consistent with a severe weathering history affecting the source rocks.

Chapter 8. Results of Garnet-Biotite Thermometry and P-T Modeling

P-T conditions were calculated using whole rock data from thirteen metasedimentary samples using the Theriak/Domino software of Capitani and Petrakakis, (2010). Estimated temperatures of garnet growth were calculated on four garnet porphyroblasts from a staurolite-garnet-mica-quartz schist (BR060912-02) using the garnet-biotite thermometer of Perchuk and Lavrent'Eva (1983). Whole rock data used to calculate equilibrium assemblage diagrams is

located in Appendix E, Table E-6 and EPMA data used for thermodynamic modeling are located in Appendix F.

Thirteen samples were utilized for P-T modeling and consist of the following: cordierite-mica-quartz schist (BR061513-06, BR061613-08), cordierite-garnet-mica-quartz schist (BR061513-03), garnet-mica-quartz schist (BR061213-04, BR061413-02, BR061513-01, BR061713-01, BR011314-03, BR011414-04), garnet-biotite-quartz schist (BR061313-03), sillimanite-garnet-mica-quartz schist (BR061213-01, BR061213-05), and staurolite-garnet-mica-quartz schist (BR060912-02). Andalusite-bearing schist was also collected at Blue Ridge, but whole-rock data was not obtained for this samples. Equilibrium assemblages were calculated for each sample (Figure 47) and the subsequent intersection of all combined assemblages define three distinct P-T regimes (Figure 48). The highest pressure P –T regime is defined by the mineral assemblage quartz + muscovite + biotite + chlorite + garnet + staurolite + ilmenite + feldspar and displays a maximum P and T of 5.2 kb and 570 ^{o}C. The intermediate pressure P – T regime is defined by the mineral assemblage quartz + muscovite + biotite + garnet + sillimanite + ilmenite + feldspar and displays a maximum P and T of 4.6 kb and 635 ^{o}C and straddles the kyanite-anadalusite stability field, transecting the triple point and extending into the sillimanite stability field. The lowest pressure P-T regime is defined by the mineral assemblage quartz + muscovite + biotite + garnet + cordierite + ilmenite + feldspar and displays a maximum P of 3.9 kb at 620 ^{o}C.

Garnet core and rim temperatures were calculated from EPMA data of four garnets from sample BR060912-02 at pressures of 4, 5 and 6 kb and display a temperature range of 550 – 640 ^{o}C (Figure 49). These temperatures overlap with the upper temperature P-T conditions defined by the highest and medium pressure equilibrium mineral assemblages listed above. Isopleths

were calculated for the almandine, pyrope, and grossular fractions of garnet using whole rock and electron microprobe data from sample BR060912-02 in order to further constrain the P-T conditions of formation. The intersection of the isopleths infers the P-T conditions ideal for garnet growth. Almandine concentration was calculated at 87%, pyrope 12%, and grossular 1%, which intersects at ~5kb and 600 ^{o}C (Figure 50), well within the P and T limits determined from Grt-Bt thermometry above.

Petrographic analysis on samples from each P-T regime reveals reaction textures that show a clockwise P-T evolution. In Figure 51A, muscovite is present as a pseudomorph after staurolite. Biotite is seen breaking down to sillimanite (fibrolite) (Figure 51B), and poikiloblastic cordierite is visibly consuming quartz and mica in Figure 51C. The reaction muscovite forming from staurolite breakdown has been reported by Guidotti (1968) and is defined by the reaction:

$$Staurolite + muscovite + quartz = sillimanite + biotite + muscovite + albite + H_2O \pm garnet$$

The reaction reported by Guidotti (1968) can also be used to explain the presence of sillimanite and biotite. The following reaction reported by Deer (1992) is similar to that of Guidotti (1968) and can be applied to the formation of sillimanite and biotite as well as the initial garnet forming reaction:

$$Staurolite + muscovite + quartz = garnet + Al_2SiO_5 + biotite + H_2O$$

Cordierite formation occurs at the expense of garnet or staurolite during decompression and cooling and is explained by the reaction reported by Garcia-Casco et al. (1999):

$$Staurolite + garnet + biotite + muscovite + plagioclase + rutile = cordierite + biotite + muscovite + plagioclase + ilmenite$$

An inferred P-T evolution is presented in Figure 52 which follows a clockwise path starting with garnet formation at ~5 kb and 570 ^{o}C, maximum temperature reached at ~625 ^{o}C, and subsequent cooling and decompression thereafter.

Chapter 9. Results of Electron Probe Micro-Analysis Garnet Transects

Garnet transects were produced on four garnets from staurolite-garnet-mica-quartz schist sample BR060912-02 and are displayed in Figure 53. Garnets are euhedral to subhedral and up to 1cm. Three of the four garnets are poikiloblastic, with inclusions of quartz and mica. The garnet composition consists of 80% almandine, 12% pyrope, 7% spessartine, and 1% grossular. Garnets show no signs of consistent core-rim zoning and are relatively homogeneous. The profiles in all garnets follow the same general trend, displaying slight increases in X_{FE}, Sps, and Grs toward the rim, and a slight decrease in Py. The increase in X_{FE} at the garnet rims can be associated with minimal resorption and retrograde diffusion back into the porphyroblast.

Chapter 10. Results of Heavy Mineral Analysis by QEMSCAN®

A northern granite (BR060913-04A), northern syenite (BR060913-04B), northern foliated granite (BR060913-05), two samples of QPC (BR060913-07 and -08), and three quartzite samples (BR061013-01, BR061013-02, BR061113-07) were analyzed for heavy mineral type and abundance using QEMSCAN®. QPC and overlying quartzite have been interpreted to result from a single-cycle of weathering and deposition sourced from and deposited onto the adjacent granite, forming a nonconformable depositional contact (Jones et al., 2009). This study analyzed the heavy mineral content of these rocks in order to determine if a source-sink relationship exists between igneous and sedimentary units. Zircon, rutile, apatite, monazite, ilmenite, and Fe oxide concentrations were normalized to 100% and compared. Heavy

mineral/zircon ratios were also evaluated and contrasted between samples (Figure 54). Heavy mineral contents varied between the units. Zircon concentrations are highest in the northern granite (BR060913-04A) at ~52%, and are lower in all other samples, ranging from 6 – 32%. Fe-oxide content is ~10% or less in all granitoid and QPC samples, but increases sharply in the quartzite, ranging from 60 – 90%. Apatite concentrations are high in the granitoid and the QPC samples at 37 – 64%, but are significantly lower in the quartzite samples at <3%. Monazite is noticeably absent from the quartzite samples, but present in the QPC and granitoid samples. Ilmenite and rutile are found in two granitoid samples and two quartzite samples but is present only in trace amounts in the QPC samples. Heavy mineral to zircon ratios display similar trends, with very high apatite/zircon in the granitoid and QPC samples and very low ratios in quartzite samples. Monazite/zircon ranges from 0.09 - 0.26 in the granitoids and 0.17 - 0.70 in the QPC Monazite/zircon in quartzite is noticeably low, ranging from 0.00 – 0.06. Rutile/zircon ratios are variable, with significant values in the foliated granite (BR060913-05), syenite (BR060913-04B), and two quartzite samples (BR061113-07 and BR061013-01), but very low values of 0.01 in both QPC samples. These are interpreted to show that heavy mineral content in the QPC and granite are relatively comparable, whereas the quartzite displays marked differences from both QPC and granite. A direct source-sink relationship does not present itself, but noticeable patterns do exist.

Chapter 11. Results of Granite and QPC Microstructural Analysis

Microstructures visible in quartz grains from basal QPC and adjacent granitic basement were analyzed and compared to one another in order to determine if the pebble quartz grains present in the QPC could have been sourced from this granitic basement. Initial field research showed that most quartz grains within the QPC were 1.5x to 2x the size of grains visible in the

granitoid, thus making the granitoid an unlikely direct quartz sediment source. Petrographic analysis reveals that quartz pebbles within the QPC are polycrystalline in nature and composed of sutured aggregates of once smaller quartz grains. Microtextures in the form of chessboard patterns are visible in both the QPC and granite (Figure 55), but grain boundaries and inclusion patterns differ in both (Figure 56). Grain boundaries in QPC occur at high angles, are sutured, and are commonly marked by trails of muscovite that follow the path of the suture (Figure 57). Grain boundaries in the granitoid are sharp and occur at high angles, with large muscovite grains found outlining the quartz crystals, not within the grains themselves (Figure 57). Inclusions within quartz grains in the QPC are often found in clusters, while inclusions within quartz grains in granite appear to be randomly distributed (Figure 56). Additionally, muscovite trails exist at high angles to one another within QPC grains, but are not present in the granite (Figure 58).

Chapter 12. Discussion

The research conducted for this study focused on the following goals: 1) testing the hypothesis that the basal conglomerate and overlying quartzite units are the result of erosion and first-cycle deposition from the northern granitic basement, 2) verifying the timing constraints on sediment deposition, 3) quantitatively determining the pressure/temperature conditions and trajectory during metamorphism, 4) accurately constraining the timing of deformation, metamorphism, and igneous activity. New field observations, coupled with geochronology and geochemistry, provide insight into the nature of boundary relationships at both the northern and southern contacts and further constrain the timing and conditions of metamorphism and previously undocumented igneous activity.

The Northern Boundary

Jones et al. (2009) report that the northern boundary of the Blue Ridge area is depositional in nature and represents original sedimentation of quartz-rich sediment sourced from the adjacent granitic basement onto a weathered granitic surface; and that this is a type locale for a period of very efficient and rapid weathering at 1.7 Ga due to acidic ocean chemistry and/or enhanced diagenetic alteration (Jones et al. 2009; Medaris et al. 2003; Cox et al., 2002; Canfield, 1998; Canfield and Teske, 1996). Field research and geochemistry analyses from this study only partially support the single-cycle depositional hypothesis of Jones et al. (2009). To summarize, the QPC is composed overwhelmingly of large (~2.5 cm) quartz pebbles, with an abundance of foliated muscovite present as matrix. Field research reported by Mai (2002), notes that quartz grains within the northern granitoids are much smaller than the pebbles of the QPC and therefore are not a viable source of sediment. Petrographic analysis from this study finds that quartz within the QPC is polycrystalline in nature and composed of sutured aggregates of quartz grains that display similar micro textures as quartz in the northern granitoids. The interpretation by Mai (2002) does not take into account the polycrystalline nature of the QPC. The size of the QPC pebble presents deceiving field evidence, but it is probable that smaller, weathered grains from the granitoids were sutured to form larger pebbles. The pebble aggregates in the QPC display chessboard micro textures similar to quartz grains in the granitic basement, but also contain clusters of inclusions and inclusion trails, which are absent in the granitoid quartz (Figures 55 – 58). Passchier and Trouw (1996) note that locally concentrated areas of inclusions and inclusion trails within grains outline relict grain boundaries. The high angle sutured grain boundaries trailed by muscovite visible in QPC grains are likely the result of grain boundary migration induced by high temperature deformation >500 ^{o}C (Kruhl, 1996; Passchier and Trouw,

1996). Petrographic evidence suggests that the polycrystalline quartz aggregates found within the QPC are most likely composed of smaller, weathered grains of granitic quartz that were deposited individually alongside feldspar and mica and then subjected to high temperature deformation where they were recrystallized, forming larger grains (Figure 59). This model is similar to the depositional model of Jones et al. (2009) in its single-cycle nature, but differs in that a thermal and or metamorphic event is required to form the quartz pebbles. Field reconnaissance along the northern boundary west of Gooseberry Gulch reveals exposures of QPC that contain large alkali-feldspar clasts (Figure 9), also suggesting a granitic source. The abundance of mica in the QPC is likely the result of primary deposition as well as the breakdown of feldspar grains as determined by the reaction *orthoclase* → *muscovite* + *silica* (Wibberley, 1999); thus, the presence of scattered and remnant feldspar clasts would be expected. Wibberley (1999) noted that silica released during orthoclase muscovitisation results in quartz precipitation and can actually lead to a volume gain of silica within adjacent pore space. This may also lead to an increase in quartz pebble size and account for the grain size differential between granite and QPC.

Heavy mineral comparisons between granitoid and QPC are less conclusive, but mineral concentrations and mineral ratios within the QPC display many similarities to those of the northern granitoids. Zircon, apatite, and monazite concentrations are present in notable quantities in both granite and QPC, and zircon/apatite and zircon/monazite ratios were similar. Heavy mineral signatures in quartzite were markedly different from those of the QPC, displaying an absence of apatite and monazite and an increased abundance of Fe-oxides. It should be noted that heavy mineral provenance signals can be influenced by a multitude of factors such as weathering at the source location, mechanical breakdown during transport, weathering during

alluvial storage, and diagenesis, which combined greatly reduce the efficacy of heavy mineral comparison (Morton, 1999). The transport distance for the original sediments at Blue Ridge is interpreted to be short based on the depositional model of Jones et al. (2009); therefore enhanced weathering at the source and diagenetic factors may have the largest control on heavy mineral signatures for this locale. The CIA analyses for the metasediments, which were shown to deviate from the typical granite weathering trends, provide additional evidence for diagenetic or metasomatic alterations that may also contribute to variations in heavy mineral abundance.

Multi-element and REE concentrations from metasedimentary rock samples and adjacent granitic basement were analyzed to compare/contrast potential source and deposition links. REE analyses have been established as reliable indicators of provenance due to their relative immobility both during transport and diagenesis (Taylor and McClennan, 1985, McClennan, 1989). Taylor and McClennan (1982) note that REE are effectively uniform in abundance in fine-grained sedimentary rocks and are not affected by most forms of metamorphism, inferring that metasedimentary rocks are viable indicators of continental crust exposed at the time of original deposition. Munskgaard (2002) tested REE characteristics in clay-rich sediments and found that they maintain a coherent behavior during weathering, erosion, and fluvial transport and show a high resistance to chemical mobilization. Payne et al. (2006) successfully used REE patterns from Paleoproterozoic sedimentary rocks of the Gawler Craton, Australia to identify potential provenance zones, and Garver (1995) effectively used REE patterns in shales located in southern British Columbia to infer the nature of adjacent crustal blocks and noted that fine-grained clastic sediment can homogenize the geochemical characteristics of the source material, resulting in a robust signal. The multi-element patterns of the northern granite (BR060913-04A) and northern syenite (BR060913-04B) were variable, with the syenite showing increased Rb, Ba,

Ta, and Nb. However, the multi-element patterns of the 16 metasediments [mica-quartz schist (BR011314-01, BR061313-01), cordierite-mica-quartz schist (BR061513-06, BR061613-08), cordierite-garnet-mica-quartz schist (BR061513-03), garnet-mica-quartz schist (BR061213-04, BR061413-02, BR061513-01, BR061713-01, BR011314-03, BR011414-04), garnet-biotite-quartz schist (BR061313-03, BR011414-03), sillimanite-garnet-mica-quartz schist (BR061213-01, BR061213-05), and staurolite-garnet-mica-quartz schist (BR060912-02)] match well with the northern granite (BR060913-04A). REE patterns for the northern granite and syenite are comparable to one another and match well with most of the metasediments, displaying slightly negative Eu-anomalies and showing overall LREE enrichment and HREE depletion. There is, however, variability in the HREE patterns of metasediments, with both flat and slightly positive trends. Asiedu et al. (2003) studied Paleoproterozoic metasedimentary rocks in southern Ghana and reported flat HREE trends which the author states as being similar to patterns seen in Archaen shales and possibly the result of provenance mixing. The closest Archaen source rocks to Blue Ridge lie in the Wyoming Province to the north (Figure 1), and detrital zircon analysis revealed a small Archean input, so it cannot be ruled out that a small degree of sediment mixing may have occurred.

U-Pb geochronology using LA-ICP-MS techniques was used to the test age constraints previously reported by Jones et al. (2009). Zircons were analyzed from the northern granitic basement, the basal QPC, and overlying quartzite and schist samples presumably located higher in the original stratigraphy. The age of the northern granitic basement reported by Jones et al. (2009) is 1706 ± 5 Ma, which overlaps the 1702 ± 6 Ma (MSWD of 1.3, n = 31) upper intercept age of the northern foliated granite (BR060913-05) and the 1699.7 ± 8.4 Ma (MSWD of 2.3, n = 24) upper intercept age of the northern granite (BR060913-04A) calculated from this study.

Jones et al. (2009) defined the granite age as the maximum QPC depositional age. Detrital U-Pb zircon ages reported for the QPC and an overlying quartzite by Jones et al. (2009) were dominantly Paleoproterozoic in age with definitive peaks at 1722 Ma and 1743 Ma, and youngest detrital ages of 1701 ± 16 Ma and 1707 ± 18 Ma, respectively. Detrital U-Pb ages calculated in this study are also dominated by Paleoproterozoic ages, with concordia ages of 1720.1 ±4.8 Ma (MSWD of 0.88, n = 32) for QPC-07 (BR060913-07), 1707.2 ±4.7 Ma (MSWD of 0.61, n = 56) for QPC-08 (BR060913-08), and 1710.4 ±3.4 Ma (MSWD of 1.14, n = 45) for the grt-mica-qtz schist (BR061213-01). The quartzite sample (BR061013-01) has a large range of Paleoproterozoic ages, but the three youngest concordant analyses have a concordia age of 1696.6 ± 7.5 Ma (MSWD of 1.05). The youngest concordant detrital ages for the QPC and schist sample overlap the calculated concordia ages and offer no younger concordant analyses than those already reported. Thus, the youngest quartzite age of 1696.6 ± 7.5 Ma is inferred to constrain the maximum age of sediment deposition at Blue Ridge, which is the same as the Jones et al. (2009) estimate of 1701 ± 3 Ma.

Jones et al. (2009) indicate that the northern boundary is depositional in nature and evidence from this study in the form of K-feldspar rich QPC supports this, but field evidence in the form of ductiley deformed pegmatite and visibly deformed QPC in Gooseberry Gulch (Figure 12) suggest that the QPC/granite contact has been strongly deformed, possibly multiple times. This indicates that the boundary was originally depositional but was later activated as a shear zone. Published ages from the southern contact constrain pegmatite emplacement at ca. 1436 Ma (Jones et al., 2009), which infers that the pegmatite located in Gooseberry Gulch was emplaced and deformed, along with QPC, at or about that same time. However, a pegmatite located in Maverick Gulch (Figure 11) cuts directly across the QPC/granite contact into QPC that

appears to have already experienced grain alignment and recrystallization. This suggests that the QPC was subjected to a deformational event prior to pegmatite emplacement. Zircons separated from foliated granite (BR061613-03, BR073015-01) collected near the inferred QPC/granite contact in Gooseberry Gulch were analyzed using CL and LA-ICP-MS for possible metamorphic overgrowths to test the age of deformation at the northern boundary. Three analyses provide within error identical concordia ages of 1710.8 ± 3.9 Ma, 1713.6 ± 7.2 Ma, and 1718.3 ± 7.2 Ma, but no younger populations. One analysis gives a concordant age of 1447 ± 13 Ma, but the existence of younger contaminants prevents this age from being conclusive. P-T and thermodynamic modeling have established that temperatures at Blue Ridge did not exceed 5.2 kb or 635 ^{o}C during metamorphism, so conditions necessary for the formation of partial melts and therefore ideal for growth of new zircon were likely not attained. Thus, a definitive age of deformation at the northern boundary has not been concluded.

The Southern Boundary and Additional Structural Marker Units

Field research at the southern boundary displays ductiley deformed pegmatite that has been emplaced into augen gneiss and adjacent quartzite at a visibly sheared contact (Figure 14 and 15). The augen gneiss is deformed with a sinistral sense of shear. The pegmatite parallels the deformation fabric of the augen gneiss, inferring that deformation and shear zone activation occurred synkinematically with pegmatite emplacement. Age constraints on the pegmatite have been established by Jones et al. (2009) at ca. 1436 Ma, suggesting shear zone activation and igneous activity occurred at this time. U-Pb zircon data was obtained for this study from two pegmatites (BR061113-05, BR072815-02) emplaced within meters of the shear zone, however, the analyses <3% discordant yield concordia ages of 1716.6 ± 5.1 Ma (BR061113-05) and 1724.1 ± 7.9 Ma (BR072815-02). Mesoproterozoic ages were not found in either sample,

suggesting that the concordia ages represent significant inheritance from adjacent granodiorite or quartzite. Zircons were also obtained from the augen gneiss with the aim of testing evidence for shear zone reactivation at ~1.4 Ga. Grains <3% discordant yielded concordia ages of 1712.4 ± 6.3 Ma and 1717.4 ± 8.3 Ma, with no Mesoproterozoic ages present. The age of the augen gneiss determined by Jones et al. (2009) is 1698 ± 4 Ma, slightly younger than the ages obtained in this study. A granodiorite (BR061113-02A) was acquired ~15m from the shear zone and yielded a concordia age of 1702.5 ± 4.3 Ma, which is within error identical to the augen gneiss result by Jones et al. (2009). The U-Pb zircon geochronology obtained in this study does not directly support the hypothesis that an episode of deformation accompanied pegmatite emplacement at 1436 Ma, but the field evidence coupled with age data of Jones et al. (2009) is a strong indicator for such Mid-Proterozoic activity. The reactivation of Proterozoic shear zones has also been well documented in the Homestake shear zone (HSZ) located approximately 100 km northwest of Blue Ridge in the northern Sawatch Range (Shaw, 2005; Shaw and Allen, 2007), and in the Moose Mountain Shear Zone located in the northern Colorado Front Range (Selverstone et al., 2000). Studies from the HSZ define two episodes of deformation: the first at ~1.7 Ga, which produced structures associated with viscous flow, and again at ~1.4 Ga, producing an overprint of localized plastic flow and brittle failure visible in mylonite and ultramylonite (Shaw and Allen, 2007).

A previously undescribed amphibole-bearing leucosome (BR060913-01, BR072815-01) was identified at the southern contact within close proximity to the deformed pegmatite. This leucosome cross-cuts both augen gneiss and quartzite, lacks a definitive foliation, and contains large, randomly oriented phenocrysts of hornblende (Figure 14 and 15). The lack of mineral orientation or foliation suggests that it post-dates pegmatite emplacement and major ductile

deformation at the southern boundary contact. This leucosome also lacks a chilled margin, indicating that the augen gneiss was at an elevated temperature and did not behave in a brittle fashion at the time of leucosome intrusion. U-Pb zircon data yields discordia lower intercept ages of 1097 ± 93 and 1109 ± 43 Ma (Figure 28 and 31). Upper intercept calculations yield discordia ages of 1695 ± 17 Ma, 1695 ± 19 Ma, 1687.1 ± 7 Ma, 1667 ± 34 Ma, 1681.3 ± 8 Ma, 1679 ± 19 Ma, 1704.9 ± 7.8 Ma, and 1693 ± 10 Ma (Figures 28 – 32). U-Pb apatite data define a line with a lower intercept of 1185 ± 39 Ma. The three lower intercept ages are interpreted as crystallization ages for the amphibole-bearing leucosome and are inferred to be related to emplacement of the Pike's Peak batholith at 1085.6 ± 2.5 Ma (Smith et al., 1999). The average upper intercept and weighted average ages represent inheritance from the southern granitic basement. Since metamorphic conditions in the Blue ridge area likely never exceeded minimum melting conditions, this magma is interpreted to have been derived from a distant deeper and hotter source while the rock it intruded into was still ductile and hot enough not to provide a high enough temperature contrast to produce a chilled margin and constrict the melt to a well-defined dike.

In order to further elucidate the origin of the amphibole-bearing leucosome, geochemical data was compared to the northern granite (BR060913-04A), northern syenite (BR060913-04B), southern granite (BR061113-01), southern granodiorite (BR061113-02), as well as Average Upper Crust (AUC) values of Taylor and McLennan (1981). In multi-element diagrams the amphibole-bearing leucosome followed the general trend of the granite and AUC, but showed lower values of Nb and Sm and a relative depletion in Y. Depletion in Y suggests that garnet is present in the source. The REE pattern for the leucosome was noticeably different from the granitoids and AUC, displaying LREE enrichment and HREE depletion, indicating different

sources for each. When La/Yb ratios are compared, the leucosome has a ratio of 60:1, and the granites 8:1. The Gd/Lu ratio of the amphibole-bearing leucosome is 3.348, which is noticeably higher than the granitoids that have an average Gd/Lu of 2. Rocks with very high La/Yb ratios are categorized as adakites. Adakites are characterized by intermediate SiO_2 (>56%), elevated Al_2O_3 (>15%), Sr/Y (>40), and La/Yb (>20), and low Y (<18 ppm) and Yb (<1.9 ppm) (Yu, 2009). Increased La/Yb ratios are attributed to interaction of felsic melt with mantle material and/or deep melting with residual garnet present wherein plagioclase releases Yb which is subsequently trapped by garnet (Moyen 2009).These types of melts were originally defined as granitoid magmas formed by partial melting of young (<25 Ma) hot and fluid-rich oceanic slab in convergent margin settings, but they have also been found to form in non-subduction settings as a result of partial melting of thickened lower crust and from fractional crystallization processes associated with basaltic magmas (Yu, 2009).The amphibole-bearing leucosome has the following concentrations which fall within the adakitic range: SiO_2 (64%), Al_2O_3 (15.4%), Sr/Y (41), La/Yb (60), Y (6.2 ppm), and Yb (0.48 ppm). Geochemical data coupled with the results of geochronology suggest that the amphibole-bearing leucosome is the result of partial melting associated with the Pike's Peak anorogenic event at ~1.1 Ga.

Additional structural marker units in the form of a granodiorite and a diabase dike are also attributed to the Pike's Peak event. Results of Nd isotopic analysis of the diabase show a T_{DM} age of 1182 Ma and an εNd path independent of the surrounding granitic basement. A U-Pb apatite lower-intercept age of 1016 ± 65 Ma is also temporally related to Pike's Peak magmatism. Research by Smith et al. (1999) reports that the Pike's Peak magmatic event was highly variable in composition, with gabbro and diabase dikes emplaced concurrently with sodic and potassic granites. DePaolo (1981) indicates that the Pike's Peak granite is a representative

end product of an exceptionally complex magmatic history, which likely began with mantle-derived basaltic magma. Bright et al. (2014) report that the Pike's Peak batholith, which consists of granite, syenite, gabbro and diabase dikes, is a prime example of coeval silicic magmatism in the Colorado Front Range initiated by partial melting of the lower crust by mafic underplating. This suggests that the diabase dike at Blue Ridge may have evolved in a similar fashion and that the granodiorite, diabase dike, and amphibole melt are cogenetic and was emplaced at approximately the same time. These are the first indications of Pike's Peak age magmatic activity for the Blue Ridge area.

Chapter 13. Summary and Conclusions

The Blue Ridge area offers rare exposure of a Proterozoic depositional basin in the south central Colorado Front Range. Field studies coupled with geochronologic and geochemical analyses have confirmed some of the findings of prior research and revealed several important new insights that further refine the Paleo- and Mesoproterozoic history in the area. This study concludes the following: 1) the northern boundary is depositional in nature and represents original sedimentation of quartz-rich sediment sourced from the adjacent granitic basement onto a weathered granitic surface; 2) the maximum depositional age of the original sediment is constrained at 1696.6 ± 7.5 Ma, based on the youngest concordant zircon population from a quartzite metasedimentary unit; 3) two stages of deformation affected Blue Ridge with the first occurring shortly after the maximum depositional age and again at ~1.4 Ga during a regional tectonothermal event that reactivated existing shear zones, 4) amphibolite-grade metamorphism was attained in the area with a clockwise P-T evolution attaining a maximum pressure of 5.2 kb and maximum temperature of 635 ^{o}C, 5) an additional pulse of coeval silicic and mafic magmatism resulted in emplacement of cogenetic granodioritic magmas, a diabase dike, and an

adakitic amphibole-bearing leucosome associated with the Pike's Peak magmatic event at 1120 ± 20 Ma.

References Cited

Anders, E., Grevesse, N., 1989, Abundances of the elements: Meteoritic and solar: Geochimica et Cosmochimica acta, v. 53, no. 1, p. 197-214.

Anderson, J. L., Cullers, R. L., 1999, Paleo-and Mesoproterozoic granite plutonism of Colorado and Wyoming: Rocky Mountain Geology, v.34, no 2, p. 149-164.

Asiedu, D. K., Dampare, S. B., Sakyi, P. A., Banoeng-Yakubo, B., Osae, S., Nyarko, B. J. B., Manu, J. , 2004, Geochemistry of Paleoproterozoic metasedimentary rocks from the Birim diamondiferous field, southern Ghana: Implications for provenance and crustal evolution at the Archean-Proterozoic boundary: GEOCHEMICAL JOURNAL-JAPAN-., v. 38, no 3, p. 215-228.

Barnhart, K. R., Mahan, K. H., Blackburn, T. J., Bowring, S. A., Dudas, F. O., 2012, Deep crustal xenoliths from central Montana, USA: Implications for the timing and mechanisms of high-velocity lower crust formation: Geosphere, v. 8, no. 6, p. 1408-1428.

Bennett, V.C., DePaolo, D.J., 1987, Proterozoic crustal history of the western United States as determined by neodymium isotopic mapping: Geological Society of America Bulletin, v. 99, p. 674-685.

Bickford, M.E., Van Schmus, W.R., 1986, Proterozoic history of the midcontinent region of North America: Geology, v. 14, p. 492-496.

Bright, R.M., Amato, J.M., Denyszyn, S.W., Ernst, R.E., 2014, U-Pb geochronology of 1.1 Ga diabase in the southwestern United States: Testing models for the origin of a post-Grenville large igneous province: Lithosphere, L335-1.

Capitani, C., Petrakakis, K., 2010, The computation of equilibrium assemblage diagrams with Theriak/Domino software: American Mineralogist, v. 95, p. 1006-1016.

Canfield, D.E., Teske, A., 1996, Late Proterozoic rise in atmospheric oxygen concentration inferred from phylogenetic and sulphur-isotope studies: Nature, v. 382, p. 127-132.

Canfield, D.E., 1998, A new model for Proterozoic ocean chemistry: Nature, v. 396, p. 450-453.

Charnock, R., Kuiper, Y. D., Möller, A., Buchwaldt, R., Hepburn, J. C., 2014, A structural and U-Pb zircon geochronology investigation of the Harvard conglomerate, Vaughn Hill Formation, Vaughn Hill conglomerate, and Ayer granite: implications for post-Acadian deformation in the Merrimack belt, eastern Massachusetts: Geological Society of America Abstracts with Programs, v. 46, no. 2, p. 119.

Condie, K. C., 1982, Plate-tectonics model for Proterozoic continental accretion in the southwestern United States: Geology, v. 10, no. 1, p. 37-42.

Cox, R., Gutmann, E.D., Hines, P.G., 2002, Diagenetic origin for quartz-pebble conglomerates: Geology, v. 30, no. 4, p. 323-326.

Deer, W. A., Howie, R. A., Zussman, J., 1992, An introduction to the rock-forming minerals: London: Longman, pp 696.

DePaolo, D. J., 1981, Neodymium isotopes in the Colorado Front Range and crust–mantle evolution in the Proterozoic: Nature, v. 291, p. 193-196.

Dickinson, W. R., & Gehrels, G. E., 2009, Use of U–Pb ages of detrital zircons to infer maximum depositional ages of strata: a test against a Colorado Plateau Mesozoic database: Earth and Planetary Science Letters, v. 288, no 1, p. 115-125.

Foster, D. A., Mueller, P. A., Mogk, D. W., Wooden, J. L., & Vogl, J. J., 2006, Proterozoic evolution of the western margin of the Wyoming craton: implications for the tectonic and magmatic evolution of the northern Rocky Mountains: Canadian Journal of Earth Sciences, v. 43, no 10, p.- 1601-1619.

Frei, D., Gerdes, A., 2009, Precise and accurate *in-situ* U-Pb dating of zircon with high sample throughput by automated LA-SF-ICP-MS: Chemical Geology, v. 261, p. 261-270.

García-Casco, A., Torres-Roldán, R. L., 1999, Natural metastable reactions involving garnet, staurolite and cordierite: implications for petrogenetic grids and the extensional collapse of the Betic-Rif Belt: Contributions to Mineralogy and Petrology, v. 136, p. 131-153.

Garver, J. I., Scott, T. J., 1995, Trace elements in shale as indicators of crustal provenance and terrane accretion in the southern Canadian Cordillera: Geological Society of America Bulletin, v. 107, no. 4, p. 440-453.

Gleadow, A., Harrison, M., Kohn, B., Lugo-Zazueta, R., Phillips, D., 2015, The Fish Canyon Tuff: A new look at an old low-temperature thermochronology standard. *Earth and Planetary Science Letters*, *424*, 95-108.

Gromet, L. P., Haskin, L. A., Korotev, R. L., Dymek, R. F., 1984, The "North American shale composite": its compilation, major and trace element characteristics: Geochimica et Cosmochimica Acta, v. 48, no.12, p. 2469-2482.

Guidotti, C.V., 1968, Prograde muscovite pseudomorphs after staurolite in the Rangeley-Oquossoc Areas, Maine: The American Mineralogist, v. 53, p. 1368-1376.

Jones, J.V., III., Connelly, J.N., Karlstrom, K.E., Williams, M.L., Doe, M.F., 2009, Age, provenance, and tectonic setting of Paleoproterozoic quartzite successions in the southwestern United States: Geological Society of America Bulletin, v. 121, no. 1/2, p. 247-264.

Jones, J.V., III., Rogers, S.A., Connelly, J.N., 2010, U-Pb geochronology of Proterozoic granites in the Sawatch Range, central Colorado, U.S.A: RockyMountain Geology, v. 45, no. 1, p. 1-22.

Jones, J. V., Siddoway, C. S., Connelly, J. N., 2010, Characteristics and implications of ca. 1.4 Ga deformation across a Proterozoic mid-crustal section, Wet Mountains, Colorado, USA: Lithosphere, v. 2, no. 2, p. 119-135.

Jones, J.V., III., Thrane, K., 2012, Correlating Proterozoic synorogenic metasedimentary successions in southwestern Laurentia: New insights from detrital zircon U-Pb geochronology of Paleoproterozoic quartzite and metaconglomerate in central and northern Colorado, U.S.A.: Rocky Mountain Geology, v. 47, no. 1, p. 1-35.

Karlstrom, K. E., Bowring, S. A., 1988, Early Proterozoic assembly of tectonostratigraphic terranes in southwestern North America: The Journal of Geology, v. 96, p. 561-576.

Kleemann, U., Reinhardt, J., 1994, Garnet-biotite thermometry revisited: The effect of AlVI and Ti in biotite: European Journal of Mineralogy, p. 925-942.

Knepper, D.H., Jr., 1972, Stratigraphy and macroscopic structure of the metasedimentary rocks of the Blue Ridge area, Fremont County, Colorado [M.S. Thesis]: Lawrence, Kansas, University of Kansas, 53p.

Kruhl, J. H., Peternell, M., 2002, The equilibration of high-angle grain boundaries in dynamically recrystallized quartz: the effect of crystallography and temperature: Journal of Structural geology, v. 24, no. 6, p. 1125-1137.

Ludwig, K. R., 2003, User's manual for Isoplot 3.00: a geochronological toolkit for Microsoft Excel (No. 4). Kenneth R. Ludwig.

Mai, K., 2002, Microstructural and kinematic analyses of a Proterozoic quartzite-schist sequence in Blue Ridge, Colorado [M.S. Thesis]: Norman, Oklahoma, University of Oklahoma, 105p.

Mattinson, J. M., 2005, Zircon U–Pb chemical abrasion (“CA-TIMS”) method: combined annealing and multi-step partial dissolution analysis for improved precision and accuracy of zircon ages: Chemical Geology, v. 220, no.1, p. 47-66.

McLennan, S. M., & Taylor, S. R., 1982, Geochemical constraints on the growth of the continental crust. *The Journal of Geology*, 347-361.

McLennan, S. M., 1989, Rare earth elements in sedimentary rocks; influence of provenance and sedimentary processes: Reviews in Mineralogy and Geochemistry, v. 21, no. 1, p. 169-200.

McClennan, S.M., Hemming, S.R., Taylor, S.R., Eriksson, K.A., 1995, Early Proterozoic crustal evolution: Geochemical and Nd-Pb isotopic evidence from metasedimentary rocks, southwestern North America: Geochimica et Cosmochimica Acta, v. 59, p. 1153-1177.

McCoy, A.M., Karlstrom, K.E., Shaw, C.A., 2005, The Proterozoic Ancestry of the Colorado Mineral Belt: 1.4 Ga Shear Zone System in Central Colorado: The Rocky Mountain Region: An Evolving Lithosphere Geophysical Monograph Series 154, p. 71-90.

Medaris, L.G., Jr., Singer, B.S., Dott, R.H., Jr., Naymark, A., Johnson, C.M., Schott, R.C., 2003, Late Proterozoic Climate, Tectonics, and Metamorphism in the Southern Lake Superior Region and Proto-North America: Evidence from Baraboo Interval Quartzites: The Journal of Geology, v. 111, p. 243-257.

Morton, A. C., Hallsworth, C. R., 1999, Processes controlling the composition of heavy mineral assemblages in sandstones: Sedimentary Geology, v. 124, no. 1, p. 3-29.

Moyen, J. F., 2009, High Sr/Y and La/Yb ratios: the meaning of the "adakitic signature": Lithos, v. 112, no. 3, p. 556-574.

Munksgaard, N. C., Lim, K., Parry, D. L., 2003, Rare earth elements as provenance indicators in North Australian estuarine and coastal marine sediments: Estuarine, Coastal and Shelf Science, v. 57, no.3, p. 399-409.

Nesbitt, H.W., Young, G.M., 1982, Early Proterozoic climates and plate motions inferred from major element chemistry of lutites: Nature, v. 299, p. 715-717.

Nesbitt, H.W., Young, G.M., 1984, Prediction of some weathering trends of plutonic and volcanic rocks based on thermodynamic and kinetic considerations: Geochim. Cosmochim. Acta, v. 48, p. 1523-1534.

Nesbitt, H.W., Young, G.M., 1989, Formation and diagenesis of weathering profiles: Journal of Geology, v 97, p. 129-147.

Passchier, C. W., Trouw, R. A., 1996, Microtectonics v. 2 Berlin: Springer.

Payne, J.L., Barovich, K.M., Hand, M., 2006, Provenance of metasedimentary rocks in the northern Gawler Craton, Australia: Implications for Palaeoproterozoic reconstructions: Precambrian Research, v. 148, p. 275-291.

Perchuk, L. L., Lavrent'Eva, I. V., 1983, Experimental investigation of exchange equilibria in the system cordierite-garnet-biotite: In Kinetics and equilibrium in mineral reactions, Springer New York, p. 199-239.

Reche, J., Martinez, F. J., 1996, GPT: an Excel spreadsheet for thermobarometric calculations in metapelitic rocks: Computers & Geosciences, v. 22, no. 7, p. 775-784.

Reuss, R.L., 1970, Geology and Petrology of the Wilson Park Area, Fremont County, Colorado [Ph.D. Dissertation]: Ann Arbor, Michigan, University of Michigan, 184p.

Reuss, R.L., 1974, Precambrian quartzite-schist succession in Wilson Park, Fremont County, Colorado: Mountain Geologist, v. 11 p. 45-58.

Rubatto, D., 2002, Zircon trace element geochemistry: partitioning with garnet and the link between U–Pb ages and metamorphism: Chemical Geology, v. 184, no. 1, p. 123-138.

Schmitz, M. D., Bowring, S. A., 2001, U-Pb zircon and titanite systematics of the Fish Canyon Tuff: an assessment of high-precision U-Pb geochronology and its application to young volcanic rocks: Geochimica et Cosmochimica Acta, v. 65, no.15, p. 2571-2587.

Selverstone, J., Hodgins, M., Aleinikoff, J. N., Fanning, C. M., 2000, Mesoproterozoic reactivation of a Paleoproterozoic transcurrent boundary in the northern Colorado Front Range: Implications for~ 1.7-and 1.4-Ga tectonism: Rocky Mountain Geology, v. 35, no. 2, p. 139-162.

Shaw, C.A., Karlstrom, K.E., 1999, The Yavapai-Mazatzal crustal boundary in the Southern Rocky Mountains: Rocky Mountain Geology, v. 34, p. 37-52.

Shaw, C.A, Karlstrom, K.E., Williams, M.L., Jercinovic, M.J., McCoy, A.M., 2001, Electron-microprobe monazite dating of ca. 1.71-1.63 Ga and ca. 1.45-1.38 Ga deformation in the Homestake shear zone, Colorado: Origin and early evolution of a persistent intracontinental tectonic zone: Geology, v. 29, no. 8, p. 739-742.

Shaw, C. A., Heizler, M. T., Karlstrom, K. E., 2005, 40Ar/39Ar thermochronologic record of 1.45–1.35 Ga intracontinental tectonism in the southern Rocky Mountains: Interplay of conductive and advective heating with intracontinental deformation: The Rocky Mountain Region: An Evolving Lithosphere Tectonics, Geochemistry, and Geophysics, Geophysical Monograph Series 154, p.163-184.

Shaw, C. A., Allen, J. L., 2007, Field rheology and structural evolution of the Homestake shear zone, Colorado: Rocky Mountain Geology, v. 42, no. 1, p. 31-56.

Sitek, B.C., Berndt, T.R., Clayton, J.K., Walker, J.D., Möller, A, 2014, Quartzites and granitic basement: examining the depositional contact hypothesis at Blue Ridge, CO using microstructural evidence: Geological Society of America Rocky Mountain Section Abstracts with Programs, v.46, no 5, p. 33.

Smith, D. R., Noblett, J., Wobus, R. A., Unruh, D., Chamberlain, K. R., 1999, A review of the Pikes Peak batholith, Front Range, central Colorado A "type example" of A-type granitic magmatism: Rocky Mountain Geology, v. 34, no. 2, p. 289-312.

Sun, S. S., McDonough, W. F., 1989, Chemical and isotopic systematics of oceanic basalts: implications for mantle composition and processes: Geological Society, London, Special Publications, v. 42, no. 1, p. 313-345.

Talavera-Mendoza, O., Ruiz, J., Gehrels, G. E., Valencia, V. A., & Centeno-García, E., 2007, Detrital zircon U/Pb geochronology of southern Guerrero and western Mixteca arc successions (southern Mexico): New insights for the tectonic evolution of southwestern North America during the late Mesozoic: Geological Society of America Bulletin, v. 119, no 9-10, p. 1052-1065.

Taylor, S. R., McLennan, S. M., Armstrong, R. L., Tarney, J., 1981, The composition and evolution of the continental crust: rare earth element evidence from sedimentary rocks [and discussion]: Philosophical Transactions of the Royal Society of London A: Mathematical, Physical and Engineering Sciences, v. 301, p. 381-399.

Tera, F., & Wasserburg, G. J., 1972, U-Th-Pb systematics in three Apollo 14 basalts and the problem of initial Pb in lunar rocks: Earth and Planetary Science Letters, v.14, no 3, p. 281-304.

Thomson, S. N., Gehrels, G. E., Ruiz, J., & Buchwaldt, R., 2012, Routine low-damage apatite U-Pb dating using laser ablation–multicollector–ICPMS: Geochemistry, Geophysics, Geosystems, v. 13, no 2.

Van Schmus, W.R., Bickford, M.E., Condie, K.C., 1993, Early Proterozoic crustal evolution, in Reed, J.C., et al., Precambrian: Conterminous U.S.: Geological Society of America, Decade of North American Geology (DNAG), v. C-2, p. 270-281.

Wetherill, G. W., 1956, Discordant uranium-lead ages, I: Eos, Transactions American Geophysical Union, v. 37, no 3, p. 320-326.

Whitmeyer, S. J., Karlstrom, K. E., 2007, Tectonic model for the Proterozoic growth of North America: Geosphere, v. 3, no. 4, p. 220-259.

Wibberley, C., 1999, Are feldspar-to-mica reactions necessarily reaction-softening processes in fault zones?: Journal of Structural Geology, v. 21, p. 1219-1227.

Wilson, M., 1989, Igneous Petrogenesis: A Global Tectonic Approach, 466 pp.

Wobus, R.A., Epis, R.C., Scott, G.R., 1979, Geologic Map of the Cover Mountain Quadrangle, Fremont, Park, and Teller Counties, Colorado, United States Geological Survey, scale 1:62,500.

Yu, S., Zhang, J., Del Real, P. G., 2012, Geochemistry and zircon U–Pb ages of adakitic rocks from the Dulan area of the North Qaidam UHP terrane, north Tibet: constraints on the timing and nature of regional tectonothermal events associated with collisional orogeny: Gondwana Research, v. 21, no. 1, p. 167-179.

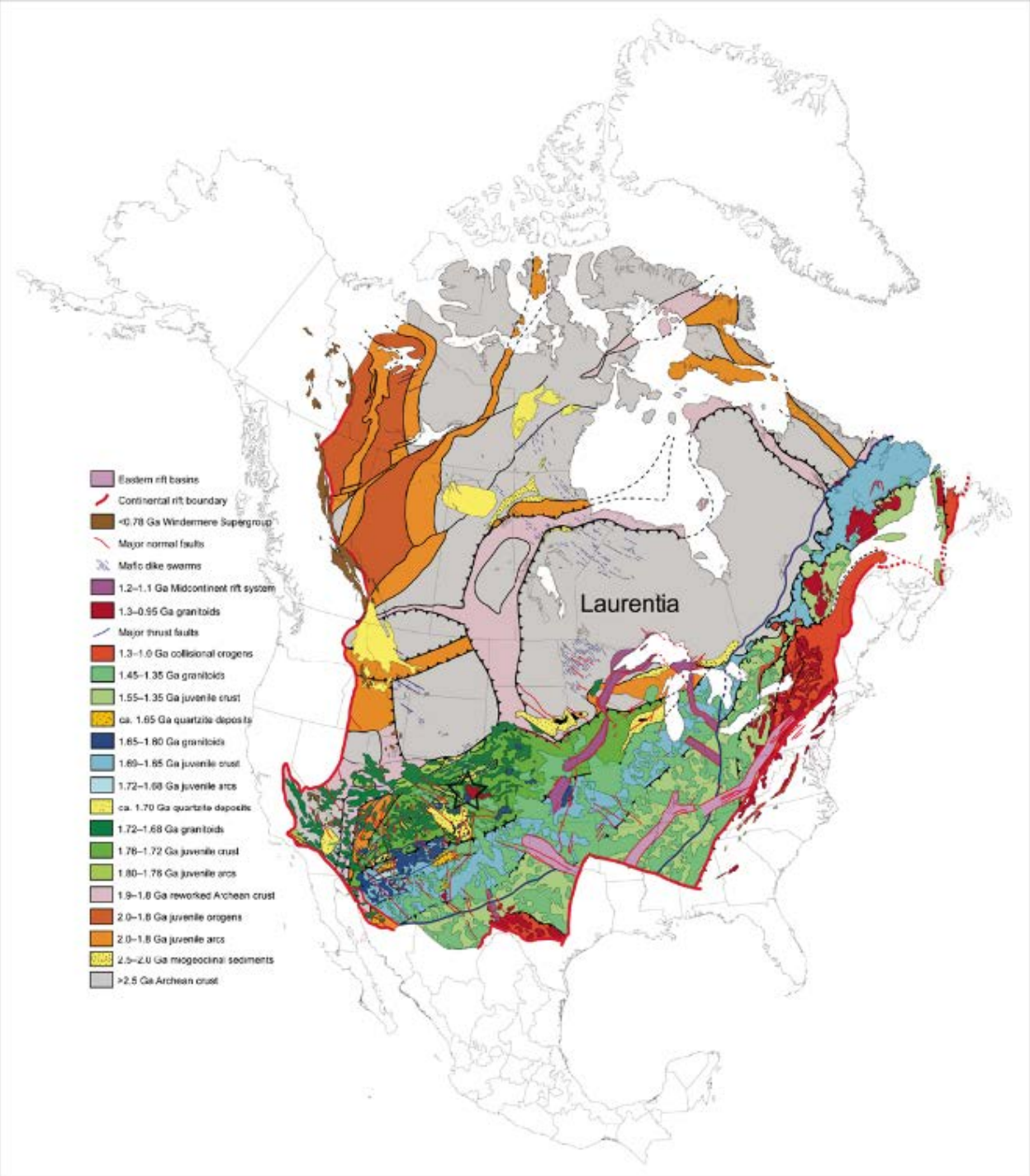

Figure 1. Archean through Neoproterozoic map showing Precambrian features of North America. The black star denotes the approximate location of Blue Ridge. Map from Whitmeyer and Karlstrom (2007)

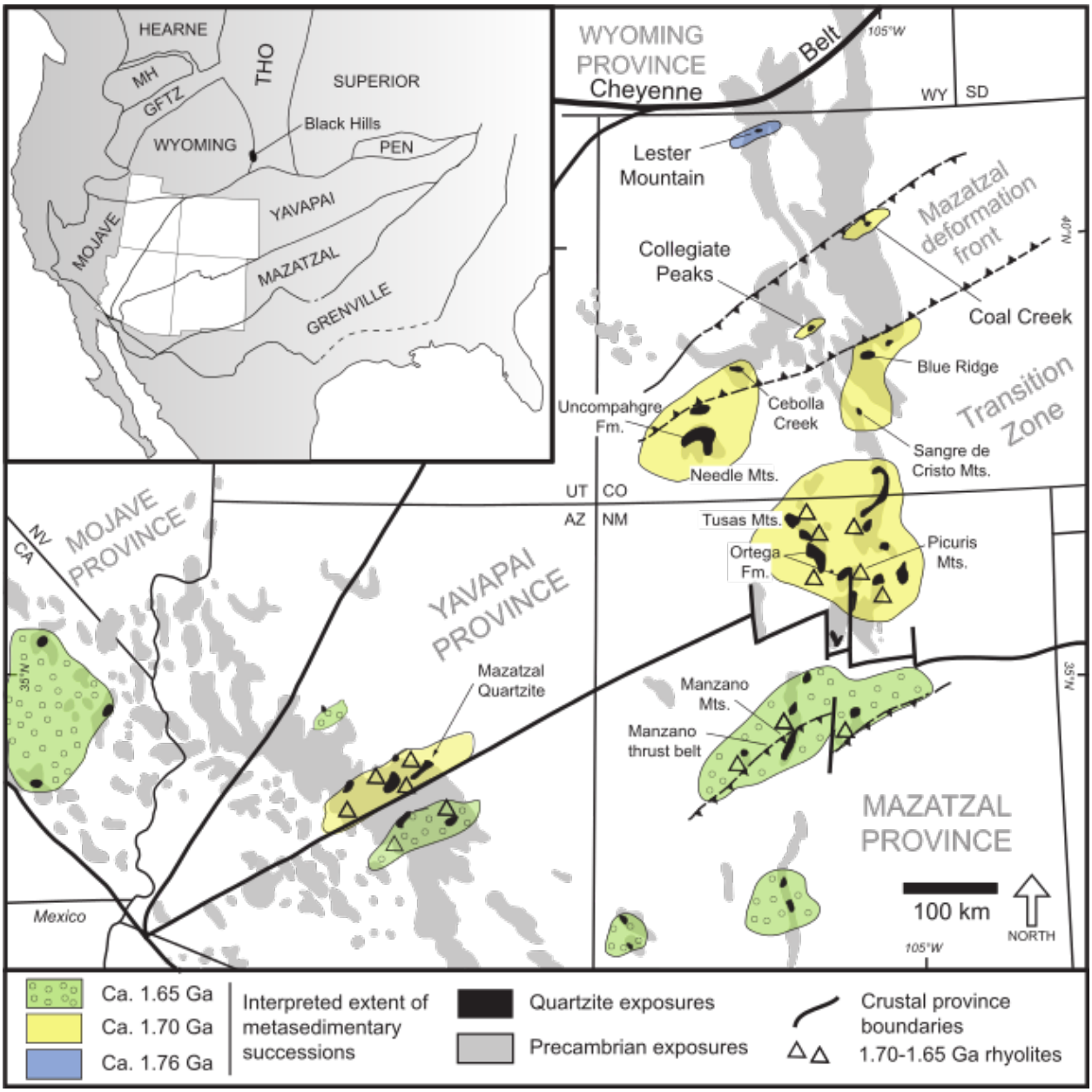

Figure 2. Paleoproterozoic quartzite locations exposed in the southern Rocky Mountains, U.S.A. Inset map shows the extent of the southern Laurentia Yavapai and Mazatzal accretionary terranes and infers that quartzite depositional regimes stretch from the Great Lakes region to western Arizona. (Map from Jones and Thrane, 2012, based on Jones et al., 2009. Inset map based on Karlstrom and Bowring, 1988; Condie, 1992; Van Schmus et al., 1993; Foster et al., 2006; Whitmeyer and Karlstrom, 2007)

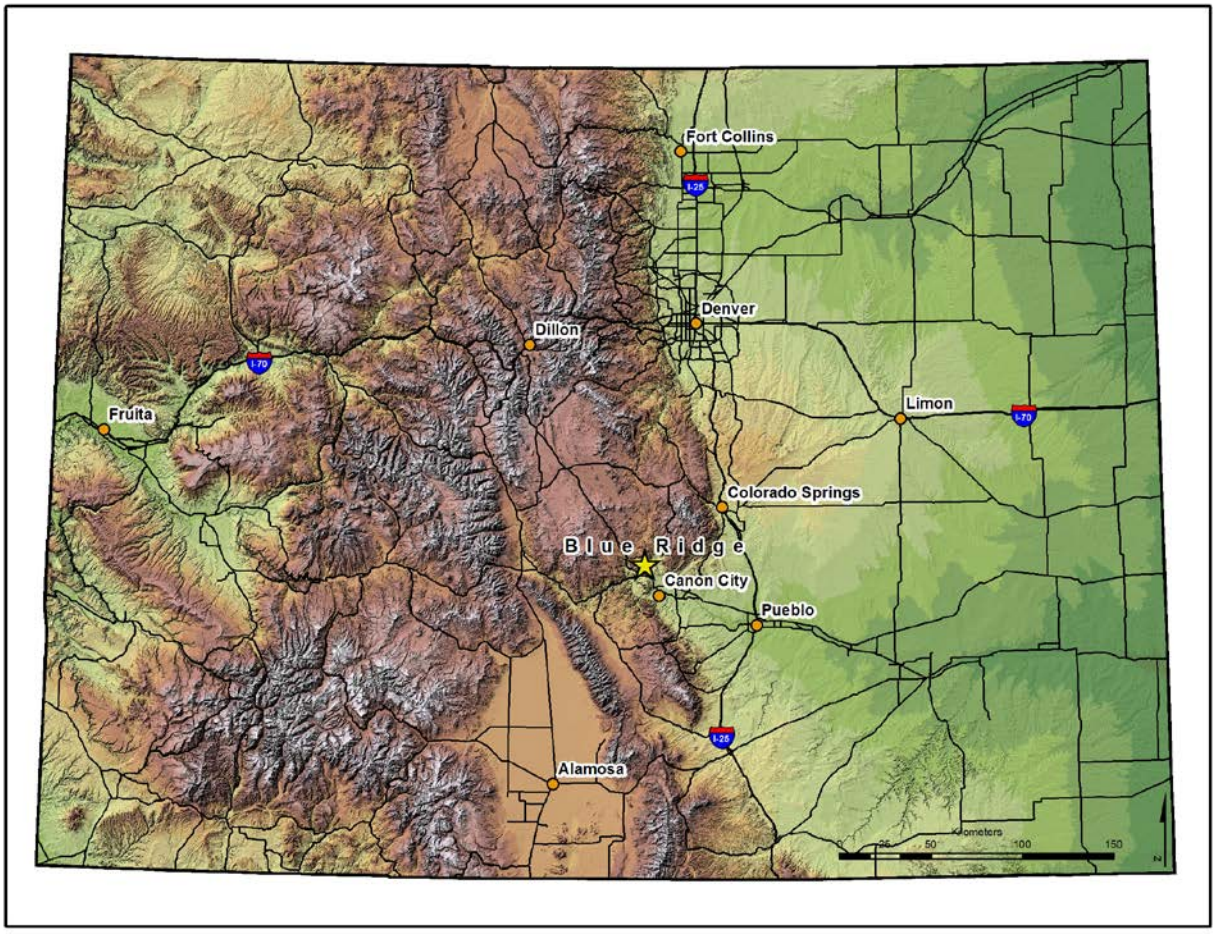

Figure 3. State map of Colorado showing location of Blue Ridge (yellow star). Blue Ridge is situated along the south-central Colorado Front Range. Map created in ArcGIS. Data sources: Coloradoview.org, Environmental Systems Research Institue (ESRI), DeLorme, NAVTEQ, TomTom, Intermap, Increment P Corp., GEBCO, USGS, FAO, NPS, NRCAN, GeoBase, IGN, Kadaster NL, Ordnance Survey, Esri Japan, METI, Esri China (Hong Kong), swisstopo, GIS User Community.

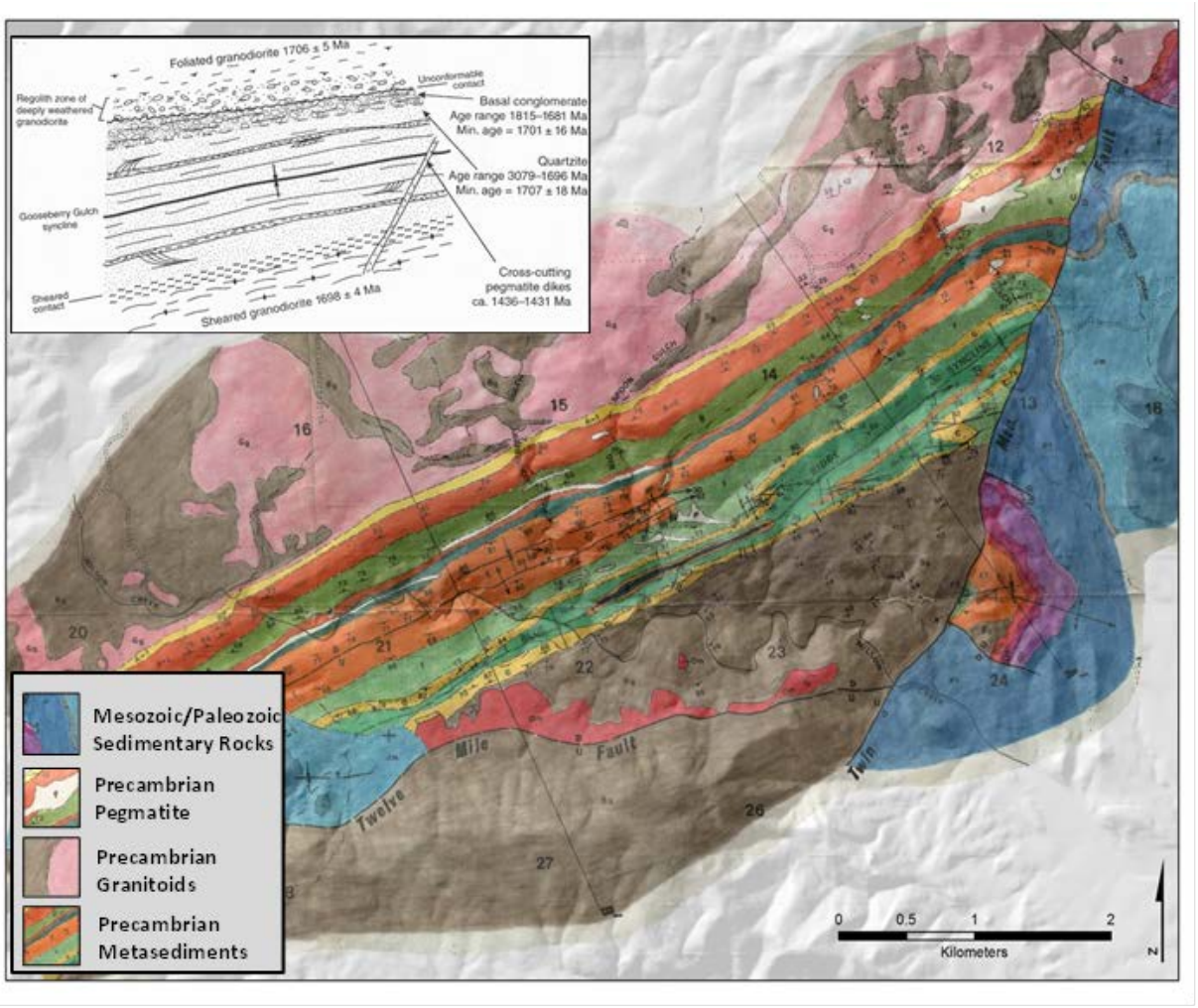

Figure 4. Geologic map of the Blue Ridge area (from Knepper, 1972, with modified legend). Inset shows geological summary sketch and age data (from Jones et al., 2009, after Reuss, 1970). Data sources: Colotadoview.org.

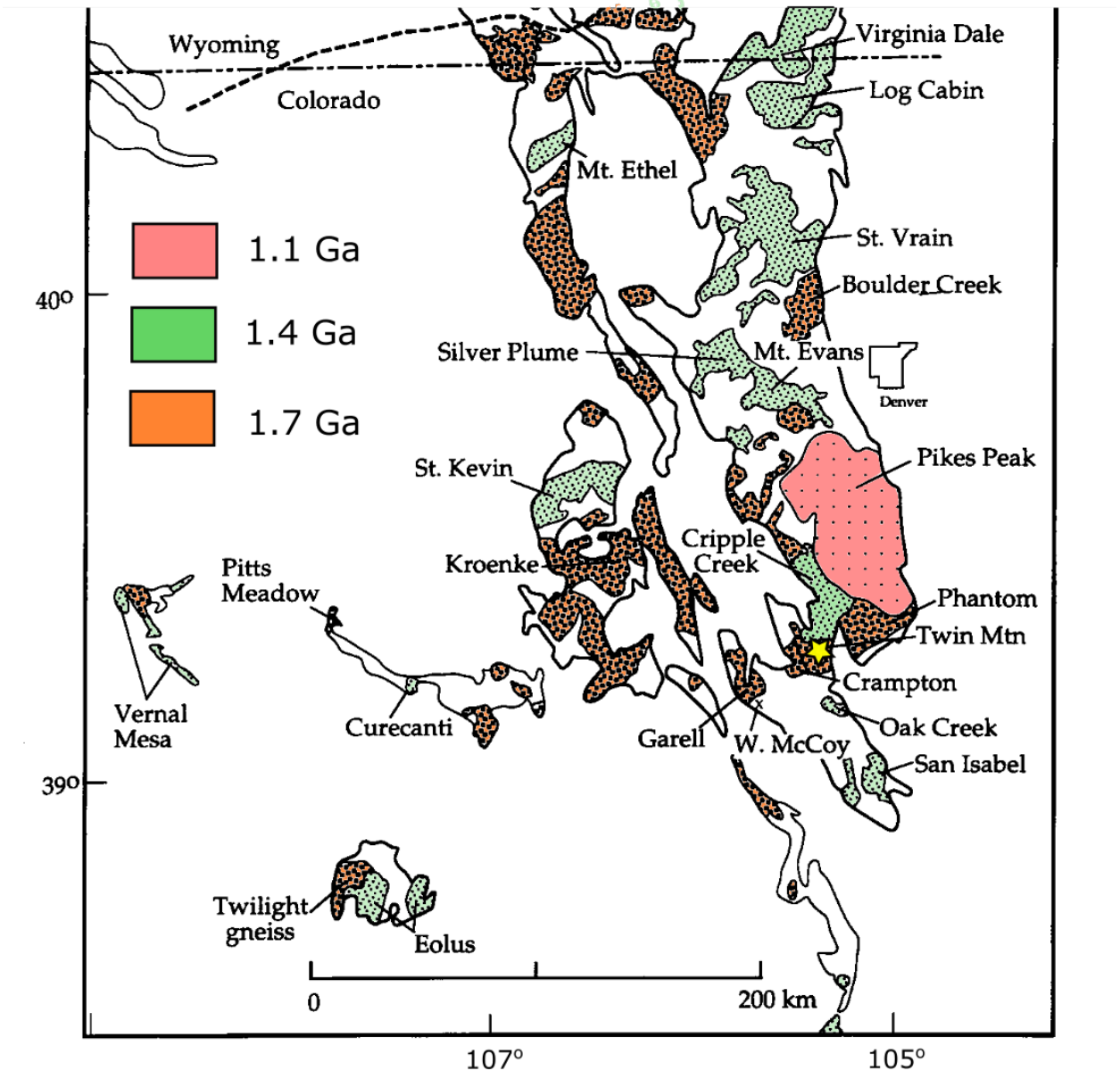

Figure 5. Distribution of 1.1 – 1.7 Ga plutons in Colorado and southern Wyoming. Map from Anderson and Cullers (1999), with color added to delineate plutons. The Blue Ridge area is noted by the yellow star. Blue Ridge sits within the 1.7 Ga Twin Mtn. pluton. Both 1.4 and 1.1 Ga plutons have been emplaced within close proximity to Blue Ridge.

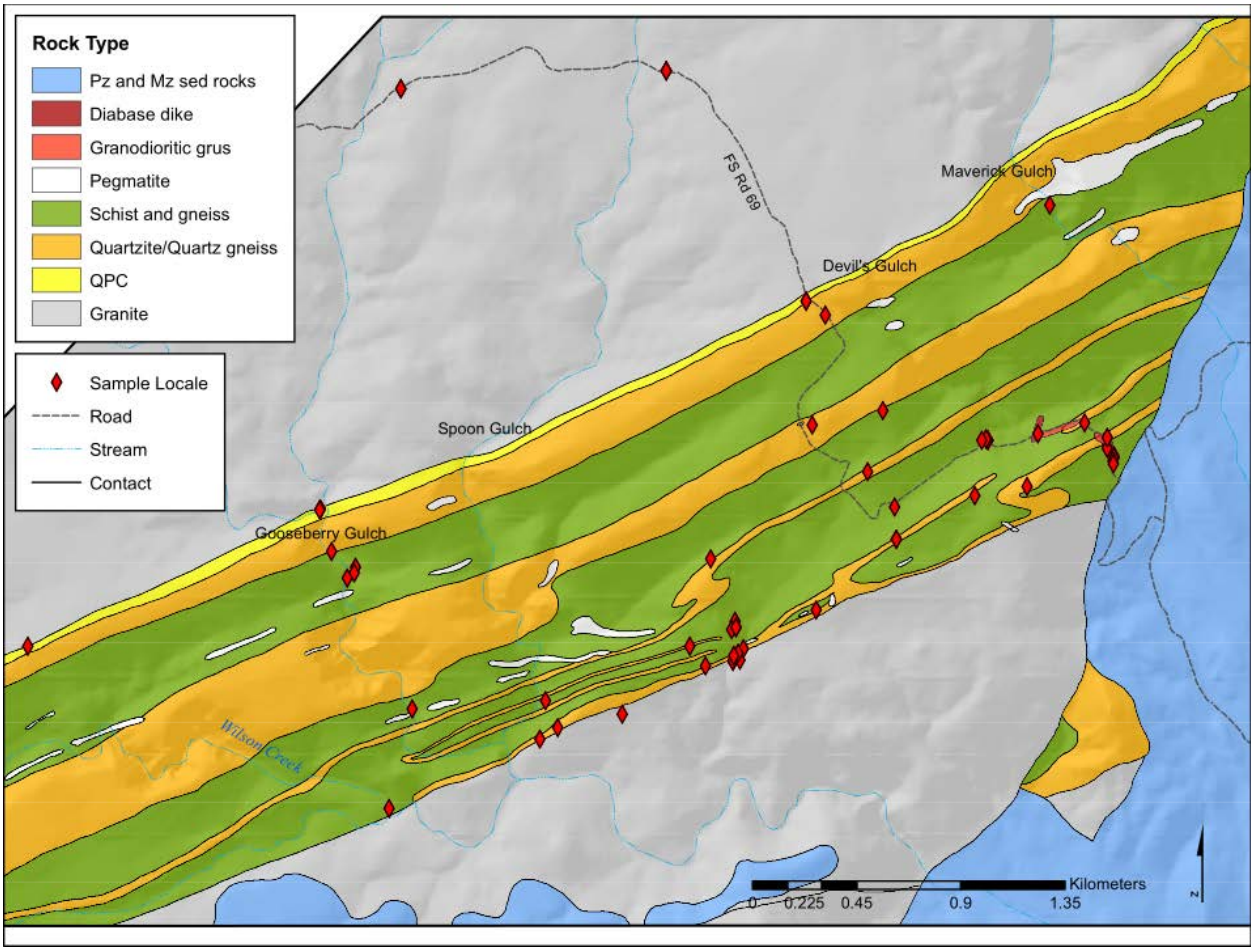

Figure 6. Geologic map showing distribution and location of all samples collected at Blue Ridge. Sample name, rock type, and location listed in Appendix A. Map modified after Knepper (1972) (Pz = Paleozoic; Mz = Mesozoic; QPC = Quartz Pebble Conglomerate). Data sources: Coloradoview.org.

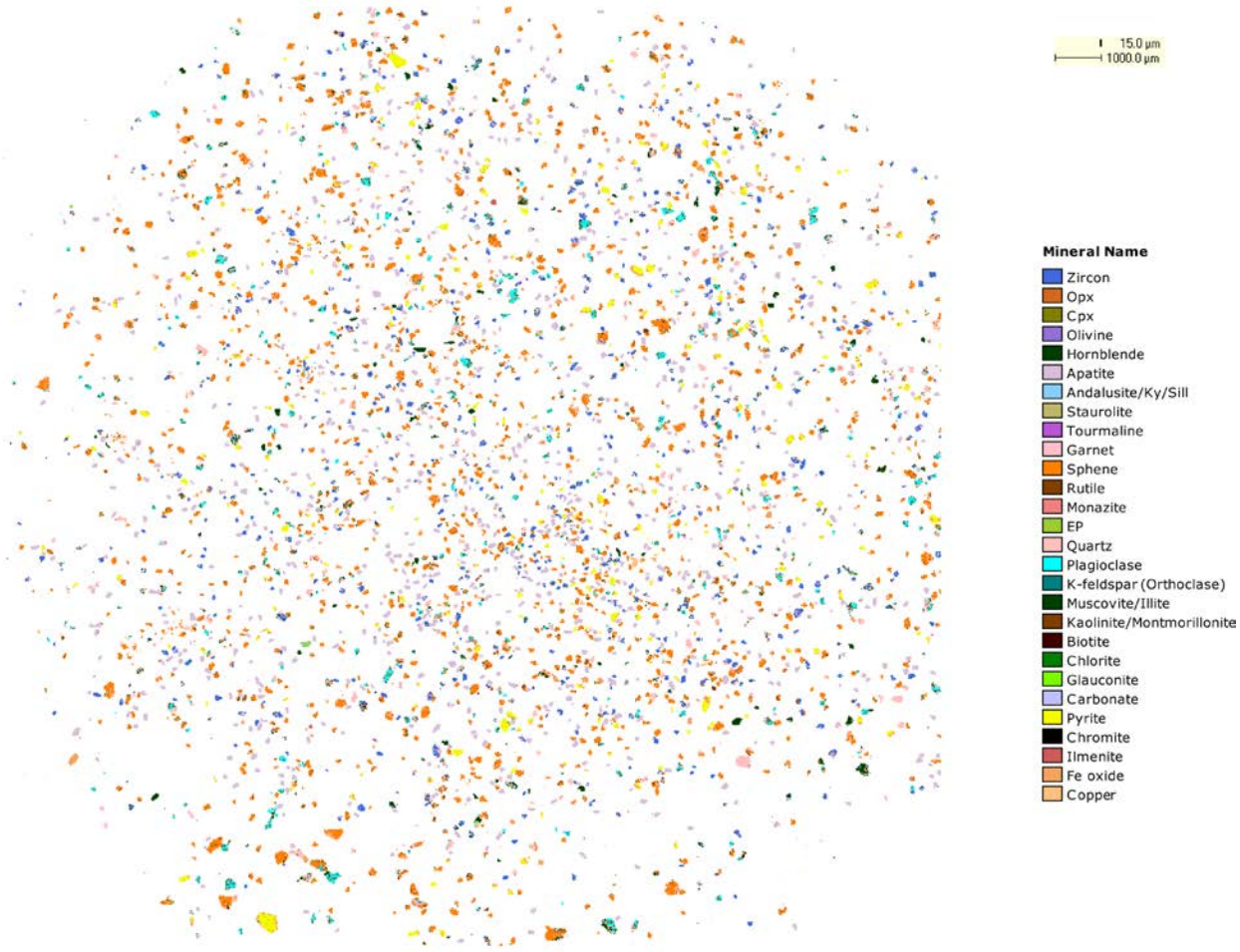

Figure 7. Color coded mineral map of amphibole-bearing leucosome (BR060913-01) produced by QEMSCAN® analysis. The heavy mineral fraction for this sample contains abundant zircon, apatite, and Fe oxide. Large pyrite grains (yellow) are also visible in this false color image.

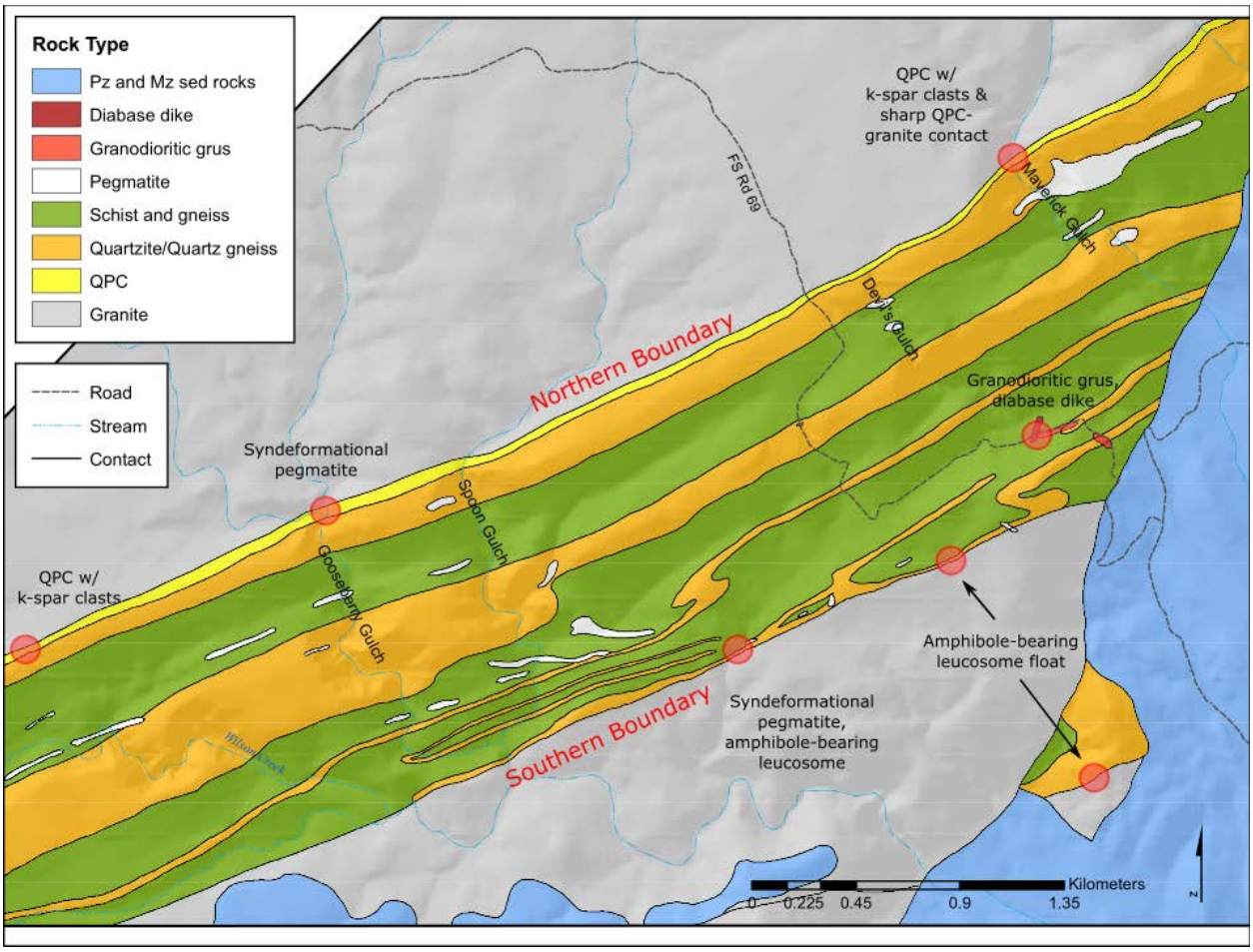

Figure 8. Geological map of Blue Ridge area with location and brief description of important field relationships and structural marker units as noted by red circles. . Map modified after Knepper (1972) (Pz = Paleozoic; Mz = Mesozoic; QPC = Quartz Pebble Conglomerate). Data sources: Coloradoview.org.

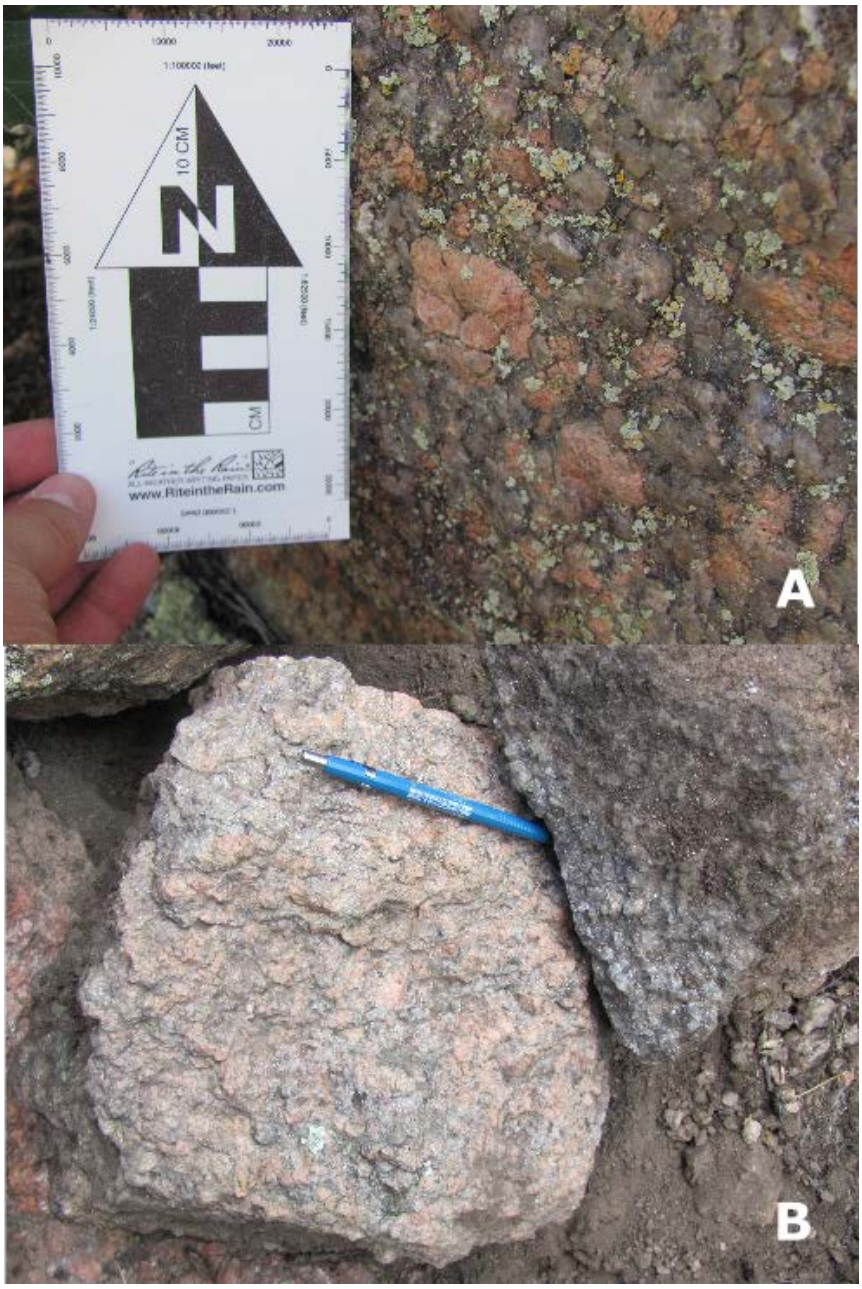

Figure 9. Quartz pebble conglomerate (QPC) with large k-feldspar clasts. A) Meter scale outcrop of upright QPC located 1.3 km west of Gooseberry Gulch (see Figure 8 for location). K-feldspar clasts are abundant and up to 5cm in length. B) QPC float located in Maverick Gulch within 10 meters of the northern contact. K-feldspar clasts are seen in pink up to 2 cm long.

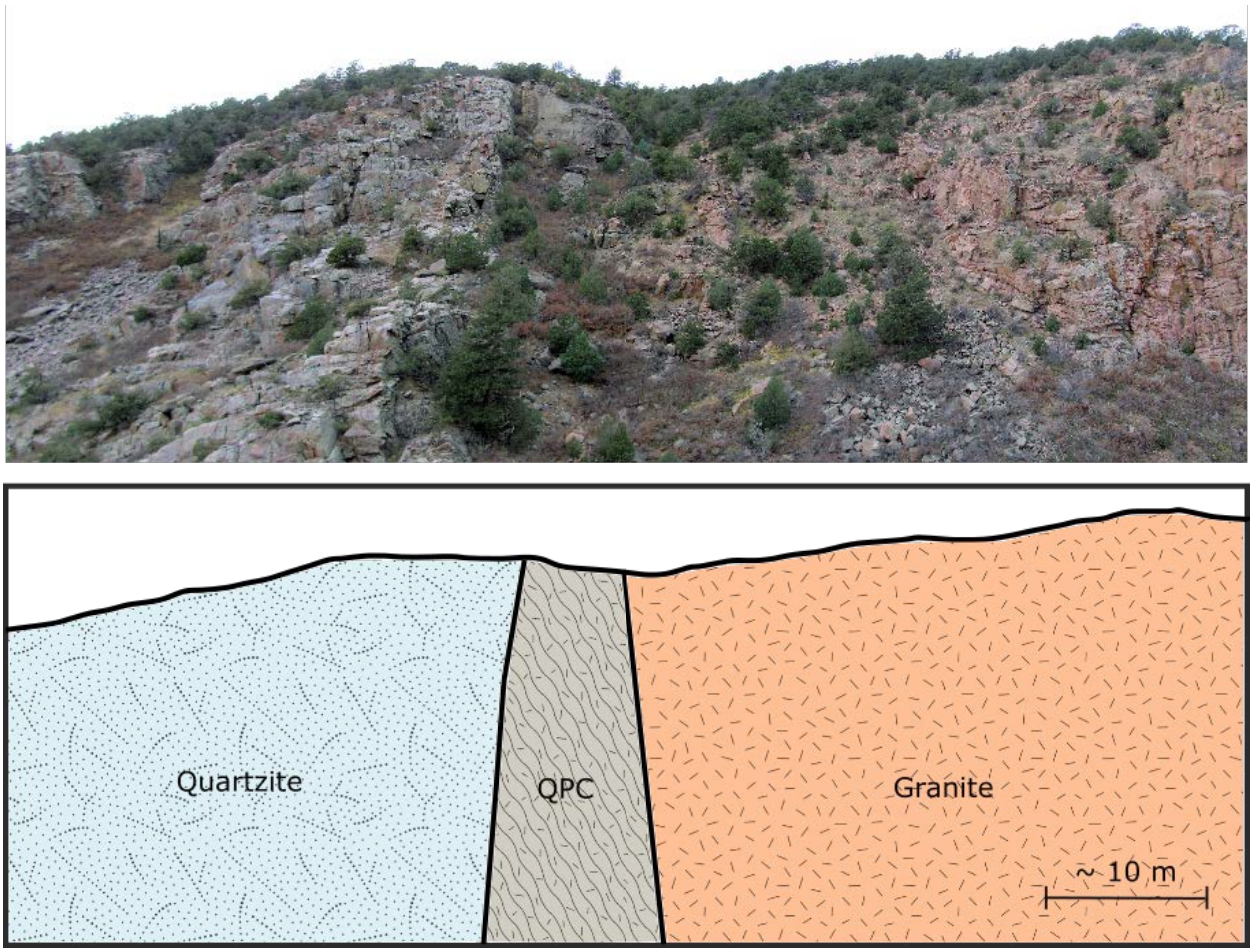

Figure 10. View to the southwest along strike in Maverick Gulch. The top image shows the transition from granite to QPC to quartzite. The QPC is less competent than the surrounding units and exposures are generally weathered or covered. Refer to Figure 8 for location.

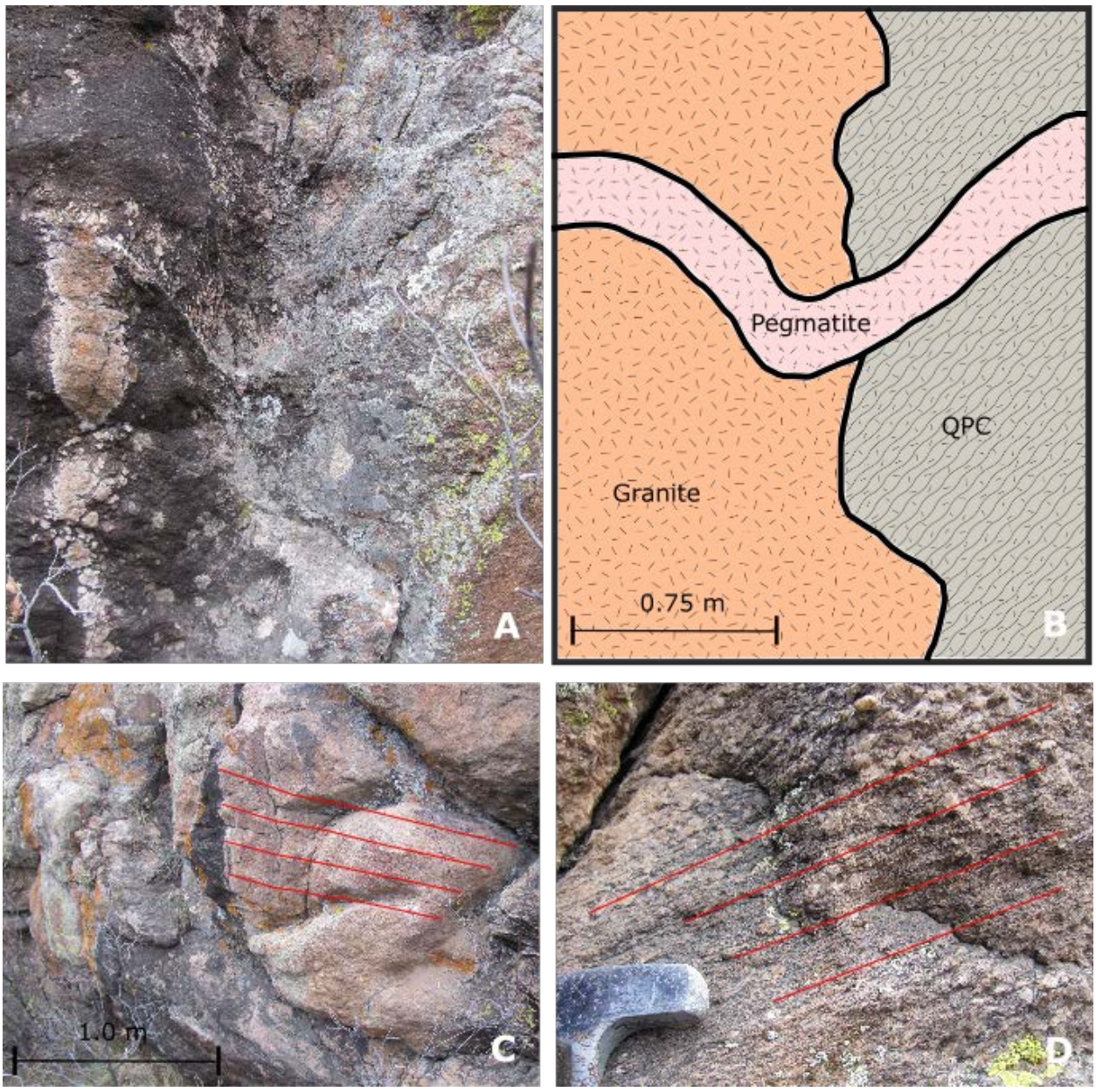

Figure 11. QPC/granite contact in Maverick Gulch. A, B) Photo and associated illustration delineate the contact between the two units. A later-stage pegmatite dike cross-cuts both rock types. C) Exposure of biotite granodiorite (entire image). Red lines are oriented parallel to foliation. Strike and dip by right-hand-rule (RHR) is 315/24. D) Exposure of QPC. There is a marked reduction in grain size from right to left as you near the contact. Red lines are oriented parallel to foliation. Strike and dip by RHR is 270/28. All views are to the NE along strike. Refer to Figure 8 for location.

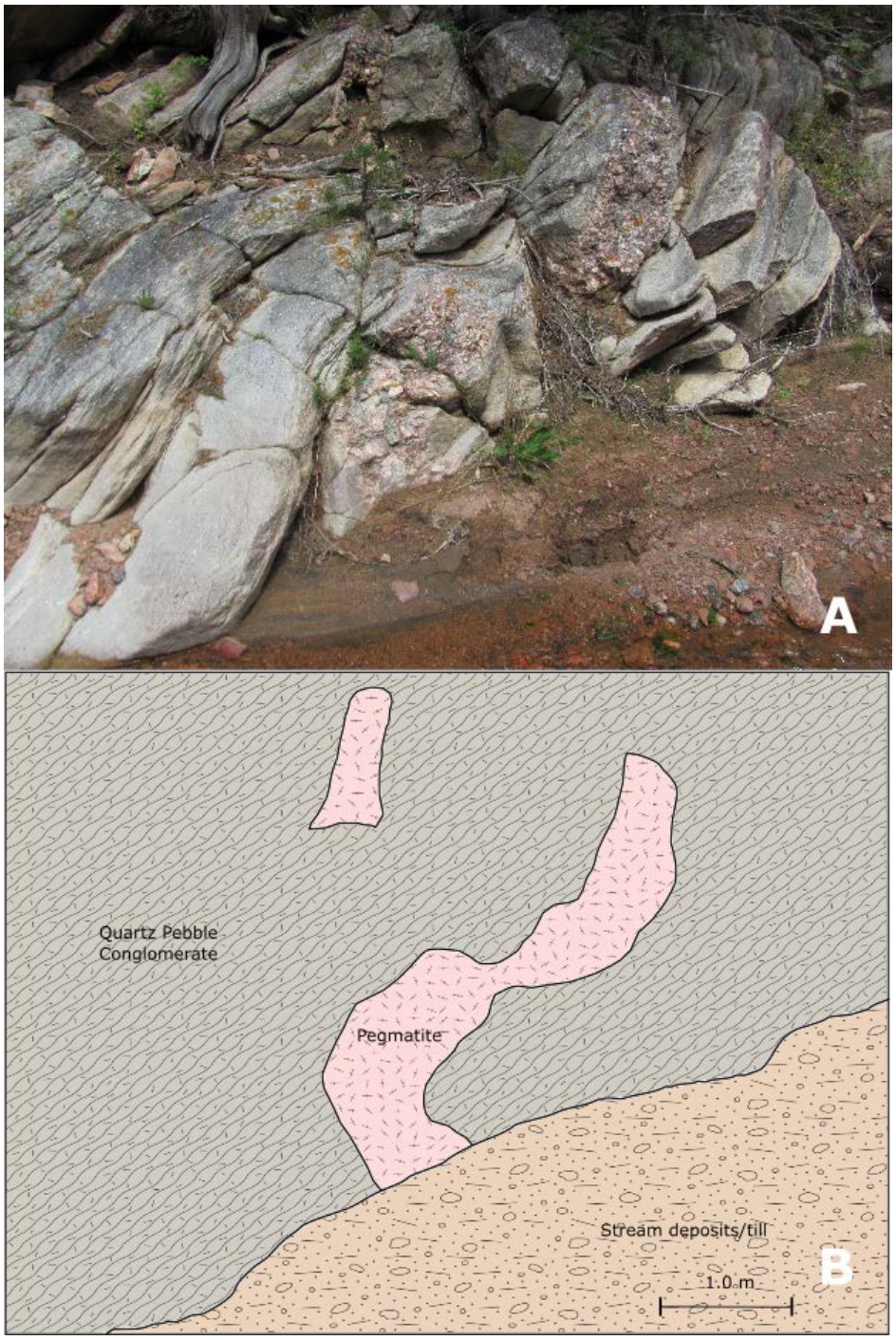

Figure 12. View to the NE along strike in Gooseberry Gulch. A, B) Photo and illustration of QPC and pegmatite relationship. The QPC and pegmatite are visibly deformed, with the QPC appearing to flow around boudinaged/stretched sections of pegmatite. Refer to Figure 8 for location.

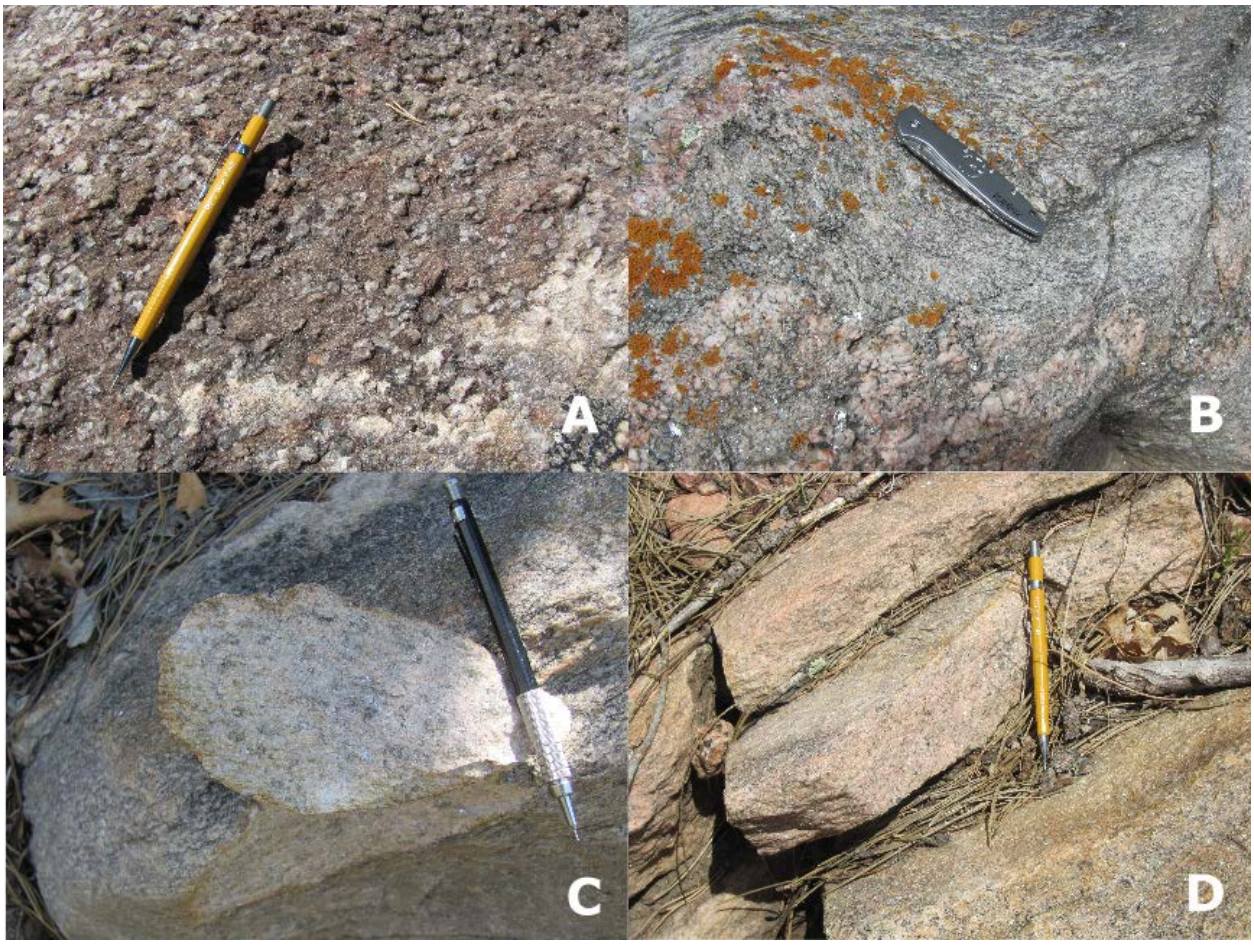

Figure 13. Gradational grain size changes visible in QPC in Gooseberry Gulch. A) Outcrop located ~ 10m from inferred QPC/granite contact. Pebble size is ~ 2.5cm. B) Close up of deformed QPC and pegmatite ~ 5m from inferred QPC/granite contact. Pebble size is ~0.5cm or less. C) QPC within ~ 1-2m of inferred QPC/granite contact. Grains visible at mm scale. D) Foliated quartz-rich granitoid with no visible biotite at or just north of inferred contact with QPC. Grain size of quartz and texture of rock in C and D are strikingly similar. Refer to Figure 8 for location.

Figure 14. Rock units at the southern boundary of the Blue Ridge area in unnamed gulch (see Figure 8 for location). A) Amphibole-bearing leucosome float. B) Amphibole-bearing leucosome intruding quartzite and augen gneiss. C) Attenuated and deformed pegmatite within augen gneiss.

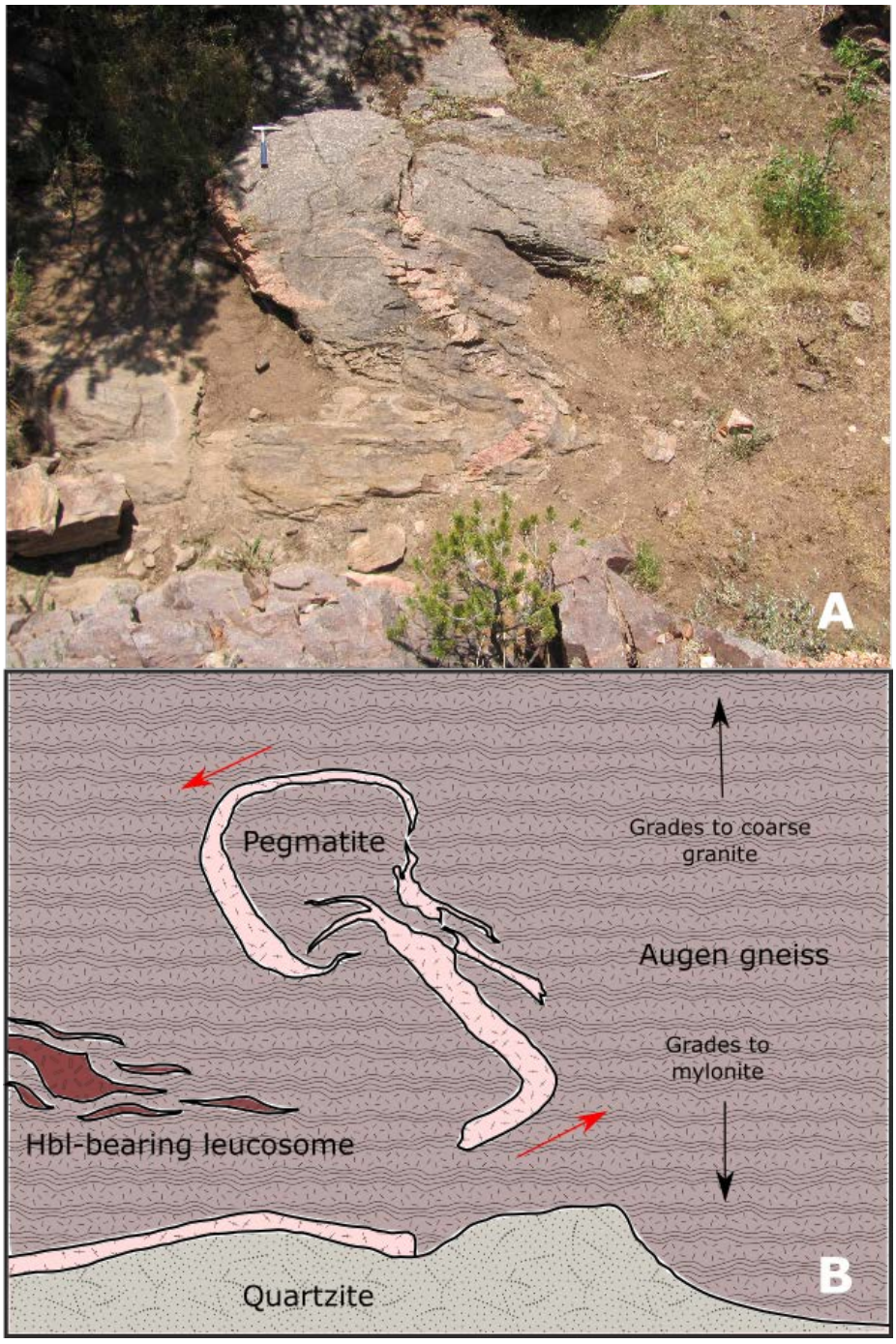

Figure 15. Geologic relationships at the southern boundary of the Blue Ridge area in unnamed gulch (see Figure 8 for location). A) Photo of attenuated pegmatite dike within augen gneiss (hammer for scale). B) Illustration showing location and distribution of geologic units seen in photo above. The pegmatite follows the foliation of the augen-gneiss, indicating a sinistral sense of shear. The amphibole-bearing leucosome is aligned with strike (NE-SW), but is undeformed, showing no preferred mineral orientation.

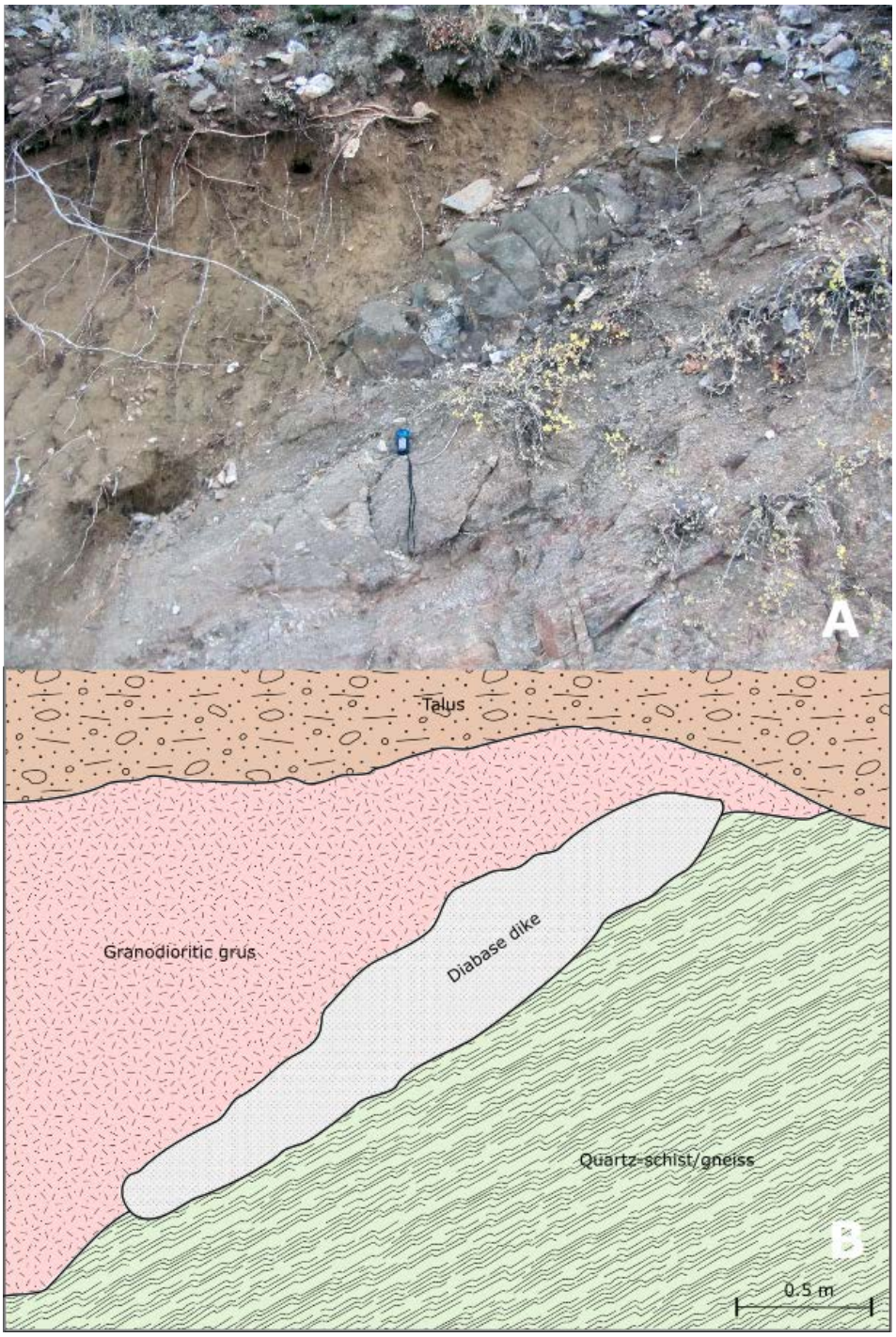

Figure 16. Structural marker units exposed along FS Road 69 (see Figure 8 for location). A, B) Photo and illustration showing position of granodioritic grus and diabase dike and adjacent metasediment. The granodiorite appears to intrude the quartz-schist unit. The diabase dike appears to have intruded along the granodiorite-schist contact.

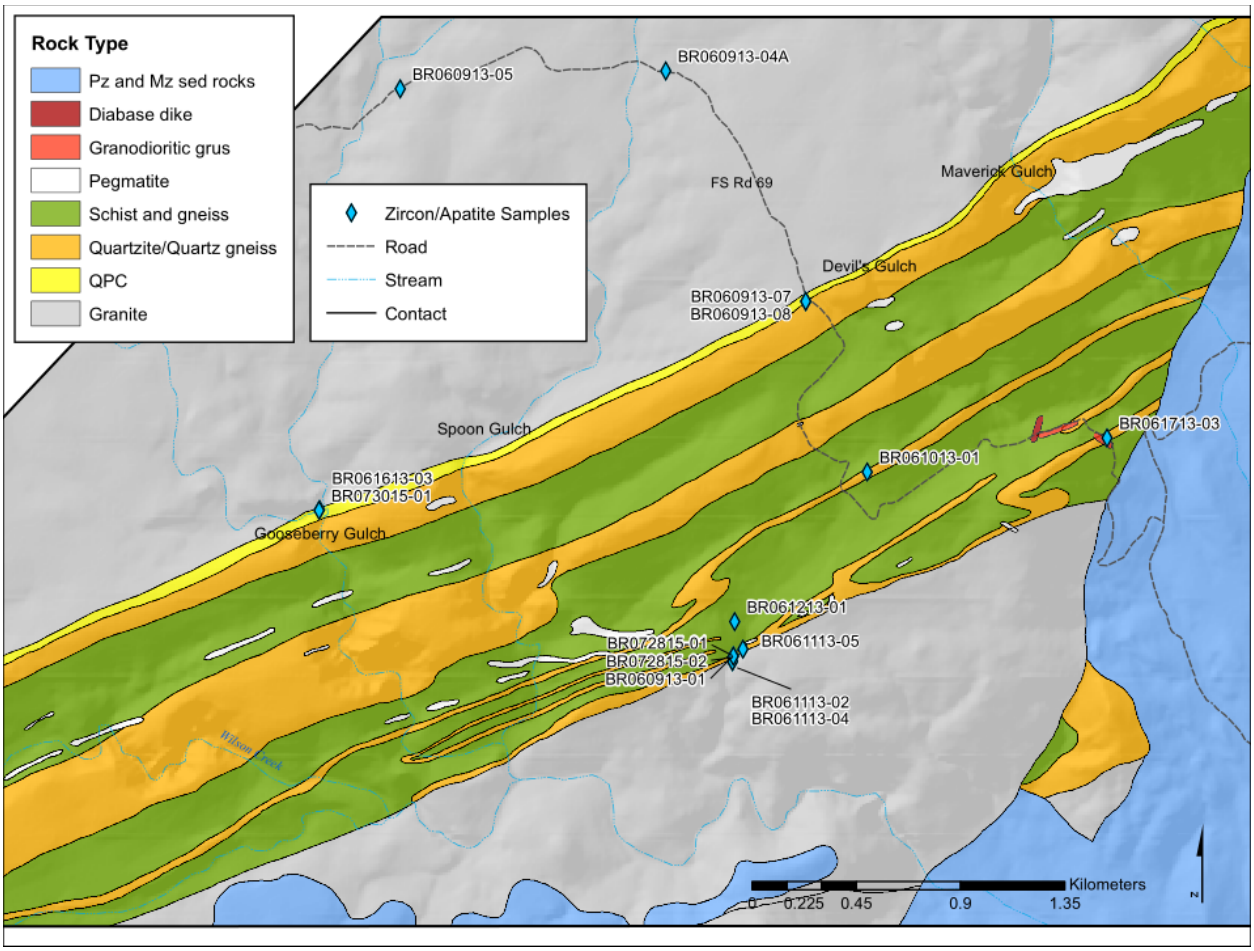

Figure 17. Geological map of the Blue Ridge area with location of samples collected for U-Pb zircon and apatite geochronology and sample numbers (BR060913-04A granite; BR060913-05 foliated granite; BR060913-07, -08 quartz-pebble-conglomerate; BR060913-01 & BR072815-01 amphibole-bearing leucosome; BR061013-01 quartzite; BR061213-01, grt-mica-quartz-schist; BR061713-03 granodioritic grus; BR061613-03 & BR073015-01 foliated granite; BR061113-05 & BR072815-02 pegmatite 1 & 2, respectively; BR061113-02 granodiorite; BR061113-04 augen gneiss). Pz = Paleozoic; Mz = Mesozoic; QPC = Quartz Pebble Conglomerate. Map modified after Knepper (1972). Map data sources: Coloradoview.org.

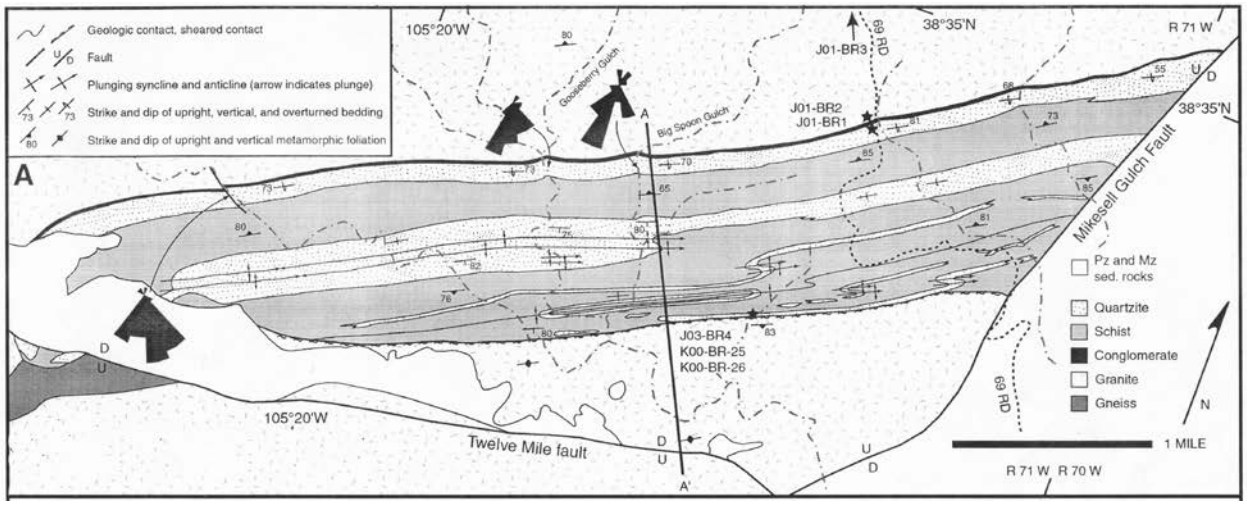

Figure 18. Location of U-Pb geochronology samples collected by Jones et al. (2009) with sample numbers. Samples are marked with black stars. Map after Reuss (1970, 1974). (J01-BR1 Quartzite; J01-BR2 Basal conglomerate; J01-BR3 Foliated granodiorite; J03-BR4 Pegmatite; K00-BR-25 Sheared granodiorite; K00-BR-26 Pegmatite)

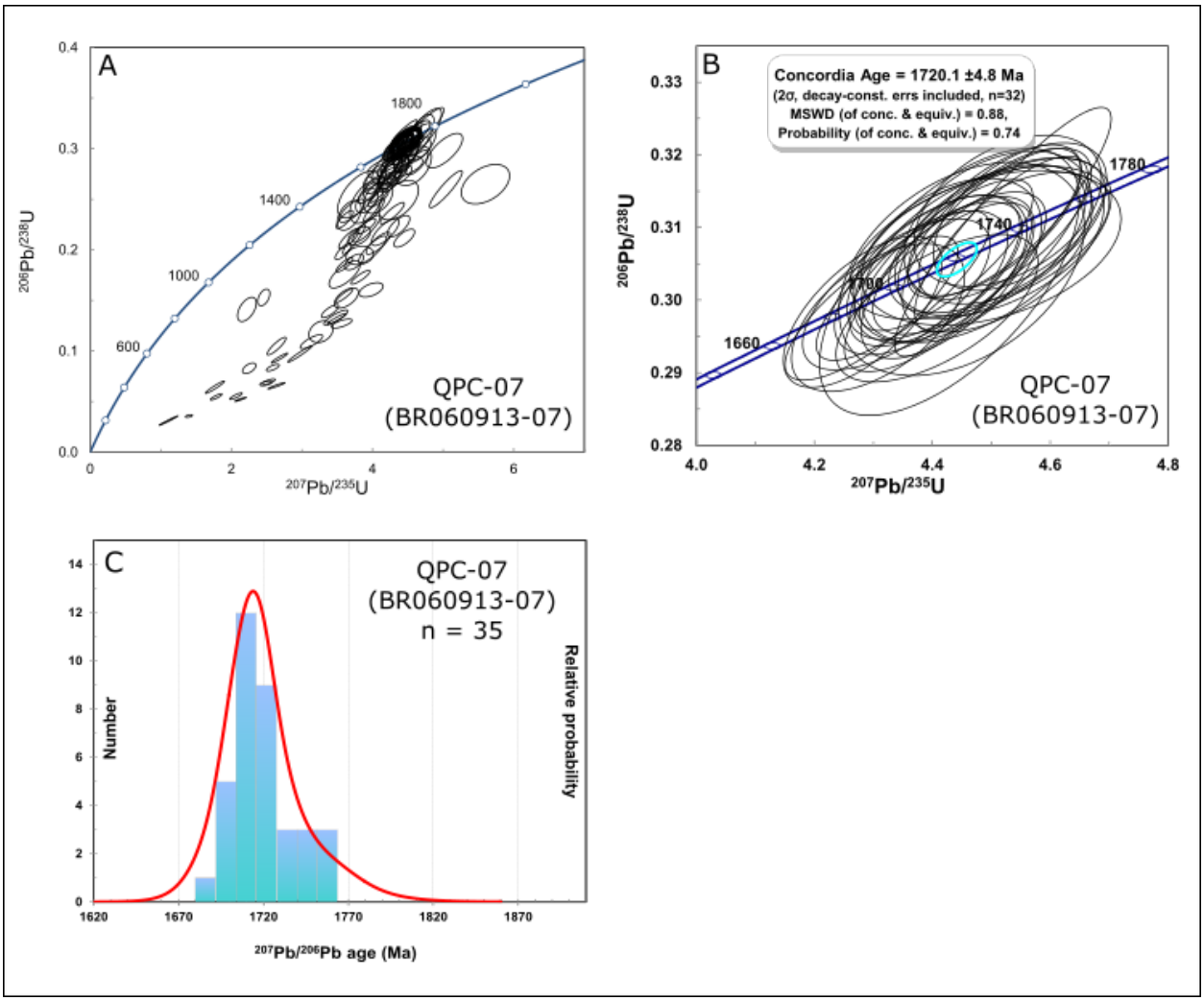

Figure 19. U-Pb zircon concordia and relative probability diagrams for QPC-07 (BR060913-07) collected along FS Road 69 (see Figure 17 for location). A) Concordia diagram showing all analyses. B) Concordia age calculated on grains <3% discordant. C) Probability density diagram and histogram of grains <3% discordant.

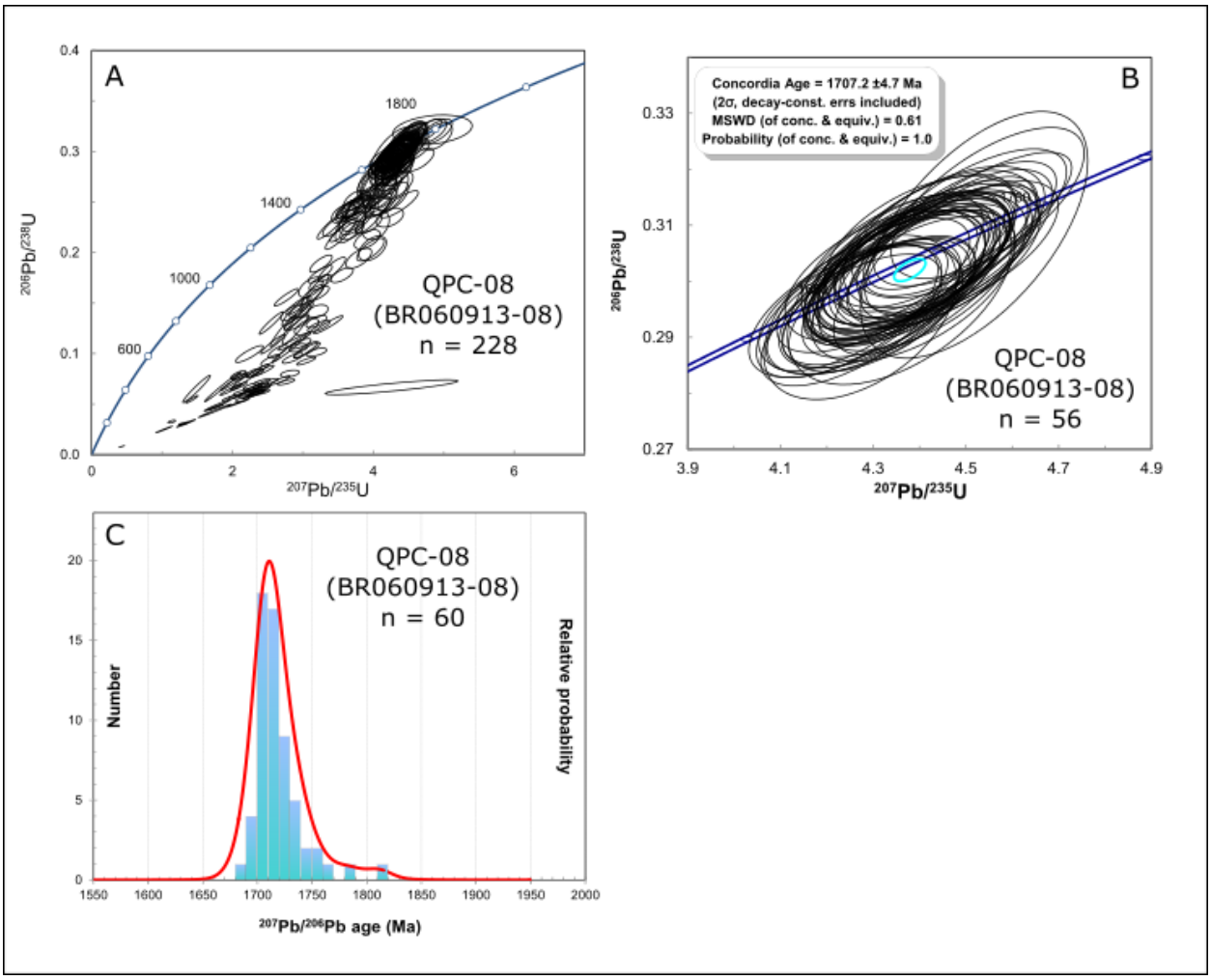

Figure 20. . U-Pb zircon concordia and relative probability diagrams for QPC-08 (BR060913-08) collected along FS Road 69 (see Figure 17 for location). A) Concordia diagram showing all analyses. B) Concordia age calculated on grains <3% discordant. C) Probability density diagram and histogram of grains <3% discordant.

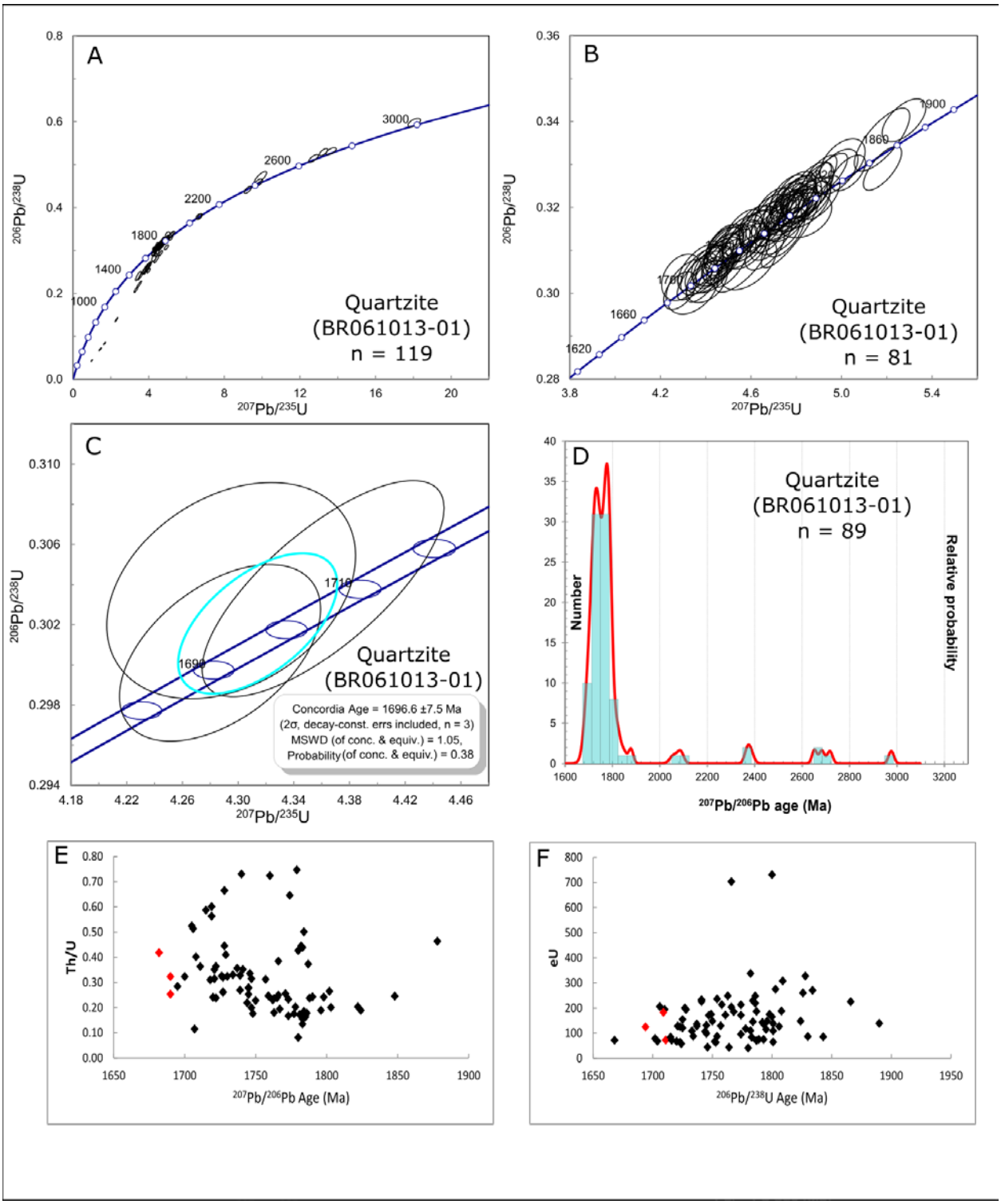
A
Quartzite
(BR061013-01)
n = 119
3000
2600
2200
1800
1400
1000
$^{206}Pb/^{238}U$
$^{207}Pb/^{235}U$
B
Quartzite
(BR061013-01)
n = 81
1900
1860
1780
1660
1620
C
Quartzite
(BR061013-01)
1716
1690
Concordia Age = 1696.6 ±7.5 Ma
(2σ, decay-const. errs included, n = 3)
MSWD (of conc. & equiv.) = 1.05,
Probability (of conc. & equiv.) = 0.38
D
Quartzite
(BR061013-01)
n = 89
Number
Relative probability
$^{207}Pb/^{206}Pb$ age (Ma)
E
Th/U
$^{207}Pb/^{206}Pb$ Age (Ma)
F
eU
$^{206}Pb/^{238}U$ Age (Ma)

Figure 21. . U-Pb zircon concordia and relative probability diagrams (A-D) and Th/U vs. Age and effective U (eU) vs. Age diagrams (E & F) for quartzite (BR061013-01) collected from a prominent quartzite ridge east of FS Road 69 in the Blue Ridge area (see Figure 17 for location). A) Concordia diagram showing all analyses. B) Concordia diagram showing range of Proterozoic ages calculated on grains <3% discordant. C) Concordia age calculated for the three youngest grains <3% discordant from diagram B. D) Probability density diagram for grains <3% discordant. E) Th/U vs. $^{207}Pb/^{206}Pb$ age diagram for grains <3% discordant from diagram B. Red dots represent the three youngest grains from diagram C. F) eU vs. $^{206}Pb/^{238}U$ age diagram for grains <3% discordant from diagram B. Red dots represent the three youngest grains from diagram C.

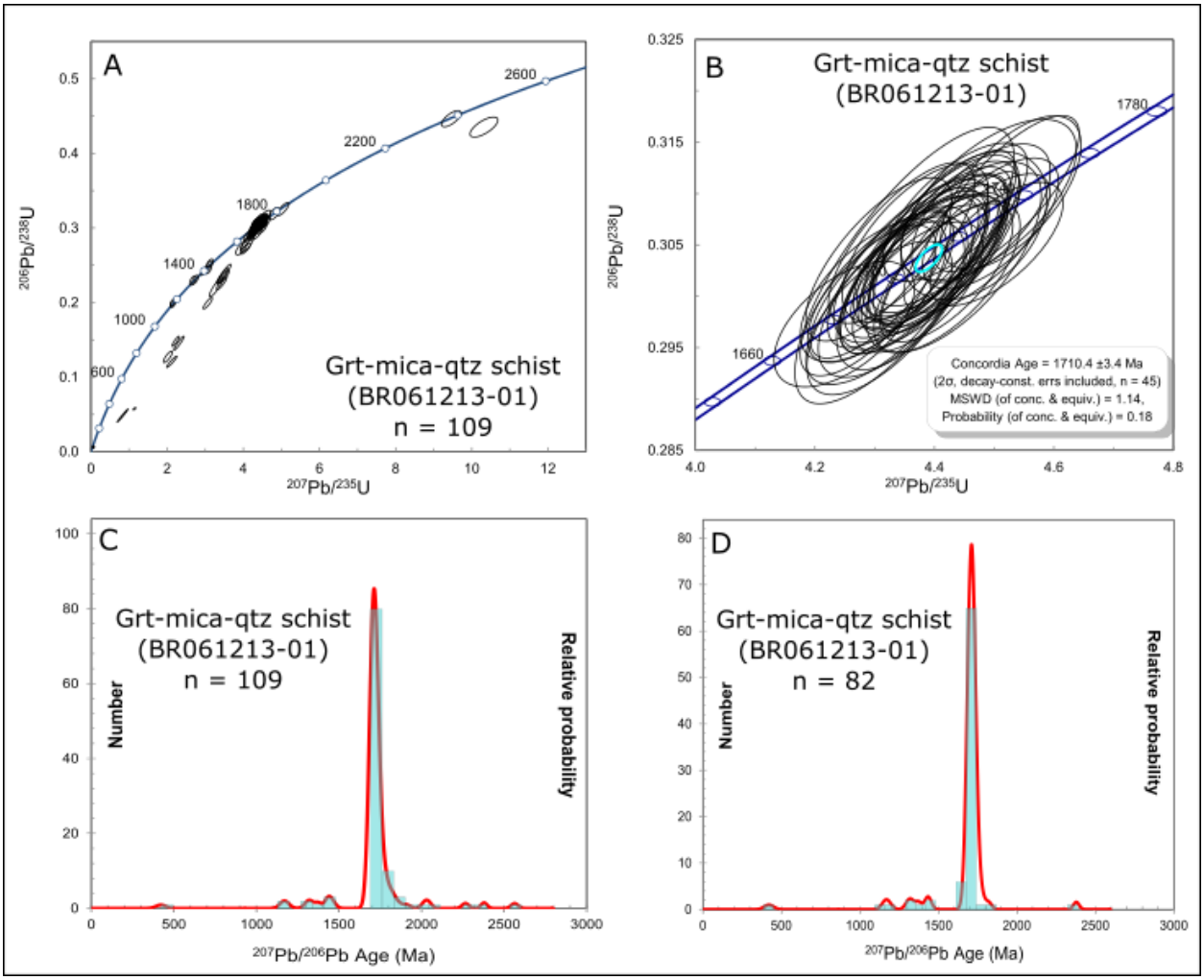

Figure 22. . U-Pb zircon concordia and relative probability diagrams for grt-mica-qtz schist (BR061213-01) collected in the south-central exposure of the Blue Ridge area (see Figure 17 for location). A) Concordia diagram showing all analyses. B) Concordia age calculated on grains <1.5% discordant between 1680 – 1740 Ma. C) Probability density diagram for all analyses. D) Probability density diagram for grains <3% discordant.

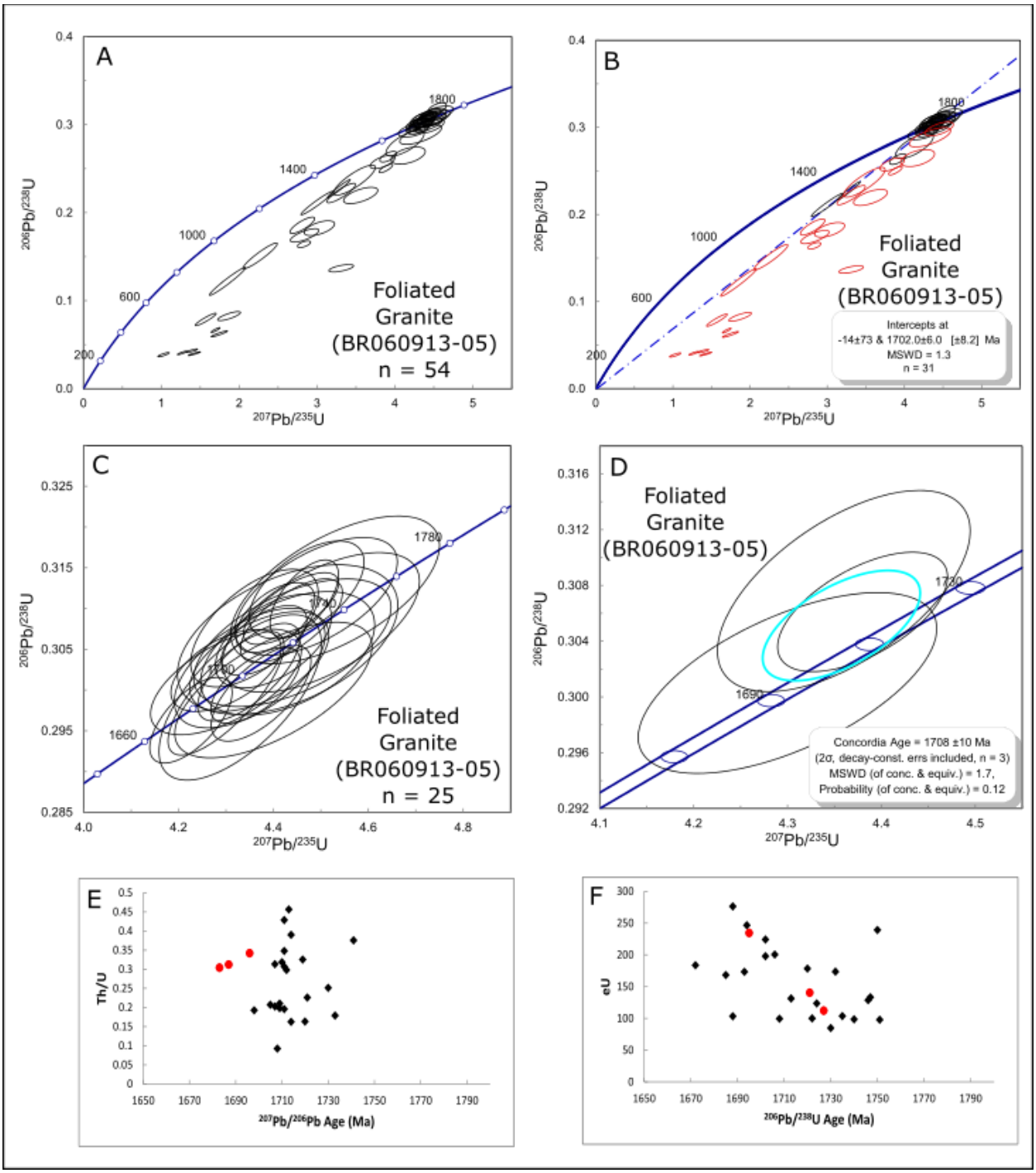
A
Foliated
Granite
(BR060913-05)
n = 54
B
Foliated
Granite
(BR060913-05)
Intercepts at
-14±73 & 1702.0±6.0 [±8.2] Ma
MSWD = 1.3
n = 31
C
Foliated
Granite
(BR060913-05)
n = 25
D
Foliated
Granite
(BR060913-05)
Concordia Age = 1708 ±10 Ma
(2σ, decay-const. errs included, n = 3)
MSWD (of conc. & equiv.) = 1.7,
Probability (of conc. & equiv.) = 0.12
E
Th/U
207Pb/206Pb Age (Ma)
F
eU
206Pb/238U Age (Ma)

Figure 23. U-Pb zircon concordia diagrams (A-D) and Th/U vs. Age and effective U (eU) vs. Age diagrams (E & F) for northern foliated granite (BR060913-05) collected along FS Road 69 (see Figure 17 for location). A) Concordia diagram showing all analyses B) Concordia diagram with intercept age based on selected analyses. Red ellipses represent analyses that have been removed from age calculations. C) Concordia diagram showing grains <3% discordant. D) Concordia age calculated from the three youngest grains <3% discordant. E) Th/U vs. $^{207}Pb/^{206}Pb$ age diagram for grains <3% discordant found in diagram B. Red dots represent the three youngest grains from diagram D. F) eU vs. $^{206}Pb/^{238}U$ age diagram for grains <3% discordant from diagram B.Red dots represent the three youngest grains from diagram C.

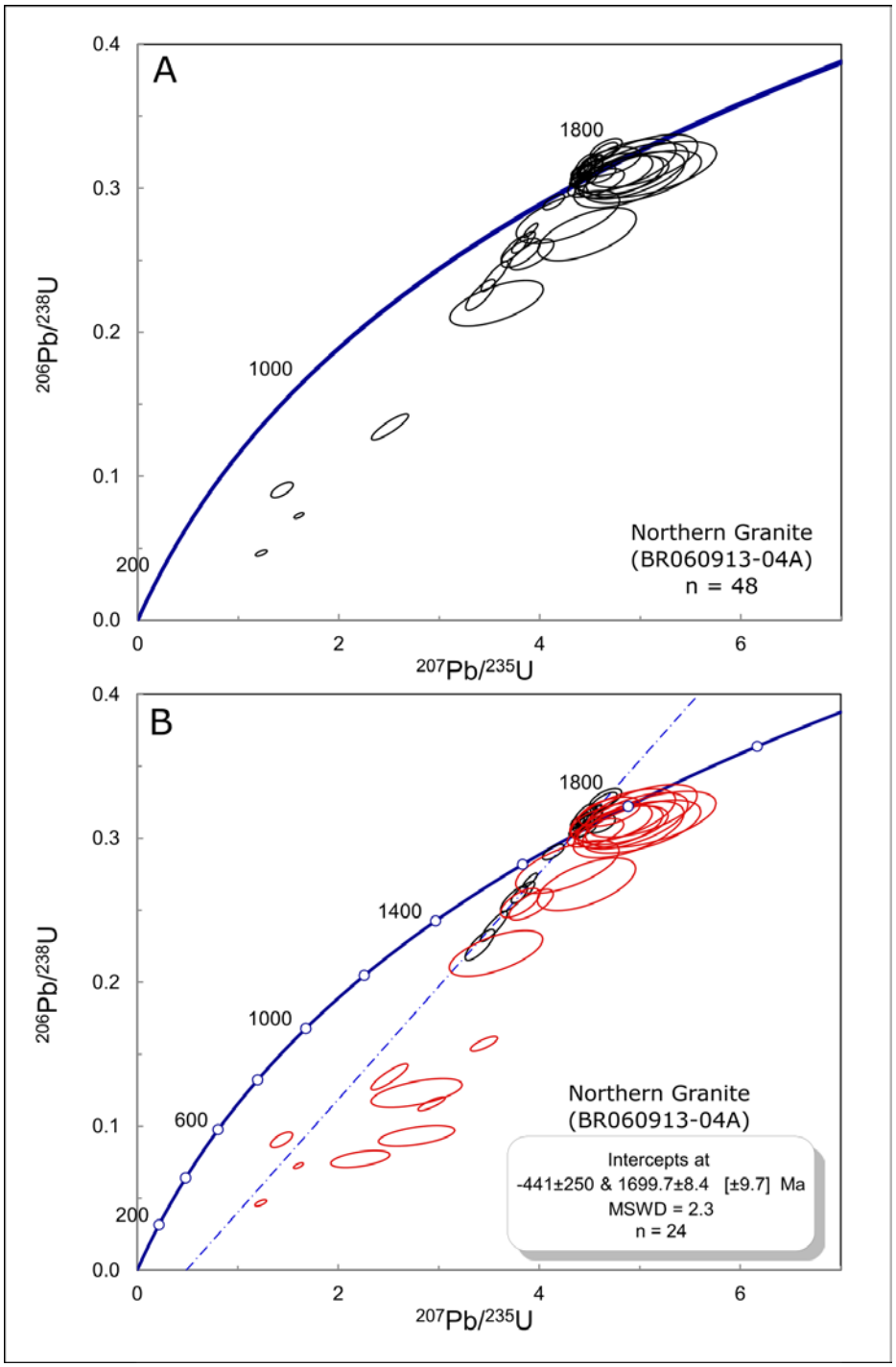

Figure 24. U-Pb zircon concordia diagrams for northern granite (BR060913-04A) collected along FS Road 69 (see Figure 17 for location). A) Concordia diagram with intercept age based on all analyses B) Concordia diagram with intercept age based on selected analyses. Red ellipses represent analyses that have been removed from age calculations.

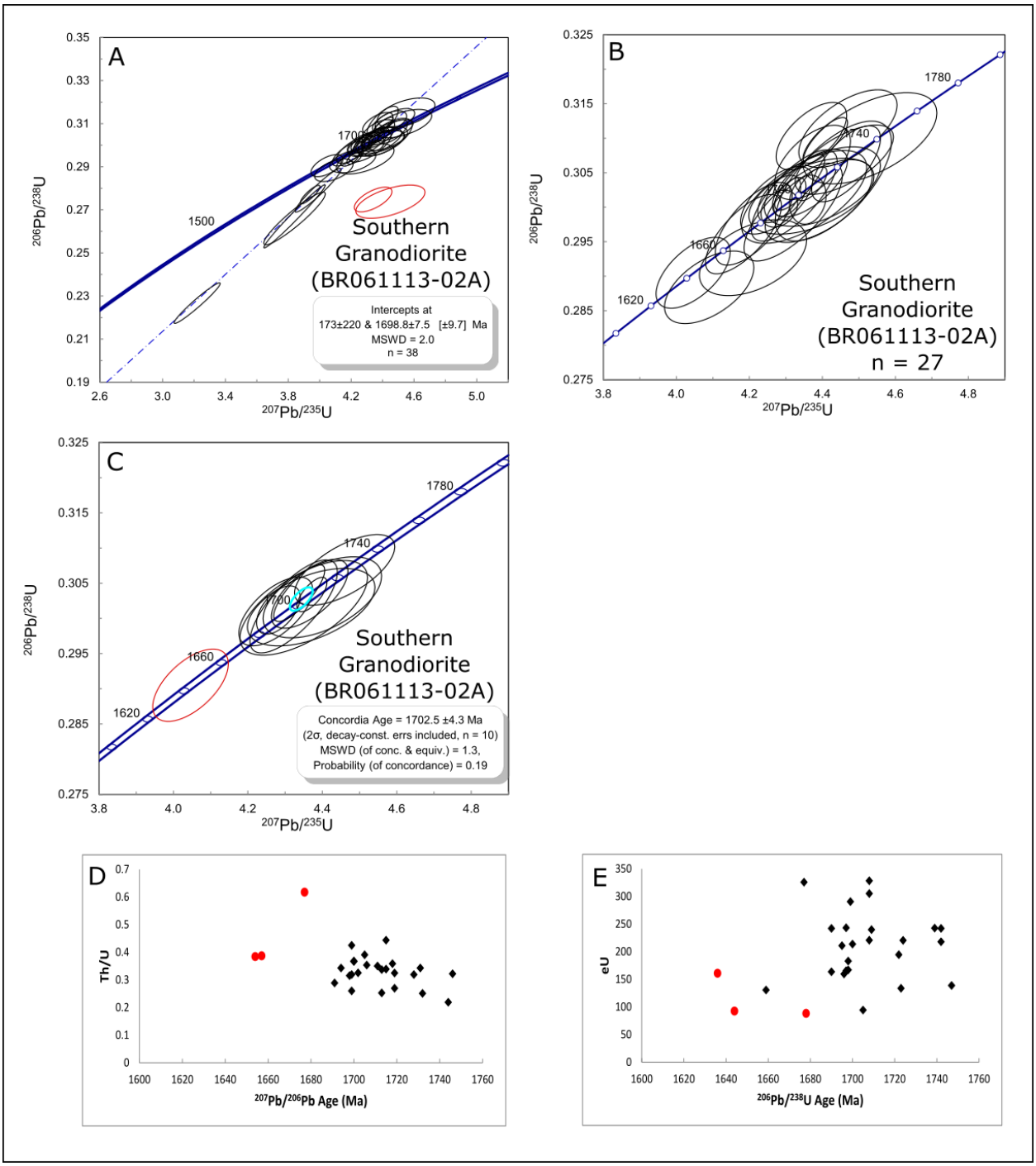
A
Southern Granodiorite (BR061113-02A)
Intercepts at 173±220 & 1698.8±7.5 [±9.7] Ma
MSWD = 2.0
n = 38
1500
1700
B
Southern Granodiorite (BR061113-02A)
n = 27
1620
1660
1700
1740
1780
C
Southern Granodiorite (BR061113-02A)
Concordia Age = 1702.5 ±4.3 Ma
(2σ, decay-const. errs included, n = 10)
MSWD (of conc. & equiv.) = 1.3,
Probability (of concordance) = 0.19
D
Th/U
207Pb/206Pb Age (Ma)
E
eU
206Pb/238U Age (Ma)
206Pb/238U
207Pb/235U

Figure 25. U-Pb zircon concordia diagrams (A-C) and Th/U vs. Age and effective U (eU) vs. Age diagrams (D & E)for southern granodiorite (BR061113-02A) collected ~15m southeast of the southern boundary in the Blue Ridge area (see Figure 17 for location). A) Concordia diagram with intercept age based on selected analyses. Red ellipses represent analyses that have been removed from age calculations. B) Concordia diagram showing grains <3% discordant. The three youngest analyses display ages between 1654 and 1677 Ma. C) Concordia age calculated on grains <1% discordant, excluding the youngest grain. D) Th/U vs. $^{207}Pb/^{206}Pb$ age diagram calculated for grains <3% discordant found in diagram B. Red dots represent the three youngest grains from diagram B. E) eU vs. $^{206}Pb/^{238}U$ age diagram for grains <3% discordant found in diagram B. Red dots represent the three youngest grains from diagram B.

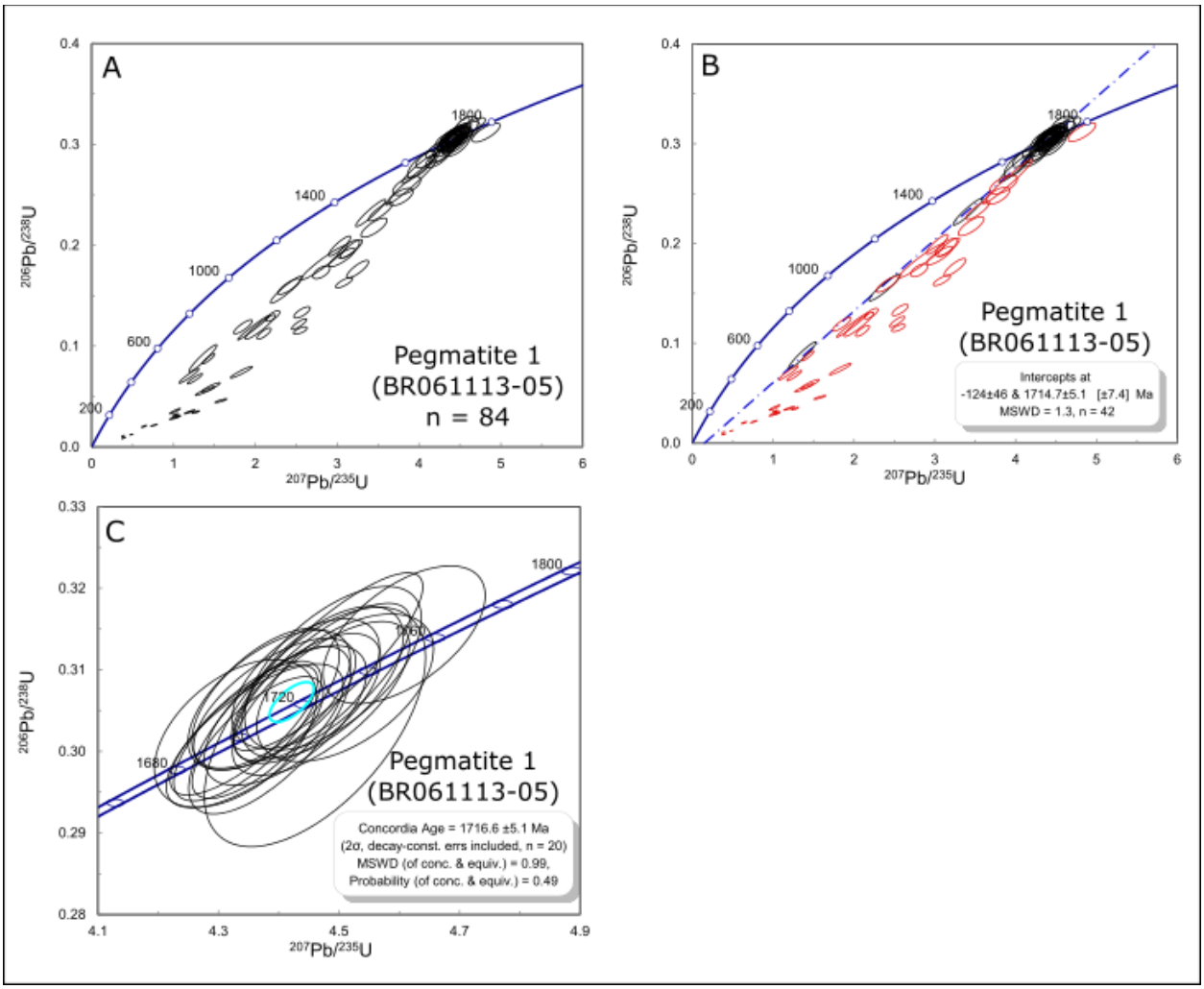

Figure 26. U-Pb zircon concordia diagrams for pegmatite 1 (BR061113-05) collected in an unnamed gulch near the southern boundary of the Blue Ridge area (see Figure 17 for location). A) Concordia diagram showing all analyses B) Concordia diagram with intercept age based on selected analyses. Red ellipses represent analyses that have been removed from age calculations. C) Concordia age calculated on grains <2% discordant.

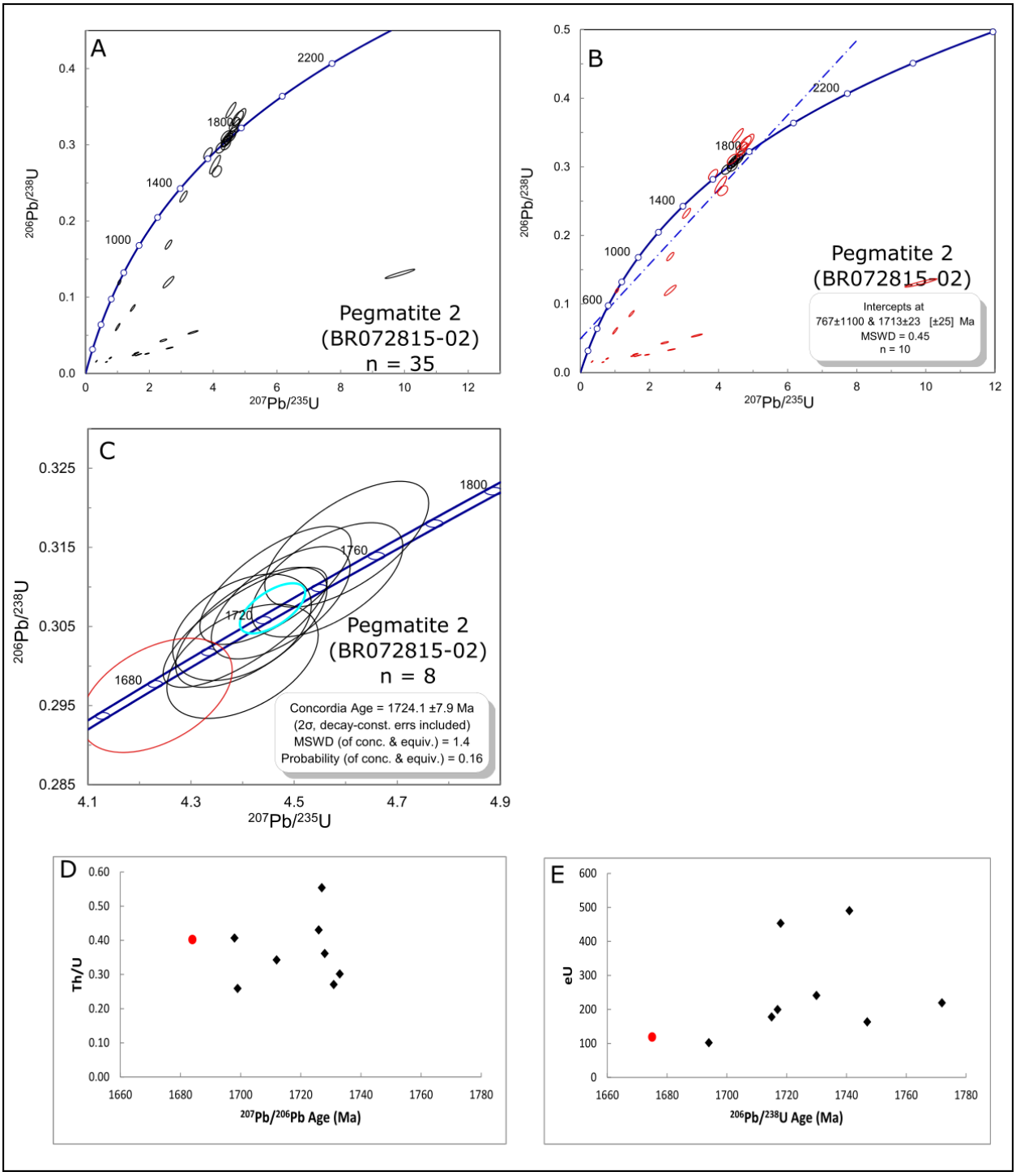
A
Pegmatite 2
(BR072815-02)
n = 35
B
Pegmatite 2
(BR072815-02)
Intercepts at
767±1100 & 1713±23 [±25] Ma
MSWD = 0.45
n = 10
C
Pegmatite 2
(BR072815-02)
n = 8
Concordia Age = 1724.1 ±7.9 Ma
(2σ, decay-const. errs included)
MSWD (of conc. & equiv.) = 1.4
Probability (of conc. & equiv.) = 0.16
D
Th/U
207Pb/206Pb Age (Ma)
E
eU
206Pb/238U Age (Ma)

Figure 27. U-Pb zircon concordia diagrams (A-C) and Th/U vs. Age and effective U (eU) vs. Age diagrams (D & E) for pegmatite 2 (BR072815-02) collected in an unnamed gulch at the southern boundary of the Blue Ridge area (see Figure 17 for location). A) Concordia diagram showing all analyses. B) Concordia diagram with intercept age based on selected analyses. Red ellipses represent analyses that have been removed from age calculations. C) Concordia age diagram calculated from grains <3% discordant. Red ellipse represents the youngest concordant analysis removed from age calculations. . D) Th/U vs. $^{207}Pb/^{206}Pb$ age diagram calculated for grains <3% discordant found in diagram C. Red dot represents the youngest grain from diagram C. E) eU vs. $^{206}Pb/^{238}U$ age diagram for grains <3% discordant found in diagram C. Red dot represents the youngest grain from diagram C.

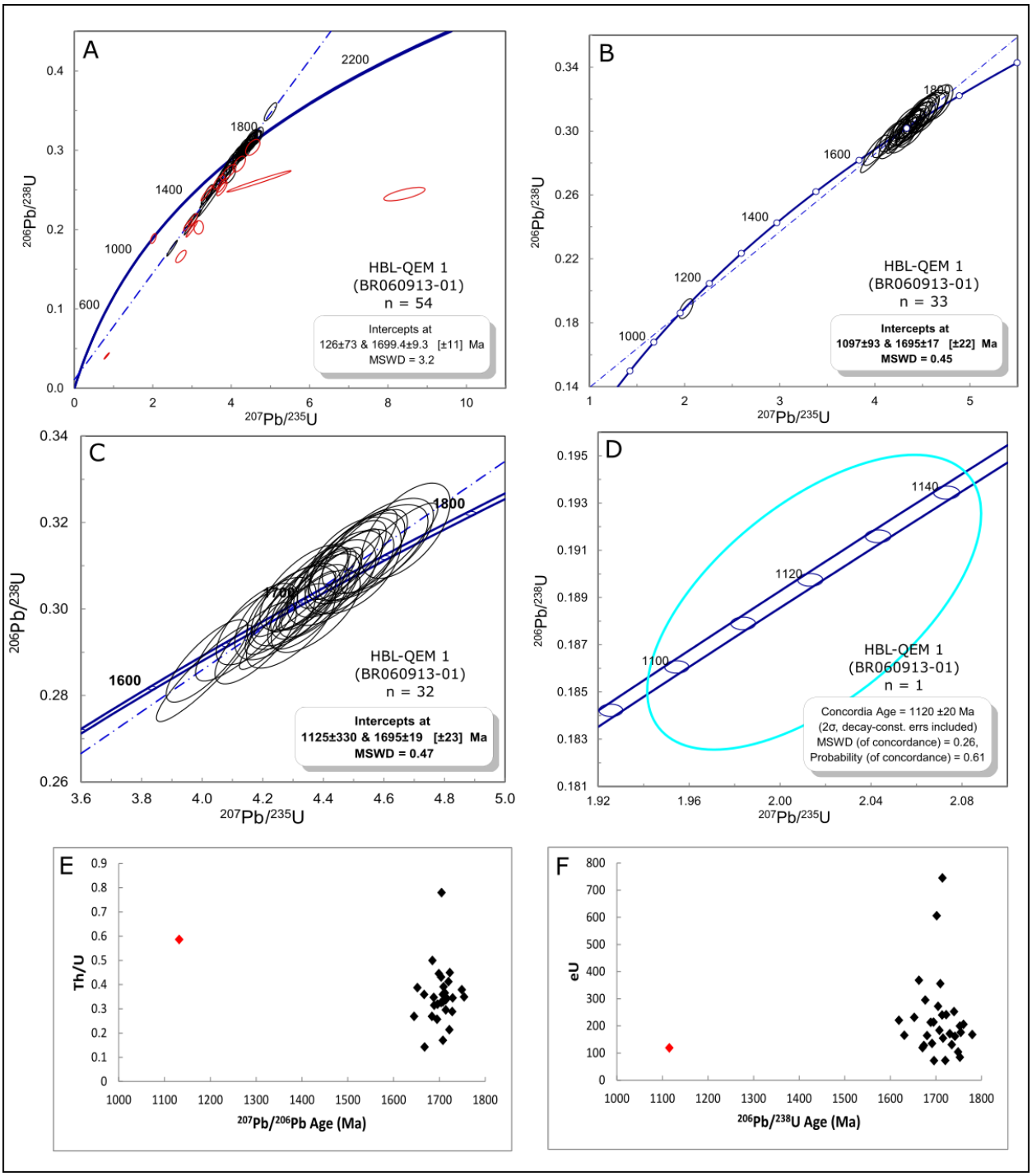
A
2200
1800
1400
1000
600
HBL-QEM 1
(BR060913-01)
n = 54
Intercepts at
126±73 & 1699.4±9.3 [±11] Ma
MSWD = 3.2
206Pb/238U
207Pb/235U
B
1800
1600
1400
1200
1000
HBL-QEM 1
(BR060913-01)
n = 33
Intercepts at
1097±93 & 1695±17 [±22] Ma
MSWD = 0.45
206Pb/238U
207Pb/235U
C
1800
1700
1600
HBL-QEM 1
(BR060913-01)
n = 32
Intercepts at
1125±330 & 1695±19 [±23] Ma
MSWD = 0.47
206Pb/238U
207Pb/235U
D
1140
1120
1100
HBL-QEM 1
(BR060913-01)
n = 1
Concordia Age = 1120 ±20 Ma
(2σ, decay-const. errs included)
MSWD (of concordance) = 0.26,
Probability (of concordance) = 0.61
206Pb/238U
207Pb/235U
E
Th/U
207Pb/206Pb Age (Ma)
F
eU
206Pb/238U Age (Ma)

Figure 28. U-Pb zircon concordia diagrams (A-D) and Th/U vs. Age and effective U (eU) vs. Age diagrams (E & F)for amphibole-bearing leucosome HBL-QEM1 (BR060913-01) collected in an unnamed gulch at the southern boundary of the Blue Ridge area (see Figure 17 for location). A) Concordia diagram with intercept age based on selected analyses. Red ellipses represent analyses that have been removed from age calculations. B) Concordia diagram with upper and lower intercept ages calculated from grains <3% discordant including young analyses. C) Concordia diagram with upper and lower intercept ages calculated from grains <3% discordant and older than 1600 Ma. D) Concordia age calculated on single youngest grain <3% discordant found in diagram B. E) Th/U vs. $^{207}Pb/^{206}Pb$ age diagram calculated for grains <3% discordant found in diagram B. Red dot represents the youngest grain from diagram B. F) eU vs. $^{206}Pb/^{238}U$ age diagram for grains <3% discordant found in diagram B. Red dot represents the youngest grain from diagram B.

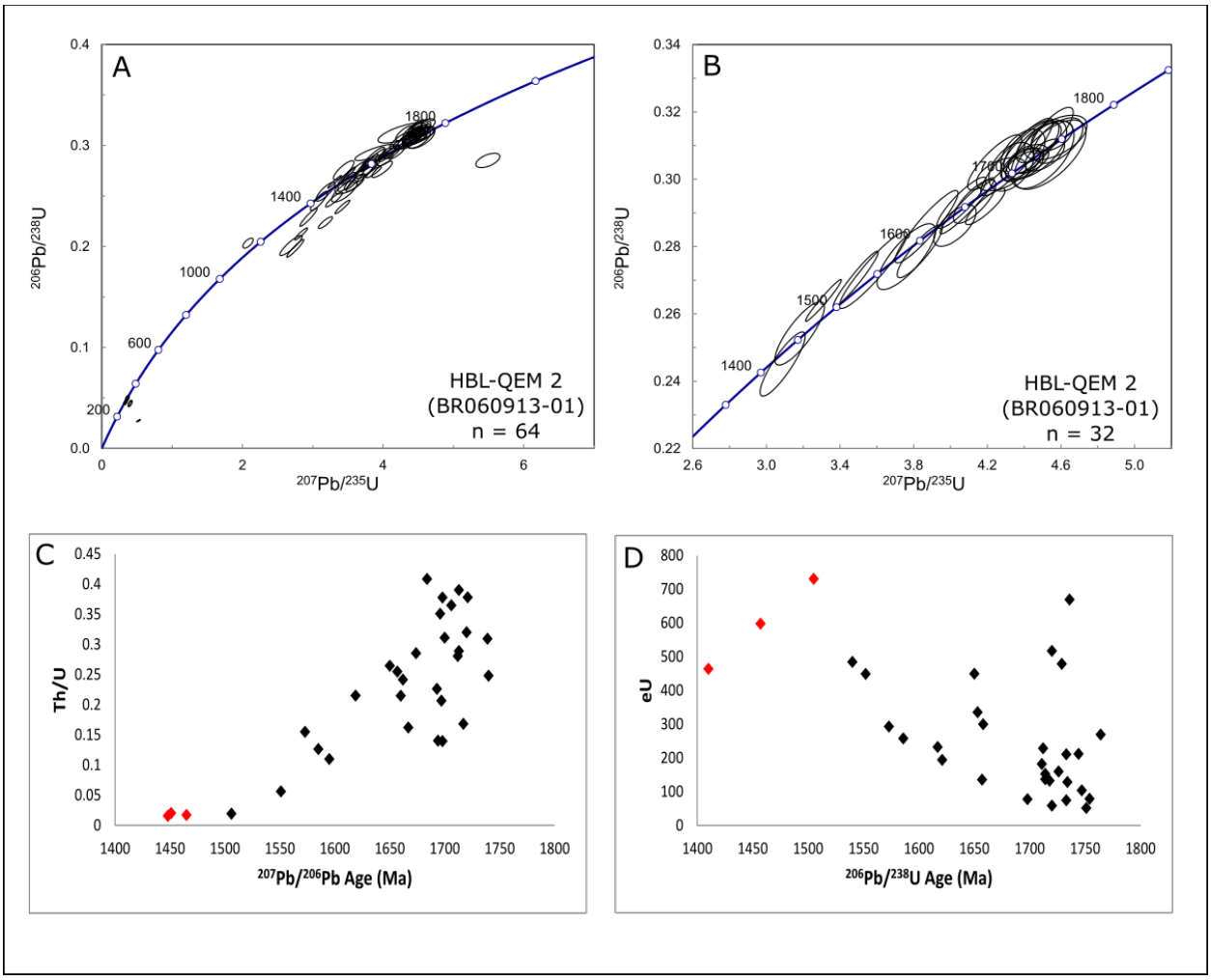

Figure 29. U-Pb zircon concordia diagrams (A & B) and Th/U vs. Age and effective U (eU) vs. Age diagrams (C & D) for amphibole-bearing leucosome HBL-QEM2 (BR060913-01) collected in an unnamed gulch at the southern boundary of the Blue Ridge area (see Figure 17 for location). A) Concordia diagram showing all analyses. B) Concordia diagram showing grains <3% discordant. C) Th/U vs. $^{207}Pb/^{206}Pb$ age diagram calculated for grains <3% discordant found in diagram B. Red dots represent the youngest three grains from diagram B. D) eU vs. $^{206}Pb/^{238}U$ age diagram for grains <3% discordant found in diagram B. Red dost represent the youngest three grains from diagram B.

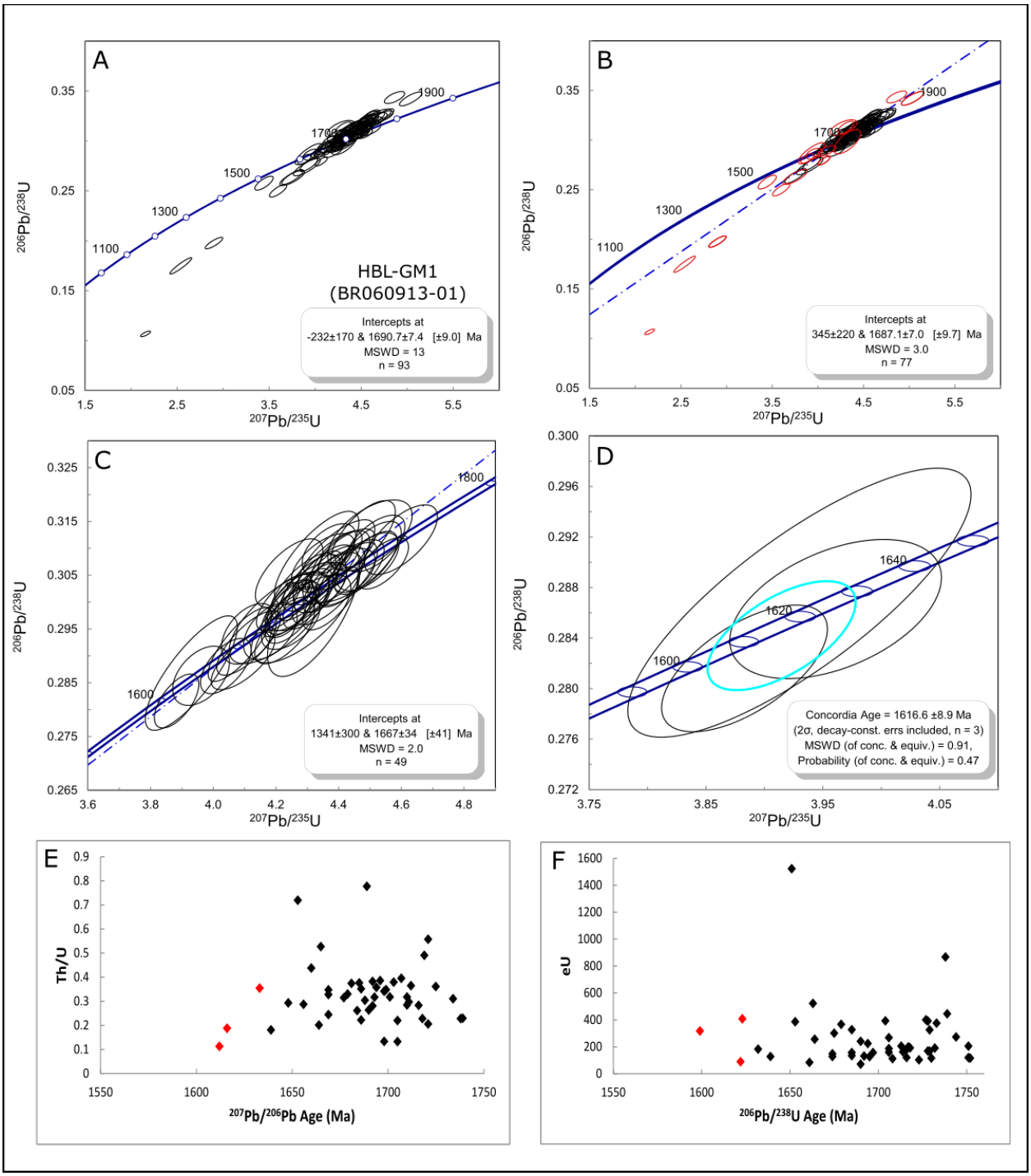
A
HBL-GM1
(BR060913-01)
Intercepts at
-232±170 & 1690.7±7.4 [±9.0] Ma
MSWD = 13
n = 93
1100
1300
1500
1700
1900
206Pb/238U
207Pb/235U
B
Intercepts at
345±220 & 1687.1±7.0 [±9.7] Ma
MSWD = 3.0
n = 77
C
Intercepts at
1341±300 & 1667±34 [±41] Ma
MSWD = 2.0
n = 49
1600
1800
D
Concordia Age = 1616.6 ±8.9 Ma
(2σ, decay-const. errs included, n = 3)
MSWD (of conc. & equiv.) = 0.91,
Probability (of conc. & equiv.) = 0.47
1600
1620
1640
E
Th/U
207Pb/206Pb Age (Ma)
F
eU
206Pb/238U Age (Ma)

Figure 30. U-Pb zircon concordia diagrams (A - D) and Th/U vs. Age and effective U (eU) vs. Age diagrams (E & F) for amphibole-bearing leucosome HBL-GM1 (BR060913-01) collected in an unnamed gulch at the southern boundary of the Blue Ridge area (see Figure 17 for location). A) Concordia diagram showing all analyses. B) Concordia diagram with intercept age based on selected analyses. Red ellipses represent analyses that have been removed from age calculations. C) Concordia diagram with upper and lower intercept ages calculated from grains <3% discordant. D) Concordia age calculated on three youngest grains <3% discordant from diagram C. E) Th/U vs. $^{207}Pb/^{206}Pb$ age diagram calculated for grains <3% discordant found in diagram C. Red dots represent the youngest three grains from diagram C. F) eU vs. $^{206}Pb/^{238}U$ age diagram for grains <3% discordant found in diagram B. Red dots represent the youngest three grains from diagram C.

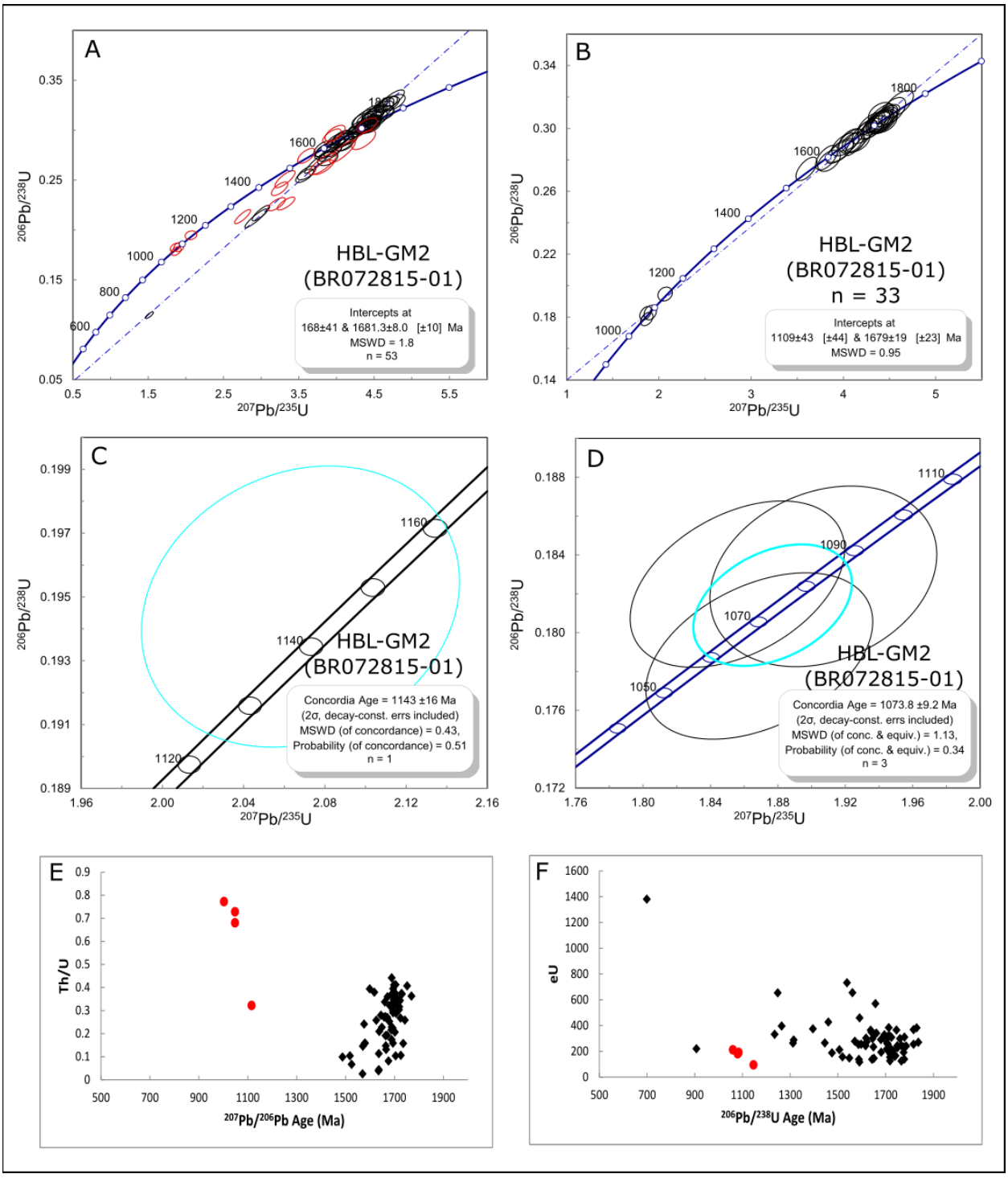
A
HBL-GM2
(BR072815-01)
Intercepts at
168±41 & 1681.3±8.0 [±10] Ma
MSWD = 1.8
n = 53
B
HBL-GM2
(BR072815-01)
n = 33
Intercepts at
1109±43 [±44] & 1679±19 [±23] Ma
MSWD = 0.95
C
HBL-GM2
(BR072815-01)
Concordia Age = 1143 ±16 Ma
(2σ, decay-const. errs included)
MSWD (of concordance) = 0.43,
Probability (of concordance) = 0.51
n = 1
D
HBL-GM2
(BR072815-01)
Concordia Age = 1073.8 ±9.2 Ma
(2σ, decay-const. errs included)
MSWD (of conc. & equiv.) = 1.13,
Probability (of conc. & equiv.) = 0.34
n = 3
E
Th/U
207Pb/206Pb Age (Ma)
F
eU
206Pb/238U Age (Ma)

Figure 31. U-Pb zircon concordia diagrams (A - D) and Th/U vs. Age and effective U (eU) vs. Age diagrams (E & F) for amphibole-bearing leucosome HBL-GM2 (BR072815-01) collected in an unnamed gulch at the southern boundary of the Blue Ridge area (see Figure 17 for location). A) Concordia diagram with intercept age based on selected analyses. Red ellipses represent analyses that have been removed from age calculations. B) Concordia diagram with upper and lower intercept age calculated from grains <3% discordant with young ages included. C) Concordia age calculated on single grain from diagram B. D) Concordia age calculated on single grain with three analyses from diagram B. E) Th/U vs. $^{207}Pb/^{206}Pb$ age diagram calculated for grains <3% discordant from diagram B. Red dots represent the youngest four analyses from diagram B. F) eU vs. $^{206}Pb/^{238}U$ age diagram for grains <3% discordant found in diagram B. Red dots represent the youngest four analyses from diagram B.

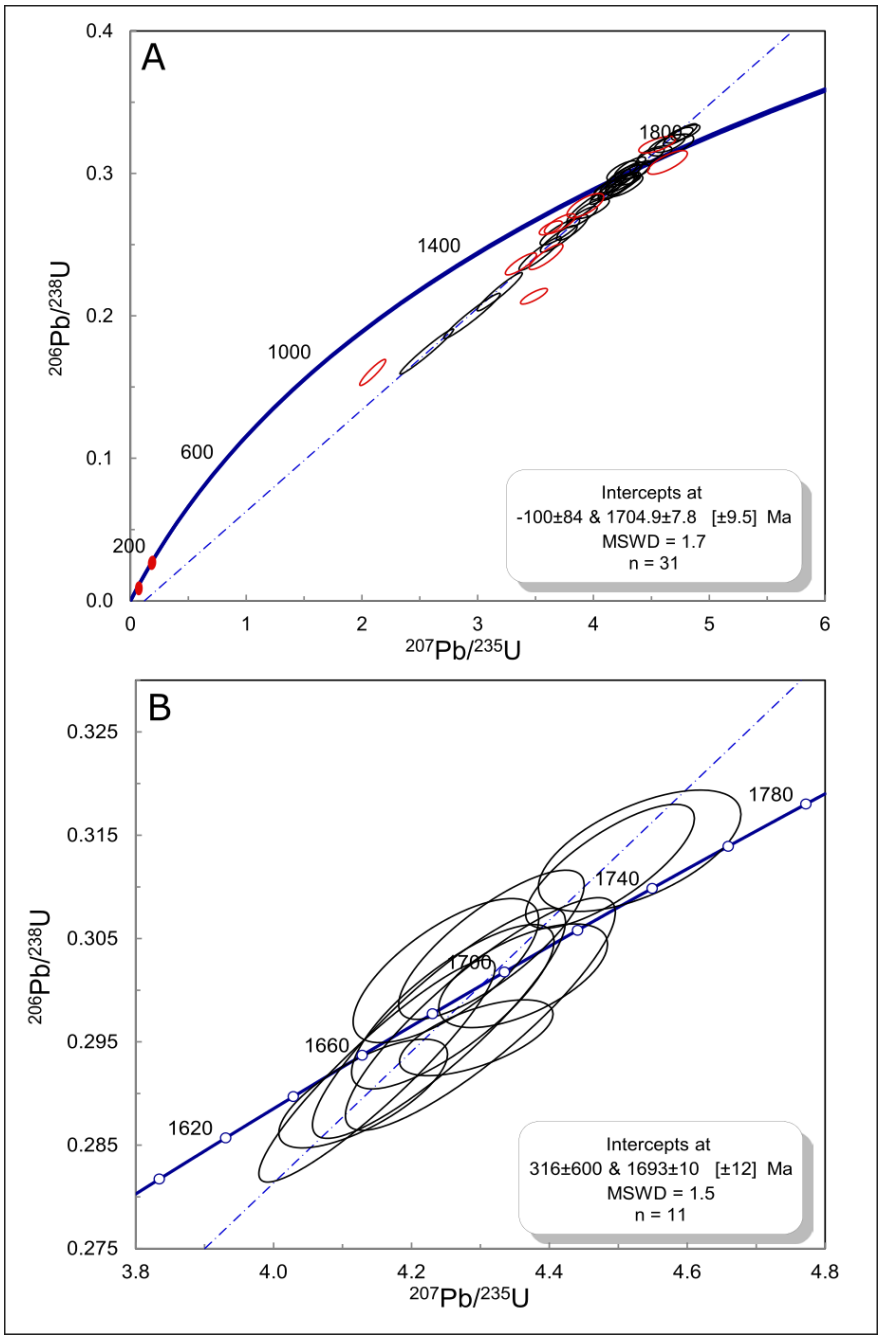

Figure 32. U-Pb zircon concordia diagrams for amphibole-bearing leucosome HBL-TM (BR060913-01) collected in an unnamed gulch at the southern boundary of the Blue Ridge area (see Figure 17 for location). A) Concordia diagram with intercept age based on selected analyses. Red ellipses represent analyses that have been removed from age calculations. B) Concordia diagram with upper intercept age calculated from grains <3% discordant.

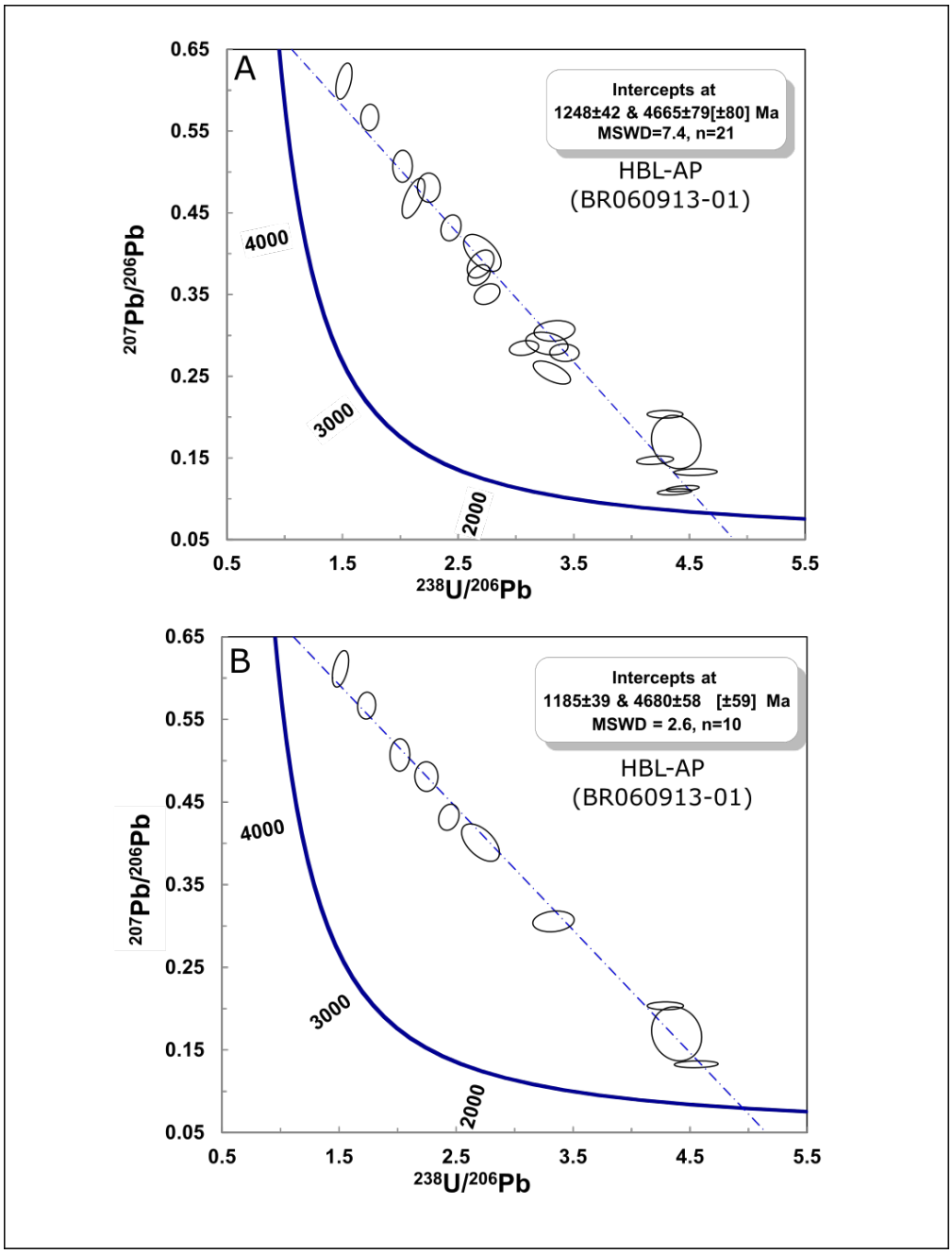

Figure 33. Tera-Wasserburg (TW) (1972) concordia diagrams for U-Pb analyses on apatite for amphibole-bearing leucosome HBL-TM (BR060913-01) collected in an unnamed gulch at the southern boundary of the Blue Ridge area (see Figure 17 for location). A) TW diagram with intercept ages based on all analyses. B) TW diagram with intercept ages based on young analyses only.

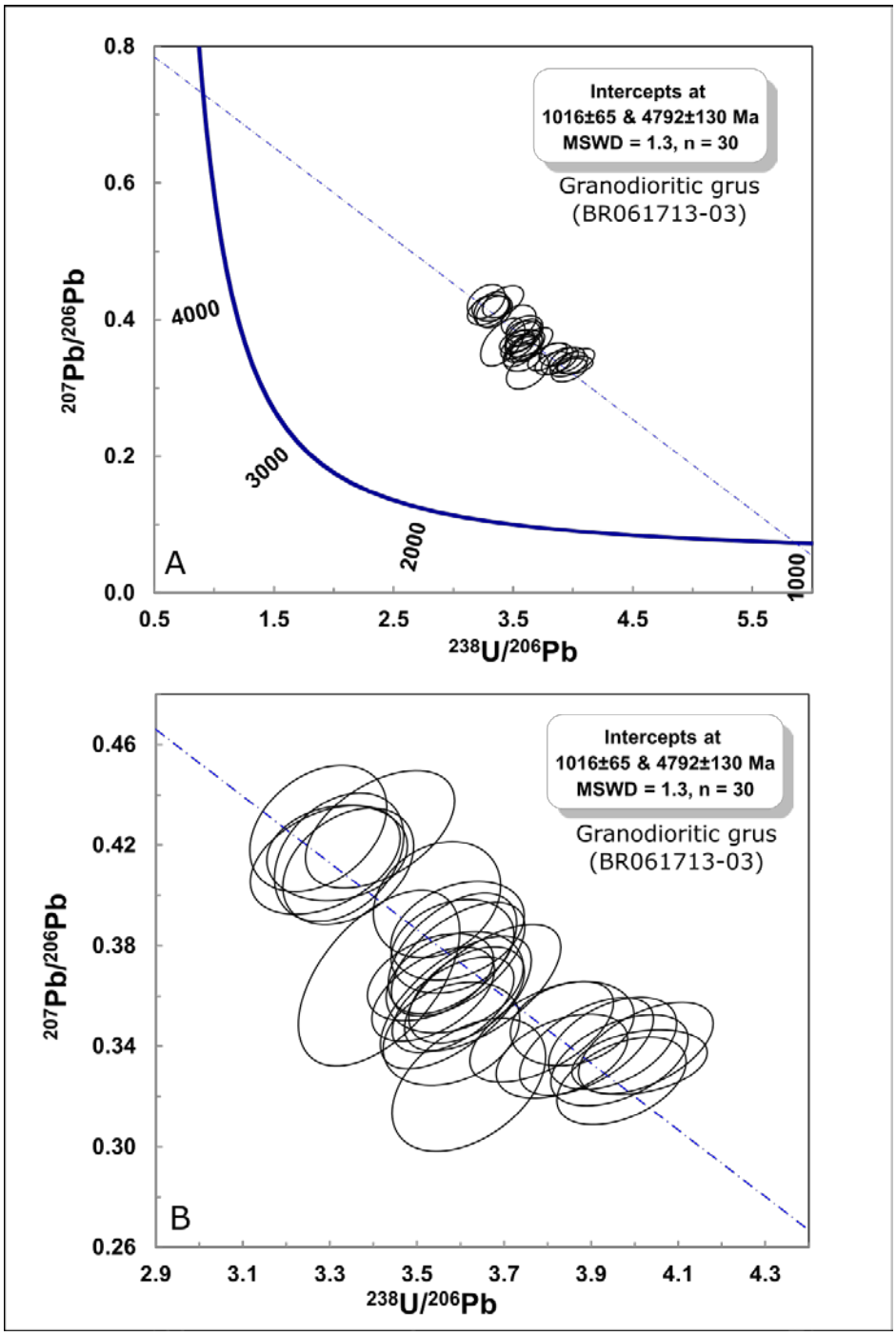

Figure 34. Tera-Wasserburg (TW) (1972) concordia diagrams for U-Pb analyses on apatite for granodioritic grus (BR061713-03) collected along FS Road 69 (see Figure 17 for location).Both diagrams show the calculated intercept ages, with the lower diagram zoomed in on the analyses to illustrate homogeneity of analyses.

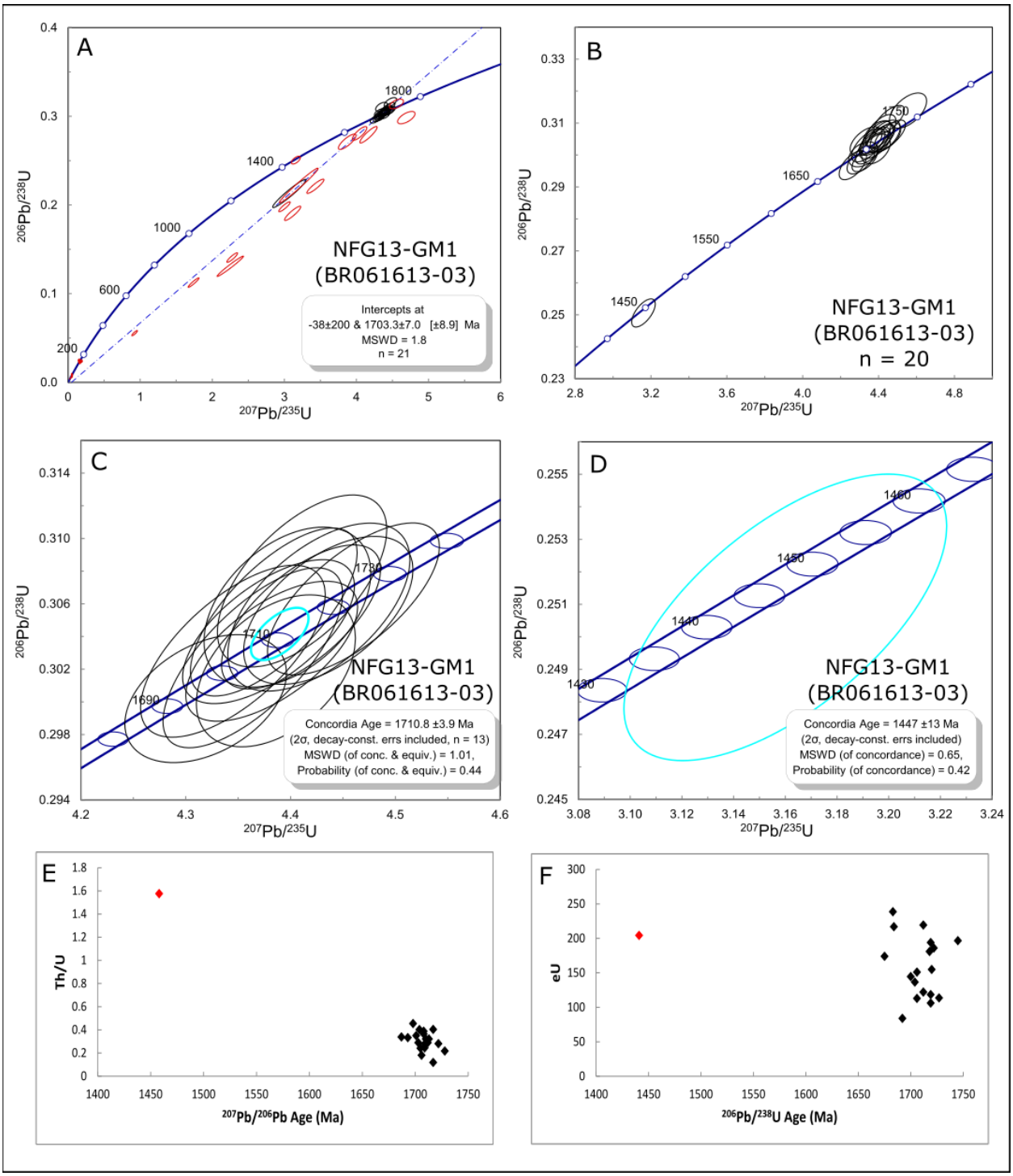
A
NFG13-GM1
(BR061613-03)
Intercepts at
-38±200 & 1703.3±7.0 [±8.9] Ma
MSWD = 1.8
n = 21
206Pb/238U
207Pb/235U
B
NFG13-GM1
(BR061613-03)
n = 20
C
NFG13-GM1
(BR061613-03)
Concordia Age = 1710.8 ±3.9 Ma
(2σ, decay-const. errs included, n = 13)
MSWD (of conc. & equiv.) = 1.01,
Probability (of conc. & equiv.) = 0.44
D
NFG13-GM1
(BR061613-03)
Concordia Age = 1447 ±13 Ma
(2σ, decay-const. errs included)
MSWD (of concordance) = 0.65,
Probability (of concordance) = 0.42
E
Th/U
207Pb/206Pb Age (Ma)
F
eU
206Pb/238U Age (Ma)

Figure 35. U-Pb zircon concordia diagrams (A - D) and Th/U vs. Age and effective U (eU) vs. Age diagrams (E & F) for foliated granite NFG13-GM1 (BR061613-03) collected near the northern boundary of Blue Ridge in Gooseberry Gulch (see Figure 17 for location). A) Concordia diagram with intercept age based on selected analyses. Red ellipses represent analyses that have been removed from age calculations. B) Concordia diagram showing grains <3% discordant. C) Concordia age calculated from grains determined to be <1% discordant from diagram B, without the youngest grain. D) Concordia age calculated for youngest grain from diagram B. E) Th/U vs. $^{207}Pb/^{206}Pb$ age diagram calculated for grains <3% discordant found in diagram B. Red dot represents the youngest grain from diagram B. F) eU vs. $^{206}Pb/^{238}U$ age diagram for grains <3% discordant found in diagram B. Red dot represents the youngest grain from diagram B.

.

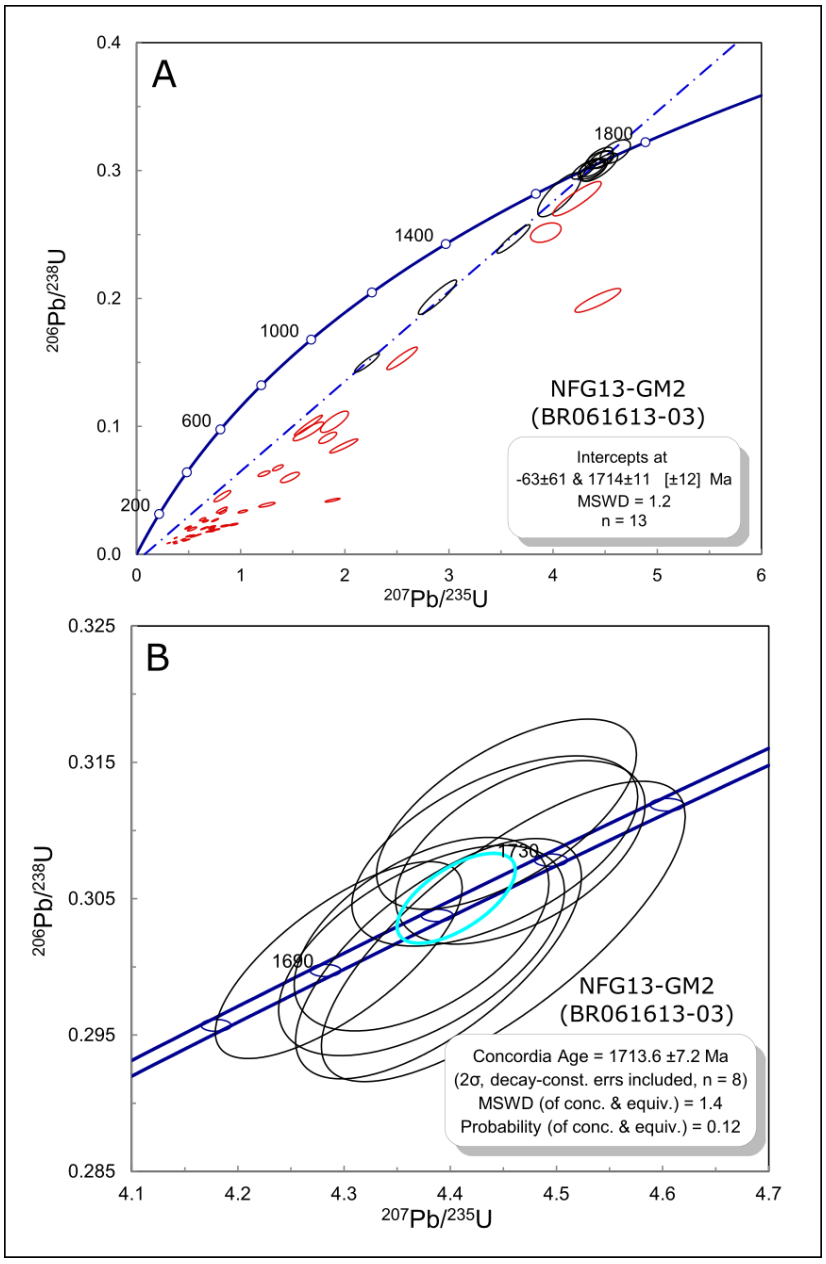

Figure 36. U-Pb zircon concordia diagrams for foliated granite NFG13-GM2 (BR061613-03) collected near the northern boundary of Blue Ridge in Gooseberry Gulch (see Figure 17 for location). A) Concordia diagram with intercept age based on selected analyses. Red ellipses represent analyses that have been removed from age calculations. B) Concordia age calculated on grains <3% discordant.

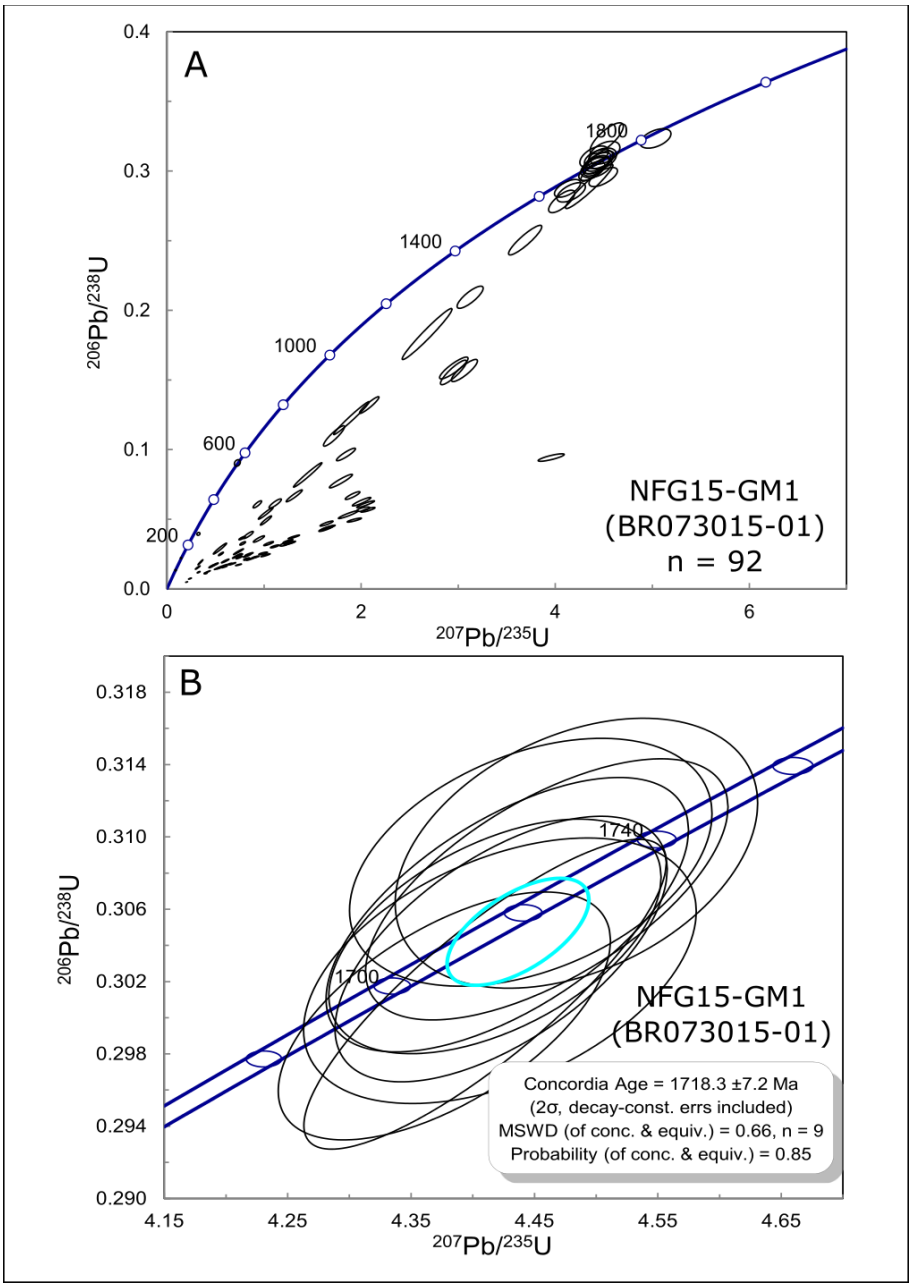

Figure 37. U-Pb zircon concordia diagrams for foliated granite NFG15-GM1 (BR061613-03) collected near the northern boundary of Blue Ridge in Gooseberry Gulch (see Figure 17 for location). A) Concordia diagram showing all analyses. B) Concordia age calculated from grains <3% discordant (grains <3% discordant with anomalously young ages and assumed to be contaminants were not included).

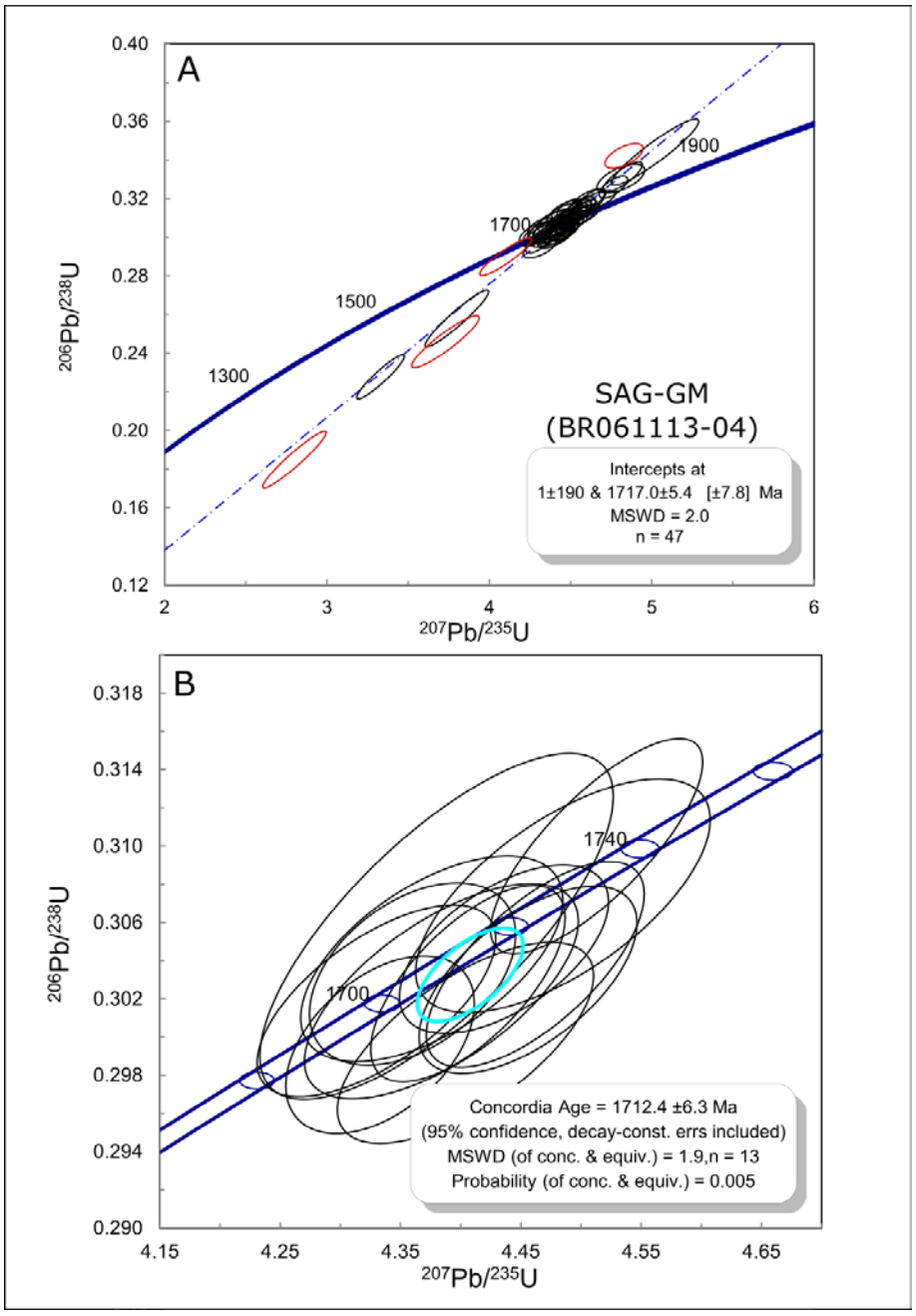

Figure 38. U-Pb zircon concordia diagrams for augen gneiss SAG-GM (BR061113-04) collected along the southern boundary of Blue Ridge in an unnamed gulch (see Figure 17 for location). A) Concordia diagram with intercept age based on selected analyses. Red ellipses represent analyses that have been removed from age calculations. B) Concordia age calculated from grains <2% discordant.

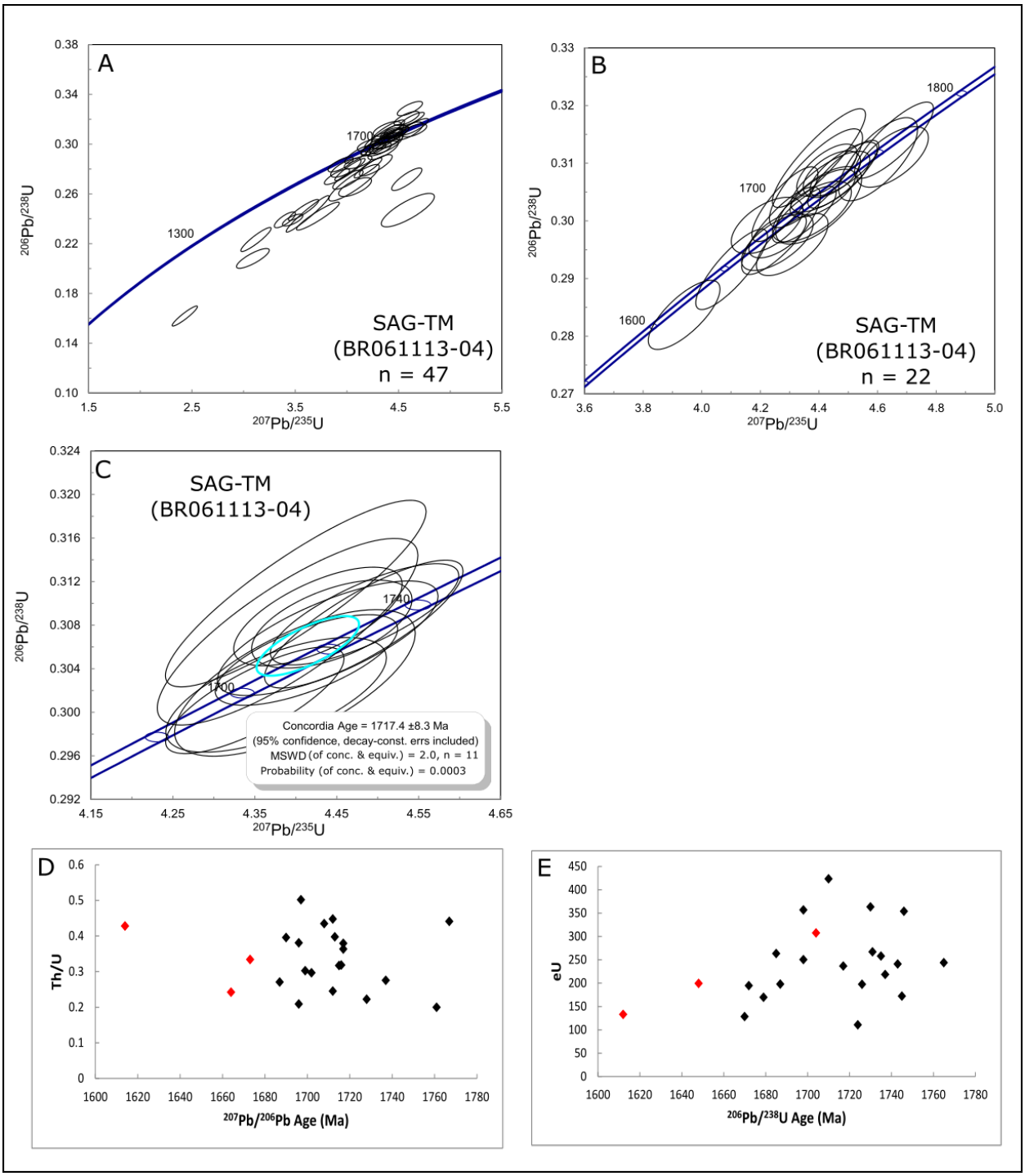
A
SAG-TM
(BR061113-04)
n = 47
1700
1300
$^{206}Pb/^{238}U$
$^{207}Pb/^{235}U$
B
SAG-TM
(BR061113-04)
n = 22
1800
1700
1600
C
SAG-TM
(BR061113-04)
1740
1700
Concordia Age = 1717.4 ±8.3 Ma
(95% confidence, decay-const. errs included)
MSWD (of conc. & equiv.) = 2.0, n = 11
Probability (of conc. & equiv.) = 0.0003
D
Th/U
$^{207}Pb/^{206}Pb$ Age (Ma)
E
eU
$^{206}Pb/^{238}U$ Age (Ma)

Figure 39. U-Pb zircon concordia diagrams (A - C) and Th/U vs. Age and effective U (eU) vs. Age diagrams (D & E) for augen gneiss SAG-TM (BR061113-04) collected along the southern boundary of Blue Ridge in an unnamed gulch (see Figure 17 for location). A) Concordia diagram showing all analyses. B) Concordia diagram showing grains <3% discordant. C) Concordia age calculated from grains determined to be <2% discordant. D) Th/U vs. $^{207}Pb/^{206}Pb$ age diagram calculated for grains <3% discordant found in diagram B. Red dots represent the three youngest grains from diagram B. E) eU vs. $^{206}Pb/^{238}U$ age diagram for grains <3% discordant found in diagram B. Red dots represent the three youngest grains from diagram B.

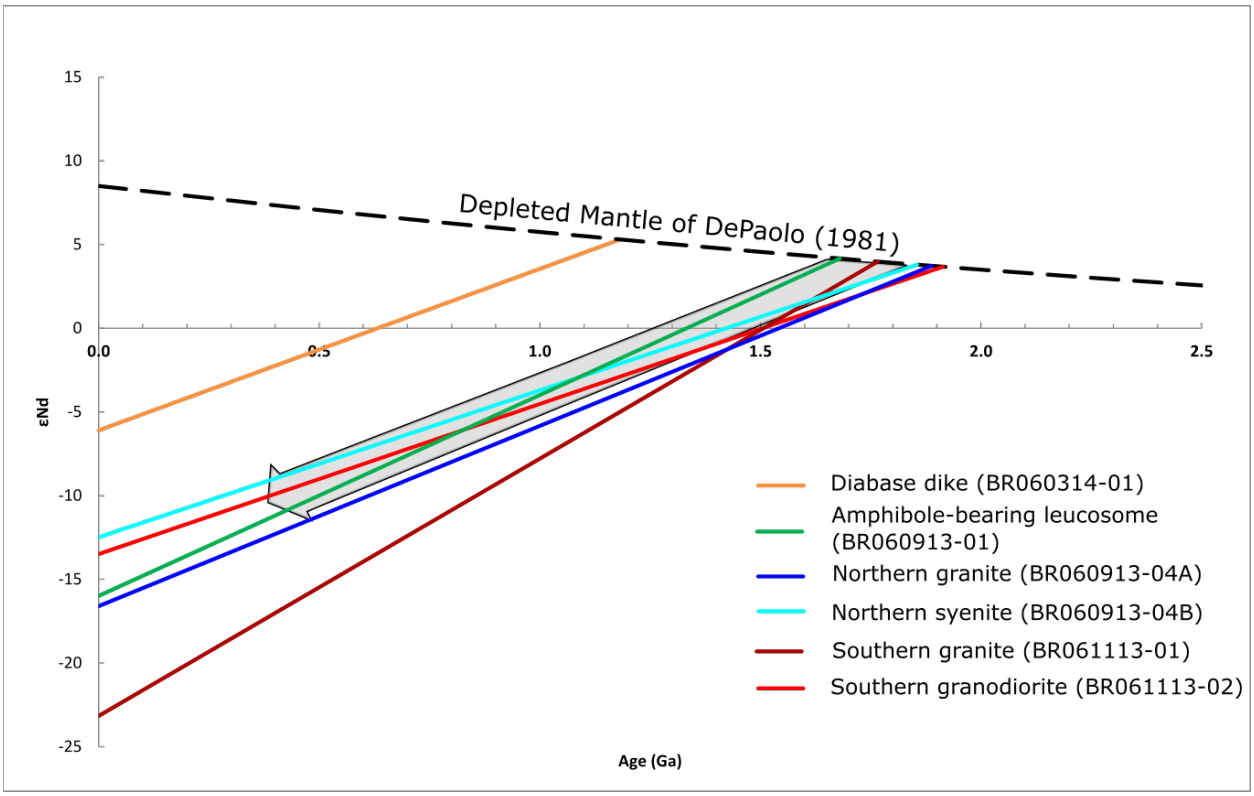

Figure 40. Neodymium isotope evolution diagram for selected igneous samples from the Blue Ridge area. The grey arrow represents the neodymium isotopic evolution path for typical 1800 Ma Colorado crust (DePaolo, 1981).

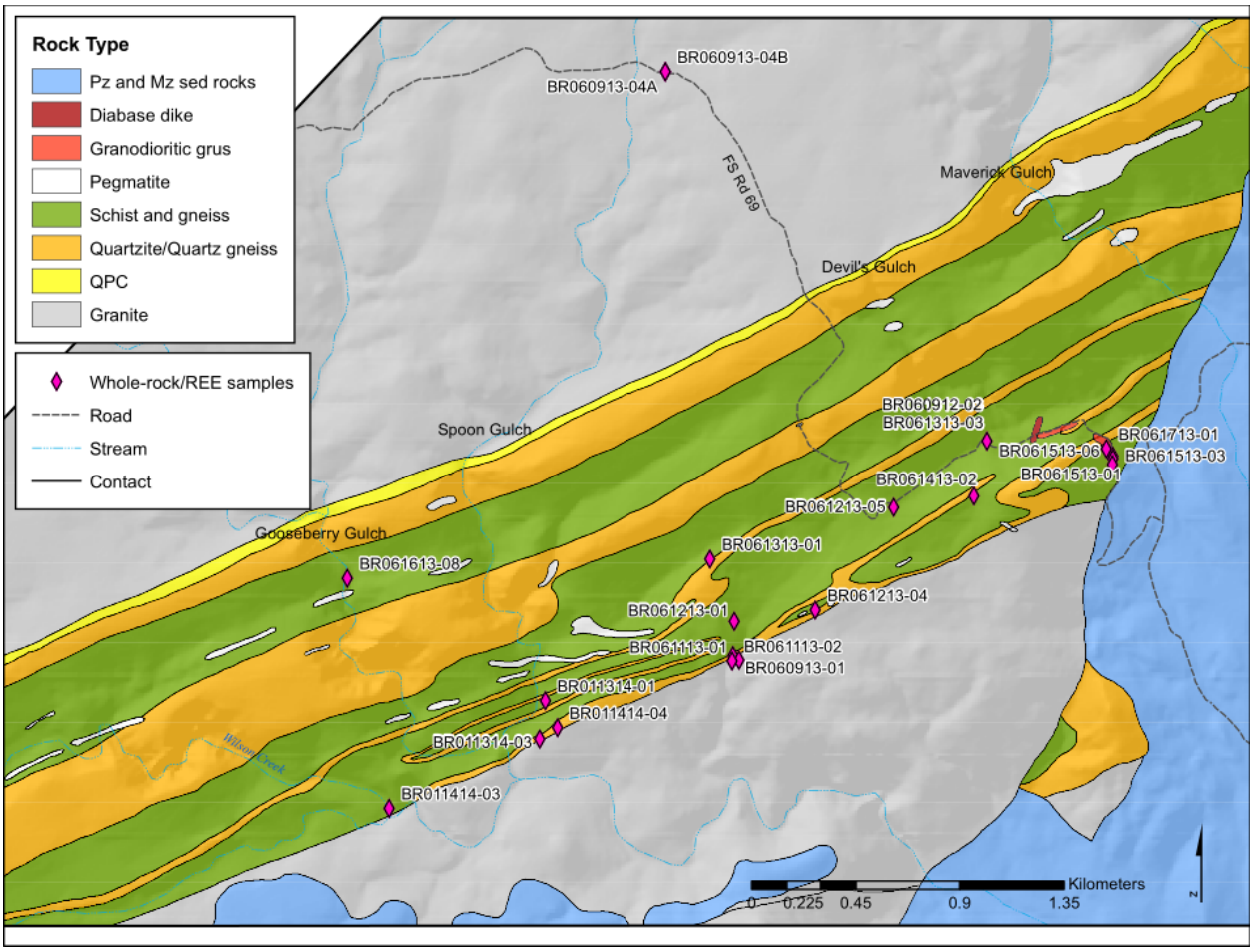

Figure 41. Geological map of the Blue Ridge area showing location and distribution of samples collected for whole-rock and REE analysis with sample numbers (BR060912-02 staur-grt-mica-qtz schist; BR060913-01 amphibole-bearing leucosome; BR060913-04A granite; BR060913-04B syenite; BR061113-01 granite; BR061113-02 granodiorite; BR061213-01 sill-grt-mica-qtz schist; BR061213-04 mica-qtz schist; BR061213-05 sill-grt-mica-qtz schist; BR061313-01 mica-qtz schist; BR061313-03 grt-mica-qtz schist; BR061413-02 grt-mica-qtz schist; BR061513-01 grt-mica-qtz schist; BR061513-03 grt-cord-mica-qtz schist; BR061513-06 cord-mica-qtz schist; BR061613-08 cord-mica-qtz schist; BR061713-01 grt-mica-qtz schist; BR011314-01 mica-qtz-schist; BR011314-03 grt-mica-qtz schist; BR011414-03 mica-qtz schist; BR011414-04 grt-mica qtz schist) (grt = garnet; staur = staurolite; cord = cordierite; qtz = quartz). Map modified after Knepper (1972) (Pz = Paleozoic; Mz = Mesozoic; QPC = Quartz Pebble Conglomerate). Map data sources: Coloradoview.org.

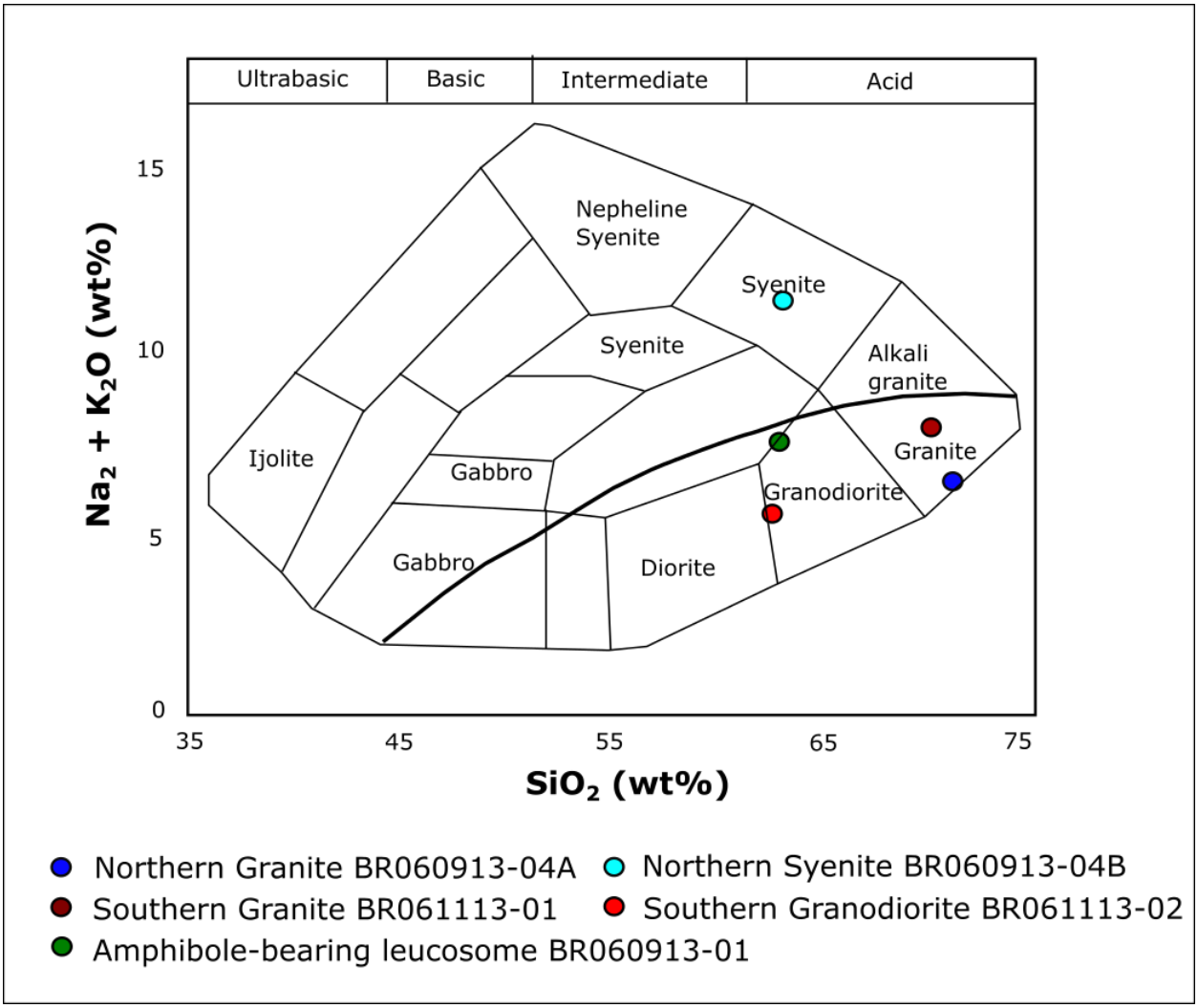

Figure 42. Total alkali versus silica (TAS) diagram for select plutonic rocks in the Blue Ridge area. The blue plots are samples from the northern granitoids and red from the southern granitoids. The green plot is the amphibole-bearing leucosome. Plot after Wilson (1989). Plots based on data in Appendix E,Table E-1. Refer to Figure 41 for sample locations.

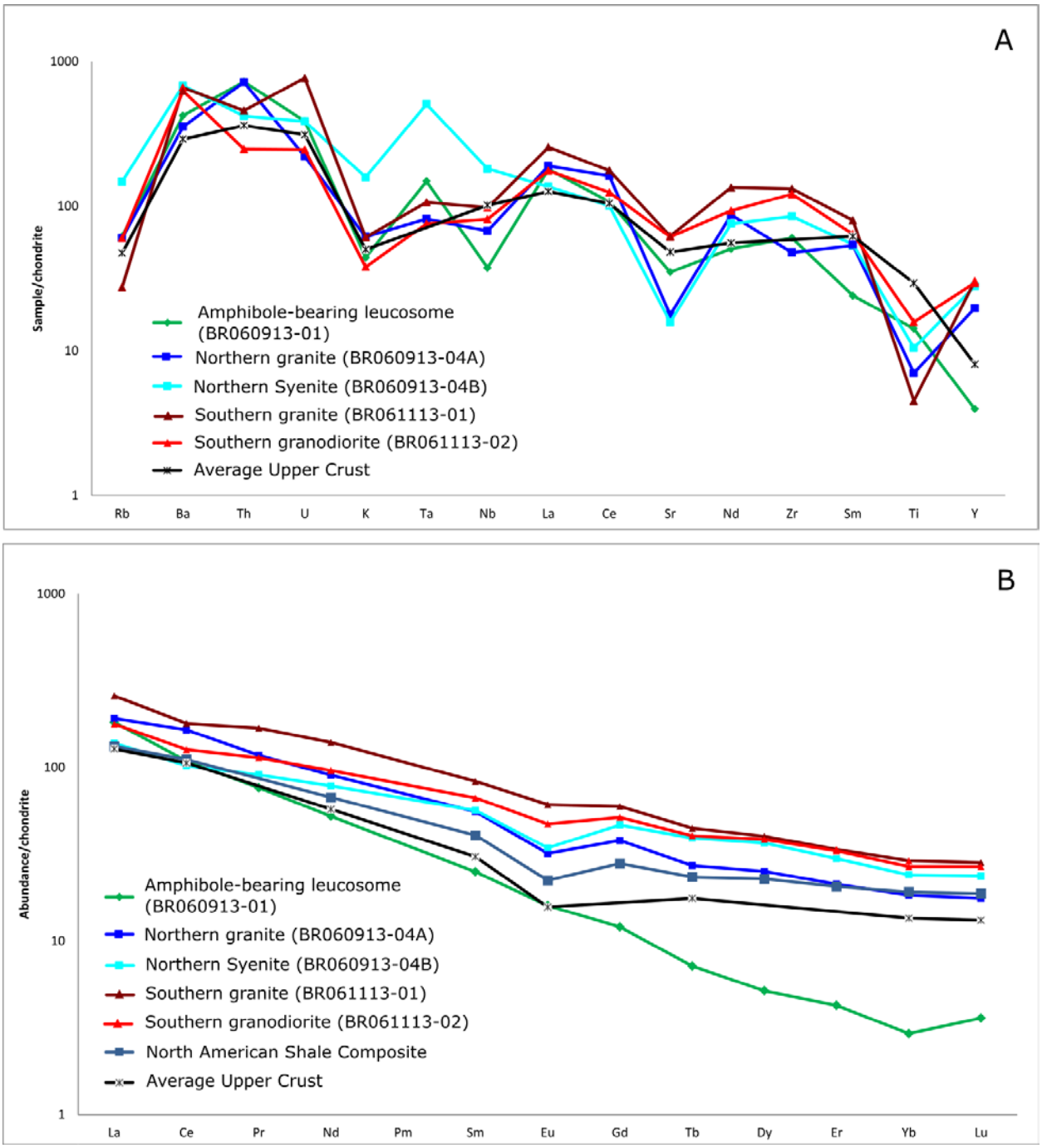

Figure 43. Multi-element (A) and REE (B) concentration diagrams of selected Blue Ridge igneous rocks based on data located in Appendix E, Table E-2 and E-3 (see Figure 41 for location). Average Upper Crust values of Taylor and McLennan (1981) and North American Shale Composite (NASC) values of Gromet et al. (1984) have been plotted for comparison. All samples and standards were normalized to the chondrite values of Sun and McDonough (1989).

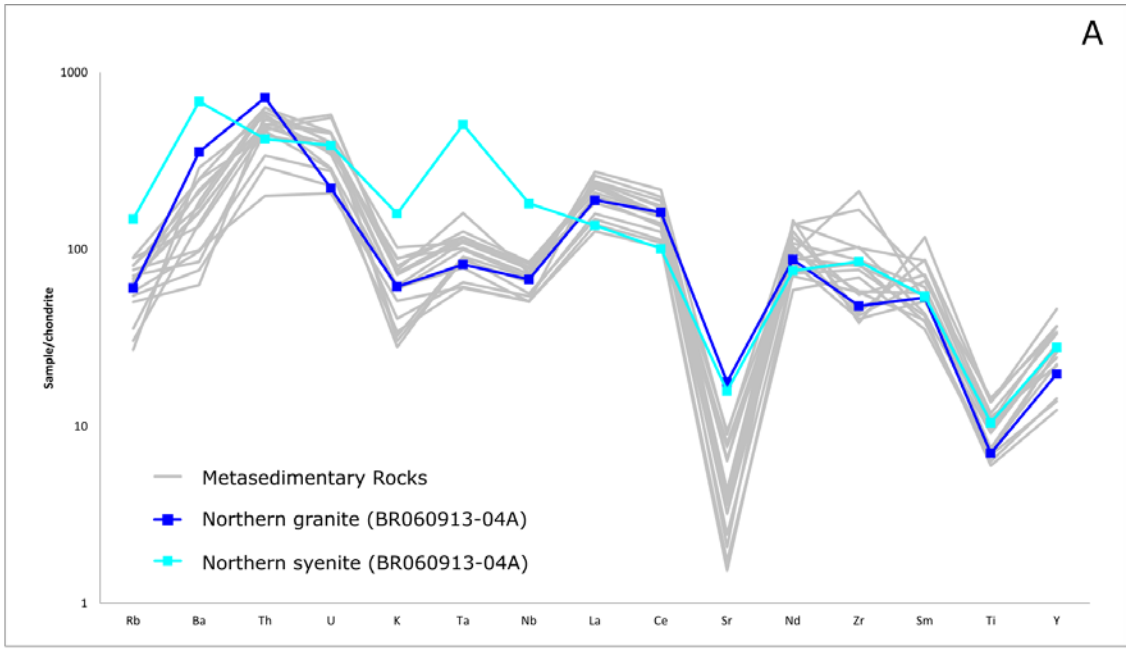
A
1000
100
10
1
Sample/chondrite
Metasedimentary Rocks
Northern granite (BR060913-04A)
Northern syenite (BR060913-04A)
Rb
Ba
Th
U
K
Ta
Nb
La
Ce
Sr
Nd
Zr
Sm
Ti
Y

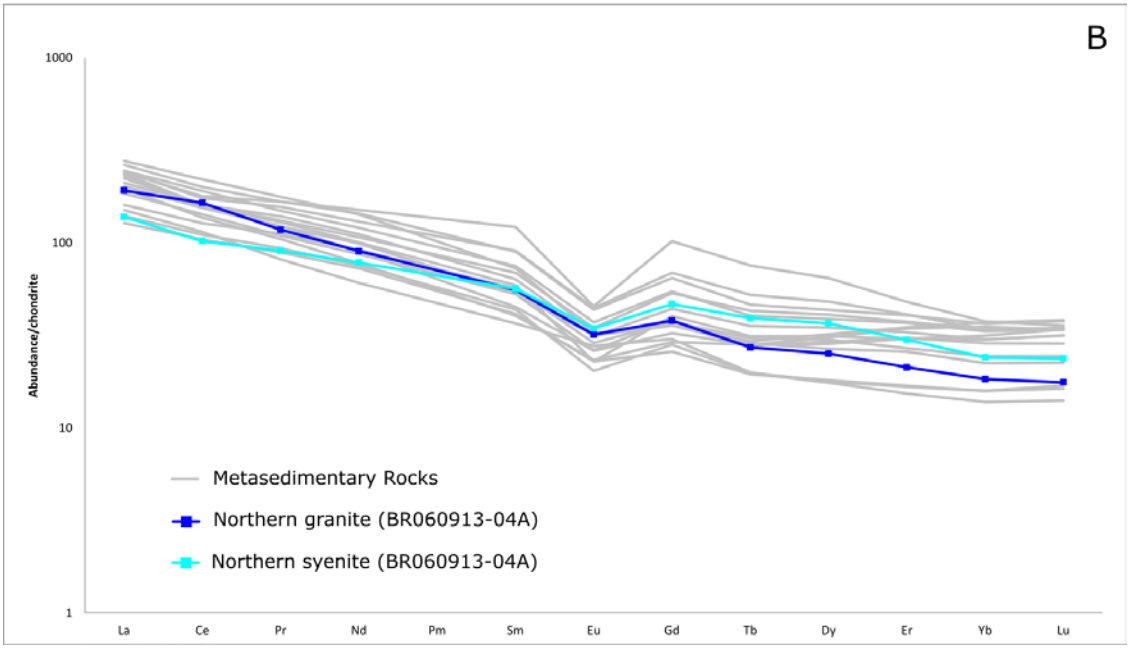
B
1000
100
10
1
Abundance/chondrite
Metasedimentary Rocks
Northern granite (BR060913-04A)
Northern syenite (BR060913-04A)
La
Ce
Pr
Nd
Pm
Sm
Eu
Gd
Tb
Dy
Er
Yb
Lu

Figure 44. Multi-element (A) and REE (B) concentration diagrams of select Blue Ridge igneous and metasedimentary rocks based on data located in Appendix E, Table E-2 and E-3 (see Figure 41 for location). The chemical signatures of the northern granitoids are being compared to that of the metasedimentary rocks for source-sink relationships. All samples were normalized to chondrite values of Sun and McDonough (1989). Metasedimentary rocks include the following: BR060912-02 staur-grt-mica-qtz schist; BR061213-01 sill-grt-mica-qtz schist; BR061213-04 mica-qtz schist; BR061213-05 sill-grt-mica-qtz schist; BR061313-01 mica-qtz schist; BR061313-03 grt-mica-qtz schist; BR061413-02 grt-mica-qtz schist; BR061513-01 grt-mica-qtz schist; BR061513-03 grt-cord-mica-qtz schist; BR061513-06 cord-mica-qtz schist; BR061613-08 cord-mica-qtz schist; BR061713-01 grt-mica-qtz schist; BR011314-01 mica-qtz-schist; BR011314-03 grt-mica-qtz schist; BR011414-03 mica-qtz schist; BR011414-04 grt-mica qtz schist (grt = garnet; staur = staurolite; cord = cordierite; qtz = quartz).

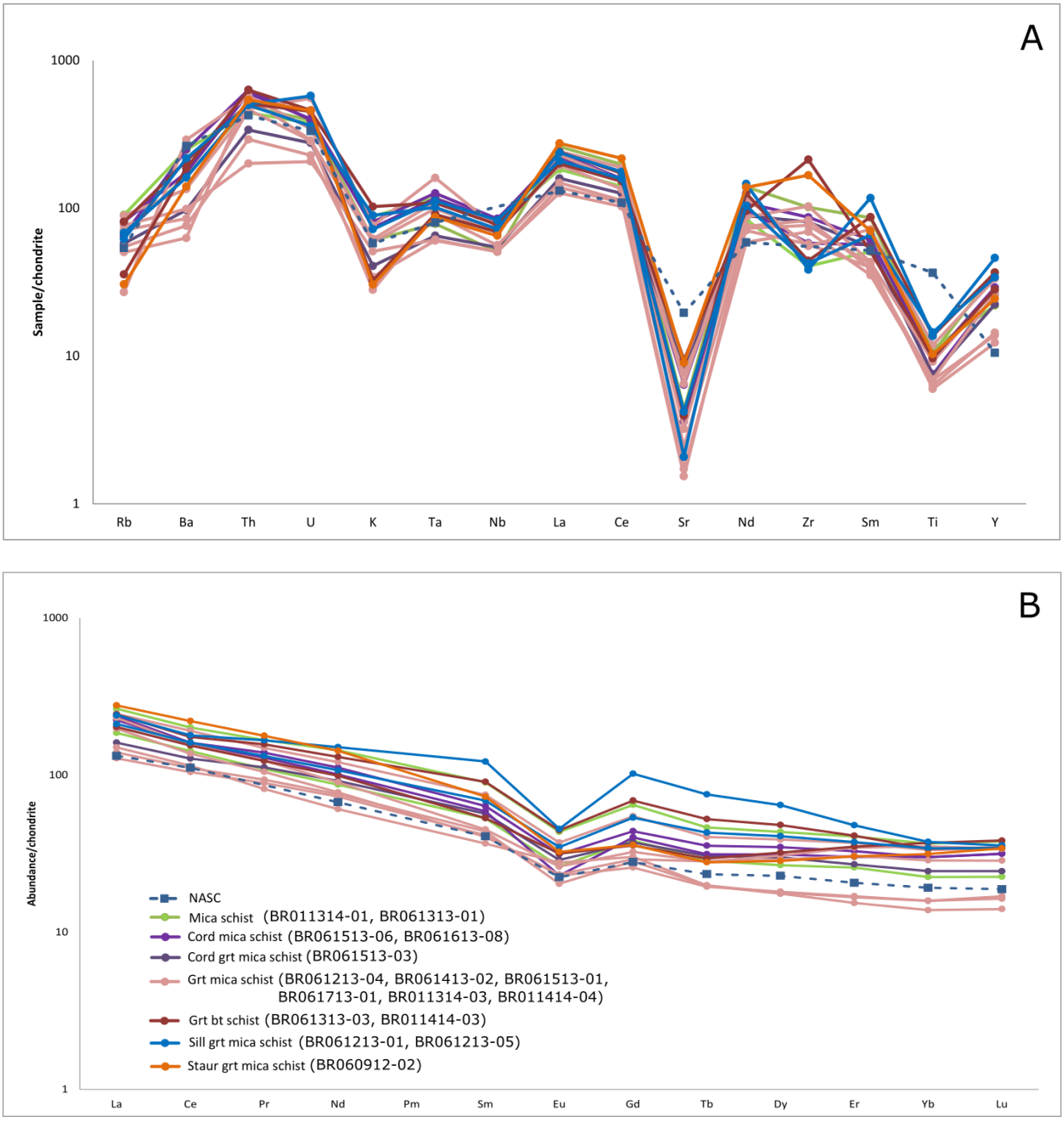

Figure 45. Multi-element (A) and REE (B) concentration diagrams of selected Blue Ridge metasedimentary rocks compared to the North American Shale Composite (NASC) of Gromet et al. (1984) (see Figure 41 for location). Diagrams are based on data located in Appendix E, Table E-2 and E-3. All samples and standards are normalized to the chondrite values of Sun and McDonough (1989). Legend applicable for both diagrams.

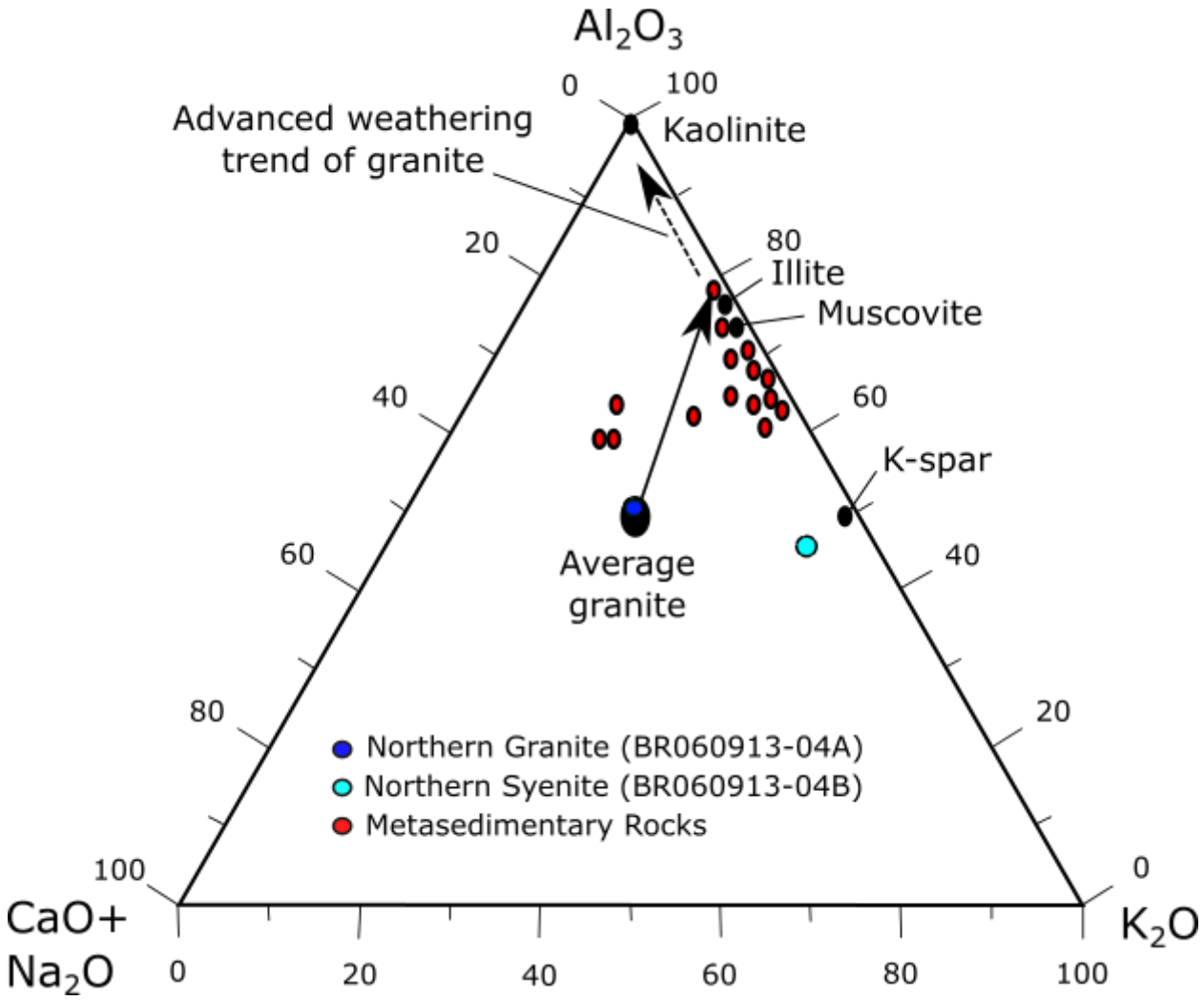

Figure 46. (Na_2O + CaO) – Al_2O_3 – K_2O ternary diagram of Nesbitt and Young (1984, 1989) showing the compositions of the northern granite and syenite and selected metasedimentary rocks from data located in Appendix E, Table E-4. The large black dot represents the initial composition of typical granite before weathering. The black arrows show the idealized weathering path for typical granite. Deviations from this path indicate diagenetic reactions/effects.

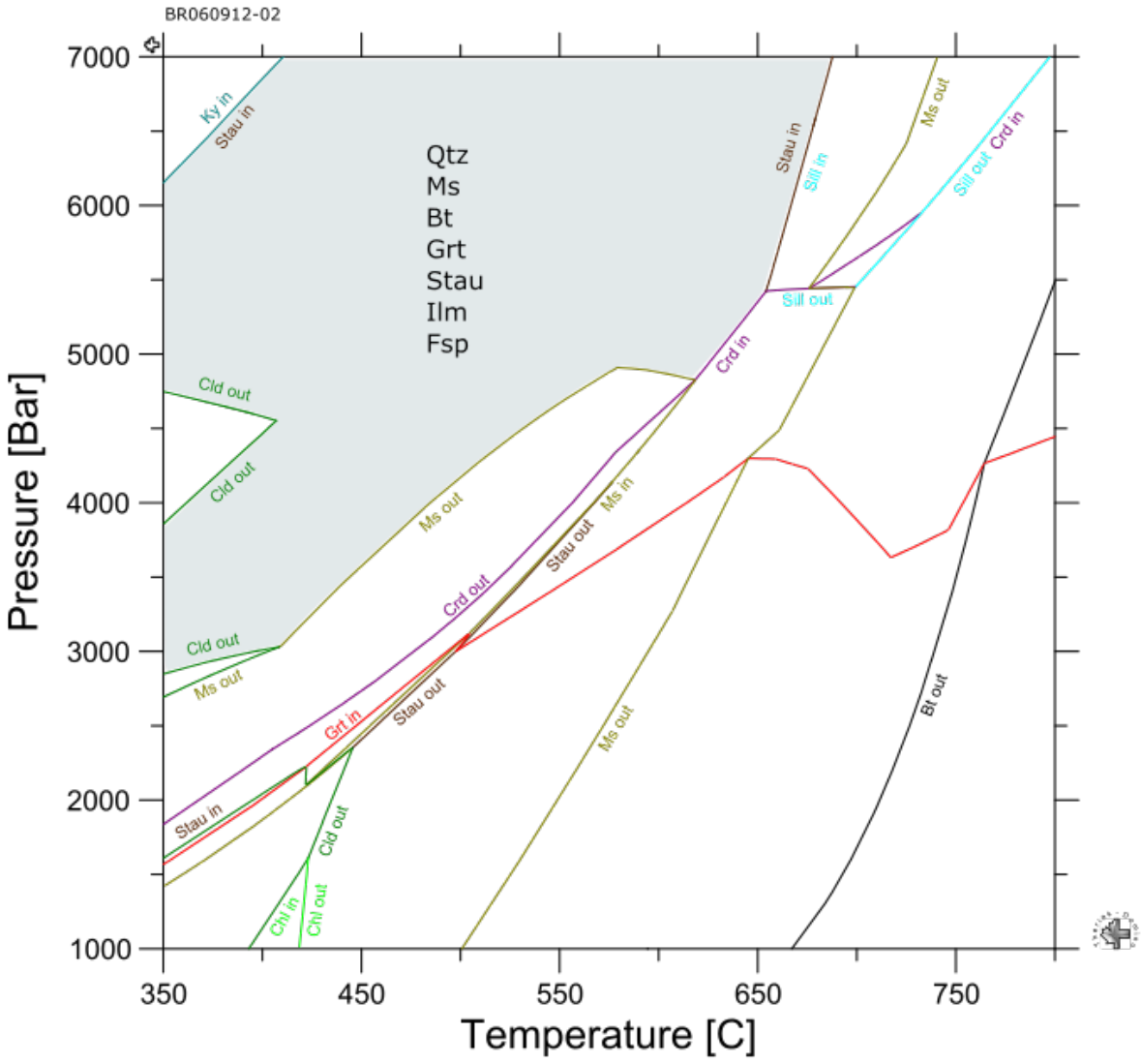

Figure 47-1. Equilibrium assemblage diagram calculated using Theriak-Domino (Capitani and Petrakakis, 2010) for a staur-grt-mica-qtz schist (BR060912-02) (see Figure 41 for location). Calculations based on data in Appendix E, Table E-5. Colored lines define the stability field of a given mineral. The stable mineral assemblage for this sample includes quartz, muscovite, biotite, garnet, staurolite, ilmenite, and feldspar. (And = Andalusite; Bt = biotite; Chl = chlorite; Cld = chloritoid; Crd = cordierite; Fsp = feldspar; Grt = garnet; Ilm = ilmenite; Ky = kyanite; Ms = muscovite; Omph = omphacite; Opx = orthopyroxene; Sill = sillimanite; Sph = sphene; Stau = staurolite).

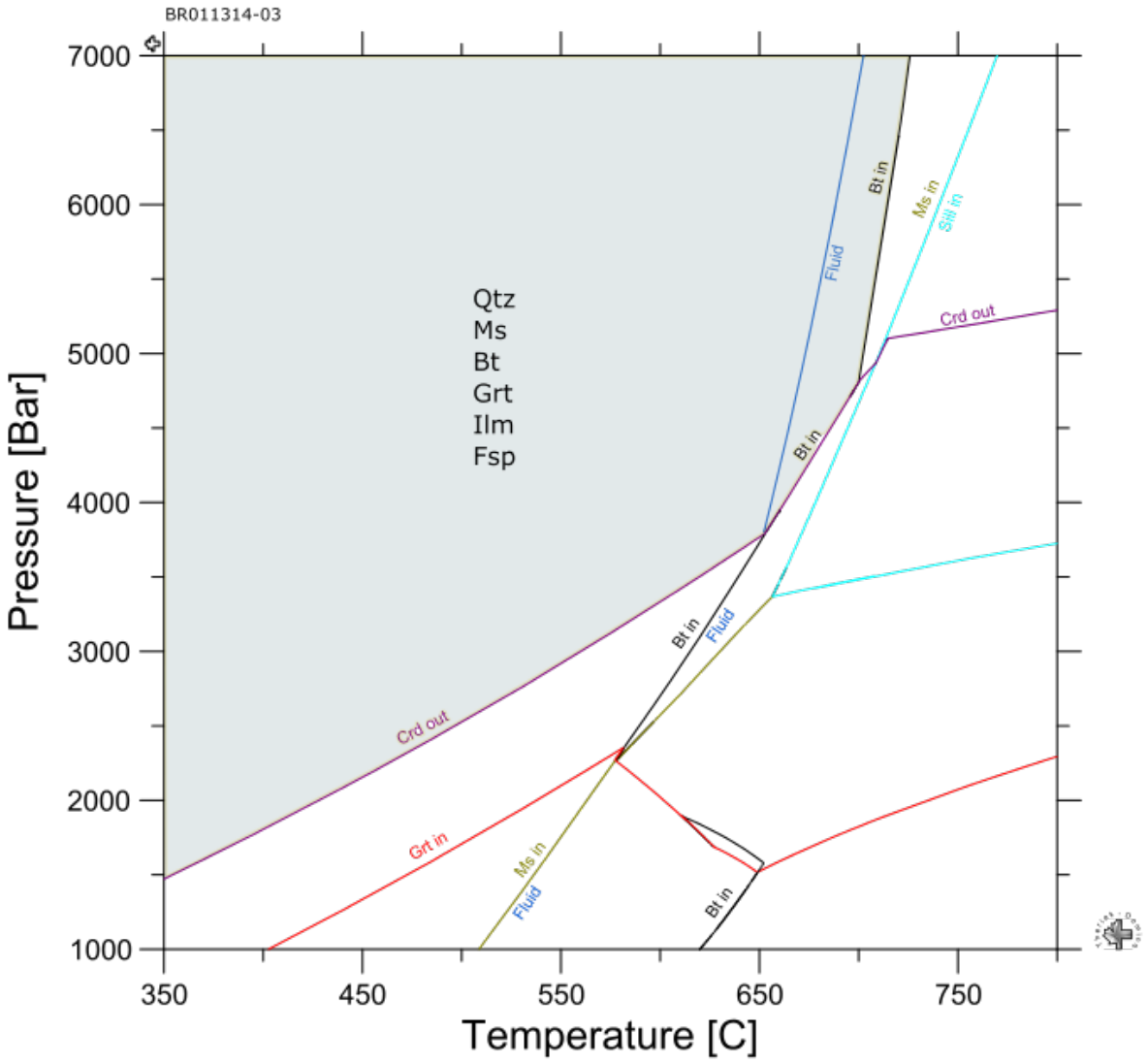

Figure 47-2. Equilibrium assemblage diagram calculated using Theriak-Domino (Capitani and Petrakakis, 2010) for a grt-mica-qtz schist (BR011314-03) (see Figure 41 for location). Calculations based on data in Appendix E, Table E-5. Colored lines define the stability field of a given mineral. The stable mineral assemblage for this sample includes quartz, muscovite, biotite, garnet, ilmenite, and feldspar. (And = Andalusite; Bt = biotite; Chl = chlorite; Cld = chloritoid; Crd = cordierite; Fsp = feldspar; Grt = garnet; Ilm = ilmenite; Ky = kyanite; Ms = muscovite; Omph = omphacite; Opx = orthopyroxene; Sill = sillimanite; Sph = sphene; Stau = staurolite)

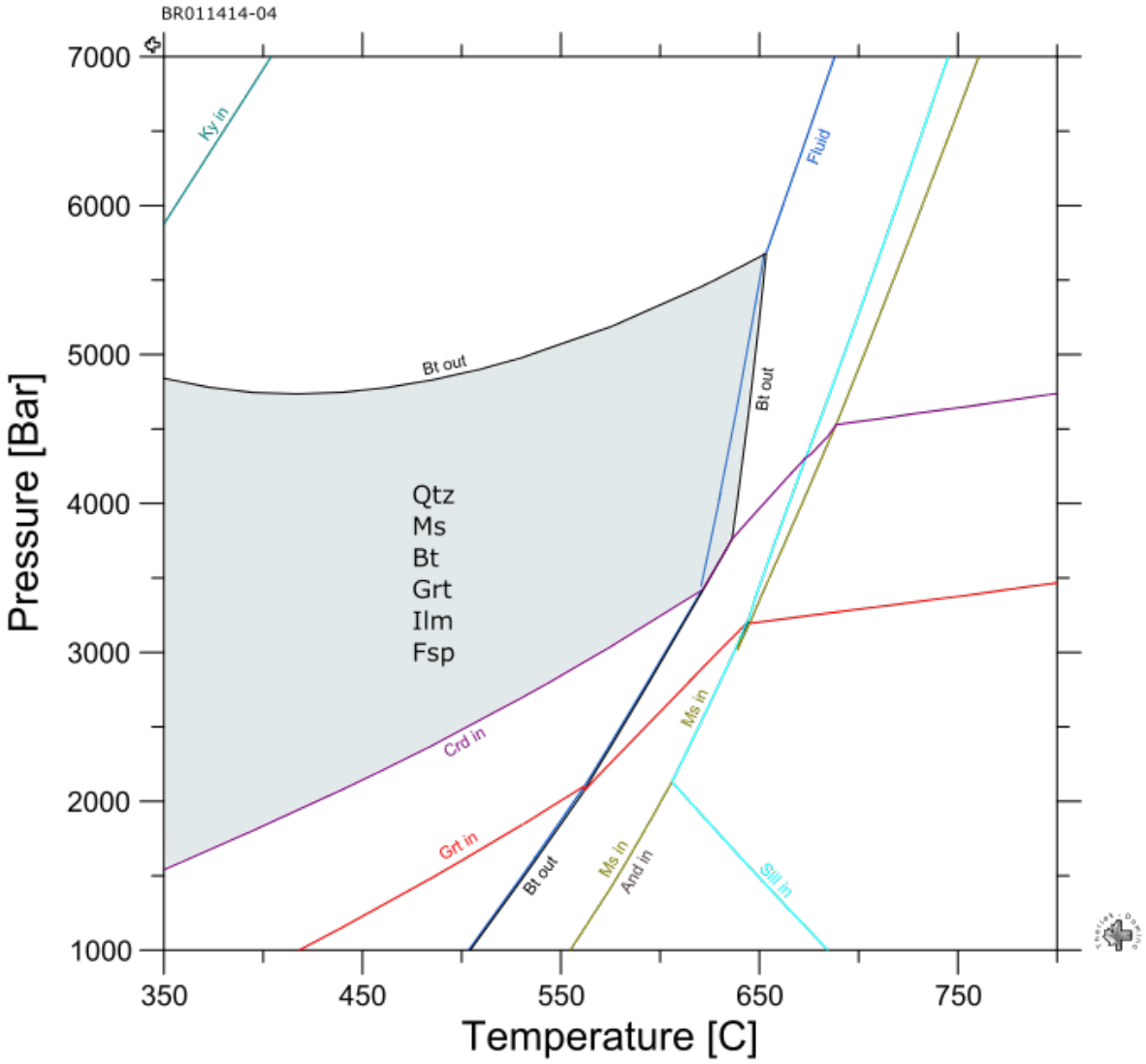

Figure 47-3. Equilibrium assemblage diagram calculated using Theriak-Domino (Capitani and Petrakakis, 2010) for a grt-mica-qtz schist (BR011414-04) (see Figure 41 for location). Calculations based on data in Appendix E, Table E-5. Colored lines define the stability field of a given mineral. The stable mineral assemblage for this sample includes quartz, muscovite, biotite, garnet, ilmenite, and feldspar. (And = Andalusite; Bt = biotite; Chl = chlorite; Cld = chloritoid; Crd = cordierite; Fsp = feldspar; Grt = garnet; Ilm = ilmenite; Ky = kyanite; Ms = muscovite; Omph = omphacite; Opx = orthopyroxene; Sill = sillimanite; Sph = sphene; Stau = staurolite)

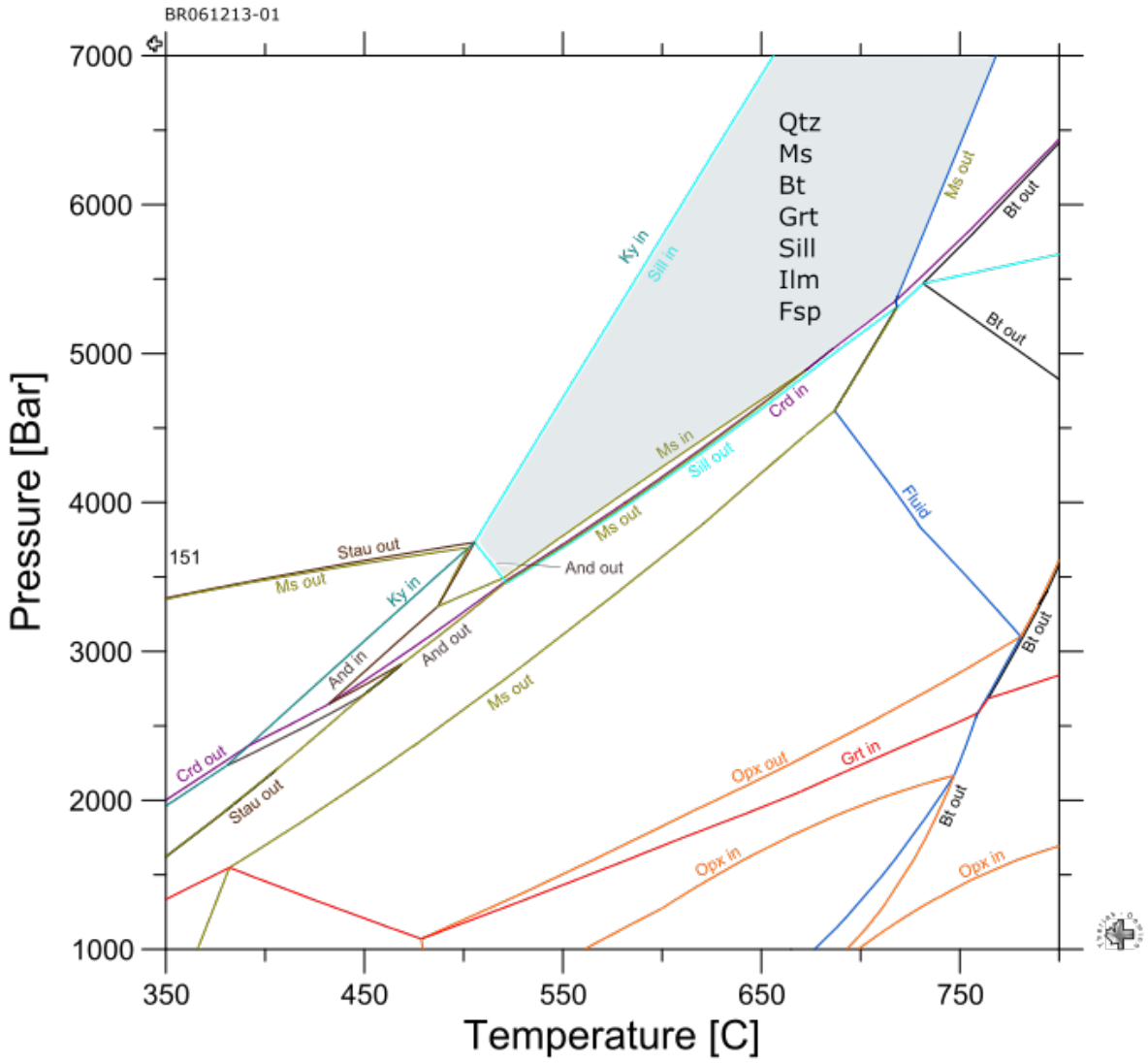

Figure 47-4. Equilibrium assemblage diagram calculated using Theriak-Domino (Capitani and Petrakakis, 2010) for a sill-grt-mica-qtz schist (BR061213-01) (see Figure 41 for location). Calculations based on data in Appendix E, Table E-5. Colored lines define the stability field of a given mineral. The stable mineral assemblage for this sample includes quartz, muscovite, biotite, garnet, sillimanite, ilmenite, and feldspar. (And = Andalusite; Bt = biotite; Chl = chlorite; Cld = chloritoid; Crd = cordierite; Fsp = feldspar; Grt = garnet; Ilm = ilmenite; Ky = kyanite; Ms = muscovite; Omph = omphacite; Opx = orthopyroxene; Sill = sillimanite; Sph = sphene; Stau = staurolite)

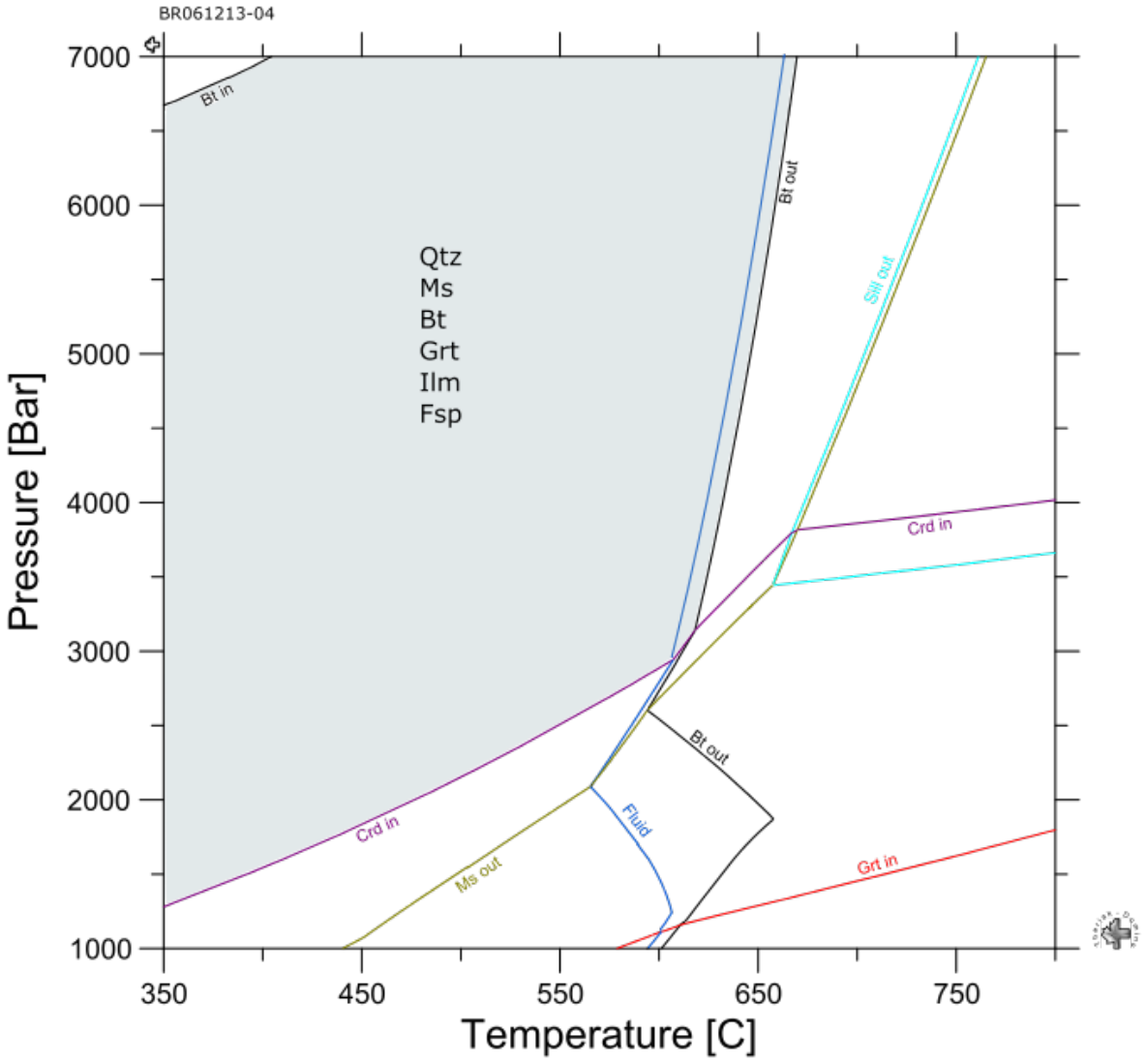

Figure 47-5. Equilibrium assemblage diagram calculated using Theriak-Domino (Capitani and Petrakakis, 2010) for a grt-mica-qtz schist (BR061213-04) (see Figure 41 for location). Calculations based on data in Appendix E, Table E-5. Colored lines define the stability field of a given mineral. The stable mineral assemblage for this sample includes quartz, muscovite, biotite, garnet, ilmenite, and feldspar. (And = Andalusite; Bt = biotite; Chl = chlorite; Cld = chloritoid; Crd = cordierite; Fsp = feldspar; Grt = garnet; Ilm = ilmenite; Ky = kyanite; Ms = muscovite; Omph = omphacite; Opx = orthopyroxene; Sill = sillimanite; Sph = sphene; Stau = staurolite)

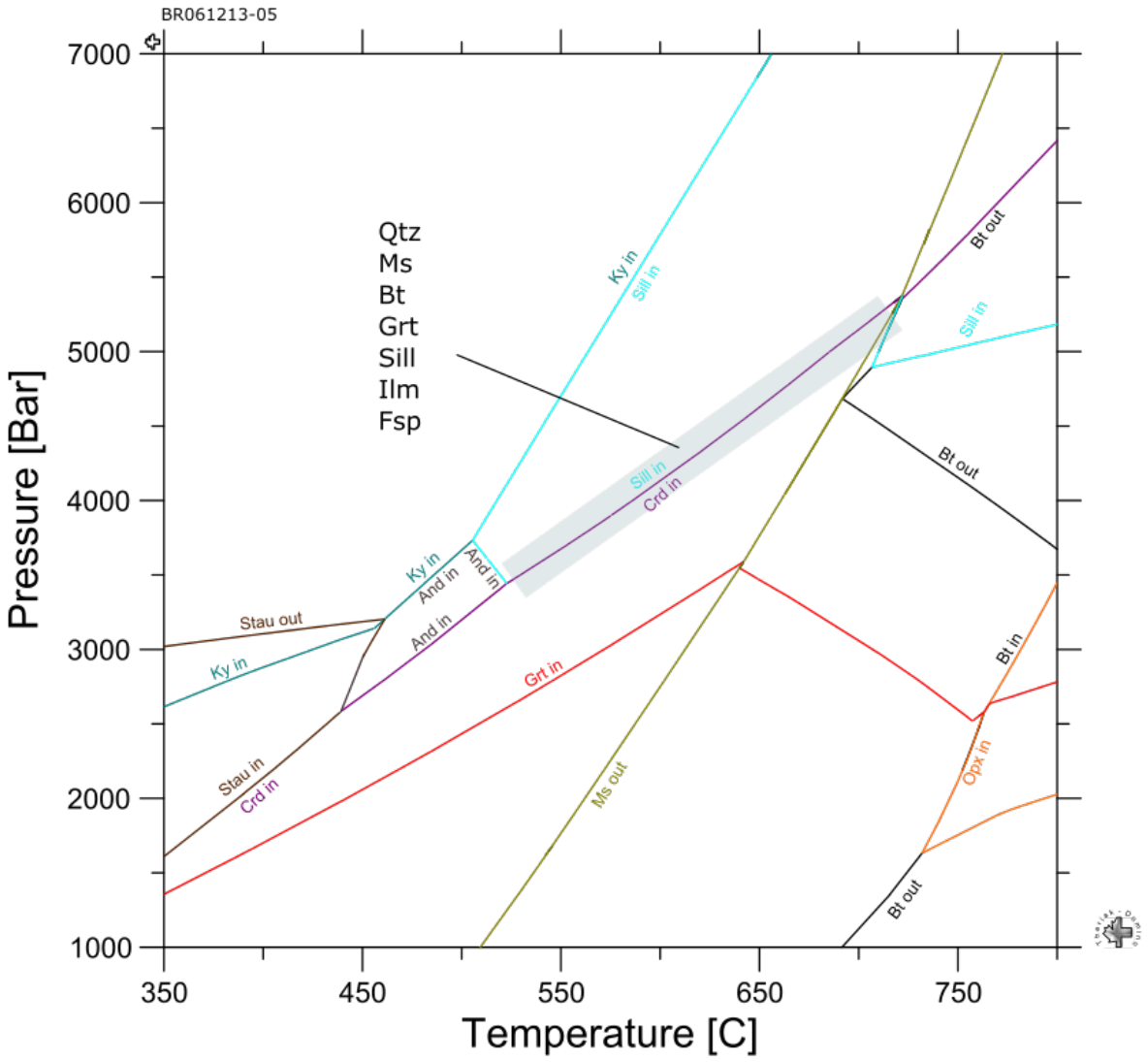

Figure 47-6. Equilibrium assemblage diagram calculated using Theriak-Domino (Capitani and Petrakakis, 2010) for a sill-grt-mica-qtz schist (BR061213-05) (see Figure 41 for location). Calculations based on data in Appendix E, Table E-5. Colored lines define the stability field of a given mineral. The stable mineral assemblage for this sample includes quartz, muscovite, biotite, garnet, sillimanite, ilmenite, and feldspar. (And = Andalusite; Bt = biotite; Chl = chlorite; Cld = chloritoid; Crd = cordierite; Fsp = feldspar; Grt = garnet; Ilm = ilmenite; Ky = kyanite; Ms = muscovite; Omph = omphacite; Opx = orthopyroxene; Sill = sillimanite; Sph = sphene; Stau = staurolite)

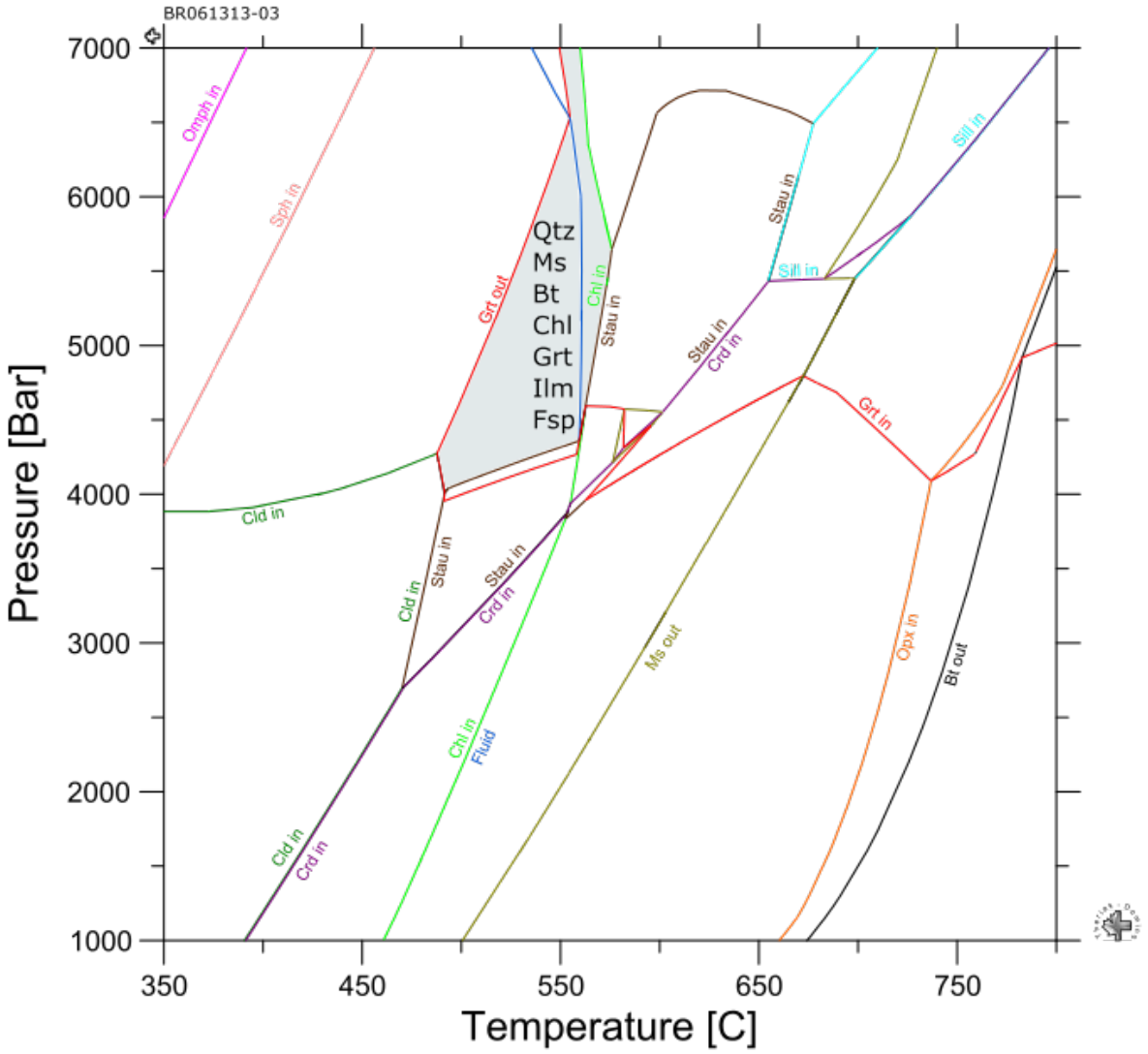

Figure 47-7. Equilibrium assemblage diagram calculated using Theriak-Domino (Capitani and Petrakakis, 2010) for a grt-mica-qtz schist (BR061313-03) (see Figure 41 for location). Calculations based on data in Appendix E, Table E-5. Colored lines define the stability field of a given mineral. The stable mineral assemblage for this sample includes quartz, muscovite, biotite, chlorite, garnet, ilmenite, and feldspar. (And = Andalusite; Bt = biotite; Chl = chlorite; Cld = chloritoid; Crd = cordierite; Fsp = feldspar; Grt = garnet; Ilm = ilmenite; Ky = kyanite; Ms = muscovite; Omph = omphacite; Opx = orthopyroxene; Sill = sillimanite; Sph = sphene; Stau = staurolite)

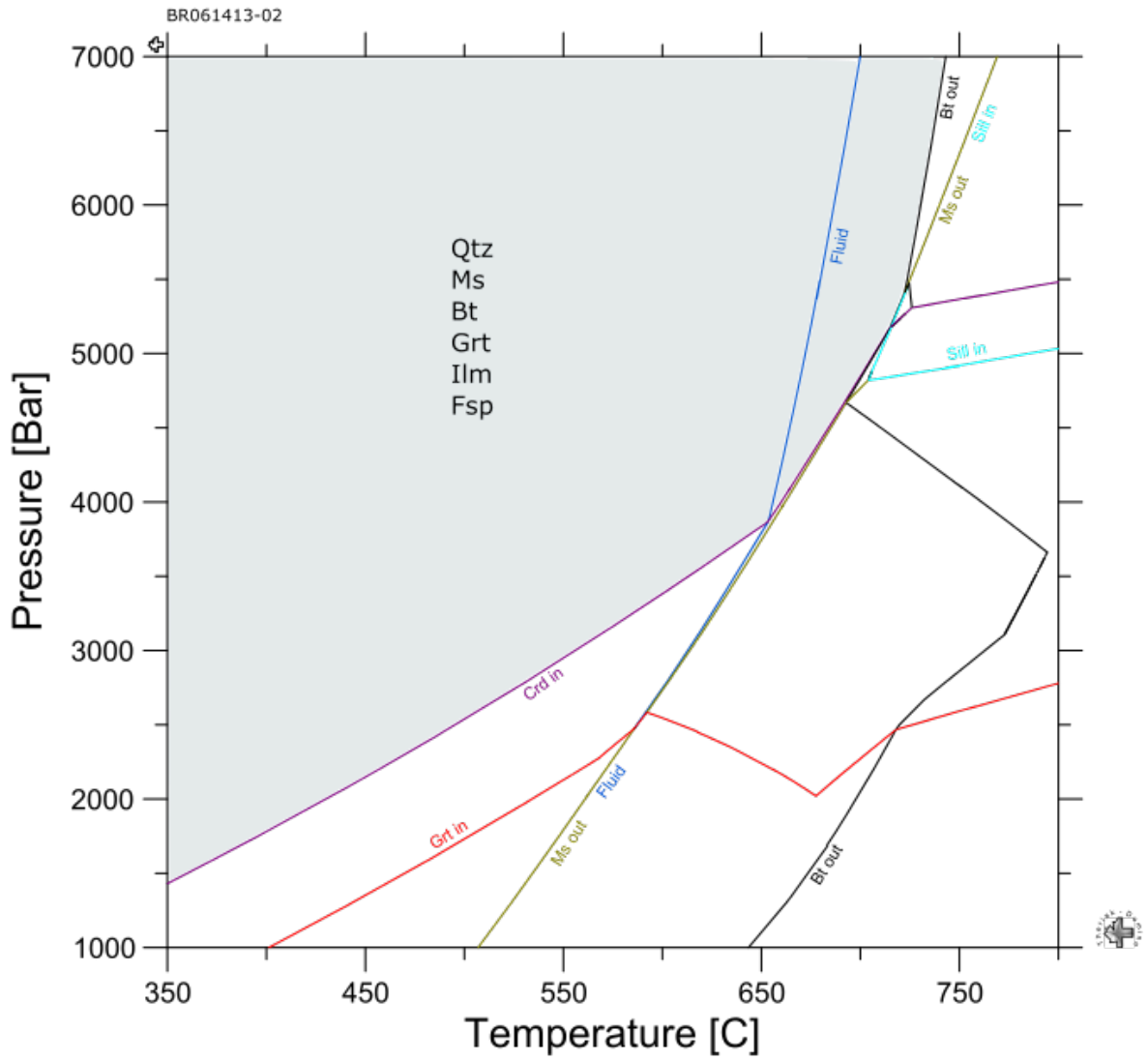

Figure 47-8. Equilibrium assemblage diagram calculated using Theriak-Domino (Capitani and Petrakakis, 2010) for a grt-mica-qtz schist (BR061413-02) (see Figure 41 for location). Calculations based on data in Appendix E, Table E-5. Colored lines define the stability field of a given mineral. The stable mineral assemblage for this sample includes quartz, muscovite, biotite, garnet, ilmenite, and feldspar. (And = Andalusite; Bt = biotite; Chl = chlorite; Cld = chloritoid; Crd = cordierite; Fsp = feldspar; Grt = garnet; Ilm = ilmenite; Ky = kyanite; Ms = muscovite; Omph = omphacite; Opx = orthopyroxene; Sill = sillimanite; Sph = sphene; Stau = staurolite)

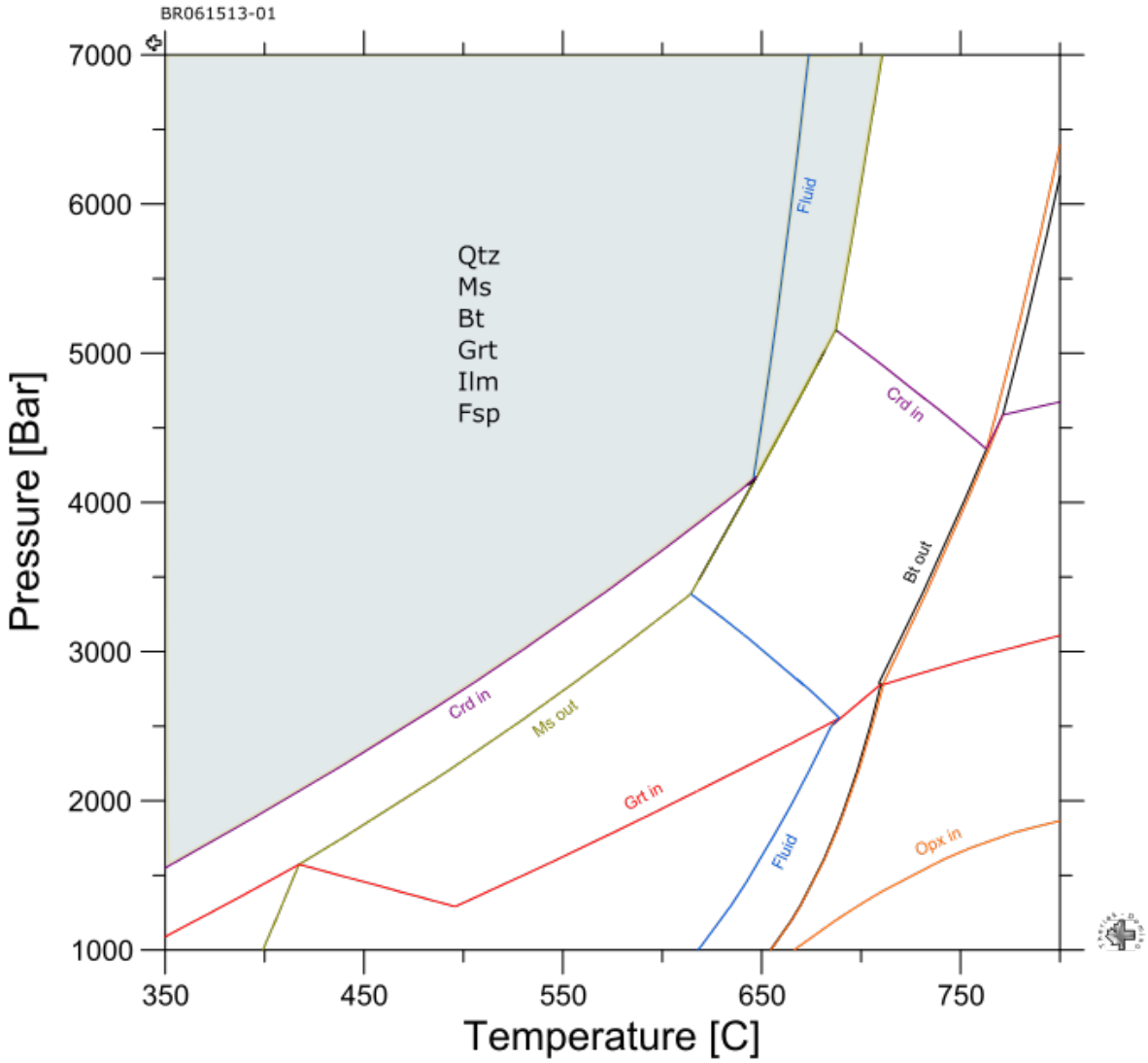

Figure 47-9. Equilibrium assemblage diagram calculated using Theriak-Domino (Capitani and Petrakakis, 2010) for a grt-mica-qtz schist (BR061513-01) (see Figure 41 for location). Calculations data in Appendix E, Table E-5. Colored lines define the stability field of a given mineral. The stable mineral assemblage for this sample includes quartz, muscovite, biotite, garnet, ilmenite, and feldspar. (And = Andalusite; Bt = biotite; Chl = chlorite; Cld = chloritoid; Crd = cordierite; Fsp = feldspar; Grt = garnet; Ilm = ilmenite; Ky = kyanite; Ms = muscovite; Omph = omphacite; Opx = orthopyroxene; Sill = sillimanite; Sph = sphene; Stau = staurolite)

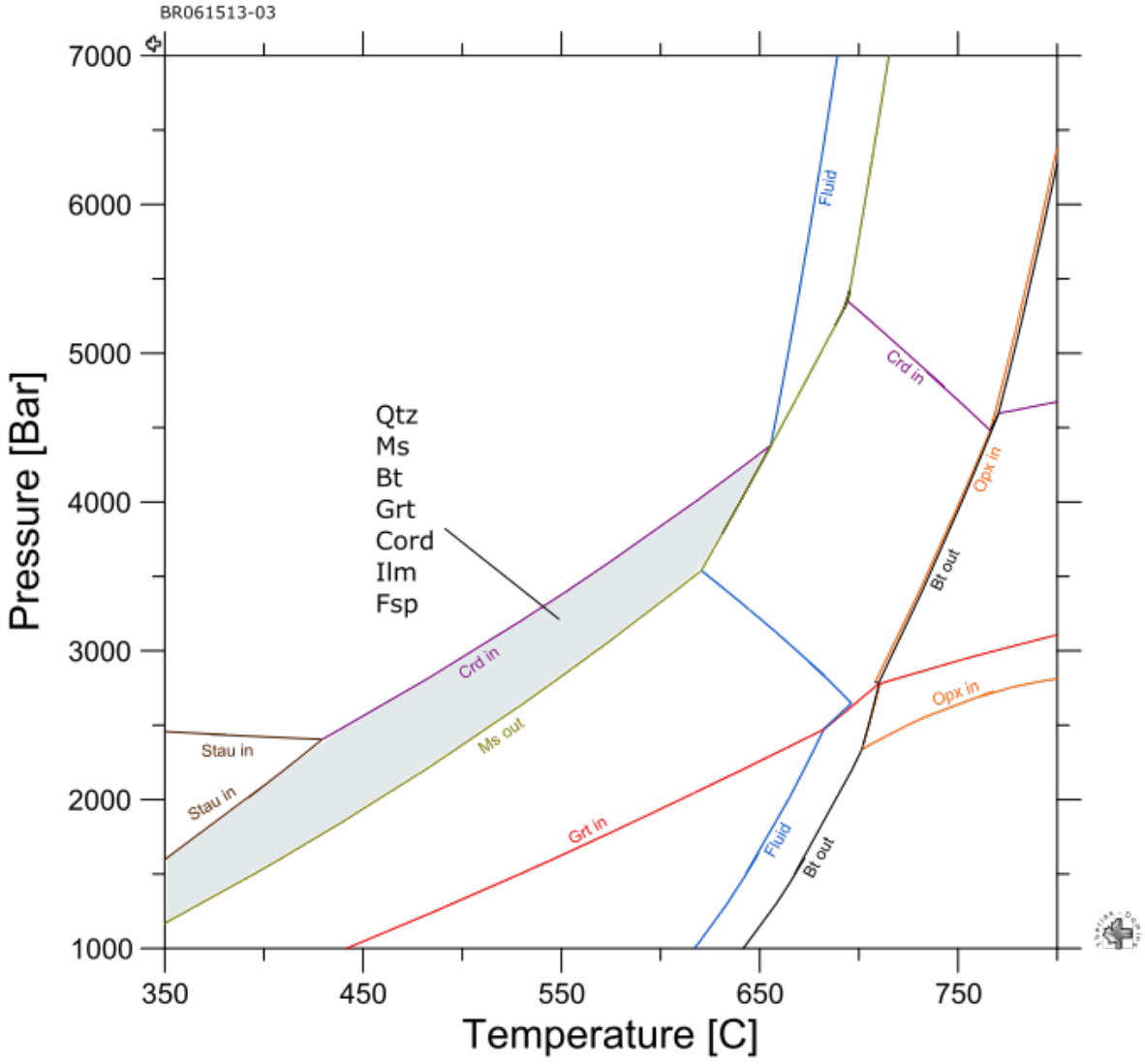

Figure 47-10. Equilibrium assemblage diagram calculated using Theriak-Domino (Capitani and Petrakakis, 2010) for a crd-grt-mica-qtz schist (BR061513-03) (see Figure 41 for location). Calculations based on data in Appendix E, Table E-5. Colored lines define the stability field of a given mineral. The stable mineral assemblage for this sample includes quartz, muscovite, biotite, garnet, cordierite, ilmenite, and feldspar. (And = Andalusite; Bt = biotite; Chl = chlorite; Cld = chloritoid; Crd = cordierite; Fsp = feldspar; Grt = garnet; Ilm = ilmenite; Ky = kyanite; Ms = muscovite; Omph = omphacite; Opx = orthopyroxene; Sill = sillimanite; Sph = sphene; Stau = staurolite)

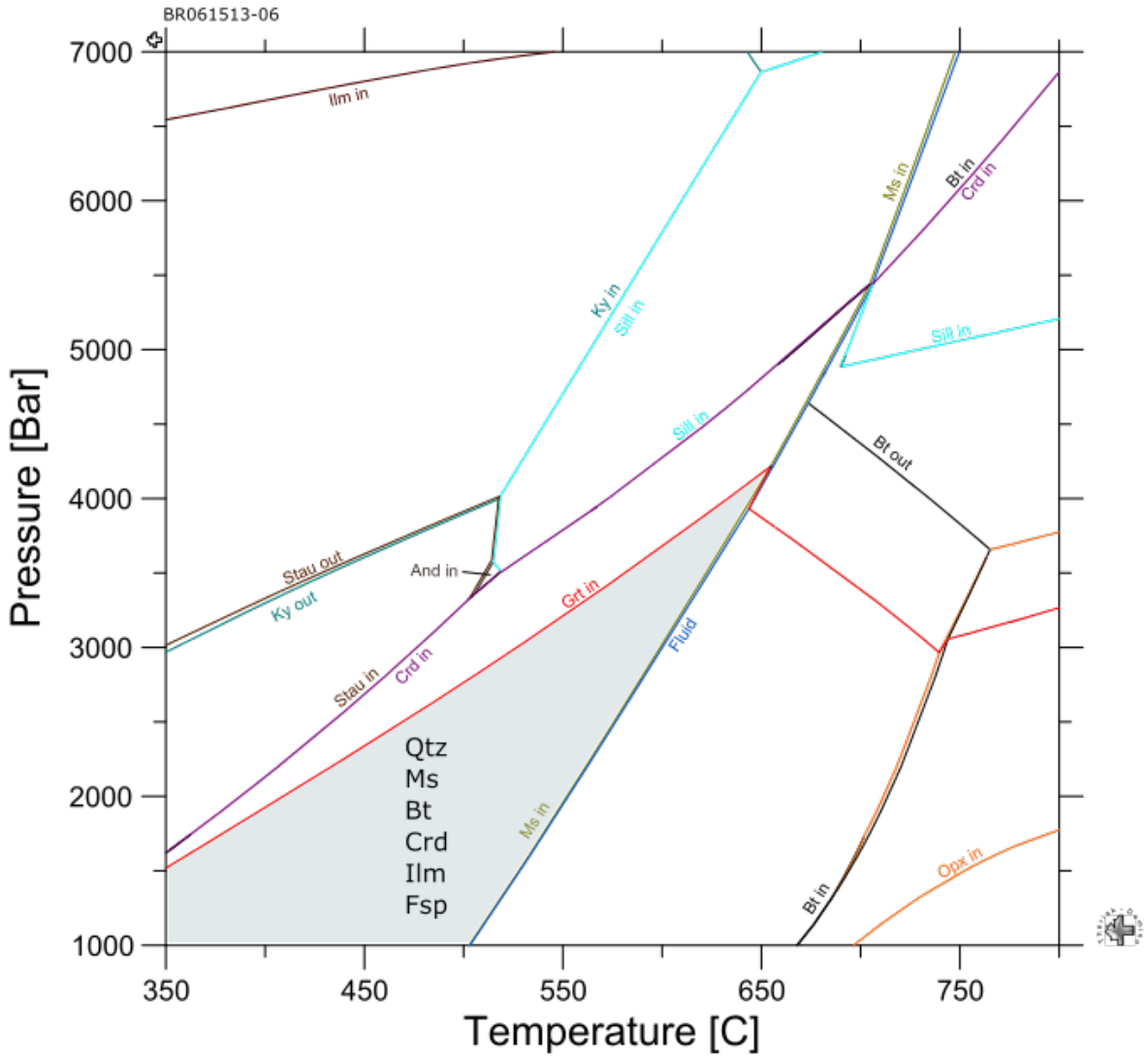

Figure 47-11. Equilibrium assemblage diagram calculated using Theriak-Domino (Capitani and Petrakakis, 2010) for a crd-mica-qtz schist (BR061513-06) (see Figure 41 for location). Calculations based on data in Appendix E, Table E-5. Colored lines define the stability field of a given mineral. The stable mineral assemblage for this sample includes quartz, muscovite, biotite, cordierite, ilmenite, and feldspar. (And = Andalusite; Bt = biotite; Chl = chlorite; Cld = chloritoid; Crd = cordierite; Fsp = feldspar; Grt = garnet; Ilm = ilmenite; Ky = kyanite; Ms = muscovite; Omph = omphacite; Opx = orthopyroxene; Sill = sillimanite; Sph = sphene; Stau = staurolite)

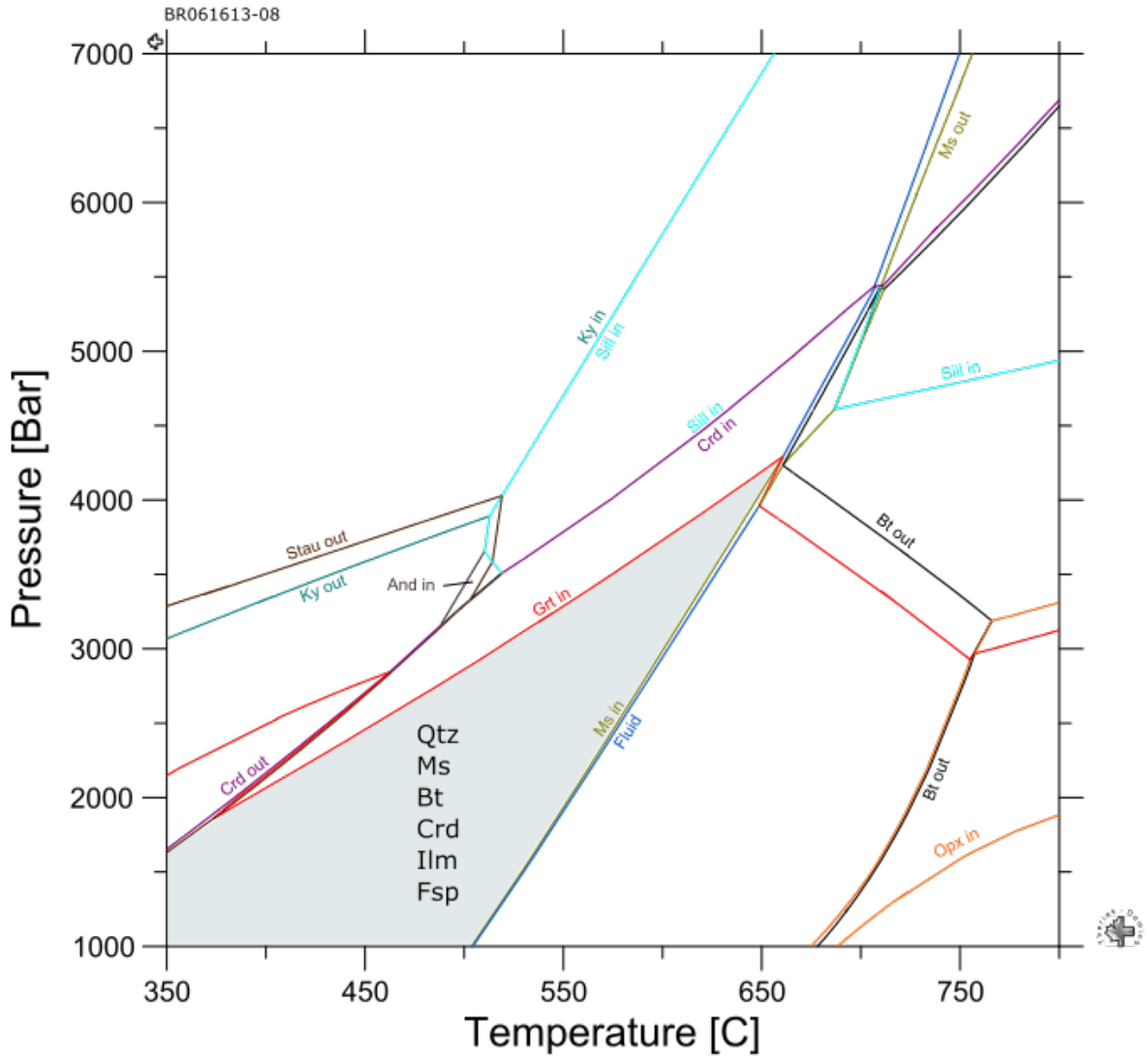

Figure 47-12. Equilibrium assemblage diagram calculated using Theriak-Domino (Capitani and Petrakakis, 2010) for a crd-mica-qtz schist (BR61613-08) (see Figure 41 for location). Calculations based on data in Appendix E, Table E-5. Colored lines define the stability field of a given mineral. The stable mineral assemblage for this sample includes quartz, muscovite, biotite, cordierite, ilmenite, and feldspar. (And = Andalusite; Bt = biotite; Chl = chlorite; Cld = chloritoid; Crd = cordierite; Fsp = feldspar; Grt = garnet; Ilm = ilmenite; Ky = kyanite; Ms = muscovite; Omph = omphacite; Opx = orthopyroxene; Sill = sillimanite; Sph = sphene; Stau = staurolite)

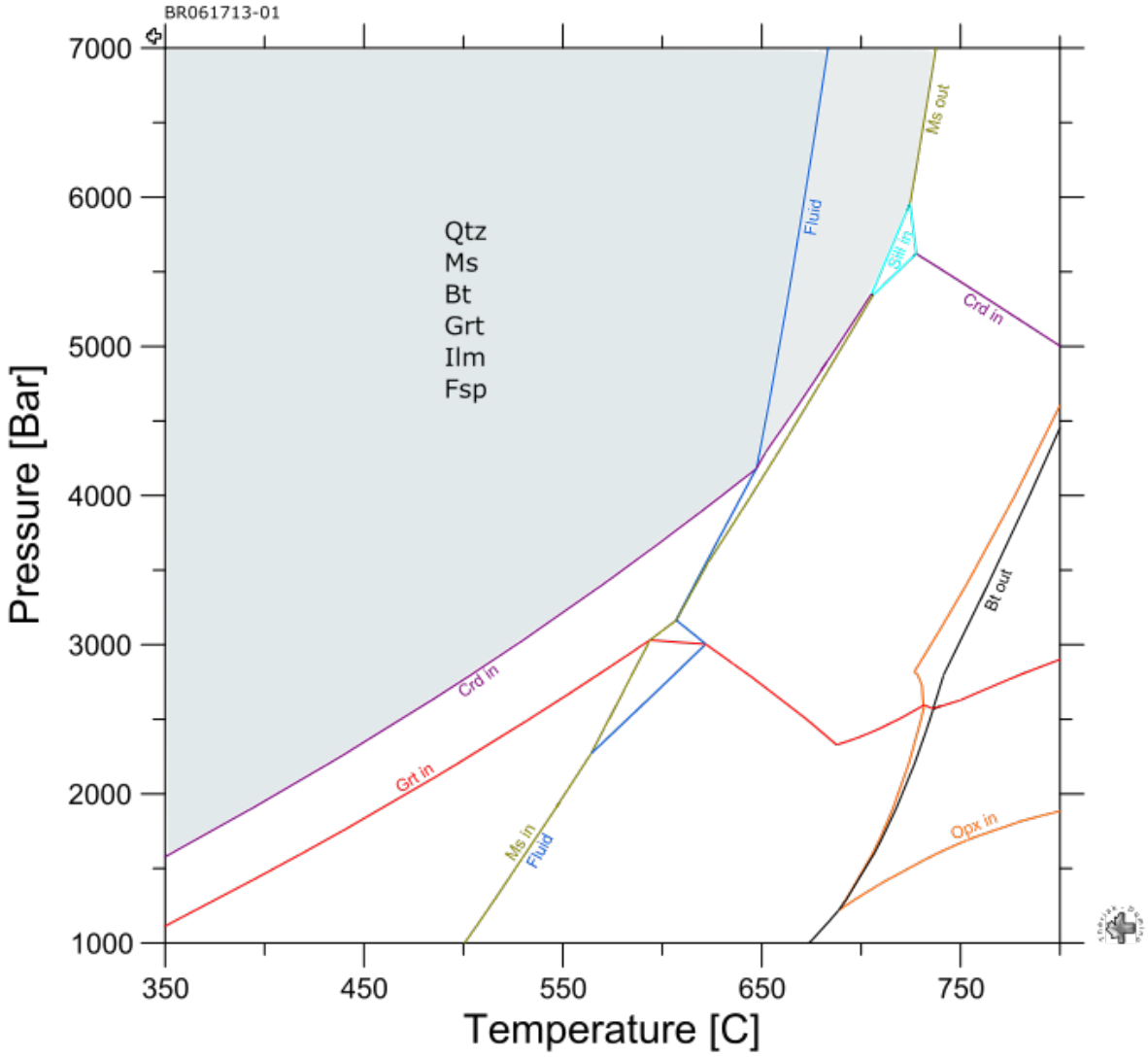

Figure 47-13. Equilibrium assemblage diagram calculated using Theriak-Domino (Capitani and Petrakakis, 2010) for a grt-mica-qtz schist (BR061713-01) (see Figure 41 for location). Calculations based on data in Appendix E, Table E-5. Colored lines define the stability field of a given mineral. The stable mineral assemblage for this sample includes quartz, muscovite, biotite, garnet, ilmenite, and feldspar. (And = Andalusite; Bt = biotite; Chl = chlorite; Cld = chloritoid; Crd = cordierite; Fsp = feldspar; Grt = garnet; Ilm = ilmenite; Ky = kyanite; Ms = muscovite; Omph = omphacite; Opx = orthopyroxene; Sill = sillimanite; Sph = sphene; Stau = staurolite)

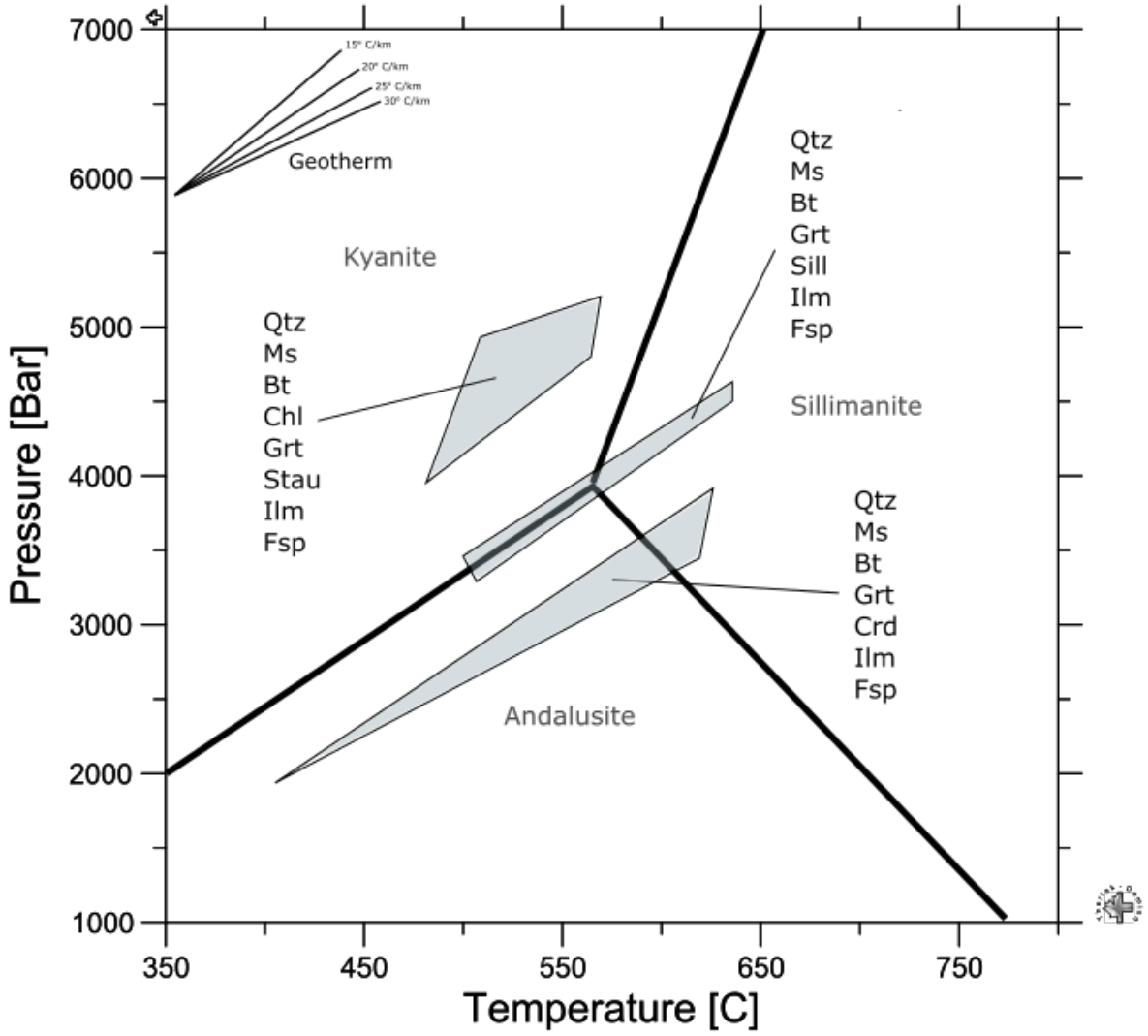

Figure 48. Interpreted areas of overlapping P and T as defined by the intersection of thirteen equilibrium mineral assemblages displayed in Figure 46. Each P-T area is defined by overlapping mineral assemblages. The three P-T areas contain quartz + muscovite + biotite + garnet + ilmenite + feldspar ± staurolite ± sillimanite ± cordierite. The high P, low T area contains staurolite, the high T, low P area contains sillimanite, and the low P-T area contains cordierite. Al_2SiO_5 triple point and geothermal gradient included for reference.

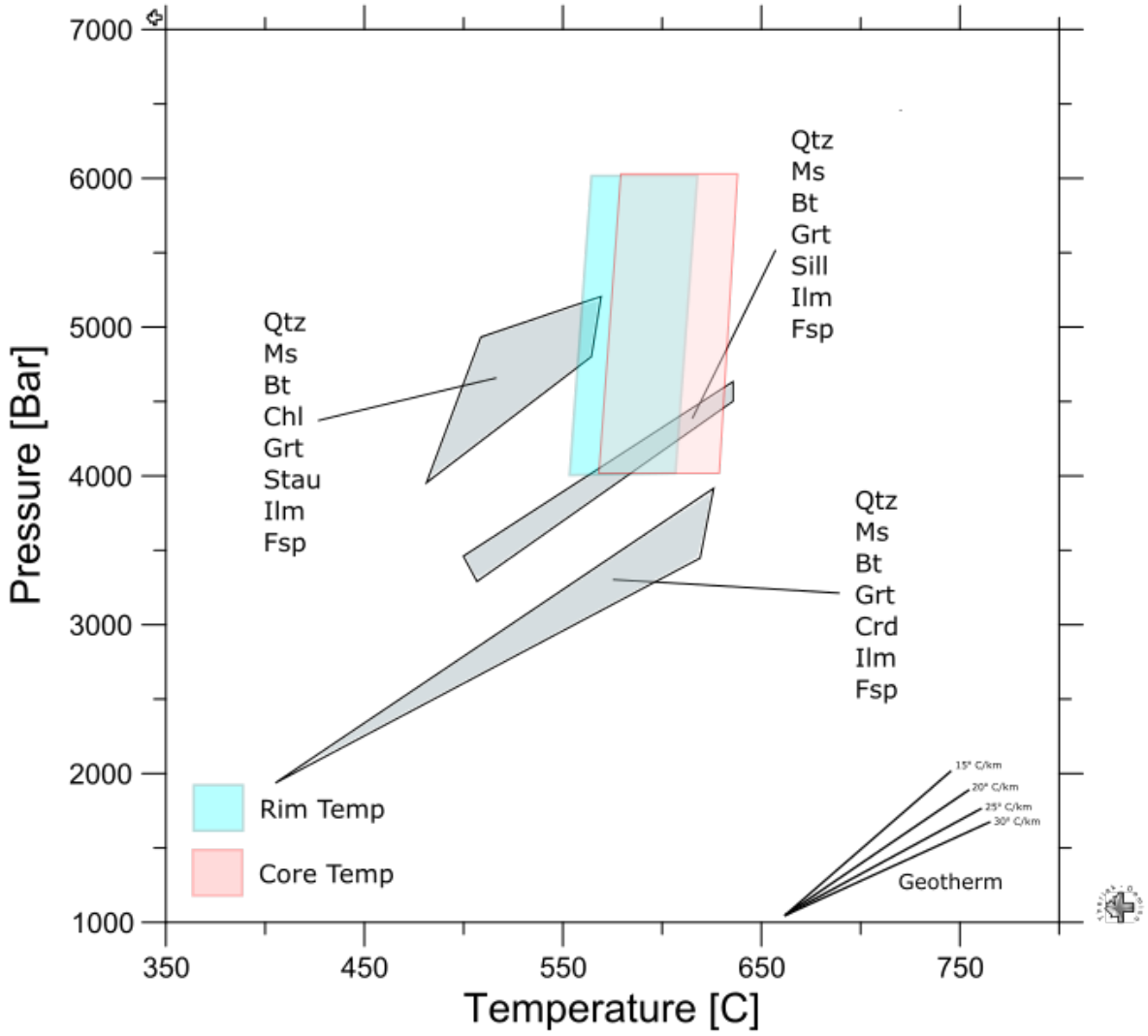

Figure 49. Calculated core and rim temperatures of four garnets from a staurolite-garnet-mica-quartz schist (BR060912-02), based on data located in Appendix F, Table F-3. Temperatures were calculated using the garnet-biotite thermometer of Perchuk and Lavrent'Eva (1983) at 4, 5, and 6 kb. The garnet core and rim temperatures are being compared to the areas of overlapping P & T in order to constrain the initial P of garnet formation.

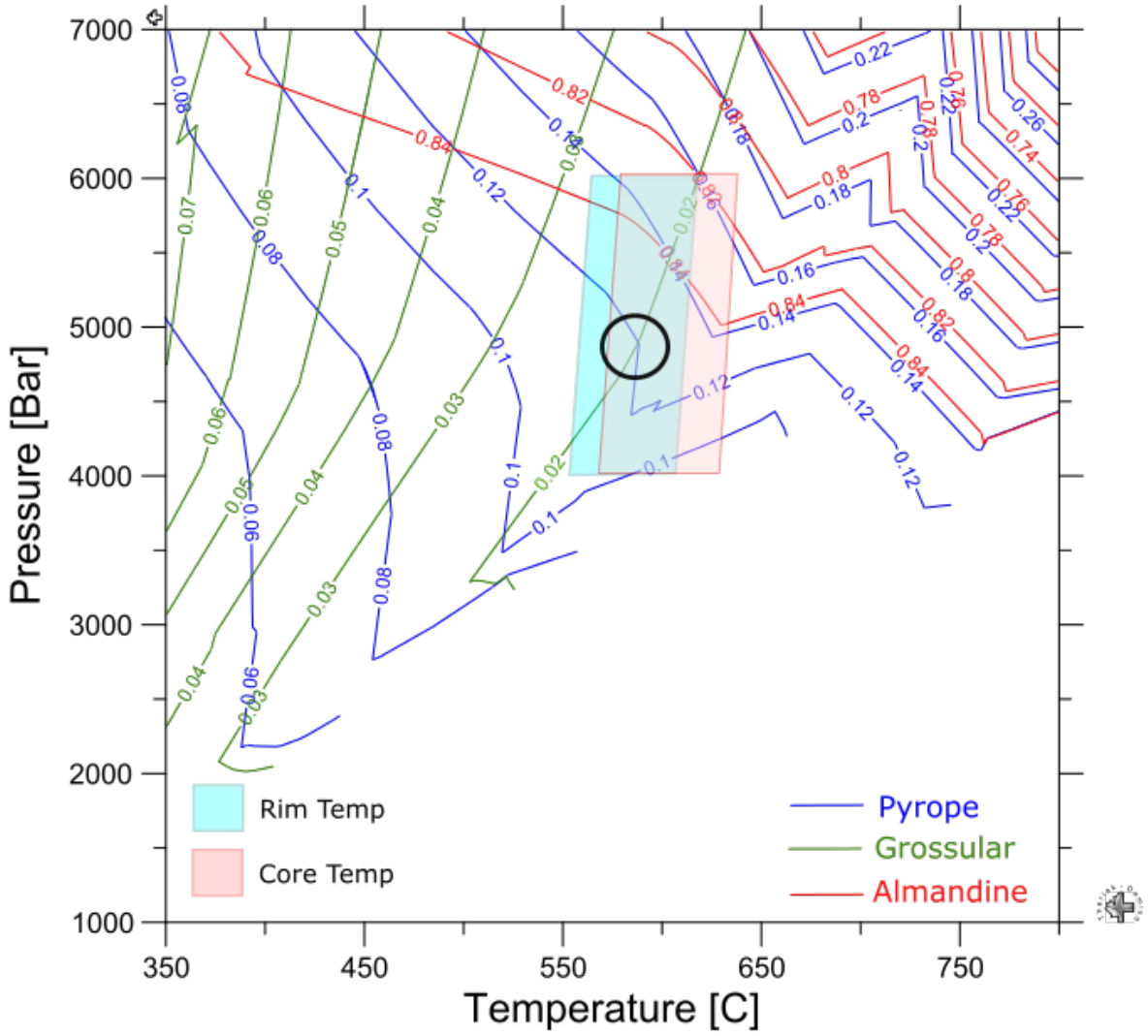

Figure 50. Garnet isopleth diagram showing intersection of calculated garnet fractions from a staurolite-garnet-mica-quartz schist (BR060912-02) based on data located in Appendix F, Table F-2. Fractions were calculated using the Garnet Pressure Temperature (GPT) Reche and Martinez Excel Spreadsheet for thermobarometric calculations in metapelitic rocks (Reche and Martinez, 1996). The black circle represents the area where garnet isopleths intersect, inferring ideal P & T conditions of formation. (Almandine 87%, Pyrope 12%, Grossular 1%).

A - Staurolite-garnet-mica-quartz schist (BR060912-02)

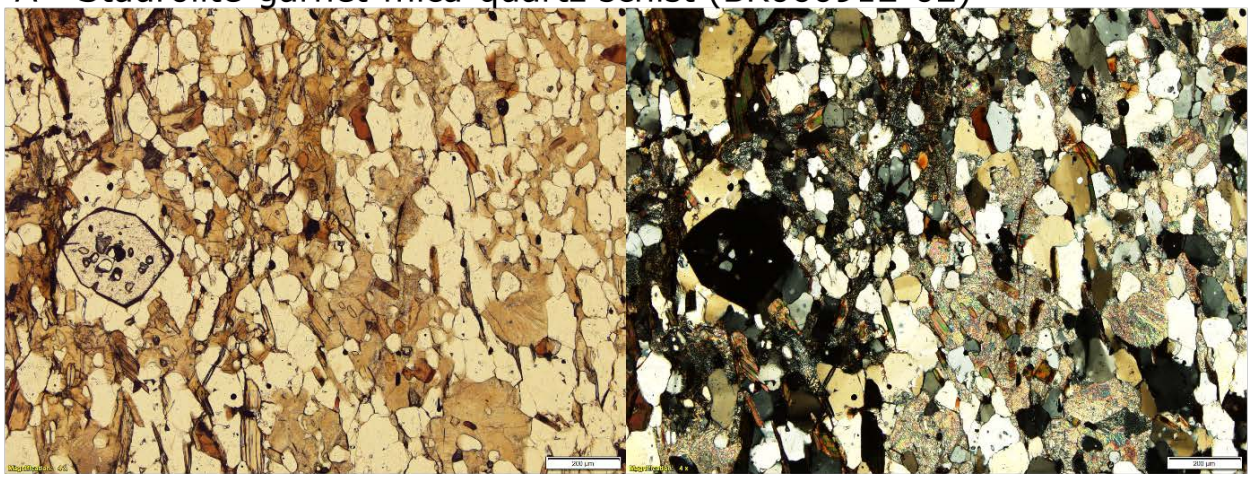

B - Sillimanite-garnet-mica-quartz schist (BR061213-05)

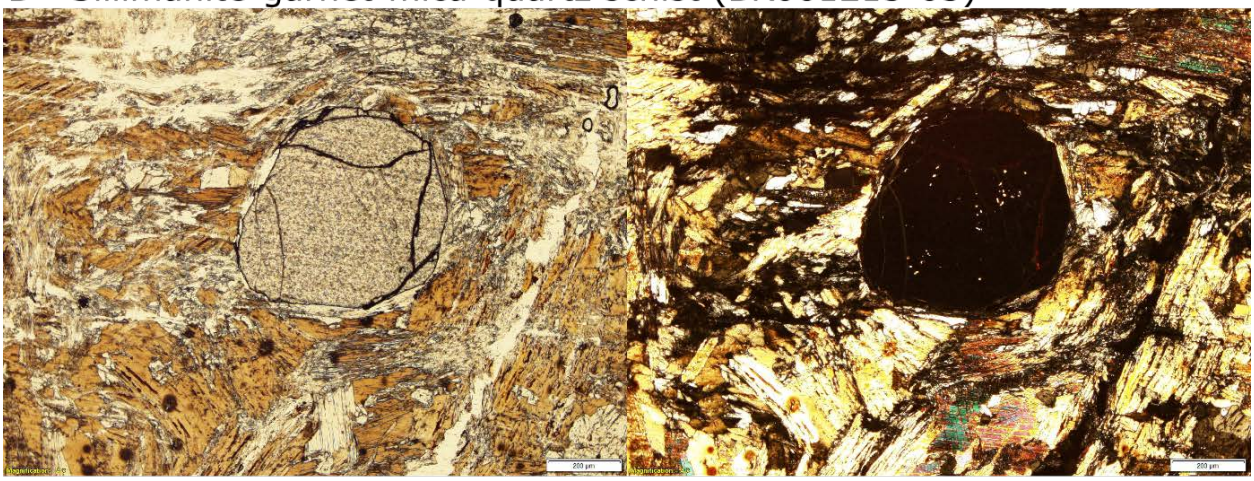

C - Cordierite-mica-quartz schist (BR061513-06)

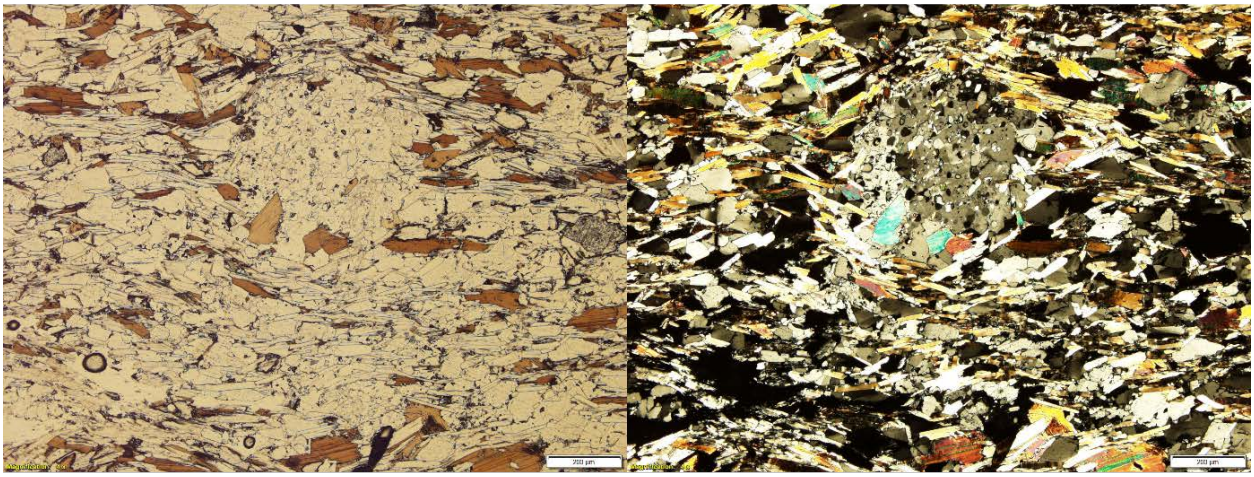

Plane Polarized Light

Cross Polarized Light

Figure 51. Reaction textures observed in metasedimentary rocks from the Blue Ridge area. A) Plane-polarize light (PPL) and cross-polarized (XPL) image of relict staurolite in a staurolite-garnet-mica-quartz schist. Staurolite is noted by its poikiloblastic texture and dark yellow coloring in PPL. The XPL image shows staurolite completely altered to fine white mica. B) PPL and XPL image showing garnet porphyroblast completely surrounded by biotite and fibrolite in a sillimanite-garnet-mica-quartz schist. Fibrolite is growing at the expense of biotite and is consuming biotite at the top of the picture. The apparent voids seen in biotite in PPL are masses of sillimanite needles. C) PPL and XPL image of a cordierite porphyroblast in a matrix of quartz, muscovite, and biotite in a cordierite-mica-quartz-schist. In PPL the cordierite is delineated by its round shape and dirty appearance. The XPL image shows the poikiloblastic nature of cordierite, with inclusions of quartz, muscovite, and biotite. All images are shown at 4x magnification. White scale bar is 200μm.

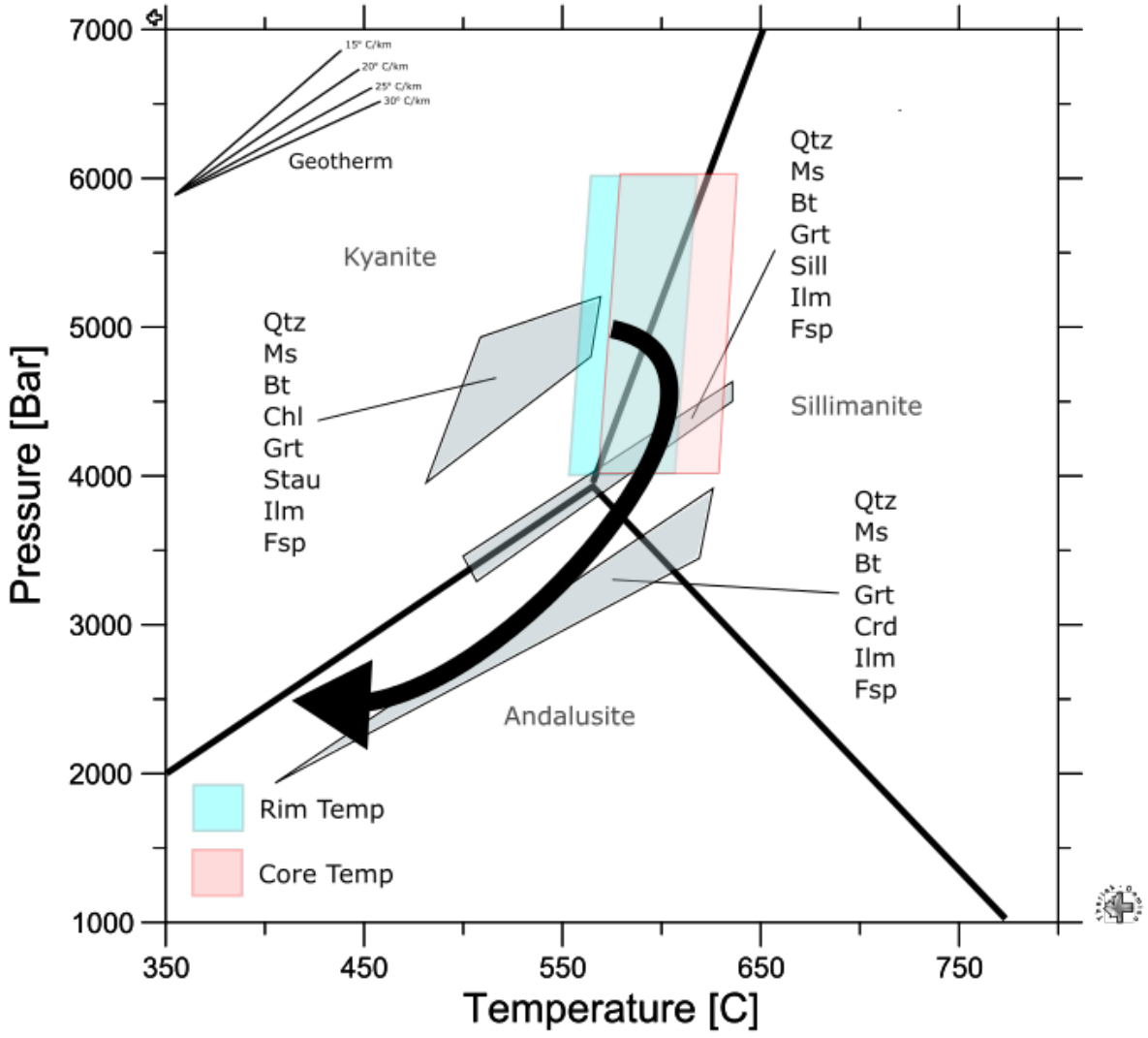

Figure 52. P-T evolution diagram showing the interpreted clockwise path for the main metamorphic event for the Blue Ridge area, based on thermodynamic equilibrium calculations and garnet-biotite thermometer temperatures. The starting point for the clockwise path coincides with garnet growth, followed by the formation of sillimanite and then cordierite.

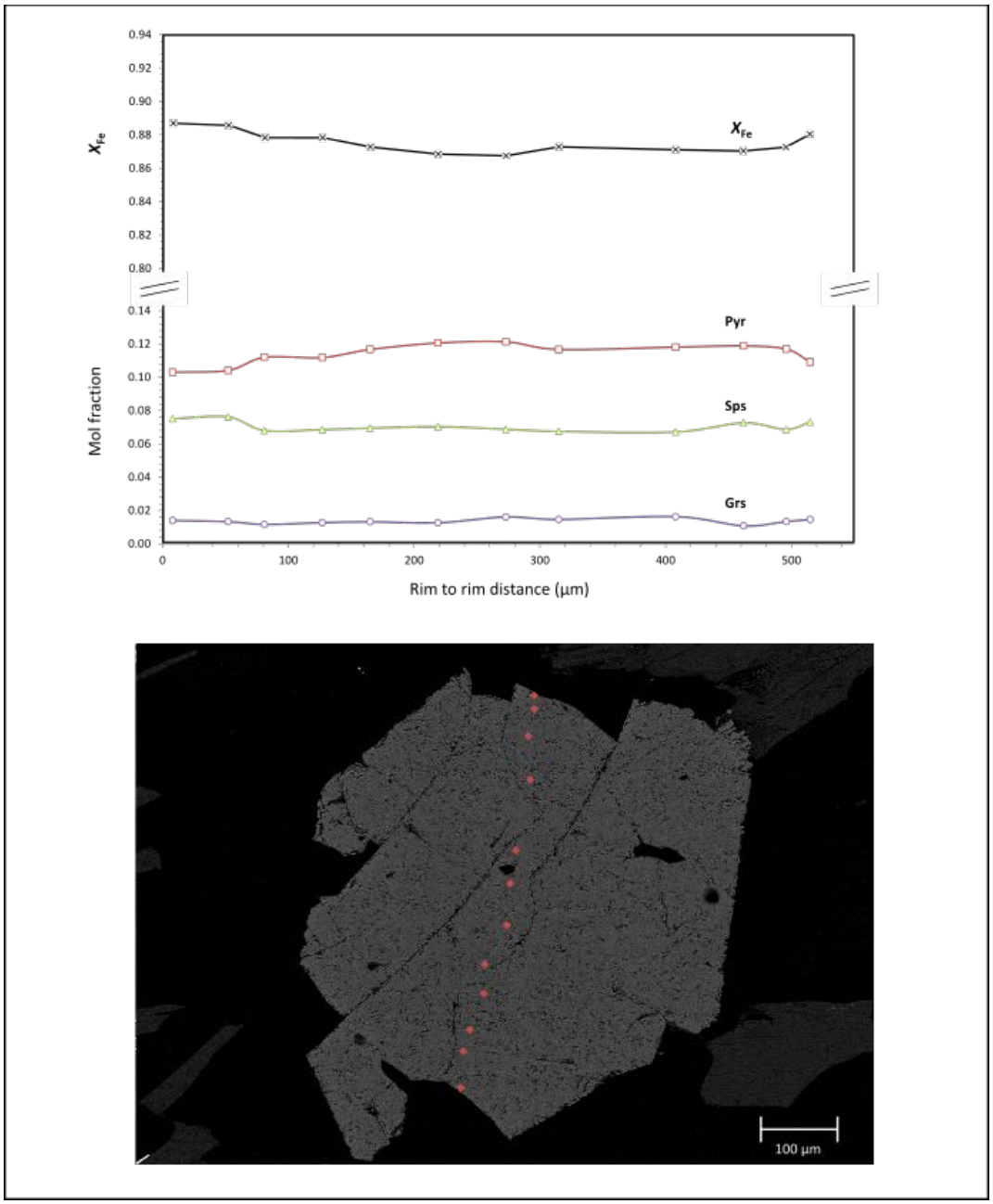

Figure 53-1. Chemical zoning profile across a garnet from a staurolite-garnet-mica-quartz schist (BR060912-02) located in the Blue Ridge area (see Figure 41 for location). Profiles based on data in Appendix F, Table F-1.

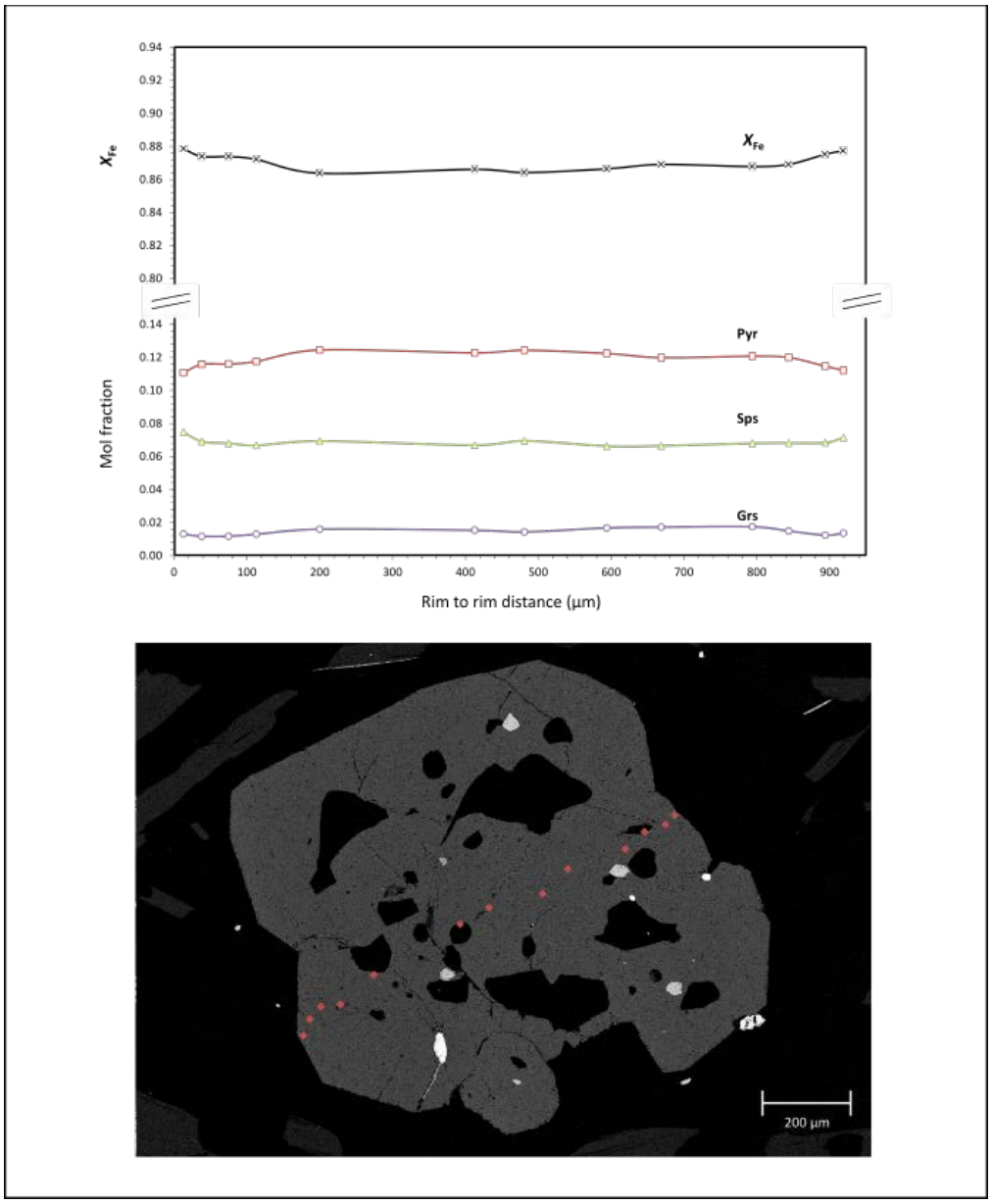

Figure 53-2. Chemical zoning profile across a garnet from a staurolite-garnet-mica-quartz schist (BR060912-02) located in the Blue Ridge area (see Figure 41 for location). Profiles based on data in Appendix F, Table F-1.

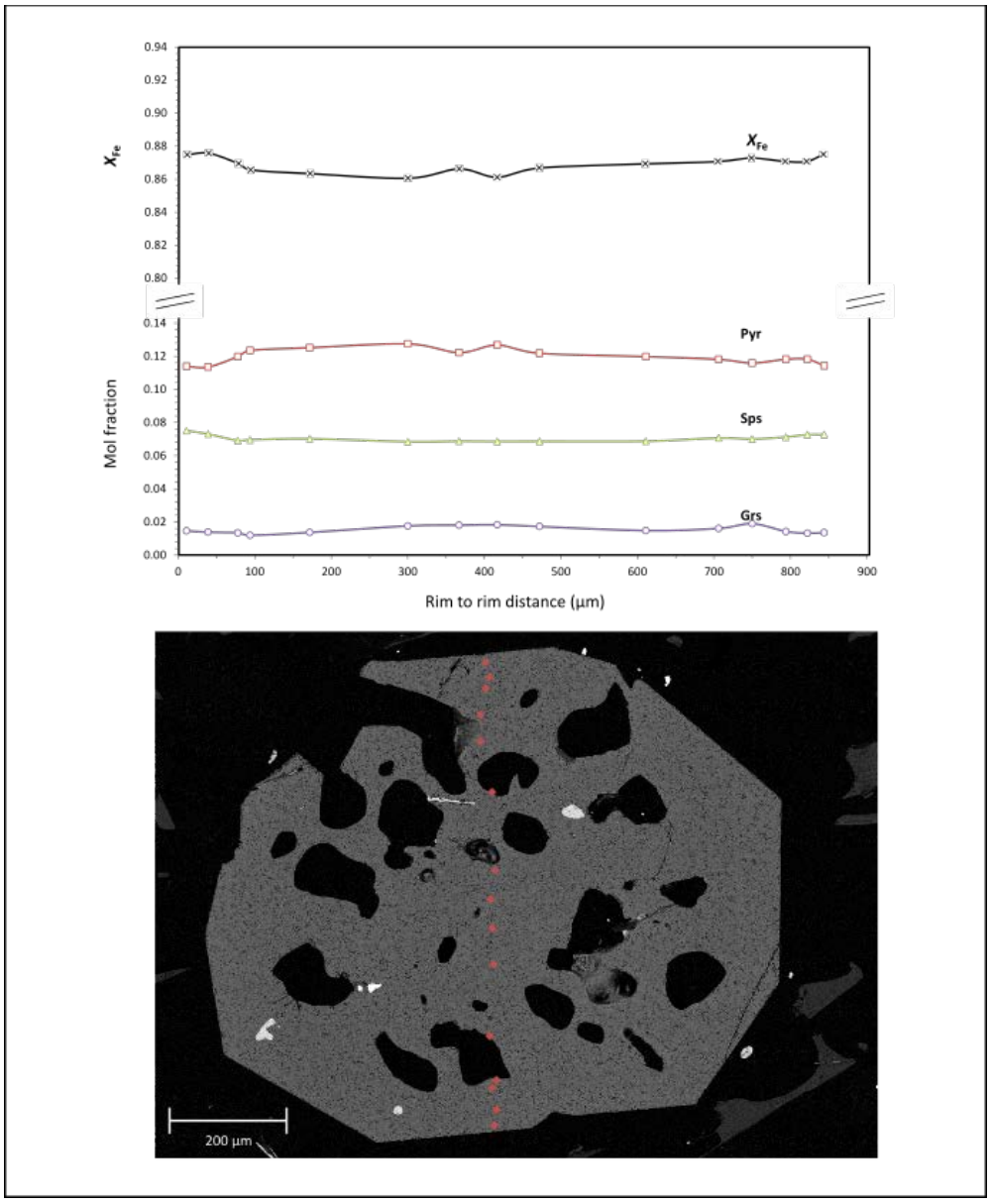

Figure 53-3. Chemical zoning profile across a garnet from a staurolite-garnet-mica-quartz schist (BR060912-02) located in the Blue Ridge area (see Figure 41 for location). Profiles based on data in Appendix F, Table F-1.

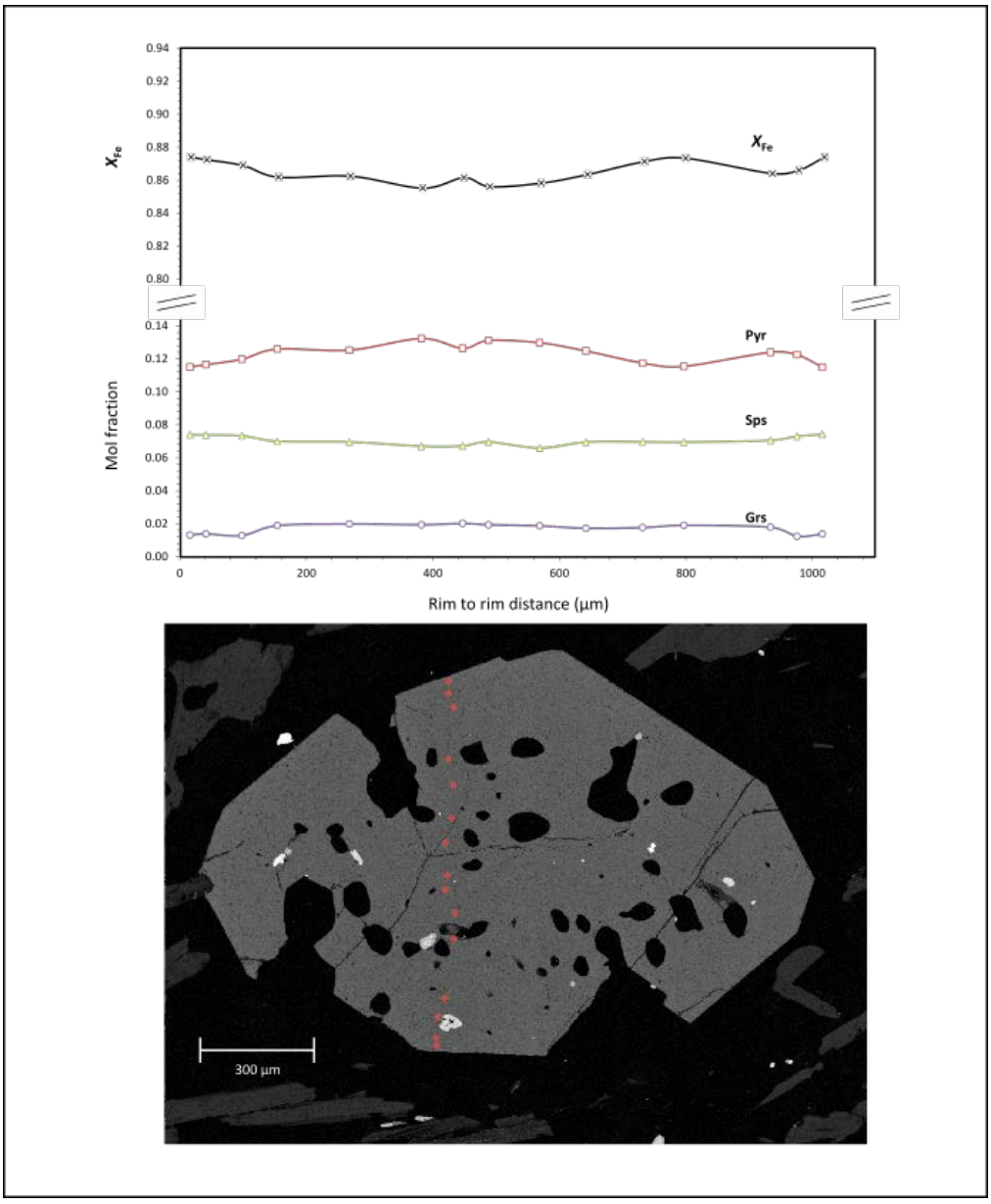

Figure 53-4. Chemical zoning profile across a garnet from a staurolite-garnet-mica-quartz schist (BR060912-02) located in the Blue Ridge area (see Figure 41 for location). Profiles based on data in Appendix F, Table F-1.

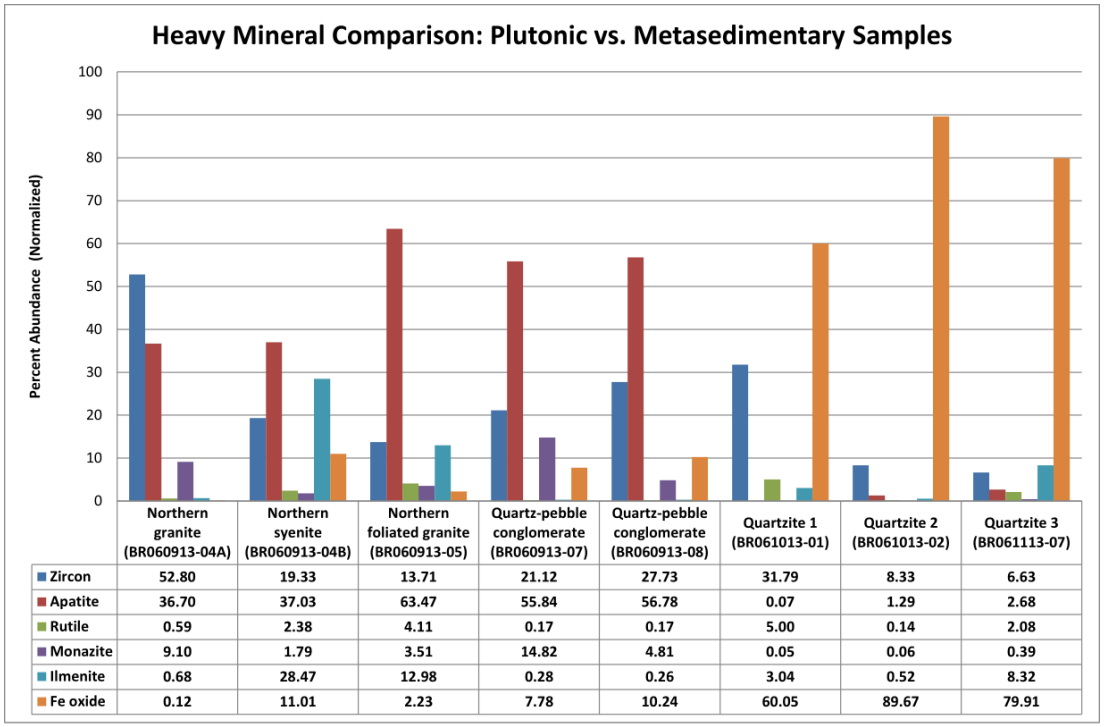

	Northern granite (BR060913-04A)	Northern syenite (BR060913-04B)	Northern foliated granite (BR060913-05)	Quartz-pebble conglomerate (BR060913-07)	Quartz-pebble conglomerate (BR060913-08)	Quartzite 1 (BR061013-01)	Quartzite 2 (BR061013-02)	Quartzite 3 (BR061113-07)
Zircon	52.80	19.33	13.71	21.12	27.73	31.79	8.33	6.63
Apatite	36.70	37.03	63.47	55.84	56.78	0.07	1.29	2.68
Rutile	0.59	2.38	4.11	0.17	0.17	5.00	0.14	2.08
Monazite	9.10	1.79	3.51	14.82	4.81	0.05	0.06	0.39
Ilmenite	0.68	28.47	12.98	0.28	0.26	3.04	0.52	8.32
Fe oxide	0.12	11.01	2.23	7.78	10.24	60.05	89.67	79.91

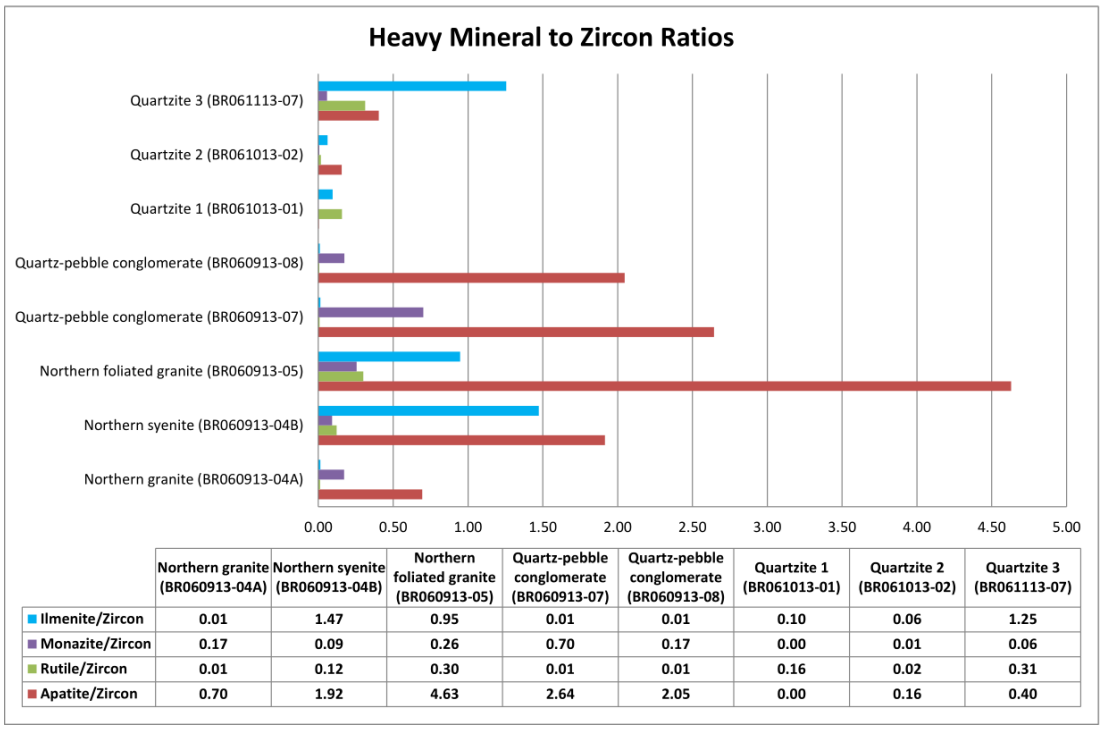

	Northern granite (BR060913-04A)	Northern syenite (BR060913-04B)	Northern foliated granite (BR060913-05)	Quartz-pebble conglomerate (BR060913-07)	Quartz-pebble conglomerate (BR060913-08)	Quartzite 1 (BR061013-01)	Quartzite 2 (BR061013-02)	Quartzite 3 (BR061113-07)
Ilmenite/Zircon	0.01	1.47	0.95	0.01	0.01	0.10	0.06	1.25
Monazite/Zircon	0.17	0.09	0.26	0.70	0.17	0.00	0.01	0.06
Rutile/Zircon	0.01	0.12	0.30	0.01	0.01	0.16	0.02	0.31
Apatite/Zircon	0.70	1.92	4.63	2.64	2.05	0.00	0.16	0.40

Figure 54**.** Results of heavy mineral analysis by QEMSCAN®. The minerals selected for comparison are chosen to reflect weathering resistant fractions. Fe-oxide is possibly a product of weathering or replacement. Charts are based on data in Appendix G, Table G-2.

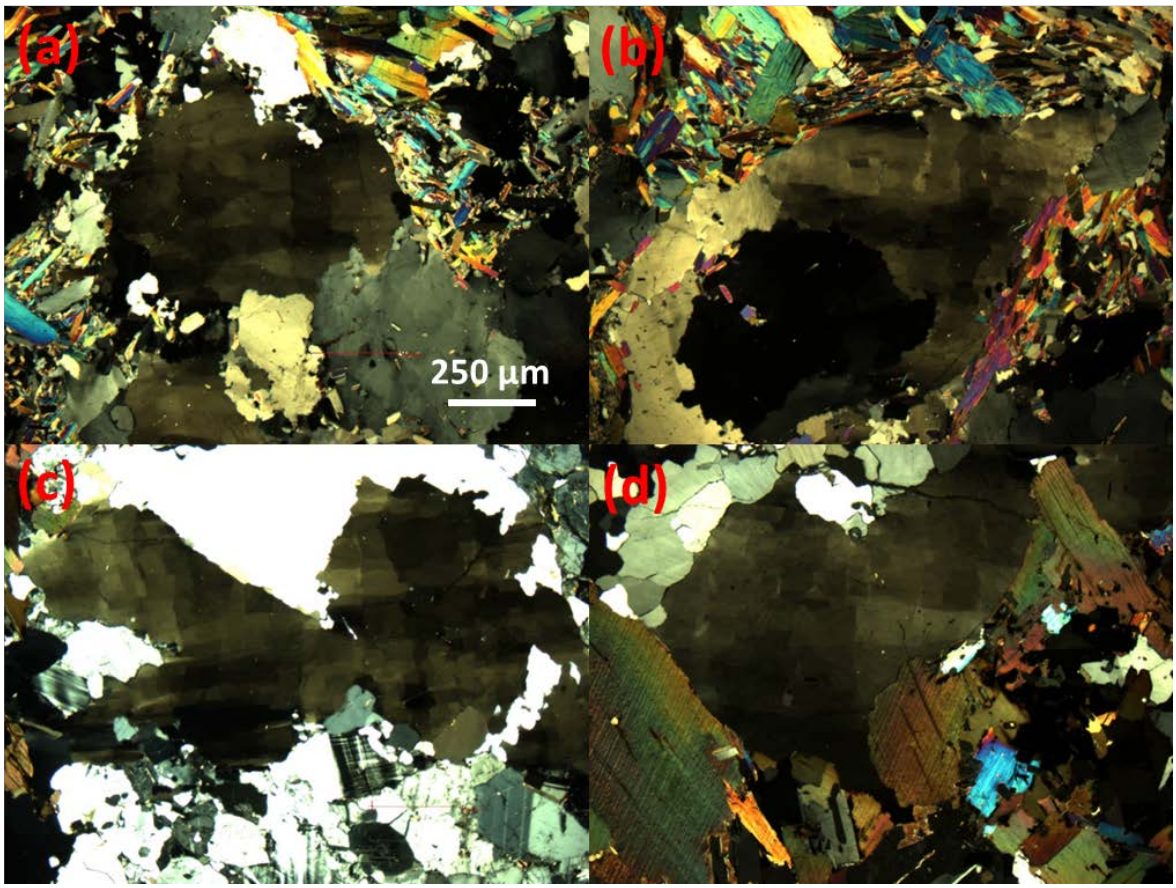

Figure 55. Chessboard microtextures observed in quartz grains. A and B) QPC (BR060913-07). C) Foliated granite (BR060913-05). D) Granite (BR060913-04A). (Photos courtesy of Brian Sitek)

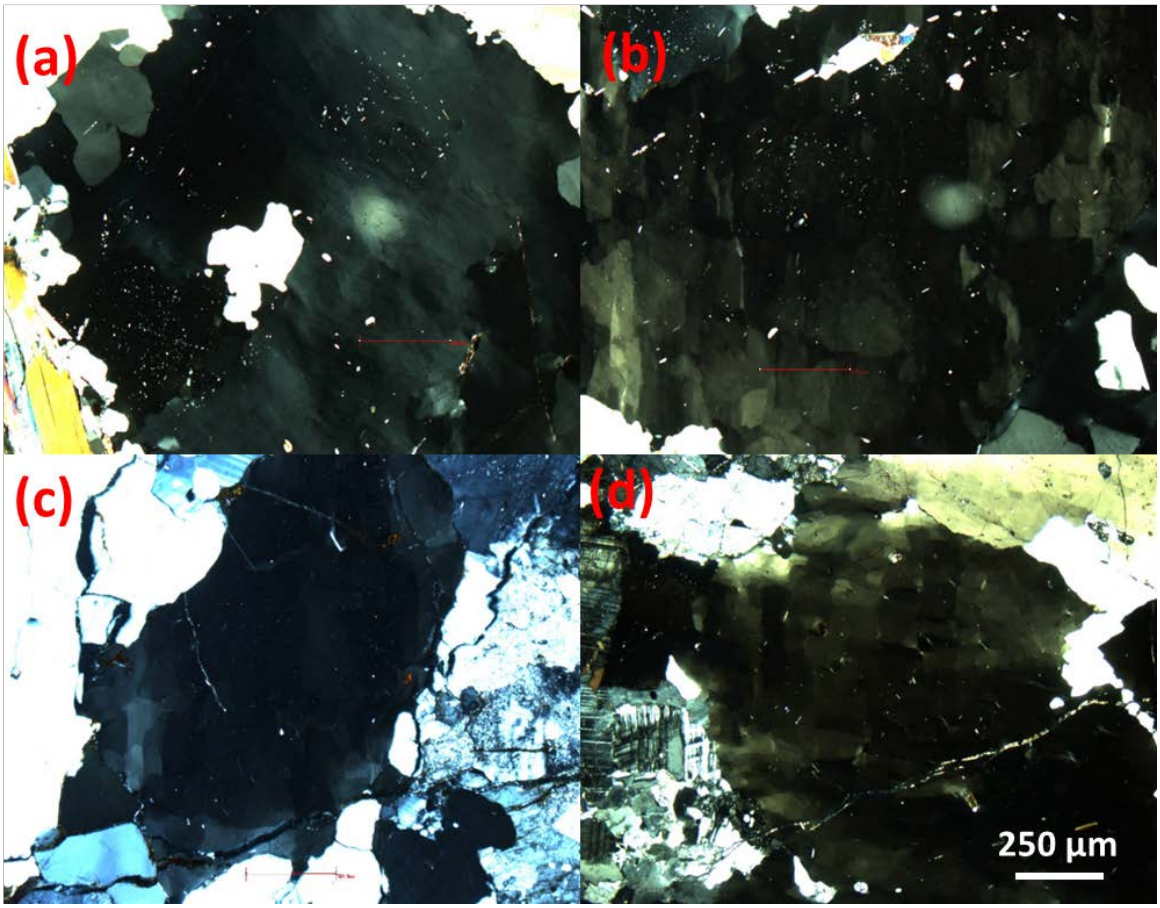

Figure 56. Inclusions patterns in northern granitoids and QPC. A and B) Centrally concentrated inclusions in quartz grains of QPC (BR060913-07) that indicate the existence of former subgrains. C) Inclusions in granite (BR060913-04A). D) Inclusions in foliated granite (BR060913-05). Inclusion clusters are noticeably lacking in the granitoids. (Photos courtesy of Brian Sitek)

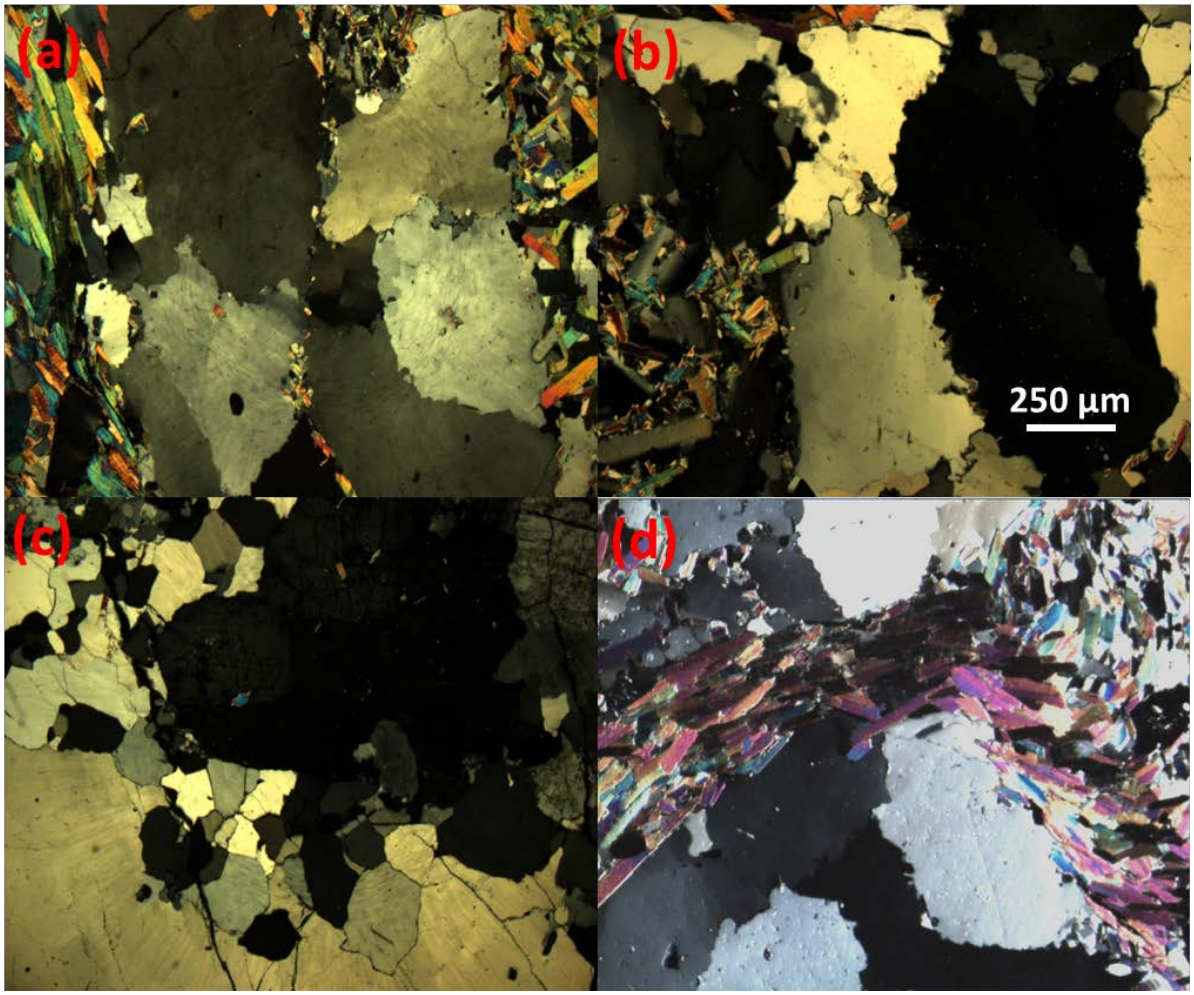

Figure 57. Microtextures from QPC (BR060913-07) and northern granite (BR060913-04A). A) Polycrystalline quartz grains in QPC showing sutured boundaries with muscovite trailing the boundaries. B) High angle suturing in the QPC. C) Monocrystalline quartz grains with high angle, sharp grain boundaries in granite. D) Muscovite grains outlining quartz in granite. (Photos courtesy of Brian Sitek)

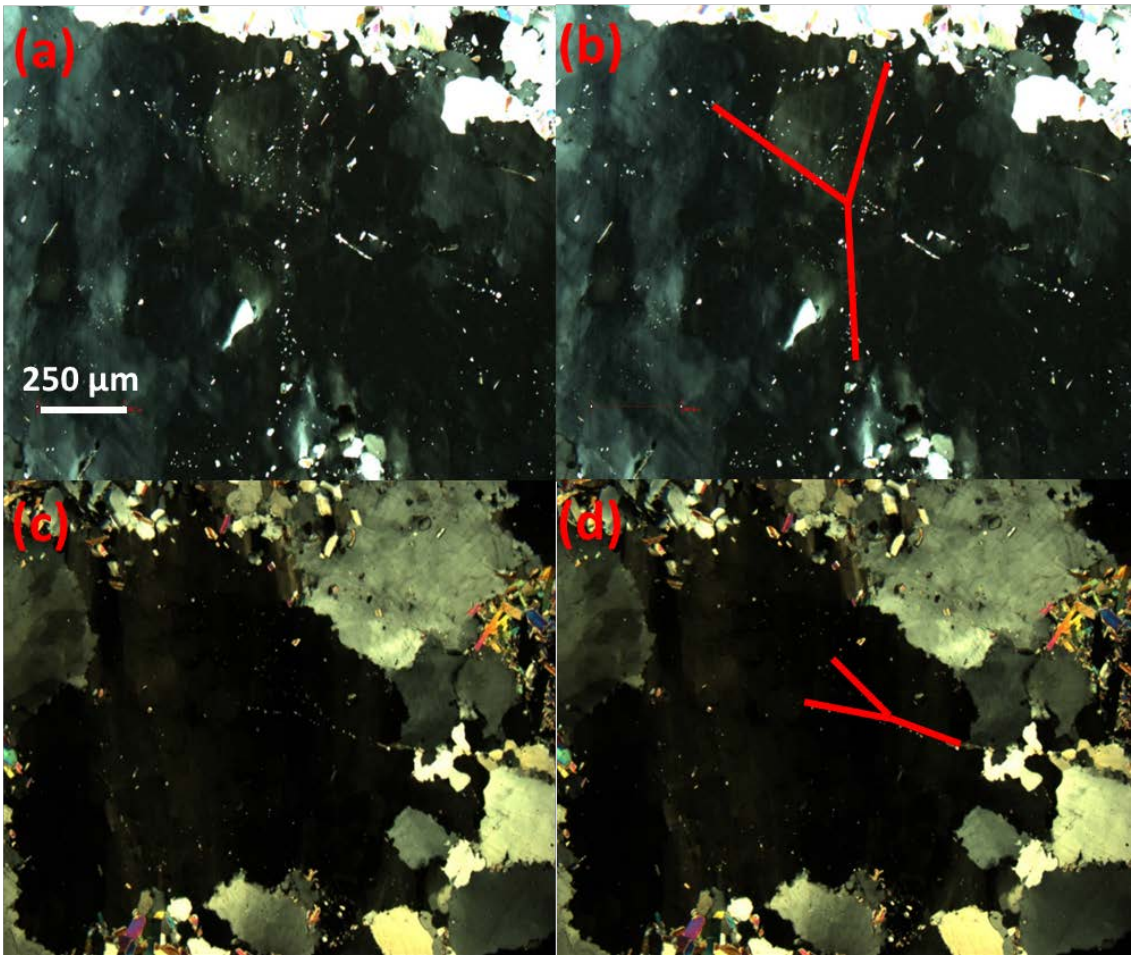

Figure 58. Muscovite trails within internal structure of quartz pebbles. (a) Muscovite trails in quartz pebble of QPC(BR060913-07). B) Muscovite trail outline. C) Muscovite trail within pebble of QPC with high angle boundaries. D) Muscovite trail outline. (Photos courtesy of Brian Sitek)

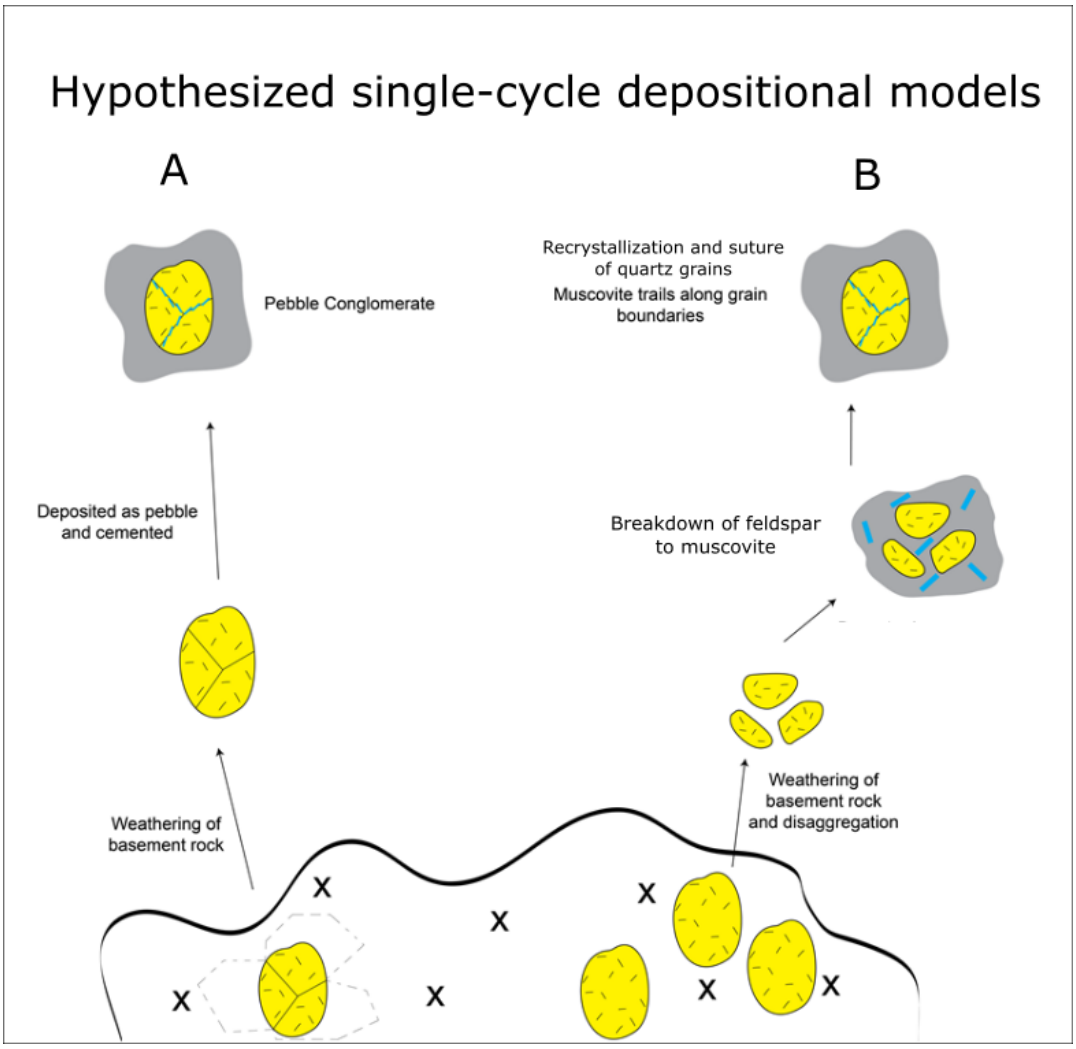

Figure 59. Hypothesized single-cycle depositional models for the quartz-pebble conglomerate (QPC). Model A follows the interpretations of Jones et al. (2009) and model B follows the interpretation for this study. Both involve a single-cycle of weathering and deposition, but model B requires a high heat (>500 ^{o}C) event to recrystallize and suture quartz grains to form QPC. Image modified after Sitek (2014).

Appendix A: Location of samples collected at Blue Ridge. All coordinates in WGS 1984.

Sample ID	Rock Type	Latitude	Longitude	Analysis
BR060912-02	Schist	38.56977	-105.28874	Geochemistry
BR060913-01	Amphibole-bearing leucosome	38.56132	-105.30118	Geochemistry, Geochronology, Qemscan
BR060913-02	Schist	38.56242	-105.30109	
BR060913-03	Foliated granite	38.58405	-105.30464	
BR060913-04A	Granite	38.58405	-105.30464	Geochronology, Geochemistry, Qemscan
BR060913-04B	Syenite	38.58405	-105.30464	Geochemistry, Qemscan
BR060913-05	Foliated granite	38.58333	-105.31779	Geochronology, Qemscan
BR060913-06	Foliated granite	38.58333	-105.31779	
BR060913-07	Quartz-Pebble-Conglomerate	38.57512	-105.29766	Geochronology, Qemscan
BR060913-08	Quartz-Pebble-Conglomerate	38.57512	-105.29766	Geochronology, Qemscan
BR061013-01	Quartzite	38.5685	-105.29459	Geochronology, Qemscan
BR061013-02	Quartzite	38.5703	-105.29733	Qemscan
BR061013-03	Ore deposit	38.56587	-105.29316	
BR061013-04	Quartzite	38.56587	-105.29316	
BR061113-01	Granite	38.56115	-105.30088	Qemscan
BR061113-02	Granodiorite	38.56112	-105.30123	Geochronology, Qemscan
BR061113-03	Amphibole-bearing leucosome	38.56112	-105.30123	Geochronology
BR061113-04	Augen gneiss	38.56112	-105.30123	Geochronology
BR061113-05	Pegmatite	38.5616	-105.30072	Geochronology, Qemscan
BR061113-06	Quartzite	38.56142	-105.30098	
BR061113-07	Quartzite	38.57458	-105.2967	Qemscan
BR061213-01	Schist	38.56267	-105.30113	Geochemistry, Geochronology
BR061213-02	Quartzite	38.5617	-105.30338	
BR061213-03	Schist	38.56234	-105.3013	
BR061213-04	Schist	38.56311	-105.29712	Geochemistry
BR061213-05	Schist	38.56712	-105.29325	Geochemistry
BR061213-06	Schist	38.57043	-105.28384	

Appendix A: (continued)

Sample ID	Rock Type	Latitude	Longitude	Analysis
BR061313-01	Schist	38.56508	-105.30235	Geochemistry
BR061313-02	Schist	38.56973	-105.28864	
BR061313-03	Schist	38.56973	-105.28864	Geochemistry
BR061313-04	Schist	38.56973	-105.28864	
BR061413-01	Schist	38.56794	-105.28669	
BR061413-02	Schist	38.56758	-105.28927	Geochemistry
BR061513-01	Schist	38.56916	-105.28239	Geochemistry
BR061513-02	Schist	38.56906	-105.28239	
BR061513-03	Schist	38.56906	-105.28239	Geochemistry
BR061513-04	Schist	38.56908	-105.28239	
BR061513-05	Schist	38.56895	-105.28243	
BR061513-06	Schist	38.56884	-105.2824	Geochemistry
BR061613-01	Quartz-Pebble-Conglomerate	38.56697	-105.32171	
BR061613-02	Foliated granite	38.56697	-105.32171	
BR061613-03	Granite	38.56697	-105.32171	Geochronology
BR061613-04	Quartz-Pebble-Conglomerate	38.56697	-105.32171	
BR061613-05	Schist	38.56532	-105.32113	
BR061613-06	Schist	38.56472	-105.31995	
BR061613-07	Schist	38.5645	-105.32001	
BR061613-08	Schist	38.56429	-105.32035	Geochemistry
BR061713-01	Schist	38.56944	-105.28271	Geochemistry
BR061713-02	Schist	38.56944	-105.28271	
BR061713-03	Granodioritic Grus	38.56984	-105.28272	Geochronology
BR061713-04	Schist	38.56979	-105.28872	
BR061713-05	Schist	38.56979	-105.28872	
BR060314-01	Diabase	38.56999	-105.28614	Geochemistry, Geochronology
BR060314-02	Granodioritic Grus	38.56984	-105.28272	
BR060314-03	Schist	38.56242	-105.30109	
BR060314-04	Schist	38.56242	-105.30109	
BR060314-05	Schist	38.56242	-105.30109	
BR011314-01	Schist	38.55956	-105.31052	Geochemistry
BR011314-02	Schist	38.55921	-105.31712	
BR011314-03	Schist	38.55806	-105.31078	Geochemistry
BR011414-01	Schist	38.56093	-105.30259	
BR011414-02	Schist xenolith	38.55904	-105.3067	

Appendix A: (continued)

Sample ID	Rock Type	Latitude	Longitude	Analysis
BR011414-03	Schist	38.55534	-105.31824	Geochemistry
BR011414-04	Schist	38.55851	-105.30991	Geochemistry
BR110614-01	Quartzite	38.57088	-105.29385	
BR110714-01	Schist	38.57888	-105.28561	
BR072815-01	Amphibole-bearing leucosome	38.56132	-105.30118	Geochronology
BR072815-02	Pegmatite	38.56132	-105.30118	Geochronology
BR072915-01	Quartz-Pebble-Conglomerate	38.5616	-105.33618	
BR073015-01	Foliated Granite	38.56694	-105.32173	Geochronology

Appendix B: Zircon/Apatite LA-ICP-MS U-Pb Isotopic Data and Ages

Table B-1. QPC (BR060913-07) Zr

Grain # - Spot #	U [ppm]	Th [ppm]	Th/U	Corrected isotope ratios[a] $^{207}Pb/^{235}U$	±2s	$^{206}Pb/^{238}U$	±2s	Rho	$^{207}Pb/^{206}Pb$	±2s	Ages (Ma) $^{207}Pb/^{235}U$	±2s	$^{206}Pb/^{238}U$	±2s	$^{207}Pb/^{206}Pb$	±2s	Disc. %[b]
003-002r	287	124	0.43	4.3	0.18	0.2758	0.013	0.6942	0.1121	0.0045	1691	35	1569	64	1835	57	14.50
004-003r	341	70	0.21	4.31	0.17	0.2799	0.012	0.6580	0.11	0.0043	1697	26	1590	64	1796	59	11.47
005-004c	136	58.9	0.43	4.51	0.15	0.3089	0.0087	0.5898	0.1048	0.002	1732	29	1737	43	1704	35	-1.94
005-005r	89.1	40.4	0.45	5.02	0.21	0.298	0.014	0.7037	0.1205	0.0037	1819	41	1680	73	1963	49	14.42
007-006r	220.7	67.2	0.30	4.426	0.12	0.3031	0.0091	0.6417	0.1058	0.0016	1716	23	1706	46	1726	26	1.16
009-008r	259.1	100.1	0.39	3.71	0.15	0.2387	0.0094	0.7493	0.1134	0.0025	1570	32	1377	49	1852	39	25.65
009-009r	418	127	0.30	4.58	0.21	0.2831	0.016	0.4492	0.1181	0.0048	1746	46	1607	84	1926	61	16.56
010-010r	1101	697	0.63	3.27	0.14	0.1192	0.0088	0.2641	0.1984	0.0082	1473	31	726	49	2811	70	74.17
011-011c	412	558	1.35	2.22	0.11	0.1412	0.0098	0.5260	0.1137	0.015	1189	45	852	58	1864	130	54.29
011-012r	418	263	0.63	3.92	0.13	0.2484	0.0097	0.4877	0.1145	0.0032	1616	29	1430	52	1859	48	23.08
012-013r	277	51.9	0.19	4.08	0.17	0.2518	0.013	0.4235	0.1173	0.0047	1648	37	1447	69	1907	60	24.12
013-014r	1066	306.4	0.29	3.135	0.13	0.1093	0.0057	0.7861	0.2092	0.007	1439	39	669	34	2897	44	76.91
014-015r	213.3	70.5	0.33	4.24	0.14	0.2828	0.0091	0.7223	0.1095	0.0021	1685	29	1605	47	1792	33	10.44
015-016r	374	71.6	0.19	4.37	0.23	0.2492	0.016	0.5131	0.1281	0.0071	1708	55	1434	88	2066	74	30.59
016-017r	406	74.2	0.18	4.32	0.32	0.2817	0.0099	0.4862	0.1101	0.0048	1694	51	1600	50	1803	67	11.26
017-018r	368.5	87.1	0.24	4.189	0.16	0.2813	0.013	0.6466	0.1089	0.0035	1671	38	1598	71	1778	46	10.12
018-019r	276	36.8	0.13	4.27	0.13	0.2816	0.0086	0.4649	0.1094	0.0022	1684	25	1603	43	1783	36	10.10
019-020r	1169	332.5	0.28	3.564	0.12	0.1272	0.0037	0.6991	0.2028	0.0035	1538	26	772	21	2842	28	72.84
021-021r	714	480	0.67	3.98	0.14	0.1605	0.0058	0.5072	0.1827	0.0049	1633	28	959	32	2663	44	63.99
022-022r	223.7	39.7	0.18	4.52	0.14	0.3066	0.009	0.5697	0.106	0.0023	1732	27	1723	45	1725	38	0.12
023-023c	166	62	0.37	4.41	0.13	0.3018	0.0095	0.7401	0.1044	0.0028	1710	26	1699	49	1700	43	0.06
023-024r	167.5	67.4	0.40	4.5	0.18	0.3072	0.0087	0.3745	0.1051	0.0031	1733	32	1729	43	1705	50	-1.41
024-025r	137	34	0.25	4.52	0.15	0.3087	0.0089	0.5001	0.1046	0.002	1731	28	1737	45	1698	37	-2.30
025-026r	154	39.6	0.26	4.528	0.13	0.3123	0.0085	0.4229	0.1049	0.0018	1734	24	1754	43	1706	31	-2.81
026-027r	576	126.2	0.22	3.91	0.19	0.2471	0.017	0.5049	0.1132	0.012	1617	51	1423	94	1854	120	23.25
027-028r	232.6	51.1	0.22	4.45	0.15	0.2944	0.01	0.4484	0.1087	0.0022	1718	30	1663	51	1767	35	5.89
028-029c	172.2	60.5	0.35	4.408	0.14	0.2989	0.0083	0.6239	0.1062	0.0018	1710	27	1685	41	1731	31	2.66
028-030r	878	170	0.19	3.74	0.11	0.1881	0.0065	0.5798	0.1426	0.004	1581	24	1110	36	2252	40	50.71
030-031c	177.5	60.7	0.34	4.63	0.16	0.3005	0.0095	0.3743	0.1113	0.004	1756	30	1693	48	1819	60	6.93
030-032r	612	75	0.12	4.14	0.14	0.26	0.011	0.9374	0.1203	0.009	1659	39	1491	63	1957	85	23.81
031-033r	1440	397	0.28	2.641	0.11	0.1049	0.0072	0.8870	0.1872	0.0074	1304	30	650	41	2680	64	75.75
032-034r	4210	1109	0.26	1.399	0.041	0.0358	0.0011	0.5391	0.2828	0.0046	889	18	227	6.7	3386	26	93.30
033-035r	160.4	39.9	0.25	4.62	0.16	0.3146	0.011	0.7721	0.1073	0.0018	1750	29	1761	53	1761	30	0.00
034-036r	498	287	0.58	4.45	0.15	0.3162	0.01	0.9275	0.10203	0.0011	1723	29	1769	49	1659	20	-6.63
035-037r	98	37.5	0.38	4.66	0.2	0.3055	0.016	0.5900	0.1103	0.0046	1754	40	1718	84	1795	65	4.29
037-038r	197	246	1.25	3.67	0.14	0.2341	0.012	0.4755	0.1122	0.0093	1562	30	1355	64	1827	100	25.83

Appendix B: Zircon/Apatite LA-ICP-MS U-Pb Isotopic Data and Ages

Table B-1. QPC (BR060913-07) Zr

Grain # - Spot #	U [ppm]	Th [ppm]	Th/U	Corrected isotope ratios[a] $^{207}Pb/^{235}U$	±2s	$^{206}Pb/^{238}U$	±2s	Rho	$^{207}Pb/^{206}Pb$	±2s	Ages (Ma) $^{207}Pb/^{235}U$	±2s	$^{206}Pb/^{238}U$	±2s	$^{207}Pb/^{206}Pb$	±2s	Disc. %[b]
038a-039r	218.4	126.5	0.58	4.23	0.13	0.2719	0.0075	0.5416	0.1119	0.0019	1675	26	1550	39	1827	30	15.16
038b-040r	175.8	55.7	0.32	4.45	0.17	0.3043	0.012	0.3986	0.106	0.0022	1722	34	1712	60	1723	36	0.64
041-042r	369	49.6	0.13	4.325	0.12	0.286	0.0078	0.4578	0.1101	0.0017	1698	23	1621	40	1795	28	9.69
041-043r	368	68.8	0.19	4.385	0.14	0.2741	0.008	0.6121	0.115	0.0021	1706	27	1561	40	1883	33	17.10
042-044r	192	106.2	0.55	4.34	0.14	0.2834	0.0079	0.6376	0.1119	0.0021	1702	28	1608	40	1821	33	11.70
043-045r	1338	708	0.53	2.252	0.078	0.083	0.0043	0.5377	0.2067	0.0071	1198	24	513	26	2873	58	82.14
045-046r	1146	286	0.25	2.682	0.095	0.0931	0.004	0.9579	0.2097	0.0039	1321	29	574	24	2902	27	80.22
046-047r	1160	296	0.26	3.63	0.14	0.1524	0.0082	0.5707	0.1694	0.0079	1553	39	914	48	2546	61	64.10
047-048r	833	960	1.15	3.398	0.1	0.1395	0.0052	0.7827	0.1737	0.0037	1502	25	844	30	2595	33	67.48
048-049c	416	211	0.51	3.82	0.16	0.1945	0.0075	0.1779	0.1444	0.0071	1591	33	1145	41	2236	84	48.79
048-050r	335	132.2	0.39	4.45	0.12	0.2116	0.0073	0.6951	0.1527	0.0065	1718	28	1237	42	2372	52	47.85
049-051c	306	112.7	0.37	4.006	0.11	0.2698	0.0075	0.6336	0.10772	0.00097	1635	22	1539	39	1760	16	12.56
050-052r	158.8	42.9	0.27	4.503	0.14	0.2925	0.013	0.8304	0.11163	0.0051	1731	28	1654	71	1832	64	9.72
050-053c	99.8	38.42	0.38	4.48	0.18	0.3079	0.0086	0.5272	0.10549	0.0021	1727	29	1730	44	1722	32	-0.46
051-054c	102.4	50.97	0.50	4.549	0.12	0.3115	0.0083	0.5039	0.10487	0.00093	1740	22	1748	41	1714	16	-1.98
052-055c	99.2	24.14	0.24	13.66	0.96	0.42	0.021	0.8938	0.2361	0.013	2718	120	2268	100	3087	120	26.53
053-056r	335	111.3	0.33	4.029	0.13	0.2668	0.014	0.5938	0.10887	0.007	1640	28	1524	77	1780	84	14.38
054-057c	208	36.4	0.18	4.517	0.12	0.3077	0.0099	0.7734	0.10641	0.0017	1735	23	1729	50	1740	27	0.63
055-058c	213	103	0.48	4.35	0.12	0.302	0.0084	0.7973	0.1047	0.00087	1704	23	1700	42	1711	15	0.64
055-059r	594	89.9	0.15	4.08	0.14	0.2065	0.0089	0.8088	0.1431	0.0045	1653	32	1210	50	2262	47	46.51
056-060r	3570	2470	0.69	2.638	0.1	0.0657	0.0026	0.9589	0.2928	0.002	1312	32	410	16	3432	11	88.05
057-061r	145.8	64.3	0.44	4.71	0.22	0.3165	0.019	0.7747	0.107	0.0058	1768	48	1772	100	1747	72	-1.43
059-062r	828	231.4	0.28	3.829	0.11	0.1729	0.0056	0.8708	0.1601	0.0019	1598	26	1028	31	2459	19	58.19
060-063r	964	425	0.44	3.493	0.11	0.1318	0.0045	0.9468	0.1927	0.0021	1527	27	798	26	2765	17	71.14
061-064c	139.2	59.5	0.43	4.414	0.12	0.3043	0.0083	0.5175	0.10464	0.0012	1714	22	1712	40	1706	20	-0.35
061-065r	315	109.7	0.35	4.257	0.12	0.2692	0.0074	0.7896	0.1145	0.001	1684	23	1536	38	1873	16	17.99
062-066c	154	30.88	0.20	4.505	0.12	0.3106	0.0084	0.7184	0.10513	0.00096	1731	22	1745	41	1715	17	-1.75
064-067r	205	60.2	0.29	4.297	0.12	0.2989	0.0081	0.7861	0.1043	0.00087	1692	22	1686	39	1701	15	0.88
064-068c	100.6	36.3	0.36	4.506	0.12	0.311	0.0085	0.6624	0.10556	0.0011	1732	23	1745	42	1722	18	-1.34
065-069r	292	51	0.17	4.472	0.14	0.293	0.014	0.5779	0.1104	0.0052	1727	28	1656	76	1805	67	8.25
066-070r	246.5	84.27	0.34	4.666	0.17	0.313	0.017	0.6659	0.1067	0.0049	1761	36	1755	87	1747	65	-0.46
069-071c	3840	831	0.22	2.13	0.067	0.0523	0.0017	0.9441	0.2968	0.0021	1160	22	329	10	3454	11	90.48
071-072r	272	121.5	0.45	4.082	0.12	0.2512	0.0071	0.7578	0.1185	0.0017	1645	21	1444	37	1929	22	25.14
072-073c	169.6	113.5	0.67	3.813	0.13	0.2138	0.0075	0.4929	0.1293	0.0022	1595	31	1249	41	2086	29	40.12
072-074r	745	262	0.35	3.481	0.14	0.1332	0.0061	0.8561	0.1897	0.0023	1522	38	806	35	2738	19	70.56
073-075r	2601	866	0.33	2.53	0.074	0.0698	0.0022	0.7350	0.2594	0.0039	1281	22	435	13	3241	23	86.58

Appendix B: Zircon/Apatite LA-ICP-MS U-Pb Isotopic Data and Ages

Table B-1. QPC (BR060913-07) Zr

				Corrected isotope ratios[a]							Ages (Ma)						
Grain # - Spot #	U [ppm]	Th [ppm]	Th/U	$^{207}Pb/^{235}U$	±2s	$^{206}Pb/^{238}U$	±2s	Rho	$^{207}Pb/^{206}Pb$	±2s	$^{207}Pb/^{235}U$	±2s	$^{206}Pb/^{238}U$	±2s	$^{207}Pb/^{206}Pb$	±2s	Disc. %[b]
074-076r	311.7	69.4	0.22	4.631	0.13	0.2863	0.01	0.7427	0.1166	0.0035	1754	24	1623	52	1903	47	14.71
075-077r	365	138.3	0.38	5.04	0.19	0.26	0.015	0.9173	0.1405	0.013	1815	37	1489	83	2226	100	33.11
077-078c	201	28.98	0.14	4.52	0.15	0.3094	0.014	0.9083	0.1076	0.0052	1737	29	1736	73	1757	64	1.20
078-079r	399	196	0.49	4.002	0.16	0.2004	0.011	0.8377	0.146	0.0061	1634	42	1178	61	2298	55	48.74
080-080r	403.7	200.7	0.50	3.584	0.094	0.1984	0.0066	0.7952	0.129	0.0031	1545	22	1170	36	2083	37	43.83
081-081r	263.5	64.8	0.25	4.523	0.12	0.3105	0.0085	0.6704	0.10582	0.0012	1736	22	1743	42	1728	20	-0.87
081-082c	145.5	41.93	0.29	4.681	0.27	0.3161	0.02	0.9104	0.10754	0.0026	1763	65	1770	110	1759	40	-0.63
082-083r	703	338	0.48	3.599	0.1	0.1548	0.0056	0.9073	0.1699	0.0028	1549	23	927	31	2553	27	63.69
084-084r	329	52.7	0.16	4.031	0.11	0.2644	0.0072	0.6408	0.11038	0.001	1640	22	1514	37	1805	17	16.12
086-085r	349	164	0.47	3.737	0.13	0.2105	0.012	0.9173	0.1291	0.0073	1577	29	1231	66	2084	75	40.93
086-086c	430	203	0.47	3.912	0.11	0.2234	0.0062	0.8142	0.12649	0.0011	1616	22	1300	33	2048	15	36.52
088-087c	351.1	110.5	0.31	4.429	0.18	0.3025	0.015	0.6155	0.1062	0.0031	1717	40	1703	78	1731	44	1.62
088-088r	1810	419	0.23	2.97	0.14	0.0971	0.0066	0.9739	0.2245	0.0062	1396	37	595	39	3020	43	80.30
089-089r	334	204	0.61	2.46	0.07	0.153	0.0068	0.4640	0.1171	0.0081	1259	21	917	39	1907	89	51.91
089-090r	381	225.4	0.59	4.257	0.13	0.2778	0.011	0.7184	0.1102	0.0038	1685	29	1580	60	1802	51	12.32
090-091r	476	289	0.61	3.606	0.1	0.23	0.0073	0.8121	0.1143	0.0035	1550	24	1334	40	1867	44	28.55
092-092c	2210	1407	0.64	1.785	0.067	0.0547	0.0025	0.8745	0.2444	0.0049	1039	24	343	15	3149	33	89.11
092-093r	500	153.1	0.31	3.912	0.16	0.2208	0.011	0.8548	0.1277	0.0021	1614	37	1285	60	2063	28	37.71
094-094c	315	76.6	0.24	4.258	0.14	0.274	0.014	0.5608	0.1121	0.0062	1687	29	1561	74	1831	75	14.75
094-095r	650	159	0.24	3.604	0.097	0.1853	0.0058	0.8395	0.1401	0.0016	1550	22	1095	31	2235	20	51.01
095-096r	452	97.2	0.22	4.369	0.13	0.2234	0.0087	0.6935	0.1417	0.0037	1707	26	1300	48	2247	40	42.15
096-097r	228.8	38.97	0.17	4.406	0.12	0.3036	0.0081	0.6468	0.1054	0.00086	1713	21	1709	39	1720	15	0.64
096-098c	200	65.3	0.33	4.277	0.11	0.2908	0.0077	0.7409	0.10698	0.00089	1689	22	1645	39	1748	15	5.89
098-099r	493	124.6	0.25	4.02	0.12	0.239	0.0095	0.8597	0.1239	0.0057	1636	28	1374	52	2011	64	31.68
099-100r	672	116.7	0.17	4.18	0.16	0.2177	0.011	0.7454	0.1406	0.0051	1669	38	1269	64	2230	53	43.09
101-101c	173	63.5	0.37	4.381	0.12	0.3024	0.0081	0.6008	0.1047	0.0011	1710	22	1703	40	1706	20	0.18
102-102c	483.9	120.8	0.25	3.604	0.18	0.1758	0.011	0.7111	0.1481	0.0029	1550	46	1044	61	2322	32	55.04
104-103r	107.7	60.6	0.56	4.282	0.11	0.2984	0.0085	0.6418	0.1038	0.0015	1689	22	1683	43	1691	25	0.47
105-104r	3960	2730	0.69	1.11	0.11	0.0313	0.0039	0.9885	0.294	0.012	735	49	198	24	3403	62	94.18
105-105r	257.9	192.3	0.75	5.6	0.28	0.2649	0.016	0.4235	0.1531	0.0078	1916	58	1515	90	2378	66	36.29
107-106c	235.4	31	0.13	4.446	0.12	0.3051	0.008	0.6476	0.10549	0.00096	1720	22	1716	40	1721	17	0.29
107-107r	2950	1087	0.37	2.489	0.07	0.06814	0.0019	0.5351	0.2664	0.0032	1270	20	425	11	3284	19	87.06
109-108c	178.9	101.5	0.57	4.424	0.12	0.3062	0.0085	0.7689	0.10481	0.00096	1716	23	1723	42	1710	17	-0.76
109-109r	2043	557	0.27	1.767	0.11	0.0643	0.005	0.9610	0.2005	0.0049	1027	41	400	30	2831	39	85.87
111-110r	254	29.81	0.12	4.44	0.13	0.3001	0.013	0.5673	0.10772	0.0043	1720	27	1692	70	1760	58	3.86
113-111r	3248	1120	0.34	2.065	0.072	0.0554	0.0027	0.8764	0.2702	0.0054	1136	23	347	16	3302	32	89.49

Appendix B: Zircon/Apatite LA-ICP-MS U-Pb Isotopic Data and Ages

Table B-1. QPC (BR060913-07) Zr

				Corrected isotope ratios[a]							Ages (Ma)						
Grain # - Spot #	U [ppm]	Th [ppm]	Th/U	$^{207}Pb/^{235}U$	±2s	$^{206}Pb/^{238}U$	±2s	Rho	$^{207}Pb/^{206}Pb$	±2s	$^{207}Pb/^{235}U$	±2s	$^{206}Pb/^{238}U$	±2s	$^{207}Pb/^{206}Pb$	±2s	Disc. %[b]
115-112c	163.5	110	0.67	3.929	0.11	0.2561	0.0083	0.7416	0.1105	0.0017	1619	24	1470	43	1807	26	18.65
116-113c	190	63.5	0.33	4.339	0.13	0.3008	0.0085	0.6539	0.1051	0.00099	1700	24	1695	43	1717	17	1.28
118-114c	120.7	37	0.31	4.402	0.12	0.3045	0.0081	0.5727	0.1043	0.0012	1713	22	1713	40	1701	21	-0.71
119-115r	306	222.9	0.73	3.668	0.12	0.2111	0.0082	0.8300	0.1247	0.0021	1561	26	1236	44	2018	29	38.75
119-116c	130	40	0.31	4.426	0.13	0.3055	0.0092	0.4325	0.1045	0.0017	1715	25	1718	46	1704	29	-0.82
120-117r	700	92.8	0.13	4.28	0.14	0.2363	0.0086	0.8731	0.1304	0.0028	1694	33	1367	47	2102	32	34.97
121-118r	1971	798	0.40	2.587	0.075	0.0836	0.0028	0.7234	0.2234	0.0037	1295	21	517	16	3007	27	82.80
122-119r	156.5	32.5	0.21	4.308	0.12	0.2976	0.0083	0.5520	0.1047	0.0011	1694	23	1679	42	1707	19	1.64
125-120r	154	42.7	0.28	4.501	0.13	0.308	0.0086	0.5418	0.1057	0.0015	1729	24	1730	43	1727	23	-0.17
126-121c	191	32.09	0.17	4.511	0.13	0.31	0.0086	0.3746	0.1044	0.0017	1731	25	1742	42	1706	29	-2.11
126-122r	206	27.7	0.13	3.8	0.24	0.2547	0.019	0.6079	0.1081	0.009	1591	75	1462	110	1765	98	17.17
132-123r	190	27.1	0.14	4.476	0.16	0.3064	0.01	0.5303	0.1042	0.002	1726	31	1722	52	1699	34	-1.35

[a]U-Pb fractionation correction and correction for background interference based on GJ-1 zircon standard (Jackson et al., 2004)

[b]Discordance % for 206Pb/238U ages >1Ga calculated as ((1-(206Pb/238U)/(207Pb/206Pb))*100)

Appendix B: Zircon/Apatite LA-ICP-MS U-Pb Isotopic Data and Ages

Table B-2. QPC (BR060913-08) Zr

Grain # - Spot #	U [ppm]	Th [ppm]	Th/U	Corrected isotope ratios[a]							Ages (Ma)						
				$^{207}Pb/^{235}U$	±2s	$^{206}Pb/^{238}U$	±2s	Rho	$^{207}Pb/^{206}Pb$	±2s	$^{207}Pb/^{235}U$	±2s	$^{206}Pb/^{238}U$	±2s	$^{207}Pb/^{206}Pb$	±2s	Disc. %[b]
001-1r	377	154.2	0.40902	3.256	0.13	0.189	0.007	0.77659	0.1253	0.0018	1469	32	1115	38	2031	25	45.1
002-1r	1990	1950	0.9799	2.02	0.16	0.0723	0.0073	0.98402	0.2171	0.0072	1093	54	446	44	2935	54	84.8
003-2c	488	505	1.03484	2.91	0.17	0.142	0.012	0.89787	0.1548	0.0064	1371	47	851	65	2384	71	64.3
004-2c	1914	744	0.38871	2.814	0.11	0.0802	0.0028	0.44101	0.2551	0.0048	1360	29	497.4	16	3209	30	84.5
005-1r	141	42.2	0.29929	4.9	0.18	0.3199	0.01	0.64718	0.1106	0.0014	1803	32	1789	51	1811	23	1.2
005-2m	165.5	51.51	0.31124	4.387	0.17	0.3033	0.0099	0.58051	0.1049	0.0014	1710	31	1707	49	1713	24	0.4
005-3c	178.8	57.8	0.32327	4.03	0.21	0.2714	0.016	0.58348	0.107	0.0029	1638	54	1548	86	1747	45	11.4
006-1r	159.8	25.81	0.16151	4.311	0.17	0.2966	0.0094	0.63256	0.1048	0.0015	1693	32	1674	47	1715	26	2.4
006-2c	84	59	0.70238	3.55	0.19	0.219	0.013	0.91232	0.1202	0.0062	1542	55	1272	74	1959	71	35.1
007-1r	437	232.1	0.53112	3.96	0.16	0.2029	0.0092	0.72163	0.1405	0.004	1623	35	1190	51	2227	47	46.6
007-2c	768	611	0.79557	2.88	0.19	0.1121	0.0071	0.96371	0.1869	0.0026	1357	48	682	41	2716	24	74.9
008-1c	136.3	42.5	0.31181	4.359	0.16	0.3019	0.0098	0.66472	0.1047	0.001	1703	31	1702	48	1707	18	0.3
008-2r	185	36.8	0.19892	4.171	0.16	0.2893	0.0094	0.70191	0.1046	0.0014	1670	31	1637	47	1705	25	4.0
009-1c	207	183.8	0.88792	3.76	0.16	0.2451	0.0094	0.7831	0.1126	0.0018	1581	35	1412	50	1837	29	23.1
010-1r	2480	1196	0.48226	2.327	0.11	0.0605	0.0029	0.90685	0.279	0.0031	1218	39	378.4	18	3356	18	88.7
010-2c	137.1	37.29	0.27199	4.366	0.17	0.3007	0.0098	0.56286	0.1046	0.0015	1704	32	1694	49	1709	26	0.9
011-1r	3360	1860	0.55357	1.75	0.19	0.0434	0.0054	0.9921	0.3022	0.0058	1002	68	272	33	3477	30	92.2
012-1c	281	85.4	0.30391	4.09	0.21	0.2674	0.018	0.61415	0.109	0.01	1650	52	1527	99	1787	110	14.5
013-1c	646	350	0.5418	2.91	0.14	0.1301	0.0056	0.74593	0.1597	0.0029	1378	35	788	33	2449	32	67.8
014-1r	112.3	32	0.28495	4.279	0.17	0.2951	0.0096	0.56742	0.1042	0.0017	1686	33	1666	48	1705	30	2.3
014-2c	118	38.6	0.32712	4.24	0.17	0.2947	0.0097	0.59078	0.1044	0.0015	1679	33	1664	48	1701	28	2.2
015-1c	180.6	68.4	0.37874	4.28	0.18	0.2551	0.012	0.64212	0.1225	0.0048	1694	37	1464	62	1988	57	26.4
016-1r	2090	1309	0.62632	2.143	0.08	0.05457	0.0018	0.5997	0.2842	0.0029	1164	27	342.5	11	3387	16	89.9
016-2c	2250	1160	0.51556	2.4	0.13	0.0646	0.0039	0.982	0.2708	0.0036	1235	41	403	24	3307	21	87.8
017-1c	218	35.1	0.16101	4.368	0.16	0.3027	0.0096	0.61705	0.1045	0.0011	1705	31	1706	47	1709	19	0.2
018-1c	145	48.2	0.33241	4.365	0.17	0.3016	0.01	0.66124	0.1061	0.0014	1710	32	1698	50	1729	23	1.8
019-1r	257	57.5	0.22374	4.228	0.22	0.259	0.018	0.63195	0.119	0.0099	1678	53	1484	100	1934	100	23.3
019-2c	266	107	0.40226	2.55	0.14	0.1303	0.0091	0.95749	0.1413	0.0032	1280	40	786	51	2234	40	64.8
020-1r	2780	1729	0.62194	2.359	0.098	0.0611	0.0023	0.91808	0.2799	0.0028	1229	30	382.2	14	3360	16	88.6
020-2c	144.9	35.42	0.24444	4.265	0.16	0.2954	0.0093	0.69496	0.104	0.001	1685	31	1668	46	1696	18	1.7
021-1r	173.9	63.6	0.36573	4.9	0.18	0.3151	0.011	0.51609	0.114	0.002	1798	33	1765	54	1855	31	4.9
022-1m	374.1	76.4	0.20422	4.2	0.19	0.2825	0.016	0.68787	0.1114	0.0087	1672	48	1603	90	1826	94	12.2
022-2c	170	145.6	0.85647	4.076	0.21	0.2641	0.017	0.40115	0.1111	0.0091	1649	55	1511	95	1816	97	16.8
023-1c	219.8	137	0.62329	3.567	0.15	0.2217	0.0091	0.88335	0.1163	0.0014	1542	34	1295	48	1896	22	31.7
023-2r	1970	1641	0.83299	2.245	0.12	0.0633	0.0034	0.97386	0.2576	0.0024	1186	37	395	20	3230	15	87.8
024-1c	337	109.3	0.32433	3.936	0.15	0.2283	0.0077	0.6398	0.1247	0.0016	1622	31	1325	40	2025	23	34.6
025-1c	174	20.3	0.11667	3.795	0.14	0.2461	0.011	0.67841	0.1121	0.006	1590	31	1417	59	1827	75	22.4
026-1c	105.1	38.52	0.36651	4.318	0.17	0.3011	0.0096	0.55115	0.104	0.0014	1698	31	1696	48	1699	25	0.2
027-1r	176	26.71	0.15176	4.244	0.16	0.2947	0.0097	0.62211	0.105	0.0016	1681	33	1665	49	1713	28	2.8
028-1c	310	85.7	0.27645	4.356	0.18	0.2828	0.014	0.60842	0.1116	0.0056	1702	35	1605	74	1823	69	12.0

Appendix B: Zircon/Apatite LA-ICP-MS U-Pb Isotopic Data and Ages

Table B-2. QPC (BR060913-08) Zr

Grain # - Spot #	U [ppm]	Th [ppm]	Th/U	Corrected isotope ratios[a] $^{207}Pb/^{235}U$	±2s	$^{206}Pb/^{238}U$	±2s	Rho	$^{207}Pb/^{206}Pb$	±2s	Ages (Ma) $^{207}Pb/^{235}U$	±2s	$^{206}Pb/^{238}U$	±2s	$^{207}Pb/^{206}Pb$	±2s	Disc. %[b]
029-1r	386	247.2	0.64041	4.031	0.16	0.2274	0.012	0.33324	0.1279	0.0089	1639	33	1320	68	2061	92	36.0
029-2c	114.2	87.8	0.76883	4.135	0.16	0.2648	0.0092	0.55522	0.1135	0.0017	1661	32	1513	47	1862	27	18.7
030-1c	168.5	29.8	0.17685	4.454	0.17	0.3053	0.0098	0.6509	0.1053	0.0013	1722	32	1717	48	1719	23	0.1
030-2c	121.2	38.88	0.32079	4.358	0.17	0.3006	0.0098	0.66741	0.1046	0.0012	1705	31	1694	48	1705	21	0.6
031-1r	1920	1340	0.69792	2.179	0.093	0.0605	0.0026	0.85581	0.2645	0.0042	1171	29	378	16	3268	26	88.4
031-2c	107	30.5	0.28505	4.306	0.16	0.2951	0.0094	0.65924	0.1053	0.001	1693	30	1666	46	1720	18	3.1
032-1c	1980	976	0.49293	2.296	0.1	0.0659	0.0028	0.90778	0.2536	0.0027	1208	33	411	17	3205	17	87.2
033-1c	124.3	34.13	0.27458	4.345	0.16	0.3001	0.0096	0.5439	0.1053	0.0013	1702	30	1692	48	1718	22	1.5
034-1r	4140	2410	0.58213	1.029	0.096	0.0249	0.0027	0.99405	0.3068	0.0067	697	45	158	17	3506	33	95.5
035-1r	145	52.54	0.36234	4.435	0.18	0.3028	0.013	0.72496	0.1066	0.0035	1719	36	1705	70	1745	54	2.3
036-1r	454	86.3	0.19009	4.232	0.16	0.2347	0.0077	0.42381	0.131	0.0026	1679	31	1359	41	2107	33	35.5
036-2c	164.4	43.36	0.26375	4.654	0.17	0.2919	0.0092	0.65883	0.1157	0.0013	1760	32	1650	46	1892	20	12.8
037-1c	113	36.07	0.3192	4.57	0.17	0.3168	0.01	0.63483	0.1041	0.0011	1743	31	1774	49	1698	19	-4.5
038-1c	131	33.48	0.25557	4.378	0.17	0.3008	0.0098	0.67457	0.1063	0.0013	1708	32	1695	49	1733	22	2.2
038-2c	111.9	29.6	0.26452	4.389	0.17	0.3018	0.0098	0.70064	0.1056	0.0013	1708	32	1699	48	1724	23	1.5
039-1c	255	225.5	0.88431	3.8	0.16	0.2429	0.011	0.57561	0.1126	0.0053	1590	35	1401	58	1836	65	23.7
039-2r	1303	1220	0.9363	3.046	0.11	0.0926	0.0031	0.8607	0.2372	0.0017	1418.2	28	571.8	18	3100	12	81.6
040-1c	292	56.9	0.19486	4.235	0.16	0.272	0.0087	0.44586	0.1126	0.0015	1681	31	1550	44	1841	24	15.8
041-1r	228	24.86	0.10904	4.27	0.16	0.2952	0.0093	0.59423	0.1054	0.0012	1686	31	1667	46	1725	20	3.4
041-2c	93.6	33.05	0.3531	4.273	0.18	0.2949	0.0093	0.50791	0.1052	0.0019	1686	33	1666	45	1713	32	2.7
042-1c	2400	1110	0.4625	1.86	0.21	0.067	0.012	0.99158	0.249	0.014	1019	65	411	69	3101	98	86.7
043-1c	154.8	26.64	0.17209	4.398	0.17	0.3041	0.0097	0.61915	0.1049	0.0011	1711	31	1711	48	1714	20	0.2
043-2r	2000	1290	0.645	2.42	0.09	0.06526	0.0021	0.75744	0.2688	0.0024	1248.6	26	407.5	13	3298	14	87.6
044-1c	238.3	70.6	0.29627	4.291	0.29	0.2951	0.024	0.61391	0.1064	0.012	1690	78	1670	130	1734	130	3.7
045-1c	420	190	0.45238	3.247	0.13	0.1704	0.0064	0.72658	0.1381	0.0021	1469	31	1013	35	2203	27	54.0
045-2r	1501	671	0.44704	2.261	0.088	0.068	0.0026	0.82977	0.2412	0.0029	1200	28	425.2	15	3130	19	86.4
046-1c	214.7	96	0.44714	4.333	0.18	0.2814	0.012	0.56355	0.1115	0.0029	1697	35	1598	63	1819	45	12.1
046-2r	1693	515	0.30419	2.402	0.091	0.06841	0.0023	0.79648	0.2545	0.0025	1246	26	426.5	14	3211	16	86.7
047-1c	149.9	52.91	0.35297	4.387	0.16	0.2892	0.0091	0.51645	0.1104	0.0013	1710	30	1639	46	1804	21	9.1
047-2r	1540	601	0.39026	1.425	0.07	0.0548	0.003	0.95134	0.1905	0.003	895	29	343	18	2747	25	87.5
048-1c	109	40	0.36697	4.84	0.46	0.3216	0.012	0.2649	0.1088	0.0067	1787	62	1797	59	1767	89	-1.7
048-2r	104.6	22.68	0.21683	4.547	0.17	0.314	0.011	0.65606	0.1057	0.0013	1738	32	1759	52	1726	23	-1.9
049-1r	1366	1769	1.29502	2.325	0.096	0.0814	0.0034	0.64297	0.206	0.004	1218	30	504.3	21	2874	29	82.5
049-2c	1174	1230	1.0477	2.086	0.099	0.0677	0.0033	0.91394	0.2218	0.0035	1141	33	422	20	2991	25	85.9
050-1c	153.1	86.7	0.5663	4.37	0.22	0.2478	0.011	0.85274	0.1283	0.0017	1702	48	1427	60	2076	24	31.3
051-1r	1226	359	0.29282	3.192	0.12	0.1014	0.0033	0.57334	0.2283	0.0027	1454	29	622.3	19	3041	19	79.5
051-2m	185.9	155.5	0.83647	3.646	0.14	0.2423	0.0078	0.58399	0.1088	0.0014	1565	32	1398	41	1783	23	21.6
051-3r	298	189.7	0.63658	3.68	0.18	0.2279	0.015	0.65428	0.1177	0.0066	1564	49	1331	81	1925	76	30.9
052-1r	2890	1823	0.6308	1.306	0.056	0.03091	0.0011	0.85131	0.3105	0.0046	848	25	196.2	7	3519	23	94.4
053-1c	194.2	65.9	0.33934	4.264	0.16	0.2909	0.0094	0.5464	0.1058	0.0016	1684	32	1646	48	1724	28	4.5
053-2r	209.6	28.1	0.13406	4.14	0.17	0.2584	0.012	0.50353	0.1161	0.0047	1661	36	1482	67	1892	61	21.7

Appendix B: Zircon/Apatite LA-ICP-MS U-Pb Isotopic Data and Ages

Table B-2. QPC (BR060913-08) Zr

				Corrected isotope ratios[a]							Ages (Ma)						
Grain # - Spot #	U [ppm]	Th [ppm]	Th/U	$^{207}Pb/^{235}U$	±2s	$^{206}Pb/^{238}U$	±2s	Rho	$^{207}Pb/^{206}Pb$	±2s	$^{207}Pb/^{235}U$	±2s	$^{206}Pb/^{238}U$	±2s	$^{207}Pb/^{206}Pb$	±2s	Disc. %[b]
054-1c	84.3	30.7	0.36418	4.335	0.17	0.2951	0.0095	0.57232	0.1056	0.0017	1697	33	1666	48	1727	29	3.5
054-2m	283	30.6	0.10813	4.319	0.17	0.289	0.0093	0.61943	0.1078	0.0015	1699	32	1636	47	1761	26	7.1
055-1c	88.4	32.41	0.36663	4.3	0.17	0.2993	0.0098	0.65107	0.1042	0.0015	1695	33	1687	48	1695	26	0.5
056-1c	1160	811	0.69914	2.854	0.12	0.0954	0.0041	0.7927	0.2144	0.0041	1367	31	587	24	2942	31	80.0
057-1c	152	222	1.46053	3.674	0.15	0.2439	0.0084	0.81482	0.1091	0.0014	1565	33	1406	44	1784	23	21.2
058-1c	1208	1297	1.07368	1.98	0.13	0.0644	0.0046	0.96891	0.2257	0.004	1100	45	401	28	3021	28	86.7
059-1c	73.9	25.56	0.34587	4.315	0.17	0.2952	0.0095	0.45179	0.1062	0.0016	1696	31	1667	47	1729	27	3.6
060-1c	187.2	194	1.03632	3.41	0.17	0.2269	0.011	0.92054	0.1113	0.0016	1505	40	1314	59	1820	27	27.8
061-1r	143.4	32.78	0.22859	4.224	0.16	0.2906	0.0093	0.5648	0.1052	0.0015	1681	32	1644	47	1718	27	4.3
061-2c	211	29.3	0.13886	3.772	0.21	0.2362	0.015	0.64568	0.1152	0.0052	1584	56	1372	85	1883	65	27.1
062-1r	166.4	27.3	0.16406	4.313	0.17	0.2962	0.0095	0.60154	0.1051	0.0014	1694	32	1672	47	1711	24	2.3
063-1c	188	27.7	0.14734	4.253	0.16	0.2931	0.0096	0.63002	0.1045	0.0015	1683	31	1657	46	1700	26	2.5
063-1r	326	93	0.28528	3.913	0.15	0.2131	0.0078	0.55224	0.1318	0.0024	1616	32	1245	42	2117	31	41.2
064-1c	1058	652	0.61626	2.536	0.11	0.0935	0.0045	0.80808	0.1994	0.0047	1281	32	575	27	2808	40	79.5
064-1r	1080	327	0.30278	3.06	0.15	0.1033	0.0063	0.89209	0.2177	0.0059	1425	36	632	37	2958	45	78.6
065-1c	145.7	70.5	0.48387	3.898	0.15	0.2503	0.01	0.53266	0.1118	0.0027	1611	34	1440	55	1832	39	21.4
066-1c	214.5	91	0.42424	3.112	0.14	0.1657	0.0083	0.55572	0.1352	0.0031	1434	37	988	47	2171	36	54.5
066-2r	332	91.7	0.2762	3.697	0.14	0.2218	0.0075	0.61111	0.1201	0.0018	1572	30	1291	40	1959	26	34.1
067-1r	384	156	0.40625	3.41	0.16	0.1832	0.01	0.85533	0.1379	0.0036	1506	34	1085	57	2196	45	50.6
067-2c	149.1	34.5	0.23139	4.217	0.16	0.2901	0.0096	0.63814	0.105	0.0013	1677	33	1644	48	1713	24	4.0
068-1c	91.5	28.3	0.30929	4.314	0.16	0.2957	0.0097	0.58218	0.1051	0.0015	1697	32	1670	49	1712	25	2.5
069-1r	388	238	0.6134	3.792	0.15	0.1944	0.0082	0.62303	0.1404	0.0032	1594	32	1143	44	2229	40	48.7
069-2c	603	690	1.14428	2.24	0.16	0.0996	0.0068	0.86777	0.1691	0.0062	1192	50	610	40	2553	61	76.1
070-1c	145.3	28.8	0.19821	4.23	0.17	0.2858	0.011	0.5567	0.1057	0.0016	1678	35	1620	57	1722	28	5.9
071-1c	199	72.4	0.36382	3.977	0.16	0.2705	0.01	0.64134	0.107	0.0016	1630	35	1548	54	1744	26	11.2
072-1r	249	31.8	0.12771	4.173	0.16	0.2866	0.0093	0.53238	0.1054	0.0014	1668	32	1624	46	1722	25	5.7
072-2r	169.1	70.7	0.4181	4.336	0.16	0.2908	0.0093	0.59603	0.1071	0.0011	1699	31	1645	47	1751	19	6.1
072-3c	91.3	86.5	0.94743	3.578	0.14	0.2386	0.0077	0.5144	0.1078	0.0016	1546	31	1379	40	1764	27	21.8
073-1c	101.3	32.7	0.3228	4.293	0.16	0.296	0.0094	0.57827	0.1042	0.0012	1693	32	1671	47	1702	22	1.8
074-1c	53.8	22.5	0.41822	4.272	0.17	0.2936	0.012	0.45473	0.1045	0.0021	1686	34	1659	59	1709	35	2.9
075-1r	1760	990	0.5625	2.42	0.096	0.0719	0.0025	0.7316	0.2438	0.0033	1247	28	447.4	15	3146	21	85.8
075-2c	148.1	74.5	0.50304	4.23	0.17	0.286	0.011	0.68846	0.1079	0.0021	1681	32	1621	57	1760	34	7.9
076-1r	2820	1164	0.41277	2.412	0.095	0.06177	0.0021	0.76416	0.2839	0.0032	1246	28	386.3	13	3382	17	88.6
076-2c	98.9	34.25	0.34631	4.13	0.16	0.2856	0.0095	0.63303	0.1045	0.0015	1660	32	1619	47	1708	26	5.2
077-1c	137.3	139.4	1.01529	3.738	0.15	0.2449	0.0079	0.57934	0.1097	0.0014	1579	31	1412	41	1793	23	21.2
078-1c	114.2	34	0.29772	4.388	0.17	0.303	0.0097	0.63457	0.1045	0.0014	1710	32	1706	48	1700	24	-0.4
079-1m	973	1013	1.04111	2.081	0.088	0.079	0.0034	0.76755	0.1917	0.0039	1142	29	490	20	2755	32	82.2
079-2c	703	532	0.75676	3.191	0.12	0.1317	0.005	0.62924	0.1779	0.0033	1453	30	799	29	2629	30	69.6
080-1c	124.3	47.5	0.38214	4.153	0.15	0.2888	0.0093	0.62481	0.1047	0.0011	1664	30	1635	47	1707	19	4.2
081-1c	107.9	54	0.50046	4.809	0.19	0.3202	0.01	0.59064	0.1091	0.0015	1784	33	1790	50	1783	24	-0.4

Appendix B: Zircon/Apatite LA-ICP-MS U-Pb Isotopic Data and Ages

Table B-2. QPC (BR060913-08) Zr

Grain # - Spot #	U [ppm]	Th [ppm]	Th/U	Corrected isotope ratios[a]							Ages (Ma)						
				$^{207}Pb/^{235}U$	±2s	$^{206}Pb/^{238}U$	±2s	Rho	$^{207}Pb/^{206}Pb$	±2s	$^{207}Pb/^{235}U$	±2s	$^{206}Pb/^{238}U$	±2s	$^{207}Pb/^{206}Pb$	±2s	Disc. %[b]
082-1c	119.9	38.4	0.32027	4.433	0.17	0.3053	0.0097	0.71383	0.1047	0.0011	1717	31	1717	48	1707	19	-0.6
082-2r	201.3	30.59	0.15196	4.401	0.16	0.3036	0.0095	0.59201	0.10518	0.00089	1712.6	30	1709	47	1717	15	0.5
083-1c	268.8	36.7	0.13653	4.319	0.16	0.2876	0.0094	0.61605	0.1089	0.0012	1699	30	1629	47	1781	21	8.5
084-1c	214	163.6	0.76449	3.7	0.14	0.2442	0.0081	0.63388	0.1105	0.0018	1569	31	1408	43	1806	28	22.0
085-1c	113.3	49.4	0.43601	4.491	0.17	0.3059	0.0098	0.63778	0.1058	0.0012	1728	31	1722	49	1727	20	0.3
085-2r	66.4	20.99	0.31611	4.447	0.17	0.3129	0.01	0.64791	0.1041	0.0012	1725	32	1756	50	1697	21	-3.5
086-1c	294	135.3	0.4602	4.344	0.18	0.2664	0.011	0.60768	0.1186	0.0027	1701	38	1522	59	1934	37	21.3
087-1c	150.1	50.8	0.33844	4.341	0.16	0.3035	0.0098	0.60377	0.1037	0.0012	1701	31	1708	48	1691	21	-1.0
088-1c	255.6	155.4	0.60798	2.765	0.14	0.1557	0.007	0.92473	0.1278	0.0017	1340	38	931	39	2064	23	54.9
088-2r	2470	587	0.23765	2.762	0.1	0.07183	0.0023	0.79314	0.2796	0.0025	1344	28	447.1	14	3359	14	86.7
089-1c	773	503	0.65071	2.641	0.11	0.1021	0.0054	0.7876	0.1901	0.0053	1309	31	626	32	2729	47	77.1
089-2r	2345	1079	0.46013	2.335	0.1	0.061	0.0027	0.91769	0.2822	0.0034	1221	31	381	16	3375	19	88.7
090-1c	75.6	39.7	0.52513	4.509	0.17	0.3114	0.01	0.66308	0.105	0.001	1731	31	1749	49	1711	18	-2.2
090-2r	259.4	72.2	0.27833	4.214	0.16	0.2782	0.0091	0.71469	0.1091	0.0011	1676	31	1582	46	1784	19	11.3
091-1r	127.1	45.8	0.36035	4.385	0.17	0.3027	0.0098	0.64243	0.105	0.0013	1709	32	1704	49	1717	24	0.8
092-1c	70.3	29.91	0.42546	4.543	0.17	0.3153	0.01	0.69629	0.105	0.0011	1737	32	1766	50	1711	20	-3.2
092-2r	500	148.8	0.2976	3.555	0.13	0.1777	0.006	0.64991	0.1476	0.002	1538	30	1054	33	2317	24	54.5
093-1c	176.4	53	0.30045	4.354	0.17	0.2867	0.0097	0.66467	0.1099	0.0018	1702	33	1624	49	1797	31	9.6
093-2r	201.7	25.89	0.12836	4.452	0.17	0.3039	0.0098	0.60574	0.1068	0.0014	1720	32	1710	49	1751	23	2.3
094-1c	2830	1090	0.38516	1.78	0.15	0.0486	0.0046	0.98085	0.2793	0.0068	1020	56	304	28	3351	38	90.9
095-1c	160.3	65	0.40549	4.57	0.17	0.3081	0.01	0.66003	0.1077	0.0014	1746	32	1731	49	1756	24	1.4
095-2r	175	48	0.27429	4.238	0.18	0.2891	0.018	0.65597	0.1065	0.0082	1680	36	1637	94	1742	100	6.0
096-1c	600	169	0.28167	3.211	0.12	0.1421	0.0051	0.37324	0.1623	0.0036	1458	30	856	29	2477	38	65.4
096-2m	128	24.3	0.18984	4.313	0.16	0.2969	0.0095	0.59513	0.1058	0.0011	1696	31	1675	47	1728	19	3.1
096-3r	308	296.5	0.96266	3.246	0.14	0.1787	0.007	0.83446	0.1338	0.0018	1466	33	1059	38	2144	24	50.6
097-1c	280	42	0.15	4.33	0.17	0.283	0.0094	0.63233	0.1104	0.0015	1697	32	1606	47	1804	24	11.0
098-1c	68.5	22.56	0.32934	4.538	0.17	0.317	0.01	0.61878	0.1037	0.0012	1738	31	1775	49	1694	22	-4.8
098-2m	203.4	35.8	0.17601	4.518	0.2	0.3083	0.018	0.59517	0.1063	0.0076	1732	37	1732	92	1732	96	0.0
098-3r	4430	2340	0.52822	1.34	0.11	0.031	0.0031	0.9871	0.3272	0.0072	846	45	196	19	3598	34	94.6
099-1c	142	34.4	0.24225	4.411	0.16	0.3072	0.0097	0.59489	0.1047	0.00093	1713	31	1727	48	1709	17	-1.1
099-2r	1205	459	0.38091	2.101	0.084	0.0773	0.0028	0.71842	0.195	0.0028	1147	27	479.6	16	2783	23	82.8
100-1c	89.5	32.9	0.3676	4.347	0.16	0.301	0.0095	0.5366	0.1053	0.0013	1702	32	1696	47	1717	23	1.2
100-2r	1990	1174	0.58995	2.035	0.078	0.05757	0.0019	0.76508	0.2587	0.0027	1129	27	360.8	12	3240	16	88.9
101-2c	105.1	53.9	0.51284	4.203	0.16	0.2923	0.0094	0.58842	0.1047	0.0013	1673	31	1653	47	1706	23	3.1
101-2r	96.6	29.9	0.30952	4.393	0.17	0.3042	0.0098	0.57215	0.1043	0.0013	1709	32	1712	48	1700	23	-0.7
102-1c	167.7	174	1.03757	3.842	0.16	0.2539	0.0096	0.86732	0.1096	0.0013	1598	32	1457	49	1794	21	18.8
102-2r	142.5	25.28	0.1774	4.487	0.17	0.3094	0.0098	0.69661	0.1049	0.0012	1727	32	1738	48	1709	21	-1.7
103-1c	79.4	30.24	0.38086	4.435	0.17	0.3045	0.0097	0.5308	0.1048	0.0013	1717	31	1713	48	1707	22	-0.4
103-2r	303	181	0.59736	3.946	0.16	0.2567	0.011	0.8906	0.1123	0.0014	1624	33	1475	55	1836	23	19.7
104-1c	740	644	0.87027	2.57	0.14	0.1093	0.0078	0.95507	0.1755	0.0046	1281	40	666	45	2613	46	74.5

Appendix B: Zircon/Apatite LA-ICP-MS U-Pb Isotopic Data and Ages

Table B-2. QPC (BR060913-08) Zr

				Corrected isotope ratios[a]							Ages (Ma)						
Grain # - Spot #	U [ppm]	Th [ppm]	Th/U	$^{207}Pb/^{235}U$	±2s	$^{206}Pb/^{238}U$	±2s	Rho	$^{207}Pb/^{206}Pb$	±2s	$^{207}Pb/^{235}U$	±2s	$^{206}Pb/^{238}U$	±2s	$^{207}Pb/^{206}Pb$	±2s	Disc. %[b]
104-2r	2050	1119	0.54585	2.341	0.097	0.0646	0.0023	0.92605	0.2639	0.0026	1224	30	403.6	14	3268	15	87.6
105-1c	139.5	47.5	0.3405	4.479	0.17	0.3065	0.011	0.66827	0.106	0.0015	1727	33	1723	53	1729	26	0.3
105-2r	2940	1242	0.42245	1.761	0.093	0.0471	0.0025	0.96752	0.2747	0.0029	1029	35	297	16	3333	17	91.1
106-1c	238	40.5	0.17017	4.209	0.16	0.2874	0.0092	0.60908	0.1061	0.0013	1674	31	1628	46	1732	22	6.0
107-1c	313	163.8	0.52332	2.956	0.12	0.1424	0.006	0.62549	0.1508	0.0035	1394	30	857	34	2355	39	63.6
107-2r	415	61.3	0.14771	4.14	0.16	0.2498	0.011	0.67737	0.1202	0.0036	1665	34	1437	58	1963	46	26.8
108-1c	103.2	80.5	0.78004	4.04	0.18	0.2737	0.016	0.65428	0.1069	0.0063	1640	43	1559	84	1744	76	10.6
108-2r	175.1	78	0.44546	4.235	0.16	0.2832	0.0089	0.47317	0.1084	0.0014	1683	30	1607	45	1775	23	9.5
109-1c	1360	1070	0.78676	2.36	0.13	0.0829	0.0056	0.95893	0.2143	0.0056	1238	40	515	34	2930	41	82.4
109-2r	536	249	0.46455	3.224	0.13	0.1271	0.0047	0.73907	0.1823	0.0028	1462	30	771	27	2674	26	71.2
110-1c	87.3	24.25	0.27778	4.388	0.16	0.3041	0.0097	0.62851	0.10441	0.0009	1710.1	30	1711	48	1704	16	-0.4
110-2r	248	50.4	0.20323	4.353	0.16	0.3011	0.0095	0.64081	0.1058	0.0012	1702	31	1696	47	1724	21	1.6
111-1c	124.6	75.7	0.60754	4.36	0.2	0.2987	0.014	0.50372	0.1057	0.003	1710	39	1684	73	1727	47	2.5
111-2r	1290	560	0.43411	2.72	0.15	0.123	0.013	0.96276	0.19	0.013	1322	42	743	73	2630	110	71.7
112-1c	21.3	7.4	0.34742	4.26	0.77	0.0667	0.006	0.84809	0.409	0.043	1493	99	406	30	3820	140	89.4
112-2m	552	324.7	0.58822	2.922	0.13	0.1472	0.0071	0.86965	0.1465	0.0032	1385	34	883	40	2300	37	61.6
112-3r	2710	1194	0.44059	2.245	0.087	0.0576	0.002	0.91905	0.2829	0.002	1195	27	360.7	12	3379	11	89.3
113-1c	173.3	52.6	0.30352	4.37	0.35	0.2972	0.013	0.68417	0.1059	0.0046	1704	31	1677	66	1731	48	3.1
113-2r	1850	701	0.37892	2.2	0.17	0.0754	0.0081	0.96833	0.2274	0.0085	1156	53	465	48	3015	62	84.6
114-1c	204	207	1.01471	3.452	0.14	0.2259	0.008	0.73894	0.1107	0.0015	1519	31	1314	42	1809	24	27.4
115-1c	727	465	0.63961	2.937	0.11	0.1057	0.0034	0.39603	0.2017	0.0031	1393	29	647.7	20	2838	26	77.2
116-1c	134.1	50.1	0.3736	4.155	0.18	0.2837	0.0099	0.35329	0.1064	0.0024	1666	34	1610	50	1743	37	7.6
116-2re	100.2	29.63	0.29571	4.747	0.18	0.3201	0.01	0.75721	0.1067	0.0011	1774	33	1792	51	1744	19	-2.8
117-1c	114.9	38.3	0.33333	4.346	0.16	0.3007	0.0097	0.5367	0.1049	0.0012	1701	31	1696	47	1713	21	1.0
118-1c	223	140	0.6278	3.632	0.14	0.2405	0.008	0.67178	0.1094	0.0013	1556	30	1389	42	1790	20	22.4
119-1c	349.3	162.1	0.46407	4.071	0.16	0.2467	0.01	0.69832	0.1206	0.0024	1648	31	1419	52	1962	35	27.7
119-2r	1790	919	0.51341	2.116	0.084	0.0611	0.0023	0.68951	0.2521	0.0038	1152	27	382.3	14	3198	24	88.0
120-1c	86	32.8	0.3814	4.423	0.17	0.3036	0.0098	0.50865	0.105	0.0014	1715	32	1709	49	1716	24	0.4
121-1c	605	416	0.6876	2.94	0.17	0.137	0.011	0.94029	0.1643	0.0056	1388	45	824	62	2478	58	66.7
121-2r	650	479	0.73692	2.843	0.13	0.1405	0.0065	0.68891	0.1511	0.0043	1363	36	850	36	2344	50	63.7
122-1r	225.6	32.7	0.14495	4.367	0.18	0.2999	0.011	0.66909	0.1053	0.0017	1705	35	1691	56	1716	28	1.5
123-1c	239	202.3	0.84644	3.728	0.14	0.231	0.008	0.59769	0.1165	0.0016	1577	30	1339	43	1906	25	29.7
123-2r	3180	2252	0.70818	1.138	0.043	0.03269	0.0012	0.64259	0.2571	0.0043	772	21	207.3	7.6	3228	26	93.6
124-1c	71.9	23.8	0.33102	4.513	0.17	0.314	0.01	0.5292	0.1044	0.0015	1731	32	1760	49	1705	26	-3.2
124-2c	178	39.5	0.22191	4.256	0.16	0.2922	0.0094	0.62475	0.1054	0.0012	1685	31	1652	48	1722	21	4.1
125-1c	195.2	32.92	0.16865	4.383	0.17	0.2978	0.0097	0.63771	0.1068	0.0013	1707	31	1680	47	1747	22	3.8
126-1c	7120	4270	0.59972	0.428	0.032	0.00804	0.0007	0.99052	0.3891	0.0062	357	22	51.6	4.4	3866	24	98.7
127-1c	119.8	37	0.30885	4.462	0.17	0.3088	0.0096	0.53224	0.1049	0.0012	1726	32	1734	47	1712	21	-1.3
128-1c	1610	1440	0.89441	2.81	0.2	0.105	0.011	0.98303	0.2113	0.0092	1339	53	645	63	2888	70	77.7
129-1r	221.2	66.7	0.30154	4.268	0.16	0.2862	0.01	0.56464	0.1075	0.0021	1686	31	1622	51	1757	33	7.7

Appendix B: Zircon/Apatite LA-ICP-MS U-Pb Isotopic Data and Ages

Table B-2. QPC (BR060913-08) Zr

Grain # - Spot #	U [ppm]	Th [ppm]	Th/U	Corrected isotope ratios[a]							Ages (Ma)						
				$^{207}Pb/^{235}U$	±2s	$^{206}Pb/^{238}U$	±2s	Rho	$^{207}Pb/^{206}Pb$	±2s	$^{207}Pb/^{235}U$	±2s	$^{206}Pb/^{238}U$	±2s	$^{207}Pb/^{206}Pb$	±2s	Disc. %[b]
129-2c	176.3	158.4	0.89847	3.746	0.14	0.2518	0.0081	0.55963	0.1078	0.0013	1580	30	1447	41	1759	21	17.7
130-1c	2430	587	0.24156	2.684	0.11	0.0737	0.0036	0.91364	0.2654	0.0051	1321	30	458	21	3276	31	86.0
130-2r	3350	1150	0.34328	2.06	0.12	0.0507	0.0031	0.99071	0.2964	0.0023	1125	43	318	19	3450	12	90.8
131-1c	1430	920	0.64336	2.89	0.15	0.124	0.012	0.91647	0.194	0.012	1377	40	755	70	2700	100	72.0
132-1c	120.5	34.7	0.28797	4.508	0.18	0.3108	0.01	0.77295	0.1046	0.0012	1730	32	1744	51	1703	21	-2.4
132-2r	230	31	0.13478	4.461	0.16	0.3062	0.0097	0.53998	0.1063	0.0012	1724	31	1722	48	1736	20	0.8
133-1c	554	429	0.77437	3.052	0.14	0.1266	0.0066	0.61446	0.1768	0.0061	1420	34	770	37	2616	59	70.6
133-2r	331	142	0.429	4.203	0.16	0.2656	0.0087	0.60344	0.1139	0.0014	1674	31	1518	44	1864	23	18.6
134-1c	553	335	0.60579	3.16	0.17	0.16	0.015	0.92245	0.165	0.012	1444	44	943	83	2420	110	61.0
135-1c	164	33.7	0.20549	4.365	0.16	0.3018	0.0095	0.46048	0.1045	0.0014	1705	31	1700	47	1701	25	0.1
135-2r	1074	437	0.40689	3.041	0.14	0.104	0.0067	0.89173	0.2176	0.0055	1414	36	636	39	2959	42	78.5
137-1c	238.5	24.6	0.10314	4.387	0.18	0.2992	0.011	0.56408	0.1066	0.003	1708	34	1687	55	1738	40	2.9
137-2r	1322	427	0.323	2.431	0.13	0.0828	0.0046	0.93291	0.2152	0.0034	1251	38	512	27	2940	25	82.6
138-1r	3050	1180	0.38689	2.329	0.096	0.0607	0.0022	0.89888	0.2788	0.0027	1223	29	379.5	14	3354	15	88.7
138-2c	633	245	0.38705	3.136	0.13	0.1587	0.0077	0.80632	0.1449	0.0036	1437	33	955	43	2278	42	58.1
139-1c	202	28.7	0.14208	4.426	0.17	0.3055	0.0097	0.58097	0.1059	0.0016	1715	32	1718	48	1723	28	0.3
140-1c	2260	1730	0.76549	1.954	0.08	0.0556	0.0021	0.83542	0.2564	0.0032	1097	28	348.8	13	3224	19	89.2
140-2r	914	562	0.61488	2.968	0.12	0.1098	0.0041	0.73511	0.1966	0.0032	1398	31	671	24	2795	27	76.0
141-1c	220	75.3	0.34227	3.99	0.2	0.237	0.015	0.8614	0.1269	0.0038	1630	42	1361	80	2031	54	33.0
142-1c	486	129.3	0.26605	3.989	0.16	0.2042	0.01	0.48195	0.1451	0.0045	1631	33	1199	55	2277	54	47.3
143-1c	102.1	32.89	0.32214	4.402	0.17	0.3067	0.0099	0.53486	0.1034	0.0013	1711	32	1724	49	1681	24	-2.6
144-1c	1300	1130	0.86923	1.49	0.16	0.065	0.011	0.96984	0.193	0.011	893	60	401	63	2707	97	85.2
144-2r	1794	1290	0.71906	2.514	0.11	0.0722	0.0025	0.81258	0.25	0.0044	1274	32	449.2	15	3181	28	85.9
145-1c	833	330	0.39616	3.36	0.17	0.1286	0.0073	0.94691	0.1901	0.0035	1490	40	777	42	2746	30	71.7
147-1c	454	120.1	0.26454	3.215	0.13	0.1592	0.006	0.75133	0.1472	0.002	1460	30	952	33	2321	24	59.0
148-1c	148.1	64.7	0.43687	4.391	0.17	0.2996	0.0098	0.56783	0.1065	0.0013	1709	33	1693	49	1737	22	2.5
149-1c	123.5	26.7	0.21619	4.444	0.17	0.3076	0.01	0.52541	0.1055	0.0016	1723	34	1728	49	1720	29	-0.5

[a]U-Pb fractionation correction and correction for background interference based on GJ-1 zircon standard (Jackson et al., 2004)

[b]Discordance % for 206Pb/238U ages >1Ga calculated as ((1-(206Pb/238U)/(207Pb/206Pb))*100)

Appendix B: Zircon/Apatite LA-ICP-MS U-Pb Isotopic Data and Ages

Table B-3. Quartzite (BR061013-01) Zr

				Corrected isotope ratios[a]							Ages (Ma)						
Grain # - Spot #	U [ppm]	Th [ppm]	Th/U	$^{207}Pb/^{235}U$	±2s	$^{206}Pb/^{238}U$	±2s	Rho	$^{207}Pb/^{206}Pb$	±2s	$^{207}Pb/^{235}U$	±2s	$^{206}Pb/^{238}U$	±2s	$^{207}Pb/^{206}Pb$	±2s	Disc. %[b]
002r	166	40	0.24096	4.493	0.062	0.3118	0.0035	0.44146	0.1055	0.0015	1729.8	11	1749	17	1720	26	-1.7
003r	242	82.5	0.34091	4.672	0.066	0.3208	0.0042	0.76878	0.10629	0.0013	1761.2	12	1793	20	1739	22	-3.1
006c	164	48.3	0.29451	4.637	0.06	0.3188	0.0036	0.56713	0.1058	0.0014	1757	11	1785	18	1728	24	-3.3
006r	225	43.8	0.19467	4.641	0.073	0.2938	0.0049	0.78597	0.1143	0.0015	1756	13	1659	24	1868	24	11.2
007r	293.9	149.3	0.508	3.7	0.21	0.25	0.015	0.97914	0.108	0.0015	1558	47	1432	78	1765	25	18.9
008c	130.2	26.4	0.20276	4.82	0.062	0.3208	0.0037	0.51059	0.10874	0.0014	1788.5	11	1793	18	1778	23	-0.8
009c	58.8	39.4	0.67007	6.713	0.1	0.3803	0.0047	0.52692	0.1295	0.0019	2074	13	2077	22	2088	26	0.5
010r1	91.4	16.93	0.18523	4.76	0.072	0.3169	0.004	0.58353	0.109	0.0015	1778	13	1774	20	1784	24	0.6
010r2	71.9	12.37	0.17204	4.807	0.076	0.32	0.0036	0.59051	0.1089	0.0015	1785	13	1789	18	1781	26	-0.4
013c	699	136.2	0.19485	4.809	0.061	0.3222	0.0034	0.68705	0.10815	0.0012	1786.8	11	1800	16	1767	21	-1.9
014c	115.8	37.4	0.32297	4.287	0.059	0.3006	0.0036	0.49322	0.1037	0.0014	1690.9	11	1694	18	1690	25	-0.2
016c	38.9	7.82	0.20103	4.838	0.097	0.3182	0.0043	0.34211	0.1101	0.0022	1792	17	1780	21	1803	37	1.3
018c	63.7	35.83	0.56248	4.284	0.1	0.2954	0.0058	0.71884	0.1052	0.0019	1688	20	1668	29	1719	33	3.0
019c	180.8	57.9	0.32024	4.421	0.062	0.3039	0.0031	0.48676	0.1059	0.0015	1718.6	11	1710	15	1727	27	1.0
019r	111.7	40.1	0.359	4.687	0.07	0.3208	0.0041	0.52138	0.1057	0.0016	1767	13	1793	20	1728	27	-3.8
020c	222	18.07	0.0814	4.661	0.07	0.3102	0.0039	0.60966	0.109	0.0014	1759	13	1741	19	1780	24	2.2
024r	178.2	31.53	0.17694	4.675	0.068	0.3157	0.0041	0.67157	0.1069	0.0014	1762	12	1768	20	1748	24	-1.1
025c1	105.2	40.4	0.38403	4.788	0.081	0.3213	0.0045	0.59947	0.108	0.0017	1781	14	1795	22	1766	27	-1.6
025c2	64.3	27.44	0.42675	4.78	0.083	0.3196	0.0043	0.64367	0.1091	0.0017	1781	14	1787	21	1780	29	-0.4
028c	98.7	43.9	0.44478	4.812	0.065	0.3223	0.0041	0.44624	0.1092	0.0016	1786.1	11	1801	20	1782	27	-1.1
029c	55.2	41.2	0.74638	4.821	0.074	0.3225	0.0041	0.38282	0.1086	0.0017	1787	13	1801	20	1779	29	-1.2
029r	199.4	87.5	0.43882	4.806	0.068	0.3193	0.004	0.62023	0.1089	0.0015	1787.1	12	1786	19	1783	24	-0.2
031c	130.9	32.16	0.24568	5.276	0.079	0.3403	0.0041	0.5959	0.1132	0.0016	1865	13	1890	19	1848	26	-2.3
033c	48.3	17.56	0.36356	5.004	0.1	0.3366	0.0057	0.35802	0.1088	0.0026	1821	17	1869	28	1773	43	-5.4
033r	163	35.7	0.21902	4.647	0.081	0.3169	0.005	0.74521	0.1065	0.0015	1758	15	1774	24	1744	24	-1.7
034c	121.2	42.5	0.35066	4.486	0.066	0.3105	0.004	0.55854	0.1053	0.0015	1728.4	12	1745	20	1721	26	-1.4
034r	90.5	36.37	0.40188	4.483	0.066	0.311	0.0036	0.44964	0.1047	0.0015	1727	12	1745	18	1708	27	-2.2
036c	137.3	44.4	0.32338	4.593	0.061	0.3119	0.0036	0.65421	0.10586	0.0014	1747	11	1750	18	1730	23	-1.2
038c	159.3	29.69	0.18638	4.351	0.065	0.2954	0.0039	0.67742	0.1064	0.0014	1703	12	1668	20	1741	25	4.2
038r	213.2	163.6	0.76735	3.326	0.083	0.2087	0.0052	0.8663	0.1162	0.0017	1484	20	1221	28	1895	26	35.6
044c	158	29.9	0.18924	4.908	0.07	0.3223	0.0042	0.65024	0.1099	0.0015	1803.7	12	1800	20	1796	25	-0.2
046c	78.4	25.3	0.3227	4.406	0.079	0.3049	0.004	0.49133	0.1042	0.0018	1711	15	1715	20	1700	31	-0.9
046r	91.3	23.69	0.25947	4.275	0.092	0.2927	0.005	0.52748	0.105	0.0021	1688	18	1657	25	1715	36	3.4
048c	139	41.3	0.29712	9.91	0.27	0.47	0.012	0.7935	0.1544	0.003	2427	25	2482	52	2396	33	-3.6
050c1	129.1	33.8	0.26181	3.86	0.17	0.258	0.011	0.92162	0.1082	0.0022	1626	36	1494	61	1768	36	15.5
050c2	257	80.8	0.3144	3.95	0.17	0.259	0.012	0.96469	0.1107	0.0016	1615	36	1478	60	1811	25	18.4
051c	201.6	134.1	0.66518	4.521	0.068	0.3102	0.0039	0.71826	0.10583	0.0014	1733	12	1741	19	1728	24	-0.8
052r	124.5	14.25	0.11446	4.429	0.07	0.3062	0.0041	0.53756	0.1048	0.0016	1720	13	1721	20	1707	28	-0.8
053r	403	32.72	0.08119	3.98	0.13	0.2634	0.0087	0.8022	0.1097	0.0027	1629	27	1505	45	1786	44	15.7
054r	139.9	33.3	0.23803	4.86	0.076	0.3213	0.0039	0.65095	0.1094	0.0015	1795	13	1796	19	1788	26	-0.4

Appendix B: Zircon/Apatite LA-ICP-MS U-Pb Isotopic Data and Ages

Table B-3. Quartzite (BR061013-01) Zr

				Corrected isotope ratios[a]							Ages (Ma)						
Grain # - Spot #	U [ppm]	Th [ppm]	Th/U	$^{207}Pb/^{235}U$	±2s	$^{206}Pb/^{238}U$	±2s	Rho	$^{207}Pb/^{206}Pb$	±2s	$^{207}Pb/^{235}U$	±2s	$^{206}Pb/^{238}U$	±2s	$^{207}Pb/^{206}Pb$	±2s	Disc. %[b]
057c	179	63.7	0.35587	4.487	0.068	0.3075	0.0043	0.73435	0.1063	0.0014	1727	13	1728	21	1737	25	0.5
057r	219	43.8	0.2	4.688	0.07	0.3186	0.0047	0.73654	0.1071	0.0014	1766	13	1784	23	1747	24	-2.1
058c	95.1	48.8	0.51314	4.486	0.075	0.3108	0.0043	0.59785	0.1046	0.0014	1727	14	1744	21	1706	25	-2.2
058r	69.2	23.5	0.3396	4.455	0.072	0.3125	0.0051	0.43124	0.1042	0.002	1722	13	1752	25	1698	35	-3.2
059c	202	147.6	0.73069	4.564	0.062	0.3128	0.0035	0.59564	0.10653	0.0014	1743.7	11	1754	17	1740	24	-0.8
059r	79.7	38	0.47679	4.768	0.077	0.3262	0.0047	0.65301	0.1052	0.0015	1779	14	1821	23	1719	26	-5.9
061c	60.6	27	0.44554	4.588	0.093	0.3126	0.0056	0.6572	0.1059	0.0017	1746	16	1752	28	1728	31	-1.4
062c	69.8	51.8	0.74212	13.25	0.18	0.5293	0.0069	0.6792	0.1833	0.0024	2696	13	2737	29	2683	22	-2.0
065c	235	170.2	0.72426	4.767	0.068	0.3228	0.004	0.58388	0.1075	0.0015	1778.2	12	1803	19	1760	26	-2.4
066Ac	104	23.75	0.22837	4.714	0.08	0.3185	0.005	0.37585	0.107	0.0019	1769	14	1782	24	1750	34	-1.8
068c	59	21.4	0.36271	4.431	0.077	0.3065	0.0039	0.39491	0.105	0.0018	1719	14	1723	19	1711	32	-0.7
069c	589	256.1	0.4348	1.437	0.055	0.07	0.0027	0.91013	0.1478	0.0026	901	23	436	17	2324	30	81.2
070c	128.2	82.8	0.64587	4.927	0.081	0.3271	0.0045	0.77279	0.10833	0.0013	1808	13	1824	22	1774	24	-2.8
071c	72.3	31.5	0.43568	4.733	0.077	0.3216	0.0047	0.52768	0.1062	0.0017	1773	14	1797	23	1736	29	-3.5
072c	80.6	21.33	0.26464	5.005	0.081	0.3306	0.0044	0.45695	0.1102	0.0019	1822	14	1843	21	1802	31	-2.3
072r	186	47.5	0.25538	3.998	0.073	0.253	0.0046	0.8107	0.1136	0.0015	1635	15	1453	24	1856	24	21.7
074c	481	153.5	0.31913	1.668	0.045	0.0836	0.0023	0.87149	0.1432	0.0021	996	17	518	13	2266	26	77.1
074r	766	144.9	0.18916	0.992	0.032	0.0435	0.0017	0.89172	0.1646	0.0035	698	16	274	11	2499	36	89.0
082c	110	30.7	0.27909	4.751	0.081	0.3177	0.0045	0.62259	0.107	0.0016	1775	14	1778	22	1745	28	-1.9
082c2	57.4	7.41	0.12909	4.276	0.092	0.2815	0.0058	0.44006	0.109	0.0026	1686	18	1598	29	1797	43	11.1
083c	143.5	45.1	0.31429	4.56	0.1	0.3071	0.0056	0.73435	0.1068	0.0019	1741	18	1725	28	1747	32	1.3
083r	199	64.6	0.32462	4.559	0.072	0.3138	0.0047	0.59682	0.1059	0.0016	1743	14	1758	23	1726	27	-1.9
085c	54.6	13.61	0.24927	4.591	0.1	0.3068	0.0049	0.52776	0.1083	0.0019	1745	19	1724	24	1766	33	2.4
086c	63.1	19.84	0.31442	4.405	0.074	0.3027	0.004	0.41357	0.1054	0.0018	1713	14	1704	20	1721	30	1.0
088Br	241	32.4	0.13444	4.753	0.071	0.3142	0.0047	0.63338	0.1091	0.0016	1778	13	1763	24	1783	25	1.1
088c	173	43.8	0.25318	4.361	0.071	0.3038	0.0044	0.74406	0.1037	0.0014	1706	13	1709	22	1690	25	-1.1
089c	115.6	40.6	0.35121	4.503	0.067	0.3065	0.0042	0.6769	0.1065	0.0014	1731	13	1723	21	1741	25	1.0
091c	121.6	21.94	0.18043	4.797	0.072	0.3234	0.0041	0.54988	0.1079	0.0016	1783	13	1806	20	1763	26	-2.4
092c	58.8	19.26	0.32755	4.568	0.076	0.3127	0.0045	0.47262	0.1063	0.0017	1742	14	1753	22	1739	28	-0.8
093c	50.3	24.19	0.48091	18.05	0.27	0.5979	0.0084	0.5792	0.2197	0.0031	2993	14	3020	34	2976	23	-1.5
095c	72.2	12.64	0.17507	4.845	0.086	0.3208	0.0045	0.52091	0.109	0.0018	1791	15	1793	22	1777	31	-0.9
096r	175.2	59.9	0.34189	4.41	0.11	0.2799	0.0073	0.8797	0.1132	0.0018	1712	21	1589	37	1851	28	14.2
097c	180.7	32.21	0.17825	4.861	0.085	0.324	0.0054	0.62193	0.1094	0.0019	1794	15	1808	26	1786	31	-1.2
097r	132.8	22.26	0.16762	4.856	0.077	0.3223	0.004	0.66088	0.1092	0.0015	1795	14	1801	20	1785	24	-0.9
098c	59.7	31.3	0.52429	4.37	0.076	0.306	0.0044	0.62014	0.1044	0.0017	1706	14	1720	22	1705	29	-0.9
099r	105.5	63.4	0.60095	4.463	0.061	0.3069	0.0039	0.53269	0.1054	0.0014	1723.1	11	1725	19	1719	25	-0.3
100r	174.2	54.4	0.31228	4.737	0.075	0.3197	0.0052	0.69334	0.1077	0.0016	1773	13	1787	25	1757	27	-1.7
101c	71.9	26.14	0.36356	4.342	0.095	0.3016	0.0053	0.3832	0.1055	0.0024	1704	17	1702	25	1722	40	1.2
101r	65.7	27.5	0.41857	4.295	0.073	0.3037	0.0044	0.32278	0.103	0.0018	1693	15	1711	22	1682	34	-1.7
102c	36.9	17.5	0.47425	13.65	0.22	0.5315	0.0068	0.63293	0.1872	0.0027	2728	15	2750	29	2717	23	-1.2
104c	71	15.47	0.21789	12.72	0.21	0.5146	0.0075	0.74255	0.1798	0.0023	2661	16	2678	32	2652	21	-1.0

Appendix B: Zircon/Apatite LA-ICP-MS U-Pb Isotopic Data and Ages

Table B-3. Quartzite (BR061013-01) Zr

				Corrected isotope ratios[a]							Ages (Ma)						
Grain # - Spot #	U [ppm]	Th [ppm]	Th/U	$^{207}Pb/^{235}U$	±2s	$^{206}Pb/^{238}U$	±2s	Rho	$^{207}Pb/^{206}Pb$	±2s	$^{207}Pb/^{235}U$	±2s	$^{206}Pb/^{238}U$	±2s	$^{207}Pb/^{206}Pb$	±2s	Disc. %[b]
105c	244	113.1	0.46352	5.181	0.069	0.3291	0.0042	0.71538	0.11469	0.0014	1848.7	11	1834	20	1878	20	2.3
105r	447	7.93	0.01774	2.292	0.061	0.1387	0.004	0.93435	0.1201	0.0016	1206	18	836	23	1958	23	57.3
106c	118.5	30.19	0.25477	4.486	0.075	0.2971	0.0048	0.69886	0.1095	0.0017	1728	14	1679	24	1789	28	6.1
107c	134	69.2	0.51642	3.45	0.12	0.2408	0.009	0.85587	0.1061	0.0022	1514	28	1389	47	1730	38	19.7
108c	159.7	53.5	0.335	4.614	0.064	0.3143	0.004	0.55067	0.1068	0.0015	1753.1	12	1761	20	1746	27	-0.9
109c	235	56.2	0.23915	4.752	0.067	0.3194	0.0039	0.64442	0.1081	0.0014	1775.4	12	1786	19	1765	24	-1.2
110c	43.4	23.63	0.54447	9.25	0.16	0.4414	0.0068	0.72153	0.1519	0.0022	2362	16	2364	31	2369	25	0.2
110r	26.76	12.6	0.47085	9.8	0.18	0.4579	0.0075	0.62526	0.1535	0.0026	2418	18	2428	33	2383	28	-1.9
111c1	128.4	33.5	0.2609	4.489	0.087	0.3095	0.0053	0.70407	0.1058	0.0016	1730	17	1737	26	1727	29	-0.6
111c2	194.6	51	0.26208	4.394	0.066	0.3032	0.0043	0.70906	0.1059	0.0014	1711	13	1706	21	1727	25	1.2
112A	320	75.4	0.23563	4.743	0.066	0.3185	0.004	0.81491	0.1079	0.0012	1773.8	12	1782	19	1763	21	-1.1
112Bc	200.3	55.5	0.27708	4.661	0.068	0.3168	0.0037	0.60181	0.1069	0.0014	1759	12	1774	18	1745	24	-1.7
112Br	666	161	0.24174	4.78	0.11	0.3155	0.0078	0.85828	0.11	0.0016	1779	19	1766	38	1798	27	1.8
113c	259	61.5	0.23745	3.49	0.11	0.2208	0.0068	0.93393	0.1144	0.0016	1518	24	1288	36	1868	25	31.0
114c	168.6	28.1	0.16667	4.846	0.075	0.3218	0.0041	0.64275	0.1084	0.0015	1793	13	1798	20	1773	25	-1.4
115c	124.5	19.32	0.15518	4.718	0.079	0.3135	0.0037	0.56258	0.1086	0.0016	1770	14	1757	18	1783	26	1.5
115r	84.3	13.62	0.16157	4.689	0.075	0.3129	0.0043	0.64242	0.1092	0.0015	1766	13	1754	21	1785	26	1.7
116c	189.9	45.3	0.23855	4.439	0.068	0.3074	0.0043	0.74435	0.10545	0.0014	1718	13	1727	21	1722	24	-0.3
117Bc	118.9	36.9	0.31034	4.475	0.067	0.3093	0.0036	0.55227	0.1052	0.0014	1726	13	1737	18	1718	26	-1.1
117c	312	63.6	0.20385	5.03	0.062	0.328	0.0034	0.58655	0.11147	0.0013	1827.3	9.7	1828	17	1822	22	-0.3
118c	67.4	19.15	0.28412	4.385	0.078	0.3051	0.0045	0.57572	0.104	0.0017	1709	15	1716	22	1695	30	-1.2
118r	41.8	11.27	0.26962	4.579	0.084	0.3112	0.0046	0.4923	0.1067	0.0018	1745	15	1746	22	1739	31	-0.4
119A	182.7	91.5	0.50082	4.697	0.067	0.3153	0.0036	0.6048	0.109	0.0014	1768.6	12	1766	18	1784	23	1.0
119Bc	79.8	18.41	0.2307	4.763	0.077	0.3187	0.0042	0.5318	0.1078	0.0017	1777	14	1783	20	1762	29	-1.2
119Cc	406	190.2	0.46847	4.79	0.071	0.326	0.0044	0.78012	0.10546	0.0013	1783	13	1821	22	1724	23	-5.6
120Ac	291	70.7	0.24296	4.866	0.073	0.3241	0.0051	0.75502	0.1094	0.0014	1796	13	1809	25	1790	23	-1.1
120Bc	79.5	29.62	0.37258	4.978	0.077	0.3283	0.0043	0.56176	0.1088	0.0017	1817	13	1830	21	1787	27	-2.4
121c	41.2	10.42	0.25291	4.645	0.079	0.3149	0.0045	0.19618	0.1065	0.0022	1758	15	1764	22	1745	39	-1.1
122c	37.8	34.5	0.9127	6.65	0.12	0.3786	0.0054	0.44911	0.1267	0.0023	2071	16	2069	25	2059	34	-0.5
123c	80.4	32.98	0.4102	4.478	0.063	0.3088	0.0043	0.54333	0.1059	0.0015	1725.9	12	1734	21	1729	27	-0.3
124c	247	57.6	0.2332	4.9	0.065	0.3271	0.0041	0.71291	0.10834	0.0014	1802.4	11	1826	20	1773	23	-3.0
124r	134.8	34.4	0.25519	4.77	0.065	0.3207	0.004	0.61378	0.108	0.0014	1778.6	11	1792	20	1771	24	-1.2
124r2	137.5	33.93	0.24676	4.727	0.06	0.3189	0.0034	0.51836	0.1076	0.0014	1771.3	11	1784	17	1759	24	-1.4
125c	203	30.13	0.14842	4.426	0.098	0.2933	0.0058	0.7247	0.1092	0.0019	1716	18	1657	29	1793	32	7.6
126Ac	158.7	52.4	0.33018	4.549	0.066	0.3113	0.0037	0.64581	0.10623	0.0013	1738.9	12	1747	18	1734	23	-0.7
126Br	95.6	56.07	0.58651	4.471	0.07	0.3086	0.0037	0.56796	0.105	0.0016	1726	13	1733	18	1715	27	-1.0
127c	216	41	0.18981	5.179	0.1	0.3358	0.006	0.74739	0.1116	0.0017	1848	17	1866	29	1824	28	-2.3
127r	258.7	71.9	0.27793	4.935	0.087	0.3071	0.0046	0.71485	0.1157	0.0017	1811	14	1726	23	1892	26	8.8

[a]U-Pb fractionation correction and correction for background interference based on GJ-1 zircon standard (Jackson et al., 2004)

[b]Discordance % for 206Pb/238U ages >1Ga calculated as ((1-(206Pb/238U)/(207Pb/206Pb))*100)

Appendix B: Zircon/Apatite LA-ICP-MS U-Pb Isotopic Data and Ages

Table B-4. Schist (BR061213-01) Zr

				Corrected isotope ratios[a]							Ages (Ma)						
Grain # - Spot #	U [ppm]	Th [ppm]	Th/U	$^{207}Pb/^{235}U$	±2s	$^{206}Pb/^{238}U$	±2s	Rho	$^{207}Pb/^{206}Pb$	±2s	$^{207}Pb/^{235}U$	±2s	$^{206}Pb/^{238}U$	±2s	$^{207}Pb/^{206}Pb$	±2s	Disc. %[b]
002c	118.9	46.2	0.38856	4.389	0.097	0.3044	0.0054	0.69748	0.1045	0.0021	1715	18	1717	27	1705	37	-0.7
002r	325	58	0.17846	3.067	0.099	0.199	0.0062	0.87688	0.1116	0.0023	1421	25	1168	33	1824	37	36.0
003c	166.4	35.5	0.21334	4.225	0.089	0.2898	0.0059	0.67194	0.1055	0.0023	1678	17	1643	30	1724	39	4.7
004c	106.6	37.2	0.34897	4.205	0.089	0.2921	0.0059	0.69024	0.1036	0.0023	1673	17	1654	29	1685	40	1.8
005ac	129.2	49.08	0.37988	4.279	0.093	0.297	0.0053	0.59287	0.1042	0.0022	1691	18	1675	26	1700	38	1.5
005ar	154	35.47	0.23032	4.106	0.086	0.2889	0.0053	0.71246	0.1038	0.0022	1656	17	1635	27	1689	39	3.2
005b	96.7	29.17	0.30165	4.517	0.1	0.3111	0.0069	0.68126	0.1047	0.0022	1731	19	1745	34	1717	42	-1.6
006c	91.3	35.4	0.38773	4.298	0.1	0.3006	0.0057	0.62637	0.1053	0.0024	1696	18	1693	28	1716	43	1.3
006r	178.4	28.9	0.162	4.372	0.089	0.3009	0.0052	0.62634	0.1051	0.0022	1707	17	1698	26	1712	38	0.8
007c	157.7	46.4	0.29423	4.352	0.09	0.3036	0.0053	0.72727	0.1033	0.0021	1706	17	1708	26	1681	37	-1.6
007r	154.4	46.51	0.30123	4.287	0.088	0.2937	0.0054	0.70475	0.1046	0.0022	1689	17	1659	27	1713	41	3.2
010c	105.8	38.37	0.36267	4.308	0.11	0.2976	0.0065	0.80784	0.1065	0.0023	1698	23	1678	32	1737	39	3.4
010r	351	22.1	0.06296	3.45	0.12	0.2361	0.0081	0.93789	0.1066	0.0022	1510	27	1363	42	1745	37	21.9
011r	200	46.5	0.2325	3.116	0.07	0.2526	0.0047	0.66883	0.0904	0.002	1439	17	1451	24	1435	41	-1.1
012c	112.7	39.3	0.34871	4.345	0.1	0.3052	0.0064	0.73992	0.1042	0.0023	1699	19	1715	31	1699	40	-0.9
012r	200.6	40.5	0.20189	4.335	0.088	0.2994	0.0057	0.71677	0.1051	0.0021	1698	17	1687	28	1715	38	1.6
013r	212.2	35.05	0.16517	4.369	0.095	0.3066	0.0054	0.5089	0.1035	0.0023	1706	18	1726	27	1686	40	-2.4
015c	97.7	36.4	0.37257	4.31	0.1	0.3009	0.006	0.69775	0.1045	0.0023	1698	19	1694	30	1699	41	0.3
015r	193	50.98	0.26415	4.41	0.097	0.3055	0.0058	0.70766	0.106	0.0024	1712	18	1717	29	1739	38	1.3
016c	134.9	29.1	0.21572	4.321	0.11	0.2991	0.0071	0.68286	0.1043	0.0023	1698	21	1692	34	1703	43	0.6
017c	128.4	29.42	0.22913	4.337	0.1	0.3058	0.0053	0.79545	0.1036	0.0022	1698	19	1719	26	1685	39	-2.0
018c	133.6	36.61	0.27403	4.419	0.1	0.3064	0.006	0.68926	0.1057	0.0024	1717	19	1722	30	1721	41	-0.1
019c	190	29.24	0.15389	4.289	0.093	0.2996	0.006	0.70825	0.1043	0.0022	1689	18	1688	30	1697	40	0.5
020c	102.8	41.04	0.39922	4.249	0.096	0.2973	0.005	0.56163	0.1042	0.0024	1682	18	1678	25	1698	43	1.2
022ac	128.8	43.5	0.33773	4.344	0.098	0.3058	0.0064	0.61244	0.1039	0.0025	1701	18	1718	32	1691	44	-1.6
022ar	144.1	41.7	0.28938	4.362	0.092	0.3028	0.0056	0.71615	0.1048	0.0022	1705	18	1705	28	1708	39	0.2
022bc	124.2	52.9	0.42593	4.363	0.1	0.3021	0.0063	0.70839	0.1052	0.0023	1703	19	1707	33	1722	39	0.9
022br	294	29.65	0.10085	4.406	0.096	0.3046	0.006	0.72214	0.1056	0.0023	1711	18	1713	30	1725	40	0.7
023c	54.1	34.2	0.63216	2.151	0.056	0.1981	0.0039	0.5411	0.0793	0.0021	1166	18	1164	21	1178	54	1.2
023r	81.1	61.9	0.76326	2.146	0.054	0.1999	0.0039	0.5572	0.079	0.002	1163	17	1174	21	1163	51	-0.9
024r	268	30.7	0.11455	4.352	0.1	0.2989	0.0066	0.76649	0.106	0.0022	1701	19	1691	32	1731	39	2.3
025c	108.4	44.7	0.41236	4.307	0.1	0.3036	0.0065	0.72831	0.1041	0.0023	1693	20	1711	31	1698	41	-0.8
025r1	247	74.5	0.30162	4.31	0.096	0.3012	0.0059	0.76616	0.1046	0.0022	1698	18	1699	30	1709	39	0.6
025r2	212	65.4	0.30849	3.49	0.15	0.238	0.011	0.93036	0.1065	0.0023	1522	33	1372	56	1736	40	21.0
027c	125.8	33.33	0.26494	4.342	0.1	0.3058	0.0055	0.59961	0.1035	0.0023	1702	19	1722	26	1689	41	-2.0
027r	172.6	54.72	0.31703	4.442	0.09	0.3119	0.0058	0.61227	0.1049	0.0022	1723	16	1749	28	1708	39	-2.4
028c	177.4	41.4	0.23337	4.378	0.12	0.3037	0.0067	0.68502	0.1041	0.0026	1708	21	1709	33	1701	47	-0.5

Appendix B: Zircon/Apatite LA-ICP-MS U-Pb Isotopic Data and Ages

Table B-4. Schist (BR061213-01) Zr

				Corrected isotope ratios[a]							Ages (Ma)						
Grain # - Spot #	U [ppm]	Th [ppm]	Th/U	$^{207}Pb/^{235}U$	±2s	$^{206}Pb/^{238}U$	±2s	Rho	$^{207}Pb/^{206}Pb$	±2s	$^{207}Pb/^{235}U$	±2s	$^{206}Pb/^{238}U$	±2s	$^{207}Pb/^{206}Pb$	±2s	Disc. %[b]
028r	148.4	47.4	0.31941	4.368	0.1	0.3052	0.0063	0.65263	0.1049	0.0024	1706	19	1716	31	1714	41	-0.1
029r	284	47.1	0.16585	4.478	0.11	0.3003	0.0063	0.57358	0.1087	0.0027	1726	21	1695	31	1770	45	4.2
029r2	131.9	30.41	0.23055	4.307	0.1	0.2984	0.0057	0.66142	0.1046	0.0023	1693	20	1691	30	1711	41	1.2
030r1	81.6	26.69	0.32708	4.366	0.11	0.3073	0.0058	0.55838	0.1042	0.0027	1703	22	1726	28	1695	46	-1.8
030r2	202.4	59.57	0.29432	4.4	0.14	0.3033	0.008	0.74461	0.1068	0.0026	1711	26	1705	39	1747	47	2.4
032c	103.7	28.33	0.27319	4.491	0.12	0.3094	0.0064	0.62463	0.105	0.0026	1725	22	1737	31	1721	45	-0.9
032r	149	40.48	0.27168	3.95	0.12	0.2727	0.0073	0.70019	0.1049	0.0027	1627	25	1565	38	1706	48	8.3
033c	114.9	37.6	0.32724	4.575	0.12	0.316	0.0064	0.69964	0.1051	0.0025	1747	22	1769	31	1715	44	-3.1
034c	70	19.43	0.27757	4.52	0.15	0.3078	0.0077	0.55757	0.1072	0.0034	1736	30	1729	38	1754	60	1.4
034r	254	57.8	0.22756	3.43	0.11	0.2259	0.0071	0.87631	0.1101	0.0024	1511	27	1311	37	1798	40	27.1
035ac	77.6	23.7	0.30541	4.362	0.11	0.3003	0.0062	0.58559	0.1065	0.0027	1706	21	1691	31	1738	46	2.7
035ar	407	41.5	0.10197	3.29	0.15	0.221	0.011	0.8995	0.1075	0.0029	1471	37	1303	57	1751	48	25.6
035bc	157	71.5	0.45541	4.432	0.12	0.3038	0.0076	0.64445	0.1058	0.0027	1715	22	1708	38	1726	48	1.0
035br	142.2	75.3	0.52954	4.35	0.093	0.3008	0.0065	0.61458	0.1039	0.0025	1704	18	1694	32	1703	45	0.5
036c	192	35.3	0.18385	4.39	0.12	0.3043	0.0081	0.78982	0.1053	0.0023	1707	23	1710	40	1721	42	0.6
036r	172.1	49	0.28472	4.401	0.098	0.3049	0.0056	0.72123	0.104	0.0022	1710	19	1714	28	1693	39	-1.2
037c	138.1	30.43	0.22035	4.466	0.1	0.3069	0.0059	0.37849	0.1047	0.0026	1725	18	1724	29	1713	46	-0.6
037r	207.5	65.3	0.3147	4.054	0.11	0.2723	0.0061	0.80993	0.1083	0.0023	1645	22	1552	31	1767	39	12.2
038c	139.5	84.4	0.60502	3.1	0.079	0.2489	0.0055	0.7095	0.0907	0.0021	1430	20	1432	28	1434	44	0.1
038r	148.1	71.5	0.48278	3.074	0.067	0.2441	0.0046	0.51118	0.0919	0.0021	1425	17	1407	24	1463	43	3.8
039a	206	48.2	0.23398	0.51	0.014	0.0671	0.0013	0.5943	0.0553	0.0015	418.9	9.5	418.6	8	421	60	0.6
039bc	122.5	43.04	0.35135	4.46	0.11	0.309	0.0064	0.73218	0.1045	0.0023	1720	20	1734	32	1704	40	-1.8
039br	276	25.42	0.0921	4.249	0.09	0.2924	0.0055	0.70883	0.1047	0.0021	1685	18	1655	28	1715	36	3.5
040c	163.5	54.5	0.33333	4.478	0.095	0.3081	0.0055	0.60738	0.1059	0.0023	1727	17	1730	27	1725	40	-0.3
040r	141.3	51.1	0.36164	4.435	0.099	0.3082	0.0055	0.68024	0.1053	0.0023	1720	18	1731	27	1718	39	-0.8
041c	73	22.03	0.30178	4.42	0.11	0.309	0.0065	0.73736	0.1036	0.0023	1716	20	1735	32	1690	39	-2.7
042r	118.9	25.1	0.2111	4.808	0.11	0.3192	0.0067	0.62072	0.1087	0.0024	1784	19	1788	33	1780	39	-0.4
043c	74.9	29.36	0.39199	4.255	0.09	0.2952	0.0058	0.66152	0.1049	0.0024	1683	17	1666	29	1717	42	3.0
043r1	288	28.4	0.09861	3.48	0.12	0.2342	0.0073	0.8435	0.1076	0.0025	1535	27	1358	39	1755	44	22.6
043r2	669	56.5	0.08445	2.02	0.096	0.1272	0.0063	0.82879	0.1167	0.0036	1122	31	771	36	1905	53	59.5
044c	100.3	50.6	0.50449	2.735	0.067	0.2306	0.0049	0.65684	0.0858	0.002	1337	18	1337	25	1329	46	-0.6
044c2	273	156.8	0.57436	2.955	0.063	0.242	0.0046	0.71733	0.0879	0.0018	1394	16	1399	23	1375	39	-1.7
044r	196.9	13.5	0.06856	2.673	0.068	0.2294	0.0052	0.59775	0.0849	0.002	1320	19	1331	27	1310	47	-1.6
045c	151.1	23.12	0.15301	4.535	0.094	0.3074	0.0062	0.66064	0.1069	0.0023	1738	18	1730	31	1751	42	1.2
045r	275	29.58	0.10756	4.52	0.1	0.31	0.0062	0.7671	0.106	0.0022	1736	20	1743	31	1728	39	-0.9
046c	123.8	42.12	0.34023	4.277	0.091	0.2984	0.0061	0.67462	0.1052	0.0022	1689	17	1682	30	1717	38	2.0
047c	208.4	27.75	0.13316	4.35	0.13	0.2947	0.0084	0.66808	0.1062	0.0027	1700	24	1663	42	1742	42	4.5

Appendix B: Zircon/Apatite LA-ICP-MS U-Pb Isotopic Data and Ages

Table B-4. Schist (BR061213-01) Zr

				Corrected isotope ratios[a]							Ages (Ma)						
Grain # - Spot #	U [ppm]	Th [ppm]	Th/U	$^{207}Pb/^{235}U$	±2s	$^{206}Pb/^{238}U$	±2s	Rho	$^{207}Pb/^{206}Pb$	±2s	$^{207}Pb/^{235}U$	±2s	$^{206}Pb/^{238}U$	±2s	$^{207}Pb/^{206}Pb$	±2s	Disc. %[b]
047r	137.9	28.5	0.20667	5.04	0.13	0.3252	0.0073	0.80841	0.1112	0.0024	1824	23	1814	36	1821	40	0.4
048c	166	69.6	0.41928	10.32	0.3	0.4353	0.011	0.69105	0.1712	0.0043	2466	25	2333	49	2564	42	9.0
049r	236	48.3	0.20466	4.499	0.098	0.3049	0.0061	0.62361	0.1071	0.0024	1729	18	1714	30	1748	41	1.9
050c	320	57.8	0.18063	2.12	0.11	0.1205	0.0062	0.94905	0.1263	0.0029	1141	33	731	35	2043	42	64.2
050r	138.4	37.6	0.27168	4.356	0.11	0.3032	0.0067	0.74956	0.104	0.0023	1703	20	1706	33	1699	42	-0.4
051r	116.3	57.7	0.49613	4.394	0.1	0.3032	0.0054	0.6994	0.1055	0.0023	1713	20	1706	27	1725	39	1.1
052c	467	40	0.08565	2.31	0.11	0.1455	0.0077	0.95051	0.1133	0.0025	1208	34	877	44	1854	40	52.7
053c	264	58.2	0.22045	2.223	0.077	0.1481	0.0055	0.90363	0.1096	0.0025	1187	23	889	31	1790	41	50.3
056c	116.4	63	0.54124	4.322	0.11	0.2981	0.0061	0.64831	0.1057	0.0025	1696	21	1681	30	1726	45	2.6
056r	137	53.1	0.38759	4.375	0.094	0.3029	0.0049	0.73254	0.1039	0.0021	1706	18	1705	24	1699	39	-0.4
057c	457	179.6	0.393	0.0285	0.0013	0.00461	0.00012	0.14259	0.0443	0.0023	28.5	1.3	29.63	0.8	-43	95	168.9
058r	104.1	28.68	0.2755	4.36	0.098	0.3017	0.0049	0.48911	0.1057	0.0025	1705	18	1699	24	1725	44	1.5
060c	102.1	41.74	0.40881	4.328	0.1	0.2997	0.0062	0.63146	0.1046	0.0025	1697	19	1689	30	1707	44	1.1
060r	131.9	32.08	0.24321	4.376	0.091	0.3037	0.0056	0.6252	0.1043	0.0022	1706	17	1709	28	1697	39	-0.7
061a	148.5	27.06	0.18222	4.42	0.1	0.3051	0.0066	0.67367	0.1054	0.0025	1719	17	1715	32	1715	42	0.0
061b	107.5	32	0.29767	4.376	0.11	0.3024	0.0062	0.69793	0.1048	0.0024	1712	22	1702	31	1707	42	0.3
062c1	106.7	24.99	0.23421	4.336	0.092	0.2994	0.0056	0.64887	0.1056	0.0023	1702	18	1687	28	1725	41	2.2
062c2	106.5	26.82	0.25183	4.421	0.1	0.3019	0.006	0.67869	0.1048	0.0022	1714	19	1700	30	1712	41	0.7
063c	962	58.3	0.0606	0.83	0.12	0.0484	0.0074	0.98908	0.1241	0.0029	576	61	302	45	2019	42	85.0
063r	341	33.9	0.09941	4.11	0.14	0.2804	0.01	0.73449	0.108	0.0031	1663	27	1591	50	1764	54	9.8
064a	104.1	79.8	0.76657	9.46	0.21	0.4465	0.0089	0.69502	0.1527	0.0032	2384	20	2378	40	2379	37	0.0
064b	141.7	36.41	0.25695	4.42	0.091	0.3023	0.0055	0.68739	0.1044	0.0023	1715	17	1702	27	1700	40	-0.1
065c	98.7	40.1	0.40628	4.471	0.1	0.3052	0.0055	0.72807	0.1054	0.0023	1723	19	1716	27	1720	41	0.2
065r	244	37.06	0.15189	4.428	0.095	0.3043	0.0064	0.82335	0.1053	0.0021	1719	19	1711	31	1718	37	0.4
066c	111.8	41.7	0.37299	4.4	0.1	0.3031	0.0057	0.71857	0.1046	0.0023	1715	19	1706	28	1702	40	-0.2
069c	103.4	29.3	0.28337	4.49	0.11	0.3105	0.006	0.65214	0.1044	0.0024	1727	19	1742	30	1704	41	-2.2
069r	199	36.3	0.18241	4.384	0.088	0.3039	0.0052	0.68804	0.1048	0.0022	1710	17	1710	26	1706	38	-0.2
070c	116.8	24.41	0.20899	4.494	0.093	0.3071	0.0052	0.63831	0.1061	0.0022	1731	17	1726	26	1732	37	0.3
070r	139.8	31.5	0.22532	4.504	0.091	0.3051	0.0049	0.66642	0.1059	0.0021	1730	17	1716	24	1728	37	0.7
071c	91	25.66	0.28198	4.35	0.15	0.303	0.011	0.77341	0.1036	0.0026	1705	27	1705	52	1683	47	-1.3
071r	983	70.5	0.07172	1.141	0.03	0.0576	0.0013	0.73875	0.1424	0.0032	772	14	361	7.8	2266	41	84.1
072a	210	54.66	0.26029	4.438	0.094	0.3015	0.0053	0.73056	0.1061	0.0022	1718	18	1698	26	1730	38	1.8
072bc	81.9	26.33	0.32149	4.528	0.096	0.3101	0.0061	0.61971	0.106	0.0024	1734	18	1740	30	1732	43	-0.5
072br	149.5	36.61	0.24488	4.404	0.093	0.3041	0.0055	0.68723	0.1052	0.0022	1711	18	1711	27	1718	40	0.4

[a]U-Pb fractionation correction and correction for background interference based on GJ-1 zircon standard (Jackson et al., 2004)

[b]Discordance % for 206Pb/238U ages >1Ga calculated as ((1-(206Pb/238U)/(207Pb/206Pb))*100)

Appendix B: Zircon/Apatite LA-ICP-MS U-Pb Isotopic Data and Ages

Table B-5. Foliated granite (BR060913-05) Zr

Grain # - Spot #	U [ppm]	Th [ppm]	Th/U	Corrected isotope ratios[a] $^{207}Pb/^{235}U$	±2s	$^{206}Pb/^{238}U$	±2s	Rho	$^{207}Pb/^{206}Pb$	±2s	Ages (Ma) $^{207}Pb/^{235}U$	±2s	$^{206}Pb/^{238}U$	±2s	$^{07}Pb/^{206}Pb$	±2s	Disc. %[b]
01c	131.1	39.9	0.30435	4.38	0.074	0.3061	0.0035	0.58688	0.1034	0.0014	1707	14	1721	17	1683	25	-2.3
02Ac	93.8	40.2	0.42857	4.3	0.1	0.2996	0.0062	0.77133	0.1047	0.0016	1688	20	1688	31	1711	27	1.3
02Ar	303	34.7	0.11452	3.883	0.072	0.2503	0.004	0.79603	0.1131	0.0014	1608	15	1440	21	1848	22	22.1
02Br	161.1	51.3	0.31844	4.362	0.077	0.3006	0.0038	0.64116	0.105	0.0014	1706	15	1693	19	1710	25	1.0
04c	156.3	50.8	0.32502	4.33	0.14	0.2991	0.0083	0.65523	0.1057	0.0028	1695	26	1685	41	1719	48	2.0
04r	214.2	41.9	0.19561	4.348	0.088	0.3022	0.0049	0.69353	0.1048	0.0017	1703	17	1702	24	1711	32	0.5
06r	165.6	33.5	0.20229	4.438	0.088	0.3085	0.0042	0.66987	0.1047	0.0015	1716	17	1732	21	1707	27	-1.5
09c	123	24.36	0.19805	4.465	0.059	0.3112	0.0039	0.61875	0.1048	0.0012	1724	11	1746	19	1709	22	-2.2
11r	186.3	35.7	0.19163	3.914	0.089	0.2636	0.005	0.64622	0.1073	0.0022	1614	18	1508	25	1747	38	13.7
13c	122.3	38.3	0.31316	4.43	0.15	0.3045	0.0062	0.46287	0.1041	0.003	1713	28	1713	30	1707	56	-0.4
13r	2133	74.6	0.03497	1.268	0.051	0.0407	0.0017	0.89577	0.2316	0.0042	835	24	257	10	3059	29	91.6
15c	168.5	63.4	0.37626	4.13	0.2	0.279	0.012	0.71906	0.107	0.0039	1665	41	1582	60	1735	66	8.8
17r	127.4	24.51	0.19239	4.49	0.14	0.3115	0.0059	0.58411	0.1048	0.0026	1723	27	1747	29	1698	47	-2.9
19r	217	44.6	0.20553	3.56	0.18	0.2196	0.0076	0.62049	0.1169	0.0044	1533	39	1278	40	1893	68	32.5
20c	79.1	24.25	0.30657	4.5	0.17	0.3083	0.007	0.5899	0.1059	0.0033	1721	31	1730	34	1711	57	-1.1
20r	255	38.5	0.15098	4.33	0.22	0.2887	0.0091	0.68777	0.1074	0.0041	1686	43	1640	44	1733	70	5.4
21r	454	78.7	0.17335	2.84	0.15	0.1742	0.0063	0.73835	0.1183	0.0043	1358	40	1034	34	1901	65	45.6
22c2	266.6	33.6	0.12603	3.84	0.13	0.2576	0.0062	0.61343	0.1087	0.0027	1595	27	1475	32	1775	46	16.9
22r	709	79.5	0.11213	1.87	0.12	0.0825	0.0042	0.79652	0.1666	0.007	1069	44	510	25	2499	70	79.6
23r	170.5	43.8	0.25689	4.45	0.15	0.2983	0.0066	0.61592	0.1093	0.003	1715	29	1681	33	1786	49	5.9
24r	91.1	35.52	0.3899	4.37	0.12	0.3035	0.005	0.53421	0.1054	0.0026	1701	23	1708	25	1714	45	0.4
26c	169.8	35.7	0.21025	4.4	0.1	0.306	0.0047	0.52327	0.1051	0.0024	1708	20	1720	23	1709	41	-0.6
29r	253.9	68.8	0.27097	3.31	0.15	0.2223	0.0091	0.87114	0.1091	0.0024	1473	34	1289	48	1774	41	27.3
31r	365	70.3	0.1926	2.832	0.069	0.1642	0.0031	0.60473	0.1254	0.0025	1364	18	980	17	2036	36	51.9
33c	92.4	23.21	0.25119	4.47	0.099	0.3123	0.0049	0.56357	0.1059	0.0021	1727	18	1751	24	1730	36	-1.2
33r	190.6	31.07	0.16301	4.3	0.095	0.3024	0.0041	0.54014	0.1055	0.0019	1694	18	1702	20	1720	33	1.0
38r	228.9	57.4	0.25076	2.81	0.13	0.1857	0.0076	0.81482	0.1115	0.0036	1352	35	1095	41	1800	57	39.2
39c	92.3	32.1	0.34778	4.44	0.17	0.3058	0.0064	0.55673	0.1064	0.0035	1708	31	1722	31	1711	59	-0.6
39r	234	52.8	0.22564	4.4	0.17	0.3	0.0068	0.64041	0.1069	0.0033	1708	32	1694	34	1721	56	1.6
41r	234	21.63	0.09244	4.53	0.18	0.3123	0.0074	0.60366	0.1062	0.0035	1724	33	1750	36	1708	59	-2.5
43c	93.6	42.7	0.4562	4.404	0.068	0.3089	0.0035	0.54325	0.1049	0.0016	1713	13	1735	17	1713	27	-1.3
43r	175	36.2	0.20686	4.226	0.071	0.2963	0.0043	0.64626	0.1047	0.0014	1677	14	1672	21	1705	25	1.9
44Ar	225	66.2	0.29422	3	0.17	0.211	0.011	0.96978	0.1066	0.0014	1407	42	1240	57	1739	23	28.7

Appendix B: Zircon/Apatite LA-ICP-MS U-Pb Isotopic Data and Ages

Table B-5. Foliated granite (BR060913-05) Zr

				Corrected isotope ratios[a]							Ages (Ma)						
Grain # - Spot #	U [ppm]	Th [ppm]	Th/U	$^{207}Pb/^{235}U$	±2s	$^{206}Pb/^{238}U$	±2s	Rho	$^{207}Pb/^{206}Pb$	±2s	$^{207}Pb/^{235}U$	±2s	$^{206}Pb/^{238}U$	±2s	$^{07}Pb/^{206}Pb$	±2s	Disc. %[b]
44Br	184.5	39.12	0.21203	3.28	0.12	0.2273	0.0085	0.97558	0.1062	0.00083	1468	28	1317	45	1737	14	24.2
49c	104.5	32.62	0.31215	4.36	0.11	0.3076	0.0059	0.5975	0.1039	0.0023	1705	22	1727	29	1687	41	-2.4
49r	115.5	34.4	0.29784	4.43	0.19	0.3062	0.0075	0.45913	0.1054	0.004	1717	35	1724	38	1712	70	-0.7
50r	434	77.4	0.17834	3.03	0.16	0.1824	0.0069	0.57636	0.1206	0.0054	1407	41	1078	37	1931	78	44.2
51r	138	36.8	0.26667	3.48	0.22	0.237	0.014	0.84606	0.1095	0.0042	1523	50	1363	74	1772	71	23.1
52r	239.5	32.11	0.13407	4.17	0.18	0.2649	0.008	0.48346	0.1165	0.0045	1660	35	1513	41	1900	70	20.4
53r	239	25.85	0.10816	4.24	0.16	0.2938	0.0064	0.51472	0.1064	0.0036	1671	30	1659	32	1715	62	3.3
57c	1138	123.4	0.10844	1.57	0.11	0.0787	0.0058	0.93659	0.1462	0.0035	947	45	487	35	2301	43	78.8
58c	532	68.9	0.12951	1.85	0.19	0.122	0.013	0.97378	0.114	0.0027	1047	72	743	77	1865	43	60.2
58r	995	57.6	0.05789	1.697	0.047	0.0667	0.0023	0.91037	0.188	0.0024	1006	18	416	14	2724	21	84.7
59r	578	73.7	0.12751	2.27	0.18	0.151	0.012	0.94032	0.1106	0.0026	1182	56	901	66	1796	43	49.8
60r	265	47.4	0.17887	4.374	0.086	0.2996	0.0048	0.66804	0.1059	0.0017	1704	16	1688	24	1733	31	2.6
62r	2660	127.1	0.04778	1.029	0.06	0.0387	0.002	0.8631	0.1924	0.0058	730	29	245	12	2763	49	91.1
63c2	139.8	37	0.26466	4.544	0.097	0.3185	0.0051	0.53442	0.1051	0.002	1742	19	1781	25	1706	36	-4.4
63r	2850	148.6	0.05214	1.394	0.059	0.0432	0.0016	0.85942	0.2377	0.0053	884	25	272.7	9.7	3101	36	91.2
64Ar	529	97.2	0.18374	3.31	0.13	0.1369	0.0035	0.6344	0.1763	0.0055	1475	30	827	20	2609	54	68.3
64Br	217	74.2	0.34194	4.3	0.13	0.301	0.0053	0.60343	0.1047	0.0026	1686	24	1695	26	1696	45	0.1
67c2	193	31.3	0.16218	4.35	0.13	0.3027	0.006	0.56031	0.1057	0.0026	1695	25	1706	30	1714	45	0.5
69c	90.6	34	0.37528	4.437	0.082	0.31	0.0036	0.70462	0.1064	0.0015	1721	15	1740	18	1741	27	0.1
69r	2390	115.9	0.04849	1.424	0.065	0.0398	0.0018	0.94039	0.2657	0.0043	893	27	252	11	3278	25	92.3
70r	1264	63.4	0.05016	1.745	0.086	0.0623	0.0028	0.93607	0.2077	0.0036	1021	33	389	17	2883	28	86.5

[a]U-Pb fractionation correction and correction for background interference based on GJ-1 zircon standard (Jackson et al., 2004)

[b]Discordance % for 206Pb/238U ages >1Ga calculated as ((1-(206Pb/238U)/(207Pb/206Pb))*100)

Appendix B: Zircon/Apatite LA-ICP-MS U-Pb Isotopic Data and Ages

Table B-6. Granite (BR060913-04A) Zr

				Corrected isotope ratios[a]							Ages (Ma)						
Grain # - Spot #	U [ppm]	Th [ppm]	Th/U	$^{207}Pb/^{235}U$	±2s	$^{206}Pb/^{238}U$	±2s	Rho	$^{207}Pb/^{206}Pb$	±2s	$^{207}Pb/^{235}U$	±2s	$^{206}Pb/^{238}U$	±2s	$^{207}Pb/^{206}Pb$	±2s	Disc. %[b]
01r	790	27.8	0.03519	4.565	0.047	0.3188	0.0036	0.80952	0.10536	0.00077	1743.7	8.8	1784	17	1722	13	-3.6
02r	104	43.71	0.42029	4.38	0.056	0.3114	0.0032	0.58556	0.1037	0.0011	1709	11	1747	16	1690	20	-3.4
04c	111.1	34.4	0.30963	3.909	0.059	0.2707	0.0041	0.84222	0.10603	0.00095	1617	12	1546	21	1732	16	10.7
04r	68.2	24.48	0.35894	4.447	0.06	0.3132	0.0034	0.71466	0.105	0.0011	1721	11	1756	17	1715	19	-2.4
07r	137.2	57.4	0.41837	4.72	0.33	0.311	0.011	0.46459	0.1095	0.0068	1737	59	1741	54	1700	110	-2.4
09c	121.7	57.6	0.47329	4.458	0.077	0.3106	0.0047	0.67529	0.1052	0.0013	1723	14	1743	23	1717	23	-1.5
09r	287	47.5	0.16551	4.491	0.068	0.316	0.0046	0.71156	0.1048	0.0012	1732	13	1769	22	1710	21	-3.5
11c	272	78	0.28676	3.41	0.12	0.2259	0.0088	0.80495	0.1131	0.0028	1510	28	1311	46	1846	45	29.0
14r	241	29	0.12033	3.838	0.096	0.2624	0.0061	0.81129	0.1072	0.0017	1603	19	1501	31	1752	29	14.3
15c	61.5	46.95	0.76341	4.64	0.11	0.3251	0.0055	0.71516	0.1052	0.0019	1753	20	1814	27	1711	33	-6.0
15r	469	45	0.09595	4.61	0.12	0.3101	0.0052	0.48475	0.109	0.0025	1751	21	1741	26	1775	41	1.9
16r	821	121.4	0.14787	2.93	0.11	0.1156	0.0039	0.83802	0.1875	0.0037	1396	29	704	22	2716	32	74.1
17r	299	34.9	0.11672	4.43	0.11	0.3057	0.0039	0.56763	0.1055	0.0022	1712	21	1719	19	1711	39	-0.5
19c	113.5	43.9	0.38678	4.7	0.25	0.3184	0.0083	0.50305	0.1069	0.0051	1752	46	1779	40	1693	87	-5.1
19r	323	60.8	0.18824	4.56	0.23	0.3037	0.0081	0.60853	0.1075	0.0042	1721	41	1712	39	1723	72	0.6
20r	938	50.1	0.05341	1.436	0.09	0.0905	0.0044	0.66617	0.1172	0.0057	896	35	560	25	1856	87	69.8
22r	822	266	0.3236	2.78	0.31	0.0933	0.0059	0.52931	0.201	0.019	1281	82	577	36	2720	160	78.8
23r	1240	116.5	0.09395	2.22	0.24	0.0772	0.0048	0.5024	0.207	0.02	1133	77	478	29	2680	170	82.2
24c	171	72	0.42105	3.57	0.38	0.22	0.013	0.62392	0.1163	0.0098	1499	87	1274	69	1720	160	25.9
27r	272	86.7	0.31875	4.5	0.11	0.3151	0.0061	0.67404	0.1044	0.002	1734	22	1765	30	1698	35	-3.9
30r	275	24.7	0.08982	4.446	0.059	0.3113	0.004	0.55705	0.1055	0.0012	1722	11	1747	20	1722	21	-1.5
33c	112.1	42.8	0.3818	4.444	0.063	0.3063	0.0047	0.66457	0.1062	0.0012	1720	12	1722	23	1737	22	0.9
33r	278	79.4	0.28561	3.55	0.11	0.2387	0.0086	0.87764	0.1115	0.0017	1538	25	1377	45	1822	29	24.4
34r	176.3	37.76	0.21418	4.514	0.097	0.3128	0.0053	0.51838	0.1052	0.002	1730	18	1757	27	1720	36	-2.2
35r	266.3	53.8	0.20203	4.14	0.088	0.2904	0.0044	0.69655	0.1043	0.0016	1661	18	1643	22	1696	28	3.1
36Ar	205.9	20.64	0.10024	4.66	0.13	0.3273	0.0059	0.617	0.1052	0.0024	1762	24	1824	29	1706	41	-6.9
36Br	869	76.1	0.08757	1.604	0.04	0.0726	0.0016	0.68716	0.1631	0.0033	971	15	451.5	9.5	2487	33	81.8
42r	630	74.6	0.11841	5.02	0.45	0.319	0.015	0.58302	0.1119	0.0084	1770	76	1778	71	1690	140	-5.2
43c	158.1	51	0.32258	4.79	0.36	0.308	0.012	0.53828	0.111	0.0072	1742	65	1731	58	1700	120	-1.8
43r	303	32.9	0.10858	4.83	0.37	0.309	0.011	0.50088	0.1096	0.0072	1746	65	1729	52	1700	120	-1.7
48r	497	258	0.51911	2.78	0.37	0.123	0.0082	0.57785	0.164	0.02	1310	100	746	46	2330	210	68.0
49r	235	79.7	0.33915	4.93	0.45	0.312	0.016	0.58834	0.1146	0.009	1769	79	1741	77	1740	150	-0.1
51r	128.9	29.5	0.22886	4.89	0.45	0.306	0.016	0.58409	0.116	0.0093	1756	80	1718	77	1750	150	1.8

Appendix B: Zircon/Apatite LA-ICP-MS U-Pb Isotopic Data and Ages

Table B-6. Granite (BR060913-04A) Zr

				Corrected isotope ratios[a]							Ages (Ma)						
Grain # - Spot #	**U [ppm]**	**Th [ppm]**	**Th/U**	**$^{207}Pb/^{235}U$**	**±2s**	**$^{206}Pb/^{238}U$**	**±2s**	**Rho**	**$^{207}Pb/^{206}Pb$**	**±2s**	**$^{207}Pb/^{235}U$**	**±2s**	**$^{206}Pb/^{238}U$**	**±2s**	**$^{207}Pb/^{206}Pb$**	**±2s**	**Disc. %[b]**
53Ac	188	18.2	0.09681	5.11	0.53	0.313	0.016	0.57618	0.1138	0.0099	1770	89	1747	76	1710	160	-2.2
53Br	151	33.4	0.22119	5.02	0.48	0.308	0.015	0.57106	0.1142	0.0089	1749	80	1732	74	1720	150	-0.7
54c	303	63.1	0.20825	3.81	0.16	0.2551	0.0083	0.66968	0.1079	0.0036	1583	34	1461	42	1750	62	16.5
54r	337	43.6	0.12938	3.92	0.18	0.2539	0.0087	0.70131	0.1133	0.0042	1619	36	1456	44	1835	66	20.7
56c	146.9	36.7	0.24983	4.83	0.43	0.316	0.015	0.59425	0.1088	0.008	1752	75	1762	74	1690	140	-4.3
58c	124.7	23.7	0.19006	4.28	0.42	0.28	0.015	0.62707	0.1121	0.0091	1647	81	1584	75	1700	150	6.8
58r	366	39.6	0.1082	4.47	0.4	0.268	0.015	0.59737	0.1206	0.009	1675	75	1537	78	1840	140	16.5
60c	92.9	39.4	0.42411	4.446	0.097	0.3144	0.0077	0.66453	0.1052	0.0019	1719	18	1760	38	1708	34	-3.0
60r	1174	61.8	0.05264	1.229	0.047	0.0467	0.0018	0.66868	0.1932	0.0066	811	21	294	11	2761	58	89.4
61r	358	53.9	0.15056	3.75	0.11	0.2581	0.0074	0.81075	0.1071	0.002	1576	22	1478	38	1755	33	15.8
66c	416	250	0.60096	2.51	0.15	0.1343	0.0074	0.87704	0.1367	0.0035	1266	43	811	42	2179	44	62.8
66r	534	404	0.75655	3.45	0.11	0.1572	0.0042	0.77014	0.1603	0.0032	1515	24	940	23	2454	34	61.7
70r	221	37.5	0.16968	4.439	0.045	0.3141	0.0034	0.68681	0.10443	0.00087	1720.7	8.5	1762	16	1704	15	-3.4
72c	119.4	76.1	0.63735	4.363	0.042	0.3067	0.0032	0.60929	0.10459	0.00094	1704.7	8	1726	16	1707	16	-1.1
72r	157.5	43.2	0.27429	4.348	0.041	0.3045	0.0026	0.66604	0.10507	0.00086	1701.9	7.7	1713	13	1714	15	0.1

[a]U-Pb fractionation correction and correction for background interference based on GJ-1 zircon standard (Jackson et al., 2004)

[b]Discordance % for 206Pb/238U ages >1Ga calculated as ((1-(206Pb/238U)/(207Pb/206Pb))*100)

Appendix B: Zircon/Apatite LA-ICP-MS U-Pb Isotopic Data and Ages

Table B-7. Southern Granodiorite (BR060913-04A) Zr

Grain # - Spot #	U [ppm]	Th [ppm]	Th/U	Corrected isotope ratios[a] $^{207}Pb/^{235}U$	±2s	$^{206}Pb/^{238}U$	±2s	Rho	$^{07}Pb/^{206}Pb$	±2s	Ages (Ma) $^{207}Pb/^{235}U$	±2s	$^{206}Pb/^{238}U$	±2s	$^{07}Pb/^{206}Pb$	±2s	Disc. %[b]
02r	168.5	60.4	0.35846	4.311	0.036	0.3015	0.0023	0.55854	0.10524	0.00082	1695.7	6.8	1698	11	1718	14	1.2
04c	131.7	64.2	0.48747	3.22	0.12	0.2267	0.0077	0.96787	0.10427	0.00082	1455	28	1314	41	1703	15	22.8
07c	84.9	32.6	0.38398	4.046	0.083	0.2905	0.0042	0.59302	0.102	0.0017	1640	17	1644	21	1654	31	0.6
08c	296	125.7	0.42466	4.184	0.085	0.2961	0.0047	0.7144	0.1038	0.0017	1670	17	1677	23	1699	30	1.3
11r	224	75.8	0.33839	4.32	0.11	0.2993	0.0058	0.736	0.1055	0.0019	1693	21	1690	28	1715	33	1.5
12Ac	457	148.9	0.32582	4.45	0.18	0.2738	0.0063	0.56587	0.1177	0.0042	1716	33	1559	32	1918	62	18.7
12Br	283.7	90.5	0.319	4.366	0.084	0.3035	0.004	0.66096	0.1042	0.0014	1705	16	1708	20	1699	25	-0.5
13r	184.4	40.4	0.21909	4.34	0.098	0.2748	0.0047	0.63947	0.1154	0.0021	1699	18	1567	23	1888	33	17.0
15c	263	116.6	0.44335	4.323	0.096	0.3017	0.0054	0.74081	0.1051	0.0016	1696	19	1699	27	1715	28	0.9
15r	147.5	50.5	0.34237	4.275	0.081	0.301	0.004	0.62712	0.104	0.0015	1688	15	1696	20	1694	27	-0.1
16r	274.5	91.2	0.33224	4.453	0.082	0.3112	0.0039	0.48766	0.1042	0.0018	1720	15	1746	19	1695	32	-3.0
17r	700	295	0.42143	3.84	0.16	0.266	0.01	0.93139	0.1038	0.0015	1595	33	1518	52	1698	27	10.6
18r	100.8	11.64	0.11548	4.401	0.081	0.3111	0.0057	0.71885	0.1036	0.0015	1713	16	1745	28	1690	25	-3.3
19r	80.9	31.3	0.3869	4.212	0.086	0.2976	0.0049	0.69018	0.1019	0.0015	1676	17	1678	24	1657	27	-1.3
23r	202.3	65.8	0.32526	4.37	0.079	0.3103	0.004	0.60865	0.1045	0.0016	1708	15	1742	20	1702	28	-2.4
25r	184.9	40.5	0.21904	4.465	0.077	0.3063	0.0045	0.6733	0.1067	0.0015	1722	14	1722	22	1744	24	1.3
28c	125.9	32.7	0.25973	4.373	0.085	0.3065	0.0044	0.5731	0.1041	0.0017	1710	16	1723	21	1699	30	-1.4
29r	131	33.1	0.25267	4.47	0.11	0.3114	0.0046	0.60729	0.1051	0.0018	1723	20	1747	23	1713	33	-2.0
32r	205	66	0.32195	4.43	0.13	0.3038	0.0071	0.65696	0.1059	0.0025	1711	25	1708	35	1746	43	2.2
33r	86.9	30.7	0.35328	4.4	0.13	0.303	0.0047	0.52644	0.1051	0.0026	1707	24	1705	23	1706	46	0.1
35c	201	56.8	0.28259	4.29	0.15	0.2936	0.0057	0.57441	0.1055	0.0031	1682	30	1658	28	1712	53	3.2
36r	224.8	73	0.32473	4.53	0.15	0.31	0.0054	0.55343	0.1059	0.003	1727	28	1742	26	1719	52	-1.3
37r	188.5	62.8	0.33316	4.55	0.15	0.3151	0.0056	0.51207	0.1048	0.0029	1733	27	1765	27	1694	52	-4.2
39c	122.3	35.3	0.28863	4.21	0.12	0.2927	0.0045	0.46061	0.104	0.0028	1670	24	1659	22	1691	50	1.9
40c	205	65.4	0.31902	4.46	0.11	0.3069	0.0041	0.65243	0.1061	0.0019	1718	20	1724	20	1728	33	0.2
41r	153.5	56.2	0.36612	4.37	0.14	0.3016	0.0045	0.51302	0.105	0.0028	1698	26	1698	22	1700	49	0.1
43r	198.9	62.6	0.31473	4.35	0.14	0.3015	0.0055	0.63599	0.1049	0.0027	1698	26	1700	27	1698	47	-0.1
44r	195	66.8	0.34256	4.39	0.12	0.3009	0.0049	0.60213	0.1065	0.0023	1711	22	1695	24	1731	40	2.1
46c	140.5	86.7	0.61708	4.09	0.1	0.2884	0.0043	0.54054	0.1033	0.0022	1649	20	1636	21	1677	39	2.4
47r	222	86.7	0.39054	4.408	0.05	0.3097	0.0027	0.77954	0.10446	0.00073	1712.8	9.5	1739	13	1705	13	-2.0
48c	135.7	58.2	0.42889	4.192	0.048	0.2938	0.0029	0.59612	0.105	0.001	1673.5	9.1	1660	14	1714	17	3.2
51r	185.6	67.4	0.36315	3.84	0.16	0.267	0.012	0.9852	0.10563	0.00069	1597	34	1531	58	1724	12	11.2
53c	290	117	0.40345	4.22	0.039	0.294	0.0023	0.61085	0.10537	0.00082	1677.5	7.7	1662	11	1720	14	3.4
53r	148.7	55.94	0.37619	3.99	0.12	0.2791	0.0083	0.95603	0.10388	0.00085	1625	25	1584	42	1693	15	6.4

Appendix B: Zircon/Apatite LA-ICP-MS U-Pb Isotopic Data and Ages

Table B-7. Southern Granodiorite (BR060913-04A) Zr

Grain # - Spot #	U [ppm]	Th [ppm]	Th/U	Corrected isotope ratios[a] $^{207}Pb/^{235}U$	±2s	$^{206}Pb/^{238}U$	±2s	Rho	$^{07}Pb/^{206}P$	±2s	Ages (Ma) $^{207}Pb/^{235}U$	±2s	$^{206}Pb/^{238}U$	±2s	$^{07}Pb/^{206}P$	±2s	Disc. %[b]
55r	153.6	41.4	0.26953	4.282	0.041	0.2998	0.0022	0.27784	0.1052	0.0011	1689.5	7.9	1690	11	1719	19	1.7
57r	156.3	39.25	0.25112	4.36	0.041	0.3011	0.0029	0.1689	0.1061	0.0014	1704.4	7.7	1697	14	1732	25	2.0
62r	160.5	67.4	0.41994	3.939	0.051	0.2771	0.0035	0.86152	0.10433	0.00063	1622	11	1576	18	1702	11	7.4
63r	222	74.8	0.33694	4.338	0.056	0.3036	0.0033	0.80415	0.10499	0.00077	1702	11	1709	17	1713	14	0.2
66c	223.8	82.3	0.36774	4.282	0.048	0.3012	0.0028	0.53245	0.1043	0.001	1689.4	9.2	1697	14	1700	18	0.2
66r	303	106.1	0.35017	4.372	0.033	0.3034	0.002	0.69406	0.10485	0.00053	1706.7	6.2	1708	9.7	1711	9.2	0.2

[a]U-Pb fractionation correction and correction for background interference based on GJ-1 zircon standard (Jackson et al., 2004)

[b]Discordance % for 206Pb/238U ages >1Ga calculated as ((1-(206Pb/238U)/(207Pb/206Pb))*100)

Appendix B: Zircon/Apatite LA-ICP-MS U-Pb Isotopic Data and Ages

Table B-8. Pegmatite 1 (BR061113-05) Zr

				Corrected isotope ratios[a]							Ages (Ma)						
Grain # - Spot #	U [ppm]	Th [ppm]	Th/U	$^{207}Pb/^{235}U$	±2s	$^{206}Pb/^{238}U$	±2s	Rho	$^{207}Pb/^{206}Pb$	±2s	$^{207}Pb/^{235}U$	±2s	$^{206}Pb/^{238}U$	±2s	$^{207}Pb/^{206}Pb$	±2s	Disc. %[b]
01r	108.7	42.8	0.39	4.447	0.1	0.3065	0.0065	0.6172	0.1049	0.0021	1721	19	1722	32	1709	38	-0.8
26c	142.2	40.76	0.29	4.456	0.12	0.3073	0.0068	0.7884	0.1038	0.002	1723	22	1730	34	1695	37	-2.1
02r	348	27.6	0.08	3.41	0.15	0.232	0.011	0.94389	0.1066	0.002	1497	36	1340	55	1746	36	23.3
03c	265	37	0.14	3.9	0.25	0.262	0.018	0.97424	0.1086	0.0023	1597	56	1488	93	1772	38	16.0
03r1	622	32.17	0.05	1.98	0.16	0.1183	0.01	0.98173	0.1211	0.0026	1075	54	715	57	1972	38	63.7
03r2	417.1	32.6	0.08	3.173	0.11	0.1964	0.0076	0.85507	0.1179	0.0028	1456	26	1154	41	1922	42	40.0
05r	341	54.4	0.16	3.45	0.13	0.2174	0.0078	0.77226	0.1129	0.0025	1514	28	1266	41	1846	42	31.4
06c	111.4	39.7	0.36	4.472	0.12	0.3085	0.0079	0.74869	0.1053	0.0022	1722	21	1731	39	1712	39	-1.1
07c	220	53	0.24	4.39	0.15	0.298	0.012	0.92404	0.1083	0.0023	1718	28	1679	59	1765	38	4.9
07r	354	94.4	0.27	2.38	0.16	0.156	0.011	0.93484	0.1137	0.0029	1251	46	932	60	1872	45	50.2
08r	5860	50.2	0.01	0.3806	0.01	0.00846	0.00025	0.81059	0.3249	0.0065	327.1	7.6	54.3	1.6	3595	32	98.5
09r	774	58.9	0.08	1.19	0.1	0.0704	0.0059	0.95702	0.1229	0.0032	784	46	437	35	1990	47	78.0
10c	227	28.6	0.13	2.41	0.11	0.1591	0.0064	0.82956	0.1083	0.0033	1244	35	951	36	1761	56	46.0
10r	797	27.4	0.03	1.429	0.062	0.0874	0.0041	0.91275	0.1192	0.0027	894	26	539	24	1936	41	72.2
12r	181.8	67.1	0.37	4.51	0.12	0.3078	0.0074	0.52208	0.106	0.0027	1731	23	1728	37	1725	48	-0.2
13r	427	22.94	0.05	1.849	0.093	0.1191	0.0057	0.8485	0.1127	0.0033	1061	33	725	33	1835	54	60.5
14r	157.5	63.7	0.40	4.47	0.12	0.3065	0.0077	0.6905	0.1043	0.0024	1723	22	1722	38	1707	41	-0.9
15c	117	47.1	0.40	4.472	0.11	0.3085	0.0076	0.59553	0.1046	0.0024	1724	21	1732	37	1714	42	-1.1
15c2	147	65.9	0.45	4.36	0.12	0.3019	0.0072	0.71198	0.1048	0.0023	1707	22	1703	36	1711	41	0.5
15r	429	45.7	0.11	1.36	0.14	0.088	0.011	0.95413	0.1161	0.0043	860	63	538	63	1892	65	71.6
16c	117	29.4	0.25	4.48	0.13	0.311	0.0089	0.84332	0.105	0.0023	1725	24	1743	44	1719	38	-1.4
16r	2060	82	0.04	1.271	0.037	0.03459	0.0011	0.81321	0.2668	0.0054	830	16	219.1	6.5	3292	33	93.3
17c	336	43.6	0.13	3.06	0.13	0.1879	0.0075	0.83664	0.1196	0.0032	1430	33	1112	40	1940	48	42.7
18c	1105	98.9	0.09	1.457	0.092	0.0591	0.0038	0.91592	0.1805	0.0046	904	38	370	23	2654	41	86.1
19r	279	75	0.27	3.85	0.14	0.2591	0.0077	0.61261	0.1075	0.0033	1597	29	1483	39	1758	53	15.6
20r	452	37.89	0.08	2.214	0.069	0.1298	0.0043	0.74027	0.1244	0.0032	1186	22	786	24	2019	44	61.1
21c	977	166.5	0.17	1.384	0.096	0.0554	0.0035	0.94893	0.1793	0.0039	865	41	349	22	2648	38	86.8
21r	339	51.8	0.15	3.14	0.11	0.1962	0.0073	0.73789	0.1162	0.0033	1440	27	1153	40	1899	50	39.3
25r	204	22.78	0.11	4.083	0.1	0.2852	0.007	0.70317	0.106	0.0023	1650	21	1616	35	1731	38	6.6
25r2	522	59.2	0.11	2.535	0.076	0.1218	0.0044	0.85985	0.1518	0.0033	1278	22	740	25	2371	39	68.8
27c	174	26.87	0.15	4.463	0.11	0.3112	0.0075	0.69171	0.1043	0.0023	1723	21	1749	37	1706	41	-2.5
27r	3580	56.8	0.02	0.762	0.034	0.02149	0.00097	0.9366	0.2558	0.0053	571	20	137	6.1	3219	32	95.7
28c	223	57	0.26	3.53	0.12	0.2333	0.0076	0.846	0.1099	0.0024	1530	26	1353	39	1797	41	24.7
28r	1871	66	0.04	1.022	0.029	0.03173	0.001	0.82846	0.2305	0.005	718	15	201.3	6.5	3057	36	93.4
29c	150	28.7	0.19	4.82	0.14	0.3117	0.0077	0.75672	0.1139	0.0026	1783	25	1747	38	1855	41	5.8

Appendix B: Zircon/Apatite LA-ICP-MS U-Pb Isotopic Data and Ages

Table B-8. Pegmatite 1 (BR061113-05) Zr

				Corrected isotope ratios[a]							Ages (Ma)						
Grain # - Spot #	U [ppm]	Th [ppm]	Th/U	$^{207}Pb/^{235}U$	±2s	$^{206}Pb/^{238}U$	±2s	Rho	$^{207}Pb/^{206}Pb$	±2s	$^{207}Pb/^{235}U$	±2s	$^{206}Pb/^{238}U$	±2s	$^{207}Pb/^{206}Pb$	±2s	Disc. %[b]
29r	490	46.7	0.10	2.106	0.07	0.1124	0.0045	0.79715	0.137	0.0035	1153	24	689	26	2186	46	68.5
31r	384	45	0.12	3.086	0.086	0.163	0.0043	0.78974	0.137	0.0029	1425	21	973	24	2189	37	55.6
32c	115.5	45.1	0.39	4.202	0.099	0.2947	0.0067	0.76648	0.1038	0.0021	1678	20	1664	33	1710	35	2.7
32r	2210	150.6	0.07	1.018	0.054	0.0355	0.0022	0.9393	0.2008	0.0052	709	27	225	14	2827	42	92.0
32r2	221	24.54	0.11	4.402	0.12	0.3011	0.0074	0.71067	0.1064	0.0022	1711	22	1698	37	1739	39	2.4
33r	177	76.9	0.43	4.378	0.1	0.3065	0.007	0.61198	0.1045	0.0022	1708	19	1722	34	1706	40	-0.9
34r	325	31.6	0.10	3.03	0.11	0.1992	0.0081	0.88449	0.1104	0.0024	1417	28	1172	43	1806	40	35.1
35r	229.4	100.6	0.44	4.46	0.15	0.303	0.012	0.57838	0.1055	0.0033	1725	29	1722	59	1724	59	0.1
36r	192	72	0.38	4	0.17	0.276	0.012	0.9439	0.1058	0.0021	1650	33	1577	61	1729	38	8.8
37c	241	40.32	0.17	4.455	0.1	0.3019	0.0073	0.81082	0.1071	0.0022	1725	20	1699	36	1752	38	3.0
37r	359.6	67.6	0.19	4.03	0.14	0.2803	0.011	0.76503	0.1062	0.0029	1640	27	1598	54	1727	50	7.5
39a	199	34.5	0.17	4.342	0.1	0.3026	0.0065	0.76916	0.1044	0.002	1699	19	1703	32	1702	35	-0.1
40c	251	26.4	0.11	4.414	0.11	0.3029	0.0076	0.66247	0.1071	0.0024	1717	21	1704	38	1744	41	2.3
40r	4910	59.4	0.01	0.384	0.014	0.01098	0.00037	0.86661	0.251	0.0057	328.9	10	70.4	2.3	3190	35	97.8
41r	236	51.1	0.22	4.385	0.11	0.3026	0.0084	0.69463	0.1059	0.0023	1709	21	1702	41	1730	39	1.6
41c	192.3	30.14	0.16	4.432	0.097	0.3097	0.0064	0.83799	0.1039	0.0019	1719	17	1738	32	1698	34	-2.4
42c	247	79.6	0.32	4.348	0.1	0.3025	0.007	0.73473	0.1048	0.0019	1700	19	1702	34	1710	34	0.5
42r	207.4	29.8	0.14	4.365	0.089	0.3017	0.0061	0.7296	0.1049	0.0018	1704	17	1699	30	1715	34	0.9
43r	87.7	43.8	0.50	4.431	0.11	0.3089	0.0064	0.70268	0.1043	0.0021	1716	20	1735	32	1698	36	-2.2
46c	182	61.8	0.34	4.23	0.12	0.2864	0.0077	0.72459	0.1066	0.0023	1680	24	1626	38	1741	38	6.6
46r1	5050	111.5	0.02	0.394	0.019	0.00913	0.00043	0.96111	0.3165	0.0061	336	13	58.6	2.7	3554	30	98.4
46r2	4970	72.1	0.01	0.485	0.016	0.01226	0.00045	0.91243	0.2908	0.0058	400.7	11	78.5	2.9	3425	31	97.7
47c	79.4	24.44	0.31	4.411	0.11	0.3044	0.007	0.61946	0.1052	0.0025	1713	21	1712	35	1713	43	0.1
47r	389	36.38	0.09	3.25	0.11	0.1763	0.0071	0.83561	0.135	0.0034	1462	26	1044	39	2162	43	51.7
51r	116.9	29.2	0.25	4.65	0.13	0.3185	0.0067	0.72079	0.1055	0.0021	1756	22	1781	33	1725	39	-3.2
52c	82.1	23.28	0.28	4.328	0.11	0.3022	0.0074	0.4825	0.1057	0.0027	1703	21	1700	37	1721	49	1.2
52r	507	48.6	0.10	2.55	0.069	0.1154	0.003	0.69507	0.1621	0.0039	1286	19	705	18	2471	40	71.5
53r	195	29.42	0.15	4.393	0.11	0.3058	0.0066	0.65151	0.1044	0.0021	1708	20	1719	33	1699	38	-1.2
55c	174.2	37.11	0.21	4.445	0.1	0.3083	0.0065	0.5386	0.1049	0.0021	1719	19	1731	32	1712	38	-1.1
55r1	2080	56	0.03	1.197	0.054	0.0348	0.0016	0.93998	0.2513	0.005	795	25	220.1	10	3192	32	93.1
55r2	3560	57.4	0.02	0.64	0.026	0.02039	0.00083	0.86373	0.2292	0.0053	500	16	130.1	5.3	3045	36	95.7
58r	142.9	57.1	0.40	4.384	0.11	0.3063	0.007	0.59673	0.1045	0.0024	1708	21	1721	34	1702	42	-1.1
62c	128.7	20.57	0.16	4.439	0.1	0.3094	0.0067	0.51596	0.1034	0.0021	1719	19	1737	33	1684	40	-3.1
62r	971	58.1	0.06	1.262	0.075	0.0676	0.0042	0.93111	0.1341	0.0034	817	33	423	25	2154	46	80.4
64r	176	29.8	0.17	4.29	0.13	0.2909	0.008	0.79911	0.1069	0.0023	1694	25	1644	40	1745	39	5.8
65c	294	173.7	0.59	4.43	0.13	0.302	0.0088	0.57479	0.1062	0.0031	1717	24	1699	44	1735	52	2.1
65r	154.3	75.9	0.49	4.575	0.12	0.3167	0.0092	0.47372	0.1064	0.0034	1746	21	1778	46	1727	59	-3.0
68r	164.3	88.7	0.54	4.33	0.13	0.2972	0.0077	0.6985	0.1051	0.0024	1698	24	1676	38	1713	44	2.2

Appendix B: Zircon/Apatite LA-ICP-MS U-Pb Isotopic Data and Ages

Table B-8. Pegmatite 1 (BR061113-05) Zr

				Corrected isotope ratios[a]							Ages (Ma)						
Grain # - Spot #	**U [ppm]**	**Th [ppm]**	**Th/U**	**$^{207}Pb/^{235}U$**	**±2s**	**$^{206}Pb/^{238}U$**	**±2s**	**Rho**	**$^{207}Pb/^{206}Pb$**	**±2s**	**$^{207}Pb/^{235}U$**	**±2s**	**$^{206}Pb/^{238}U$**	**±2s**	**$^{207}Pb/^{206}Pb$**	**±2s**	**Disc. %[b]**
71c2	2860	75.9	0.03	1.05	0.031	0.03019	0.00092	0.78371	0.254	0.0056	729	15	191.7	5.7	3211	34	94.0
71r	880	68.5	0.08	1.83	0.11	0.0741	0.0047	0.94876	0.1779	0.0039	1052	42	460	28	2635	37	82.5
73c	137.4	27.2	0.20	4.49	0.12	0.3102	0.0082	0.60734	0.1051	0.0026	1732	22	1744	41	1727	45	-1.0
73r1	389	25.89	0.07	2.84	0.23	0.183	0.014	0.95747	0.1086	0.0027	1350	63	1096	81	1772	44	38.1
74r	789	44.1	0.06	2.06	0.15	0.119	0.01	0.93116	0.1285	0.0041	1118	53	718	59	2068	60	65.3
77r	2240	90.7	0.04	1.579	0.06	0.0458	0.0016	0.8977	0.2448	0.0052	959	23	288.4	10	3154	33	90.9
79r	2660	73.4	0.03	1.015	0.053	0.029	0.0015	0.91931	0.2478	0.0059	706	26	184.4	9.6	3167	38	94.2
83r	235	50.9	0.22	2.807	0.086	0.1732	0.0053	0.60583	0.1153	0.0032	1360	23	1029	29	1880	49	45.3
90r	176	55.2	0.31	3.78	0.12	0.248	0.007	0.64069	0.1092	0.0029	1584	26	1427	36	1786	48	20.1
94c	139	37.69	0.27	4.608	0.11	0.3143	0.0069	0.5701	0.1063	0.0023	1748	20	1761	34	1738	39	-1.3
94r	450	31.3	0.07	2.57	0.082	0.1334	0.0046	0.75124	0.1389	0.0036	1289	23	807	26	2227	44	63.8

[a]U-Pb fractionation correction and correction for background interference based on GJ-1 zircon standard (Jackson et al., 2004)

[b]Discordance % for 206Pb/238U ages >1Ga calculated as ((1-(206Pb/238U)/(207Pb/206Pb))*100)

Appendix B: Zircon/Apatite LA-ICP-MS U-Pb Isotopic Data and Ages

Table B-9. Pegmatite 2 (BR072815-02) Zr

				Corrected isotope ratios[a]							Ages (Ma)						
Grain # - Spot #	U [ppm]	Th [ppm]	Th/U	$^{207}Pb/^{235}U$	±2s	$^{206}Pb/^{238}U$	±2s	Rho	$^{207}Pb/^{206}Pb$	±2s	$^{207}Pb/^{235}U$	±2s	$^{206}Pb/^{238}U$	±2s	$^{207}Pb/^{206}Pb$	±2s	Disc. %[b]
01r	3330	1250	0.38	2.439	0.089	0.0434	0.0014	0.79075	0.4133	0.0085	1252	26	273.5	8.5	3971	29	93.1
02r	1770	102.6	0.06	4.557	0.13	0.3456	0.0084	0.88966	0.09583	0.0013	1744	23	1912	40	1543	26	-23.9
03r	2440	353	0.14	3.37	0.13	0.054	0.0018	0.91621	0.4528	0.0074	1496	30	339	11	4092	24	91.7
04a	222	80.2	0.36	4.474	0.11	0.308	0.0058	0.62417	0.1059	0.0016	1727	21	1730	28	1728	28	-0.1
04b	204.5	61.6	0.30	4.602	0.13	0.3154	0.0065	0.65147	0.1063	0.0018	1749	23	1772	31	1733	32	-2.3
05r	3070	963	0.31	2.635	0.089	0.03339	0.001	0.91594	0.5752	0.0088	1306	25	211.7	6.5	4446	23	95.2
06r	3230	5260	1.63	1.511	0.042	0.02416	0.00064	0.74876	0.4559	0.0081	934	17	154.3	4.1	4103	27	96.2
07r	462	119.6	0.26	4.464	0.12	0.3102	0.0061	0.70135	0.1039	0.0017	1725	22	1741	30	1699	31	-2.5
08r	231.7	2.77	0.01	1.057	0.039	0.1195	0.0027	0.62284	0.0639	0.0016	733	19	729	16	732	51	0.4
09r	429	67.8	0.16	2.601	0.085	0.1691	0.005	0.83898	0.1127	0.002	1304	24	1009	27	1839	32	45.1
09a	727	58	0.08	1.006	0.058	0.0609	0.0039	0.93575	0.1203	0.0033	712	29	381	24	1968	48	80.6
10r	3520	1577	0.45	1.657	0.082	0.0246	0.0012	0.9711	0.4937	0.0068	990	32	156.8	7.4	4221	20	96.3
11r	5830	443	0.08	0.339	0.021	0.016	0.001	0.93626	0.1541	0.0043	295	16	102.3	6.3	2391	46	95.7
12r	5680	253	0.04	0.775	0.031	0.02031	0.00092	0.84982	0.2832	0.0068	581	18	129.6	5.8	3380	38	96.2
13r	92.6	39.84	0.43	4.4	0.12	0.3006	0.0059	0.46029	0.1056	0.0021	1712	23	1694	29	1726	37	1.9
14a	1493	61.5	0.04	1.48	0.062	0.0859	0.0036	0.92414	0.125	0.0023	925	25	533	21	2038	33	73.8
14b	6370	177	0.03	0.653	0.024	0.0151	0.00051	0.77964	0.3116	0.0075	513	15	96.6	3.2	3528	38	97.3
15c	190	61.8	0.33	4.83	0.16	0.3359	0.0096	0.78602	0.1045	0.0021	1788	28	1869	47	1703	36	-9.7
16r	401	222	0.55	4.405	0.13	0.3049	0.0062	0.76817	0.106	0.0017	1712	24	1718	30	1727	30	0.5
17r	129	44	0.34	3.839	0.11	0.2887	0.0061	0.63977	0.0958	0.0019	1600	24	1637	31	1541	38	-6.2
18r	189	51.3	0.27	4.776	0.14	0.3351	0.0078	0.68203	0.1038	0.0019	1778	24	1865	38	1701	35	-9.6
19a	197.3	69.5	0.35	4.06	0.14	0.2741	0.01	0.86182	0.1075	0.0023	1650	28	1559	50	1753	38	11.1
19b	162.3	66.02	0.41	4.399	0.11	0.3049	0.0055	0.42474	0.1042	0.0018	1712	21	1715	27	1698	32	-1.0
20r	184.5	63.2	0.34	4.417	0.12	0.3049	0.0062	0.64109	0.1051	0.0017	1717	22	1717	31	1712	30	-0.3
21r	462	51.6	0.11	3.072	0.095	0.2322	0.006	0.84065	0.0968	0.0016	1425	24	1345	32	1562	32	13.9
22c	2560	96	0.04	2.6	0.14	0.1198	0.0062	0.90207	0.1618	0.0038	1285	40	728	35	2465	40	70.5
24a	109	34	0.31	4.666	0.13	0.327	0.0074	0.56577	0.1042	0.0022	1758	24	1823	36	1701	39	-7.2
24b	115.1	32.3	0.28	4.395	0.12	0.311	0.006	0.60431	0.1032	0.0019	1715	23	1745	30	1679	35	-3.9
25r	108.6	43.7	0.40	4.233	0.12	0.2963	0.0059	0.44131	0.1032	0.0021	1680	23	1675	29	1684	37	0.5
26a	4300	89	0.02	1.928	0.056	0.02591	0.00065	0.84169	0.5407	0.0081	1090	19	164.9	4.1	4356	22	96.2
26b	3070	42.4	0.01	1.594	0.062	0.02678	0.00097	0.87727	0.4376	0.0085	967	25	170.3	6.1	4043	28	95.8
27r	359	143	0.40	4.699	0.13	0.3243	0.008	0.83669	0.1064	0.0016	1770	24	1812	39	1738	28	-4.3
29r	130.2	73.2	0.56	4.117	0.12	0.2651	0.0059	0.41339	0.114	0.0027	1655	25	1519	30	1856	43	18.2
30r	153.5	41.5	0.27	4.564	0.12	0.3109	0.0059	0.58499	0.1063	0.0019	1743	22	1747	30	1731	33	-0.9
31r	566	38.8	0.07	9.86	0.38	0.1307	0.005	0.94728	0.5499	0.0087	2443	34	794	28	4380	23	81.9

[a]U-Pb fractionation correction and correction for background interference based on GJ-1 zircon standard (Jackson et al., 2004)

[b]Discordance % for 206Pb/238U ages >1Ga calculated as ((1-(206Pb/238U)/(207Pb/206Pb))*100)

Appendix B: Zircon/Apatite LA-ICP-MS U-Pb Isotopic Data and Ages

Table B-10. HBL-QEM1 (BR060913-01) Zr

				Corrected isotope ratios[a]							Ages (Ma)						
Grain # - Spot #	U [ppm]	Th [ppm]	Th/U	$^{207}Pb/^{235}U$	±2s	$^{206}Pb/^{238}U$	±2s	Rho	$^{207}Pb/^{206}Pb$	±2s	$^{207}Pb/^{235}U$	±2s	$^{206}Pb/^{238}U$	±2s	$^{207}Pb/^{206}Pb$	±2s	Disc. %[b]
Hbl-14-01r	162.2	58.2	0.36	4.55	0.16	0.313	0.0091	0.6569	0.1052	0.002	1737	28	1755	44	1708	34	-2.8
Hbl-14-02c	260	90.8	0.35	4.58	0.15	0.3146	0.009	0.6388	0.105	0.0018	1746	26	1763	43	1706	32	-3.3
Hbl-15-03r	484	46.2	0.10	4.495	0.13	0.315	0.0091	0.8062	0.104	0.0011	1729	24	1764	44	1695	20	-4.1
Hbl-15-04c	143	49.6	0.35	4.337	0.12	0.3049	0.0081	0.6703	0.1036	0.001	1699	22	1716	40	1688	19	-1.7
Hbl-16-05r	66.1	27.24	0.41	4.427	0.12	0.3061	0.0081	0.5799	0.10499	0.001	1717	22	1721	40	1720	18	-0.1
Hbl-17-06r	228	38.35	0.17	3.847	0.13	0.2697	0.0095	0.5852	0.1028	0.00079	1602	30	1539	49	1674	14	8.1
Hbl-18-07r	682	266.3	0.39	4.396	0.11	0.3047	0.0078	0.8490	0.10473	0.00062	1712	21	1715	39	1709	11	-0.3
Hbl-19-08r	655	78.2	0.12	4.71	0.67	0.2608	0.011	0.9847	0.117	0.0075	1647	66	1490	56	1836	87	18.8
Hbl-20-09r	76.4	34.3	0.45	4.531	0.12	0.3125	0.0086	0.7207	0.10528	0.001	1737	23	1753	42	1723	18	-1.7
Hbl-20-10c	64.7	28.8	0.45	4.309	0.12	0.301	0.0078	0.6246	0.10416	0.00092	1695	22	1696	39	1699	16	0.2
Hbl-21-11r	146.7	73.3	0.50	4.242	0.11	0.2978	0.0078	0.5950	0.10333	0.00089	1682	21	1681	38	1685	16	0.2
Hbl-21-12r	117.5	42.2	0.36	4.181	0.11	0.2965	0.0077	0.6869	0.1022	0.00079	1672	20	1674	38	1667	15	-0.4
Hbl-22-13r	281.1	60	0.21	4.282	0.13	0.2974	0.0093	0.9308	0.10544	0.00091	1693	25	1677	46	1722	16	2.6
Hbl-22-14c	180.7	77.9	0.43	4.497	0.12	0.3126	0.0085	0.8212	0.10446	0.00079	1731	22	1753	42	1704	14	-2.9
Hbl-23-15r	125.9	40.1	0.32	4.294	0.12	0.3003	0.0079	0.6047	0.1041	0.0011	1691	22	1692	39	1696	20	0.2
Hbl-23-16r	197.2	68	0.34	4.375	0.12	0.2995	0.0078	0.6675	0.10583	0.00095	1708	23	1689	39	1729	16	2.3
Hbl-25-17r	280	16	0.06	3.17	0.1	0.2028	0.0069	0.0340	0.1138	0.0033	1453	24	1192	37	1842	48	35.3
Hbl-25-18r	288	19.08	0.07	3.766	0.11	0.2515	0.0072	0.8217	0.10868	0.001	1584	23	1447	37	1777	17	18.6
Hbl-26-19r	456	103.8	0.23	3.493	0.11	0.2471	0.0084	0.9316	0.10376	0.00086	1530	25	1422	43	1693	16	16.0
Hbl-27-20r	572	55.9	0.10	2.493	0.11	0.1765	0.0082	0.9729	0.10223	0.00091	1260	34	1045	45	1667	16	37.3
Hbl-28-21r	672	194.4	0.29	4.296	0.11	0.2956	0.0078	0.7637	0.10593	0.00082	1693	22	1669	39	1731	15	3.6
Hbl-29-22r	362	84.8	0.23	3.762	0.11	0.2694	0.0074	0.9227	0.10121	0.00073	1587	22	1537	38	1646	13	6.6
Hbl-30-23r	516	31.4	0.06	2.896	0.09	0.2056	0.006	0.8456	0.10173	0.0011	1378	23	1207	32	1657	19	27.2
Hbl-30-24c	396	61.1	0.15	2.947	0.11	0.2109	0.0075	0.9523	0.10178	0.00091	1394	29	1236	39	1657	16	25.4
Hbl-31-25r	320.8	103.2	0.32	4.12	0.11	0.2867	0.0075	0.7731	0.10389	0.00078	1658	21	1625	38	1695	13	4.1
Hbl-32-26r	226	49.8	0.22	3.43	0.19	0.244	0.014	0.9889	0.1045	0.0013	1503	49	1398	74	1702	23	17.9
Hbl-33-27r	416	69.6	0.17	3.023	0.098	0.2121	0.0067	0.8176	0.1025	0.0013	1412	25	1239	36	1669	22	25.8
Hbl-34-28r	212	50.4	0.24	3.634	0.12	0.2553	0.0083	0.8995	0.1039	0.0012	1559	26	1465	42	1696	22	13.6
Hbl-35-29r	312	52.7	0.17	3.693	0.12	0.2601	0.0074	0.7014	0.1024	0.0016	1571	26	1492	37	1672	30	10.8
Hbl-36-30r	1176	75.9	0.06	0.824	0.055	0.0407	0.0033	0.9686	0.152	0.0035	606	31	256	21	2366	36	89.2
Hbl-37-31r	293	47	0.16	2.719	0.11	0.1661	0.0063	0.7097	0.1155	0.002	1324	27	990	34	1884	31	47.5
Hbl-37-32r	388	132.5	0.34	2.997	0.12	0.2009	0.0085	0.9654	0.10801	0.00098	1410	30	1182	45	1766	17	33.1
Hbl-37-33c	197	71.5	0.36	4.351	0.11	0.3005	0.008	0.7069	0.10457	0.00093	1703	22	1695	40	1710	16	0.9
Hbl-38-34r	223	70.2	0.31	4.55	0.15	0.3037	0.0082	0.5419	0.1087	0.0019	1736	26	1709	40	1771	29	3.5
Hbl-39-35r	211	24	0.11	3.44	0.23	0.236	0.016	0.9872	0.1063	0.0019	1498	47	1358	79	1732	33	21.6

Appendix B: Zircon/Apatite LA-ICP-MS U-Pb Isotopic Data and Ages

Table B-10. HBL-QEM1 (BR060913-01) Zr

Grain # - Spot #	U [ppm]	Th [ppm]	Th/U	Corrected isotope ratios[a] $^{207}Pb/^{235}U$	±2s	$^{206}Pb/^{238}U$	±2s	Rho	$^{207}Pb/^{206}Pb$	±2s	Ages (Ma) $^{207}Pb/^{235}U$	±2s	$^{206}Pb/^{238}U$	±2s	$^{207}Pb/^{206}Pb$	±2s	Disc. %[b]
Hbl-40-36r	180	67.4	0.37	3.02	0.18	0.209	0.013	0.9869	0.10682	0.0011	1398	47	1216	72	1747	17	30.4
Hbl-41-37r	255	120	0.47	3.821	0.11	0.2705	0.0075	0.7279	0.1026	0.0012	1597	22	1545	39	1670	22	7.5
Hbl-41-38r	151.7	58.7	0.39	4.016	0.11	0.288	0.0078	0.8084	0.10132	0.0009	1637	22	1631	39	1652	17	1.3
Hbl-42-39r	428	99	0.23	3.751	0.099	0.2554	0.0068	0.7545	0.1061	0.00091	1582	21	1468	34	1733	16	15.3
Hbl-43-40r	168	78.7	0.47	5	0.13	0.3485	0.0094	0.8182	0.10383	0.00086	1819	23	1927	45	1692	15	-13.9
Hbl-44-41r	468	97.9	0.21	3.93	0.16	0.2724	0.0081	0.7640	0.1043	0.0026	1607	24	1552	41	1672	25	7.2
Hbl-45-42r	236.4	68.2	0.29	4.498	0.13	0.3101	0.0091	0.4862	0.1058	0.0014	1730	24	1740	44	1728	25	-0.7
Hbl-46-43c	110.4	37.2	0.34	4.293	0.12	0.2961	0.008	0.6847	0.10499	0.00097	1691	22	1671	40	1714	16	2.5
Hbl-46-44r	170	55.9	0.33	4.389	0.11	0.3034	0.0081	0.7532	0.10469	0.00081	1710	22	1708	40	1708	14	0.0
Hbl-47-45r	215.1	67.7	0.31	4.177	0.11	0.2921	0.0077	0.7553	0.1035	0.00086	1669	22	1653	38	1689	15	2.1
Hbl-47-46r	207.3	55.7	0.27	4.008	0.13	0.2851	0.0091	0.9198	0.10113	0.00091	1631	28	1619	45	1645	16	1.6
Hbl-48-47r	356	50.7	0.14	4.137	0.13	0.294	0.0087	0.8213	0.1024	0.001	1664	26	1663	44	1668	18	0.3
Hbl-49-48c	157.9	54.25	0.34	4.449	0.12	0.3081	0.0082	0.6735	0.10519	0.001	1721	23	1731	40	1716	18	-0.9
Hbl-49-49r	240	38.3	0.16	3.93	0.11	0.2793	0.0082	0.7022	0.10224	0.00092	1618	23	1587	41	1664	17	4.6
Hbl-50-50r	149	54.38	0.36	4.461	0.12	0.3103	0.0083	0.7434	0.1049	0.00099	1723	23	1742	41	1712	18	-1.8
Hbl-50-51r	261	62	0.24	3.94	0.11	0.2767	0.0075	0.6808	0.103	0.00099	1621	22	1574	38	1679	18	6.3
Hbl-51-52r	254	75.1	0.30	4.373	0.12	0.3029	0.0081	0.6755	0.10506	0.00094	1707	22	1705	40	1714	16	0.5
Hbl-52-53r	776	281	0.36	3.76	0.11	0.2652	0.0073	0.8113	0.10279	0.00088	1584	23	1516	37	1674	16	9.4
Hbl-53-54r	218	56.88	0.26	4.19	0.13	0.2881	0.0091	0.9507	0.10551	0.00091	1670	25	1631	46	1725	16	5.4
Hbl-53-55c	120.8	41.5	0.34	4.486	0.12	0.3086	0.008	0.6379	0.10506	0.00093	1729	22	1735	41	1715	16	-1.2
Hbl-54-56r	334	89.8	0.27	4.331	0.13	0.3039	0.0084	0.8971	0.10322	0.001	1697	24	1710	41	1684	18	-1.5
Hbl-55-57r	900	124.2	0.14	3.374	0.12	0.2459	0.0079	0.9454	0.09884	0.00095	1496	28	1416	40	1600	18	11.5
Hbl-56-58r	104.7	61.4	0.59	2.015	0.06	0.1888	0.0051	0.6007	0.07748	0.0011	1120	20	1115	28	1132	27	1.5
Hbl-57-59r	232	39.5	0.17	4.415	0.14	0.3068	0.0096	0.8904	0.10463	0.00099	1716	26	1723	47	1708	17	-0.9
Hbl-57-60r	227	37.9	0.17	3.366	0.11	0.2414	0.0078	0.8889	0.10198	0.001	1497	25	1395	41	1658	18	15.9
Hbl-58-61r	189	61.3	0.32	4.204	0.13	0.2826	0.0081	0.5693	0.1073	0.0015	1676	25	1604	40	1752	24	8.4
Hbl-58-62c	96.1	31.3	0.33	4.51	0.13	0.3117	0.0086	0.6558	0.1046	0.0012	1731	24	1749	42	1704	20	-2.6
Hbl-59-63r	273.3	59.5	0.22	4.487	0.14	0.313	0.0095	0.8659	0.10319	0.0011	1727	31	1755	48	1686	19	-4.1
Hbl-59-64c	123.6	53	0.43	3.977	0.11	0.2676	0.0075	0.7072	0.1076	0.0011	1628	23	1528	38	1757	19	13.0
Hbl-61-65c	512	399	0.78	4.325	0.15	0.3017	0.01	0.8704	0.10441	0.00079	1698	31	1702	51	1705	14	0.2
Hbl-61-66r	190	66.3	0.35	4.619	0.13	0.3141	0.0085	0.8782	0.10716	0.00095	1753	23	1761	42	1754	16	-0.4
Hbl-62-67r	226.2	58	0.26	4.346	0.11	0.3046	0.0081	0.7760	0.10385	0.00075	1702	22	1714	40	1695	13	-1.1
Hbl-63-68r	154.2	58.4	0.38	4.672	0.12	0.3181	0.009	0.5948	0.1072	0.0013	1763	23	1780	44	1749	22	-1.8
Hbl-64-69r	280	34.85	0.12	3.436	0.095	0.2484	0.0068	0.7678	0.10024	0.00099	1511	22	1430	35	1626	18	12.1
Hbl-65-70r	114.3	68.3	0.60	8.42	0.43	0.2447	0.0069	0.6994	0.254	0.0078	2284	44	1411	36	3201	45	55.9

[a]U-Pb fractionation correction and correction for background interference based on GJ-1 zircon standard (Jackson et al., 2004)

[b]Discordance % for 206Pb/238U ages >1Ga calculated as ((1-(206Pb/238U)/(207Pb/206Pb))*100)

Appendix B: Zircon/Apatite LA-ICP-MS U-Pb Isotopic Data and Ages

Table B-11. HBL-QEM2 (BR060913-01) Zr

Grain # - Spot #	U [ppm]	Th [ppm]	Th/U	Corrected isotope ratios[a]							Ages (Ma)						
				$^{207}Pb/^{235}U$	±2s	$^{206}Pb/^{238}U$	±2s	Rho	$^{207}Pb/^{206}Pb$	±2s	$^{207}Pb/^{235}U$	±2s	$^{206}Pb/^{238}U$	±2s	$^{207}Pb/^{206}Pb$	±2s	Disc. %[b]
1	325	45.4	0.14	4.189	0.088	0.2919	0.0044	0.87387	0.10417	0.00073	1674	17	1653	22	1698	13	2.7
2	128	32.6	0.25	4.131	0.094	0.2934	0.0053	0.76412	0.1021	0.0013	1659	18	1657	26	1657	24	0.0
3	281	65.2	0.23	3.819	0.089	0.285	0.0053	0.90484	0.09655	0.00084	1596	19	1619	27	1556	16	-4.0
4	181	26.2	0.15	3.61	0.11	0.2632	0.0071	0.85591	0.0987	0.0014	1555	24	1503	36	1596	28	5.8
5	207	29.9	0.14	3.488	0.11	0.264	0.0076	0.77657	0.0974	0.0018	1527	24	1507	39	1584	36	4.9
6	462	9.45	0.02	3.088	0.1	0.2451	0.0078	0.87249	0.091	0.0015	1428	26	1410	40	1451	31	2.8
7	500	70.2	0.14	4.36	0.16	0.3066	0.0094	0.89765	0.1039	0.0015	1701	30	1720	47	1694	27	-1.5
8	126	27.1	0.22	5.49	0.14	0.2852	0.0058	0.54456	0.1408	0.0035	1898	23	1616	29	2229	46	27.5
9	391	29.2	0.07	2.751	0.1	0.1981	0.0072	0.95062	0.1009	0.0012	1340	27	1162	39	1644	22	29.3
10	443	24.9	0.06	3.58	0.15	0.273	0.0093	0.93132	0.0964	0.003	1539	34	1552	49	1551	52	-0.1
11	285	61.3	0.22	4.06	0.11	0.293	0.0062	0.88692	0.0998	0.0011	1648	23	1658	31	1619	21	-2.4
12	394	24.5	0.06	2.834	0.075	0.2124	0.0049	0.93582	0.09629	0.00087	1367	20	1240	26	1555	17	20.3
13	460	107.1	0.23	3.867	0.09	0.2737	0.0047	0.89775	0.1031	0.00099	1604	20	1558	24	1678	18	7.2
14	463	98.3	0.21	4.43	0.12	0.3167	0.0072	0.89557	0.101	0.0011	1722	23	1771	35	1641	21	-7.9
15	333	53.7	0.16	3.45	0.15	0.2546	0.0088	0.76997	0.0988	0.0029	1506	35	1458	45	1586	54	8.1
16	986	92	0.09	0.522	0.022	0.02746	0.00099	0.86075	0.1362	0.0028	427	14	174.5	6.2	2172	36	
17	147	23.8	0.16	4.24	0.12	0.305	0.0067	0.83576	0.1019	0.0014	1686	23	1714	33	1667	26	-2.8
18	240	16.7	0.07	3.85	0.14	0.2868	0.0093	0.8942	0.0977	0.0015	1599	30	1621	46	1573	28	-3.1
19	314	53.2	0.17	3.18	0.082	0.2236	0.0048	0.86506	0.1034	0.0011	1449	20	1300	25	1684	20	22.8
20	614	8.58	0.01	4.27	0.28	0.3124	0.0082	0.71581	0.1003	0.0028	1683	35	1751	41	1632	45	-7.3
21	426	90.2	0.21	2.69	0.13	0.2009	0.0081	0.88743	0.0967	0.0021	1323	35	1182	44	1561	43	24.3
22	73	17.74	0.24	4.276	0.11	0.3015	0.004	0.47355	0.1026	0.002	1687	20	1698	20	1662	37	-2.2
22b	183	48.4	0.26	4.024	0.094	0.2862	0.005	0.65884	0.1015	0.0015	1636	19	1621	25	1650	27	1.8
23	728	12.6	0.02	3.31	0.08	0.264	0.0051	0.97309	0.09192	0.00073	1475	21	1505	26	1465	15	-2.7
24a	428	91.9	0.21	4.09	0.12	0.2921	0.0068	0.94752	0.1021	0.00088	1648	25	1650	35	1660	16	0.6
24b	426	17.94	0.04	3.422	0.087	0.2391	0.0055	0.94154	0.10321	0.00082	1508	20	1384	29	1682	15	17.7
25	172	62.2	0.36	4.451	0.085	0.3164	0.0045	0.80255	0.10216	0.00086	1722	16	1771	22	1662	16	-6.6
26	247	93.4	0.38	4.551	0.095	0.3145	0.0056	0.7856	0.1053	0.0012	1741	17	1764	28	1721	20	-2.5
27	464	34.2	0.07	3.88	0.23	0.293	0.0065	0.83061	0.0969	0.0037	1620	38	1655	32	1560	61	-6.1
28	405	12.84	0.03	2.94	0.1	0.229	0.0074	0.94198	0.0967	0.0016	1403	27	1325	39	1555	31	14.8
29	571	13.8	0.02	3.44	0.12	0.2754	0.0078	0.82022	0.0911	0.0019	1517	28	1565	40	1444	40	-8.4
30	141	37	0.26	4.57	0.14	0.3188	0.0062	0.63672	0.1038	0.0023	1741	26	1785	30	1687	41	-5.8
31	635	143.6	0.23	4.43	0.13	0.3085	0.0072	0.75124	0.104	0.0018	1716	23	1736	35	1693	32	-2.5
32	284	35.9	0.13	3.76	0.13	0.277	0.008	0.78555	0.0974	0.0019	1582	29	1573	41	1585	38	0.8
33	224	34.7	0.15	3.87	0.14	0.2859	0.0088	0.92399	0.0975	0.0011	1598	29	1617	44	1573	20	-2.8

Appendix B: Zircon/Apatite LA-ICP-MS U-Pb Isotopic Data and Ages

Table B-11. HBL-QEM2 (BR060913-01) Zr

				Corrected isotope ratios[a]							Ages (Ma)						
Grain # - Spot #	U [ppm]	Th [ppm]	Th/U	$^{207}Pb/^{235}U$	±2s	$^{206}Pb/^{238}U$	±2s	Rho	$^{207}Pb/^{206}Pb$	±2s	$^{207}Pb/^{235}U$	±2s	$^{206}Pb/^{238}U$	±2s	$^{207}Pb/^{206}Pb$	±2s	Disc. %[b]
34	596	9.42	0.02	3.18	0.11	0.2542	0.0077	0.82644	0.0913	0.002	1453	27	1457	40	1448	41	-0.6
35c	1510	200	0.13	0.353	0.015	0.0487	0.0016	0.54034	0.0529	0.0025	306	10	306	9.6	326	81	
35r1	1044	122	0.12	0.391	0.015	0.0434	0.0017	0.70683	0.0652	0.0017	335.1	11	274	11	788	54	
35r2	1480	114.2	0.08	0.35	0.012	0.0471	0.0013	0.63358	0.0546	0.0012	304	8.9	296.6	8.2	379	48	
36	127	44.4	0.35	4.383	0.086	0.3043	0.0041	0.58335	0.1041	0.0014	1707	16	1714	20	1696	25	-1.1
37	344	112.6	0.33	4.467	0.084	0.3144	0.0038	0.7067	0.1041	0.0011	1726	15	1761	19	1697	19	-3.8
37b	121	41.1	0.34	4.453	0.088	0.3128	0.004	0.68741	0.1035	0.0013	1722	16	1754	20	1687	23	-4.0
38	423	55.8	0.13	3.58	0.11	0.2653	0.0076	0.89457	0.0977	0.0012	1542	24	1514	39	1579	23	4.1
39	194	50	0.26	4.3	0.1	0.3121	0.006	0.77106	0.0994	0.0014	1692	19	1749	29	1616	26	-8.2
39b	234	58.4	0.25	3.52	0.17	0.2615	0.0077	0.69785	0.0982	0.0023	1527	33	1496	39	1585	41	5.6
40	480	32.4	0.07	3.303	0.099	0.2465	0.0061	0.90794	0.0959	0.0012	1476	23	1418	31	1541	24	8.0
41c	73	23.42	0.32	4.551	0.092	0.3128	0.0037	0.44744	0.1056	0.0015	1740	17	1754	18	1720	26	-2.0
41r	123	38.34	0.31	4.405	0.083	0.3054	0.0031	0.58619	0.1042	0.0012	1714	16	1718	15	1700	20	-1.1
42	482	9.28	0.02	3.485	0.1	0.2703	0.0068	0.95988	0.09399	0.0008	1520	23	1540	34	1506	16	-2.3
43a	50	8.32	0.17	4.57	0.14	0.3124	0.0054	0.54072	0.105	0.0024	1751	24	1751	27	1717	43	-2.0
43b	97	29.97	0.31	4.584	0.11	0.3115	0.0055	0.55314	0.1063	0.0017	1746	20	1747	27	1739	31	-0.5
44c	168	61.1	0.36	4.402	0.084	0.3041	0.0035	0.54705	0.1046	0.0013	1712	15	1711	17	1706	23	-0.3
44r	149	50.1	0.34	4.503	0.082	0.3152	0.004	0.60279	0.1037	0.0012	1731	16	1766	20	1688	21	-4.6
45	251	27.6	0.11	3.833	0.1	0.2786	0.0064	0.88154	0.0984	0.0012	1598	22	1586	32	1595	22	0.6
46r	158	42.6	0.27	4.53	0.087	0.3191	0.0037	0.62441	0.1032	0.0012	1736	16	1787	18	1682	21	-6.2
46r2	150	43.3	0.29	4.512	0.088	0.3072	0.0039	0.58932	0.105	0.0013	1735	16	1726	20	1713	23	-0.8
47a	140	25.87	0.18	4.52	0.13	0.3168	0.0064	0.55817	0.1027	0.0022	1735	24	1772	31	1666	40	-6.4
47b	192	78.4	0.41	4.46	0.14	0.3089	0.0072	0.58667	0.1033	0.0025	1722	27	1733	35	1684	45	-2.9
48r	214	61	0.29	4.331	0.1	0.3037	0.0059	0.45351	0.1032	0.0023	1696	20	1712	29	1674	40	-2.3
49	118	44.59	0.38	4.394	0.098	0.3081	0.0055	0.48512	0.1041	0.0017	1712	18	1734	27	1698	30	-2.1
50	452	112.1	0.25	4.54	0.16	0.3073	0.0084	0.6495	0.1057	0.0026	1733	29	1729	41	1740	45	0.6
51	70	19.56	0.28	4.5	0.14	0.3073	0.0082	0.58629	0.1054	0.0028	1729	26	1733	39	1712	50	-1.2
52	150	21.8	0.15	3.72	0.12	0.2731	0.0083	0.83485	0.0988	0.0016	1580	26	1553	42	1606	32	3.3
53	73	55.8	0.77	2.079	0.06	0.2033	0.004	0.65172	0.0746	0.0017	1138	20	1192	21	1051	45	-13.4
54	252	37.7	0.15	3.985	0.12	0.2763	0.0066	0.84177	0.1031	0.0013	1631	23	1571	34	1685	22	6.8
56	53	20.8	0.39	4.424	0.09	0.306	0.0035	0.43817	0.1051	0.0016	1715	17	1720	17	1713	28	-0.4
62	202	41.7	0.21	4.479	0.1	0.3108	0.0048	0.64528	0.1042	0.0016	1726	18	1744	24	1697	29	-2.8

[a]U-Pb fractionation correction and correction for background interference based on GJ-1 zircon standard (Jackson et al., 2004)

[b]Discordance % for 206Pb/238U ages >1Ga calculated as ((1-(206Pb/238U)/(207Pb/206Pb))*100)

Appendix B: Zircon/Apatite LA-ICP-MS U-Pb Isotopic Data and Ages

Table B-12. HBL-GM1 (BR060913-01) Zr

Grain # - Spot #	U [ppm]	Th [ppm]	Th/U	Corrected isotope ratios[a] $^{207}Pb/^{235}U$	±2s	$^{206}Pb/^{238}U$	±2s	Rho	$^{207}Pb/^{206}Pb$	±2s	Ages (Ma) $^{207}Pb/^{235}U$	±2s	$^{206}Pb/^{238}U$	±2s	$^{207}Pb/^{206}Pb$	±2s	Disc. %[b]
RY-04r	175	63.8	0.364571	4.491	0.089	0.3084	0.0054	0.68029	0.1046	0.0018	1731	16	1732	26	1712	32	-1.2
RY-05c	83	29.43	0.354578	3.961	0.074	0.2863	0.0045	0.45301	0.1007	0.0019	1629	15	1622	23	1633	37	0.7
RY-05r	77.8	22.32	0.286889	4.114	0.072	0.2941	0.0046	0.44935	0.102	0.0019	1657	15	1661	23	1656	35	-0.3
RY-06r	436	81.8	0.187615	3.75	0.11	0.2629	0.0062	0.79125	0.1038	0.002	1582	22	1504	32	1693	36	11.2
RY-07r	137.7	43.7	0.317357	4.247	0.076	0.2961	0.004	0.55504	0.1049	0.0019	1684	15	1674	19	1710	32	2.1
RY-09r	890	193.5	0.217416	3.444	0.082	0.2577	0.0057	0.74941	0.0975	0.0019	1519	20	1477	29	1577	38	6.3
RY-11r	67.8	9.01	0.132891	4.32	0.12	0.2984	0.01	0.67799	0.1046	0.0031	1695	23	1690	48	1698	54	0.5
RY-12c	233	100.5	0.43133	3.91	0.12	0.2738	0.0071	0.81935	0.1038	0.0022	1611	24	1558	36	1695	40	8.1
RY-13r	169.4	94.4	0.557261	4.409	0.088	0.305	0.0041	0.54845	0.1044	0.0019	1713	16	1718	21	1721	34	0.2
RY-13r2	209.9	77.9	0.371129	4.509	0.088	0.3125	0.0048	0.63308	0.1044	0.0019	1730	16	1752	24	1700	32	-3.1
RY-14r	150.9	33.19	0.219947	4.363	0.091	0.3025	0.0055	0.67569	0.104	0.0019	1706	18	1706	27	1705	31	-0.1
RY-16ac	732	569	0.777322	4.425	0.074	0.3092	0.0036	0.6655	0.1038	0.0017	1717	14	1738	17	1689	30	-2.9
RY-16ar	371	84.5	0.227763	4.493	0.081	0.3075	0.0044	0.59623	0.1061	0.0018	1728	15	1728	22	1738	31	0.6
RY-16br	154.8	49	0.316537	4.405	0.077	0.3078	0.0045	0.63593	0.104	0.0017	1713	14	1729	22	1693	30	-2.1
RY-17c	92.1	34.1	0.37025	4.36	0.11	0.309	0.0056	0.70374	0.1029	0.0022	1704	20	1735	28	1674	39	-3.6
RY-17r	116.3	43.7	0.375752	4.095	0.083	0.2891	0.0044	0.7029	0.1033	0.0017	1652	17	1639	22	1685	30	2.7
RY-17r2	116.6	37.1	0.318182	4.536	0.07	0.319	0.0048	0.58486	0.1039	0.0017	1739	13	1784	24	1697	29	-5.1
RY-18c	86	41.48	0.482326	4.495	0.079	0.3176	0.0037	0.58944	0.1044	0.0017	1728	15	1778	18	1703	30	-4.4
RY-18r	159.5	17.83	0.111787	4.479	0.073	0.3146	0.0047	0.80944	0.1038	0.0016	1728	13	1762	23	1697	28	-3.8
RY-20c	129.4	36	0.278207	4.609	0.077	0.3249	0.0051	0.65612	0.1042	0.0019	1751	14	1813	25	1698	33	-6.8
RY-20r	569	69.8	0.122671	4.464	0.077	0.3117	0.0043	0.65292	0.1042	0.0017	1723	14	1748	21	1697	31	-3.0
RY-21r	127.8	39.9	0.312207	4.51	0.071	0.3174	0.0039	0.4615	0.1032	0.0016	1734	13	1777	19	1686	29	-5.4
RY-21r2	174.7	23.03	0.131826	4.428	0.078	0.3051	0.0049	0.7115	0.1045	0.0016	1716	15	1716	24	1705	28	-0.6
RY-22r	361	65	0.180055	2.54	0.097	0.1749	0.0067	0.93768	0.1068	0.0018	1279	28	1037	37	1749	31	40.7
RY-24r	140	68.7	0.490714	4.376	0.074	0.3007	0.0048	0.70536	0.1054	0.0016	1706	14	1697	24	1719	29	1.3
RY-26c	185	73.3	0.396216	4.323	0.073	0.3063	0.0045	0.71428	0.1022	0.0016	1696	14	1722	22	1664	29	-3.5
RY-32r	460	145.4	0.316087	3.929	0.079	0.2761	0.0054	0.7859	0.1025	0.0016	1617	16	1571	27	1667	29	5.8
RY-33r	188.2	65.3	0.346971	4.333	0.064	0.3045	0.0041	0.69212	0.1025	0.0015	1701	12	1713	20	1669	28	-2.6
RY-34r	262	67.18	0.256412	3.597	0.077	0.2501	0.0052	0.78455	0.1046	0.0018	1551	17	1438	27	1704	32	15.6
RY-37r	378.7	86.8	0.229205	4.541	0.067	0.3072	0.0039	0.63725	0.1064	0.0016	1737	12	1727	19	1739	27	0.7
RY-38c	113.8	30.48	0.267838	4.652	0.084	0.3234	0.0045	0.69248	0.1049	0.0017	1760	15	1806	22	1714	29	-5.4
RY-38r	255	72	0.282353	4.516	0.078	0.3109	0.0043	0.60698	0.1052	0.0018	1732	14	1744	21	1716	32	-1.6
RY-38r2	138	42.7	0.30942	4.744	0.085	0.3248	0.0045	0.66456	0.1056	0.0017	1777	15	1813	22	1724	30	-5.2
RY-39r	299	107.8	0.360535	4.487	0.082	0.3073	0.0048	0.69656	0.1057	0.0017	1731	15	1729	24	1725	29	-0.2
RY-40r	280	88.8	0.317143	4.28	0.13	0.2969	0.0067	0.70477	0.1047	0.0028	1690	26	1675	33	1701	50	1.5

Appendix B: Zircon/Apatite LA-ICP-MS U-Pb Isotopic Data and Ages

Table B-12. HBL-GM1 (BR060913-01) Zr

Grain # - Spot #	U [ppm]	Th [ppm]	Th/U	Corrected isotope ratios[a]							Ages (Ma)						
				$^{207}Pb/^{235}U$	±2s	$^{206}Pb/^{238}U$	±2s	Rho	$^{207}Pb/^{206}Pb$	±2s	$^{207}Pb/^{235}U$	±2s	$^{206}Pb/^{238}U$	±2s	$^{207}Pb/^{206}Pb$	±2s	Disc. %[b]
RY-41c	162.6	85.6	0.526445	4.04	0.066	0.2881	0.0042	0.59644	0.1023	0.0017	1644	14	1632	21	1665	31	2.0
RY-41r	367	104.3	0.284196	4.356	0.057	0.3026	0.0037	0.67555	0.1044	0.0015	1703.2	11	1704	18	1710	26	0.4
RY-42r	166.2	45.2	0.271961	5.037	0.1	0.3421	0.0057	0.79736	0.1068	0.0016	1825	17	1899	27	1742	28	-9.0
RY-43r	190	59	0.310526	4.599	0.095	0.3116	0.0053	0.66348	0.1062	0.0019	1751	17	1751	27	1734	32	-1.0
WG-01	301	65.9	0.218937	3.754	0.096	0.2639	0.0061	0.83469	0.1043	0.0018	1582	20	1508	31	1703	32	11.5
WG-03c	134	51.5	0.384328	4.403	0.081	0.3129	0.0053	0.69448	0.1027	0.0017	1714	16	1757	26	1673	32	-5.0
WG-03r	208.2	29.7	0.142651	4.68	0.12	0.3248	0.0058	0.72285	0.1043	0.0021	1765	22	1812	28	1699	37	-6.7
WG-04r	206.8	72	0.348162	4.302	0.065	0.3006	0.0046	0.62565	0.1043	0.0017	1693	13	1694	23	1699	30	0.3
WG-05c	107.2	39.9	0.372201	4.554	0.079	0.3195	0.0052	0.6556	0.1036	0.0017	1739	14	1786	26	1685	31	-6.0
WG-05r	307.2	80.2	0.261068	4.242	0.072	0.2988	0.0043	0.6968	0.1034	0.0016	1681	14	1685	21	1684	29	-0.1
WG-08c	106	34.6	0.326415	4.187	0.084	0.3001	0.0044	0.48864	0.1006	0.002	1669	16	1691	22	1639	37	-3.2
WG-08r	169.4	61.4	0.362456	4.428	0.077	0.3149	0.0042	0.5705	0.1027	0.0018	1715	14	1764	21	1675	33	-5.3
WG-08r2	124.4	24.98	0.200804	4.271	0.08	0.3002	0.0045	0.57306	0.1023	0.0018	1686	15	1692	22	1664	34	-1.7
WG-10r	117.7	34.45	0.292693	4.282	0.095	0.301	0.0052	0.72435	0.1014	0.0018	1689	18	1695	26	1648	34	-2.9
WG-11r	151.2	45.9	0.303571	4.34	0.11	0.3049	0.0068	0.83412	0.1035	0.0019	1696	21	1714	34	1688	33	-1.5
WG-12r	197	63.3	0.32132	4.579	0.074	0.321	0.0041	0.45634	0.102	0.0017	1745	13	1796	20	1666	30	-7.8
WG-13c	156	53.2	0.341026	4.195	0.083	0.289	0.0046	0.71438	0.1054	0.0018	1672	16	1636	23	1716	31	4.7
WG-13r	491	129.2	0.263136	4.228	0.078	0.2944	0.0048	0.66862	0.1039	0.0017	1679	15	1663	24	1690	30	1.6
WG-15r	310	35	0.112903	3.883	0.058	0.2816	0.0041	0.62131	0.0994	0.0016	1611	12	1599	21	1612	29	0.8
WG-16r	240.9	58.95	0.244707	4.182	0.07	0.2946	0.0043	0.49221	0.1023	0.0017	1670	14	1664	21	1669	31	0.3
WG-17c	95	32.43	0.341368	4.434	0.091	0.3055	0.005	0.67978	0.1042	0.0018	1716	17	1723	24	1698	32	-1.5
WG-17r	106.4	27.51	0.258553	4.629	0.088	0.3191	0.0041	0.5619	0.1043	0.0019	1753	16	1785	20	1711	32	-4.3
WG-18c	109.1	42.02	0.385151	4.385	0.081	0.3051	0.0044	0.60545	0.1037	0.0018	1712	14	1716	22	1696	31	-1.2
WG-18r	99	33.6	0.339394	4.358	0.088	0.3059	0.0058	0.75049	0.1022	0.0017	1701	17	1719	29	1659	31	-3.6
WG-18r2	68.8	17.98	0.261337	4.28	0.12	0.3126	0.0065	0.61326	0.0986	0.0022	1688	21	1752	32	1595	41	-9.8
WG-21r	391	73.5	0.18798	3.93	0.12	0.2868	0.0087	0.80462	0.0998	0.0019	1616	24	1623	43	1616	36	-0.4
WG-22c	127.7	25.29	0.198042	2.9	0.078	0.1977	0.0047	0.84439	0.1061	0.0019	1379	20	1162	25	1733	34	32.9
WG-22r	1770	1071	0.605085	2.157	0.044	0.1068	0.0023	0.78489	0.1451	0.0025	1166	14	654	13	2286	29	71.4
WG-24r	1459	264	0.180946	4.085	0.083	0.2921	0.0056	0.79868	0.1009	0.0016	1652	16	1651	28	1639	29	-0.7
WG-25r	214	55.7	0.26028	4.458	0.075	0.3108	0.0051	0.76103	0.1037	0.0015	1723	14	1744	25	1692	27	-3.1
WG-26c	330	237.3	0.719091	4.113	0.083	0.2924	0.0049	0.7593	0.1017	0.0016	1655	16	1653	25	1653	29	0.0
WG-26r	120.6	40.6	0.33665	4.558	0.082	0.3153	0.0046	0.63249	0.1047	0.0018	1741	15	1766	22	1708	32	-3.4
WG-27c	219	118.5	0.541096	4.284	0.085	0.2966	0.0054	0.76876	0.1056	0.0017	1689	16	1673	27	1728	29	3.2
WG-27r	170.3	64.55	0.379037	4.341	0.069	0.3027	0.0038	0.59699	0.1042	0.0016	1701	13	1706	19	1703	30	-0.2
WG-28c	113.9	23.4	0.205443	4.478	0.084	0.3124	0.0053	0.68646	0.1052	0.0019	1726	15	1751	26	1721	33	-1.7
WG-28r	245.7	91.8	0.373626	4.287	0.085	0.303	0.005	0.72996	0.1033	0.0017	1688	16	1706	25	1681	30	-1.5
WG-29r	109	47.1	0.43211	4.862	0.09	0.3435	0.0049	0.6718	0.1041	0.0018	1797	16	1906	23	1699	32	-12.2

Appendix B: Zircon/Apatite LA-ICP-MS U-Pb Isotopic Data and Ages

Table B-12. HBL-GM1 (BR060913-01) Zr

				Corrected isotope ratios[a]							Ages (Ma)						
Grain # - Spot #	U [ppm]	Th [ppm]	Th/U	$^{207}Pb/^{235}U$	±2s	$^{206}Pb/^{238}U$	±2s	Rho	$^{207}Pb/^{206}Pb$	±2s	$^{207}Pb/^{235}U$	±2s	$^{206}Pb/^{238}U$	±2s	$^{207}Pb/^{206}Pb$	±2s	Disc. %[b]
WG-31r	231	112.6	0.487446	4.401	0.1	0.3122	0.0053	0.63185	0.1027	0.002	1711	19	1751	26	1677	35	-4.4
WG-32c	184.6	58.1	0.314735	4.242	0.088	0.3054	0.0052	0.64693	0.1027	0.002	1686	17	1717	25	1677	36	-2.4
WG-32r	109.7	25	0.227894	4.5	0.11	0.3124	0.0054	0.56674	0.1052	0.0025	1737	21	1752	26	1718	43	-2.0
WG-33c	115.4	50.5	0.437608	4.21	0.13	0.297	0.0069	0.70582	0.1018	0.0023	1669	25	1674	34	1660	42	-0.8
WG-33r	338	72	0.213018	4.51	0.11	0.3166	0.0056	0.63859	0.1046	0.0022	1730	20	1772	27	1702	39	-4.1
WG-34c	106.4	37.36	0.351128	4.33	0.11	0.3082	0.0071	0.75814	0.1035	0.0021	1701	21	1730	35	1686	36	-2.6
WG-34r	458	27.63	0.060328	4.581	0.089	0.3215	0.0046	0.49298	0.1035	0.002	1747	16	1799	22	1685	37	-6.8
WG-36r	136.6	26.81	0.196266	4.667	0.094	0.3218	0.0055	0.6583	0.1061	0.0019	1761	16	1797	27	1737	33	-3.5
WG-37r	350	103.9	0.296857	4.393	0.1	0.3086	0.0055	0.73954	0.105	0.0018	1708	19	1733	27	1711	32	-1.3
WG-38r	417	117.1	0.280815	4.369	0.07	0.3098	0.0039	0.53409	0.1037	0.0018	1707	13	1739	19	1692	32	-2.8
WG-39c	92.5	37.4	0.404324	4.544	0.092	0.3165	0.0047	0.75382	0.1048	0.0019	1738	17	1772	23	1707	35	-3.8
WG-39r	223	73.6	0.330045	4.227	0.073	0.2999	0.0043	0.69193	0.1031	0.0017	1681	14	1690	22	1679	30	-0.7
WG-40r	270	90.9	0.336667	4.733	0.1	0.3247	0.0061	0.80664	0.1067	0.0017	1771	19	1812	30	1742	29	-4.0
WG-43r	85	24.64	0.289882	4.304	0.074	0.3127	0.0052	0.68925	0.1024	0.0016	1693	14	1753	26	1665	30	-5.3
WG-44r	151	38.7	0.256291	4.592	0.077	0.3233	0.0054	0.66498	0.1044	0.0017	1746	14	1805	26	1700	29	-6.2
WG-46r	154.6	59	0.38163	4.35	0.082	0.3076	0.0042	0.63012	0.1038	0.0017	1703	16	1728	21	1692	30	-2.1
WG-48r	337	120.4	0.35727	4.247	0.067	0.2976	0.0043	0.63775	0.1039	0.0015	1682	13	1679	21	1694	27	0.9
WG-50r	121.4	47.9	0.394563	4.244	0.063	0.2988	0.0044	0.62999	0.1043	0.0016	1683	12	1685	22	1707	28	1.3
WG-50r2	144.8	47.4	0.327348	4.258	0.066	0.2989	0.004	0.72467	0.1026	0.0015	1684	13	1685	20	1669	27	-1.0
WG-51c	106.2	23.56	0.221846	4.313	0.075	0.3036	0.0043	0.69308	0.1035	0.0016	1696	15	1708	21	1686	29	-1.3
WG-51r	416	47.9	0.115144	4.067	0.055	0.2794	0.0037	0.78508	0.10606	0.0014	1646.8	11	1588	19	1731	24	8.3

[a]U-Pb fractionation correction and correction for background interference based on GJ-1 zircon standard (Jackson et al., 2004)

[b]Discordance % for 206Pb/238U ages >1Ga calculated as ((1-(206Pb/238U)/(207Pb/206Pb))*100)

Appendix B: Zircon/Apatite LA-ICP-MS U-Pb Isotopic Data and Ages

Table B-13. HBL-GM2 (BR072815-01) Zr

				Corrected isotope ratios[a]							Ages (Ma)						
Grain # - Spot #	U [ppm]	Th [ppm]	Th/U	$^{207}Pb/^{235}U$	±2s	$^{206}Pb/^{238}U$	±2s	Rho	$^{207}Pb/^{206}Pb$	±2s	$^{207}Pb/^{235}U$	±2s	$^{206}Pb/^{238}U$	±2s	$^{207}Pb/^{206}Pb$	±2s	Disc. %[b]
HBL-01	278	63.3	0.23	3.919	0.12	0.2762	0.006	0.79174	0.1038	0.0017	1620	23	1571	31	1689	30	7.0
HBL-02	165.2	61.5	0.37	4.405	0.11	0.3097	0.0056	0.39299	0.1038	0.0019	1716	20	1741	27	1691	34	-3.0
HBL-03	340	52.8	0.16	3.938	0.1	0.2941	0.0059	0.67175	0.0975	0.0015	1620	21	1661	29	1577	29	-5.3
HBL-04	1380	34.9	0.03	1.516	0.044	0.1146	0.0027	0.81021	0.0969	0.0016	935	18	699	15	1570	31	55.5
HBL-05	364	149.2	0.41	4.141	0.12	0.2885	0.0077	0.7622	0.1041	0.0019	1661	24	1637	39	1698	33	3.6
HBL-06	182.6	62.7	0.34	4.408	0.11	0.305	0.0058	0.55046	0.1053	0.0019	1712	22	1718	29	1723	33	0.3
HBL-07	254	40.2	0.16	3.818	0.098	0.2814	0.0064	0.59015	0.0978	0.0018	1597	21	1597	32	1580	34	-1.1
HBL-08A	136.9	51.9	0.38	4.02	0.12	0.2899	0.006	0.57002	0.1001	0.002	1637	24	1643	30	1618	38	-1.5
HBL-08B	117	39.4	0.34	3.87	0.13	0.2802	0.0078	0.70912	0.1018	0.0021	1605	26	1590	39	1661	38	4.3
HBL-09	327	94.2	0.29	4.321	0.11	0.3008	0.0059	0.64169	0.1048	0.0018	1696	21	1695	29	1707	31	0.7
HBL-11A	383	79	0.21	4.381	0.11	0.3045	0.0056	0.64291	0.1044	0.0016	1707	21	1713	28	1702	28	-0.6
HBL-11B	305	48.2	0.16	4.283	0.11	0.2997	0.0055	0.5282	0.1037	0.0017	1689	20	1692	27	1694	30	0.1
HBL-12A	217	70.8	0.33	4.289	0.11	0.303	0.0058	0.67268	0.1041	0.0016	1694	21	1705	29	1696	28	-0.5
HBL-12B	233.1	87.6	0.38	4.504	0.12	0.3167	0.0061	0.59306	0.1044	0.0019	1733	22	1776	31	1702	34	-4.3
HBL-13	124	46	0.37	4.6	0.13	0.3155	0.007	0.62775	0.106	0.0022	1751	23	1766	35	1731	37	-2.0
HBL-14	331	89.7	0.27	4.076	0.11	0.2926	0.0057	0.65202	0.1019	0.0016	1649	22	1654	29	1658	29	0.2
HBL-16	233.6	103.1	0.44	4.15	0.11	0.2917	0.0054	0.42812	0.1035	0.0019	1667	22	1649	27	1689	35	2.4
HBL-17	290	110	0.38	4.226	0.11	0.2978	0.0061	0.66028	0.1043	0.0018	1677	21	1680	30	1697	32	1.0
HBL-18	244	78	0.32	4.488	0.11	0.3153	0.006	0.53873	0.104	0.0018	1729	20	1766	30	1698	33	-4.0
HBL-19	368	122.4	0.33	4.662	0.12	0.3257	0.0065	0.66433	0.1039	0.0017	1759	22	1817	32	1697	31	-7.1
HBL-20	203	54.1	0.27	4.464	0.12	0.3082	0.0058	0.61449	0.1055	0.0018	1722	22	1731	29	1725	33	-0.3
HBL-21	288	117	0.41	3.33	0.096	0.2265	0.0053	0.77688	0.1071	0.0018	1489	23	1315	28	1752	32	24.9
HBL-22	228	66.1	0.29	4.461	0.11	0.3121	0.0057	0.47147	0.1035	0.0019	1722	21	1750	28	1695	33	-3.2
HBL-23	308	105.8	0.34	4.452	0.11	0.3069	0.0063	0.63901	0.1054	0.0017	1720	21	1724	31	1720	30	-0.2
HBL-24A	427	81.6	0.19	3.576	0.097	0.2543	0.0055	0.68057	0.1023	0.0018	1542	22	1460	28	1664	33	12.3
HBL-24B	459	125.2	0.27	3.953	0.1	0.2801	0.0055	0.60959	0.1022	0.0017	1626	21	1591	28	1663	30	4.3
HBL-25	153.3	39.6	0.26	4.437	0.12	0.305	0.0062	0.33421	0.1071	0.0022	1719	22	1718	30	1743	38	1.4
HBL-26	374	54.2	0.14	3.245	0.089	0.2413	0.0056	0.68651	0.0969	0.0017	1469	22	1395	29	1571	33	11.2
HBL-27	302	90.2	0.30	4.096	0.1	0.2854	0.005	0.42365	0.1039	0.0018	1655	20	1618	25	1694	31	4.5
HBL-28	270	27.8	0.10	4.73	0.14	0.3299	0.0086	0.78833	0.1047	0.0018	1772	25	1837	42	1705	32	-7.7
HBL-29	212	64.2	0.30	3.828	0.11	0.2628	0.0059	0.75355	0.1053	0.0017	1598	23	1506	30	1719	30	12.4
HBL-30	653	64	0.10	2.754	0.087	0.2134	0.0058	0.85078	0.093	0.0014	1346	22	1248	31	1488	30	16.1
HBL-31	138	46.6	0.34	4.619	0.12	0.3176	0.0057	0.28784	0.1055	0.0021	1754	21	1778	28	1719	38	-3.4
HBL-32	94.5	30.4	0.32	2.068	0.064	0.1947	0.0036	0.17888	0.0767	0.002	1140	22	1146	20	1116	52	-2.7
HBL-33	243	50.7	0.21	3.96	0.12	0.2851	0.006	0.68	0.1009	0.0018	1629	23	1616	30	1638	33	1.3
HBL-34	316	124.5	0.39	4.418	0.11	0.3039	0.0057	0.56374	0.1041	0.0016	1718	20	1710	28	1695	28	-0.9

Appendix B: Zircon/Apatite LA-ICP-MS U-Pb Isotopic Data and Ages

Table B-13. HBL-GM2 (BR072815-01) Zr

				Corrected isotope ratios[a]							Ages (Ma)						
Grain # - Spot #	U [ppm]	Th [ppm]	Th/U	$^{207}Pb/^{235}U$	±2s	$^{206}Pb/^{238}U$	±2s	Rho	$^{207}Pb/^{206}Pb$	±2s	$^{207}Pb/^{235}U$	±2s	$^{206}Pb/^{238}U$	±2s	$^{207}Pb/^{206}Pb$	±2s	Disc. %[b]
HBL-35A	187.9	52.5	0.28	3.605	0.1	0.2572	0.0057	0.67713	0.1012	0.0017	1548	23	1475	29	1645	33	10.3
HBL-36	347	125.8	0.36	4.36	0.13	0.2901	0.0078	0.67766	0.1085	0.0021	1703	25	1641	39	1770	36	7.3
HBL-37A	191	139	0.73	1.907	0.055	0.1829	0.0038	0.24156	0.0747	0.0018	1082	19	1084	21	1048	49	-3.4
HBL-37B	181.1	139.8	0.77	1.856	0.052	0.1825	0.0035	0.41581	0.0727	0.0015	1064	19	1080	19	1003	43	-7.7
HBL-37C	212	144.2	0.68	1.869	0.055	0.1788	0.0035	0.41041	0.0744	0.0016	1071	19	1060	19	1048	42	-1.1
HBL-38	125.7	51.7	0.41	4.44	0.12	0.3051	0.0069	0.58815	0.1048	0.0019	1719	22	1718	33	1705	34	-0.8
HBL-39	365	119.9	0.33	4.528	0.12	0.311	0.0071	0.565	0.1042	0.002	1737	20	1745	35	1696	36	-2.9
HBL-40	382	136.5	0.36	4.765	0.12	0.3278	0.0065	0.57674	0.1036	0.0017	1779	21	1830	32	1696	29	-7.9
HBL-41	570	205	0.36	4.19	0.14	0.2938	0.0091	0.88007	0.1026	0.0016	1671	28	1657	45	1672	28	0.9
HBL-42	157	20.55	0.13	3.82	0.15	0.2663	0.009	0.80874	0.1023	0.0021	1592	30	1519	46	1666	39	8.8
HBL-43	654	67.4	0.10	3.6	0.094	0.2743	0.0061	0.637	0.0944	0.0017	1548	21	1561	31	1518	34	-2.8
HBL-44A	264	17.5	0.07	3.316	0.11	0.2509	0.007	0.79295	0.0949	0.0018	1482	26	1445	37	1525	35	5.2
HBL-44B	137.1	53.9	0.39	3.845	0.1	0.2794	0.0055	0.49145	0.0989	0.002	1602	22	1588	28	1599	38	0.7
HBL-45	263	38.6	0.15	3.203	0.096	0.2258	0.0054	0.71397	0.1022	0.0019	1460	24	1312	28	1665	35	21.2
HBL-46	145	32.9	0.23	4.086	0.11	0.292	0.0064	0.44208	0.1014	0.0021	1654	21	1651	32	1649	39	-0.1
HBL-47	253	39.6	0.16	4.08	0.14	0.2786	0.0092	0.84075	0.1058	0.002	1647	28	1586	47	1736	36	8.6
HBL-48	240	41.6	0.17	4.584	0.14	0.3195	0.0081	0.6238	0.1036	0.0023	1749	25	1786	40	1689	40	-5.7
HBL-49	162	43.6	0.27	4.339	0.11	0.3093	0.0061	0.45942	0.1027	0.002	1699	21	1737	30	1671	36	-3.9
HBL-50	243	46.7	0.19	4.378	0.13	0.3122	0.0077	0.66705	0.1027	0.0021	1707	23	1749	38	1670	36	-4.7
HBL-51	318	112.5	0.35	4.399	0.11	0.3044	0.0059	0.47487	0.1044	0.0019	1710	22	1717	29	1710	34	-0.4
HBL-53	148	31.9	0.22	3.884	0.11	0.2715	0.0057	0.42637	0.1035	0.0022	1610	22	1548	29	1688	39	8.3
HBL-54	298	95.6	0.32	4.486	0.12	0.314	0.0059	0.61028	0.103	0.0017	1728	21	1760	29	1681	30	-4.7
HBL-55	732	188.5	0.26	3.76	0.15	0.269	0.01	0.93403	0.1002	0.0015	1580	33	1538	50	1626	28	5.4
HBL-56A	298	24.08	0.08	4.108	0.1	0.2909	0.0052	0.38153	0.1029	0.0018	1655	20	1645	26	1676	33	1.8
HBL-56B	219	48.9	0.22	4.383	0.13	0.3064	0.0075	0.76755	0.1041	0.0018	1708	25	1721	37	1693	32	-1.7
HBL-57	193	46.4	0.24	3.981	0.11	0.297	0.0065	0.61811	0.0976	0.0019	1631	24	1681	32	1576	36	-6.7
HBL-59A	331	12.71	0.04	2.93	0.12	0.2117	0.0077	0.91905	0.1009	0.0017	1386	32	1235	41	1635	32	24.5
HBL-59B	396	17.22	0.04	2.996	0.095	0.2169	0.0064	0.84217	0.1008	0.0018	1405	24	1264	34	1636	34	22.7
HBL-60	254	80.3	0.32	4.674	0.13	0.3259	0.0067	0.55775	0.1053	0.002	1762	23	1817	32	1720	34	-5.6
HBL-61	273	30.8	0.11	3.967	0.12	0.286	0.0062	0.67201	0.1009	0.002	1625	24	1621	31	1636	37	0.9
HBL-62	191	48.2	0.25	4.485	0.12	0.3171	0.0065	0.48003	0.1032	0.0021	1726	23	1775	32	1679	37	-5.7
HBL-64A	309	107.1	0.35	4.526	0.12	0.318	0.0065	0.67499	0.1043	0.0019	1737	23	1779	32	1697	33	-4.8
HBL-64B	263	97.5	0.37	4.357	0.12	0.3032	0.0062	0.63693	0.1044	0.0018	1702	22	1706	31	1699	33	-0.4
HBL-64C	255.7	95.4	0.37	4.381	0.11	0.3037	0.0057	0.44049	0.1059	0.002	1707	22	1709	28	1729	36	1.2

[a]U-Pb fractionation correction and correction for background interference based on GJ-1 zircon standard (Jackson et al., 2004)

[b]Discordance % for 206Pb/238U ages >1Ga calculated as ((1-(206Pb/238U)/(207Pb/206Pb))*100)

Appendix B: Zircon/Apatite LA-ICP-MS U-Pb Isotopic Data and Ages

Table B-14. HBL-TM (BR060913-01) Zr

				Corrected isotope ratios[a]							Ages (Ma)						
Grain # - Spot #	U [ppm]	Th [ppm]	Th/U	$^{207}Pb/^{235}U$	±2s	$^{206}Pb/^{238}U$	±2s	Rho	$^{207}Pb/^{206}Pb$	±2s	$^{207}Pb/^{235}U$	±2s	$^{206}Pb/^{238}U$	±2s	$^{207}Pb/^{206}Pb$	±2s	Disc. %[b]
HBL-01	266	48.2	0.18	3.59	0.12	0.2415	0.0073	0.8603	0.1058	0.0019	1547	27	1400	39	1727	34	18.9
HBL-02	146	51.9	0.36	3.631	0.081	0.2618	0.004	0.70511	0.0996	0.0015	1555	18	1499	20	1616	27	7.2
HBL-03	165	82.8	0.50	3.71	0.14	0.259	0.0076	0.85962	0.1038	0.0019	1571	29	1482	39	1696	34	12.6
HBL-04	242	108.4	0.45	4.3	0.16	0.2977	0.0092	0.8734	0.1033	0.0019	1695	30	1676	46	1681	35	0.3
HBL-05	157	46	0.29	4.294	0.091	0.2954	0.003	0.62561	0.1041	0.0016	1695	17	1668	15	1704	28	2.1
HBL-06	199	41.8	0.21	2.56	0.19	0.175	0.013	0.97724	0.1052	0.0018	1297	54	1042	69	1717	32	39.3
HBL-07	209	100	0.48	4.362	0.1	0.3014	0.0041	0.6115	0.1036	0.0017	1704	19	1698	20	1686	31	-0.7
HBL-08	178	110.1	0.62	4.658	0.11	0.3211	0.0051	0.65909	0.1051	0.0018	1759	20	1794	25	1713	30	-4.7
HBL-09	298	71.9	0.24	3.486	0.095	0.2138	0.0045	0.82536	0.1163	0.0022	1520	21	1254	25	1898	33	33.9
HBL-10	113	51.4	0.45	4.25	0.11	0.3019	0.0057	0.7081	0.1025	0.0018	1681	21	1699	28	1673	33	-1.6
HBL-11	245	119	0.49	4.67	0.16	0.32	0.0063	0.59534	0.1035	0.0026	1754	28	1788	31	1688	47	-5.9
HBL-12	245	87.5	0.36	3.71	0.11	0.2647	0.0057	0.76435	0.1028	0.002	1573	24	1519	28	1670	36	9.0
HBL-13	149.7	67.4	0.45	3.7	0.13	0.2542	0.0077	0.88096	0.1052	0.0018	1564	29	1457	40	1721	31	15.3
HBL-14	304	125	0.41	4.2	0.13	0.2907	0.0078	0.7983	0.1051	0.0025	1673	27	1643	39	1707	43	3.7
HBL-15	94.2	22.26	0.24	3.93	0.13	0.2774	0.007	0.72261	0.1023	0.0024	1618	27	1580	35	1658	43	4.7
HBL-16	248	50	0.20	3.373	0.11	0.2365	0.0063	0.84506	0.1043	0.0022	1498	25	1371	34	1698	38	19.3
HBL-17	476	294	0.62	2.093	0.092	0.1603	0.0075	0.92493	0.0965	0.0019	1151	31	955	41	1553	37	38.5
HBL-18	171	29.8	0.17	4.24	0.15	0.2968	0.0091	0.88332	0.1033	0.0018	1683	29	1677	45	1691	33	0.8
HBL-19	295	54.1	0.18	4.103	0.11	0.2862	0.0064	0.88962	0.1045	0.0015	1654	21	1621	32	1706	28	5.0
HBL-20	382	152.9	0.40	4.737	0.1	0.3269	0.0045	0.69119	0.1066	0.0016	1776	18	1822	22	1740	28	-4.7
HBL-21	190	39.7	0.21	2.95	0.2	0.2	0.013	0.96736	0.1063	0.0018	1395	50	1176	72	1738	30	32.3
HBL-22	166	45.9	0.28	4.64	0.14	0.3078	0.0068	0.75159	0.109	0.0022	1757	25	1728	33	1781	35	3.0
HBL-23	172	82.9	0.48	3.898	0.11	0.2695	0.006	0.84822	0.1046	0.0016	1611	23	1540	30	1708	29	9.8
HBL-25	225	51.2	0.23	4.316	0.11	0.3044	0.0059	0.80015	0.1027	0.0016	1709	21	1712	29	1676	29	-2.1
HBL-26	172.4	83.1	0.48	0.1603	0.007	0.02337	0.00049	0.20452	0.0497	0.0022	150.6	6.2	148.9	3.1	179	89	16.8
HBL-27	205	44.8	0.22	3.19	0.16	0.217	0.011	0.95732	0.1066	0.0017	1469	36	1278	57	1738	28	26.5
HBL-28	261	122.1	0.47	4.15	0.14	0.2922	0.0088	0.92474	0.1039	0.0015	1659	28	1649	44	1692	27	2.5
HBL-29	167.2	47.7	0.29	4.28	0.12	0.2912	0.006	0.78265	0.1062	0.0018	1694	23	1649	30	1738	31	5.1
HBL-30	101.6	32.7	0.32	4.55	0.13	0.3202	0.0048	0.67312	0.103	0.0019	1741	23	1790	24	1688	35	-6.0
HBL-31	84	28.2	0.34	4.531	0.12	0.3135	0.0048	0.5988	0.1049	0.002	1738	22	1757	24	1713	35	-2.6
HBL-32	216	48.5	0.22	4.13	0.1	0.29	0.0043	0.72261	0.1025	0.0016	1657	20	1641	22	1667	29	1.6
HBL-33	103.7	38.5	0.37	3.817	0.11	0.2621	0.0073	0.82418	0.1051	0.0019	1597	24	1498	37	1714	33	12.6
HBL-34	354	40.5	0.11	3.93	0.13	0.2763	0.0085	0.92507	0.1026	0.0015	1614	27	1575	44	1668	28	5.6
HBL-35	453	198	0.44	4.488	0.1	0.312	0.0049	0.77279	0.1042	0.0015	1729	20	1750	24	1702	27	-2.8
HBL-36	257	52.9	0.21	4.26	0.12	0.2927	0.0065	0.84726	0.1048	0.0016	1683	23	1656	33	1713	28	3.3

Appendix B: Zircon/Apatite LA-ICP-MS U-Pb Isotopic Data and Ages

Table B-14. HBL-TM (BR060913-01) Zr

				Corrected isotope ratios[a]							Ages (Ma)						
Grain # - Spot #	**U [ppm]**	**Th [ppm]**	**Th/U**	**$^{207}Pb/^{235}U$**	**±2s**	**$^{206}Pb/^{238}U$**	**±2s**	**Rho**	**$^{207}Pb/^{206}Pb$**	**±2s**	**$^{207}Pb/^{235}U$**	**±2s**	**$^{206}Pb/^{238}U$**	**±2s**	**$^{207}Pb/^{206}Pb$**	**±2s**	**Disc. %[b]**
HBL-37	246	144	0.59	0.041	0.0038	0.00572	0.00017	0.05111	0.0521	0.0048	40.7	3.7	36.8	1.1	290	180	87.3
HBL-38	290	77.2	0.27	4.26	0.12	0.2984	0.0065	0.79666	0.1033	0.0018	1688	23	1682	32	1681	31	-0.1
HBL-39	556	284	0.51	4.22	0.14	0.2909	0.0081	0.91253	0.105	0.0015	1680	27	1647	40	1711	26	3.7
HBL-40	186.1	63.7	0.34	3.99	0.12	0.2754	0.0057	0.75716	0.1039	0.0019	1630	24	1570	29	1688	34	7.0
HBL-41	305	42.1	0.14	4.748	0.12	0.3272	0.0063	0.85572	0.1043	0.0015	1774	21	1823	31	1708	25	-6.7
HBL-42	174	68.9	0.40	4.797	0.1	0.3288	0.0044	0.70189	0.105	0.0014	1784	18	1831	21	1715	26	-6.8
HBL-43	302	45.8	0.15	3.54	0.15	0.2438	0.0096	0.9251	0.1044	0.0019	1525	33	1402	49	1701	33	17.6

[a]U-Pb fractionation correction and correction for background interference based on GJ-1 zircon standard (Jackson et al., 2004)

[b]Discordance % for 206Pb/238U ages >1Ga calculated as ((1-(206Pb/238U)/(207Pb/206Pb))*100)

Appendix B: Zircon/Apatite LA-ICP-MS U-Pb Isotopic Data and Ages

Table B-15. HBL-AP (BR060913-01) Ap

				Corrected isotope ratios[a]							Ages (Ma)						
Grain # - Spot #	U [ppm]	Th [ppm]	Th/U	$^{207}Pb/^{235}U$	±2s	$^{206}Pb/^{238}U$	±2s	Rho	$^{207}Pb/^{206}Pb$	±2s	$^{207}Pb/^{235}U$	±2s	$^{206}Pb/^{238}U$	±2s	$^{207}Pb/^{206}Pb$	±2s	Disc. %[b]
Hbl-B-02	5.31	1.42	0.27	12.24	0.83	0.306	0.014	0.8315	0.285	0.013	2589	63	1719	69	3374	74	49.1
Hbl-B-03	1.073	0.0545	0.05	55.7	2	0.661	0.025	0.6805	0.615	0.013	4098	35	3266	98	4541	33	28.1
Hbl-B-06	1.334	0.275	0.21	45	1.9	0.576	0.021	0.8330	0.569	0.012	3887	42	2929	87	4429	31	33.9
Hbl-B-07	7.01	3.61	0.51	10.6	0.81	0.302	0.012	0.8835	0.249	0.014	2449	82	1697	57	3110	100	45.4
Hbl-B-08	3.61	0.266	0.07	19.23	0.62	0.3731	0.011	0.6058	0.3744	0.0077	3053	31	2043	51	3810	31	46.4
Hbl-B-09	1.936	0.077	0.04	29.5	1.4	0.445	0.016	0.7679	0.476	0.015	3470	47	2370	70	4165	44	43.1
Hbl-B-11	2.154	0.404	0.19	24.4	0.92	0.41	0.012	0.6255	0.4279	0.0089	3283	35	2213	55	4015	32	44.9
Hbl-B-12	2.84	0.478	0.17	19.82	0.78	0.3711	0.013	0.5322	0.3915	0.0086	3081	37	2033	60	3870	33	47.5
Hbl-B-13	5.18	0.656	0.13	11.24	0.5	0.2924	0.0089	0.7110	0.2746	0.007	2532	40	1652	44	3323	38	50.3
Hbl-B-14	5.04	0.716	0.14	12.64	0.64	0.3	0.013	0.7539	0.3019	0.008	2644	44	1690	62	3469	44	51.3
Hbl-B-16	23.81	4.58	0.19	4.83	0.17	0.2379	0.0074	0.6212	0.1484	0.0033	1787	32	1379	38	2326	37	40.7
Hbl-B-17	52.46	14.68	0.28	3.494	0.1	0.2251	0.0059	0.5199	0.1122	0.0018	1524	23	1308	31	1831	29	28.6
Hbl-B-18	1.96	0.208	0.11	30.51	1.1	0.473	0.018	0.3395	0.474	0.015	3501	35	2493	77	4160	46	40.1
Hbl-B-19	16.4	7.8	0.48	5.33	0.89	0.228	0.0091	0.3519	0.173	0.022	1854	110	1323	47	2540	170	47.9
Hbl-B-21	4.04	0.316	0.08	17.57	0.66	0.3635	0.012	0.6549	0.3494	0.0079	2971	35	2004	58	3704	34	45.9
Hbl-B-22.	3.8	0.228	0.06	20.4	1.7	0.369	0.018	0.8848	0.395	0.018	3071	77	2021	83	3896	67	48.1
Hbl-B-23	60.5	15.22	0.25	3.424	0.11	0.2287	0.0064	0.5726	0.1074	0.0019	1510	26	1327	33	1750	32	24.2
Hbl-B-24	12.72	6.26	0.49	6.54	0.23	0.2331	0.0069	0.8404	0.193	0.0065	1967	34	1350	36	2721	60	50.4
Hbl-B-25	5.56	0.612	0.11	12.78	0.48	0.3257	0.011	0.7413	0.2922	0.0047	2674	34	1816	54	3427	26	47.0
Hbl-B-26	34.9	10.6	0.30	4.02	0.16	0.2196	0.0074	0.7736	0.1311	0.003	1638	34	1279	39	2112	41	39.4
Hbl-B-27	1.329	0.259	0.19	34.6	1.6	0.495	0.017	0.7309	0.507	0.014	3614	45	2587	75	4256	41	39.2

[a]U-Pb fractionation correction and correction for background interference based on GJ-1 zircon standard (Jackson et al., 2004)

[b]Discordance % for 206Pb/238U ages >1Ga calculated as ((1-(206Pb/238U)/(207Pb/206Pb))*100)

Appendix B: Zircon/Apatite LA-ICP-MS U-Pb Isotopic Data and Ages

Table B-16. Grus (BR061713-03) Ap

				Corrected isotope ratios[a]							Ages (Ma)						
Grain # - Spot #	U [ppm]	Th [ppm]	Th/U	$^{207}Pb/^{235}U$	±2s	$^{206}Pb/^{238}U$	±2s	Rho	$^{207}Pb/^{206}Pb$	±2s	$^{207}Pb/^{235}U$	±2s	$^{206}Pb/^{238}U$	±2s	$^{207}Pb/^{206}Pb$	±2s	Disc. %[b]
Grus-01-01	1.058	3.18	3.01	13.75	0.54	0.2767	0.0083	0.2344	0.363	0.013	2730	38	1573	42	3752	52	58.1
Grus-01-02	0.907	2.61	2.88	13.72	0.51	0.2791	0.0089	0.2086	0.358	0.012	2729	37	1585	45	3736	50	57.6
Grus-01-03	0.904	2.71	3.00	14.35	0.56	0.2832	0.0095	0.4455	0.365	0.012	2768	38	1606	47	3759	50	57.3
Grus-02-01	1.28	3.63	2.84	14.83	0.98	0.293	0.013	0.0500	0.38	0.02	2805	48	1656	64	3827	64	56.7
Grus-02-02	0.95	2.64	2.78	14.05	0.68	0.2788	0.01	0.4616	0.372	0.015	2741	45	1583	53	3790	58	58.2
Grus-02-03	0.94	2.73	2.90	14.62	0.65	0.2792	0.009	0.4919	0.38	0.013	2775	42	1584	45	3836	52	58.7
Grus-03-01	0.828	2.33	2.81	14.51	0.66	0.2792	0.0094	0.1604	0.378	0.013	2765	39	1586	47	3804	52	58.3
Grus-03-02	0.922	2.649	2.87	14.06	0.53	0.2827	0.0092	0.2763	0.367	0.011	2743	34	1603	46	3779	44	57.6
Grus-03-03	0.827	2.31	2.79	14.37	0.59	0.2782	0.0097	0.1607	0.376	0.014	2767	38	1580	49	3808	53	58.5
Grus-04-01	0.882	2.48	2.81	13.73	0.64	0.2786	0.011	0.0253	0.361	0.013	2720	42	1582	55	3760	60	57.9
Grus-04-02	1.2	3.31	2.76	12.37	0.76	0.2763	0.011	0.1896	0.329	0.013	2629	47	1571	55	3602	54	56.4
Grus-04-03	1.015	2.88	2.84	13.29	0.68	0.2794	0.01	0.4173	0.346	0.012	2691	44	1591	51	3683	51	56.8
Grus-05-01	0.708	2.06	2.91	17.36	0.81	0.304	0.013	0.5489	0.413	0.015	2954	44	1711	64	3945	56	56.6
Grus-05-02	0.532	1.47	2.76	17.33	0.87	0.3015	0.012	0.6811	0.411	0.013	2945	48	1695	58	3943	45	57.0
Grus-05-03	0.536	1.46	2.72	17.24	0.89	0.3011	0.011	0.3896	0.412	0.018	2959	51	1694	56	3950	69	57.1
Grus-06-01	1.13	3.15	2.79	13.72	0.6	0.2739	0.011	0.0919	0.365	0.012	2734	38	1560	56	3758	51	58.5
Grus-06-02	0.783	2.2	2.81	17.97	0.91	0.3055	0.012	0.4504	0.425	0.015	2988	50	1708	59	3981	52	57.1
Grus-06-03	0.819	2.3	2.81	15.49	0.79	0.282	0.0095	0.4359	0.395	0.015	2840	47	1604	48	3875	55	58.6
Grus-07-01	1.42	4.16	2.93	11.47	0.43	0.2493	0.0079	0.5942	0.3287	0.0078	2562	36	1433	41	3611	37	60.3
Grus-07-02	1.42	3.95	2.78	11.33	0.46	0.2519	0.0077	0.2766	0.3229	0.0098	2549	36	1448	41	3582	44	59.6
Grus-07-03	1.22	3.41	2.80	12.09	0.48	0.2609	0.0084	0.3778	0.3342	0.0095	2610	35	1493	43	3638	45	59.0
Grus-08-01	1.091	2.95	2.70	12.48	0.55	0.2593	0.0078	0.4933	0.346	0.011	2646	41	1489	41	3685	49	59.6
Grus-08-02	1.076	3.06	2.84	12.05	0.47	0.2571	0.0083	0.1509	0.338	0.013	2601	36	1478	42	3658	55	59.6
Grus-08-03	1.27	3.6	2.83	12.59	0.5	0.2641	0.0094	0.2117	0.339	0.012	2645	35	1514	47	3651	54	58.5
Grus-09-01	0.684	1.877	2.74	14.81	0.67	0.2783	0.0097	0.4865	0.382	0.013	2794	42	1590	49	3821	52	58.4
Grus-09-02	0.552	1.578	2.86	17.21	0.75	0.2928	0.012	0.4392	0.422	0.016	2955	45	1652	59	4010	57	58.8
Grus-09-03	0.519	1.497	2.88	16.98	0.81	0.2992	0.011	0.4315	0.417	0.016	2917	46	1685	53	3979	60	57.7
Grus-10-01	1.26	3.73	2.96	11.62	0.44	0.2484	0.0078	0.2078	0.34	0.011	2567	35	1429	39	3657	51	60.9
Grus-10-02	1.35	3.9	2.89	11.63	0.47	0.2522	0.0082	0.2802	0.336	0.011	2570	37	1452	42	3656	50	60.3
Grus-10-03	1.14	3.38	2.96	11.91	0.49	0.2532	0.0077	0.2725	0.337	0.011	2594	40	1454	40	3641	49	60.1

[a]U-Pb fractionation correction and correction for background interference based on GJ-1 zircon standard (Jackson et al., 2004)

[b]Discordance % for 206Pb/238U ages >1Ga calculated as ((1-(206Pb/238U)/(207Pb/206Pb))*100)

Appendix B: Zircon/Apatite LA-ICP-MS U-Pb Isotopic Data and Ages

Table B-17. NFG13-GM1 (BR061613-03) Zr

				Corrected isotope ratios[a]							Ages (Ma)						
Grain # - Spot #	U [ppm]	Th [ppm]	Th/U	$^{207}Pb/^{235}U$	±2s	$^{206}Pb/^{238}U$	±2s	Rho	$^{207}Pb/^{206}Pb$	±2s	$^{207}Pb/^{235}U$	±2s	$^{206}Pb/^{238}U$	±2s	$^{207}Pb/^{206}Pb$	±2s	Disc. %[b]
03c	142.6	51.9	0.36	4.436	0.066	0.3056	0.0037	0.549	0.1047	0.0014	1719	12	1720	18	1708	25	-0.7
03r	211	25	0.12	4.327	0.055	0.2986	0.0031	0.61189	0.10516	0.0013	1698.7	10	1684	15	1717	23	1.9
04r	224	62	0.28	4.307	0.06	0.2985	0.0036	0.61064	0.1047	0.0013	1696.6	11	1683	18	1709	23	1.5
07r	97.2	37.7	0.39	4.397	0.065	0.3058	0.004	0.42752	0.1048	0.0016	1713	12	1719	20	1708	27	-0.6
07r2	542	96.8	0.18	2.277	0.061	0.1407	0.0044	0.90521	0.1169	0.0018	1203	19	852	25	1907	28	55.3
08c	124.7	50.2	0.40	4.364	0.07	0.3027	0.0045	0.70848	0.1044	0.0014	1704	13	1704	22	1704	25	0.0
08r	397	41.8	0.11	3.431	0.097	0.2211	0.0066	0.91024	0.1138	0.0018	1512	23	1297	35	1859	29	30.2
13c	110.1	35.3	0.32	4.427	0.071	0.3058	0.0042	0.56186	0.1051	0.0015	1718	13	1719	21	1713	27	-0.4
13r	207.2	50.7	0.24	4.379	0.067	0.3043	0.0036	0.633	0.1045	0.0015	1708	13	1712	18	1709	25	-0.2
15c	161.3	53.7	0.33	4.264	0.059	0.2968	0.0037	0.6042	0.1038	0.0014	1685.4	11	1675	18	1693	26	1.1
15r	277.9	35.38	0.13	3.115	0.092	0.1906	0.0066	0.9056	0.1184	0.0021	1432	23	1123	36	1932	31	41.9
17Ac	299	34.2	0.11	3.002	0.065	0.198	0.0046	0.90067	0.1102	0.0014	1407	17	1166	24	1804	23	35.4
17Br	565	60.5	0.11	1.741	0.062	0.1125	0.0044	0.94978	0.1122	0.0016	1017	24	686	25	1835	26	62.6
19c	181.8	50.9	0.28	4.41	0.062	0.3052	0.0036	0.66289	0.10518	0.0013	1715.6	11	1719	18	1722	23	0.2
19r	106.4	30.71	0.29	4.411	0.066	0.3074	0.0043	0.59703	0.1049	0.0016	1713	12	1727	21	1712	27	-0.9
22c	77.7	31.3	0.40	4.555	0.08	0.3139	0.0045	0.54335	0.1053	0.0018	1739	14	1759	22	1717	31	-2.4
22r	440	53.1	0.12	2.25	0.15	0.1309	0.0094	0.98145	0.1262	0.0019	1189	48	790	54	2044	27	61.4
23r	104.3	36.5	0.35	4.345	0.072	0.3031	0.0043	0.65735	0.1043	0.0015	1703	14	1706	21	1701	27	-0.3
24r	118.3	26.44	0.22	4.349	0.068	0.3105	0.0043	0.49368	0.1022	0.0017	1702	13	1743	21	1668	30	-4.5
26c	98.1	30	0.31	3.07	0.19	0.213	0.013	0.95994	0.1051	0.0021	1419	50	1239	72	1718	36	27.9
26c	833	86	0.10	0.923	0.032	0.0555	0.0024	0.89574	0.1233	0.0028	662	17	348	14	1999	40	82.6
26r	100.3	28.5	0.28	3.872	0.1	0.2713	0.0071	0.81074	0.105	0.002	1605	21	1546	36	1713	35	9.7
27r	177.7	78.5	0.44	4.167	0.098	0.2792	0.0076	0.9011	0.1078	0.0015	1664	20	1597	39	1762	27	9.4
30c	128.9	41.1	0.32	4.471	0.071	0.3156	0.0045	0.59081	0.1033	0.0016	1724	13	1767	22	1682	27	-5.1
30r	272.8	25.92	0.10	3.2	0.22	0.222	0.016	0.98215	0.1063	0.0016	1422	56	1281	85	1733	27	26.1
32c	507	253.6	0.50	0.0308	0.0015	0.00454	0.0001	0.02188	0.0498	0.0027	30.8	1.5	29.2	0.67	160	100	81.8
32r	410	206.6	0.50	0.0322	0.002	0.00439	0.0001	0.12757	0.0529	0.0032	32.2	2	28.22	0.67	280	120	89.9
33c	113.1	38.17	0.34	4.334	0.069	0.3043	0.0037	0.54302	0.1035	0.0016	1699	13	1712	18	1687	28	-1.5
33r1	173.6	31.23	0.18	4.384	0.065	0.3055	0.0042	0.70507	0.1047	0.0014	1708	12	1718	21	1706	25	-0.7
34r	272	32.5	0.12	4.692	0.099	0.2985	0.0057	0.63198	0.1144	0.0019	1767	17	1683	28	1868	29	9.9
35r	136.8	32.9	0.24	4.386	0.062	0.3019	0.0038	0.42907	0.1047	0.0017	1709.8	12	1700	19	1705	29	0.3
44c	134.5	55.1	0.41	4.044	0.082	0.2807	0.0063	0.80839	0.1052	0.0017	1641	17	1598	31	1716	29	6.9
44r	141.3	40.8	0.29	4.382	0.067	0.3031	0.0035	0.63201	0.1045	0.0014	1709	13	1706	18	1703	25	-0.2
45c	149.1	235	1.58	3.16	0.051	0.2506	0.0036	0.637	0.0917	0.0015	1449	13	1441	19	1458	30	1.2
52c	75.8	34.4	0.45	4.319	0.063	0.3002	0.0032	0.39668	0.1041	0.0015	1695.8	12	1692	16	1698	28	0.4

Appendix B: Zircon/Apatite LA-ICP-MS U-Pb Isotopic Data and Ages

Table B-17. NFG13-GM1 (BR061613-03) Zr

				Corrected isotope ratios[a]							Ages (Ma)						
Grain # - Spot #	U [ppm]	Th [ppm]	Th/U	$^{207}Pb/^{235}U$	±2s	$^{206}Pb/^{238}U$	±2s	Rho	$^{207}Pb/^{206}Pb$	±2s	$^{207}Pb/^{235}U$	±2s	$^{206}Pb/^{238}U$	±2s	$^{207}Pb/^{206}Pb$	±2s	Disc. %[b]
53c	66.9	80.7	1.21	0.1636	0.0087	0.02329	0.00055	0.02242	0.0505	0.0027	154.1	7.4	148.4	3.4	220	110	32.5
53r	75.9	57.9	0.76	0.1534	0.0093	0.02383	0.00051	0.02	0.0472	0.0031	145	8.1	151.8	3.2	80	120	-89.8
56c	156.3	58.9	0.38	4.04	0.18	0.275	0.012	0.92825	0.1073	0.0021	1636	36	1573	59	1755	36	10.4
57c	80.2	68.5	0.85	0.1572	0.0088	0.023	0.00046	0.02	0.0502	0.0031	147.6	7.7	146.6	2.9	190	120	22.8
57r	44.9	35	0.78	0.169	0.012	0.02311	0.00059	0.01508	0.0535	0.0039	158	10	147.2	3.7	320	140	54.0
62r	182.8	58.7	0.32	4.455	0.066	0.311	0.0037	0.68727	0.1047	0.0014	1721	12	1745	18	1710	25	-2.0
63c	239	53.7	0.22	4.554	0.078	0.3022	0.0037	0.47307	0.1093	0.0018	1740	14	1702	18	1784	30	4.6
64c	177	38.3	0.22	4.46	0.067	0.3063	0.0038	0.68714	0.1054	0.0014	1723	13	1722	19	1728	24	0.3

[a]U-Pb fractionation correction and correction for background interference based on GJ-1 zircon standard (Jackson et al., 2004)

[b]Discordance % for 206Pb/238U ages >1Ga calculated as ((1-(206Pb/238U)/(207Pb/206Pb))*100)

Appendix B: Zircon/Apatite LA-ICP-MS U-Pb Isotopic Data and Ages

Table B-18. NFG13-GM2 (BR061613-03) Zr

				Corrected isotope ratios[a]							Ages (Ma)						
Grain # - Spot #	U [ppm]	Th [ppm]	Th/U	$^{207}Pb/^{235}U$	±2s	$^{206}Pb/^{238}U$	±2s	Rho	$^{207}Pb/^{206}Pb$	±2s	$^{207}Pb/^{235}U$	±2s	$^{206}Pb/^{238}U$	±2s	$^{207}Pb/^{206}Pb$	±2s	Disc. %[b]
01c	188	54.5	0.29	4.06	0.17	0.281	0.014	0.77827	0.1066	0.0037	1651	31	1593	70	1745	61	8.7
01r	6770	481	0.07	0.532	0.018	0.01474	0.00041	0.85665	0.2592	0.0054	433	12	94.3	2.6	3238	33	97.1
02c	755	102.6	0.14	0.829	0.029	0.0331	0.0013	0.82237	0.1802	0.0045	612	16	210	8.2	2650	41	92.1
02r	950	106.9	0.11	1.357	0.042	0.0676	0.0019	0.7604	0.1459	0.0036	869	18	421.8	11	2294	43	81.6
03r	173	41.2	0.24	4.453	0.1	0.3112	0.0057	0.6286	0.1045	0.0021	1723	19	1746	28	1699	38	-2.8
05r	5600	193	0.03	0.375	0.012	0.01277	0.00044	0.88345	0.2175	0.0044	322.5	8.5	81.8	2.8	2965	33	97.2
06r	4850	830	0.17	0.569	0.042	0.0146	0.0011	0.97574	0.2882	0.0058	458	27	93.4	6.9	3405	31	97.3
07r	5440	501	0.09	0.728	0.019	0.01811	0.00046	0.83118	0.2907	0.0057	554.6	11	115.7	2.9	3424	31	96.6
09c	2950	217.2	0.07	0.533	0.036	0.0198	0.0013	0.8365	0.198	0.0085	431	24	126.5	7.9	2815	66	95.5
10c	3620	308	0.09	0.933	0.033	0.02334	0.00074	0.74617	0.2847	0.0075	666	18	148.7	4.7	3382	42	95.6
10r	2300	117.7	0.05	0.661	0.023	0.02596	0.00073	0.71431	0.1833	0.0052	516	14	165.2	4.6	2682	46	93.8
11r	1123	59	0.05	1.473	0.074	0.0601	0.0033	0.77161	0.1786	0.0068	917	30	376	20	2629	62	85.7
12r	328	57.5	0.18	4.23	0.19	0.278	0.011	0.89402	0.1101	0.0025	1678	38	1574	57	1800	42	12.6
14r	169	25.2	0.15	4.389	0.11	0.3006	0.0072	0.68181	0.107	0.0022	1713	21	1697	35	1744	38	2.7
16r	2400	52.5	0.02	1.252	0.064	0.0387	0.0015	0.78784	0.2305	0.0073	818	28	244.4	9.6	3048	50	92.0
17r	3420	113.8	0.03	0.495	0.025	0.02092	0.001	0.86121	0.178	0.0061	411	18	133.4	6.4	2623	57	94.9
18a	4490	726	0.16	0.652	0.03	0.02042	0.00095	0.93889	0.2348	0.0051	506	18	130.3	6	3079	35	95.8
18b	1687	250	0.15	0.819	0.043	0.0346	0.0019	0.86222	0.1755	0.0056	605	24	221	12	2603	54	91.5
20r	2748	458	0.17	0.727	0.026	0.02152	0.00074	0.82269	0.2442	0.006	553	15	137.2	4.6	3141	39	95.6
21r	5570	461	0.08	0.368	0.015	0.00977	0.00041	0.89092	0.276	0.0065	317	11	62.7	2.6	3344	37	98.1
22r	3630	337	0.09	0.754	0.027	0.02671	0.00098	0.9088	0.2067	0.0044	568	15	169.8	6.2	2878	34	94.1
23r	5950	453	0.08	0.689	0.019	0.01783	0.00046	0.8142	0.2853	0.0058	533.4	11	113.9	2.9	3388	32	96.6
25c	586	47.7	0.08	2.89	0.15	0.201	0.011	0.92548	0.1066	0.0026	1389	40	1188	58	1737	44	31.6
26r	516	52.6	0.10	1.65	0.11	0.1008	0.0065	0.96615	0.1172	0.0025	979	41	617	38	1916	36	67.8
28r	9970	720	0.07	0.309	0.013	0.00883	0.00037	0.93001	0.258	0.0051	273.8	9.8	56.7	2.4	3233	31	98.2
29r	282	116.9	0.41	4.596	0.12	0.3147	0.0076	0.55373	0.1048	0.0024	1747	22	1763	37	1708	42	-3.2
31c	72.1	25.65	0.36	4.373	0.11	0.3012	0.0063	0.56761	0.1049	0.0023	1704	20	1699	31	1707	40	0.5
31r	2820	475	0.17	1.882	0.059	0.0423	0.0012	0.84771	0.3198	0.0067	1077	20	267.2	7.3	3566	32	92.5
33r	119.1	32.06	0.27	4.442	0.11	0.3085	0.0057	0.5682	0.1044	0.0022	1717	21	1733	28	1702	39	-1.8
35r	211	41.6	0.20	2.213	0.097	0.1498	0.0061	0.91772	0.1069	0.0024	1181	29	898	34	1744	43	48.5
36r	1793	160.2	0.09	1.02	0.037	0.0335	0.00097	0.72812	0.217	0.006	713	19	212.3	6.1	2960	44	92.8
36c	425	43.1	0.10	1.836	0.07	0.0911	0.0036	0.76803	0.1433	0.0042	1060	24	561	21	2266	49	75.2
37c	954	96	0.10	1.65	0.12	0.0961	0.006	0.88391	0.1249	0.004	978	44	591	35	2017	57	70.7
37r	4170	667	0.16	0.722	0.024	0.0205	0.00056	0.6717	0.2519	0.0069	550	14	130.8	3.6	3186	43	95.9
46c	431	56.4	0.13	1.9	0.11	0.1036	0.0068	0.80141	0.1338	0.0052	1075	39	634	40	2136	67	70.3
46r	1570	144	0.09	0.824	0.066	0.0454	0.0036	0.88369	0.1302	0.0047	603	36	289	23	2087	64	86.2

Appendix B: Zircon/Apatite LA-ICP-MS U-Pb Isotopic Data and Ages

Table B-18. NFG13-GM2 (BR061613-03) Zr

				Corrected isotope ratios[a]							Ages (Ma)						
Grain # - Spot #	U [ppm]	Th [ppm]	Th/U	$^{207}Pb/^{235}U$	±2s	$^{206}Pb/^{238}U$	±2s	Rho	$^{207}Pb/^{206}Pb$	±2s	$^{207}Pb/^{235}U$	±2s	$^{206}Pb/^{238}U$	±2s	$^{207}Pb/^{206}Pb$	±2s	Disc. %[b]
49r	94.4	41	0.43	4.373	0.098	0.3024	0.0058	0.52375	0.105	0.0023	1705	19	1703	29	1714	40	0.6
50r	391	55.4	0.14	2.55	0.12	0.1532	0.0072	0.92334	0.121	0.0028	1279	34	917	41	1973	40	53.5
51c	92.7	31.3	0.34	4.466	0.096	0.3084	0.0055	0.51807	0.1057	0.0022	1725	18	1732	27	1723	38	-0.5
51r	5610	353	0.06	0.722	0.019	0.01894	0.00049	0.88264	0.2756	0.0049	552.1	11	120.9	3.1	3336	28	96.4
51r2	169.1	13.33	0.08	4.295	0.095	0.3005	0.0059	0.7345	0.1045	0.0019	1692	19	1693	29	1701	34	0.5
54c	308	26.7	0.09	3.62	0.13	0.2465	0.0091	0.93363	0.106	0.002	1549	29	1427	46	1730	35	17.5
54r	937	43.4	0.05	1.224	0.047	0.063	0.0018	0.73335	0.1409	0.0041	812	22	393.7	11	2229	50	82.3
55ra	6050	540	0.09	0.493	0.014	0.01149	0.00029	0.78678	0.3106	0.0072	406.3	9.3	73.7	1.8	3520	36	97.9
55rb	4680	339	0.07	0.774	0.02	0.01947	0.00045	0.74741	0.2893	0.0064	582.2	11	124.3	2.8	3413	35	96.4
58c	18.8	29.5	1.57	3.93	0.12	0.2515	0.0062	0.41702	0.1144	0.0034	1622	25	1445	32	1858	55	22.2
59r	6720	407	0.06	0.448	0.018	0.01169	0.00051	0.93836	0.2831	0.0058	377	13	74.9	3.2	3381	31	97.8
60c	243.9	41.7	0.17	4.45	0.14	0.3026	0.009	0.7634	0.1059	0.0025	1717	26	1708	45	1728	44	1.2
61r	1914	183.1	0.10	0.635	0.025	0.02736	0.001	0.71496	0.1659	0.0056	498	16	174	6.6	2511	56	93.1
64r	10620	1028	0.10	0.463	0.017	0.01072	0.00036	0.81429	0.3128	0.0086	385	12	68.7	2.3	3523	42	98.0
65c	2610	576	0.22	0.848	0.032	0.02228	0.00063	0.68528	0.278	0.0086	620	18	142	4	3344	48	95.8
65r	5080	467	0.09	0.503	0.023	0.01422	0.00057	0.81967	0.2585	0.0077	411	15	91	3.6	3231	47	97.2
66c1	559	33.1	0.06	1.99	0.11	0.0847	0.0045	0.92872	0.1727	0.0049	1120	39	523	27	2578	46	79.7
66c2	364	55.6	0.15	4.43	0.18	0.1985	0.0076	0.87753	0.1646	0.004	1724	35	1165	41	2498	40	53.4
66r	13420	458	0.03	0.374	0.014	0.00861	0.00027	0.79938	0.314	0.0084	322.6	10	55.3	1.7	3545	39	98.4

[a]U-Pb fractionation correction and correction for background interference based on GJ-1 zircon standard (Jackson et al., 2004)

[b]Discordance % for 206Pb/238U ages >1Ga calculated as ((1-(206Pb/238U)/(207Pb/206Pb))*100)

Appendix B: Zircon/Apatite LA-ICP-MS U-Pb Isotopic Data and Ages

Table B-19. NFG15-GM1 (BR072815-01) Zr

				Corrected isotope ratios[a]							Ages (Ma)						
Grain # - Spot #	U [ppm]	Th [ppm]	Th/U	$^{207}Pb/^{235}U$	±2s	$^{206}Pb/^{238}U$	±2s	Rho	$^{207}Pb/^{206}Pb$	±2s	$^{207}Pb/^{235}U$	±2s	$^{206}Pb/^{238}U$	±2s	$^{207}Pb/^{206}Pb$	±2s	Disc. %[b]
01r	4620	355	0.08	0.538	0.02	0.01497	0.00052	0.91126	0.2598	0.0044	436	13	95.8	3.3	3248	28	97.1
02b	222	195	0.88	0.324	0.013	0.03948	0.00084	0.22305	0.0592	0.0021	287.2	9.7	249.6	5.2	606	75	58.8
04r	432	133.5	0.31	0.1447	0.0052	0.0221	0.00045	0.0596	0.048	0.0016	137.1	4.6	140.9	2.8	102	66	-38.1
08r	5390	176	0.03	0.6	0.032	0.02	0.0011	0.94861	0.2202	0.0043	474	21	127.9	7.2	2978	31	95.7
09r	3240	285.1	0.09	0.498	0.025	0.01754	0.00088	0.91406	0.2067	0.0047	409	17	112.1	5.6	2876	37	96.1
10r	1690	109	0.06	1.02	0.047	0.0491	0.0027	0.94982	0.1517	0.0032	714	24	309	16	2360	36	86.9
11r	840	63	0.08	0.931	0.036	0.0607	0.0021	0.85152	0.1117	0.0023	668	18	380	13	1824	37	79.2
12a	122.5	52.8	0.43	5.033	0.13	0.3234	0.0057	0.48262	0.1125	0.002	1824	23	1806	28	1841	33	1.9
12b	6190	1376	0.22	0.414	0.026	0.01209	0.00079	0.9709	0.2484	0.0046	351	19	77.4	5	3171	29	97.6
13a	1400	122.5	0.09	1.792	0.097	0.0774	0.004	0.93854	0.1669	0.0033	1039	35	480	24	2523	33	81.0
13b	3290	225.6	0.07	0.722	0.039	0.0236	0.0014	0.95067	0.2193	0.0045	556	21	150.5	8.7	2977	33	94.9
14r	200.9	78.1	0.39	4.126	0.11	0.2876	0.0052	0.60449	0.1046	0.0017	1658	21	1629	26	1703	30	4.3
15r	219.1	41.8	0.19	4.377	0.11	0.3001	0.0056	0.60605	0.1056	0.0017	1708	22	1691	28	1724	30	1.9
17r	4600	355	0.08	0.592	0.023	0.0158	0.00055	0.93245	0.2719	0.0042	471	14	101.1	3.5	3321	24	97.0
18r	171.4	58.3	0.34	4.418	0.11	0.3045	0.0053	0.50482	0.106	0.0019	1717	22	1713	26	1727	33	0.8
20c	203.6	58.9	0.29	4.423	0.11	0.3038	0.006	0.60186	0.1055	0.0019	1720	21	1709	30	1726	33	1.0
21r	3870	62.2	0.02	0.326	0.012	0.01198	0.00043	0.83621	0.1993	0.0043	288.3	8.9	76.8	2.7	2819	34	97.3
22c	201	54.9	0.27	4.41	0.12	0.3013	0.007	0.84747	0.1054	0.0019	1714	24	1701	36	1726	32	1.4
23a	117	40.1	0.34	4.507	0.13	0.3132	0.0067	0.45062	0.1039	0.0024	1731	24	1755	33	1689	43	-3.9
23b	256	97.6	0.38	3.69	0.14	0.2504	0.0087	0.90442	0.1072	0.0017	1568	32	1442	45	1752	29	17.7
24r	1207	274	0.23	1.209	0.038	0.03191	0.00098	0.70564	0.2731	0.0061	804	18	202.4	6.1	3319	34	93.9
25a	3160	287	0.09	0.46	0.023	0.01624	0.0009	0.89351	0.2047	0.0052	383	16	103.8	5.7	2858	41	96.4
25b	179.1	71.4	0.40	4.428	0.12	0.3057	0.0062	0.61582	0.1052	0.0019	1717	22	1718	30	1715	33	-0.2
26r	210	38.03	0.18	4.53	0.14	0.3235	0.0091	0.77835	0.1007	0.002	1738	26	1804	44	1631	38	-10.6
27r	153.9	92.3	0.60	0.725	0.025	0.0904	0.0019	0.25646	0.0579	0.0017	555	14	558	11	510	64	-9.4
28r	1299	244	0.19	1.64	0.062	0.0433	0.0017	0.9037	0.269	0.0048	986	24	273.4	10	3297	28	91.7
29r	1620	521	0.32	1.243	0.043	0.03357	0.00096	0.86177	0.2724	0.0045	822	19	212.8	6	3317	26	93.6
30r	1524	44.4	0.03	0.774	0.027	0.03646	0.001	0.86277	0.1519	0.0029	581	15	231.8	6.1	2369	34	90.2
31r	2050	83	0.04	2.046	0.075	0.0608	0.002	0.93189	0.2415	0.0036	1129	25	380	12	3128	24	87.9
32r	2570	72	0.03	0.746	0.027	0.02415	0.00081	0.86378	0.222	0.0043	567	16	153.8	5.1	2992	31	94.9
33r	6420	297	0.05	0.237	0.012	0.00738	0.00033	0.89727	0.2342	0.0053	216.6	9.9	47.4	2.1	3077	37	98.5
34r	5490	440	0.08	0.737	0.025	0.01726	0.00048	0.91897	0.3037	0.0043	559	14	110.3	3.1	3489	21	96.8
35a	4660	389	0.08	0.872	0.043	0.0218	0.0011	0.96629	0.2818	0.0042	632	23	139.1	6.6	3373	23	95.9
35b	2960	347	0.12	1.11	0.036	0.0305	0.00085	0.85146	0.2625	0.0044	758	17	193.6	5.3	3261	27	94.1
36a	1430	99.4	0.07	1.017	0.062	0.0542	0.0034	0.96617	0.1311	0.0025	717	30	340	20	2112	33	83.9
36b	183.5	55.7	0.30	4.46	0.12	0.3071	0.0059	0.63082	0.1043	0.0017	1723	21	1726	29	1710	32	-0.9

Appendix B: Zircon/Apatite LA-ICP-MS U-Pb Isotopic Data and Ages

Table B-19. NFG15-GM1 (BR072815-01) Zr

Grain # - Spot #	U [ppm]	Th [ppm]	Th/U	Corrected isotope ratios[a] $^{207}Pb/^{235}U$	±2s	$^{206}Pb/^{238}U$	±2s	Rho	$^{207}Pb/^{206}Pb$	±2s	Ages (Ma) $^{207}Pb/^{235}U$	±2s	$^{206}Pb/^{238}U$	±2s	$^{207}Pb/^{206}Pb$	±2s	Disc. %[b]
37r	1051	327	0.31	2.005	0.078	0.0626	0.0025	0.92373	0.2305	0.0039	1113	26	391	15	3055	27	87.2
38r	3480	302	0.09	0.647	0.019	0.01784	0.0005	0.80639	0.2614	0.0047	507.2	12	114	3.1	3255	28	96.5
39a	792	96.5	0.12	3.064	0.11	0.1568	0.0065	0.85987	0.1379	0.0032	1421	28	938	36	2196	40	57.3
39b	721	145.5	0.20	2.955	0.12	0.1586	0.0064	0.87951	0.1342	0.0029	1396	29	948	36	2149	37	55.9
40r	933	17.4	0.02	1.844	0.08	0.0965	0.0037	0.90446	0.1387	0.0025	1060	29	593	22	2213	30	73.2
41r	1127	427	0.38	2.022	0.055	0.0572	0.0013	0.68345	0.2527	0.0047	1122	18	358.7	7.8	3202	29	88.8
42r	775	26.9	0.03	1.115	0.052	0.0613	0.0027	0.87675	0.1291	0.0026	757	25	383	16	2082	35	81.6
44a	736	31.9	0.04	2.084	0.082	0.132	0.0049	0.93636	0.1125	0.0021	1143	26	798	28	1835	33	56.5
44b	2680	71.5	0.03	0.991	0.037	0.02543	0.00076	0.77904	0.2833	0.0061	701	19	161.8	4.7	3385	33	95.2
45r	996	86.8	0.09	0.838	0.042	0.0387	0.0021	0.88656	0.1568	0.004	615	23	245	13	2419	43	89.9
46a	1591	228.9	0.14	0.947	0.047	0.0358	0.0019	0.90692	0.1917	0.0039	676	24	227	12	2753	33	91.8
46b	142.6	46.1	0.32	4.484	0.12	0.3091	0.0061	0.37032	0.1046	0.0021	1731	21	1735	30	1700	37	-2.1
47a	2830	346	0.12	0.821	0.023	0.02165	0.00053	0.80434	0.2754	0.0046	607.9	13	138.1	3.3	3341	26	95.9
47b	128.9	36.3	0.28	4.447	0.12	0.3086	0.0056	0.39027	0.1045	0.002	1724	22	1736	27	1706	35	-1.8
48r	985	170	0.17	1.912	0.062	0.067	0.0023	0.88603	0.2051	0.0038	1082	22	418	14	2871	29	85.4
50r	2160	96.4	0.04	0.737	0.042	0.0267	0.0017	0.97151	0.2024	0.0038	560	24	170	11	2849	32	94.0
51r	890	145.9	0.16	1.721	0.089	0.1098	0.006	0.90547	0.1141	0.0028	1012	34	671	35	1861	44	63.9
52r	2830	233	0.08	0.825	0.033	0.02386	0.00091	0.94288	0.2465	0.0041	610	18	152	5.7	3164	27	95.2
53r	2740	167.7	0.06	0.556	0.021	0.0251	0.001	0.89828	0.1601	0.0033	448	14	159.8	6.5	2456	36	93.5
54r	5440	304	0.06	0.3995	0.012	0.01111	0.0003	0.72657	0.2598	0.0051	342.6	8.4	71.2	1.9	3248	30	97.8
56r	930	43.7	0.05	1.311	0.068	0.0668	0.0035	0.9469	0.142	0.0025	849	29	417	21	2257	29	81.5
57a	2760	703	0.25	0.915	0.028	0.02291	0.00056	0.85376	0.2863	0.0044	659	15	146	3.5	3395	24	95.7
57b	2430	740	0.30	1.015	0.039	0.02415	0.00088	0.93169	0.3025	0.0049	709	19	153.8	5.6	3484	25	95.6
58r	174.7	42.5	0.24	4.422	0.13	0.3026	0.006	0.44669	0.1059	0.0024	1715	24	1704	30	1724	41	1.2
59r	273	197	0.72	0.0884	0.0053	0.01339	0.0004	0.07067	0.0491	0.0031	87.2	5.2	85.8	2.6	160	120	46.4
60r	2270	80.6	0.04	0.78	0.024	0.03266	0.001	0.80658	0.1729	0.0034	585	14	207.1	6.5	2587	33	92.0
61a	1980	168	0.08	1.307	0.048	0.0373	0.0011	0.93809	0.2531	0.0037	846	21	236.1	7	3208	22	92.6
61b	2550	110.3	0.04	1.662	0.058	0.044	0.0014	0.94061	0.2721	0.0039	991	22	277.6	8.9	3316	23	91.6
62a	2050	688	0.34	1.644	0.055	0.0469	0.0015	0.89423	0.2551	0.004	992	21	295.2	9.3	3214	25	90.8
62b	3060	787	0.26	1.867	0.083	0.0533	0.0023	0.93968	0.2583	0.0043	1075	29	334	14	3237	25	89.7
63a	3040	277	0.09	1.258	0.042	0.03276	0.00097	0.92377	0.2774	0.0041	827	19	207.8	6.1	3348	23	93.8
63b	2500	299	0.12	1.278	0.038	0.03312	0.00089	0.88854	0.2824	0.0042	834	17	210	5.5	3376	24	93.8
64c	248.1	94.4	0.38	4.164	0.12	0.2847	0.0057	0.59053	0.1053	0.002	1665	23	1614	29	1721	34	6.2
65r	4020	362	0.09	0.823	0.026	0.02126	0.00059	0.88706	0.2819	0.0042	612	14	135.6	3.7	3373	24	96.0
66a	226	83	0.37	4.066	0.11	0.2782	0.0066	0.73339	0.1051	0.0019	1645	23	1584	33	1728	31	8.3
66b	1750	91.2	0.05	0.546	0.056	0.0289	0.0032	0.96894	0.1382	0.0036	434	37	183	20	2210	46	91.7
67a	600	108.3	0.18	1.9	0.15	0.1226	0.0097	0.98307	0.1131	0.0019	1063	53	741	55	1849	31	59.9

Appendix B: Zircon/Apatite LA-ICP-MS U-Pb Isotopic Data and Ages

Table B-19. NFG15-GM1 (BR072815-01) Zr

				Corrected isotope ratios[a]							Ages (Ma)						
Grain # - Spot #	U [ppm]	Th [ppm]	Th/U	$^{207}Pb/^{235}U$	±2s	$^{206}Pb/^{238}U$	±2s	Rho	$^{207}Pb/^{206}Pb$	±2s	$^{207}Pb/^{235}U$	±2s	$^{206}Pb/^{238}U$	±2s	$^{207}Pb/^{206}Pb$	±2s	Disc. %[b]
67b	285	49.4	0.17	4.35	0.2	0.289	0.013	0.95408	0.1088	0.0019	1690	43	1633	66	1778	31	8.2
68r	715	87.5	0.12	1.45	0.12	0.0818	0.0072	0.98245	0.1291	0.0027	900	50	504	43	2080	37	75.8
69a	3350	72.1	0.02	0.317	0.02	0.0153	0.001	0.95364	0.1515	0.0035	281	16	97.7	6.5	2362	39	95.9
69b	3430	348	0.10	0.554	0.054	0.0157	0.0015	0.97941	0.2548	0.0049	434	34	100	9.6	3213	31	96.9
71r	260	57	0.22	2.68	0.21	0.183	0.015	0.97268	0.1069	0.0021	1303	60	1070	81	1747	36	38.8
72r	2900	391	0.13	0.743	0.026	0.02252	0.00078	0.89966	0.2383	0.0043	562	15	143.5	4.9	3104	28	95.4
73r	1113	56.7	0.05	0.345	0.021	0.0191	0.0015	0.97302	0.132	0.0036	299	16	121.8	9.4	2131	48	94.3
74a	1680	187.8	0.11	0.847	0.033	0.02496	0.00087	0.91438	0.2404	0.004	621	18	158.9	5.5	3122	27	94.9
74b	1340	123.2	0.09	2.07	0.06	0.0568	0.0014	0.8718	0.2673	0.004	1137	20	356.2	8.6	3288	24	89.2
75r	1850	50.2	0.03	1.93	0.06	0.0494	0.0012	0.88294	0.2822	0.0042	1089	21	311	7.6	3375	23	90.8
76r	110.2	43.46	0.39	4.4	0.12	0.3103	0.0063	0.52752	0.1038	0.0019	1710	23	1747	31	1695	34	-3.1
77r	1300	64.2	0.05	2.952	0.11	0.1554	0.0072	0.88594	0.1394	0.0034	1395	29	929	40	2218	43	58.1
81r	4690	187.3	0.04	0.2026	0.0079	0.0049	0.00017	0.94477	0.2996	0.0045	187.6	6.6	31.5	1.1	3470	23	99.1
82r	2950	144.3	0.05	1.248	0.04	0.03442	0.00093	0.93787	0.261	0.0035	822	18	218.1	5.8	3257	21	93.3
83r	848	106.5	0.13	3.958	0.11	0.0943	0.0022	0.82117	0.3035	0.0047	1623	23	581	13	3492	24	83.4
84a	5540	358	0.06	0.675	0.027	0.01804	0.00067	0.95247	0.2747	0.004	521	17	115.2	4.2	3333	23	96.5
84b	482	92	0.19	3.123	0.11	0.2094	0.0065	0.81571	0.109	0.0026	1439	27	1224	35	1781	43	31.3
88r	187	119	0.64	4.494	0.12	0.2957	0.0056	0.65279	0.1105	0.0018	1728	21	1669	28	1804	30	7.5
89r	1720	28.5	0.02	1.047	0.041	0.0325	0.0012	0.88514	0.2368	0.0046	725	20	206.1	7.7	3102	31	93.4

[a]U-Pb fractionation correction and correction for background interference based on GJ-1 zircon standard (Jackson et al., 2004)

[b]Discordance % for 206Pb/238U ages >1Ga calculated as ((1-(206Pb/238U)/(207Pb/206Pb))*100)

Appendix B: Zircon/Apatite LA-ICP-MS U-Pb Isotopic Data and Ages

Table B-20. SAG-GM (BR061113-04) Zr

				Corrected isotope ratios[a]							Ages (Ma)						
Grain # - Spot #	U [ppm]	Th [ppm]	Th/U	$^{207}Pb/^{235}U$	±2s	$^{206}Pb/^{238}U$	±2s	Rho	$^{207}Pb/^{206}Pb$	±2s	$^{207}Pb/^{235}U$	±2s	$^{206}Pb/^{238}U$	±2s	$^{207}Pb/^{206}Pb$	±2s	Disc. %[b]
06c	214	89	0.42	4.581	0.065	0.3143	0.0043	0.72703	0.10478	0.0014	1744.8	12	1761	21	1710	23	-3.0
06r	267	80.6	0.30	4.466	0.067	0.3066	0.0046	0.73919	0.1047	0.0014	1726	13	1726	23	1706	24	-1.2
07c	199.7	79.6	0.40	4.528	0.082	0.3133	0.0052	0.72559	0.1039	0.0014	1735	15	1756	25	1693	25	-3.7
07r	273	112.4	0.41	4.462	0.062	0.3091	0.0039	0.64422	0.10366	0.0013	1725	12	1736	19	1690	24	-2.7
09c	242	105.1	0.43	4.547	0.068	0.3127	0.0048	0.77941	0.1044	0.0014	1740	13	1753	24	1704	25	-2.9
10c	247	98.1	0.40	4.429	0.066	0.3086	0.0041	0.73706	0.10364	0.0012	1717	12	1733	20	1691	22	-2.5
11r	181.5	70.73	0.39	4.436	0.071	0.3046	0.0036	0.56352	0.1045	0.0015	1719	13	1715	18	1702	27	-0.8
13c	157	56.3	0.36	3.8	0.16	0.258	0.012	0.94577	0.1059	0.0017	1583	35	1474	61	1728	29	14.7
13r	371	99.9	0.27	3.33	0.12	0.2278	0.0093	0.93432	0.1056	0.0017	1482	30	1319	49	1729	30	23.7
15r	164.2	48.99	0.30	3.73	0.17	0.246	0.011	0.9194	0.1074	0.0019	1568	36	1412	56	1754	33	19.5
16c	126	50.1	0.40	4.311	0.084	0.2947	0.0044	0.64037	0.104	0.0017	1697	15	1667	22	1706	31	2.3
16r	288	105	0.36	4.456	0.074	0.303	0.004	0.60695	0.1047	0.0015	1721	14	1705	20	1708	27	0.2
17r	256	94.2	0.37	4.586	0.079	0.3119	0.0044	0.68696	0.1052	0.0016	1745	14	1749	22	1712	29	-2.2
18c	559	255	0.46	5.02	0.22	0.344	0.014	0.93123	0.1044	0.0019	1807	37	1899	68	1704	32	-11.4
18r	275	107	0.39	4.467	0.094	0.3055	0.0053	0.7244	0.1038	0.0017	1725	17	1717	26	1693	29	-1.4
19c	184.3	67.3	0.37	4.462	0.074	0.3038	0.0044	0.68475	0.1051	0.0016	1722	14	1709	22	1716	29	0.4
19r	98.7	38.6	0.39	4.376	0.089	0.3041	0.0044	0.57493	0.1041	0.0019	1705	17	1711	22	1698	33	-0.8
20r	105.7	36.2	0.34	4.287	0.084	0.3016	0.005	0.55259	0.1021	0.0017	1688	16	1698	25	1663	32	-2.1
21c	113.2	65.8	0.58	4.404	0.089	0.3014	0.0048	0.62807	0.1051	0.0018	1714	16	1698	24	1717	31	1.1
21r	214	70.4	0.33	4.404	0.087	0.2997	0.0043	0.66715	0.1038	0.0017	1712	16	1689	21	1697	30	0.5
22r	204.8	91.9	0.45	4.658	0.096	0.3191	0.0042	0.69147	0.1049	0.0017	1757	17	1785	20	1711	30	-4.3
24r	261	80.1	0.31	4.553	0.083	0.3112	0.0045	0.58894	0.1045	0.0017	1738	15	1748	22	1704	30	-2.6
26r1	150.8	71.5	0.47	4.513	0.083	0.3107	0.0046	0.67138	0.1047	0.0016	1731	15	1746	23	1709	28	-2.2
26r2	263	90.4	0.34	4.764	0.071	0.326	0.0047	0.67389	0.1049	0.0015	1777	13	1818	23	1713	26	-6.1
28Ac	143.1	62.8	0.44	4.476	0.078	0.3144	0.0038	0.60157	0.1037	0.0015	1726	15	1762	18	1690	28	-4.3
28Br	261	100.3	0.38	4.399	0.072	0.3024	0.0043	0.6573	0.1058	0.0016	1711	14	1703	21	1727	28	1.4
30r	123.3	55.7	0.45	4.33	0.081	0.3019	0.0041	0.64581	0.104	0.0016	1703	15	1700	20	1695	29	-0.3
33c	142	76.1	0.54	4.598	0.092	0.3184	0.0054	0.70822	0.1043	0.0017	1746	17	1781	26	1700	30	-4.8
33r	483	138.6	0.29	4.561	0.075	0.3153	0.0047	0.62852	0.1046	0.0015	1743	14	1766	23	1706	26	-3.5
34Ar	169	45.7	0.27	4.1	0.13	0.2899	0.0079	0.91156	0.1041	0.0019	1647	28	1646	38	1699	33	3.1
34Bc	243	84.1	0.35	4.384	0.093	0.3024	0.0046	0.65204	0.1046	0.0018	1706	18	1705	22	1708	30	0.2
35r	355	119.3	0.34	2.8	0.16	0.185	0.012	0.95285	0.1126	0.0023	1351	43	1086	64	1844	36	41.1
36c	169.9	68.7	0.40	4.461	0.087	0.3118	0.0047	0.57932	0.1045	0.0019	1723	16	1749	23	1702	34	-2.8
36r	134.7	45.9	0.34	4.394	0.08	0.3082	0.0044	0.54399	0.1044	0.0018	1715	15	1734	22	1701	32	-1.9
39c	358	86.4	0.24	4.485	0.1	0.3074	0.005	0.65014	0.1059	0.0019	1728	19	1727	25	1729	33	0.1

Appendix B: Zircon/Apatite LA-ICP-MS U-Pb Isotopic Data and Ages

Table B-20. SAG-GM (BR061113-04) Zr

				Corrected isotope ratios[a]							Ages (Ma)						
Grain # - Spot #	U [ppm]	Th [ppm]	Th/U	$^{207}Pb/^{235}U$	±2s	$^{206}Pb/^{238}U$	±2s	Rho	$^{207}Pb/^{206}Pb$	±2s	$^{207}Pb/^{235}U$	±2s	$^{206}Pb/^{238}U$	±2s	$^{207}Pb/^{206}Pb$	±2s	Disc. %[b]
40r	178	41.8	0.23	4.829	0.096	0.3421	0.0052	0.60581	0.1038	0.0019	1789	17	1896	25	1689	33	-12.3
41r	76.5	22.7	0.30	4.81	0.12	0.3303	0.0061	0.59091	0.1058	0.0023	1790	21	1839	30	1718	41	-7.0
42r	173	44	0.25	4.38	0.12	0.3058	0.0074	0.75132	0.1055	0.0023	1706	22	1719	37	1721	39	0.1
45c	112.6	26.4	0.23	4.313	0.085	0.3031	0.0047	0.75926	0.1034	0.0015	1698	16	1706	23	1685	26	-1.2
47r	167.2	81.5	0.49	4.82	0.1	0.3311	0.0064	0.82054	0.1054	0.0015	1788	18	1842	31	1719	26	-7.2
50c	103.3	44.3	0.43	4.495	0.064	0.3144	0.0043	0.49629	0.1047	0.0016	1729.1	12	1764	21	1709	28	-3.2
52r	82.7	32.88	0.40	4.429	0.078	0.302	0.0046	0.59247	0.1057	0.0017	1719	15	1700	23	1725	29	1.4
54r	106.9	40.3	0.38	4.319	0.068	0.3049	0.0041	0.52629	0.1032	0.0016	1697	13	1715	20	1685	28	-1.8
57r	239	104.8	0.44	4.605	0.092	0.3169	0.0067	0.77597	0.1062	0.0016	1749	17	1773	33	1732	28	-2.4
59r	292	96.4	0.33	4.495	0.089	0.3107	0.0057	0.81411	0.1049	0.0014	1729	17	1749	28	1714	24	-2.0
61r	490	118.3	0.24	4.513	0.072	0.31	0.0046	0.78094	0.1063	0.0014	1732	13	1740	22	1738	23	-0.1
65c	117.8	70.1	0.60	4.36	0.07	0.3033	0.0039	0.43211	0.1035	0.0016	1703	13	1707	19	1693	27	-0.8
65r	321	99.6	0.31	4.299	0.063	0.2973	0.0043	0.63307	0.1044	0.0014	1692.1	12	1677	21	1701	25	1.4
66r	149.3	53.1	0.36	4.423	0.066	0.3057	0.0045	0.59585	0.1038	0.0015	1717	13	1721	22	1695	27	-1.5
68c	117.3	35.2	0.30	4.333	0.064	0.2996	0.0038	0.46396	0.1037	0.0016	1698	12	1689	19	1694	29	0.3
68r	204	58.1	0.28	4.406	0.066	0.3028	0.0042	0.67044	0.1047	0.0015	1712	12	1705	21	1708	25	0.2
71r	136.6	40.7	0.30	4.48	0.062	0.3071	0.0038	0.53338	0.1047	0.0015	1726.3	12	1726	19	1706	26	-1.2

[a]U-Pb fractionation correction and correction for background interference based on GJ-1 zircon standard (Jackson et al., 2004)

[b]Discordance % for 206Pb/238U ages >1Ga calculated as ((1-(206Pb/238U)/(207Pb/206Pb))*100)

Appendix B: Zircon/Apatite LA-ICP-MS U-Pb Isotopic Data and Ages

Table B-21. SAG-TM (BR061113-04) Zr

				Corrected isotope ratios[a]							Ages (Ma)						
Grain # - Spot #	U [ppm]	Th [ppm]	Th/U	$^{207}Pb/^{235}U$	±2s	$^{206}Pb/^{238}U$	±2s	Rho	$^{07}Pb/^{206}Pb$	±2s	$^{207}Pb/^{235}U$	±2s	$^{206}Pb/^{238}U$	±2s	$^{07}Pb/^{206}Pb$	±2s	Disc. %[b]
1	185	61.8	0.33	4.102	0.1	0.2916	0.0057	0.83266	0.1027	0.0014	1653	20	1648	28	1673	26	1.5
2	181	112.2	0.62	4.35	0.12	0.2951	0.0061	0.74663	0.1066	0.002	1700	24	1666	30	1746	34	4.6
3	218	97.6	0.45	4.4	0.13	0.3109	0.007	0.87853	0.1048	0.0018	1715	26	1743	34	1712	33	-1.8
4	121	51.8	0.43	3.94	0.1	0.2837	0.0049	0.74453	0.0996	0.0017	1621	21	1612	25	1614	31	0.1
5	265	125.7	0.47	4.28	0.13	0.283	0.007	0.81685	0.1102	0.0021	1689	23	1605	35	1798	34	10.7
6	338	67.4	0.20	4.602	0.11	0.3107	0.0059	0.7174	0.1077	0.0018	1752	20	1746	29	1761	30	0.9
7	397	87.1	0.22	3.475	0.081	0.239	0.0039	0.71802	0.106	0.0016	1519	18	1381	21	1731	27	20.2
8	172	87.2	0.51	4.579	0.1	0.3207	0.0046	0.72219	0.1042	0.0015	1746	18	1795	23	1701	26	-5.5
9	248	65.4	0.26	3.09	0.13	0.2082	0.0065	0.8223	0.1095	0.0027	1443	32	1217	35	1788	46	31.9
10	102.8	32.7	0.32	4.439	0.11	0.3068	0.0043	0.7332	0.1049	0.0019	1717	20	1724	21	1716	33	-0.5
11	174	46.1	0.26	3.58	0.12	0.2471	0.0069	0.90783	0.1065	0.0017	1545	26	1422	36	1740	29	18.3
12	184	45.1	0.25	4.258	0.1	0.2963	0.004	0.64963	0.1052	0.0018	1683	19	1672	20	1712	31	2.3
13	186	50.3	0.27	4.223	0.1	0.2992	0.004	0.56651	0.1035	0.0018	1677	20	1687	20	1687	33	0.0
14a	107.2	40.3	0.38	4.109	0.11	0.2855	0.0043	0.66769	0.105	0.0019	1654	21	1621	21	1714	34	5.4
14b	126	30.8	0.24	3.99	0.12	0.281	0.0062	0.72606	0.1025	0.002	1627	24	1599	32	1670	37	4.3
15	266	87	0.33	3.904	0.1	0.2738	0.0051	0.8123	0.1056	0.0016	1617	22	1562	25	1723	28	9.3
16	456	104	0.23	2.431	0.1	0.1619	0.0066	0.9345	0.1107	0.0017	1247	31	965	36	1807	27	46.6
17	174	58.2	0.33	4.61	0.1	0.3286	0.0047	0.7413	0.1032	0.0015	1754	18	1833	22	1684	27	-8.8
18	313	158.1	0.51	4.38	0.13	0.3001	0.0065	0.71287	0.1081	0.0021	1711	24	1690	32	1760	36	4.0
19	251	52.4	0.21	4.271	0.11	0.2983	0.0062	0.80505	0.1039	0.0017	1690	21	1685	30	1696	30	0.6
20	234	69.4	0.30	4.376	0.11	0.3016	0.0043	0.64746	0.1043	0.0018	1708	21	1698	21	1702	33	0.2
21	181.3	69	0.38	4.39	0.13	0.3074	0.007	0.8176	0.1043	0.0018	1710	24	1726	35	1696	32	-1.8
22	474	85.7	0.18	4.59	0.21	0.247	0.011	0.80651	0.1366	0.0039	1750	39	1421	56	2181	50	34.8
23	220.2	69.8	0.32	4.413	0.091	0.3048	0.0034	0.68607	0.1052	0.0014	1714	17	1717	17	1715	25	-0.1
24	139.7	60.8	0.44	4.388	0.11	0.3123	0.0049	0.67765	0.103	0.0017	1714	21	1756	24	1682	32	-4.4
25a	321	126.5	0.39	4.635	0.094	0.3202	0.0044	0.8292	0.10461	0.0012	1755	17	1790	21	1709	21	-4.7
25b	384	166.8	0.43	4.399	0.12	0.3027	0.0055	0.67604	0.1045	0.0018	1711	21	1710	27	1708	32	-0.1
26	240	100.1	0.42	4.01	0.12	0.2715	0.0063	0.80177	0.1071	0.002	1637	24	1547	32	1746	34	11.4
27	301	114.6	0.38	4.08	0.13	0.2655	0.0062	0.69371	0.11	0.0026	1649	27	1521	32	1787	43	14.9
28	245	54.5	0.22	4.484	0.094	0.309	0.0038	0.76451	0.1058	0.0014	1726	17	1735	19	1728	24	-0.4
29	218	42	0.19	3.62	0.17	0.244	0.012	0.96127	0.1079	0.0017	1545	39	1409	63	1763	28	20.1
30	89.3	48.2	0.54	4.466	0.089	0.3106	0.0044	0.56887	0.1036	0.0016	1726	17	1743	22	1687	28	-3.3
31	203	88.1	0.43	4.205	0.11	0.2809	0.0066	0.90571	0.108	0.0015	1674	22	1594	33	1763	25	9.6
32	200	79.1	0.40	4.427	0.084	0.3088	0.0037	0.65702	0.10364	0.0013	1718.3	16	1737	19	1690	23	-2.8
33	118	44.7	0.38	4.309	0.1	0.2959	0.0044	0.66964	0.1051	0.0016	1697	19	1670	22	1717	28	2.7

Appendix B: Zircon/Apatite LA-ICP-MS U-Pb Isotopic Data and Ages

Table B-21. SAG-TM (BR061113-04) Zr

				Corrected isotope ratios[a]							Ages (Ma)						
Grain # - Spot #	U [ppm]	Th [ppm]	Th/U	$^{207}Pb/^{235}U$	±2s	$^{206}Pb/^{238}U$	±2s	Rho	$^{07}Pb/^{206}Pb$	±2s	$^{207}Pb/^{235}U$	±2s	$^{206}Pb/^{238}U$	±2s	$^{07}Pb/^{206}Pb$	±2s	Disc. %[b]
34	222.9	158.6	0.71	4.58	0.12	0.2718	0.0074	0.83809	0.1203	0.002	1743	22	1548	37	1962	31	21.1
35	332	131.9	0.40	4.483	0.099	0.3081	0.0048	0.8251	0.1051	0.0014	1729	18	1730	24	1713	24	-1.0
36	190	67.8	0.36	4.03	0.12	0.2796	0.0073	0.92771	0.1045	0.0016	1636	24	1587	37	1704	28	6.9
37	282	81	0.29	3.12	0.12	0.2234	0.0079	0.91942	0.1022	0.0018	1434	30	1298	41	1662	33	21.9
38	245.8	89.3	0.36	4.444	0.08	0.3081	0.0033	0.55985	0.1052	0.0014	1722	15	1731	16	1717	25	-0.8
39	158.5	47.9	0.30	4.259	0.08	0.2975	0.0032	0.62214	0.10428	0.0013	1685.7	15	1679	16	1699	23	1.2
40	291	70.5	0.24	4.284	0.092	0.3029	0.0053	0.80823	0.10218	0.0013	1690	18	1704	26	1664	24	-2.4
41	156	68.8	0.44	4.651	0.1	0.3111	0.0043	0.62869	0.1082	0.0016	1758	18	1745	21	1767	26	1.2
42a	382	123	0.32	3.4	0.084	0.2392	0.0052	0.78439	0.105	0.0018	1505	19	1385	26	1719	32	19.4
42b	421	107.2	0.25	3.72	0.17	0.2422	0.0092	0.93199	0.1093	0.0018	1571	35	1395	47	1792	31	22.2
43	229	63.1	0.28	4.656	0.11	0.314	0.0054	0.8334	0.1063	0.0014	1762	20	1765	27	1737	25	-1.6
44	47.7	15.22	0.32	4.07	0.2	0.269	0.012	0.88907	0.1097	0.0025	1638	40	1528	60	1788	42	14.5
45	319	160	0.50	4.35	0.089	0.3011	0.004	0.78072	0.10412	0.0013	1701	17	1698	20	1697	22	-0.1

[a]U-Pb fractionation correction and correction for background interference based on GJ-1 zircon standard (Jackson et al., 2004)

[b]Discordance % for 206Pb/238U ages >1Ga calculated as ((1-(206Pb/238U)/(207Pb/206Pb))*100)

Appendix C: Cathodoluminescence Imagery of Zircons

C-1. QPC-07 (BR060913-07)

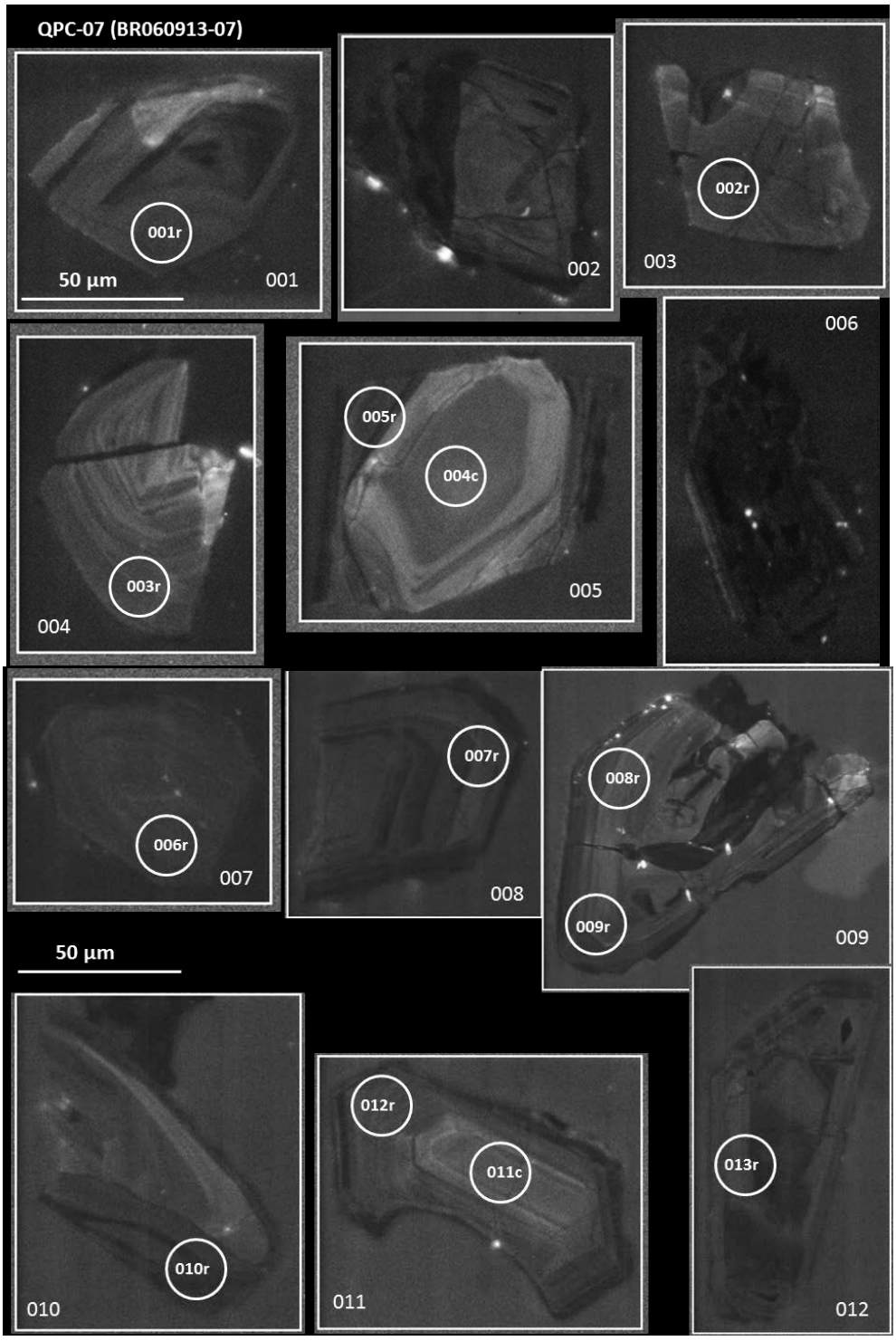

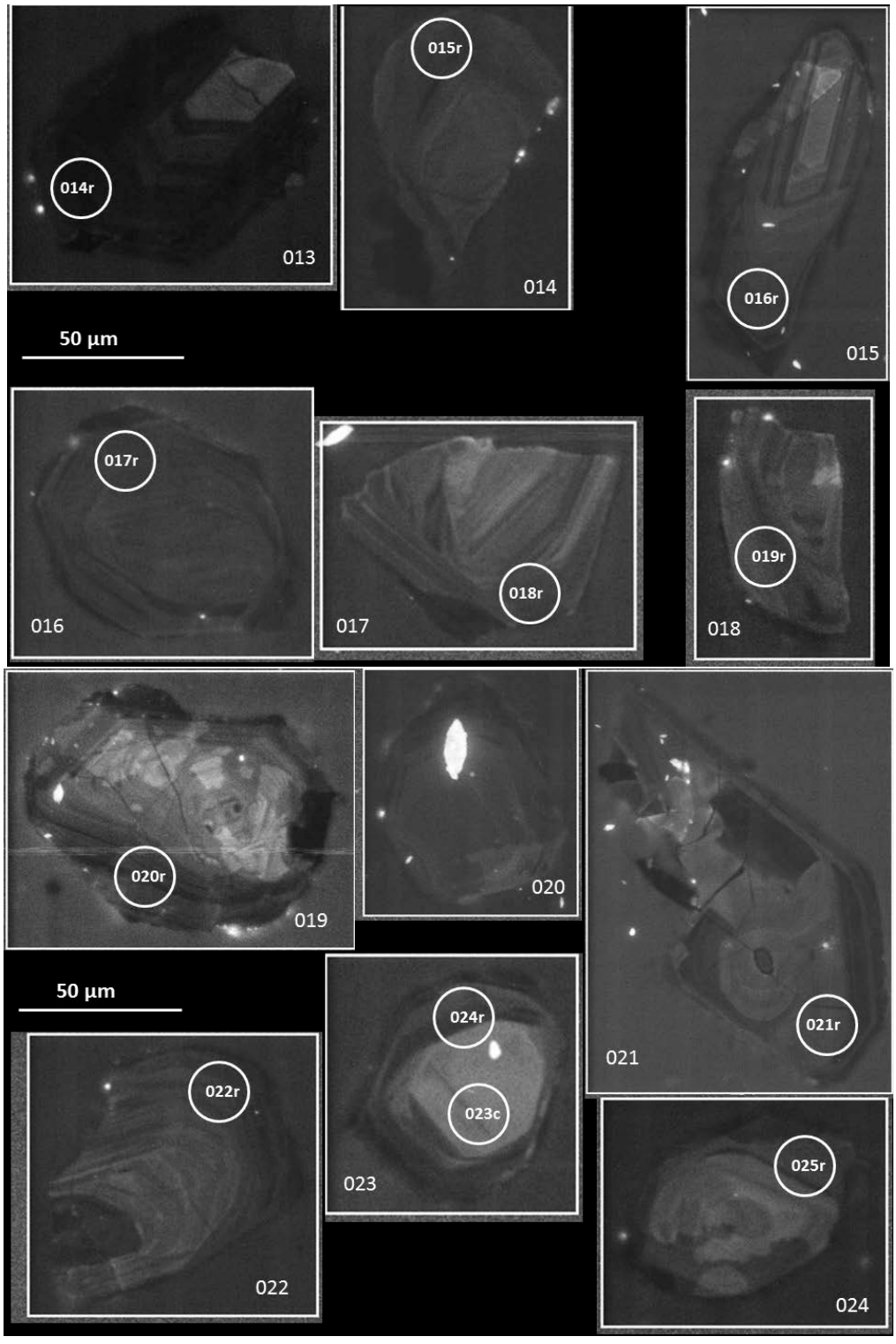
014r
013
015r
014
016r
015
50 µm
017r
016
018r
017
019r
018
020r
019
020
021r
021
50 µm
024r
023c
023
022r
022
025r
024

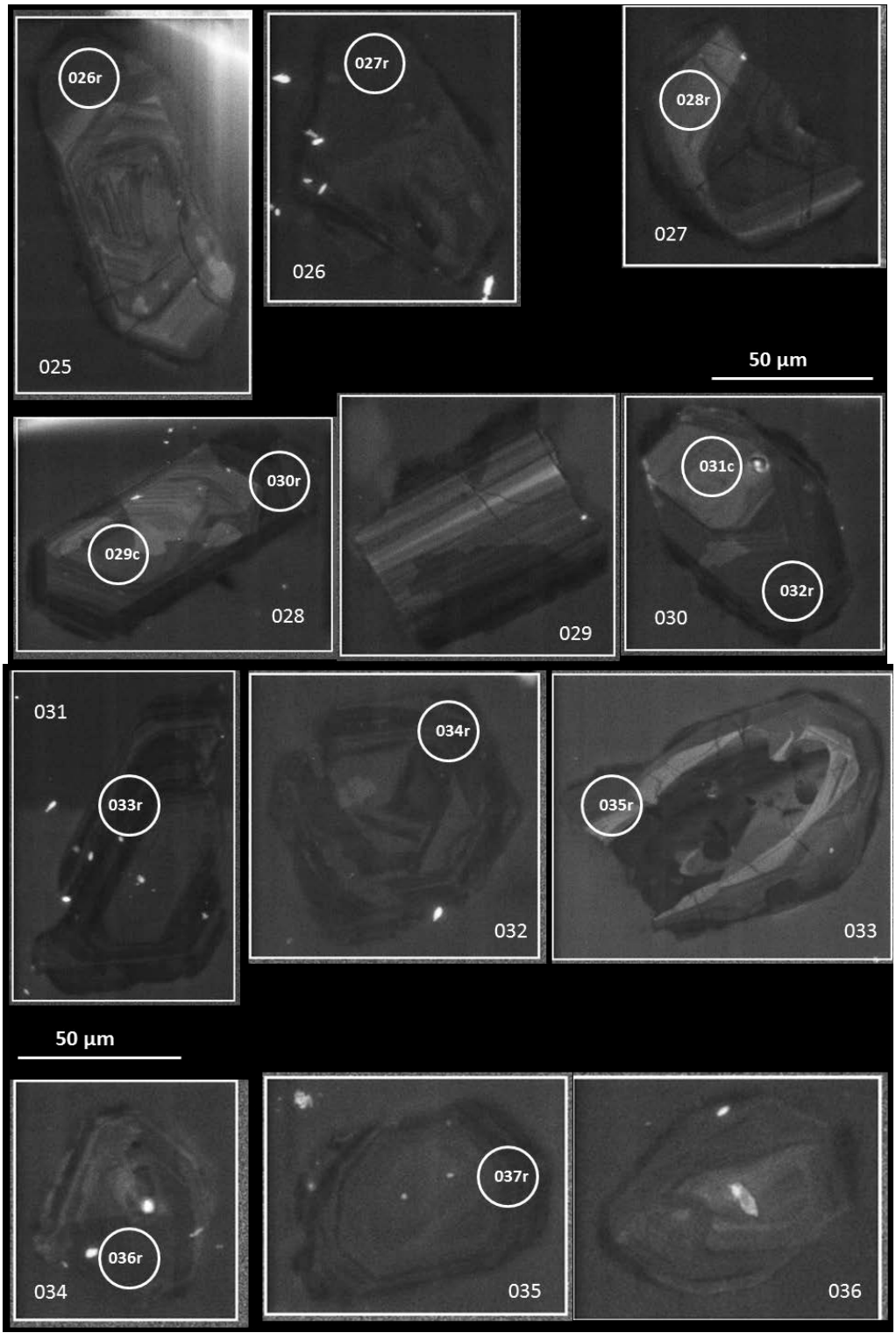
026r
025
027r
026
028r
027
50 µm
030r
029c
028
029
031c
032r
030
031
033r
034r
032
035r
033
50 µm
036r
034
037r
035
036

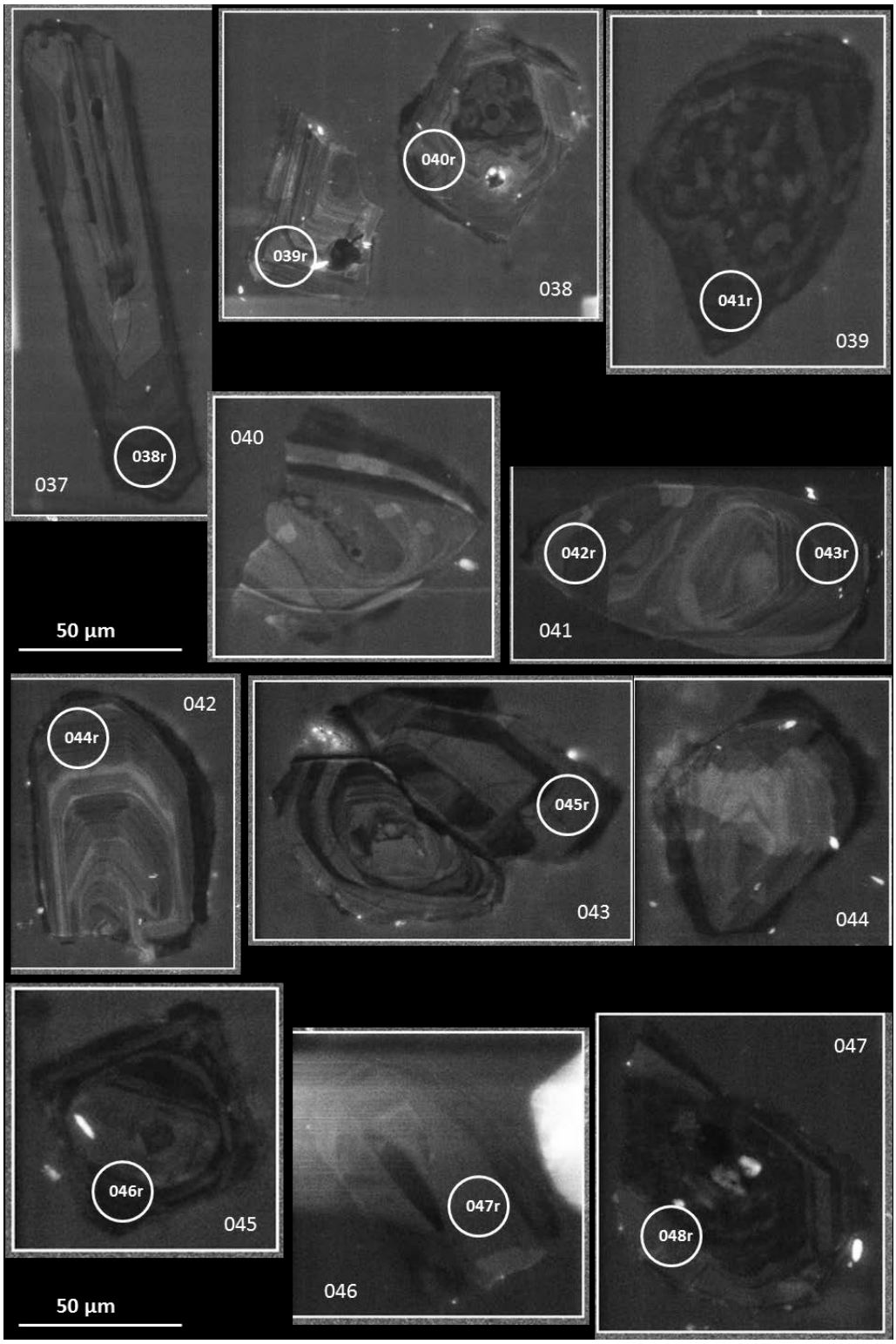
037
038r
038
039r
040r
039
041r
040
041
042r
043r
042
044r
043
045r
044
045
046r
046
047r
047
048r
50 µm
50 µm

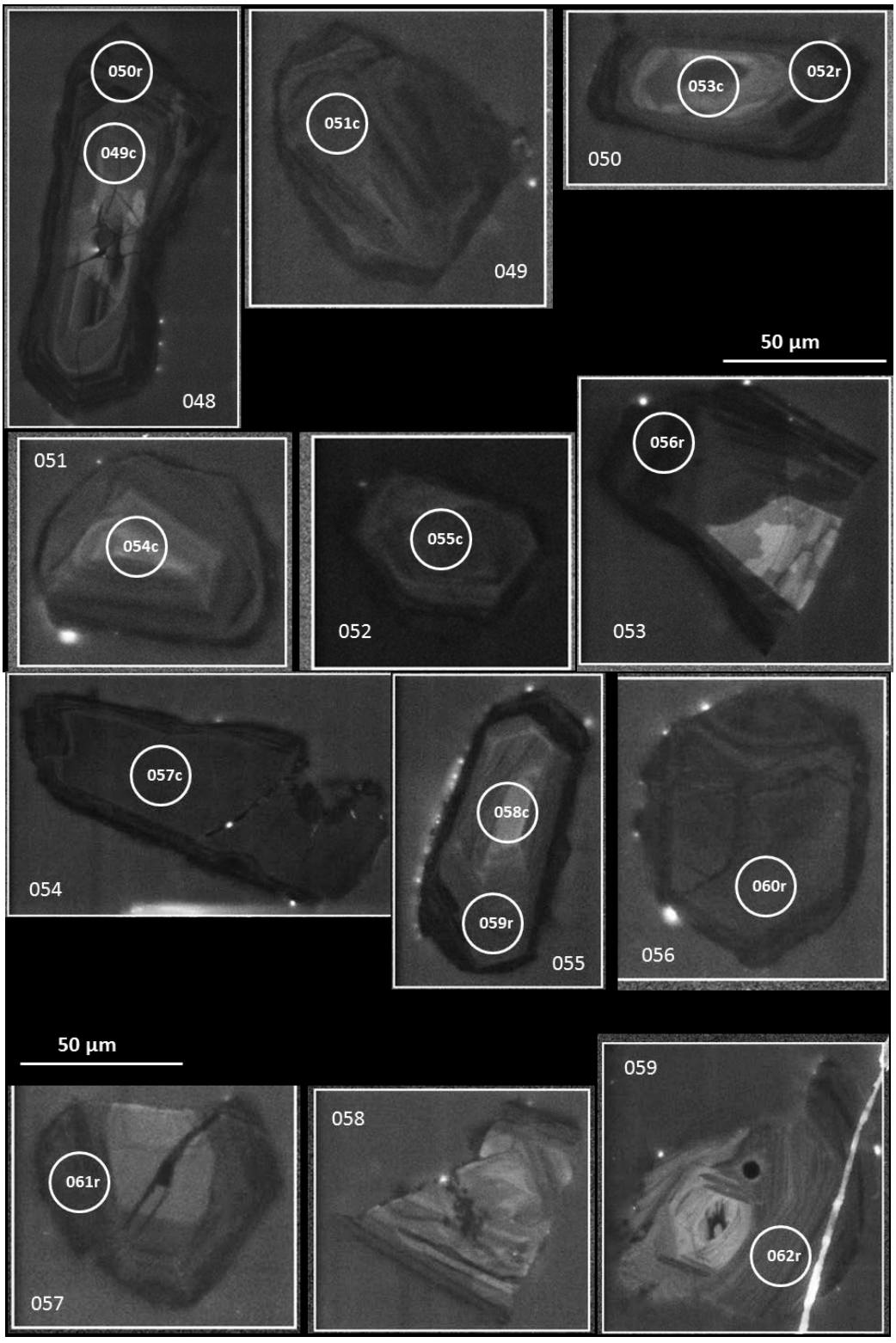
050r
049c
048
051c
049
053c
052r
050
50 µm
051
054c
055c
052
056r
053
057c
054
058c
059r
055
060r
056
50 µm
061r
057
058
059
062r

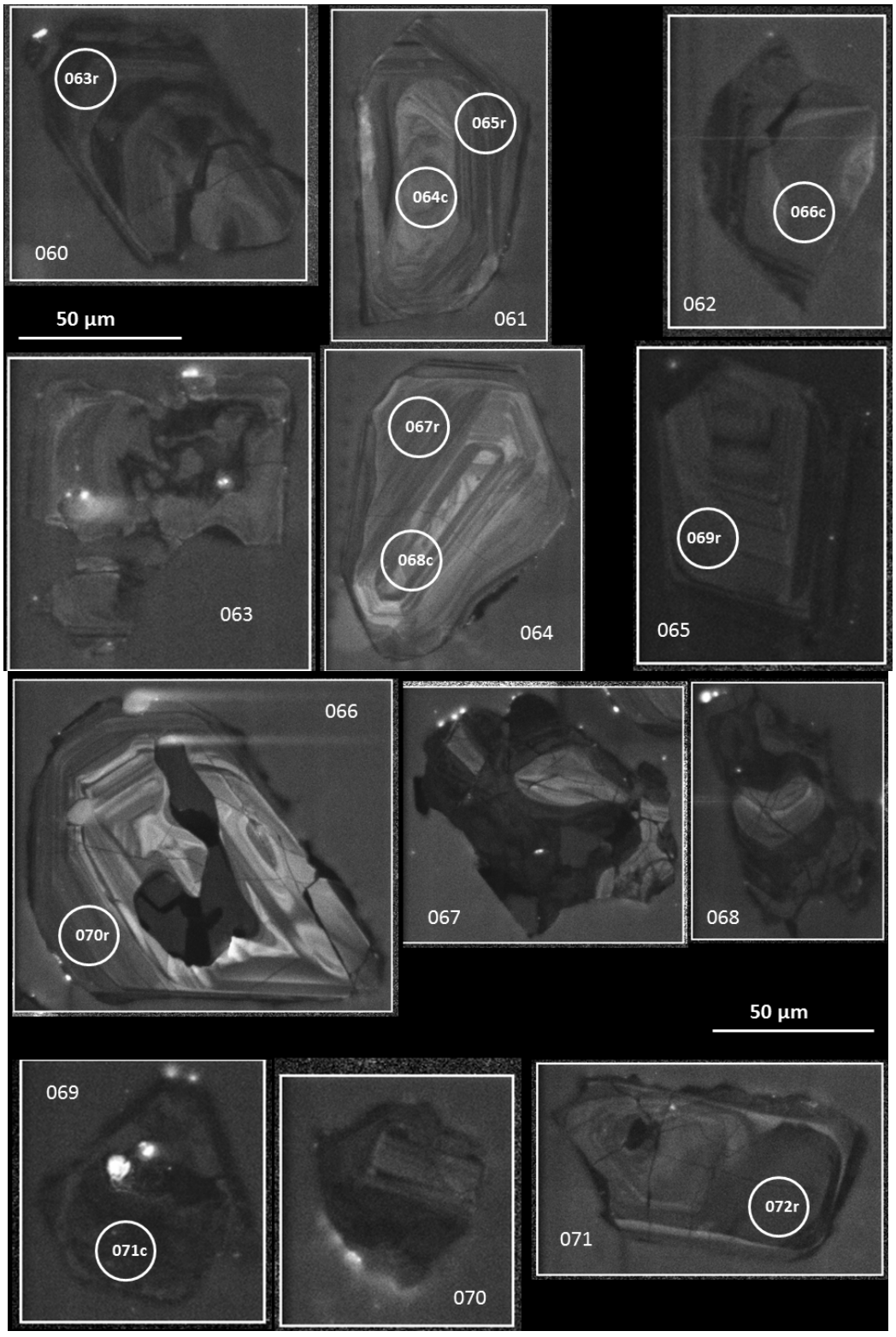
063r
060
065r
064c
061
066c
062
50 µm
067r
068c
063
064
069r
065
066
070r
067
068
50 µm
069
071c
070
072r
071

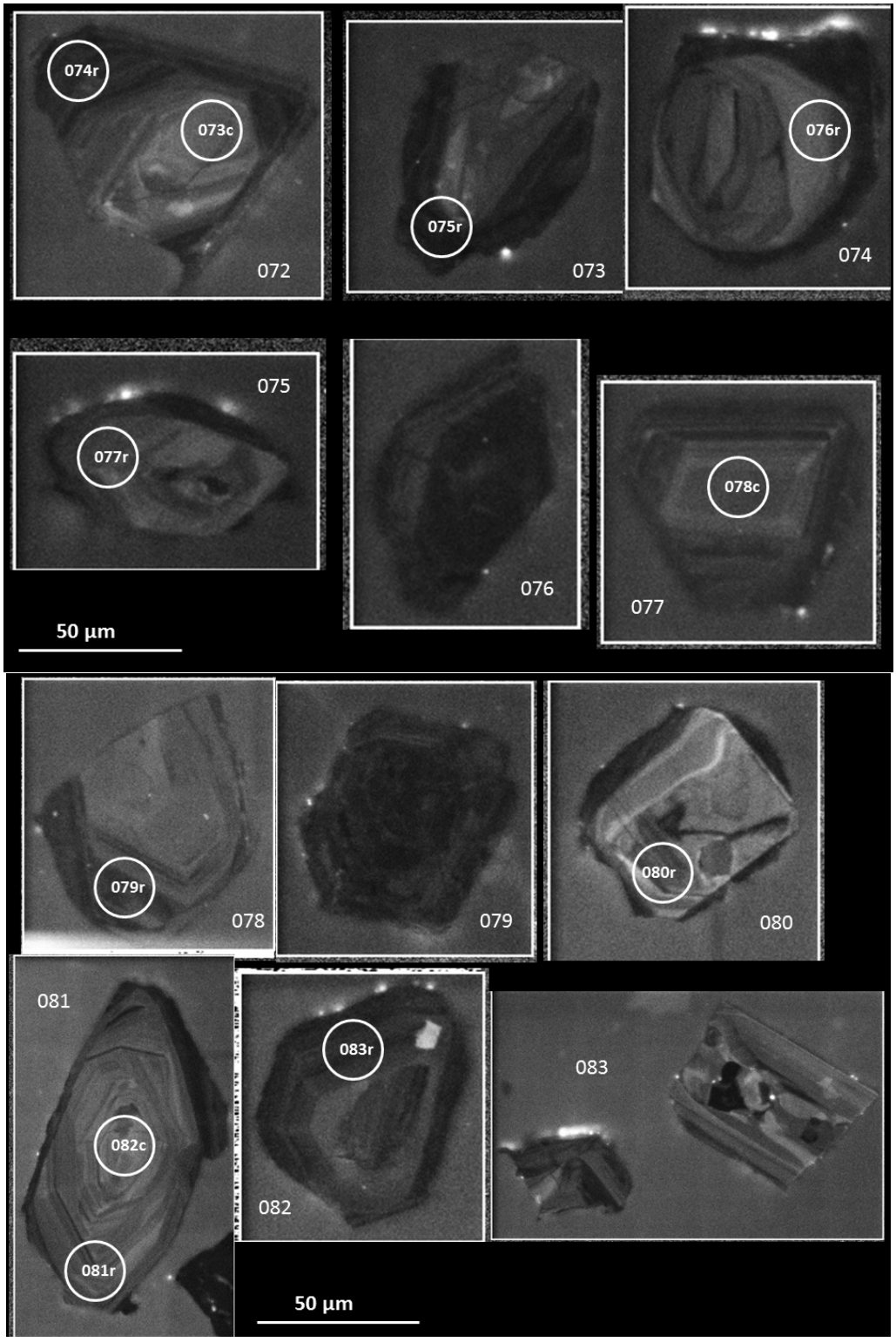
074r
073c
072
075r
073
076r
074
075
077r
076
078c
077
50 µm
079r
078
079
080r
080
081
082c
081r
083r
082
083
50 µm

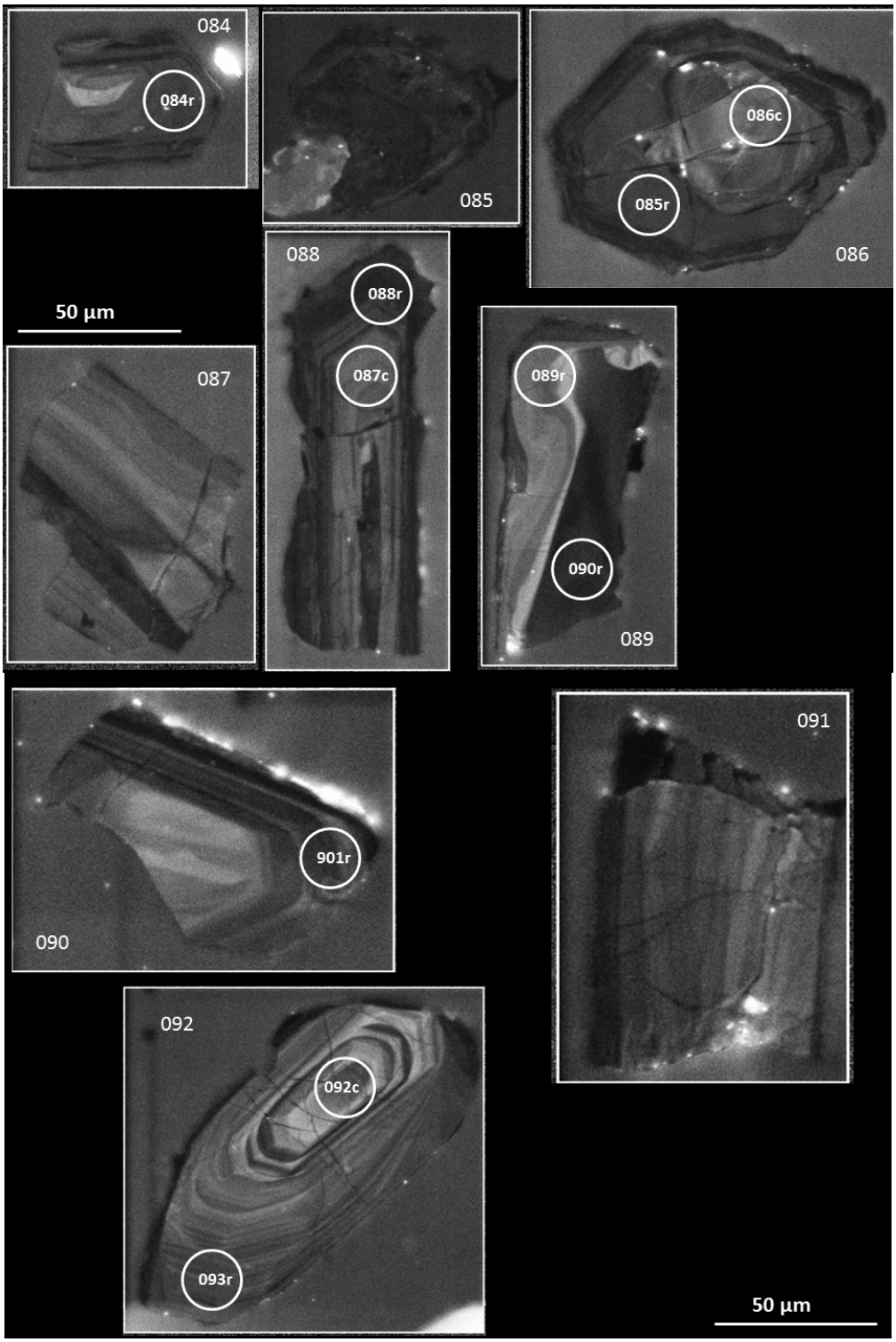
084
084r
085
086c
085r
086
088
088r
087c
50 µm
087
089r
090r
089
091
901r
090
092
092c
093r
50 µm

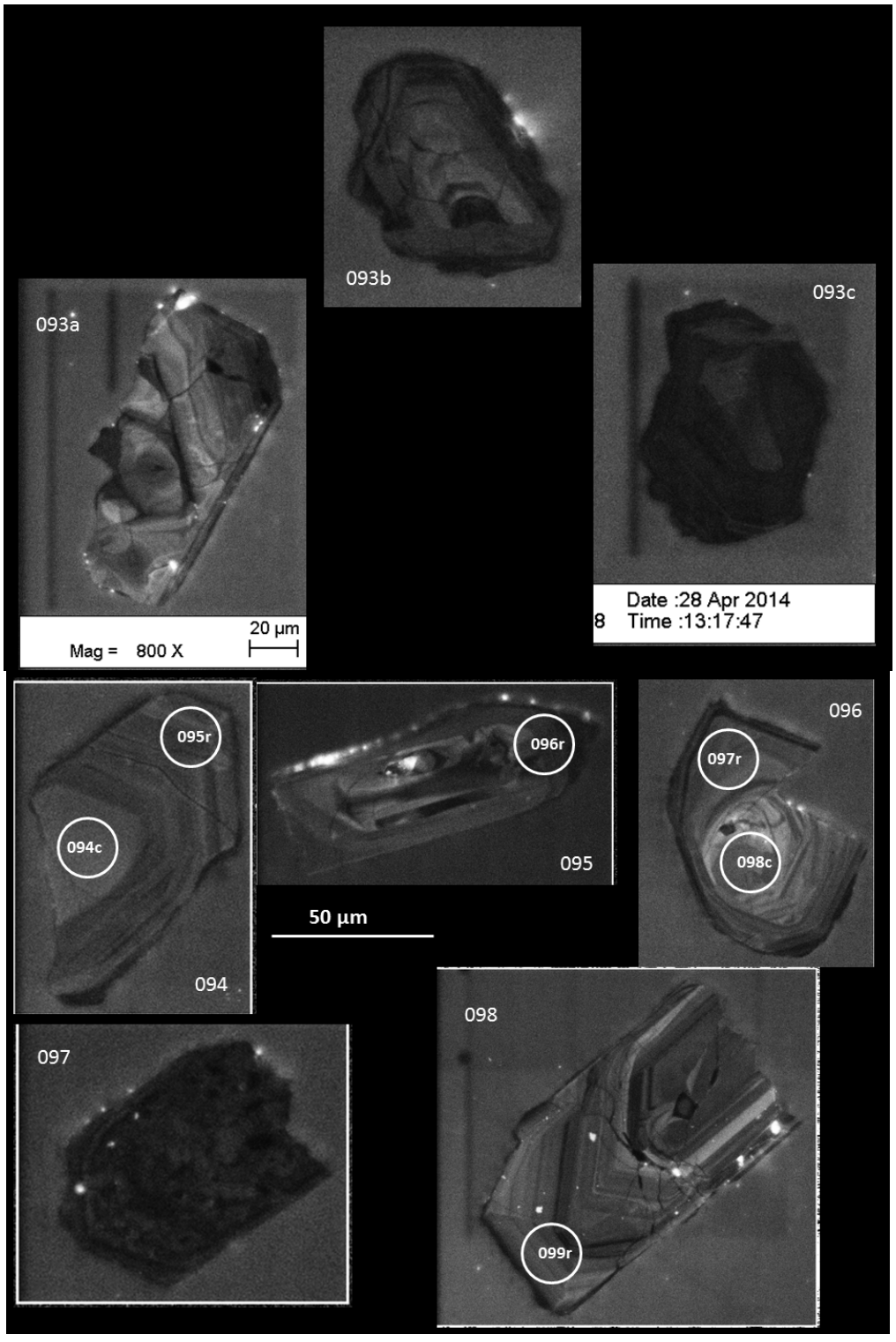
093b
093a
093c
20 µm
Mag = 800 X
Date :28 Apr 2014
Time :13:17:47
095r
094c
094
096r
095
50 µm
096
097r
098c
097
098
099r

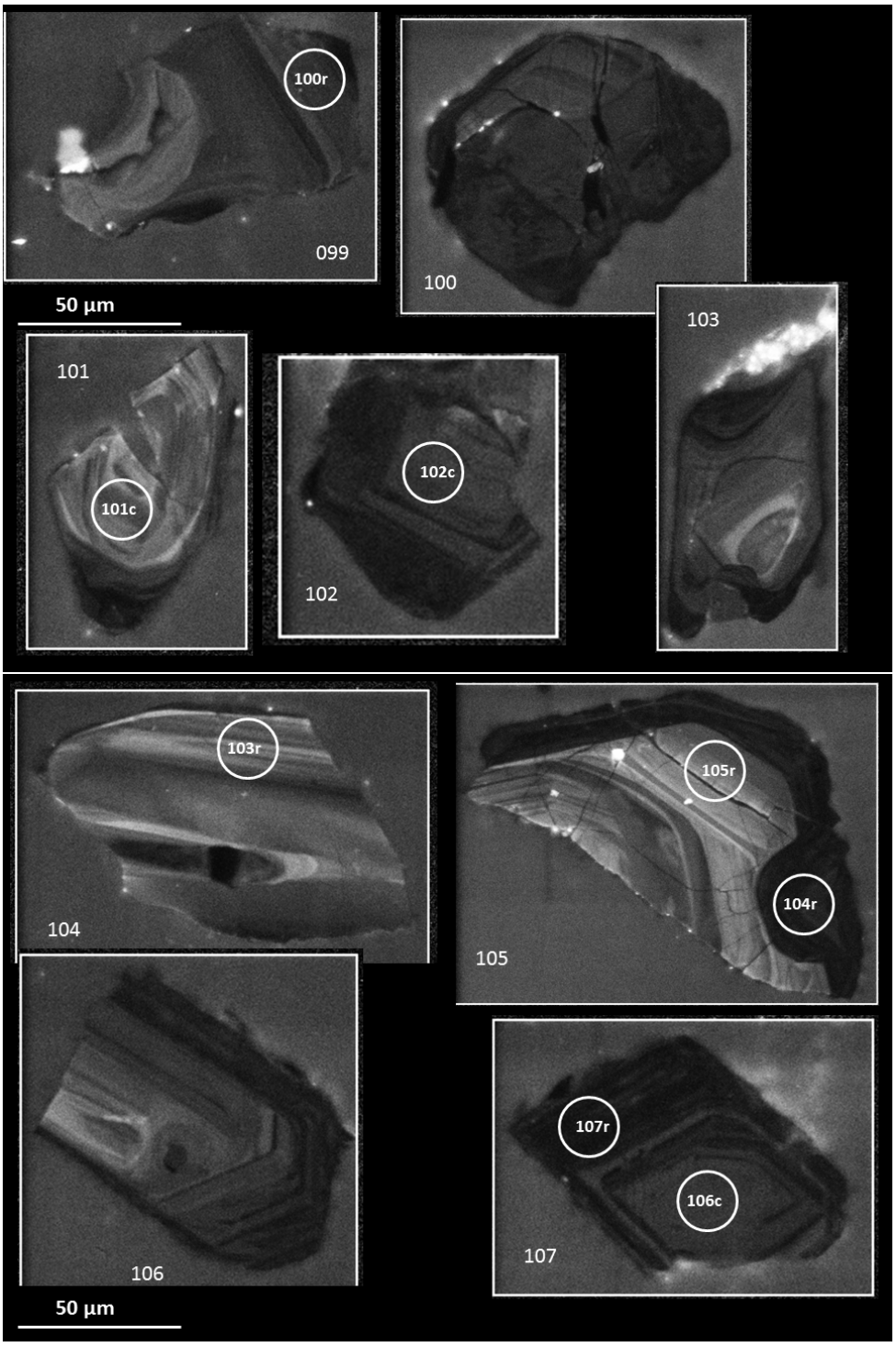
100r
099
50 µm
100
103
101
101c
102c
102
103r
104
105r
104r
105
106
107r
106c
107
50 µm

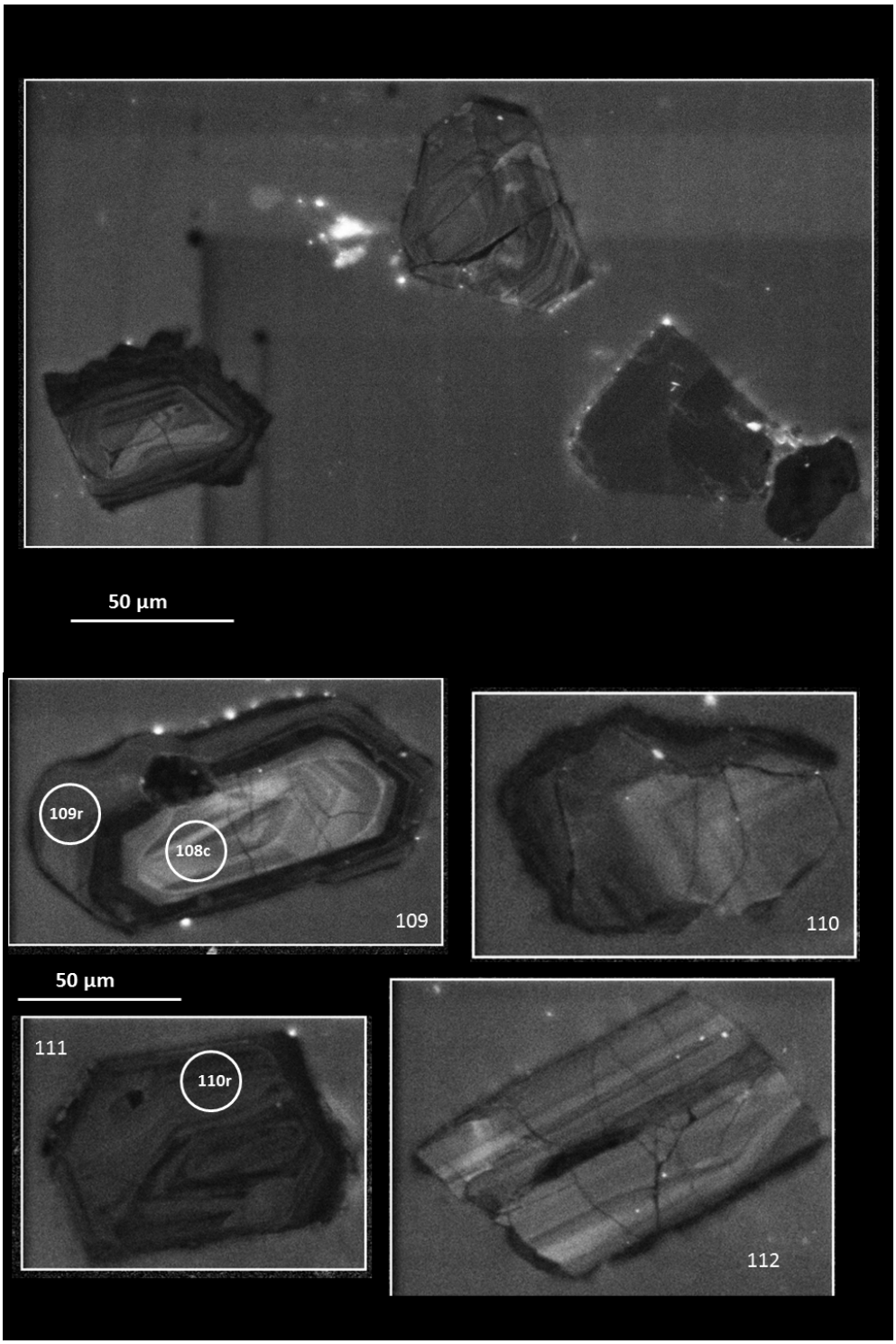
50 µm
109r
108c
109
110
50 µm
111
110r
112

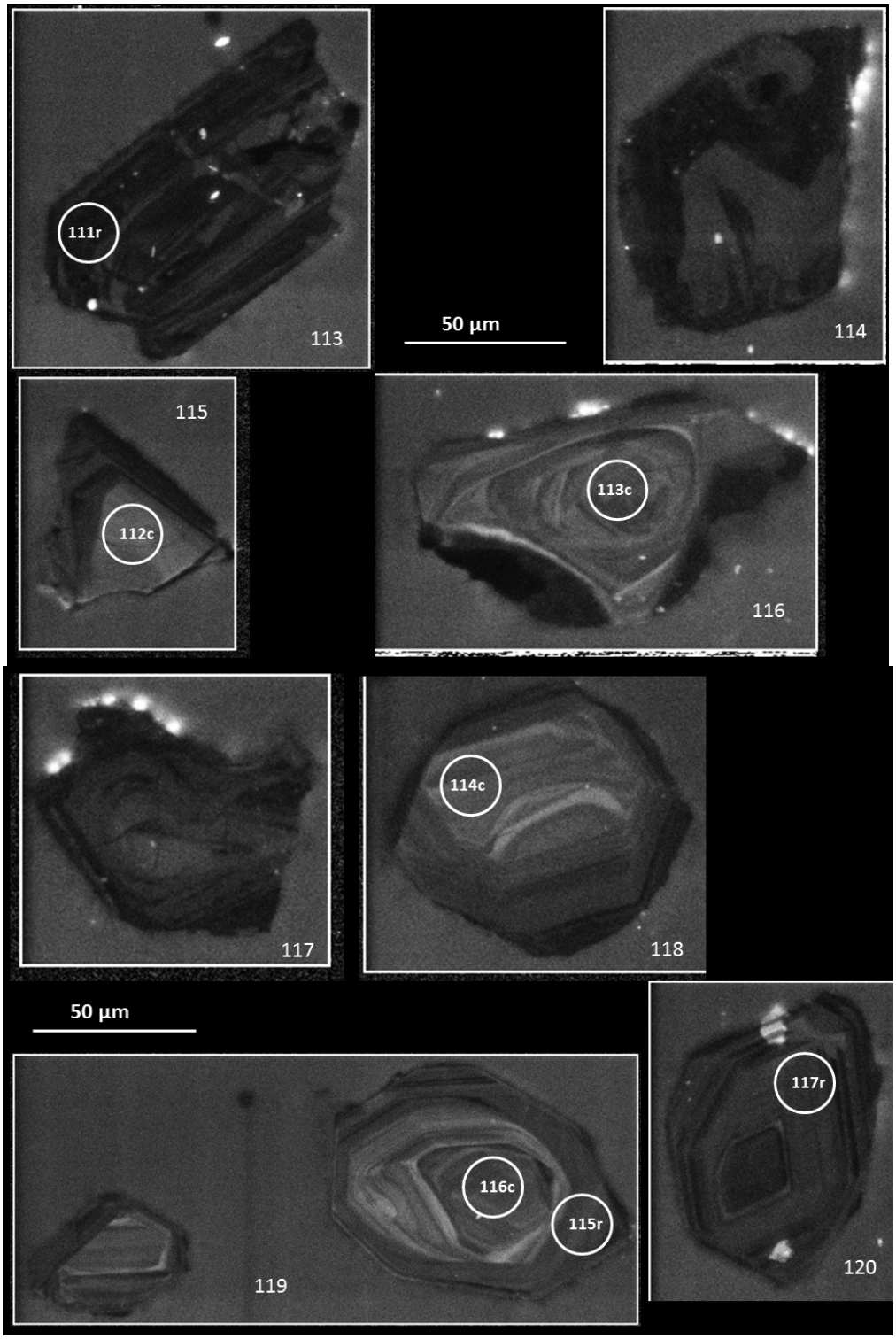
111r
113
50 µm
114
115
112c
113c
116
117
114c
118
50 µm
117r
116c
115r
119
120

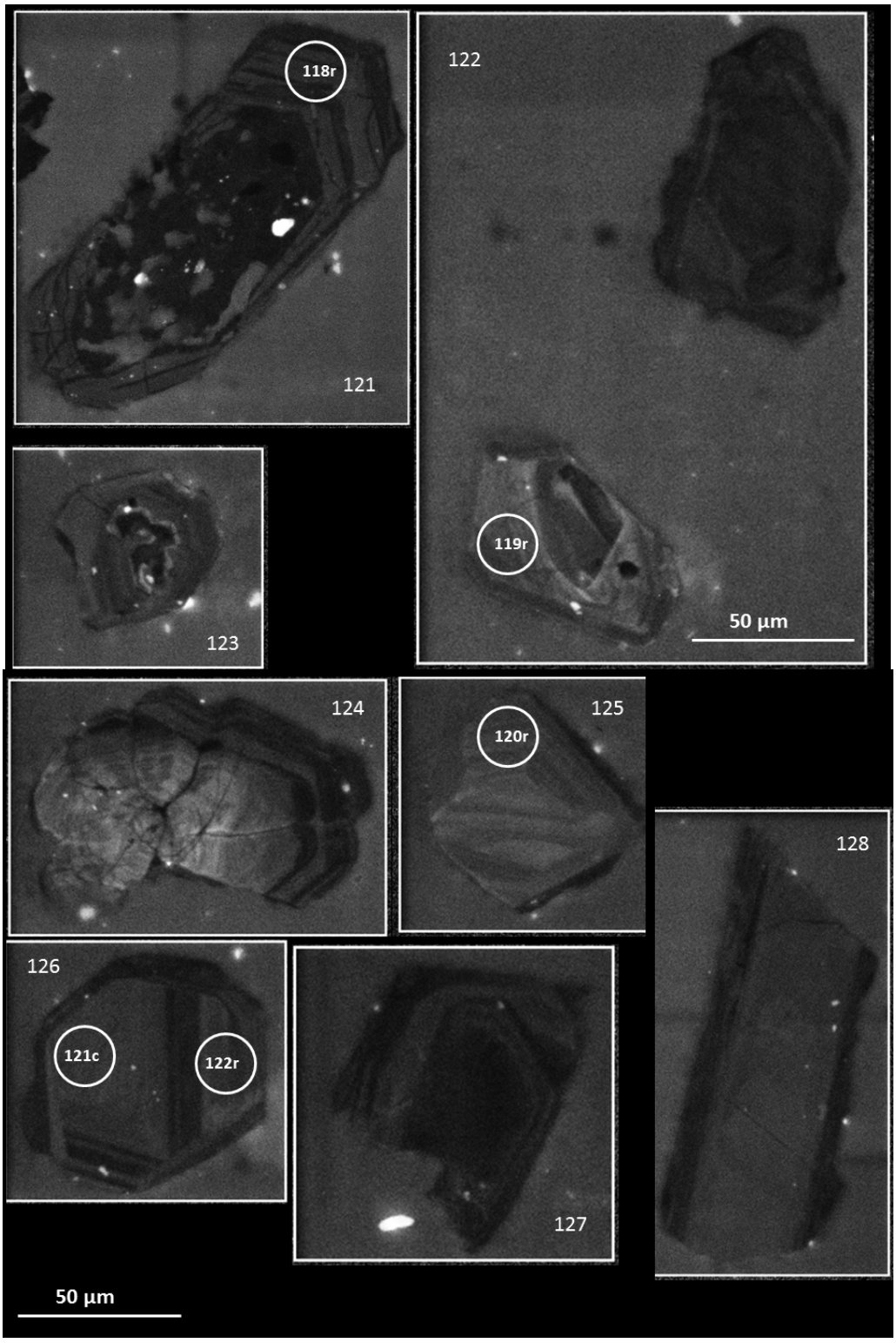
118r
121
122
119r
50 µm
123
124
125
120r
128
126
121c
122r
127
50 µm

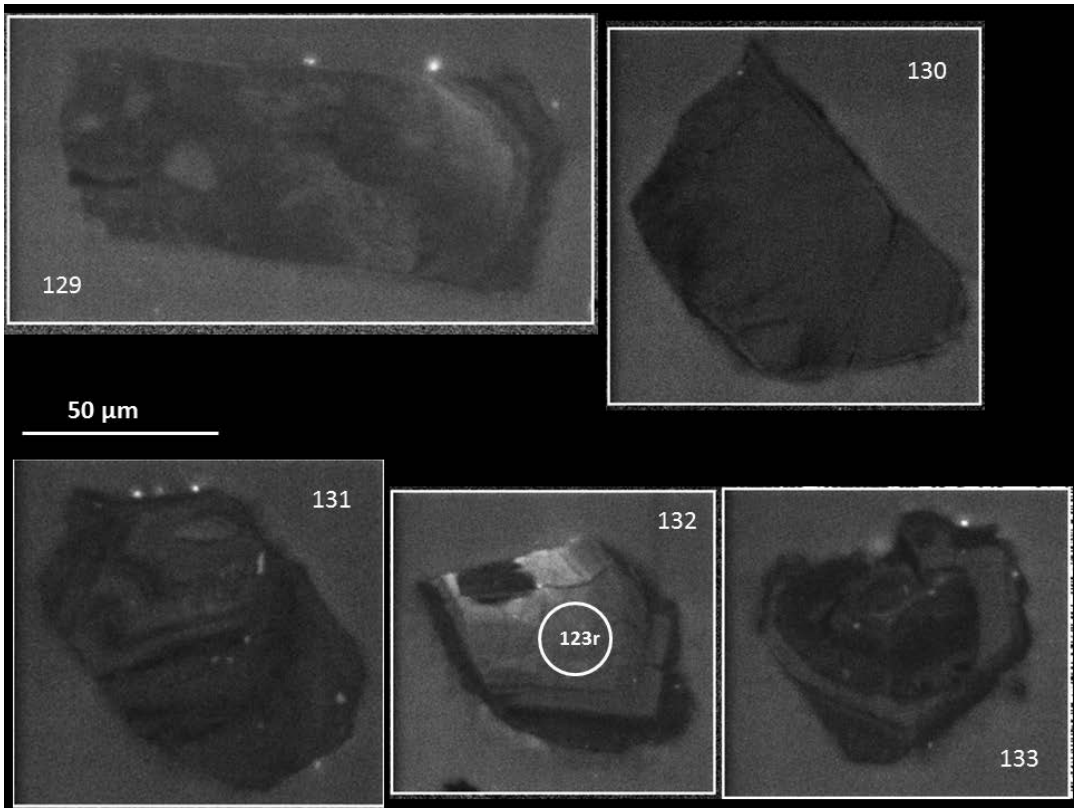
129
130
50 µm
131
132
123r
133

C-2. Quartzite (BR061013-01)

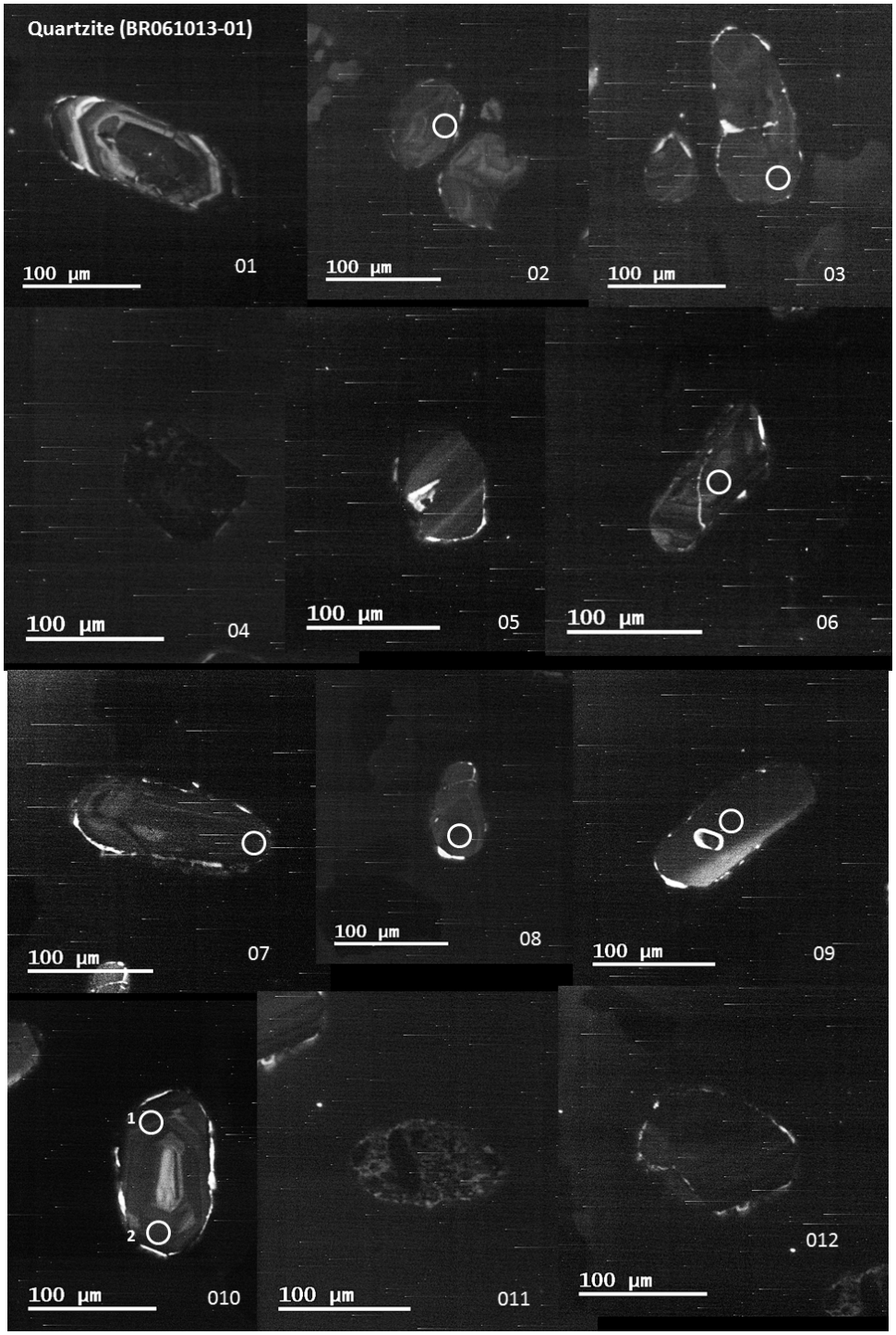

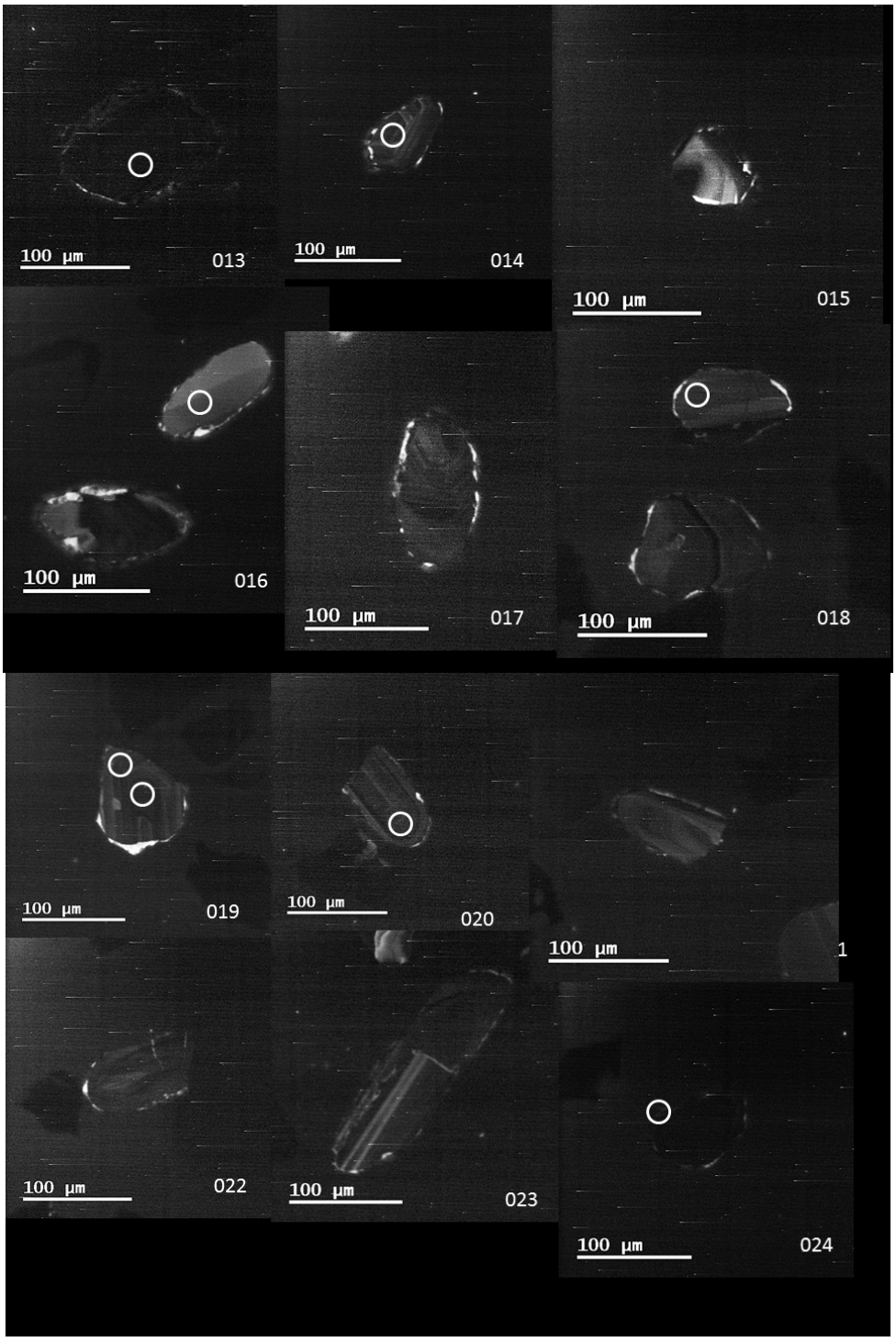
100 µm
013
100 µm
014
100 µm
015
100 µm
016
100 µm
017
100 µm
018
100 µm
019
100 µm
020
100 µm
1
100 µm
022
100 µm
023
100 µm
024

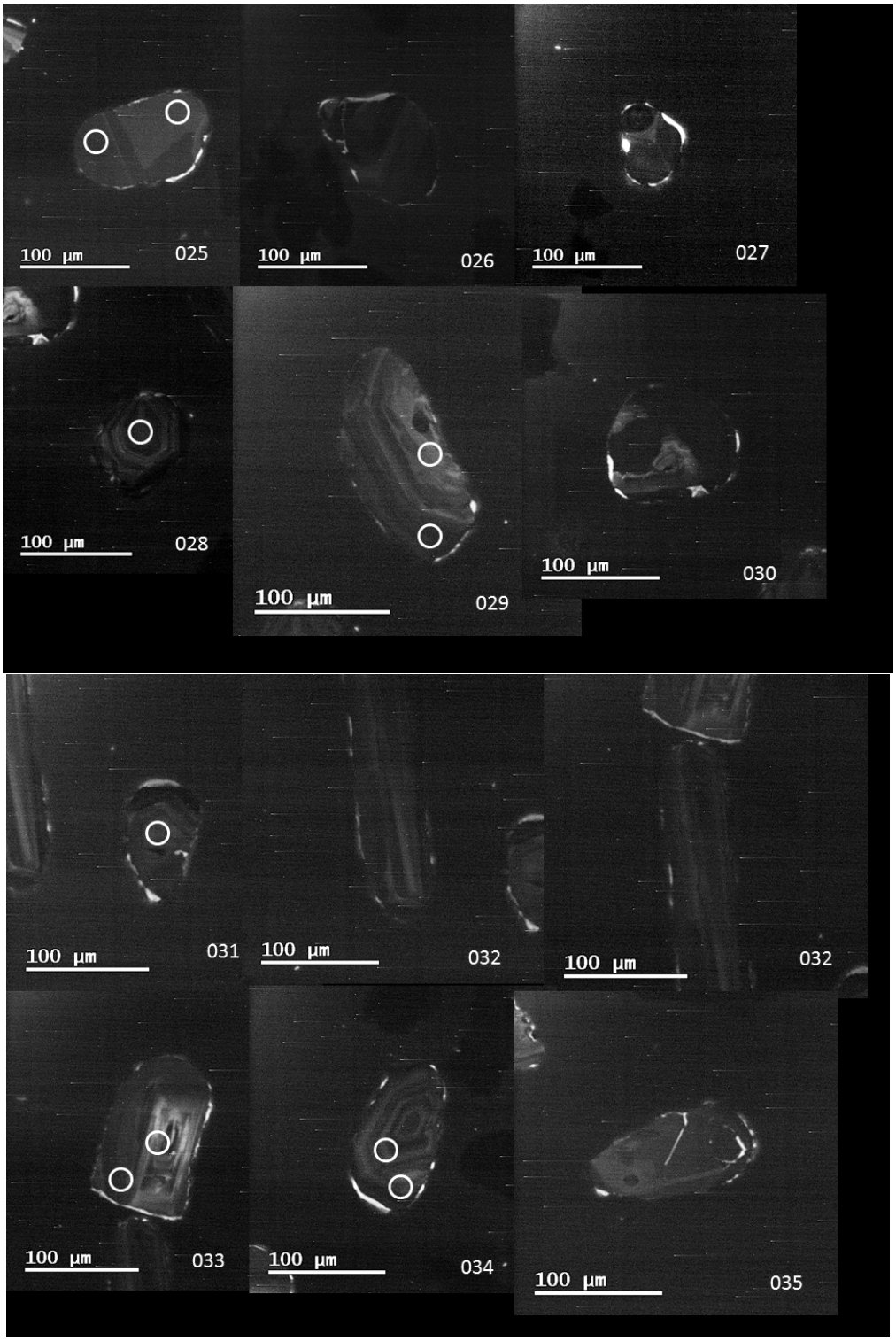
100 µm
025
100 µm
026
100 µm
027
100 µm
028
100 µm
029
100 µm
030
100 µm
031
100 µm
032
100 µm
032
100 µm
033
100 µm
034
100 µm
035

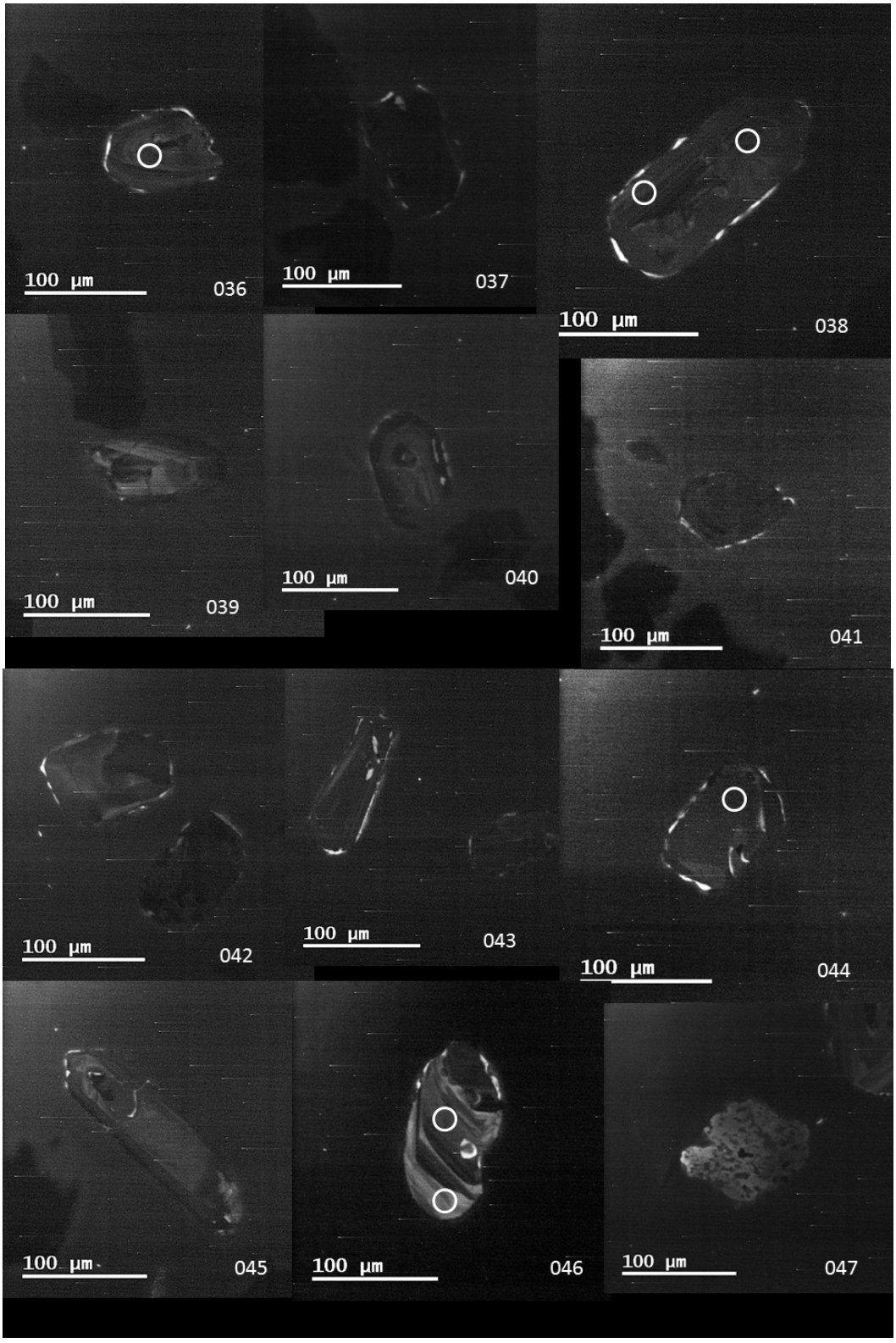
100 µm
036
100 µm
037
100 µm
038
100 µm
039
100 µm
040
100 µm
041
100 µm
042
100 µm
043
100 µm
044
100 µm
045
100 µm
046
100 µm
047

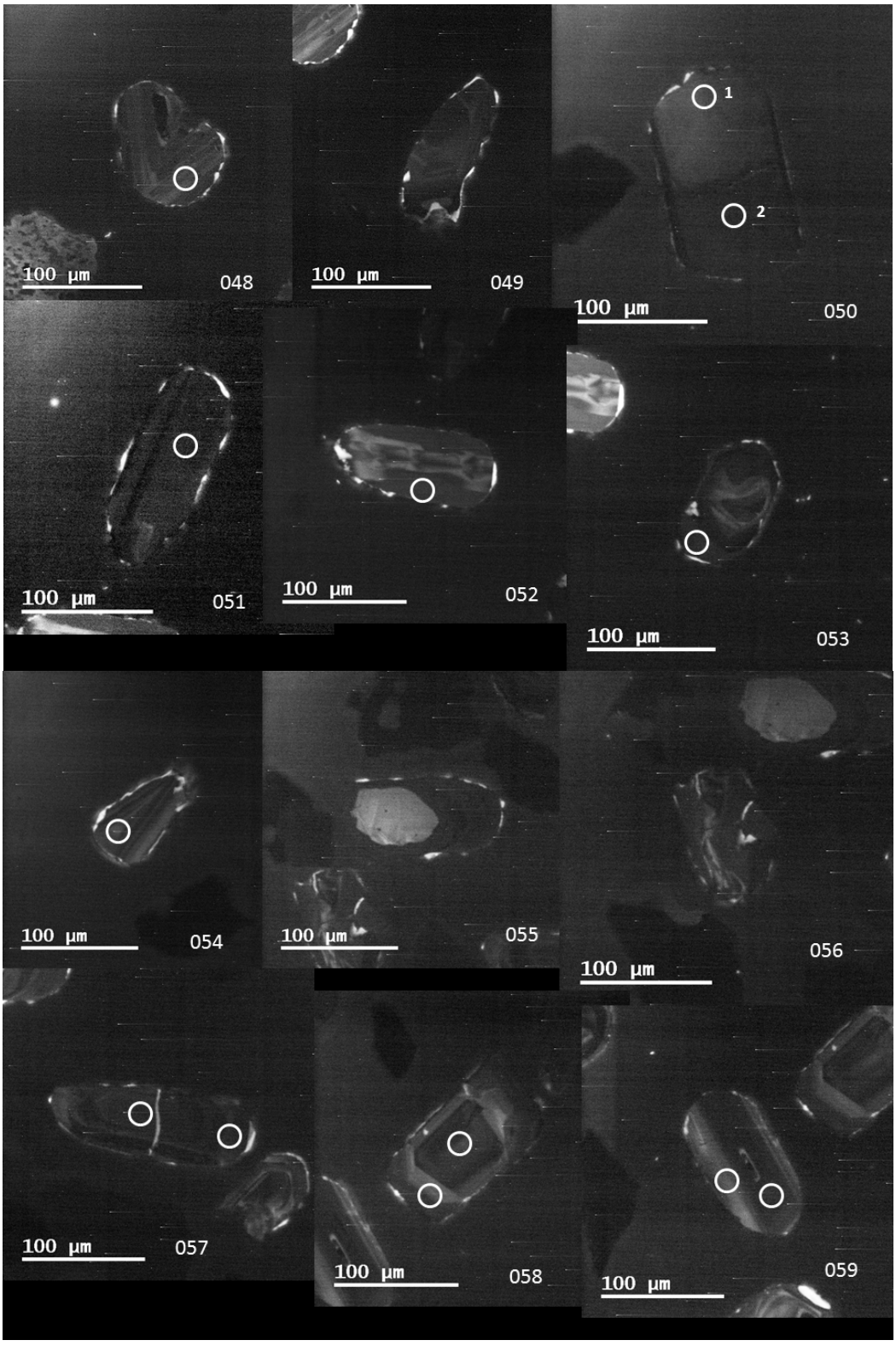
100 µm
048
100 µm
049
1
2
100 µm
050
100 µm
051
100 µm
052
100 µm
053
100 µm
054
100 µm
055
100 µm
056
100 µm
057
100 µm
058
100 µm
059

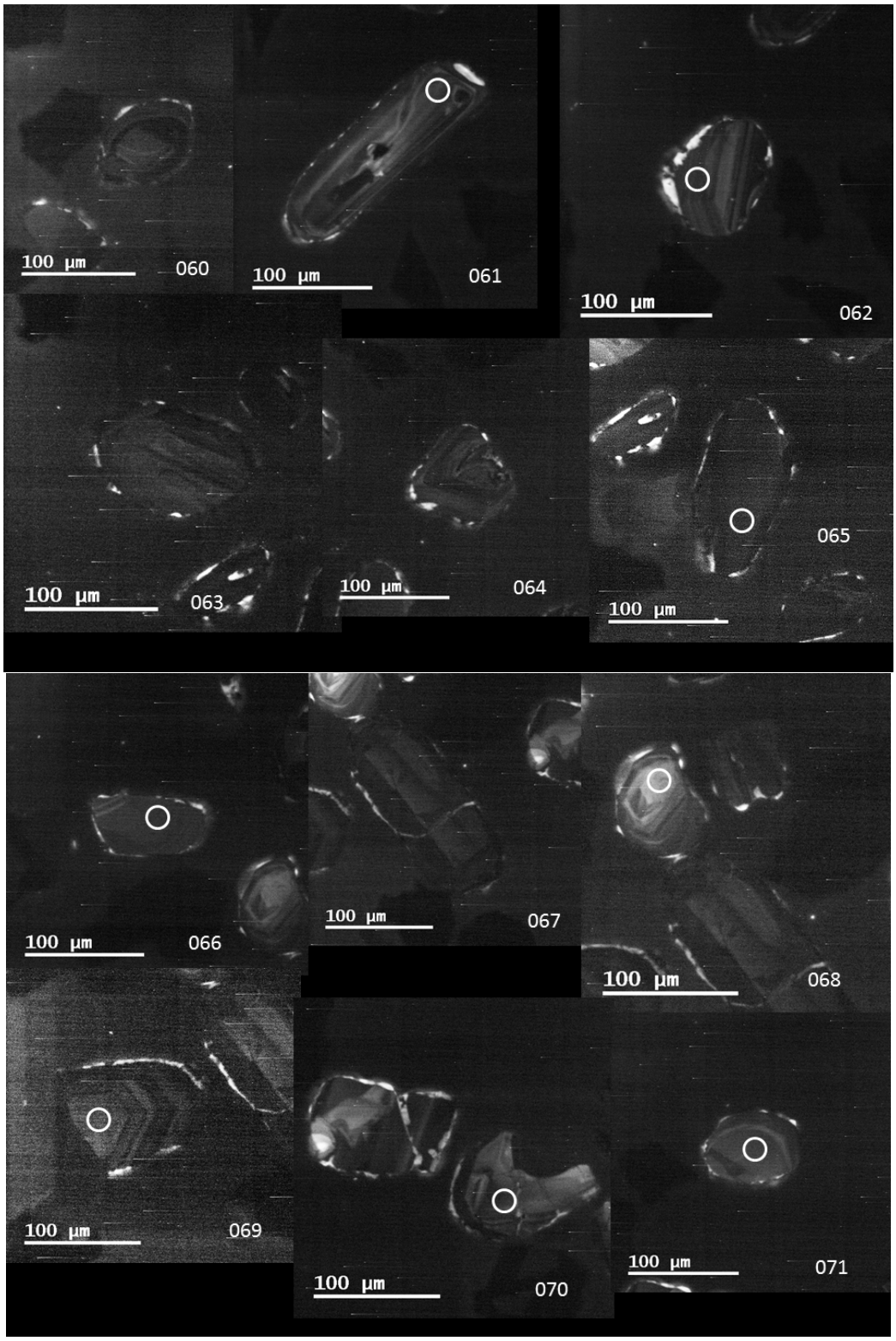
100 µm
060
100 µm
061
100 µm
062
100 µm
063
100 µm
064
065
100 µm
100 µm
066
100 µm
067
100 µm
068
100 µm
069
100 µm
070
100 µm
071

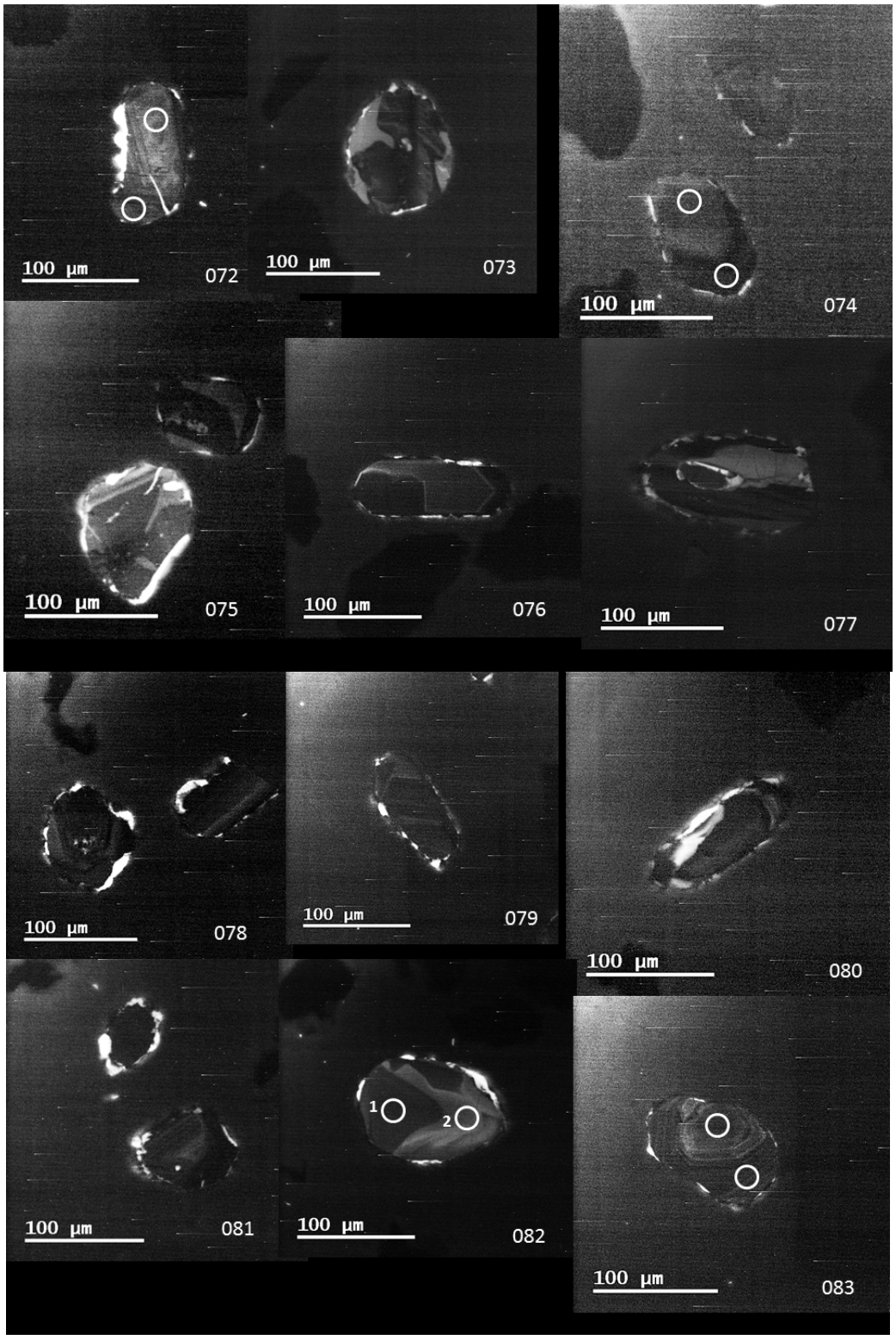
100 µm
072
100 µm
073
100 µm
074
100 µm
075
100 µm
076
100 µm
077
100 µm
078
100 µm
079
100 µm
080
100 µm
081
1
2
100 µm
082
100 µm
083

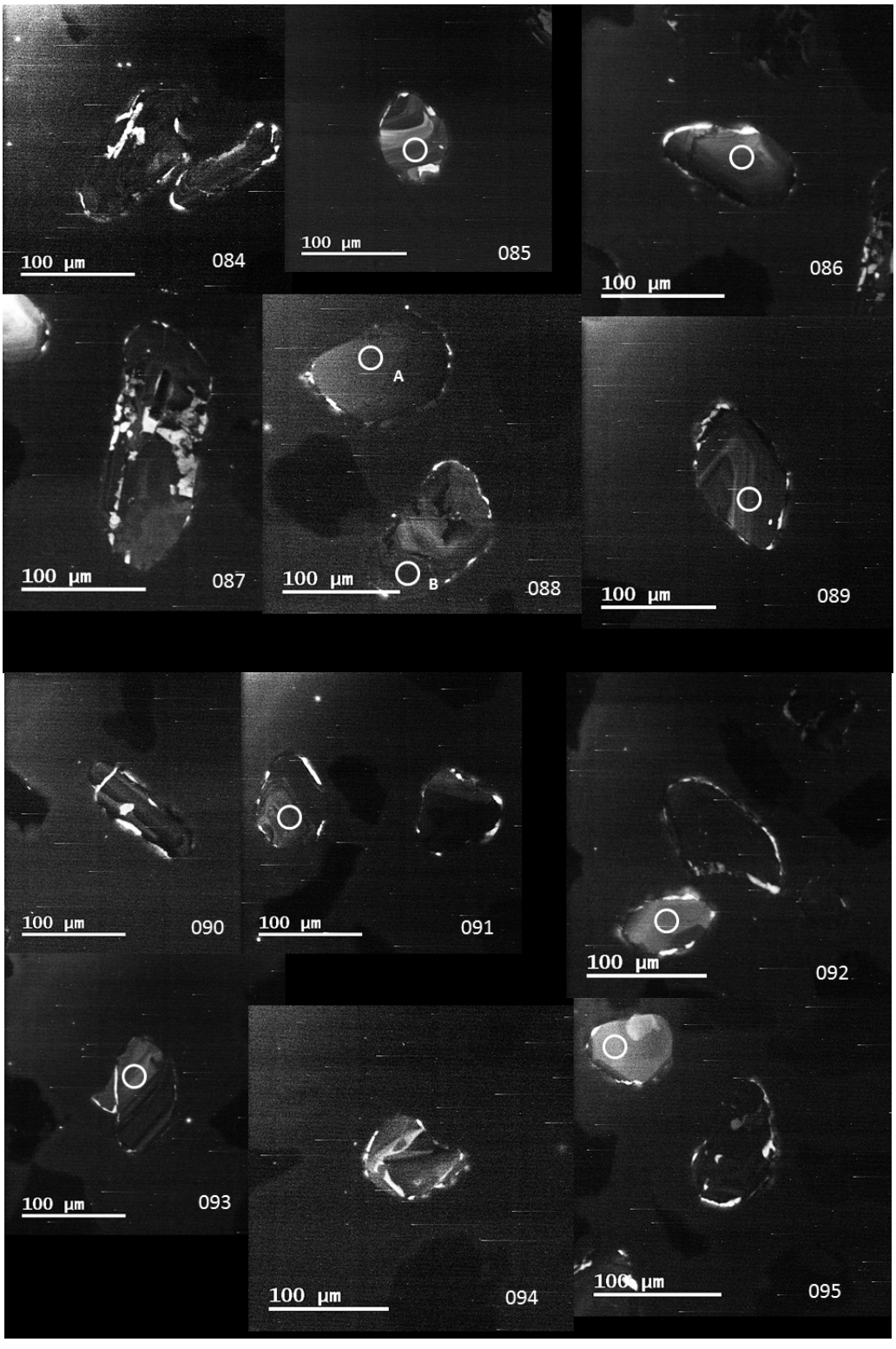
100 µm
084
100 µm
085
100 µm
086
100 µm
087
A
100 µm
B
088
100 µm
089
100 µm
090
100 µm
091
100 µm
092
100 µm
093
100 µm
094
100 µm
095

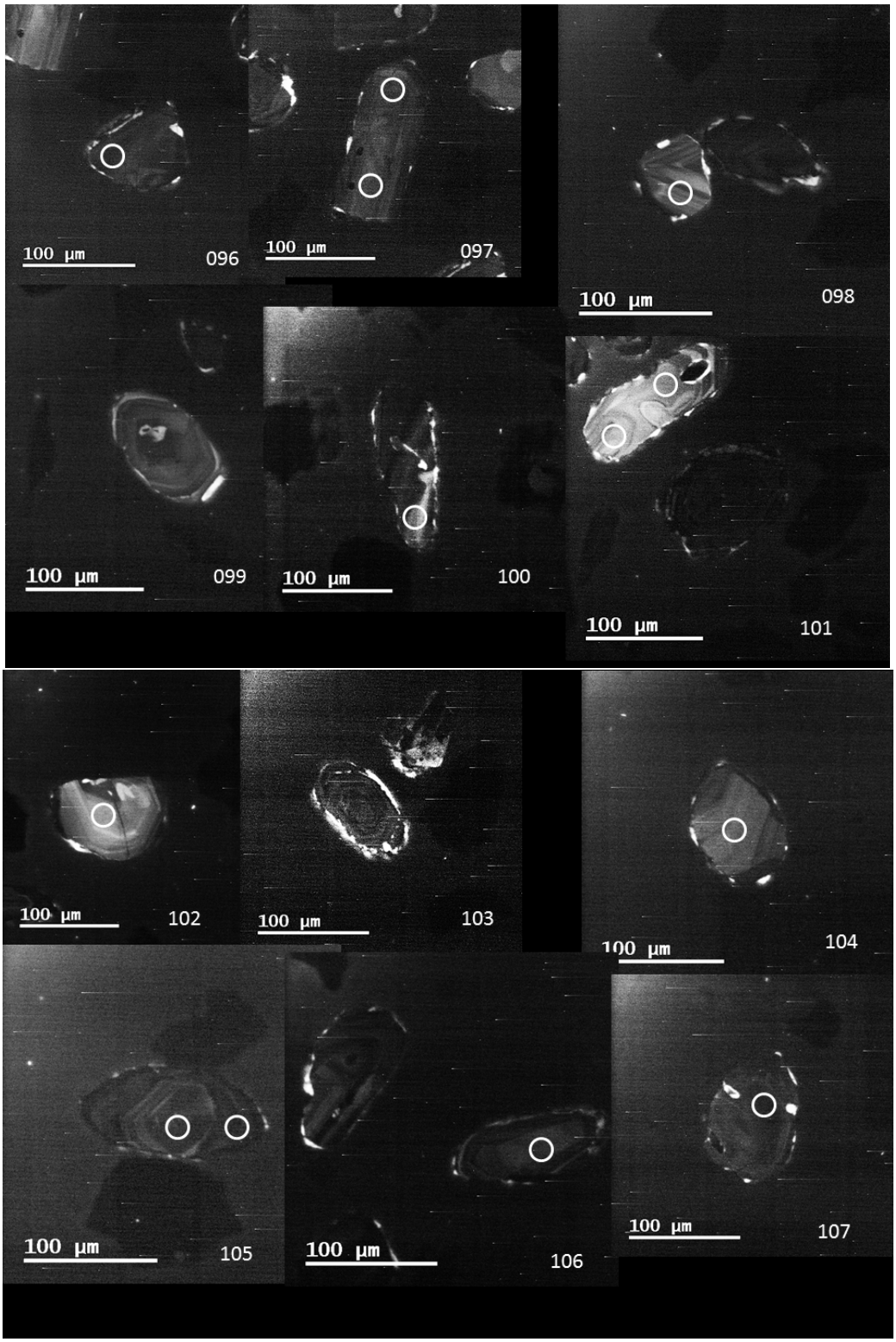
100 µm
096
100 µm
097
100 µm
098
100 µm
099
100 µm
100
100 µm
101
100 µm
102
100 µm
103
100 µm
104
100 µm
105
100 µm
106
100 µm
107

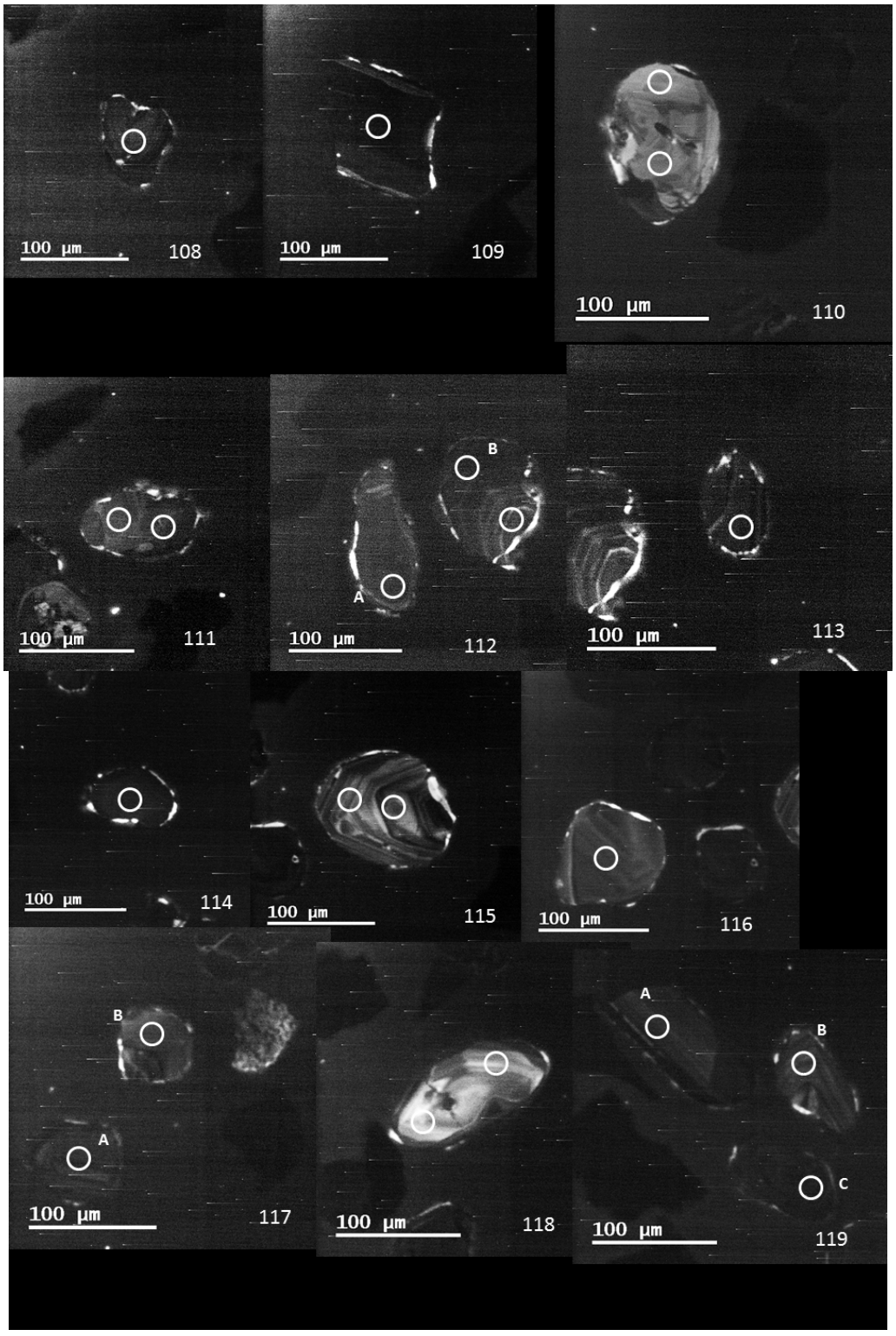
100 µm
108
100 µm
109
100 µm
110
100 µm
111
B
A
100 µm
112
100 µm
113
100 µm
114
100 µm
115
100 µm
116
B
A
100 µm
117
100 µm
118
A
B
C
100 µm
119

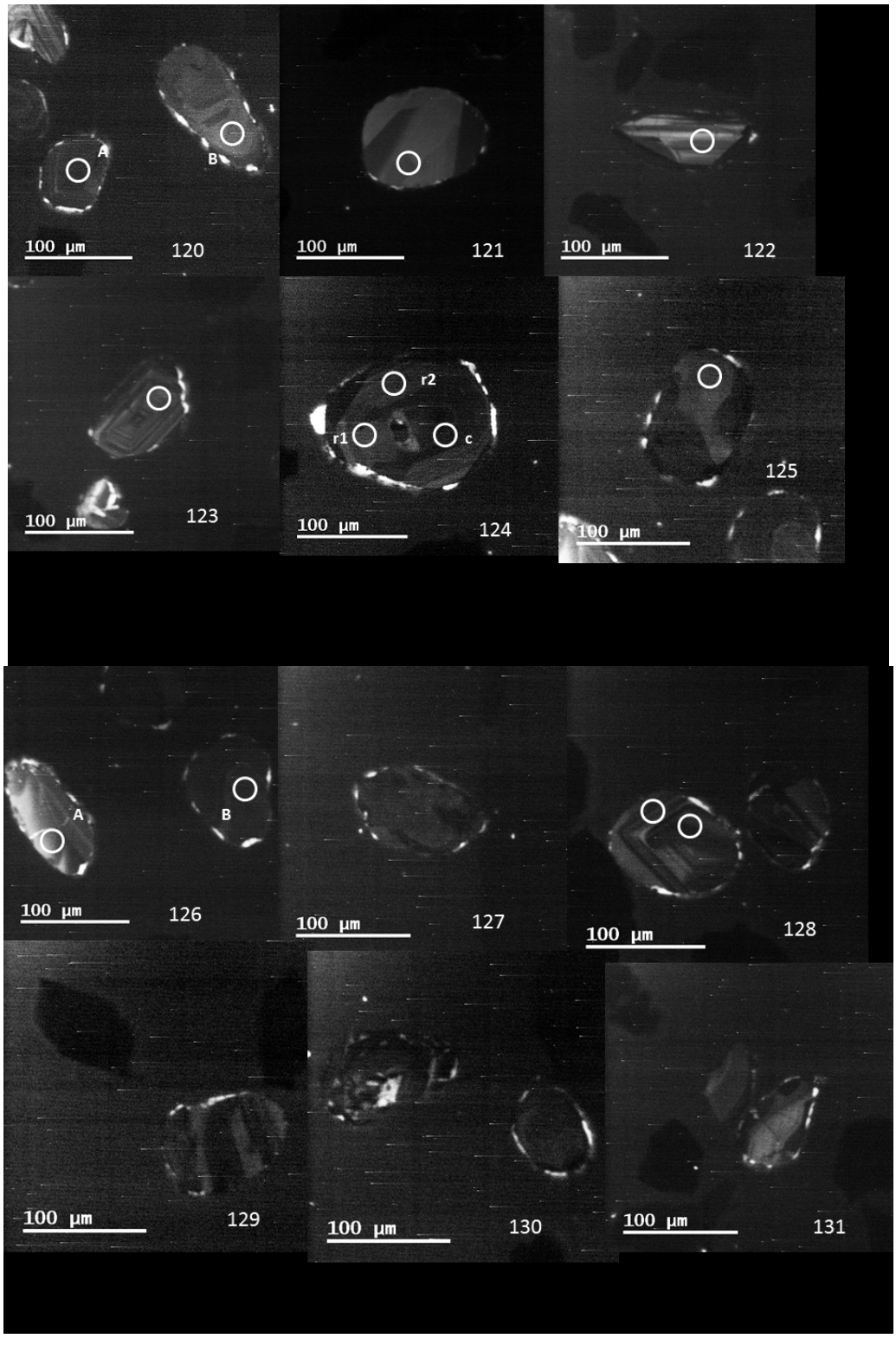
A
B
100 µm
120
100 µm
121
100 µm
122
100 µm
123
r2
r1
c
100 µm
124
125
100 µm
A
B
100 µm
126
100 µm
127
100 µm
128
100 µm
129
100 µm
130
100 µm
131

C-3. Garnet-mica-quartz schists (BR061213-01)

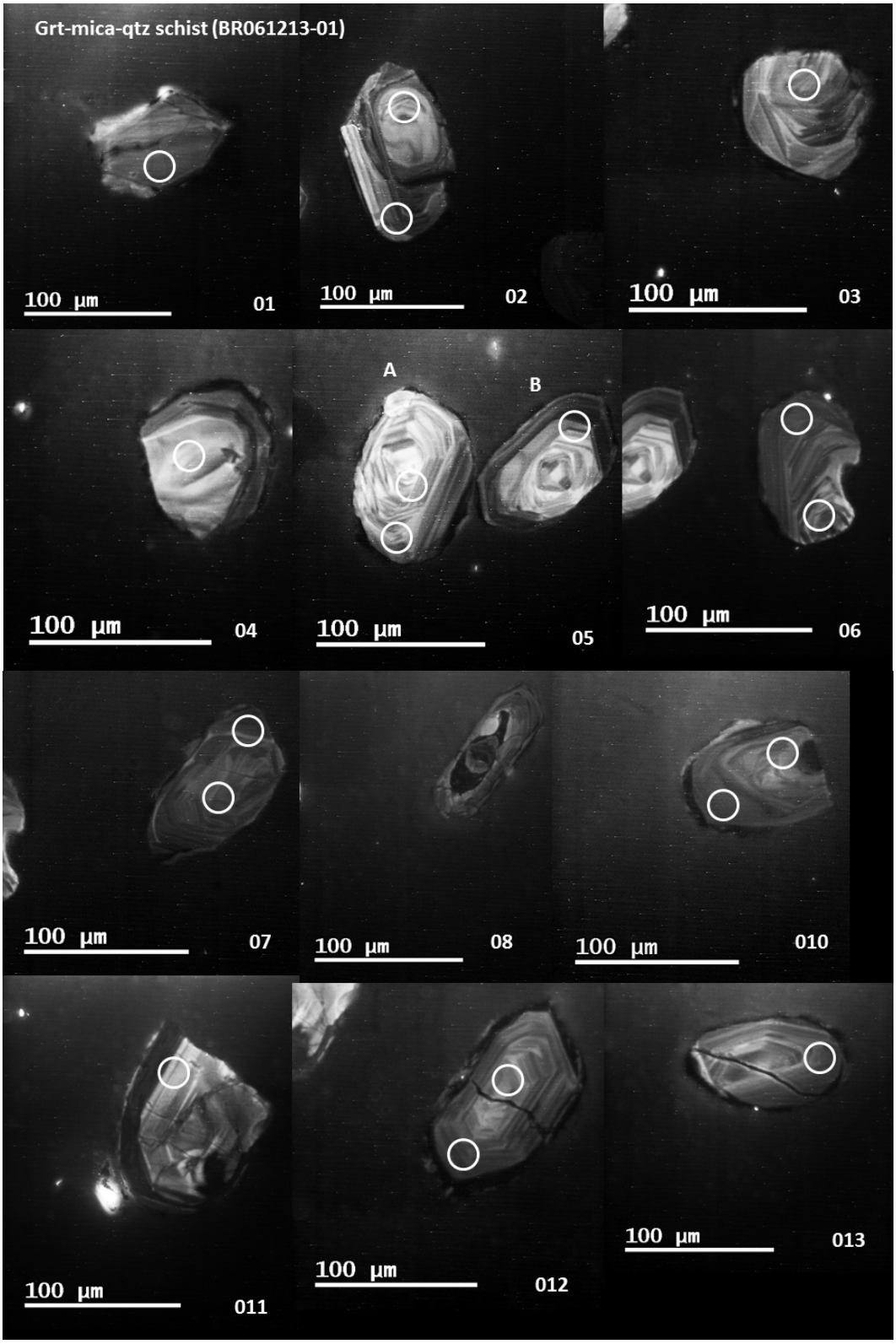

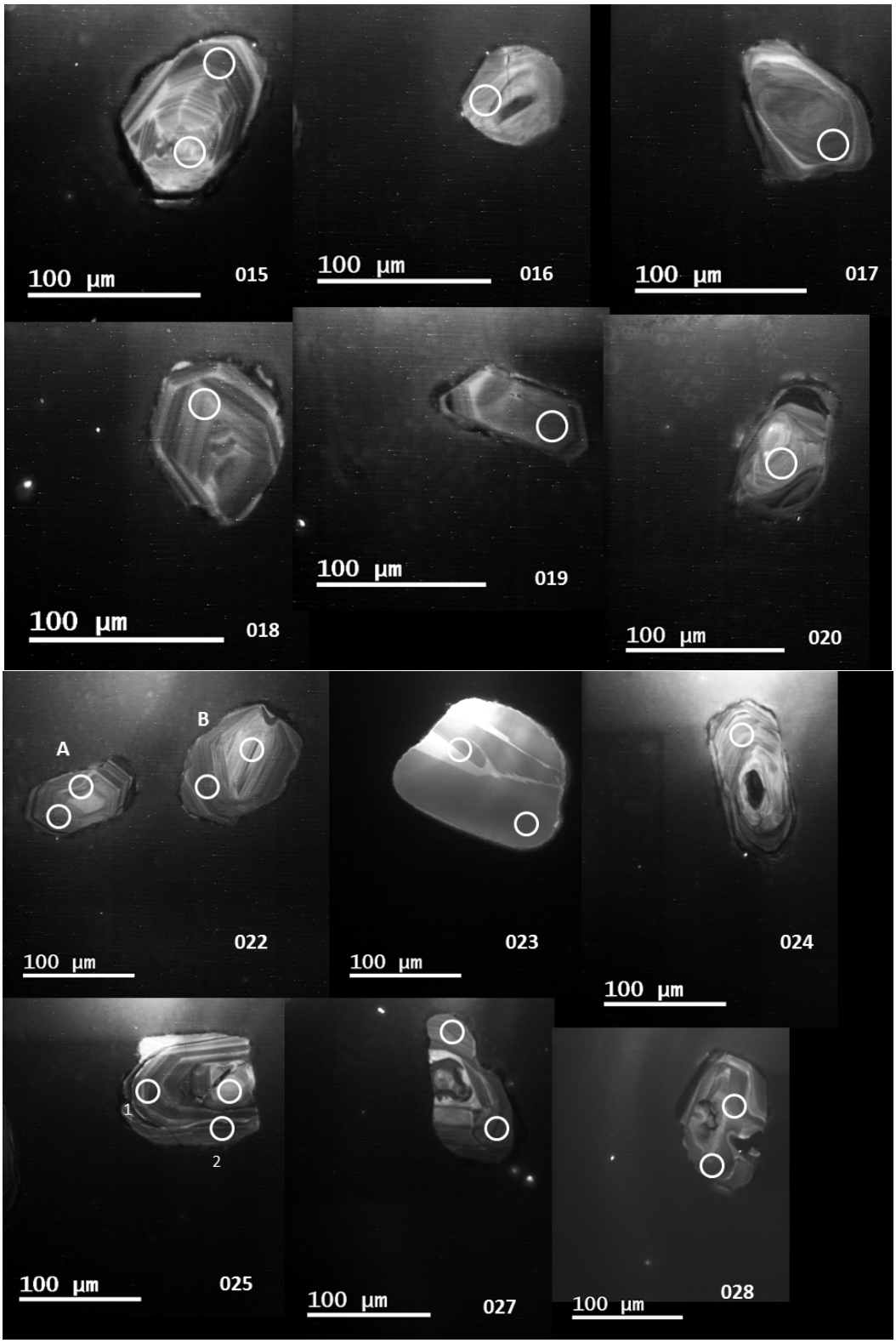
100 µm
015
100 µm
016
100 µm
017
100 µm
018
100 µm
019
100 µm
020
A
B
100 µm
022
100 µm
023
100 µm
024
1
2
100 µm
025
100 µm
027
100 µm
028

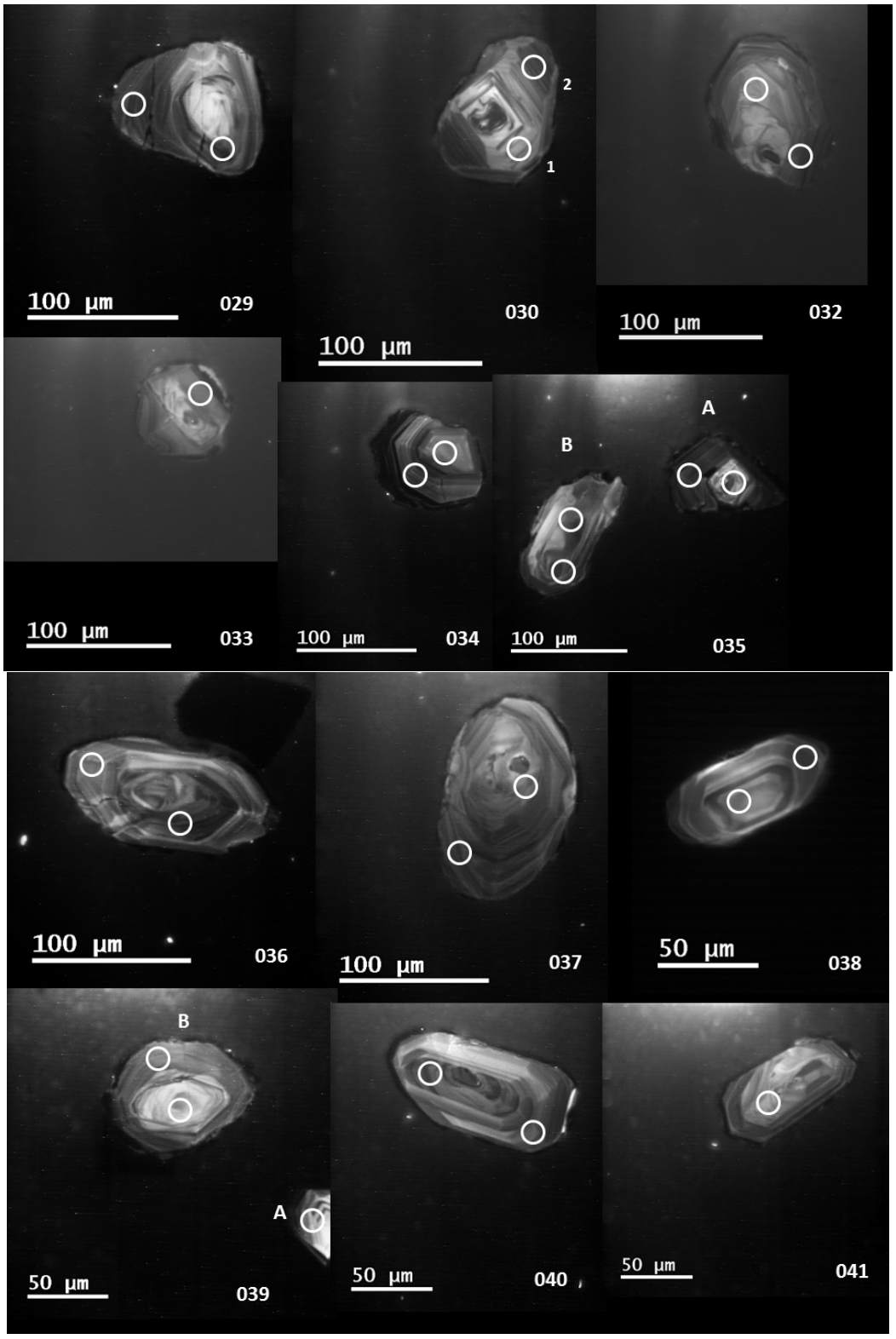
100 µm
029
2
1
030
100 µm
032
100 µm
033
100 µm
034
A
B
100 µm
035
100 µm
036
100 µm
037
50 µm
038
B
A
50 µm
039
50 µm
040
50 µm
041

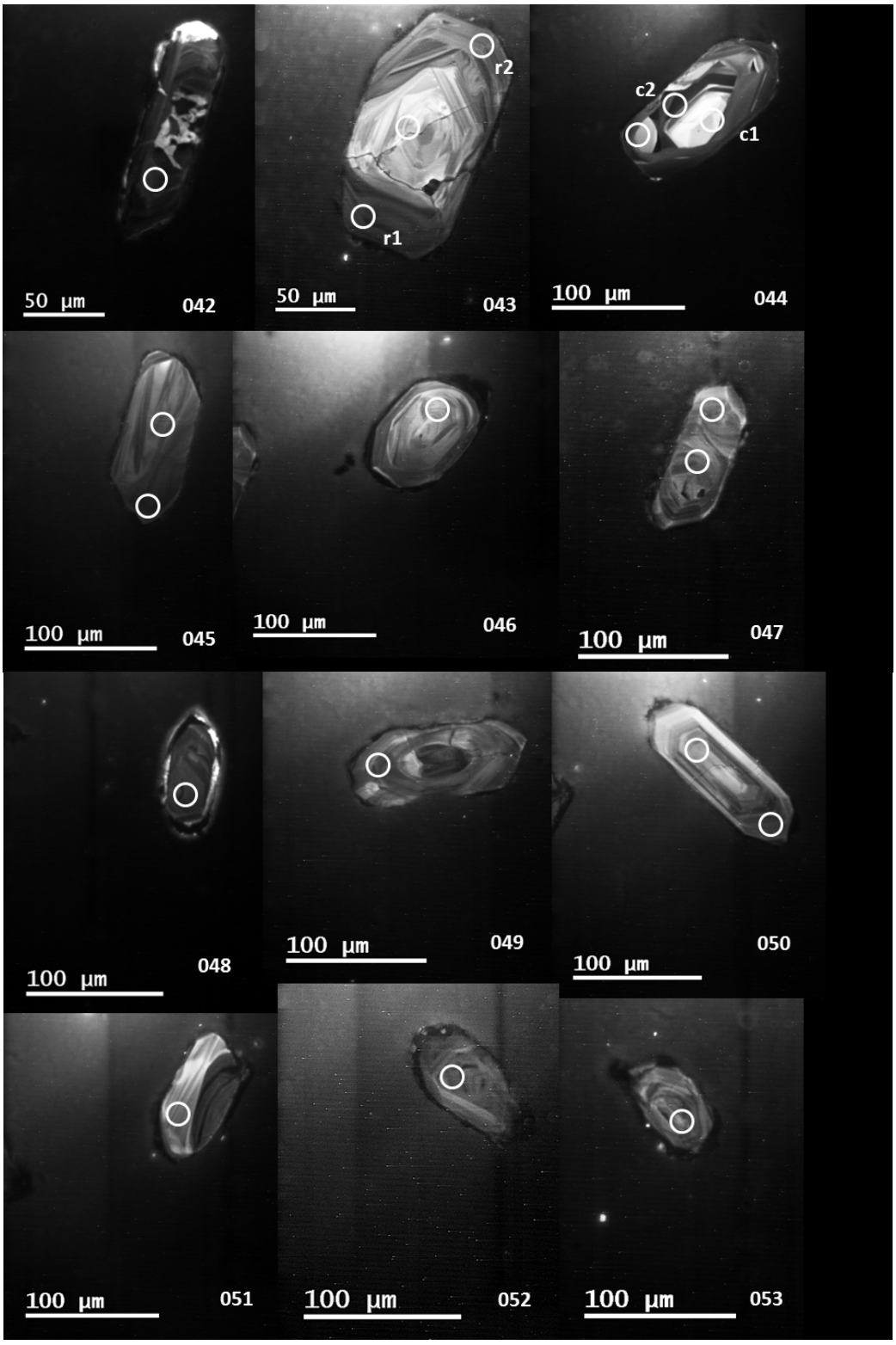
50 µm
042
r2
r1
50 µm
043
c2
c1
100 µm
044
100 µm
045
100 µm
046
100 µm
047
100 µm
048
100 µm
049
100 µm
050
100 µm
051
100 µm
052
100 µm
053

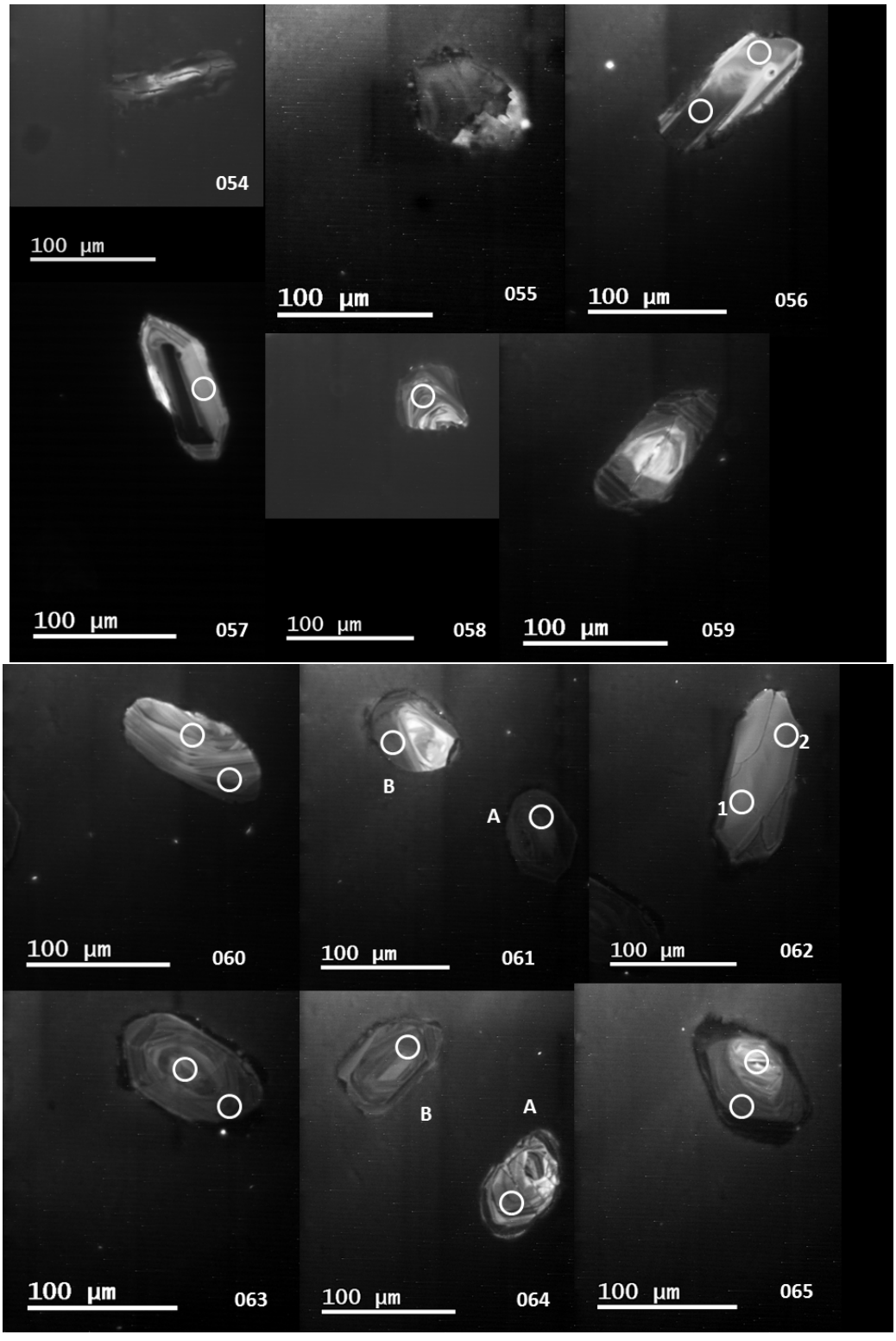
054
100 µm
100 µm
055
100 µm
056
100 µm
057
100 µm
058
100 µm
059
100 µm
060
B
A
100 µm
061
2
1
100 µm
062
100 µm
063
B
A
100 µm
064
100 µm
065

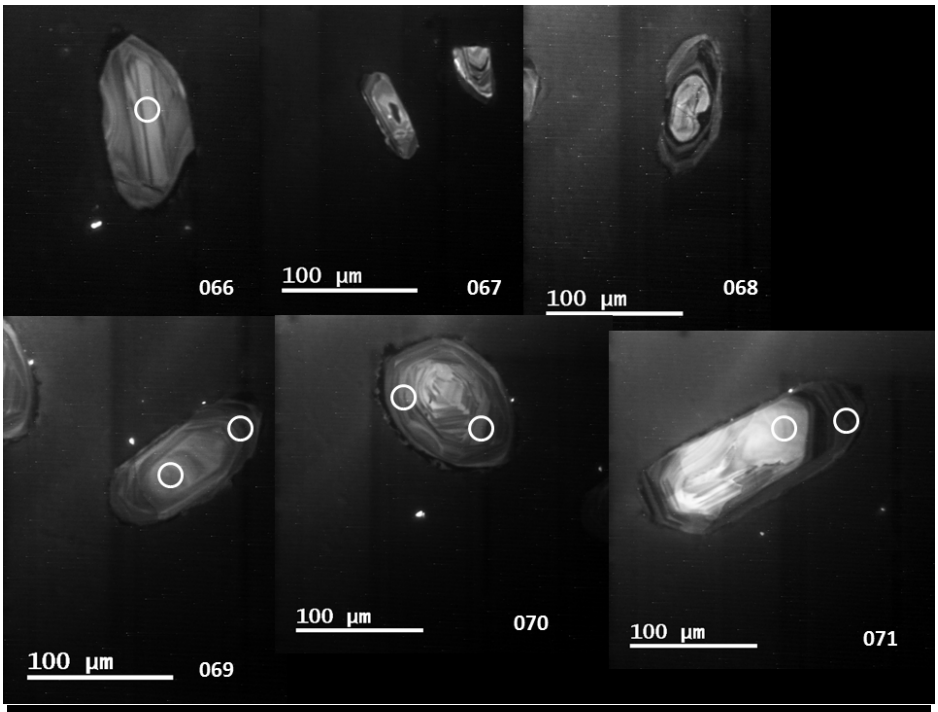
066
100 µm
067
100 µm
068
100 µm
069
100 µm
070
100 µm
071

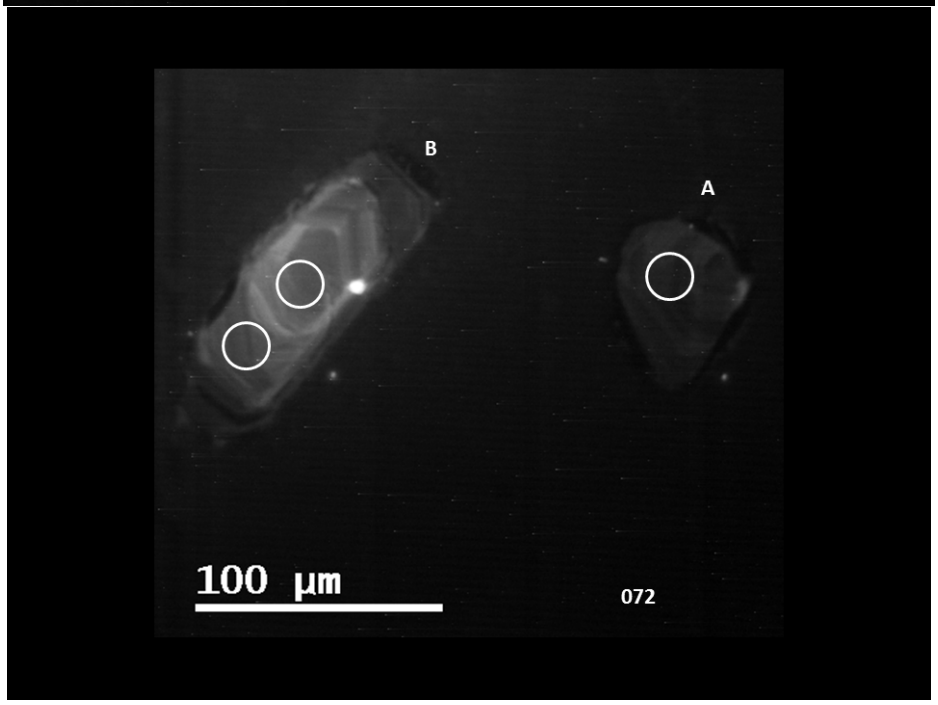
B
A
100 µm
072

C-4. Foliated granite (BR060913-05)

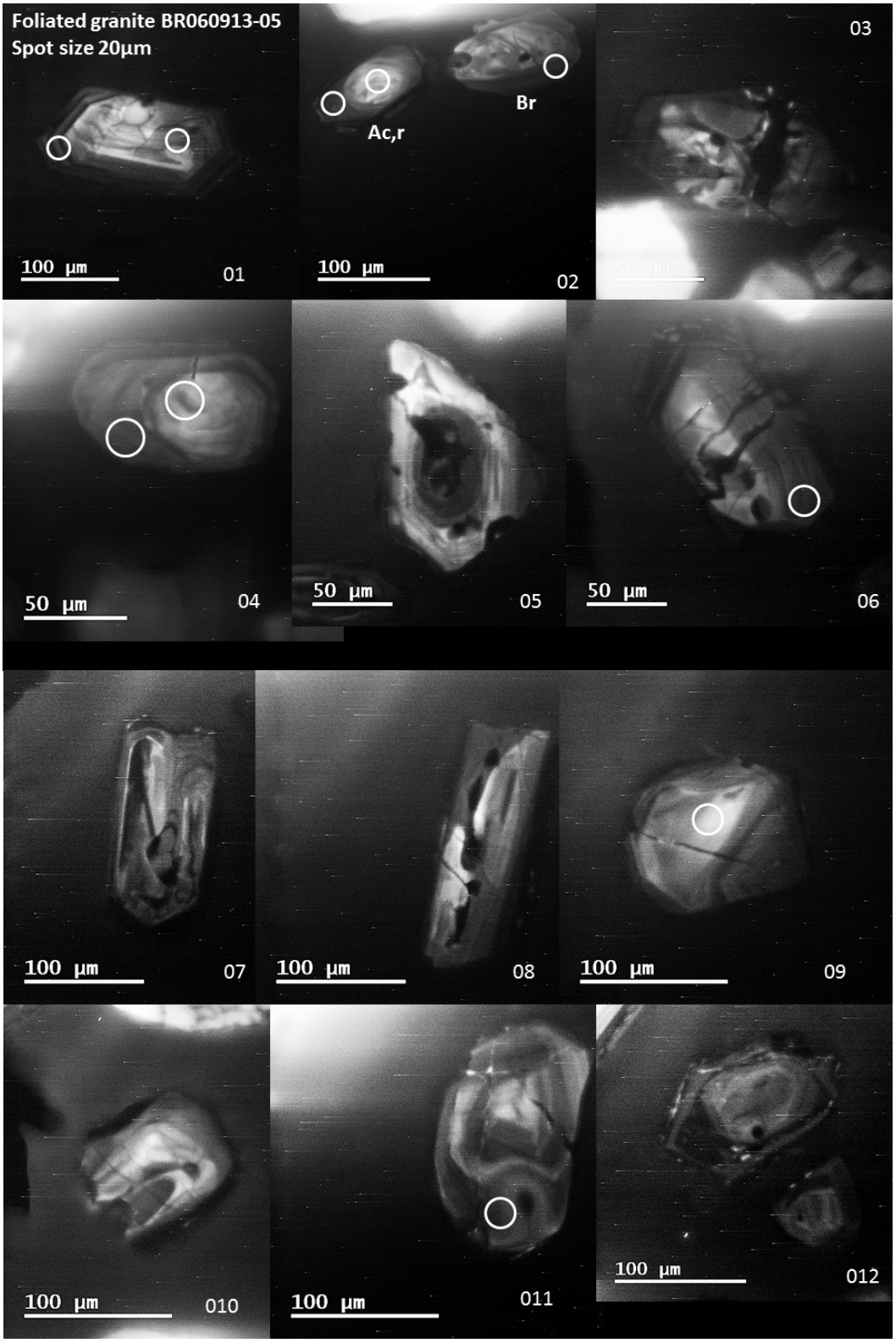

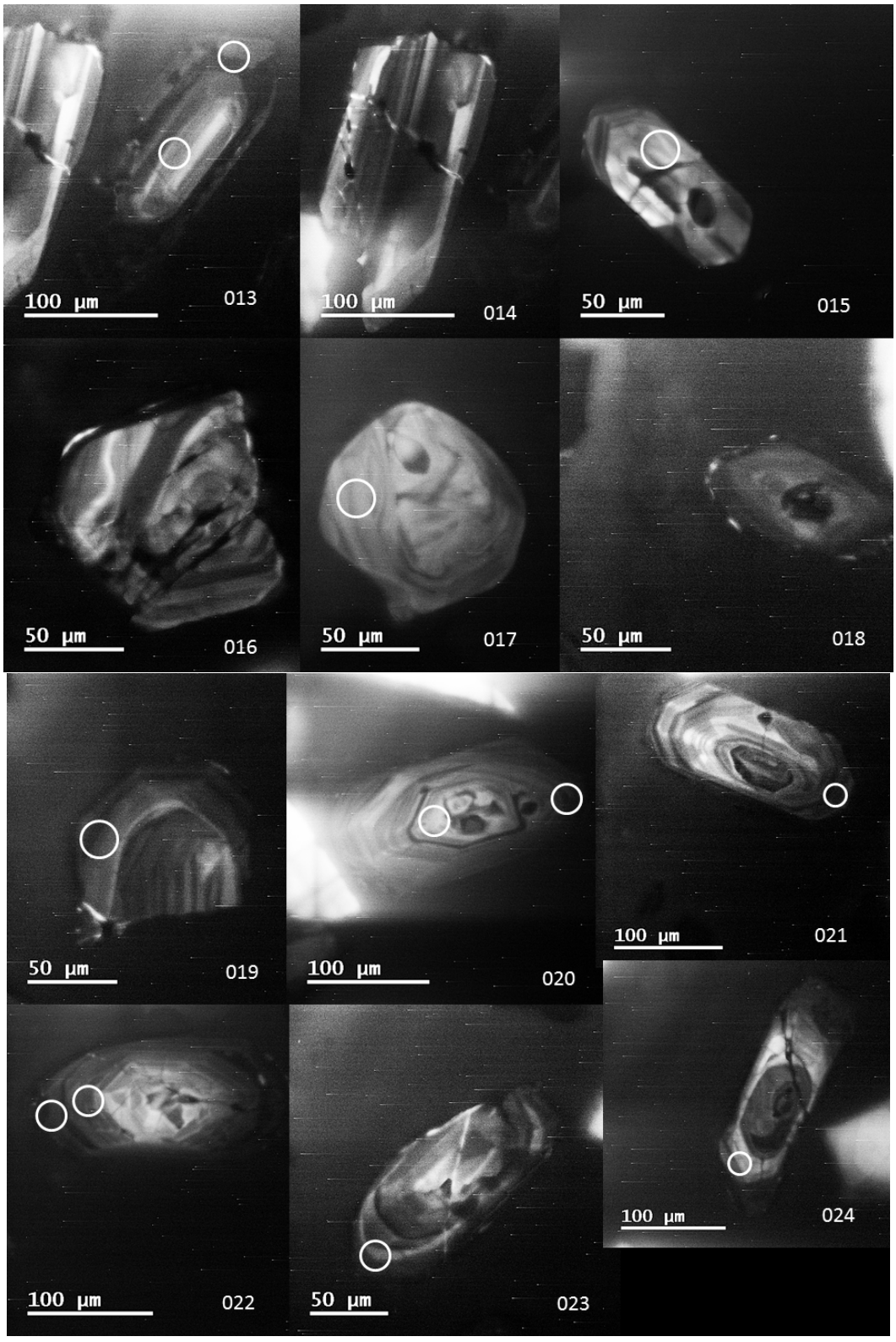
100 µm
013
100 µm
014
50 µm
015
50 µm
016
50 µm
017
50 µm
018
50 µm
019
100 µm
020
100 µm
021
100 µm
022
50 µm
023
100 µm
024

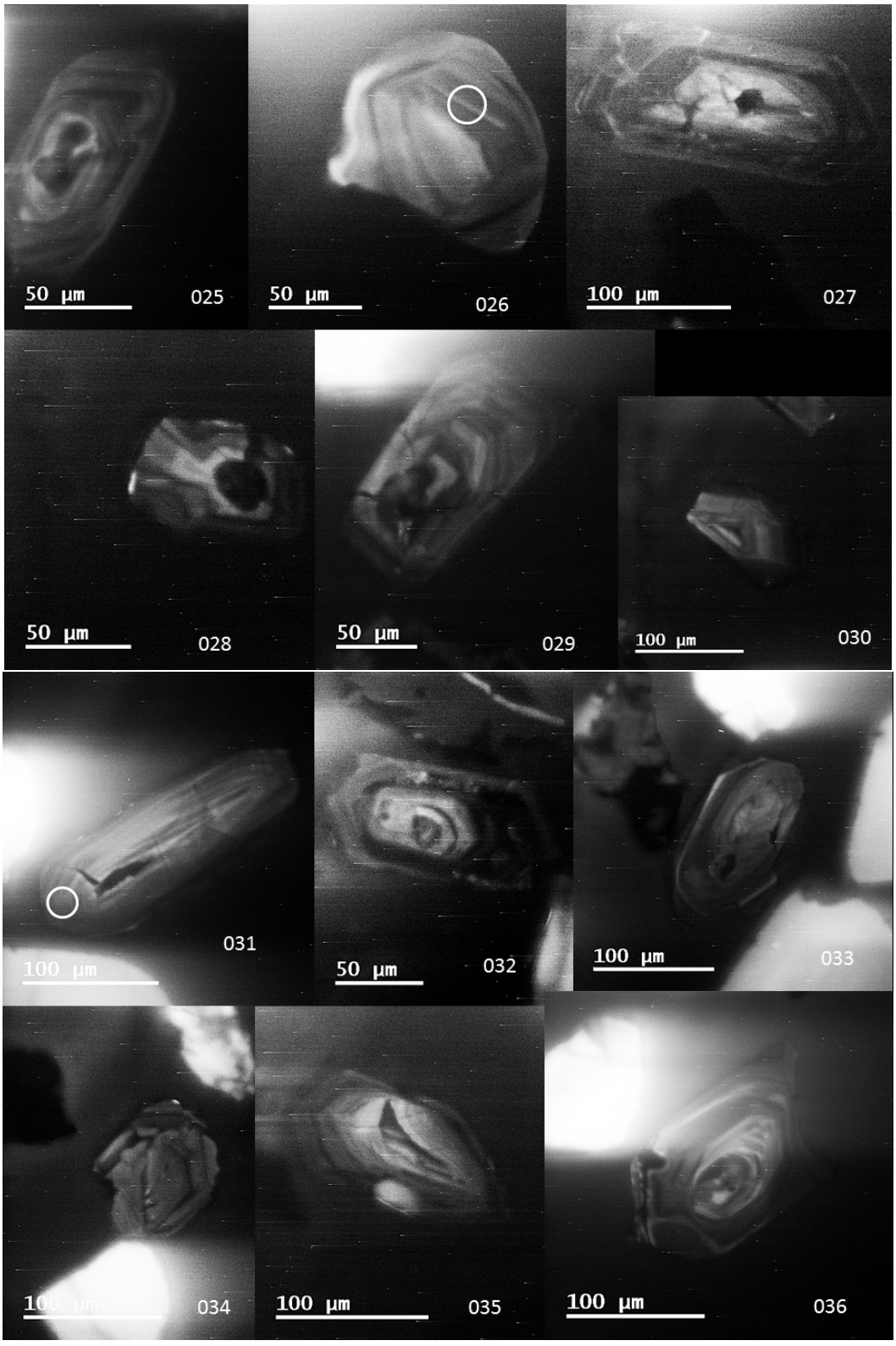
50 µm
025
50 µm
026
100 µm
027
50 µm
028
50 µm
029
100 µm
030
031
100 µm
50 µm
032
100 µm
033
100 µm
034
100 µm
035
100 µm
036

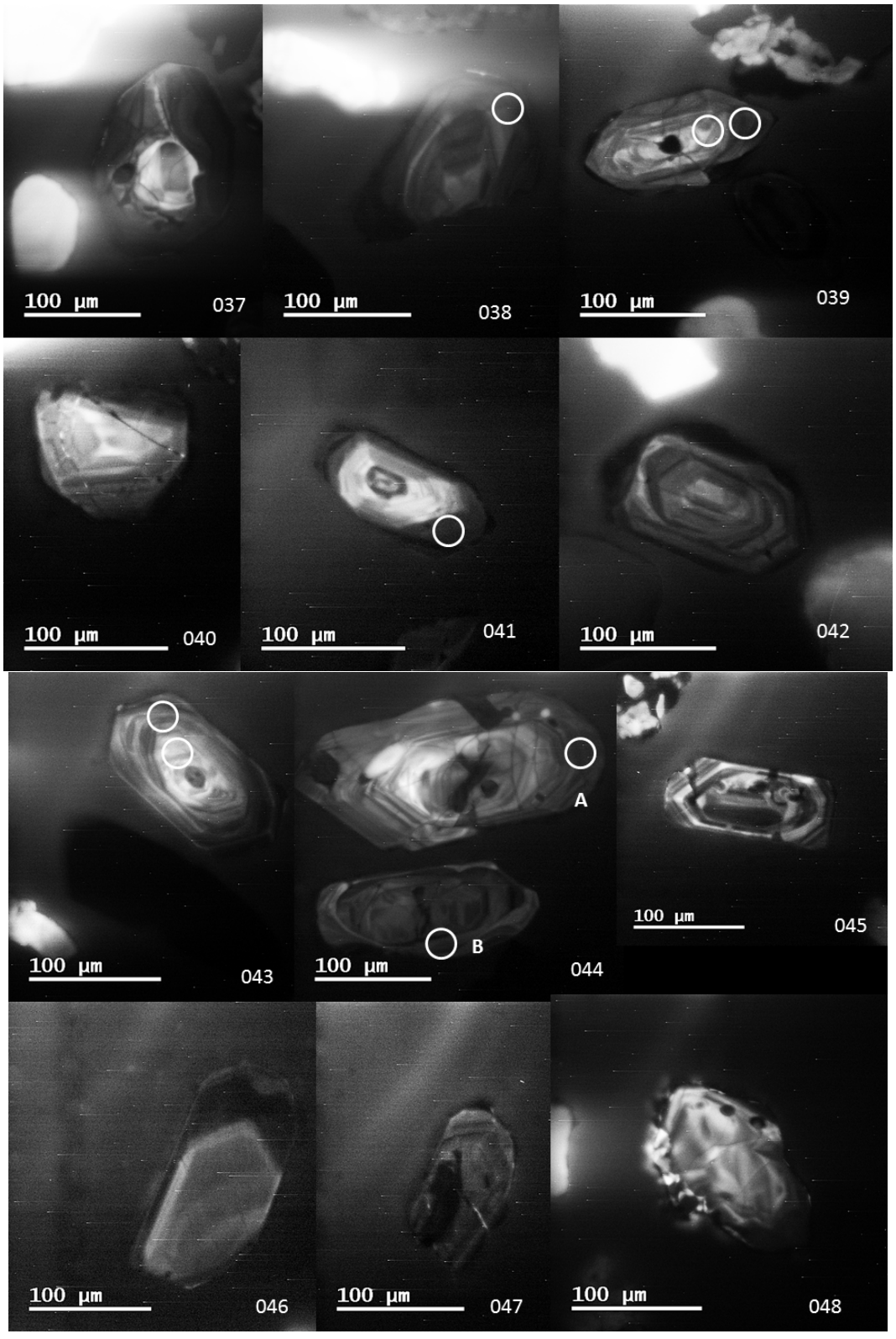
100 µm
037
100 µm
038
100 µm
039
100 µm
040
100 µm
041
100 µm
042
100 µm
043
A
B
100 µm
044
100 µm
045
100 µm
046
100 µm
047
100 µm
048

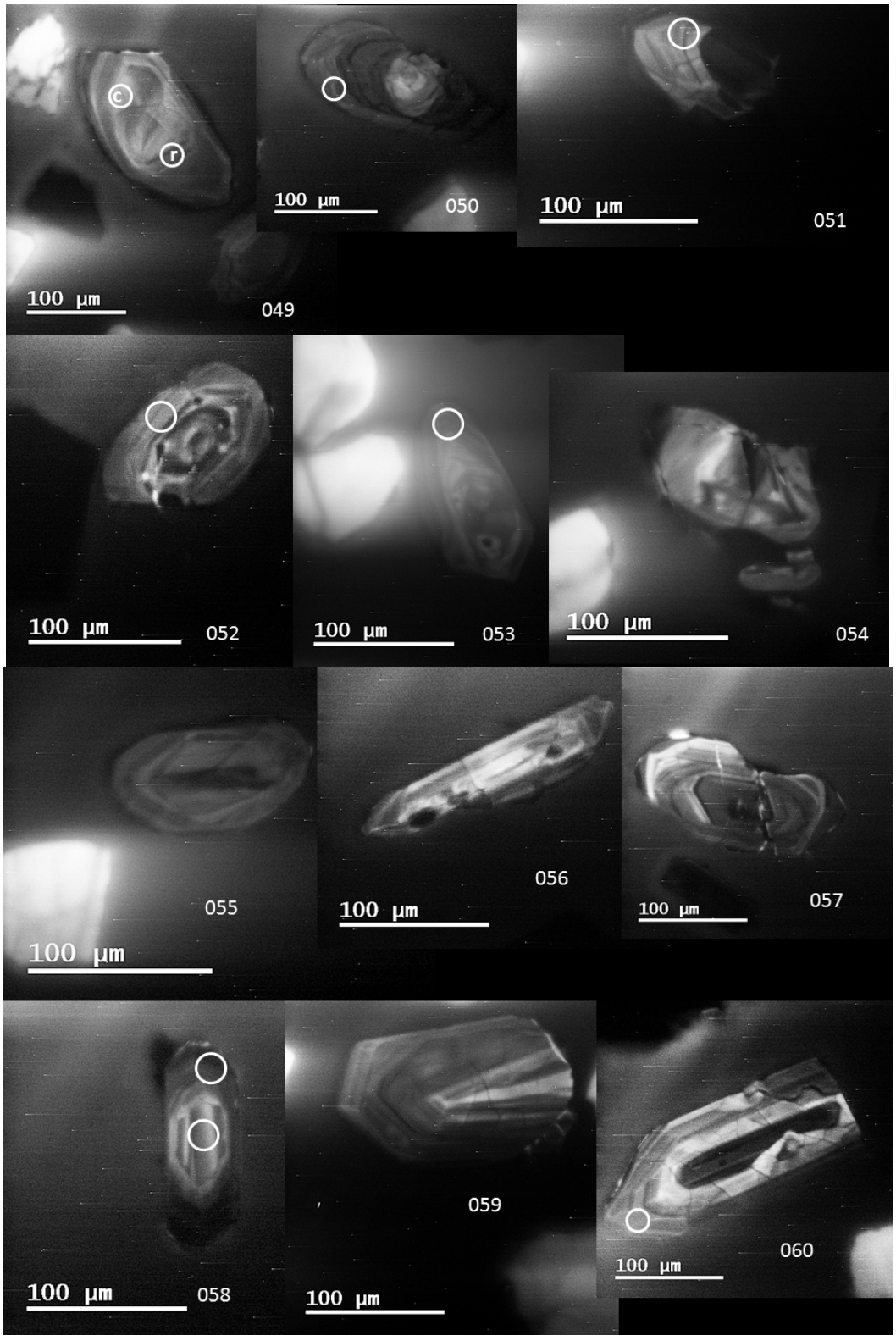
c
r
100 µm
049
100 µm
050
100 µm
051
100 µm
052
100 µm
053
100 µm
054
055
100 µm
056
100 µm
057
100 µm
058
059
100 µm
060
100 µm

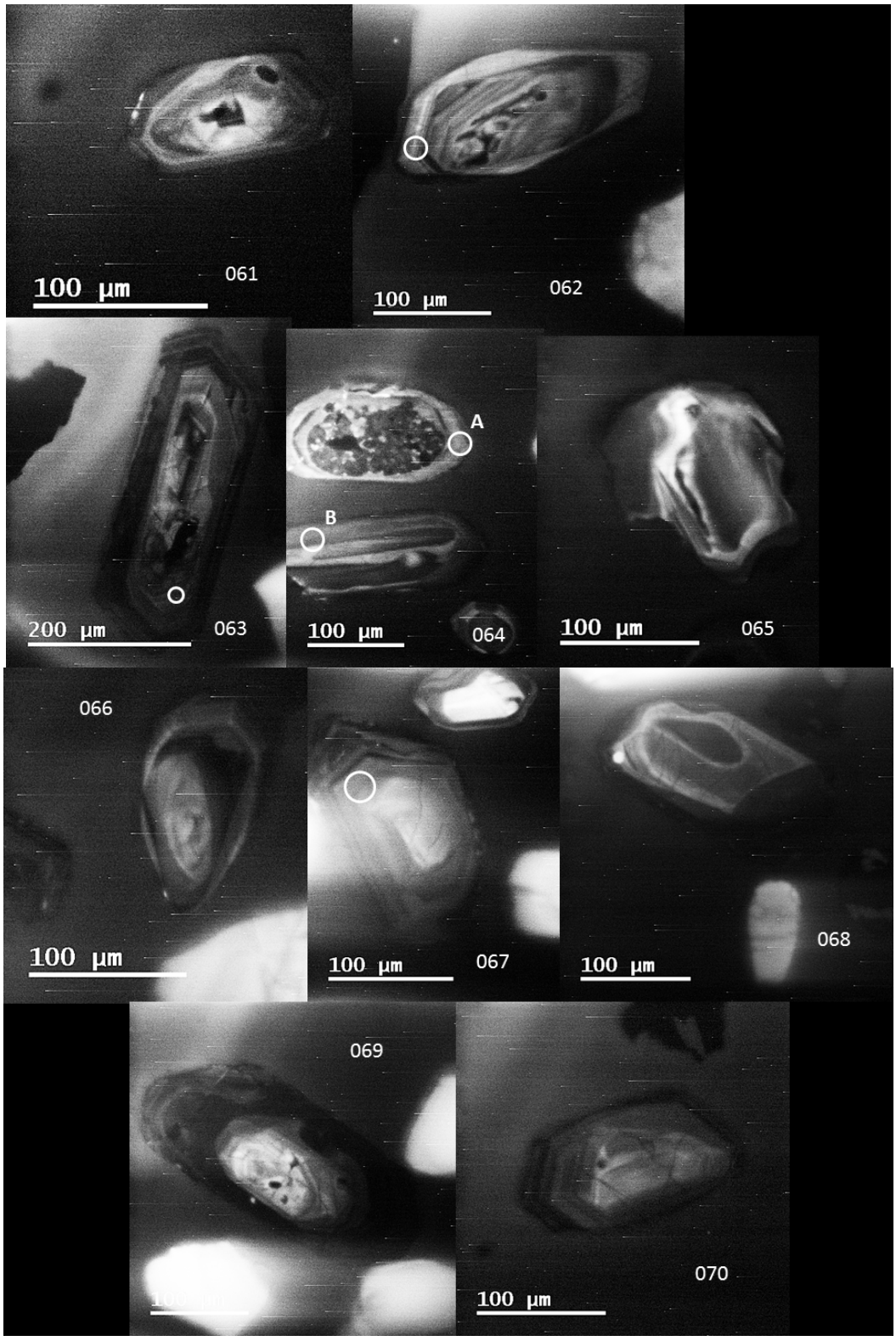
100 µm
061
100 µm
062
200 µm
063
A
B
100 µm
064
100 µm
065
066
100 µm
100 µm
067
068
100 µm
069
070
100 µm

C-5. Northern granite (BR060913-04A)

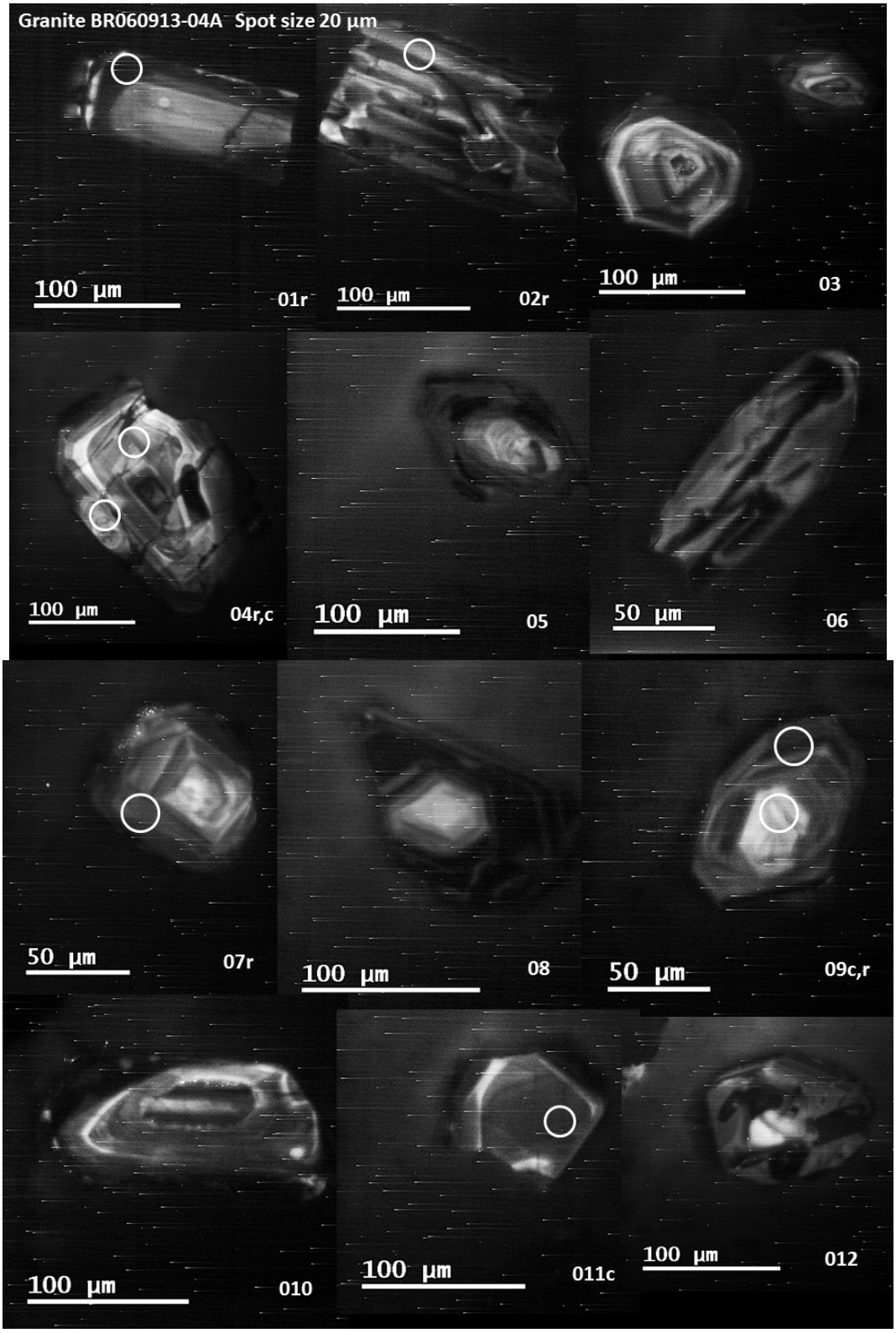

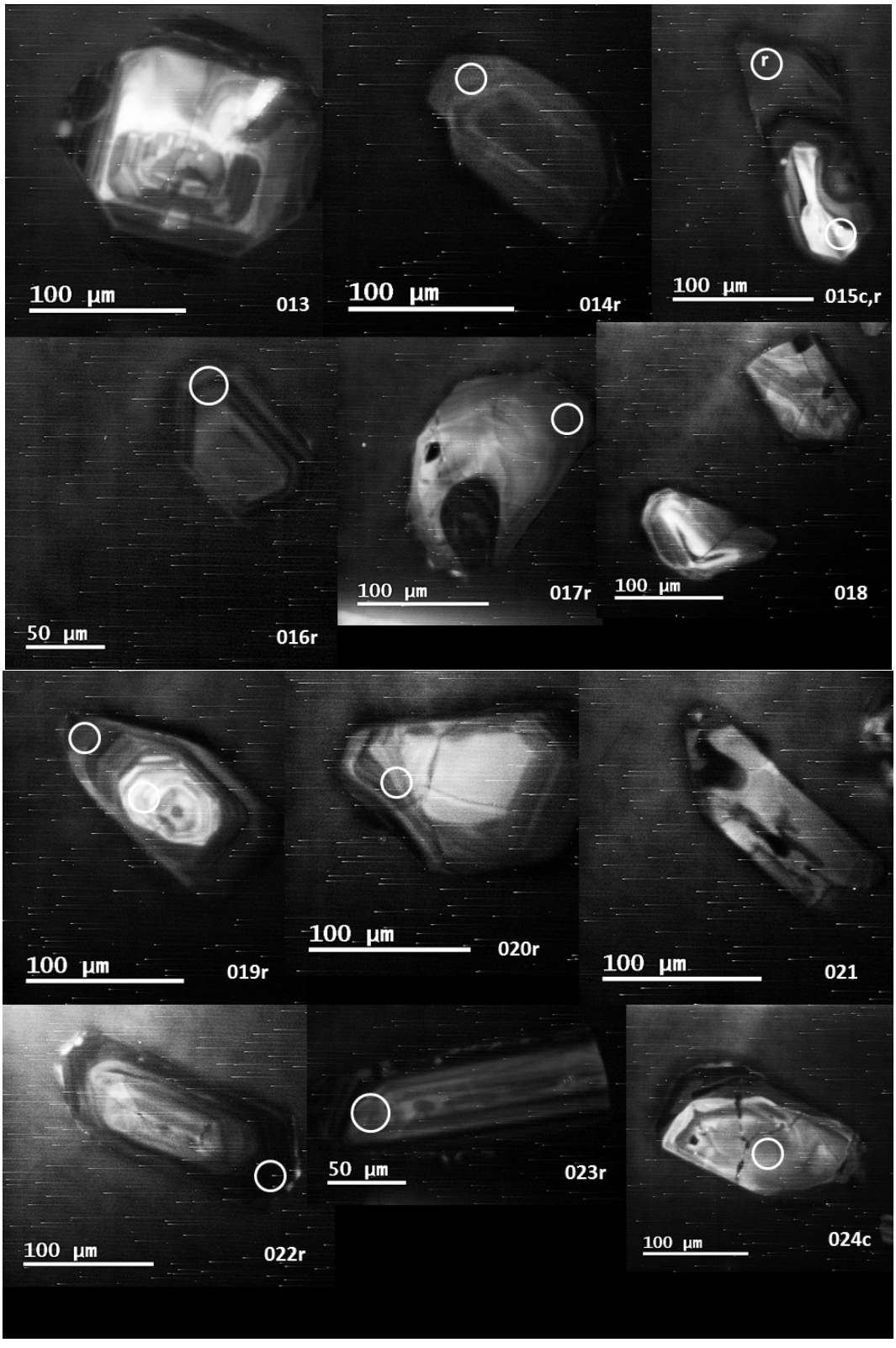
100 µm
013
100 µm
014r
r
100 µm
015c,r
50 µm
016r
100 µm
017r
100 µm
018
100 µm
019r
100 µm
020r
100 µm
021
50 µm
022r
50 µm
023r
100 µm
024c

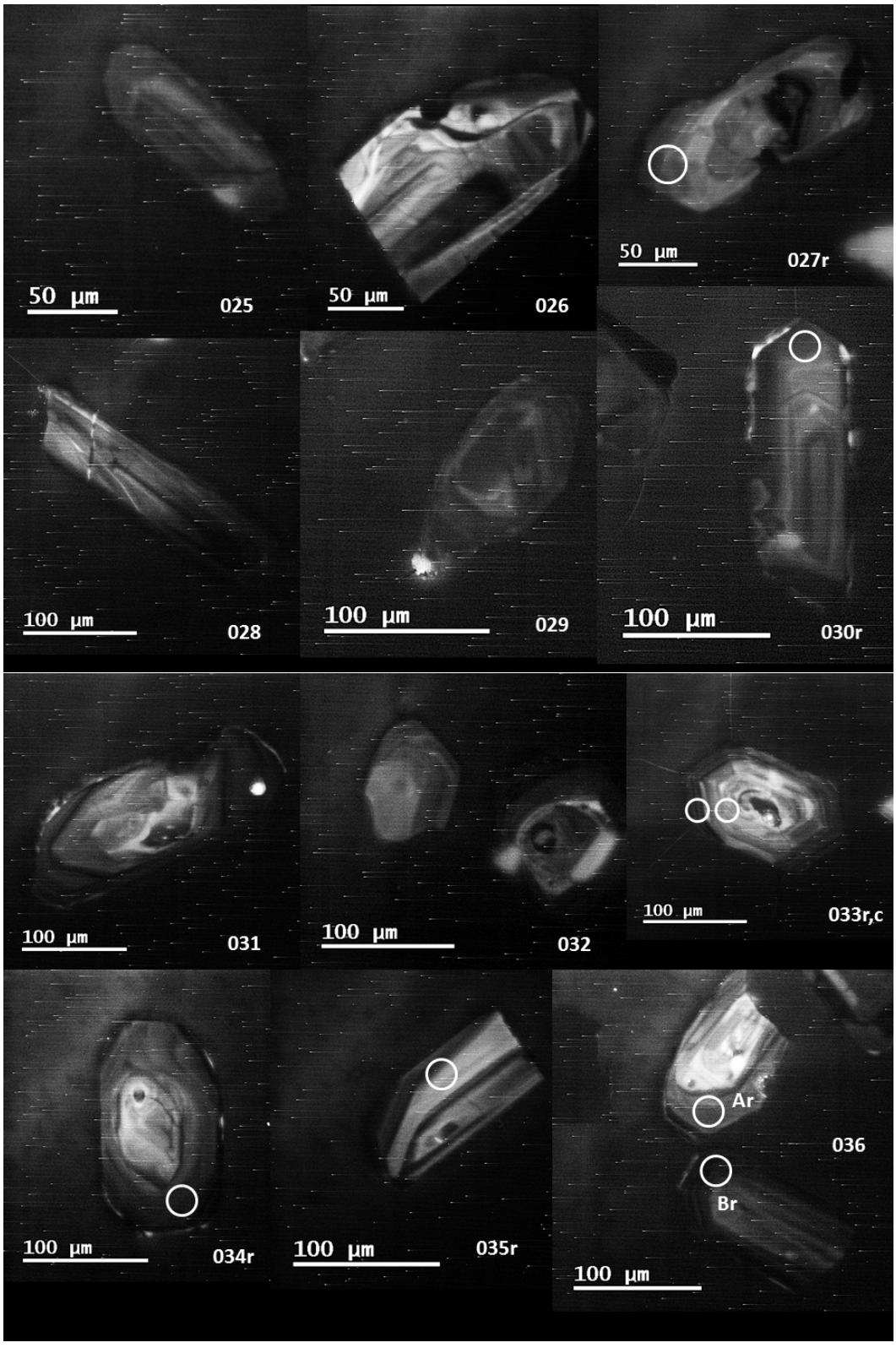
50 µm
025
50 µm
026
50 µm
027r
100 µm
028
100 µm
029
100 µm
030r
100 µm
031
100 µm
032
100 µm
033r,c
100 µm
034r
100 µm
035r
Ar
036
Br
100 µm

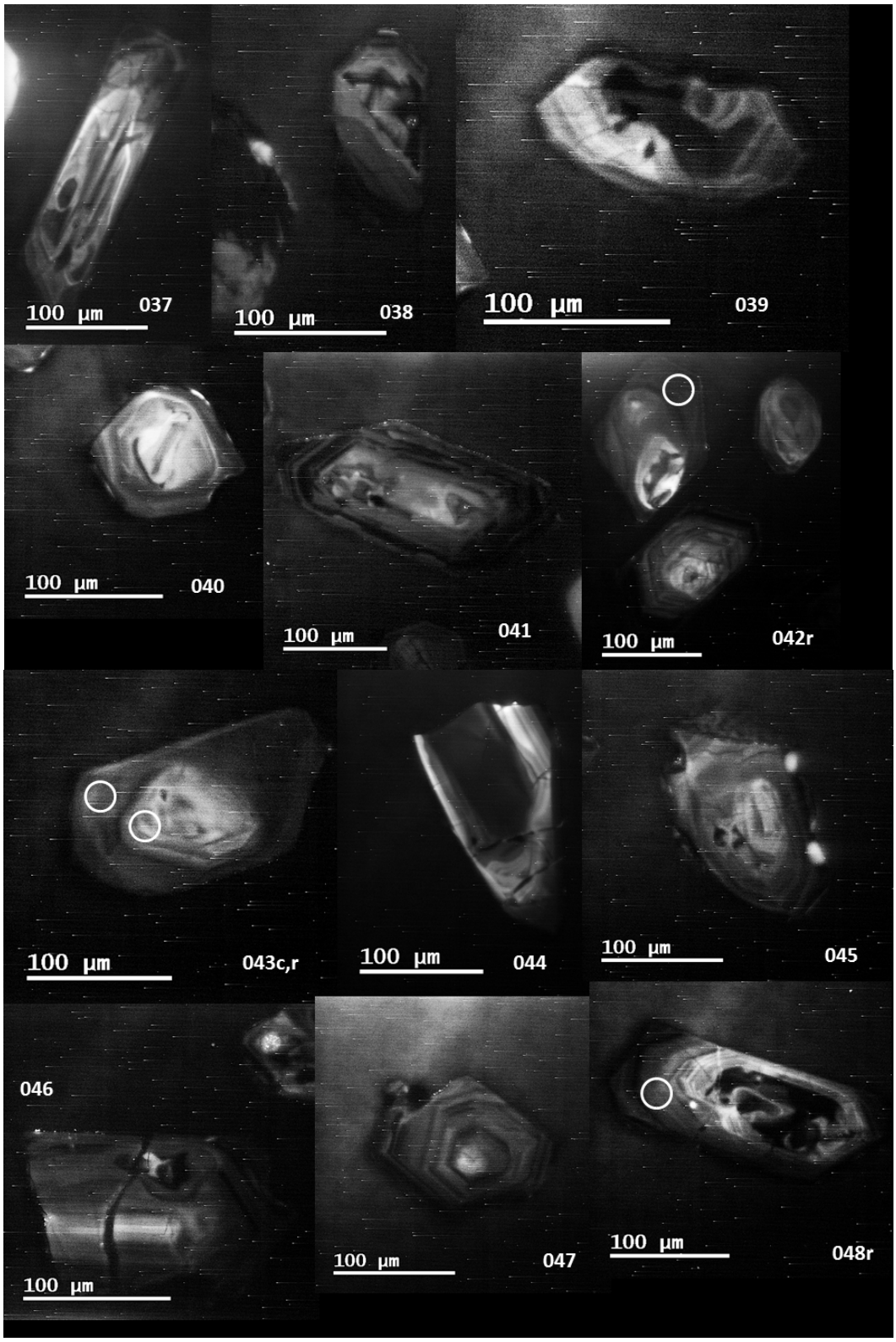
100 µm
037
100 µm
038
100 µm
039
100 µm
040
100 µm
041
100 µm
042r
100 µm
043c,r
100 µm
044
100 µm
045
046
100 µm
100 µm
047
100 µm
048r

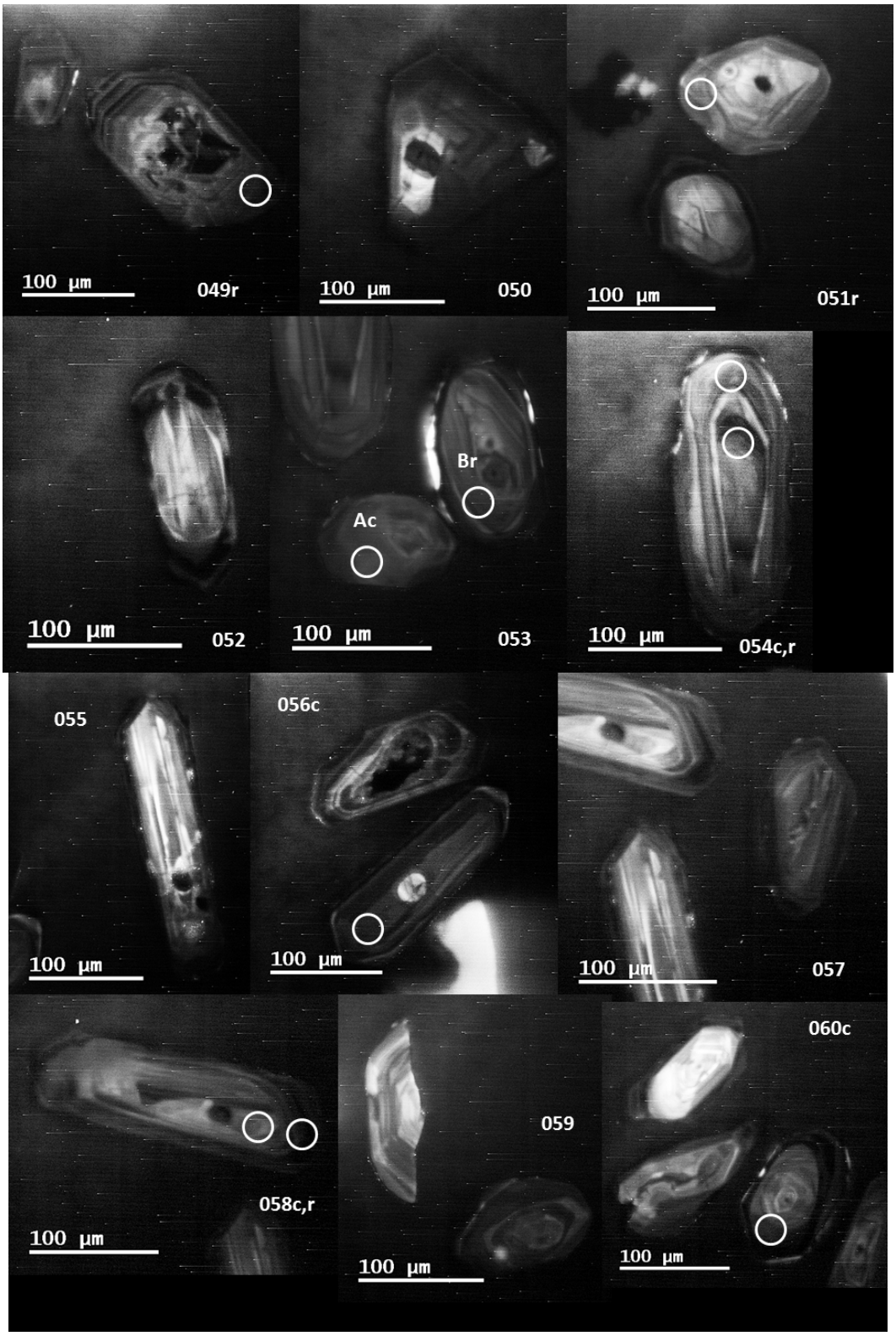
100 µm
049r
100 µm
050
100 µm
051r
100 µm
052
Br
Ac
100 µm
053
100 µm
054c,r
055
100 µm
056c
100 µm
100 µm
057
058c,r
100 µm
059
100 µm
060c
100 µm

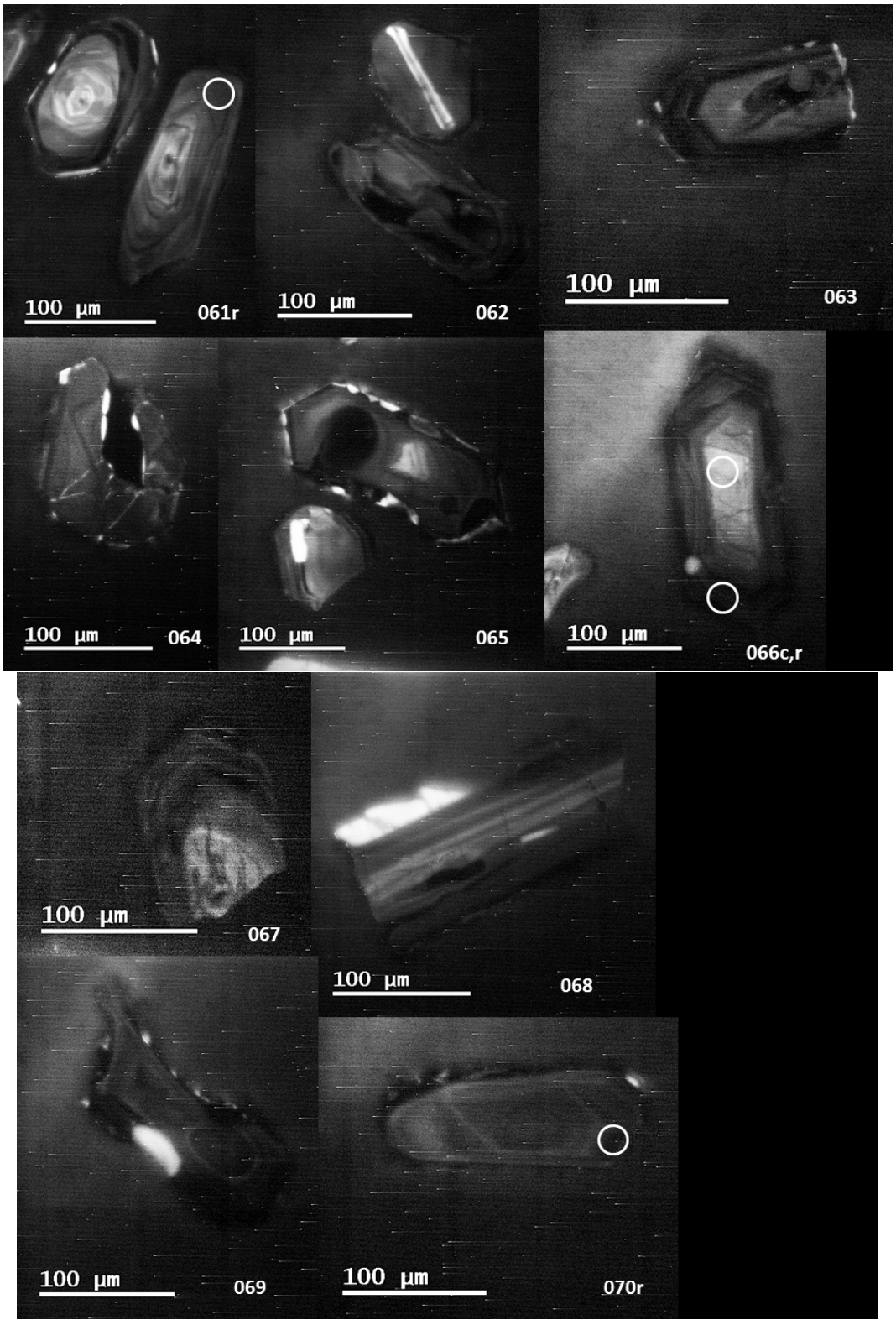
100 µm
061r
100 µm
062
100 µm
063
100 µm
064
100 µm
065
100 µm
066c,r
100 µm
067
100 µm
068
100 µm
069
100 µm
070r

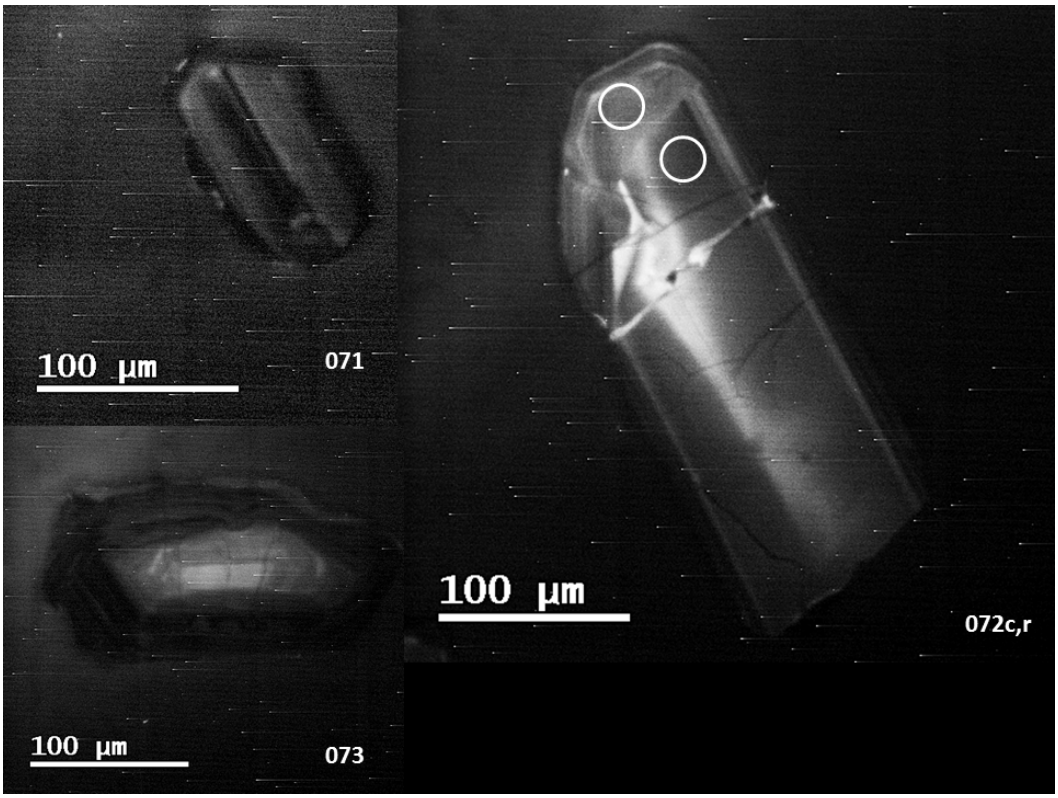
100 µm
071
100 µm
072c,r
100 µm
073

C-6. Southern granodiorite (BR061113-02A)

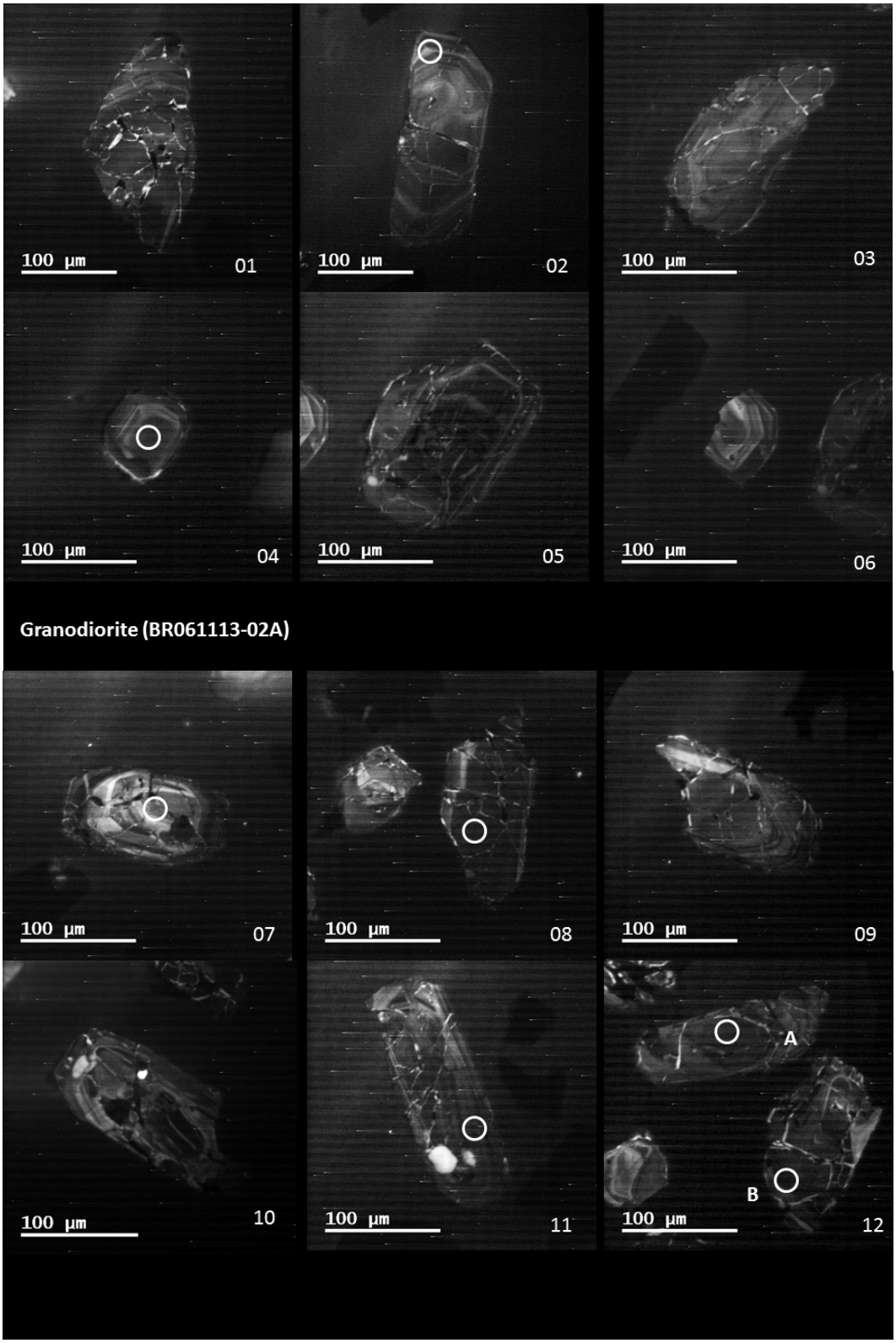

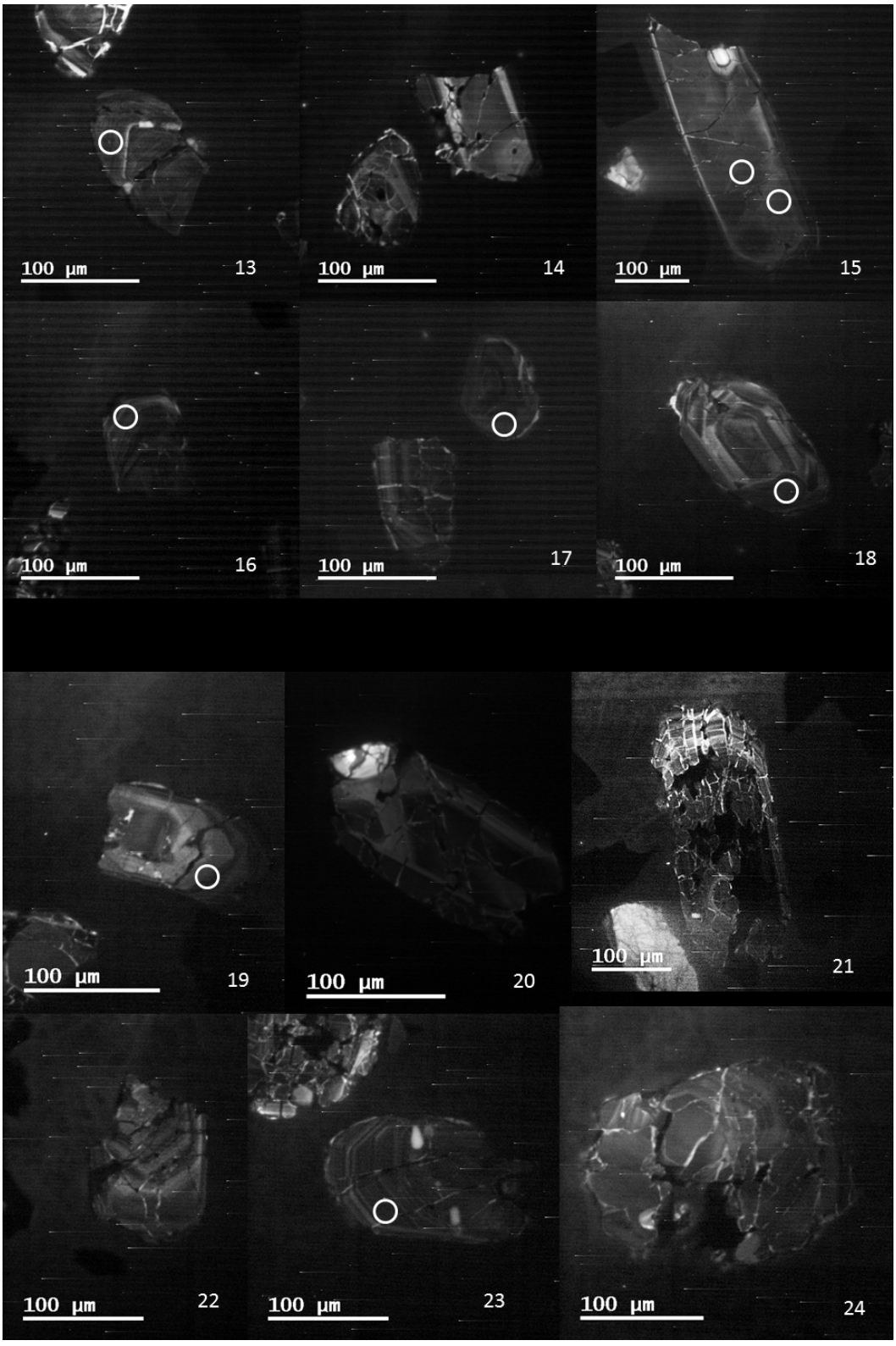
100 µm
13
100 µm
14
100 µm
15
100 µm
16
100 µm
17
100 µm
18
100 µm
19
100 µm
20
100 µm
21
100 µm
22
100 µm
23
100 µm
24

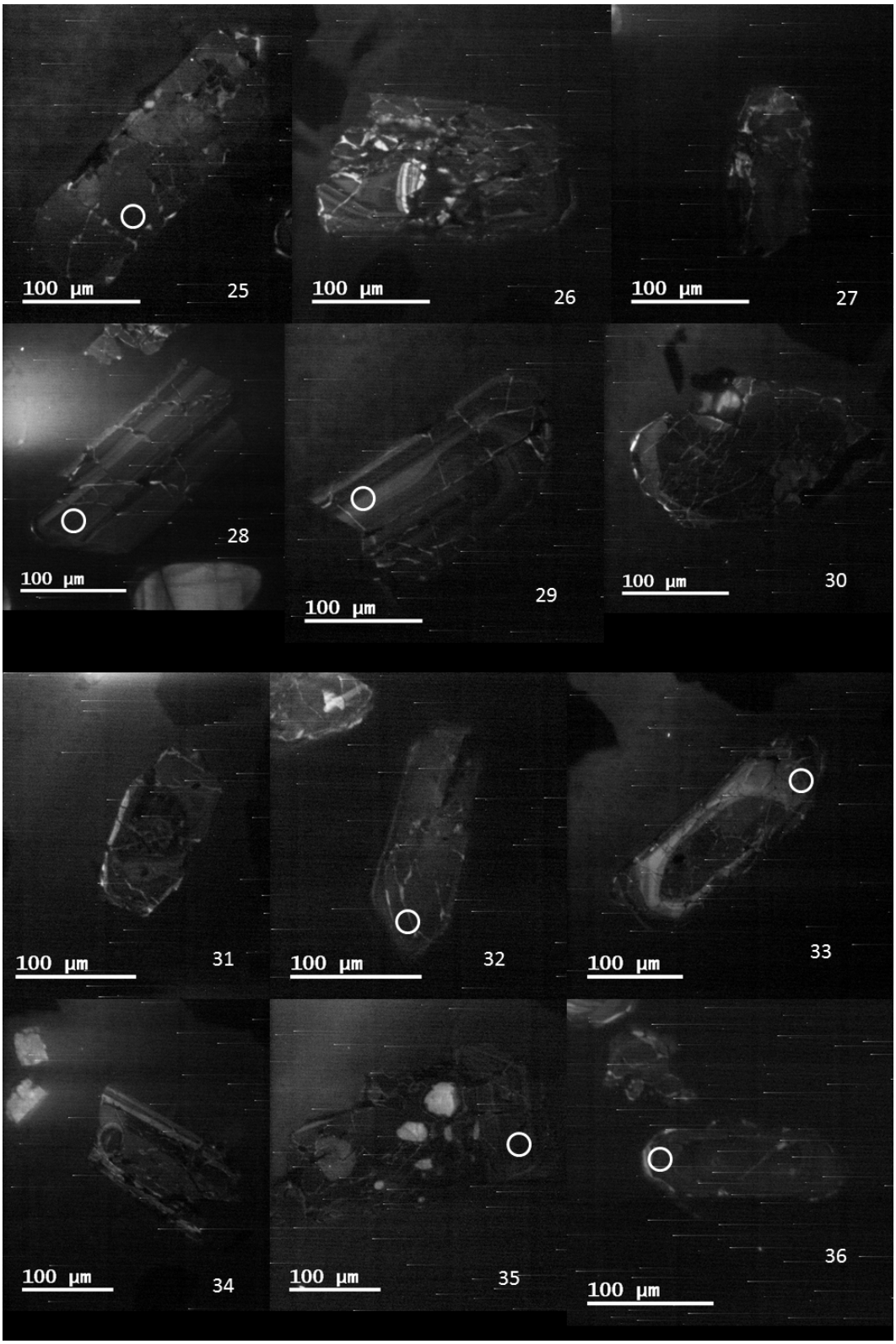
100 µm
25
100 µm
26
100 µm
27
28
100 µm
100 µm
29
100 µm
30
100 µm
31
100 µm
32
100 µm
33
100 µm
34
100 µm
35
36
100 µm

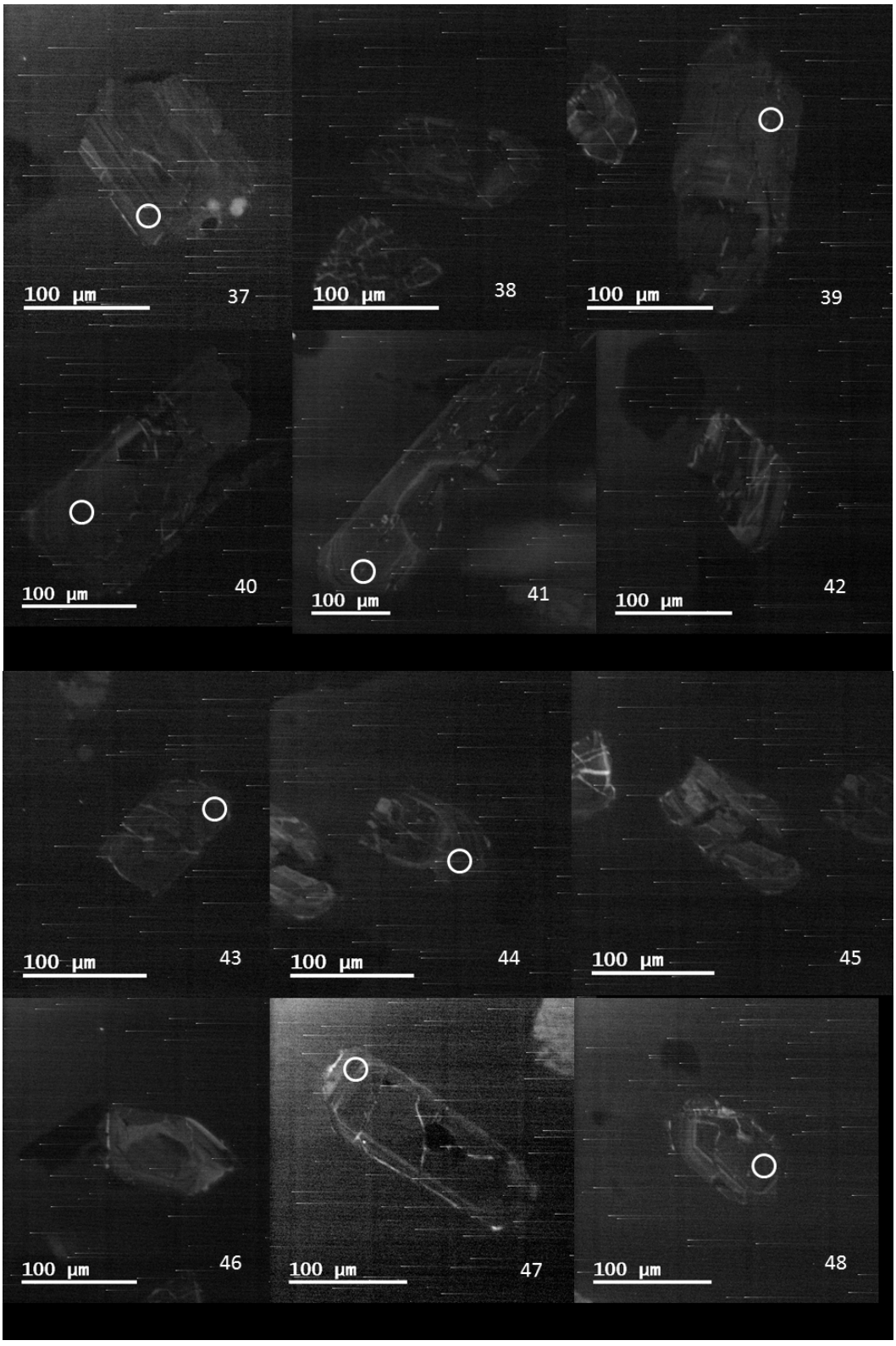
100 µm
37
100 µm
38
100 µm
39
100 µm
40
100 µm
41
100 µm
42
100 µm
43
100 µm
44
100 µm
45
100 µm
46
100 µm
47
100 µm
48

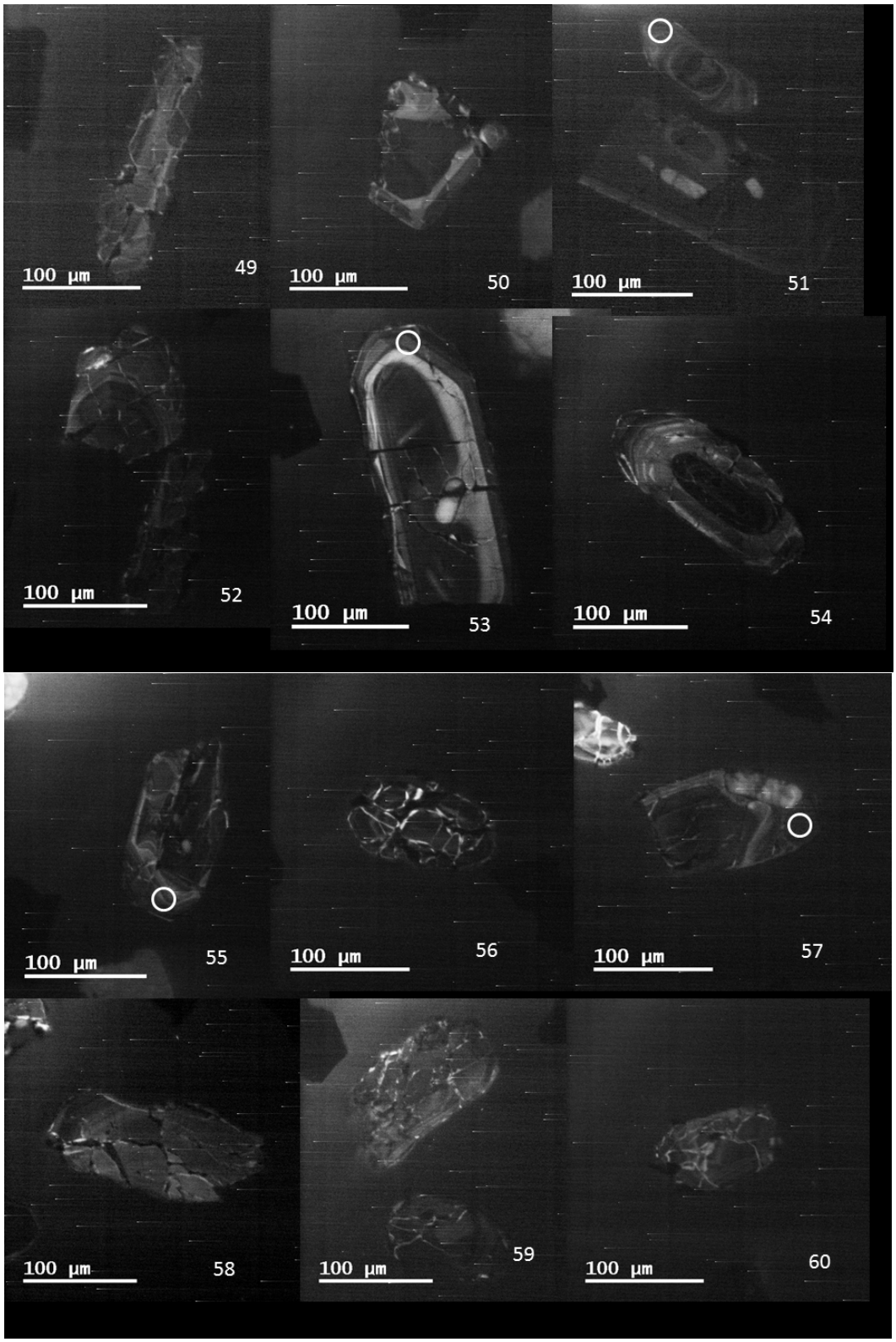
100 µm
49
100 µm
50
100 µm
51
100 µm
52
100 µm
53
100 µm
54
100 µm
55
100 µm
56
100 µm
57
100 µm
58
100 µm
59
100 µm
60

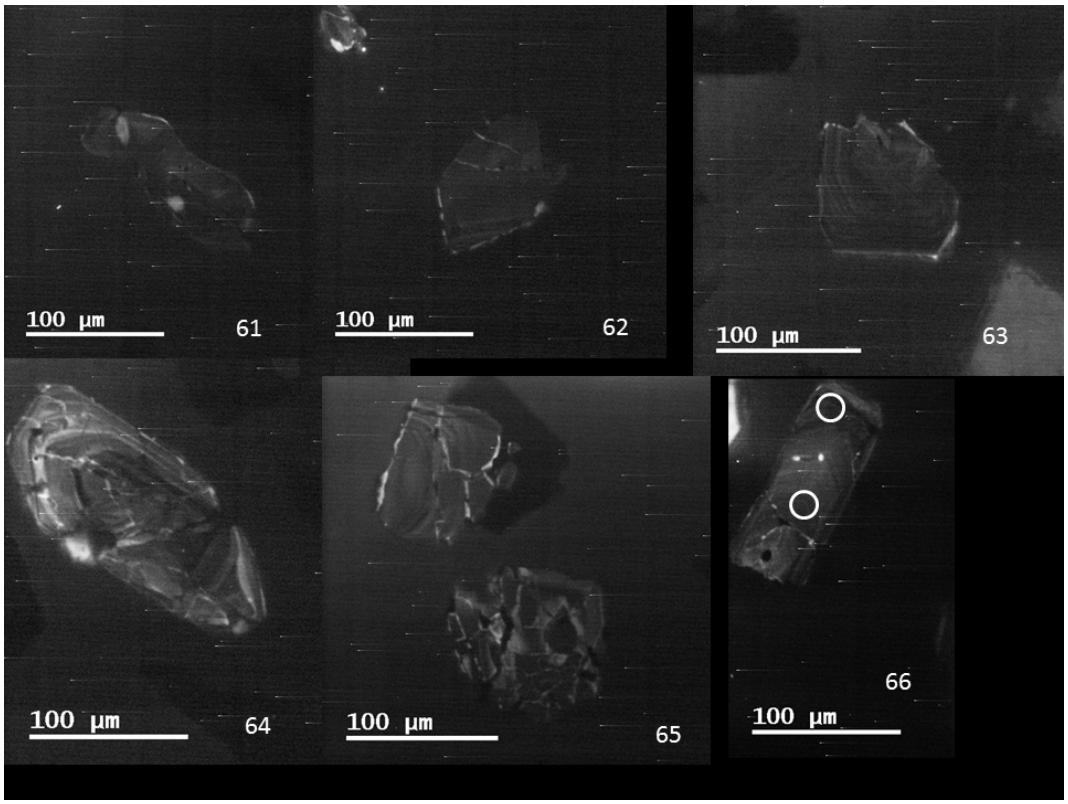
100 µm
61
100 µm
62
100 µm
63
100 µm
64
100 µm
65
66
100 µm

C-7. Pegmatite 1 (BR061113-05)

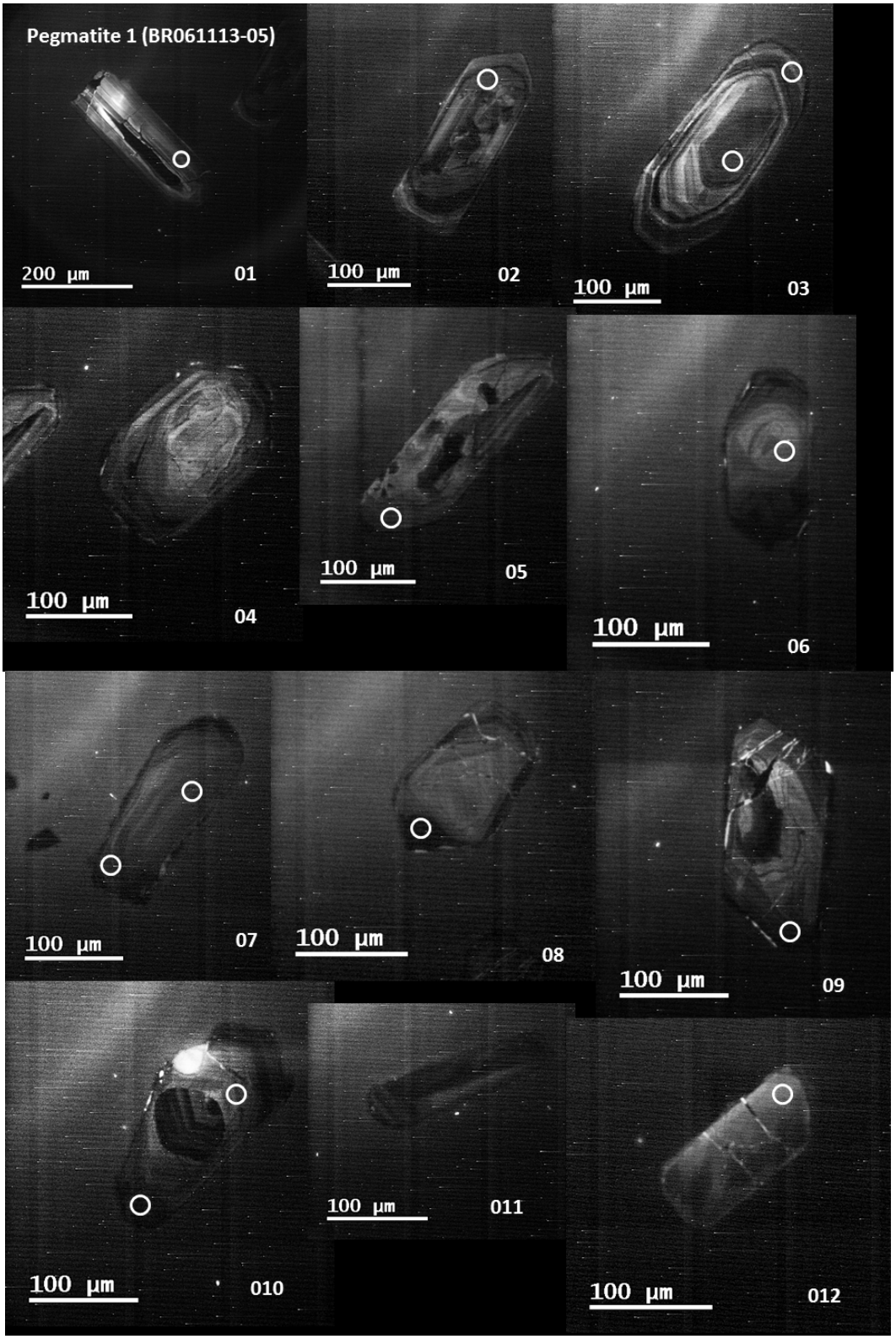

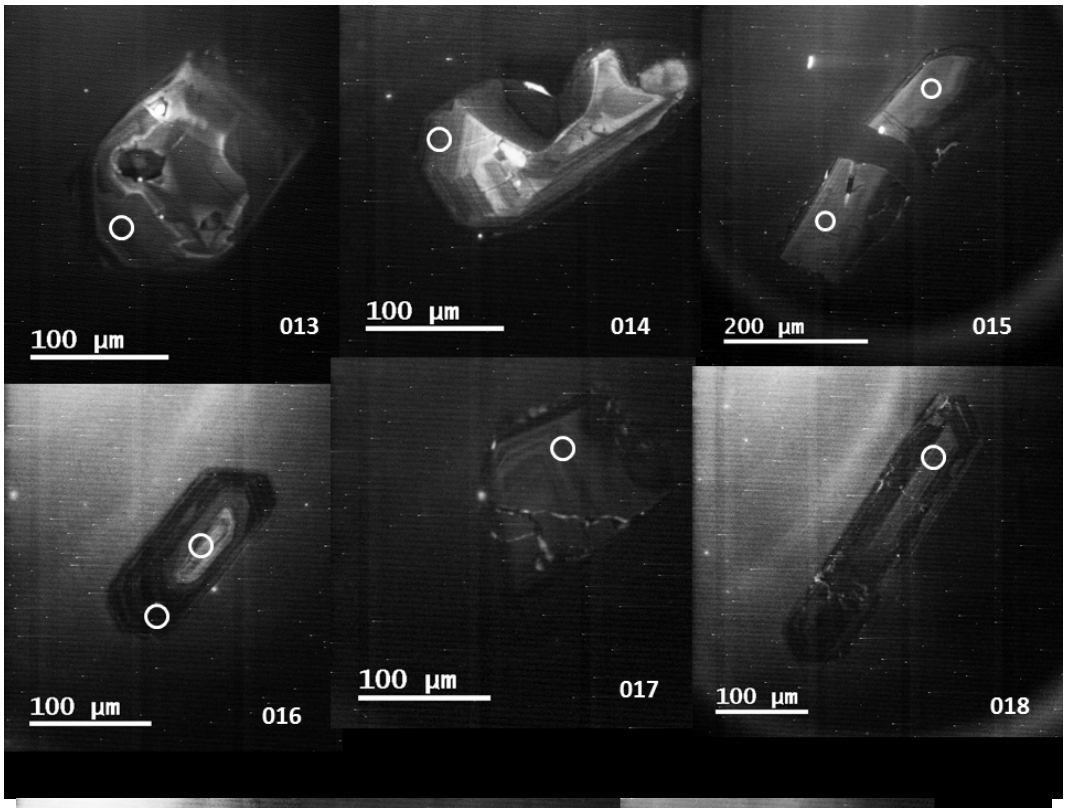
100 µm
013
100 µm
014
200 µm
015
100 µm
016
100 µm
017
100 µm
018

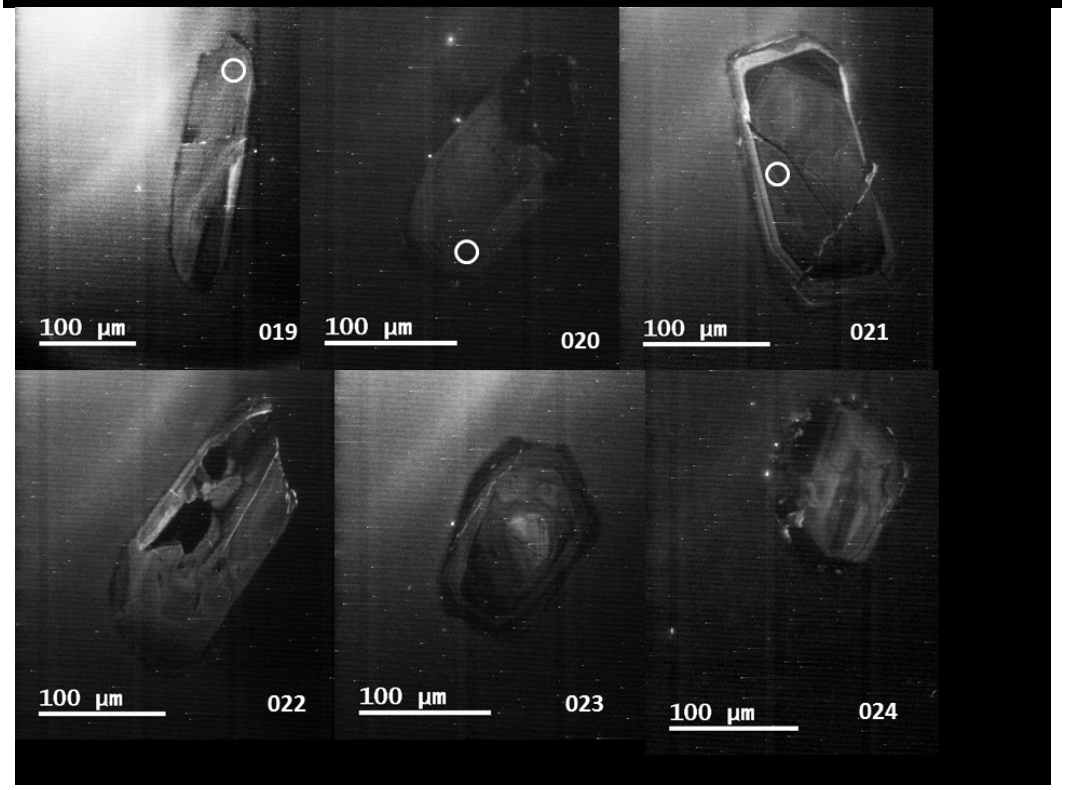
100 µm
019
100 µm
020
100 µm
021
100 µm
022
100 µm
023
100 µm
024

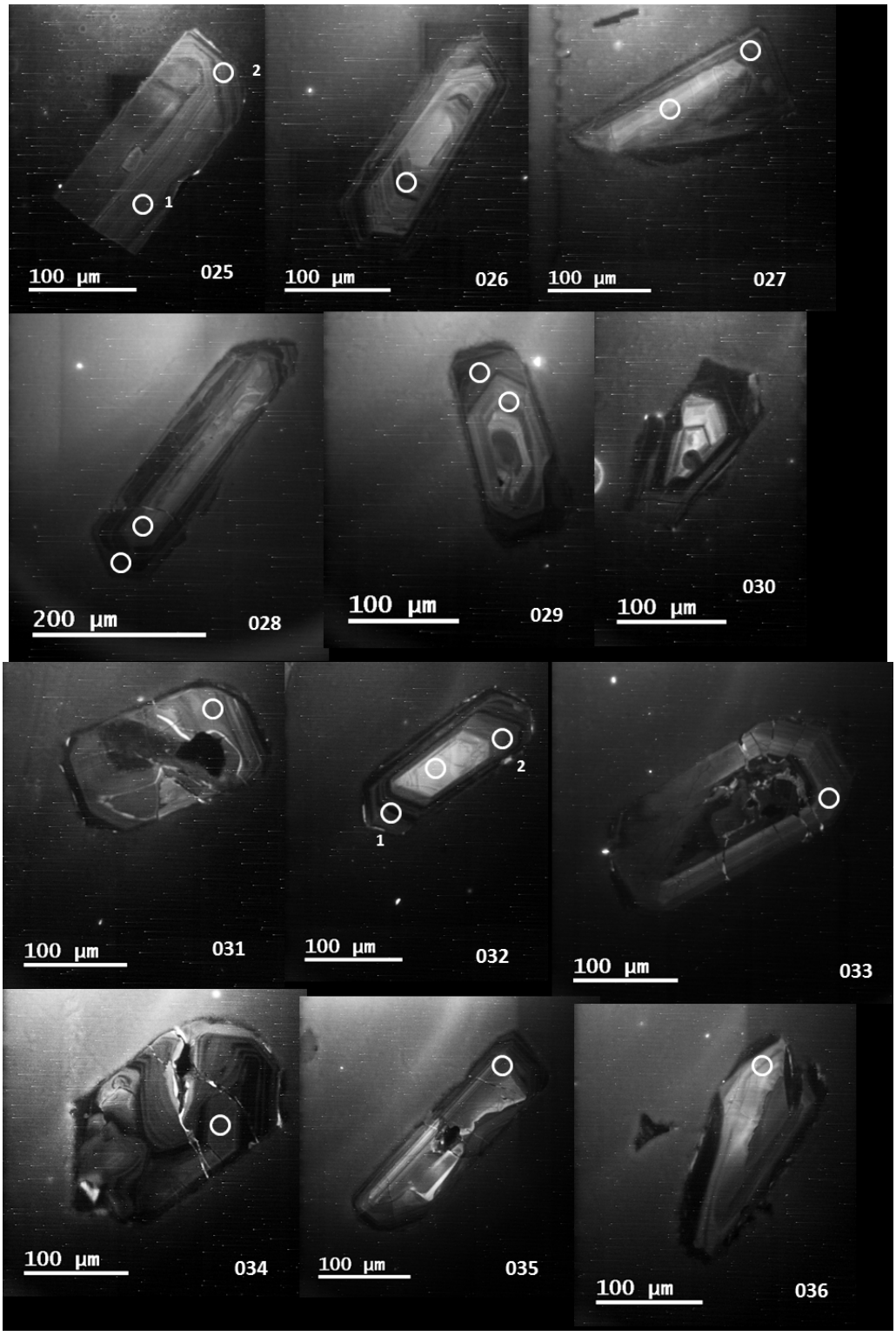
2
1
100 µm
025
100 µm
026
100 µm
027
200 µm
028
100 µm
029
100 µm
030
100 µm
031
2
1
100 µm
032
100 µm
033
100 µm
034
100 µm
035
100 µm
036

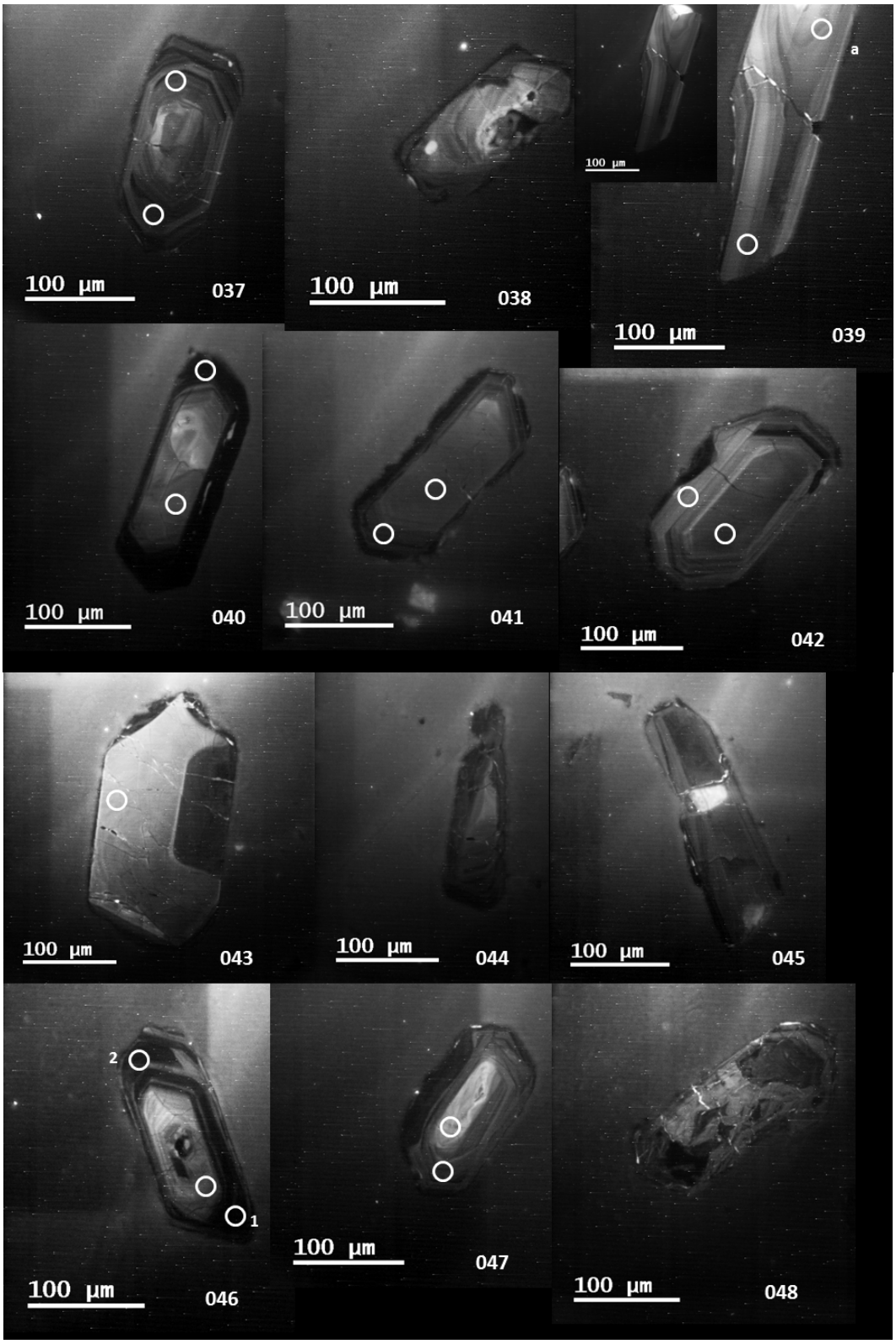
100 µm
037
100 µm
038
100 µm
a
100 µm
039
100 µm
040
100 µm
041
100 µm
042
100 µm
043
100 µm
044
100 µm
045
2
1
100 µm
046
100 µm
047
100 µm
048

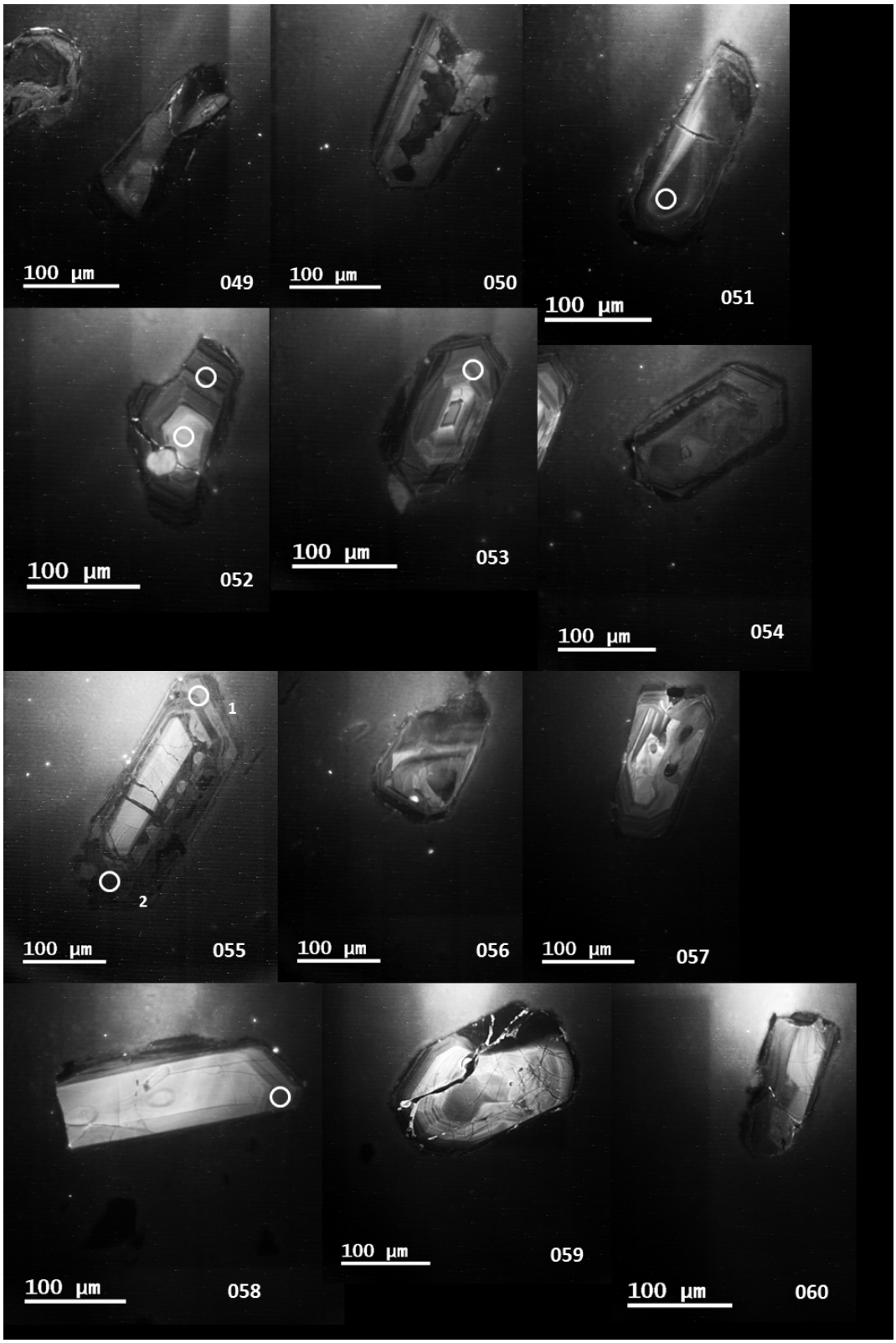
100 µm
049
100 µm
050
100 µm
051
100 µm
052
100 µm
053
100 µm
054
1
2
100 µm
055
100 µm
056
100 µm
057
100 µm
058
100 µm
059
100 µm
060

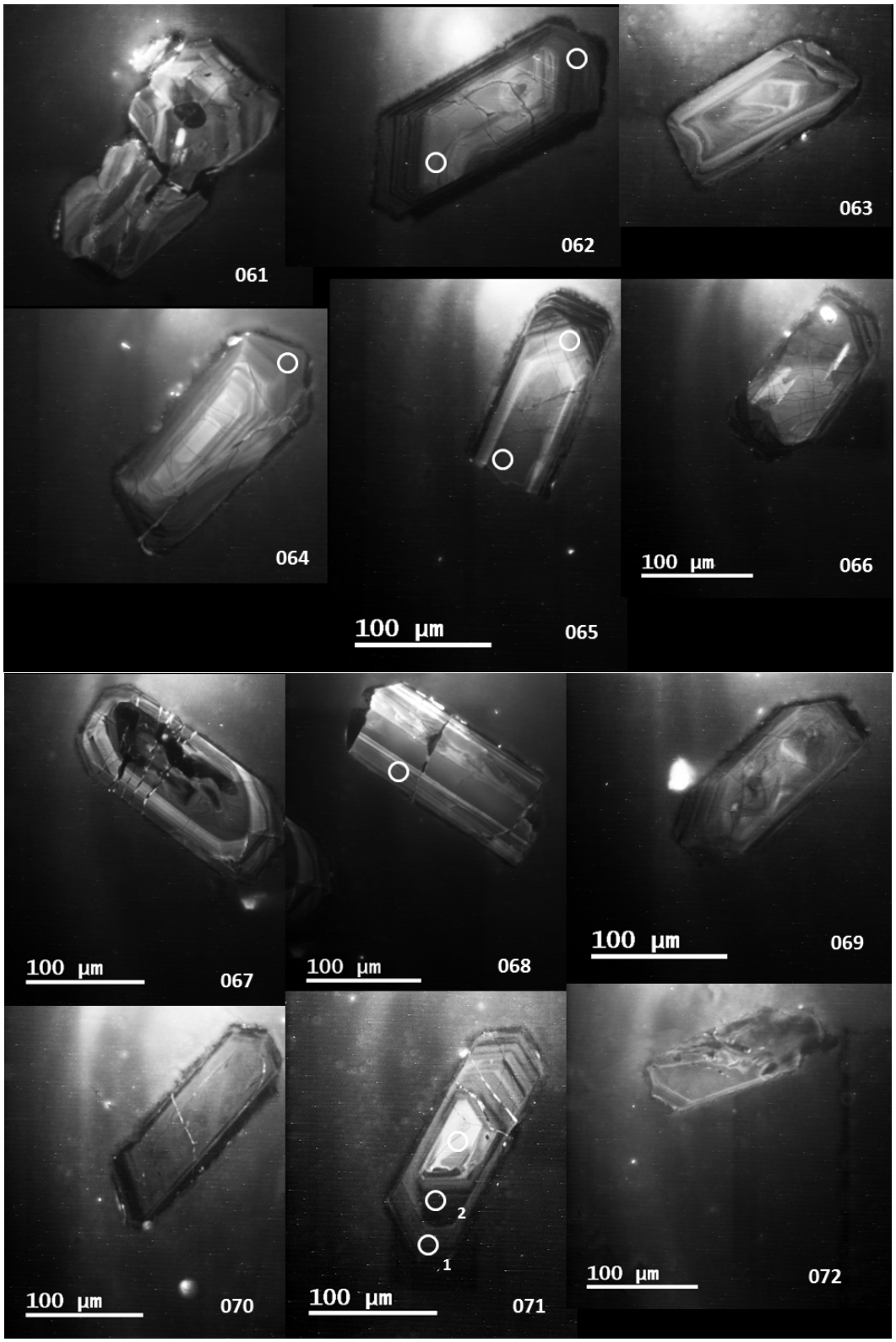
061
062
063
064
100 µm
065
100 µm
066
100 µm
067
100 µm
068
100 µm
069
100 µm
070
2
1
100 µm
071
100 µm
072

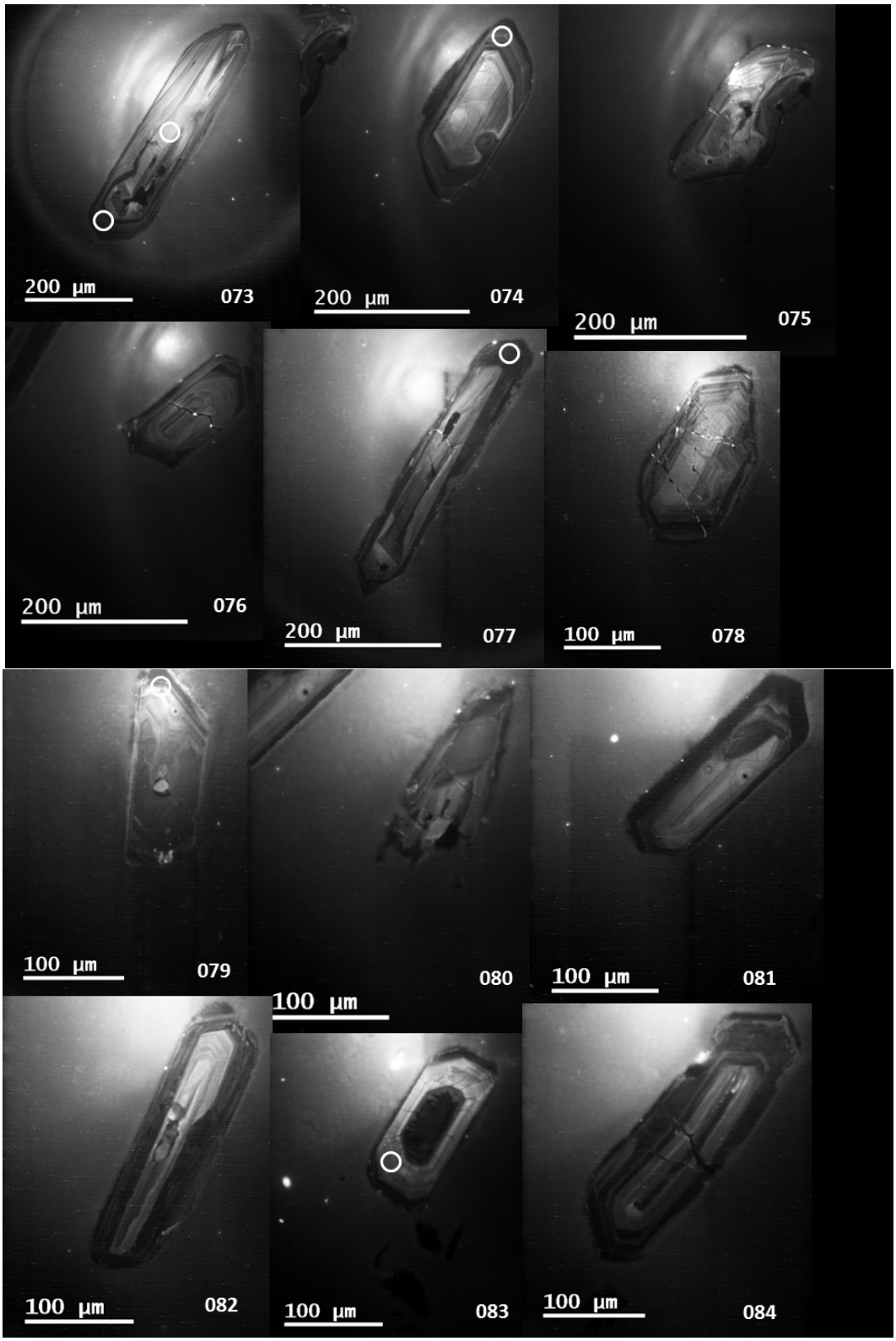
200 µm
073
200 µm
074
200 µm
075
200 µm
076
200 µm
077
100 µm
078
100 µm
079
100 µm
080
100 µm
081
100 µm
082
100 µm
083
100 µm
084

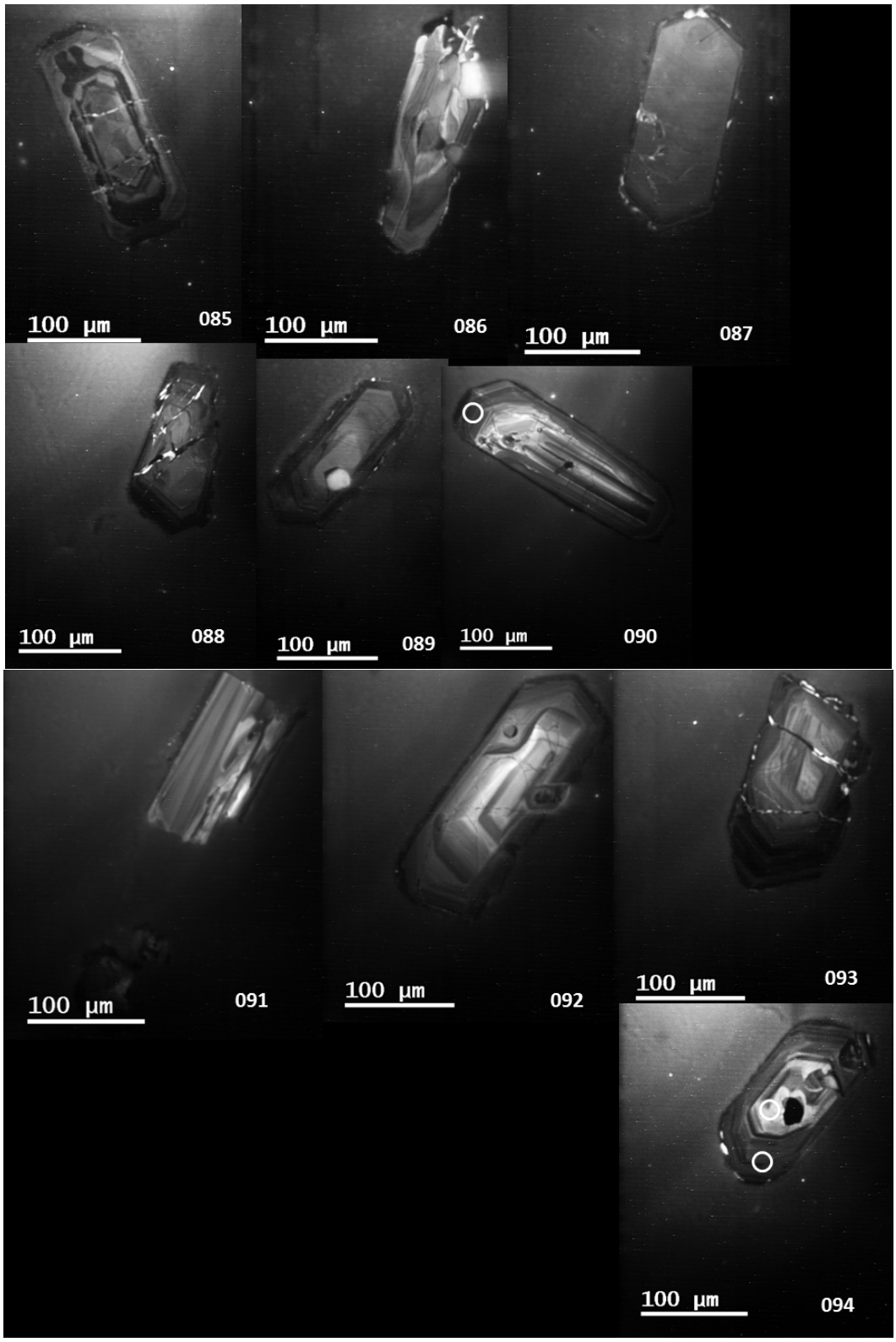
100 µm
085
100 µm
086
100 µm
087
100 µm
088
100 µm
089
100 µm
090
100 µm
091
100 µm
092
100 µm
093
100 µm
094

C-8. Pegmatite 2 (BR072815-02)

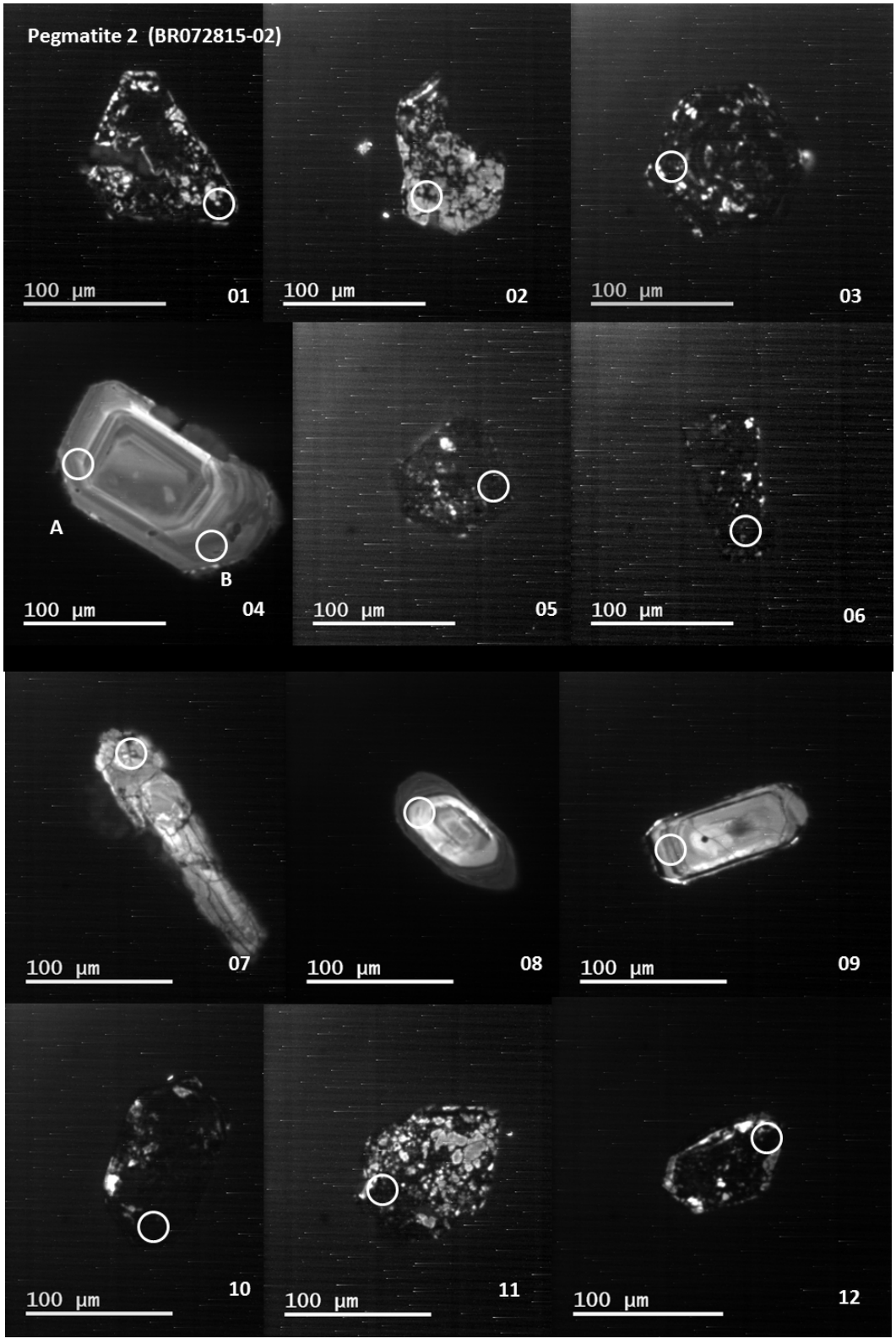

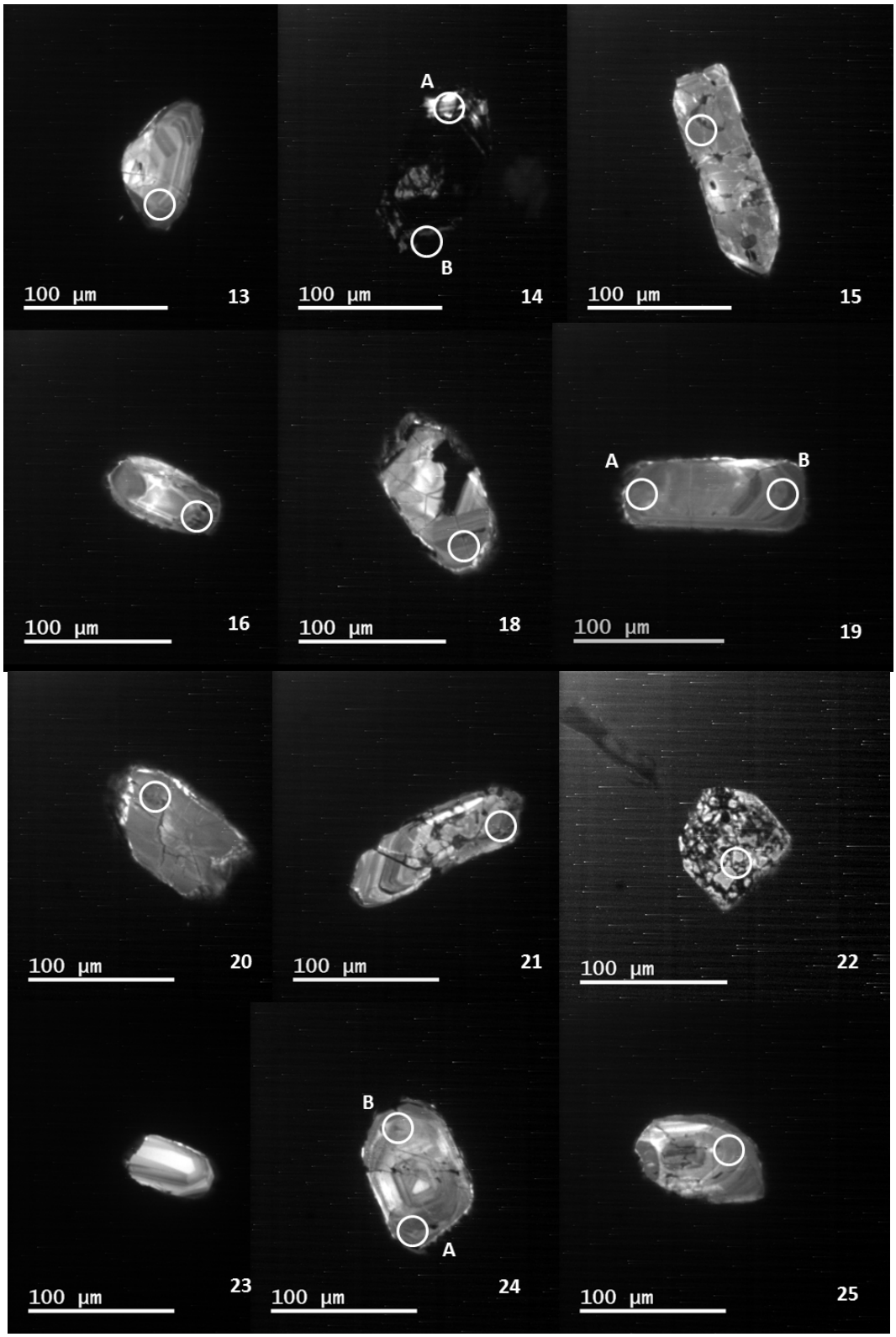
100 µm
13
A
B
100 µm
14
100 µm
15
100 µm
16
100 µm
18
A
B
100 µm
19
100 µm
20
100 µm
21
100 µm
22
100 µm
23
B
A
100 µm
24
100 µm
25

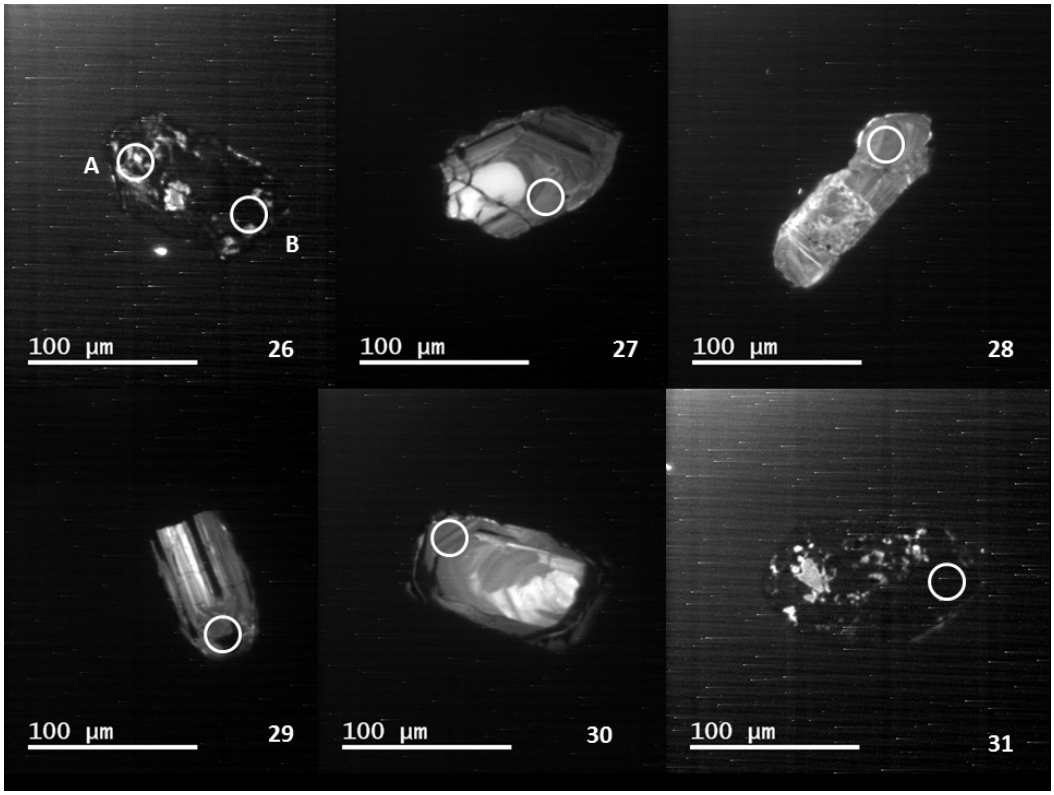
A
B
100 µm
26
100 µm
27
100 µm
28
100 µm
29
100 µm
30
100 µm
31

C-9. HBL-QEM1 (BR060913-01)

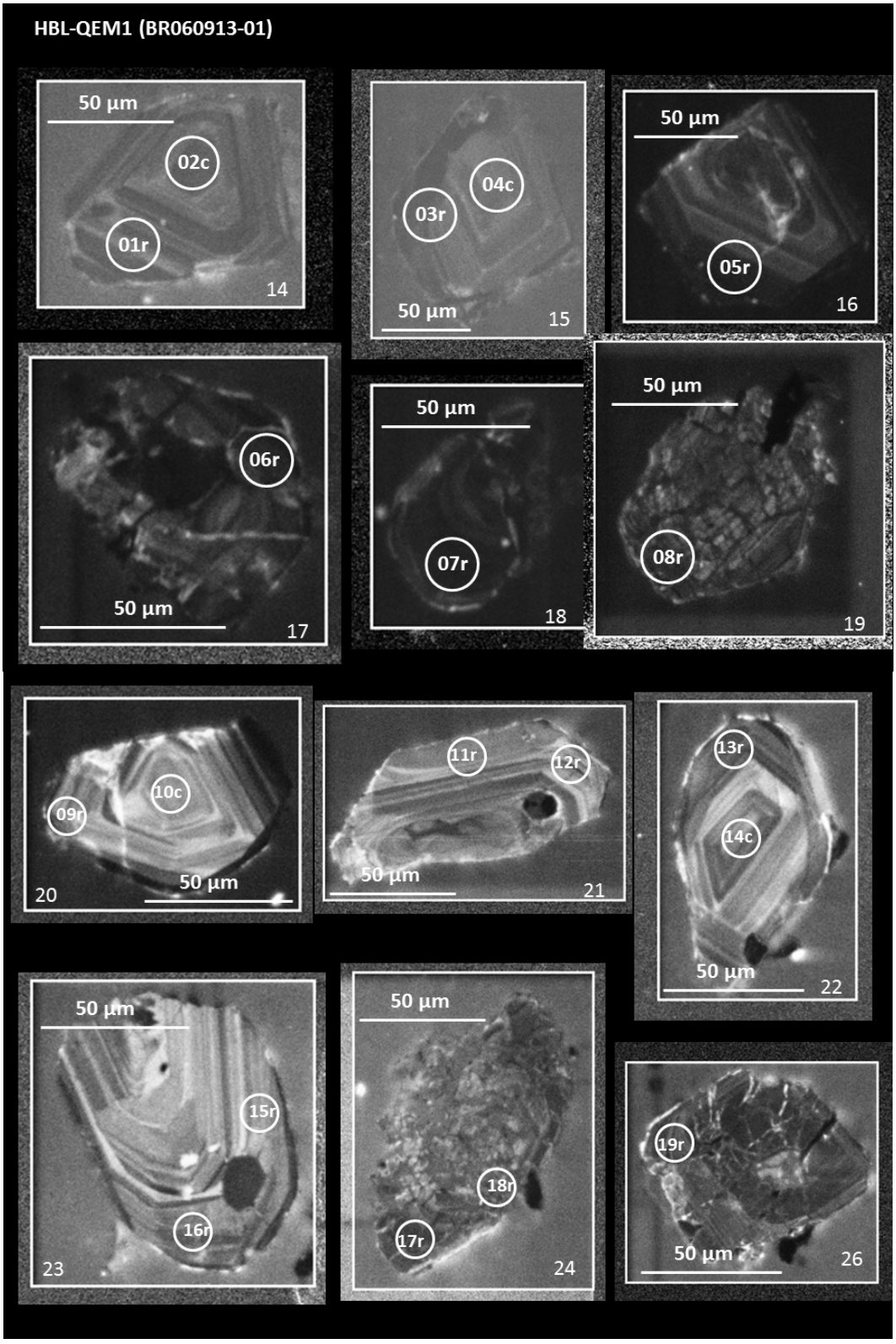

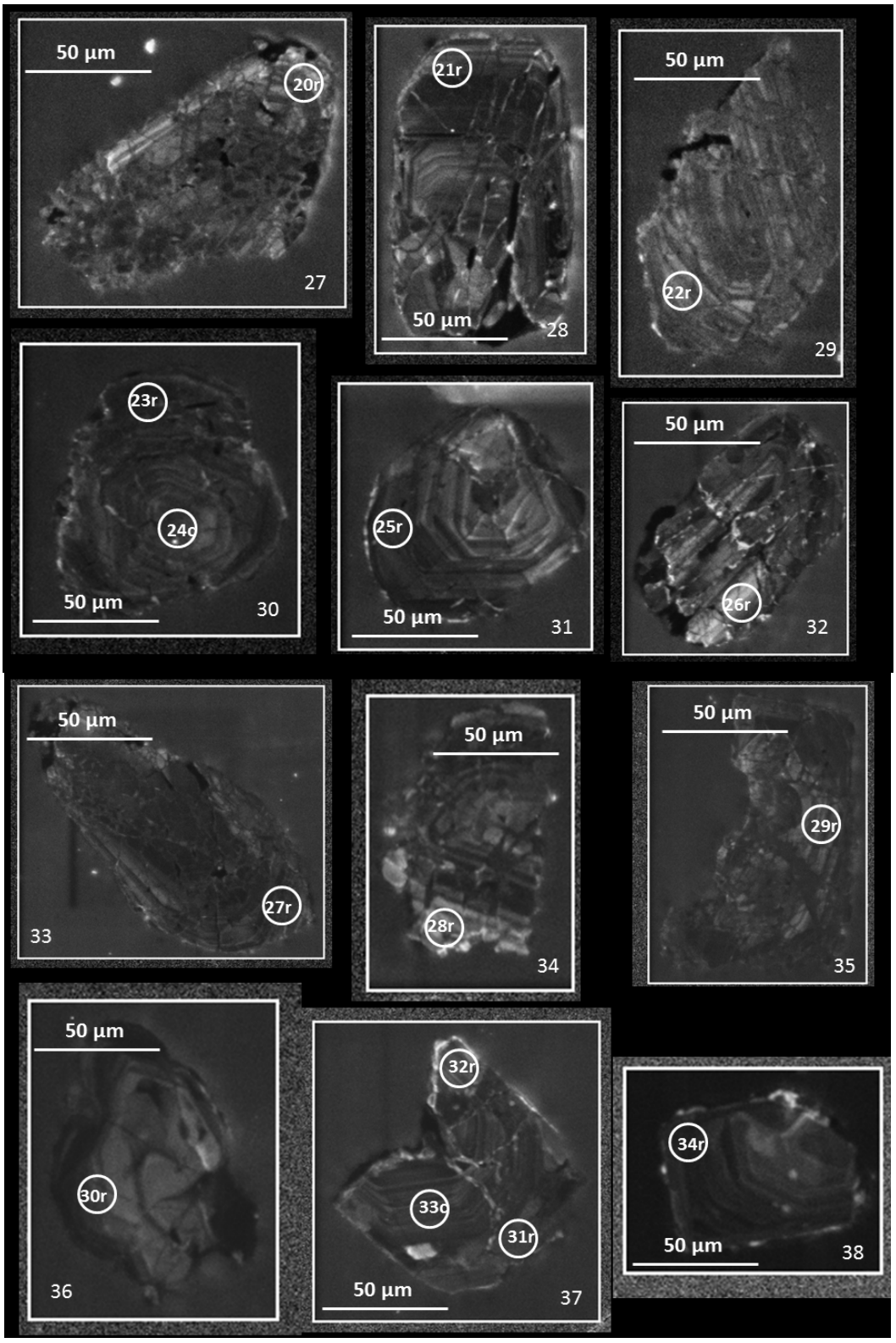
50 µm
20r
27
21r
50 µm
28
50 µm
22r
29
23r
24c
50 µm
30
25r
50 µm
31
50 µm
26r
32
50 µm
27r
33
50 µm
28r
34
50 µm
29r
35
50 µm
30r
36
32r
33c
31r
50 µm
37
34r
50 µm
38

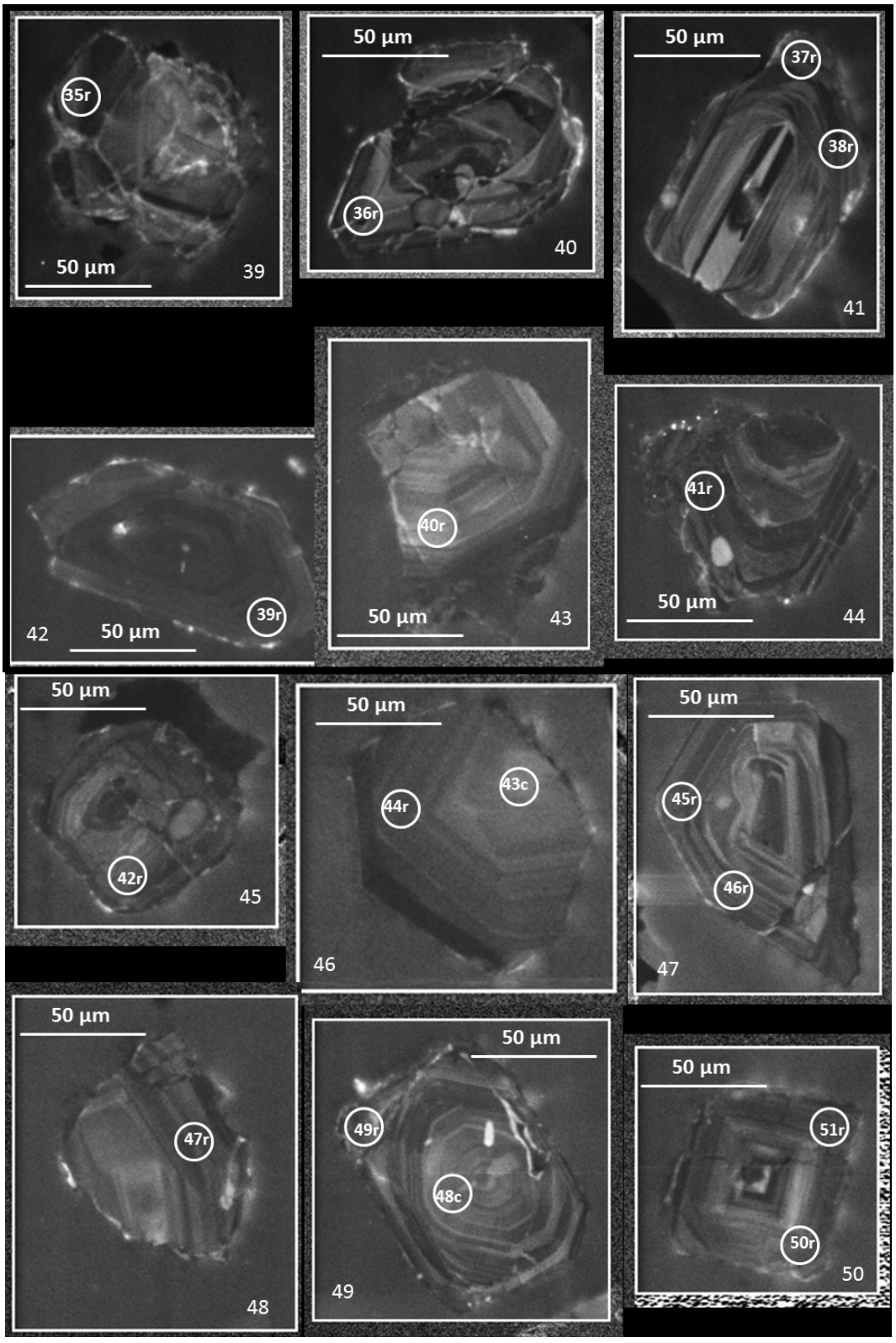
35r
50 µm
39
50 µm
36r
40
50 µm
37r
38r
41
40r
50 µm
43
39r
42
50 µm
41r
50 µm
44
50 µm
42r
45
50 µm
44r
43c
46
50 µm
45r
46r
47
50 µm
47r
48
50 µm
49r
48c
49
50 µm
51r
50r
50

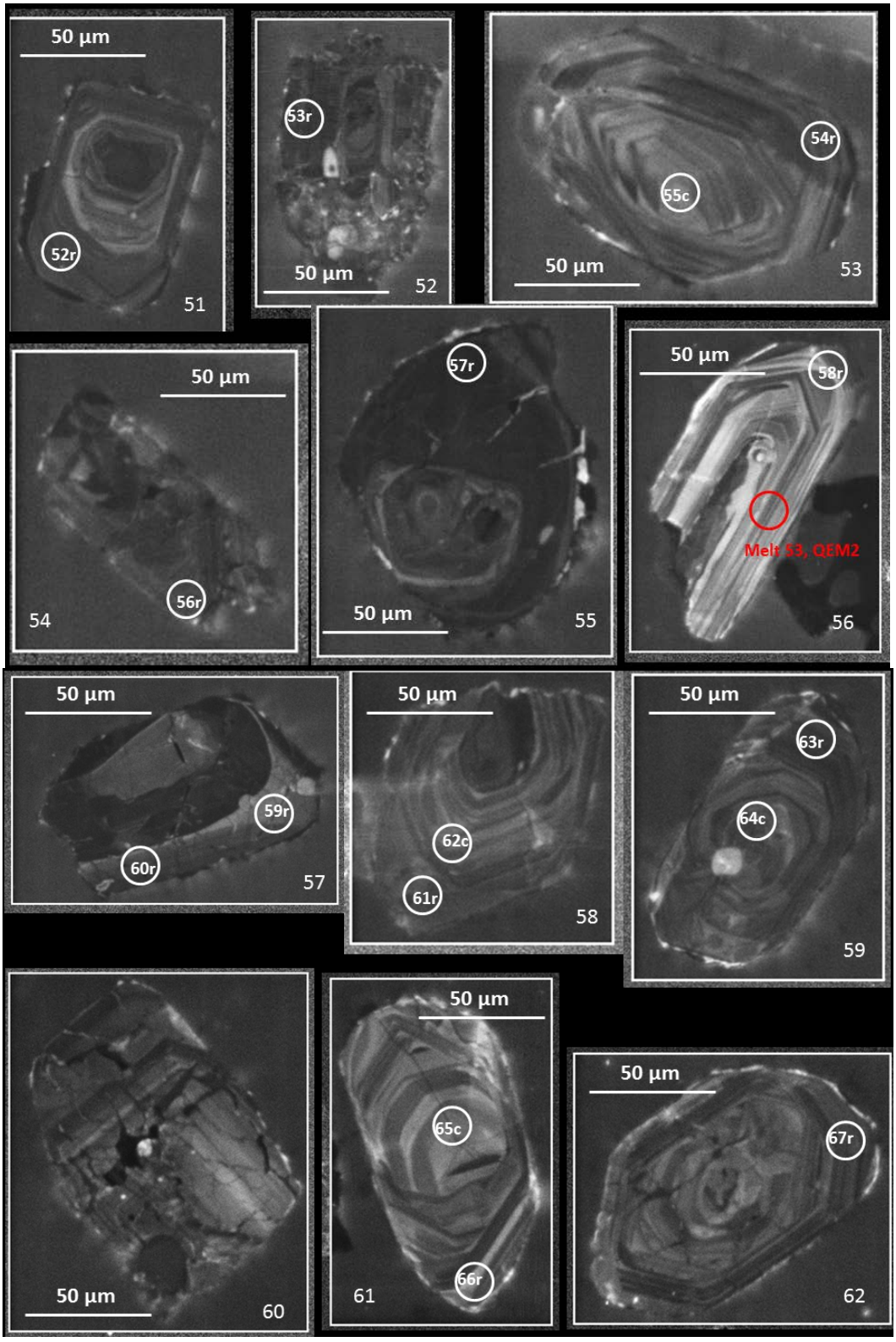
50 µm
52r
51
53r
50 µm
52
54r
55c
50 µm
53
50 µm
56r
54
57r
50 µm
55
50 µm
58r
Melt 53, QEM2
56
50 µm
59r
60r
57
50 µm
62c
61r
58
50 µm
63r
64c
59
50 µm
60
50 µm
65c
66r
61
50 µm
67r
62

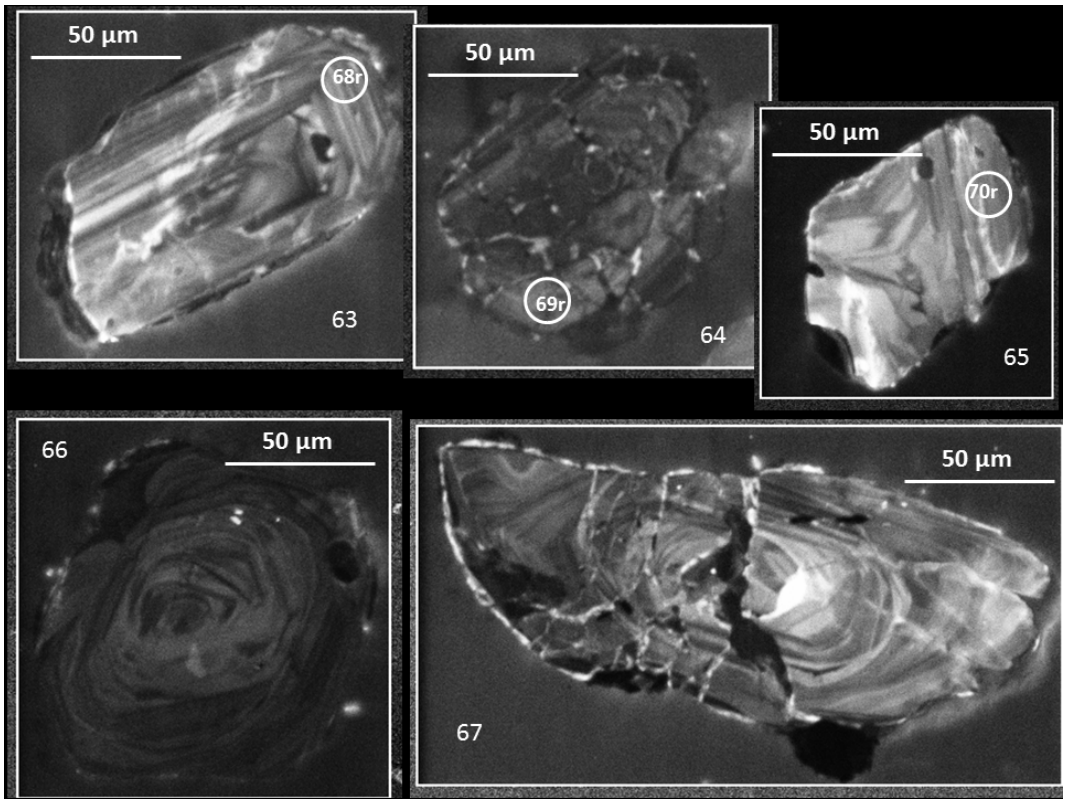
50 µm
68r
63
50 µm
69r
64
50 µm
70r
65
66
50 µm
50 µm
67

C-10. HBL-GM1 (BR060913-01)

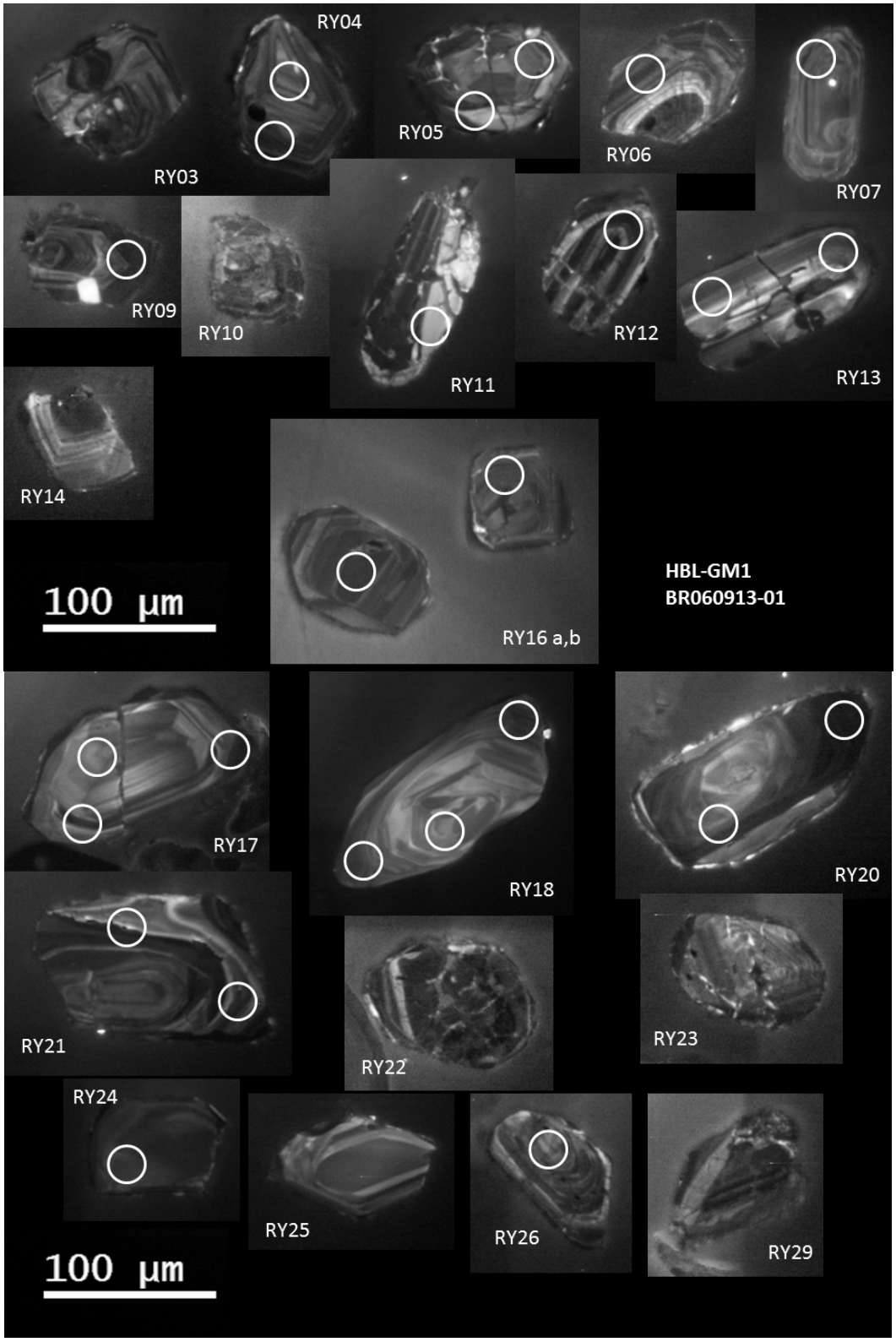

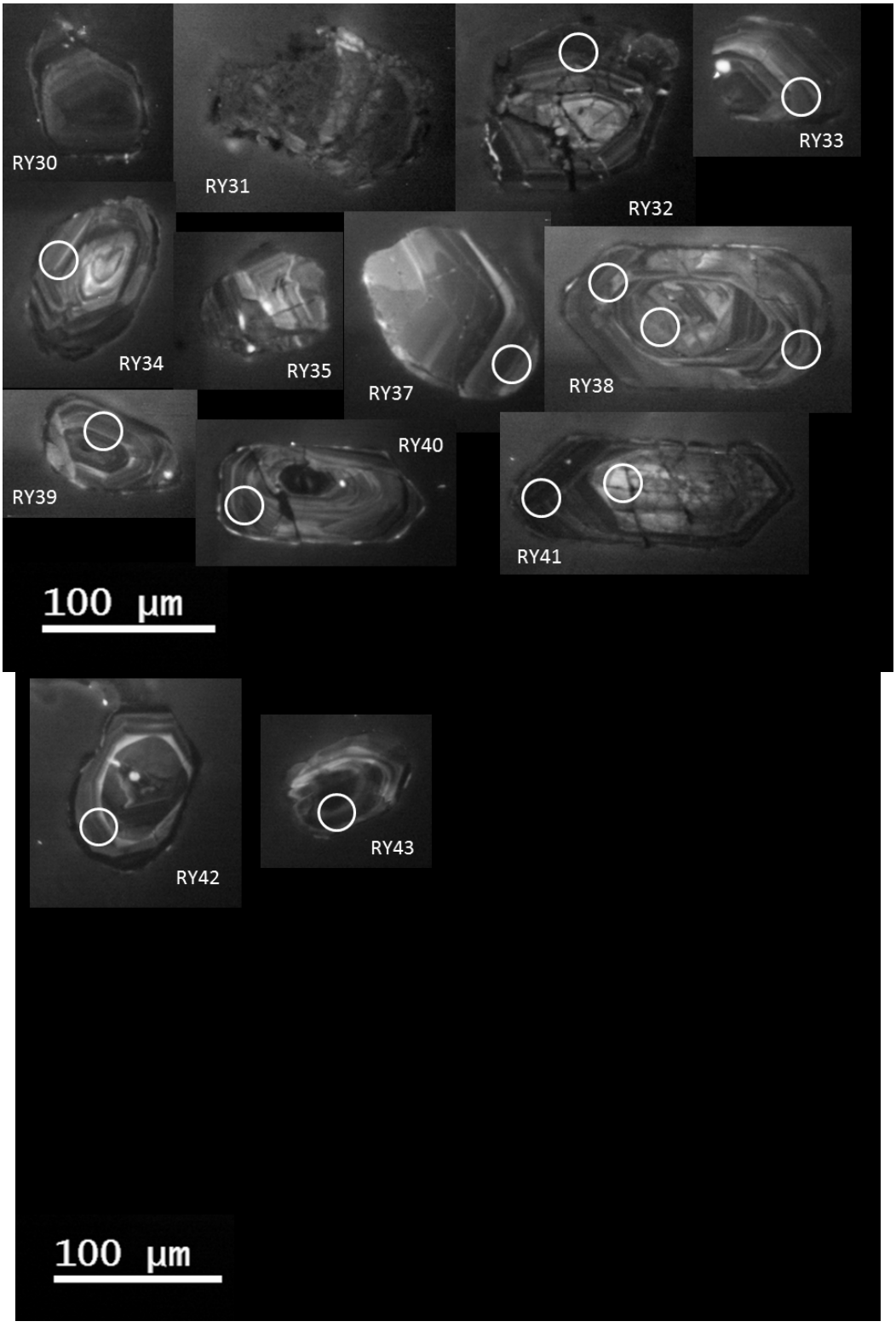
RY30
RY31
RY32
RY33
RY34
RY35
RY37
RY38
RY39
RY40
RY41
100 µm
RY42
RY43
100 µm

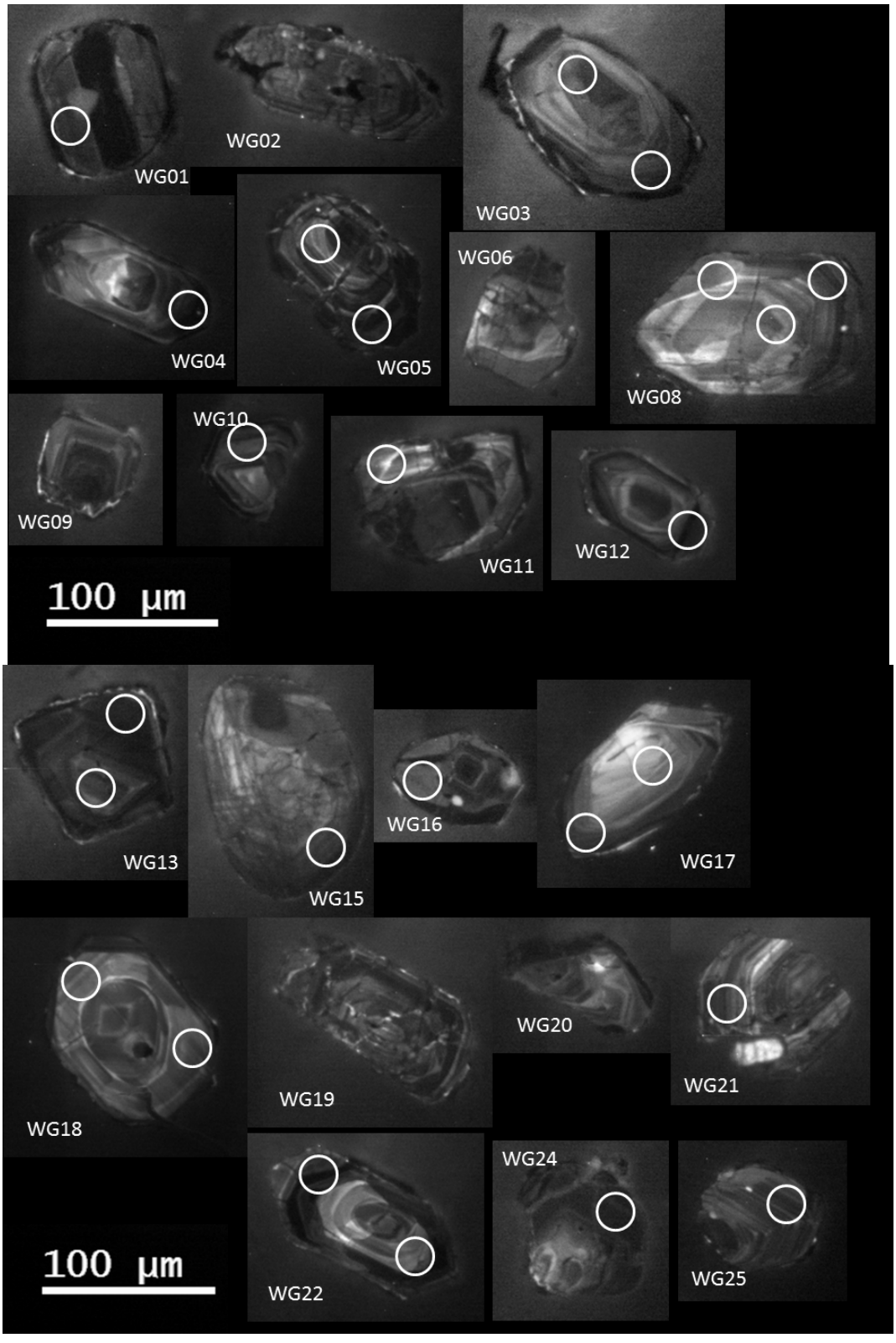
WG01
WG02
WG03
WG04
WG05
WG06
WG08
WG09
WG10
WG11
WG12
100 µm
WG13
WG15
WG16
WG17
WG18
WG19
WG20
WG21
WG22
WG24
WG25
100 µm

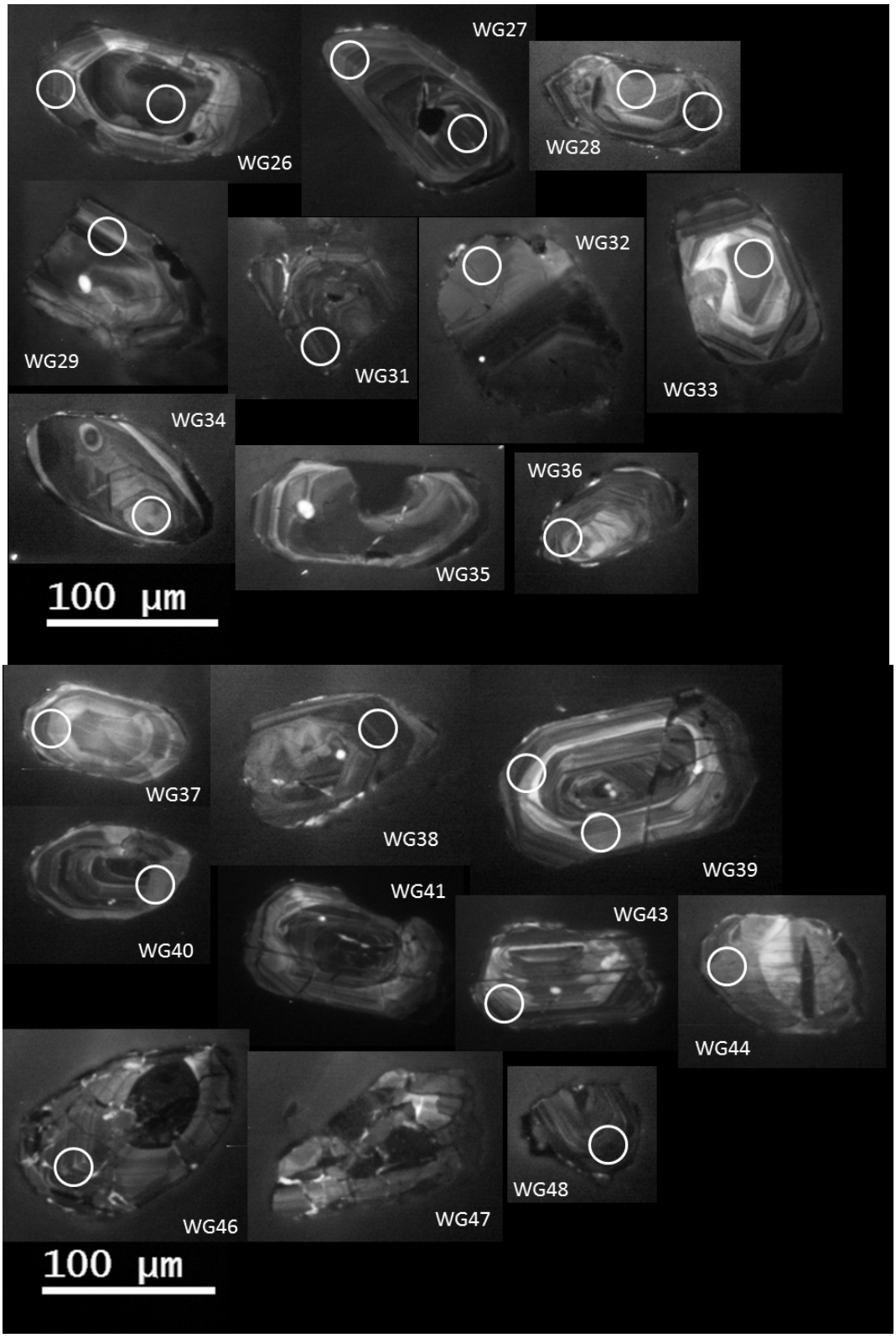
WG26
WG27
WG28
WG29
WG31
WG32
WG33
WG34
WG35
WG36
100 µm
WG37
WG38
WG39
WG40
WG41
WG43
WG44
WG46
WG47
WG48
100 µm

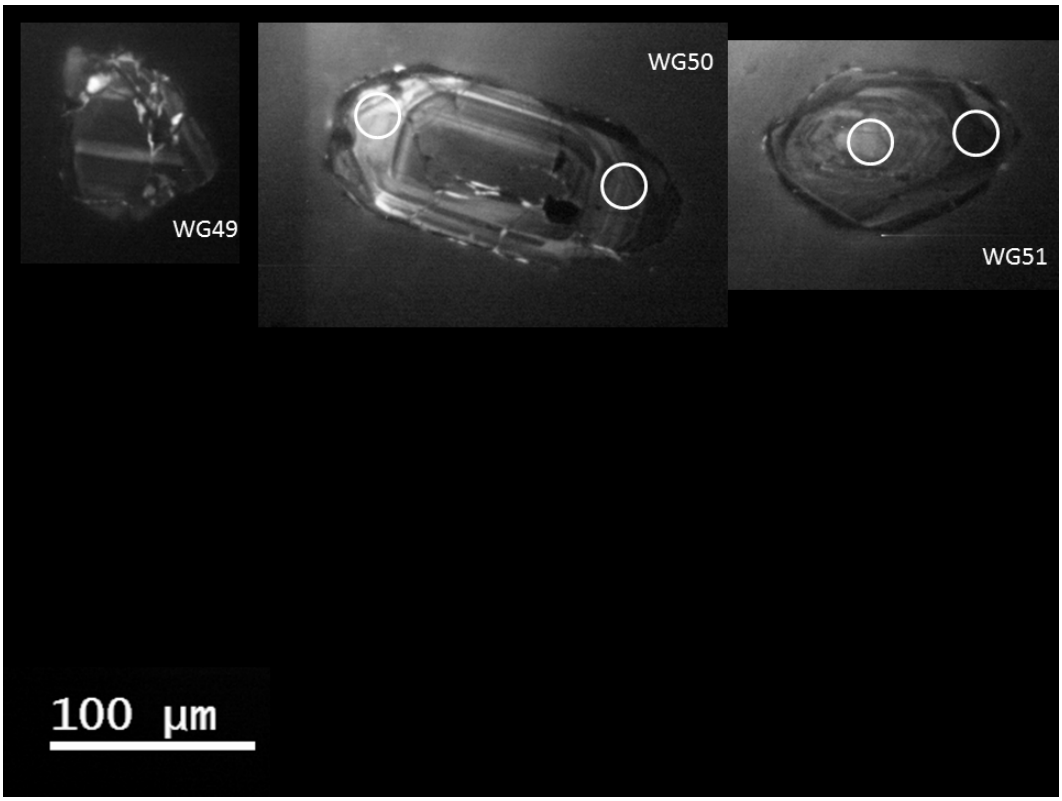
WG49
WG50
WG51
100 µm

C-11. HBL-GM2 (BR072815-01)

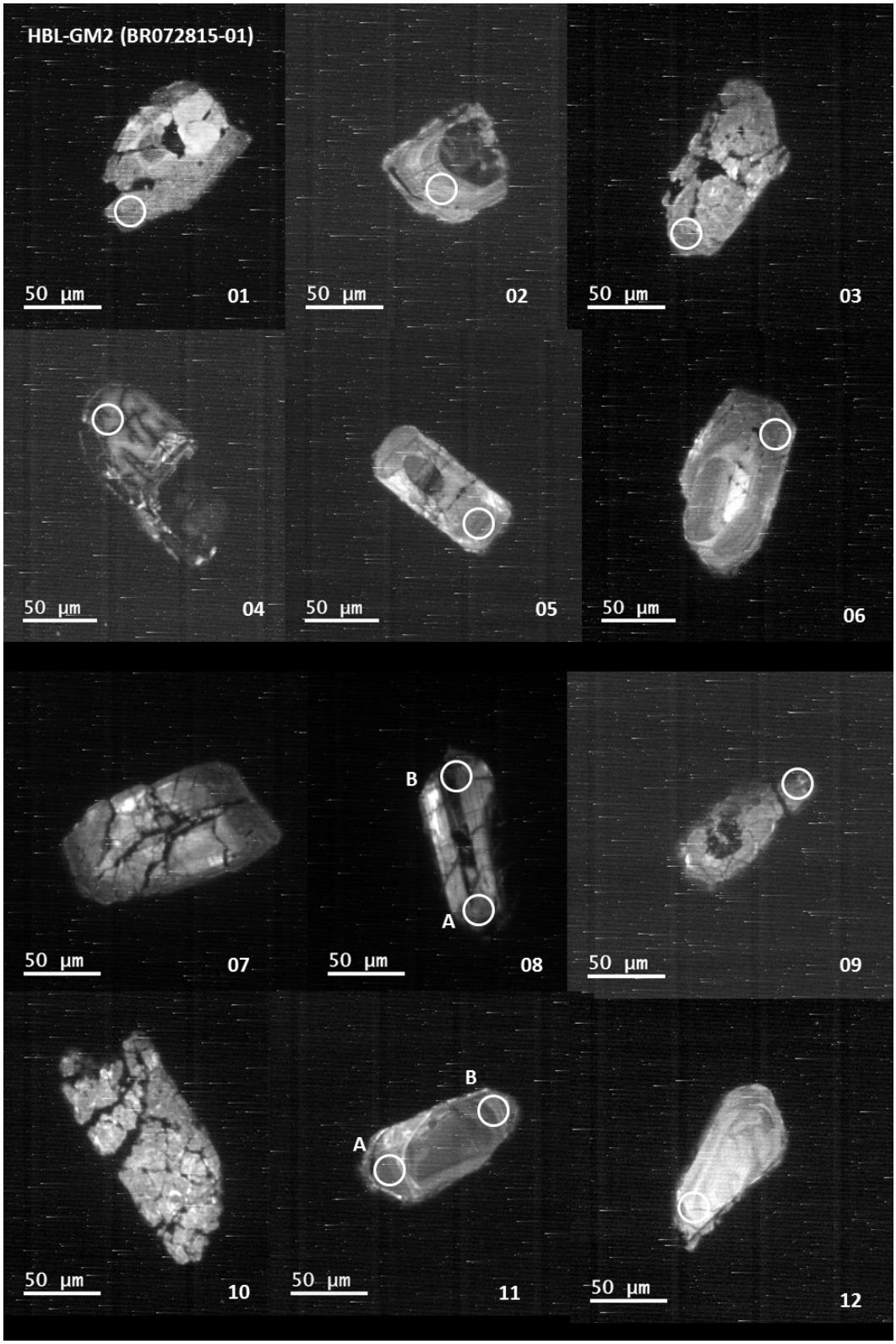

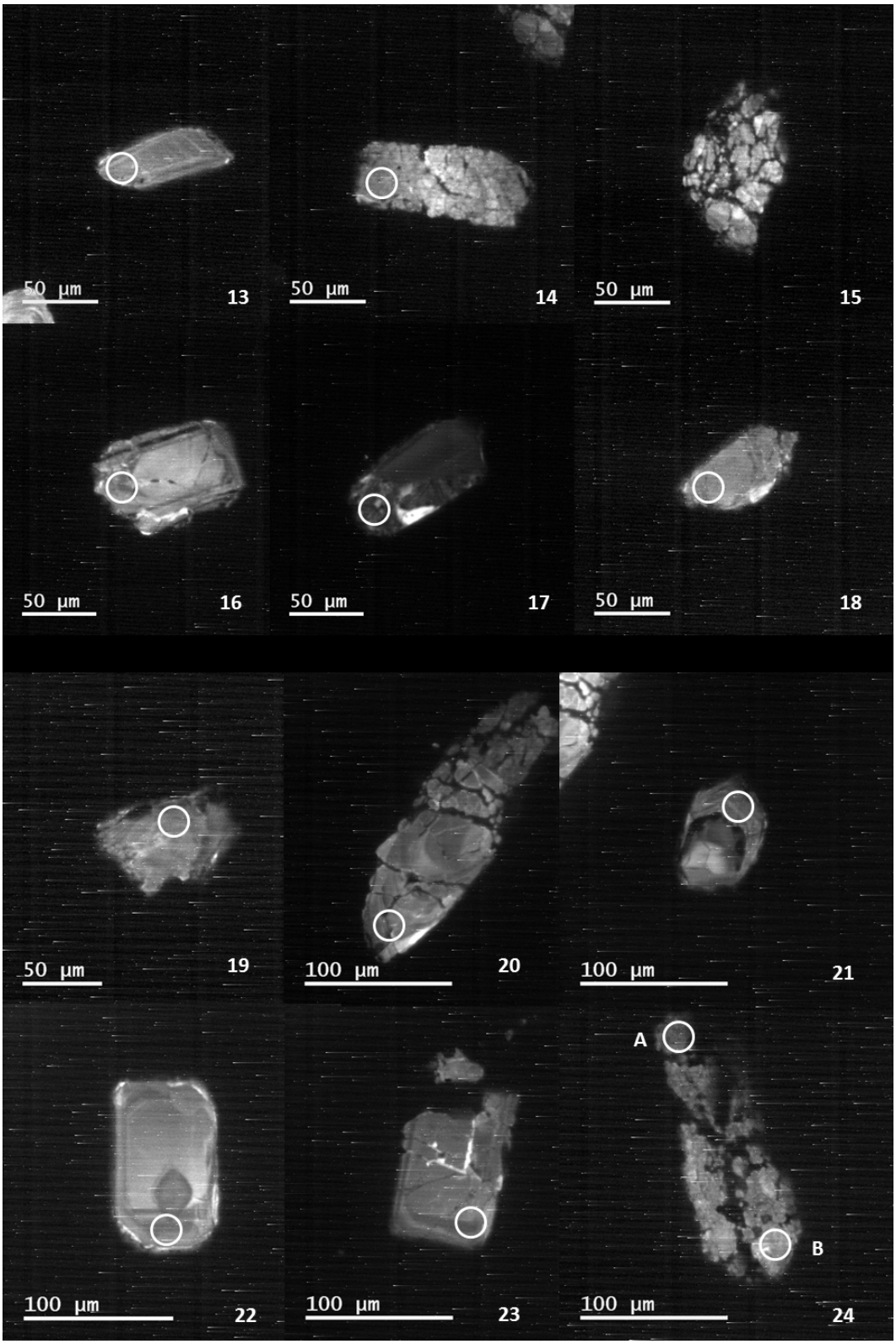
50 µm
13
50 µm
14
50 µm
15
50 µm
16
50 µm
17
50 µm
18
50 µm
19
100 µm
20
100 µm
21
100 µm
22
100 µm
23
A
B
100 µm
24

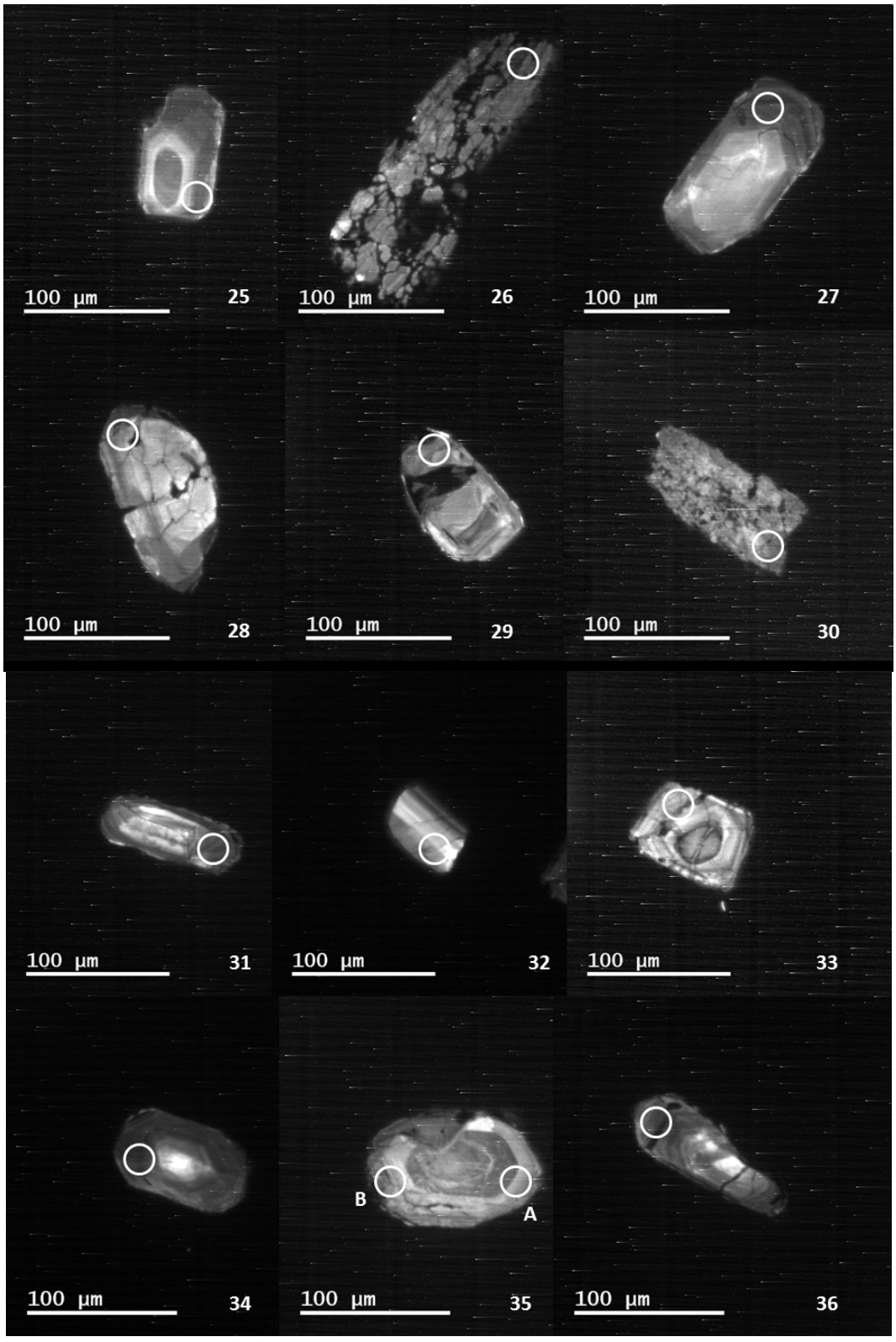
100 µm
25
100 µm
26
100 µm
27
100 µm
28
100 µm
29
100 µm
30
100 µm
31
100 µm
32
100 µm
33
100 µm
34
B
A
100 µm
35
100 µm
36

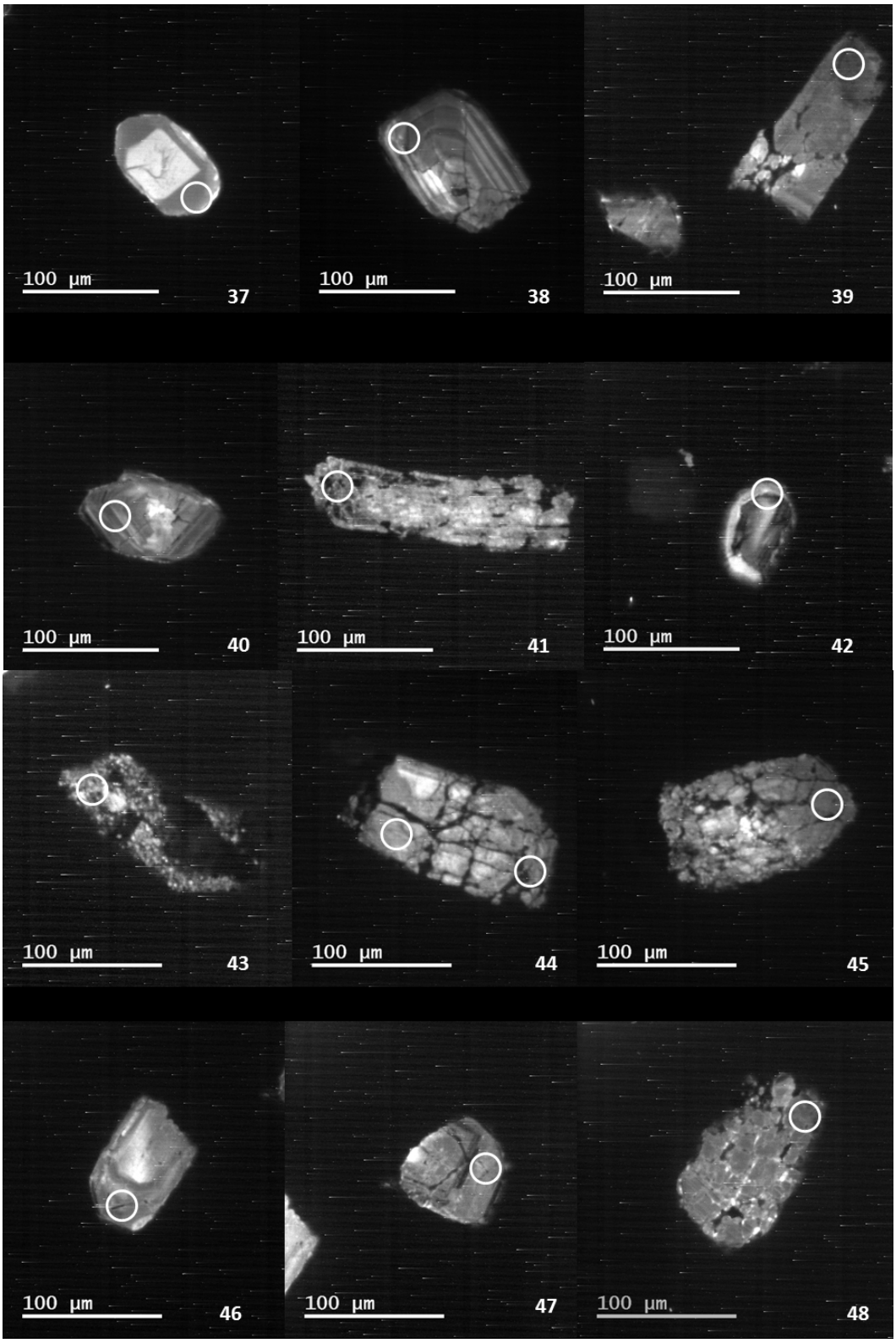
100 µm
37
100 µm
38
100 µm
39
100 µm
40
100 µm
41
100 µm
42
100 µm
43
100 µm
44
100 µm
45
100 µm
46
100 µm
47
100 µm
48

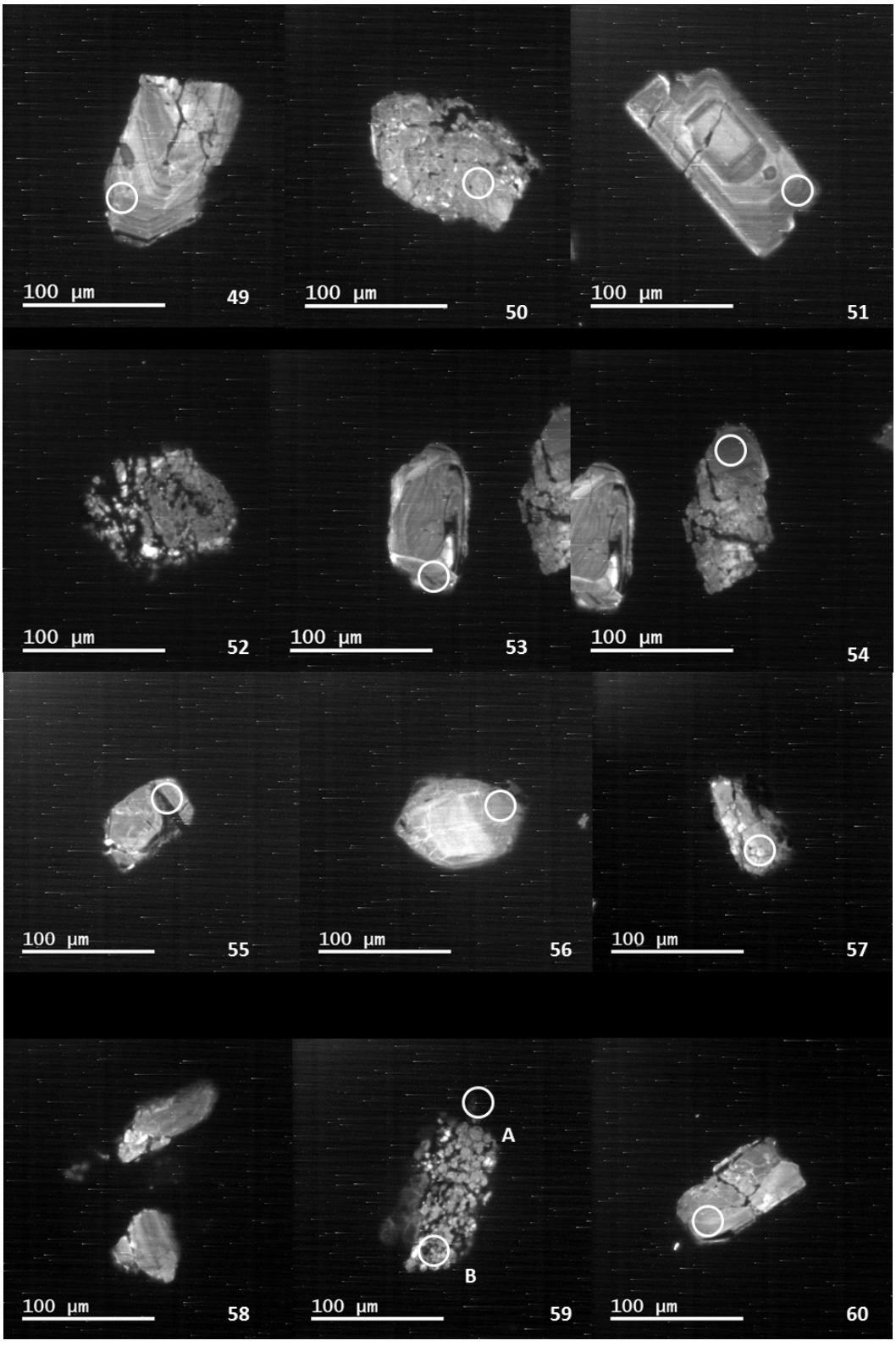
100 µm
49
100 µm
50
100 µm
51
100 µm
52
100 µm
53
100 µm
54
100 µm
55
100 µm
56
100 µm
57
A
B
100 µm
58
100 µm
59
100 µm
60

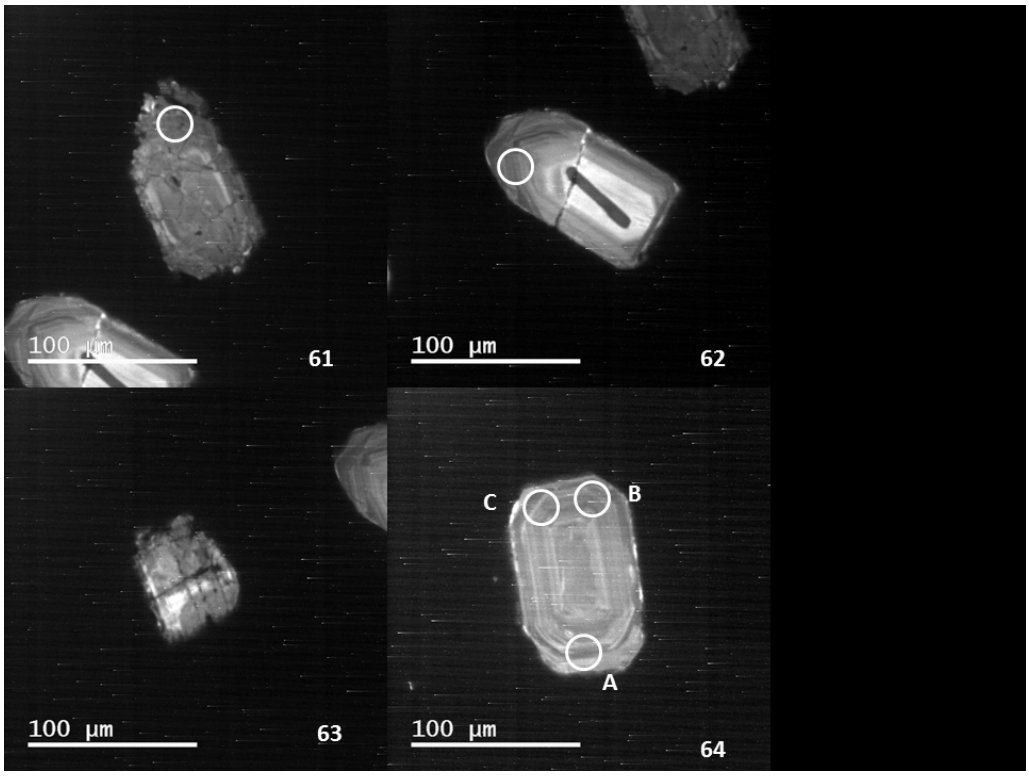
100 µm
61
100 µm
62
100 µm
63
C
B
A
100 µm
64

C-12. NFG13-GM1 & GM2 (BR061613-03)

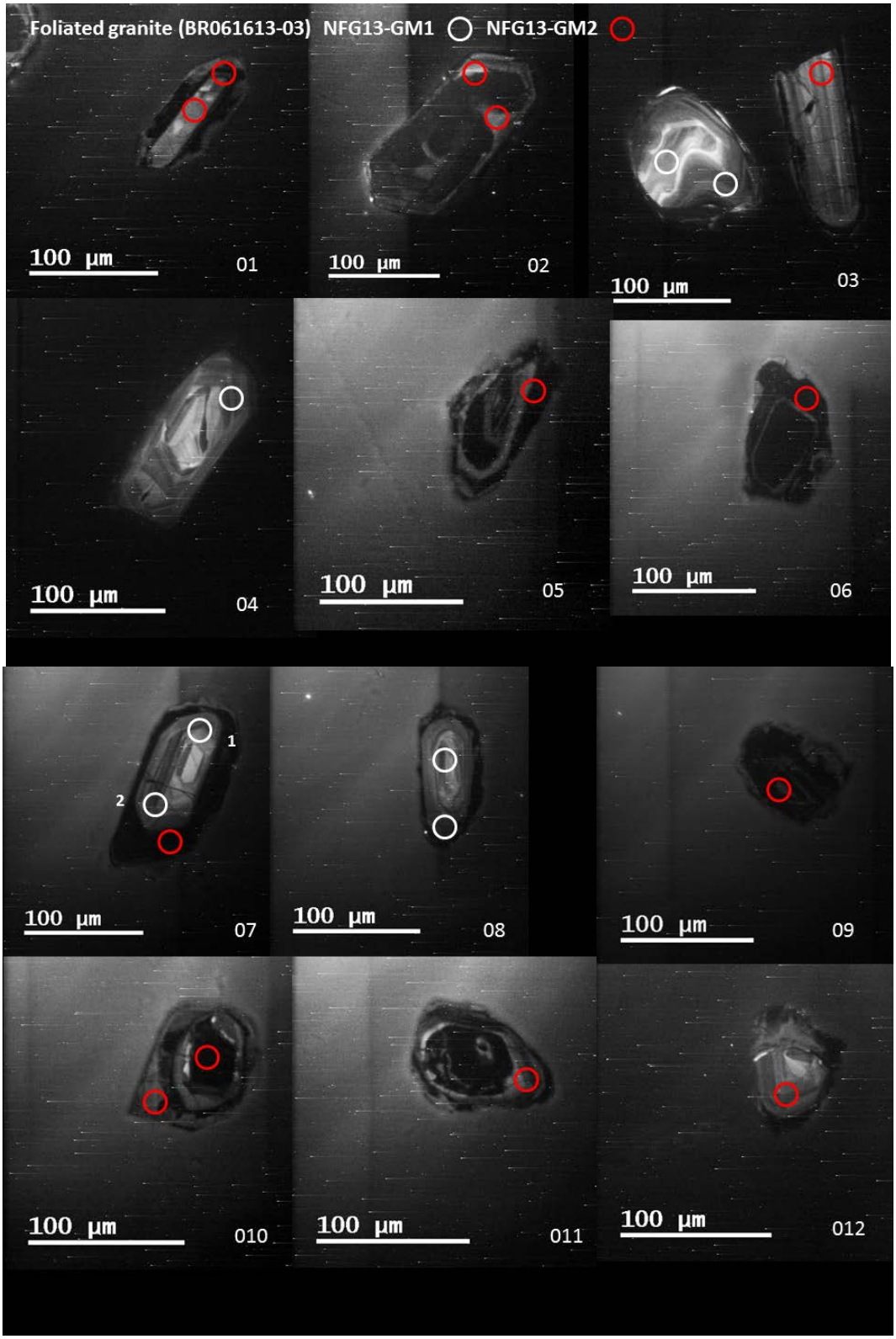

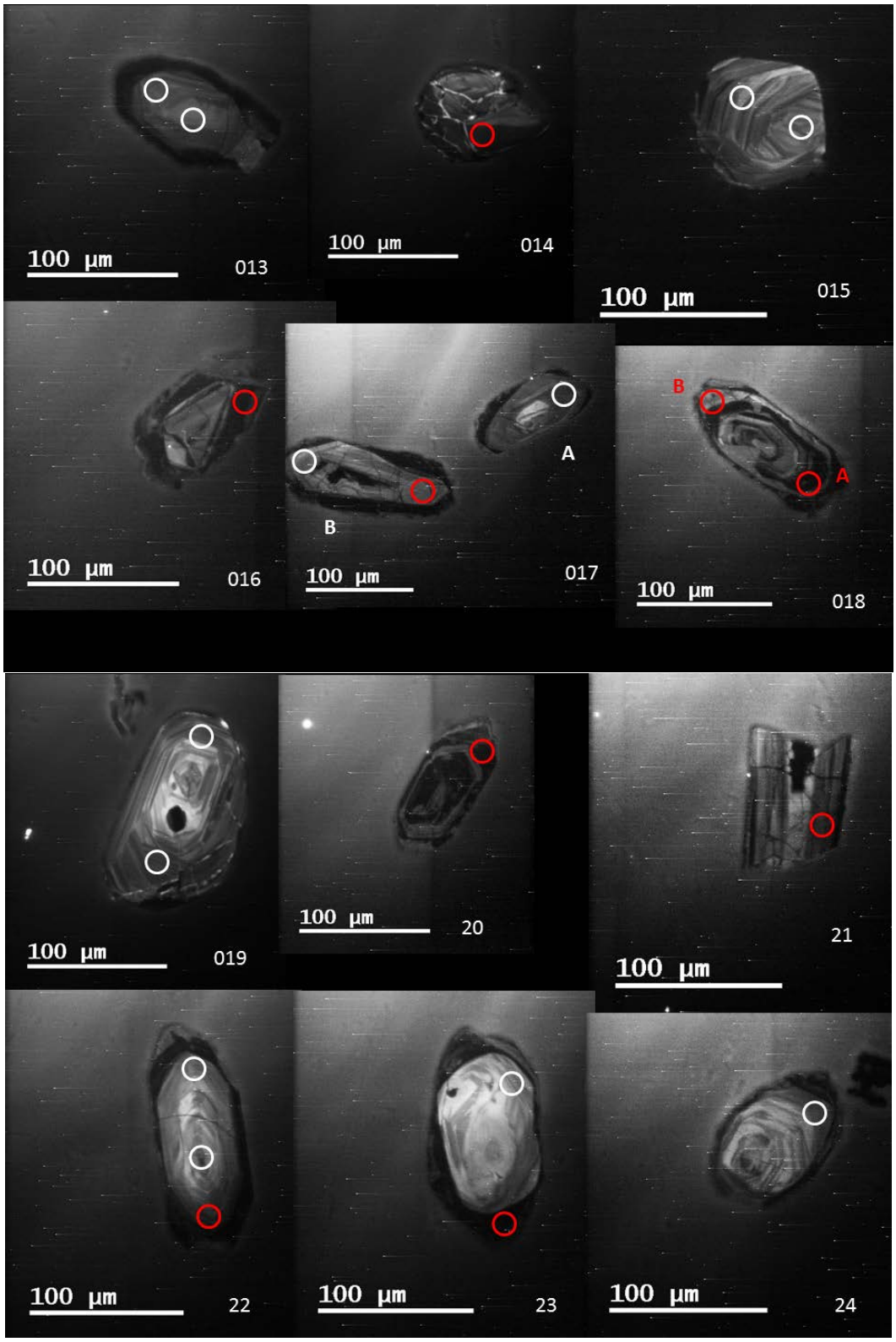
100 µm
013
100 µm
014
100 µm
015
100 µm
016
A
B
100 µm
017
B
A
100 µm
018
100 µm
019
100 µm
20
21
100 µm
100 µm
22
100 µm
23
100 µm
24

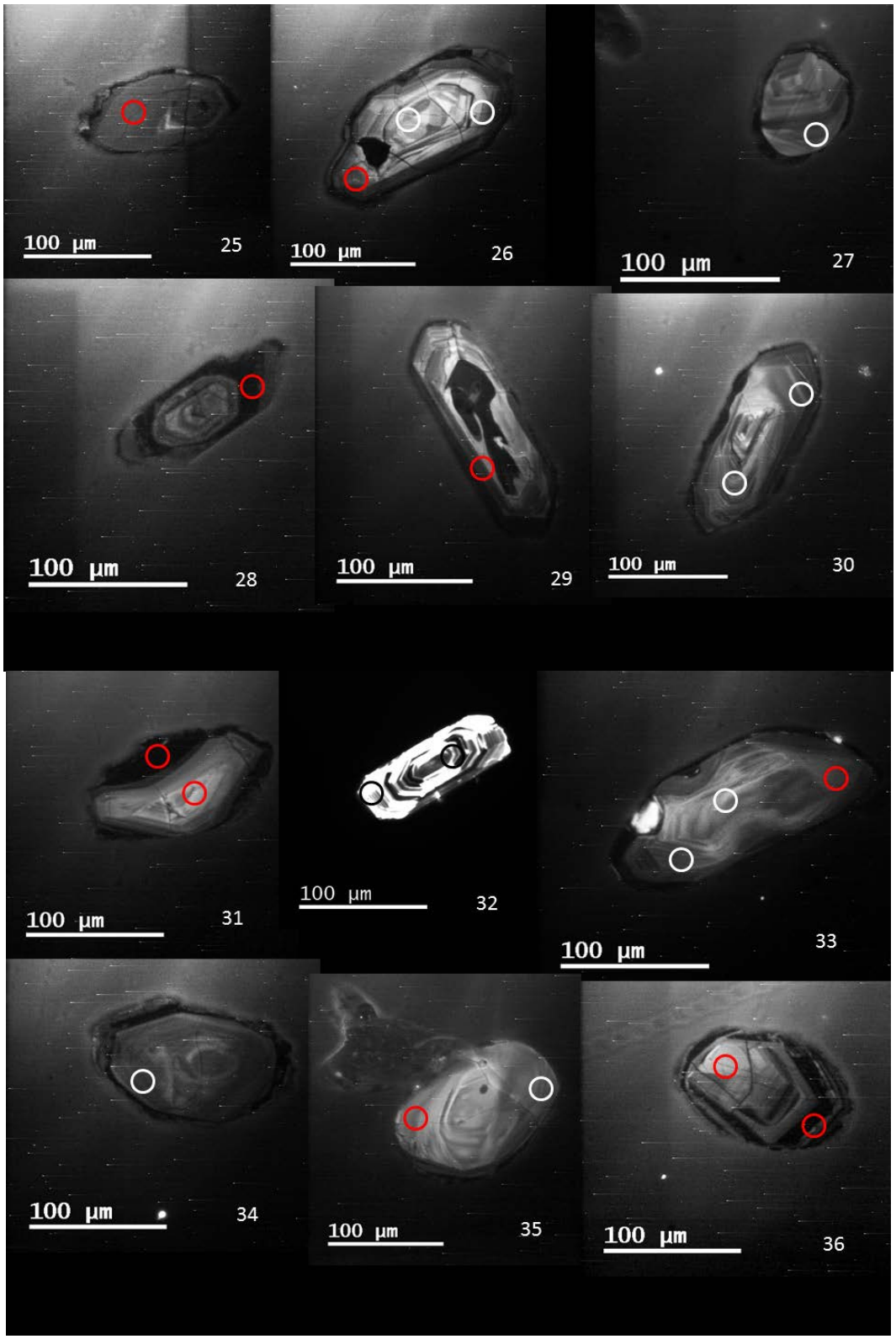
100 µm
25
100 µm
26
100 µm
27
100 µm
28
100 µm
29
100 µm
30
100 µm
31
100 µm
32
100 µm
33
100 µm
34
100 µm
35
100 µm
36

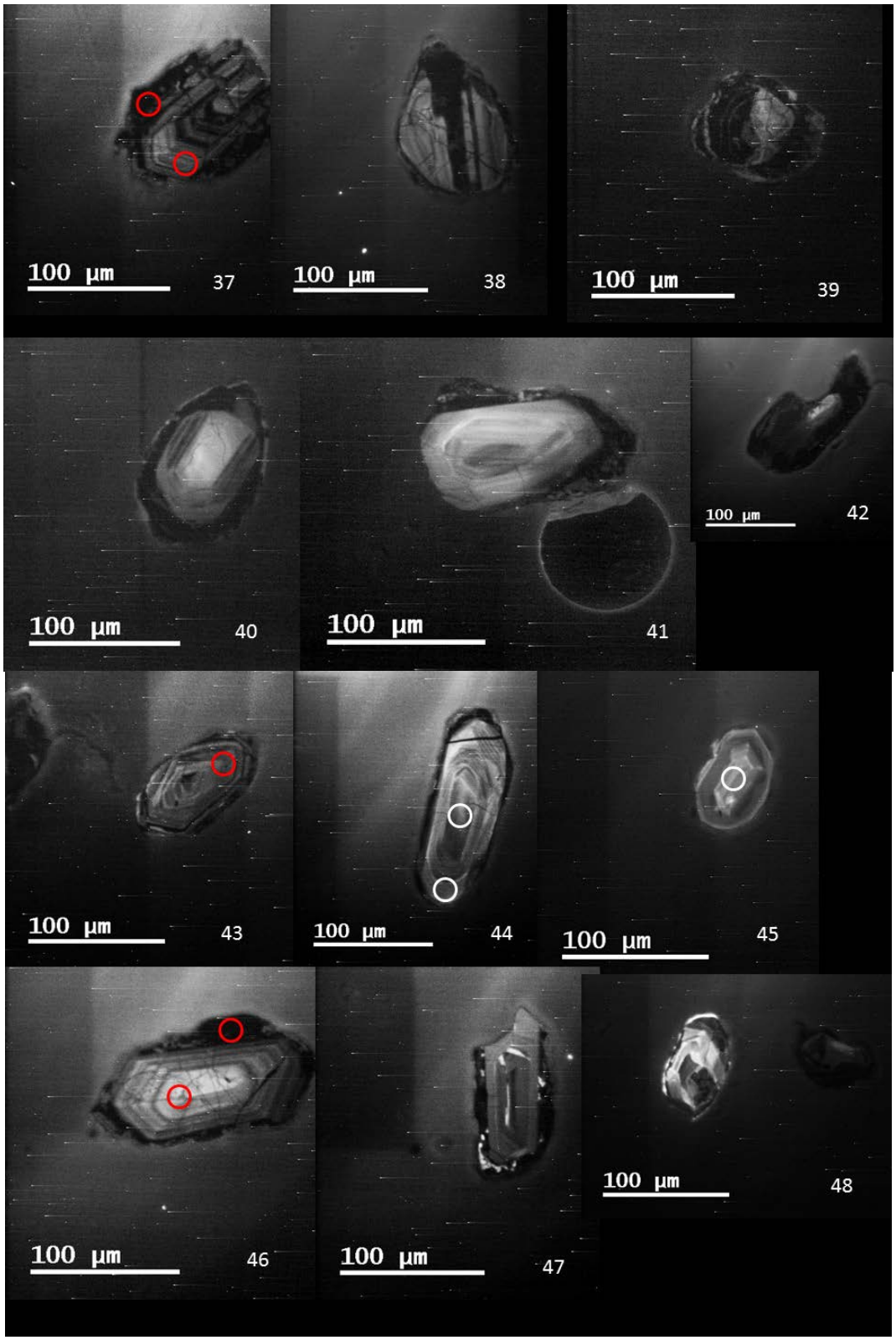
100 µm
37
100 µm
38
100 µm
39
100 µm
40
100 µm
41
100 µm
42
100 µm
43
100 µm
44
100 µm
45
100 µm
46
100 µm
47
100 µm
48

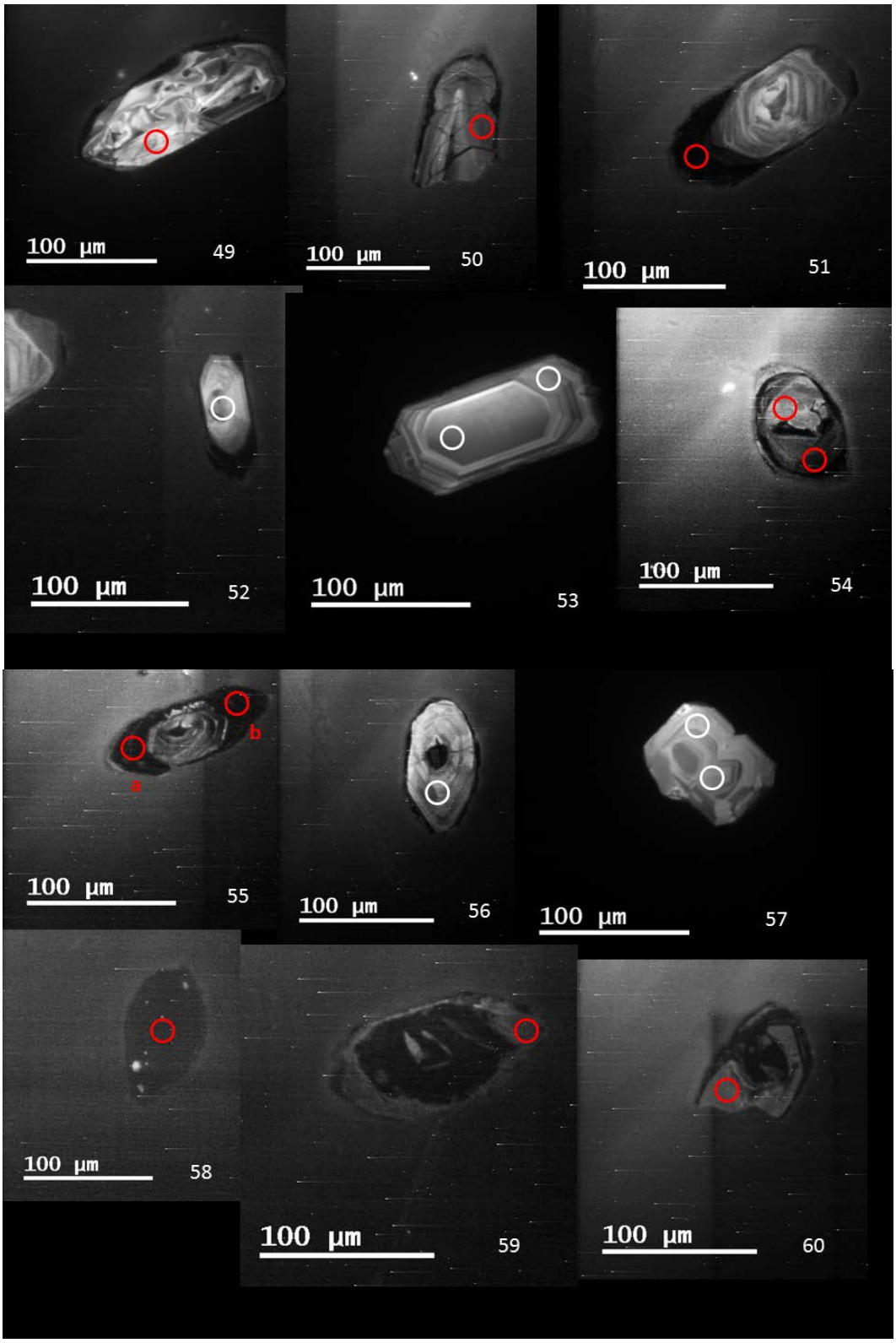
100 µm
49
100 µm
50
100 µm
51
100 µm
52
100 µm
53
100 µm
54
b
a
100 µm
55
100 µm
56
100 µm
57
100 µm
58
100 µm
59
100 µm
60

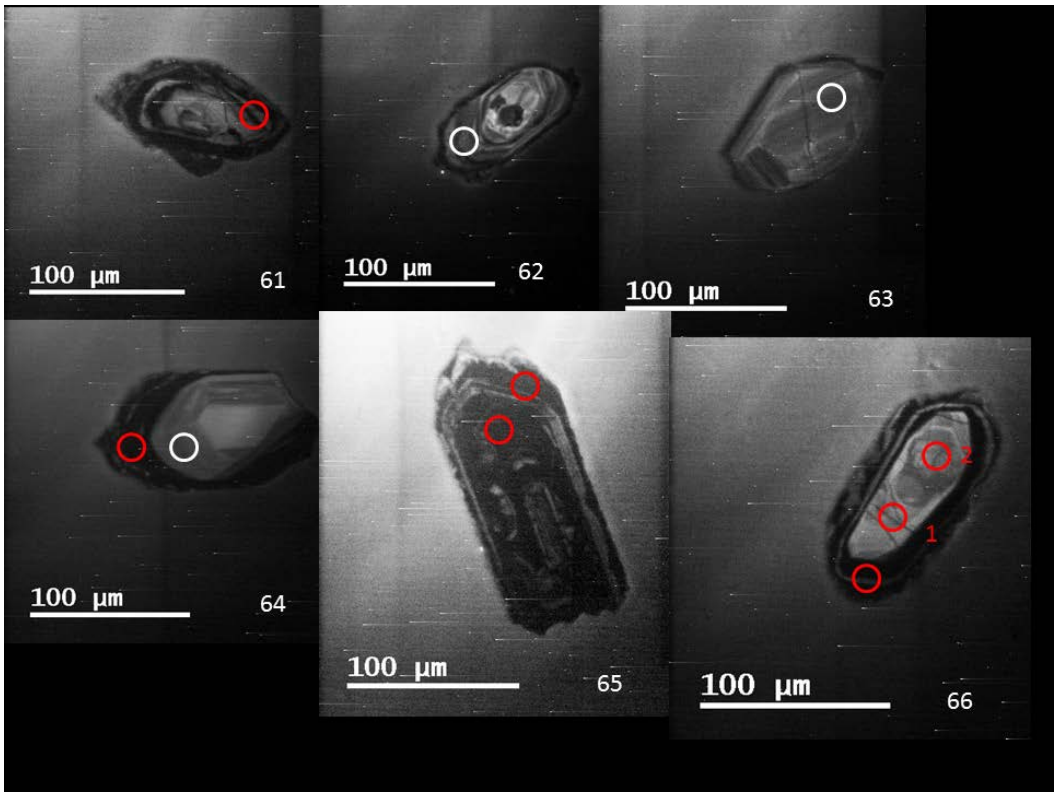
100 µm
61
100 µm
62
100 µm
63
100 µm
64
100 µm
65
2
1
100 µm
66

C-14. NFG15-GM1 (BR073015-01)

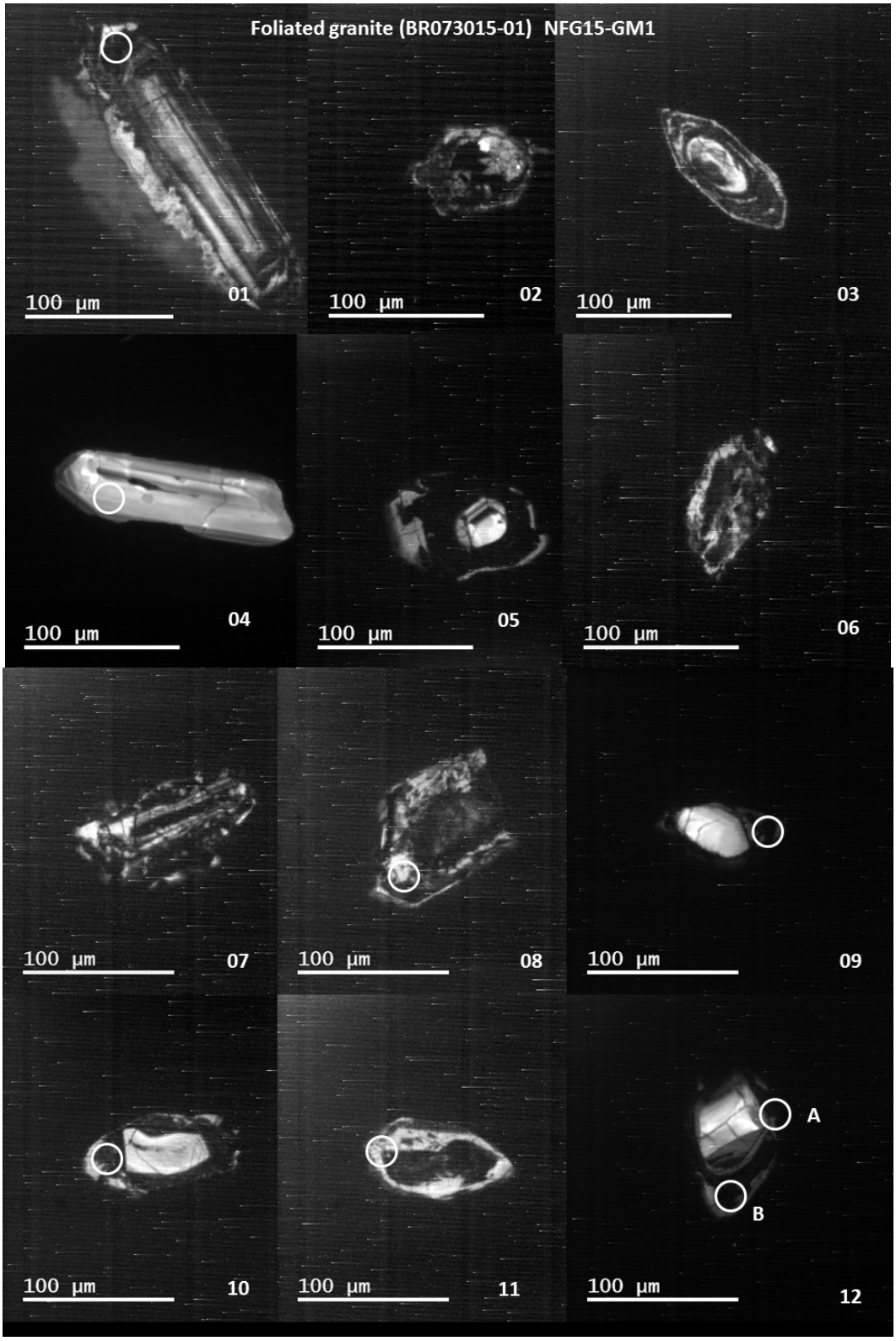

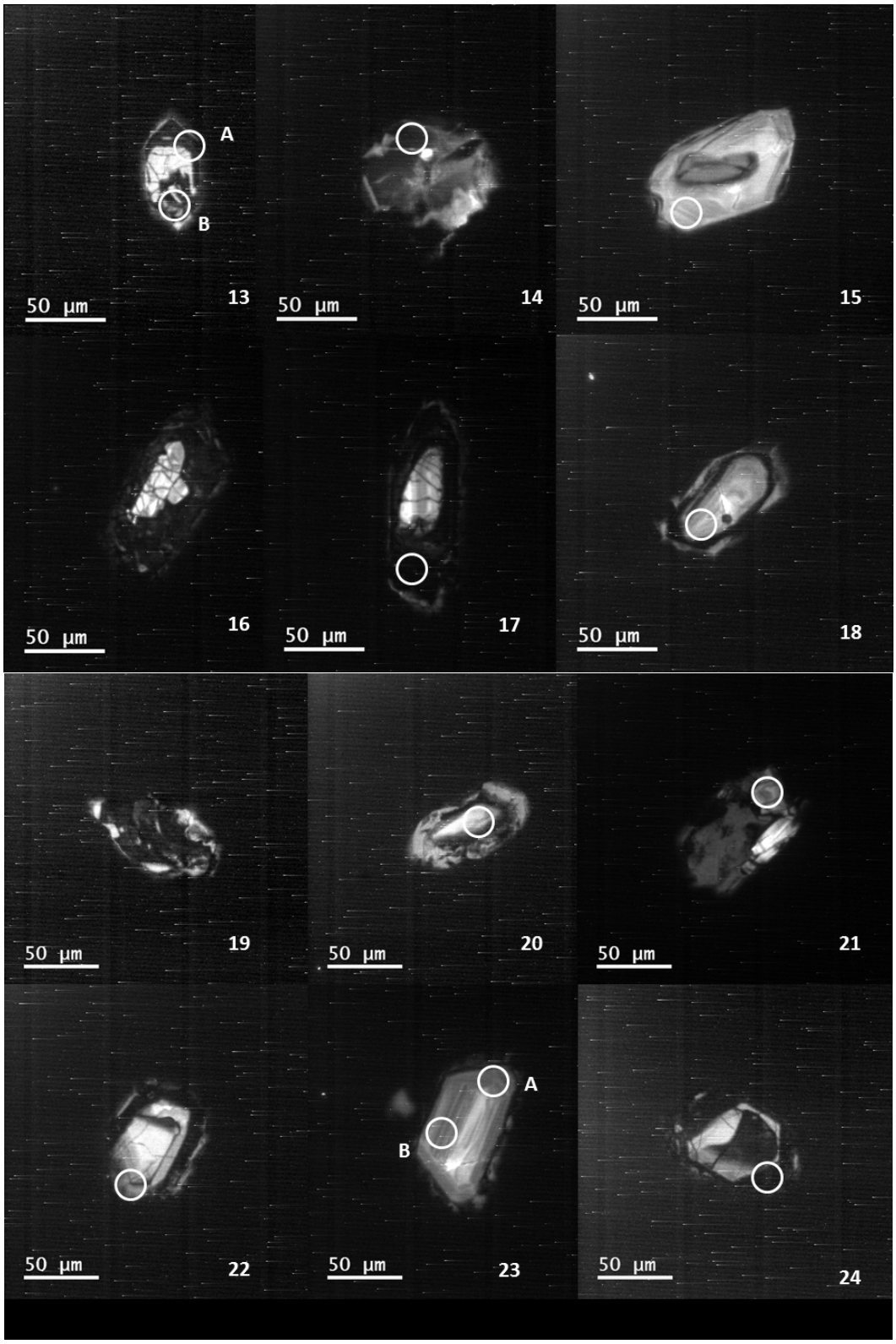
A
B
50 µm
13
50 µm
14
50 µm
15
50 µm
16
50 µm
17
50 µm
18
50 µm
19
50 µm
20
50 µm
21
50 µm
22
A
B
50 µm
23
50 µm
24

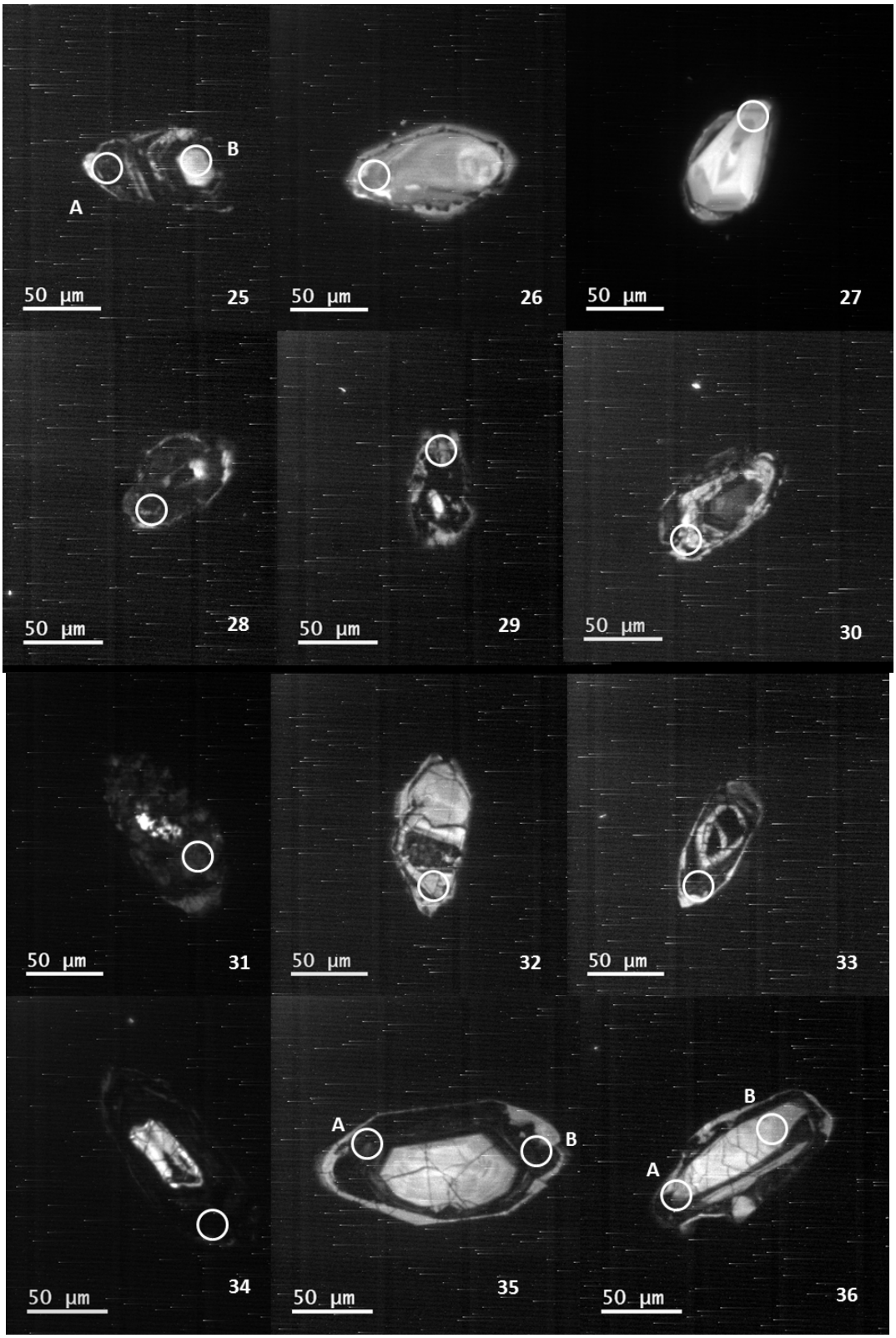
A
B
50 µm
25
50 µm
26
50 µm
27
50 µm
28
50 µm
29
50 µm
30
50 µm
31
50 µm
32
50 µm
33
50 µm
34
A
B
50 µm
35
B
A
50 µm
36

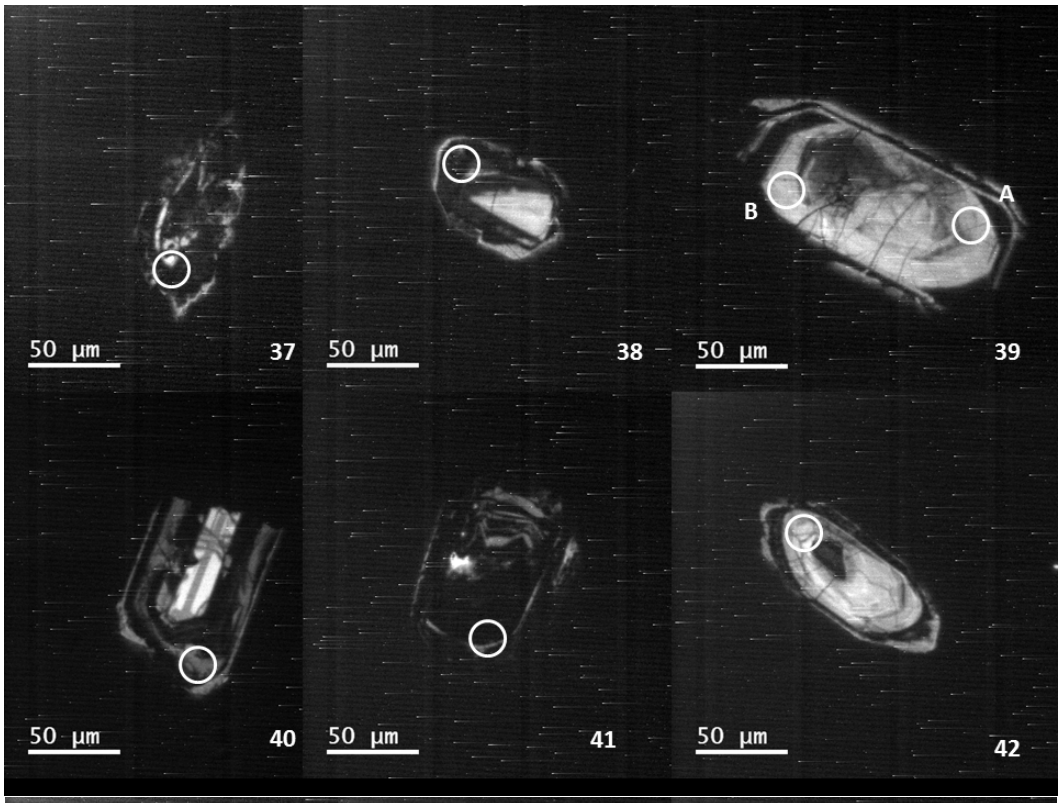
50 µm
37
50 µm
38
B
A
50 µm
39
50 µm
40
50 µm
41
50 µm
42

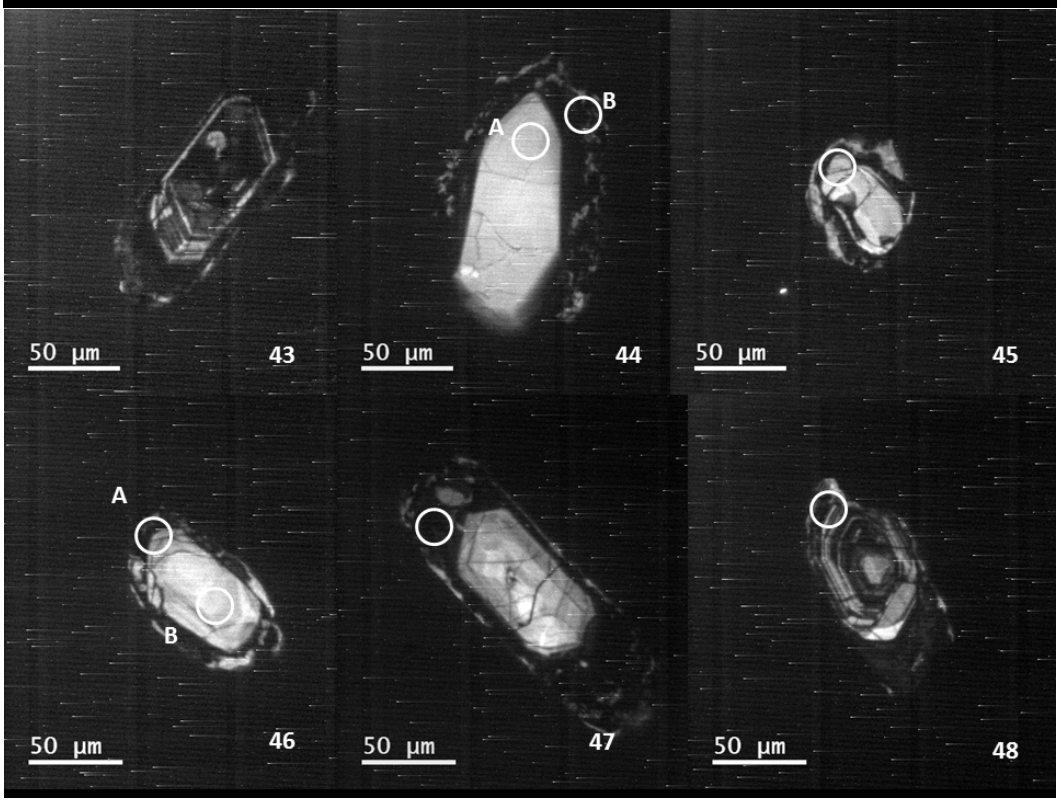
50 µm
43
A
B
50 µm
44
50 µm
45
A
B
50 µm
46
50 µm
47
50 µm
48

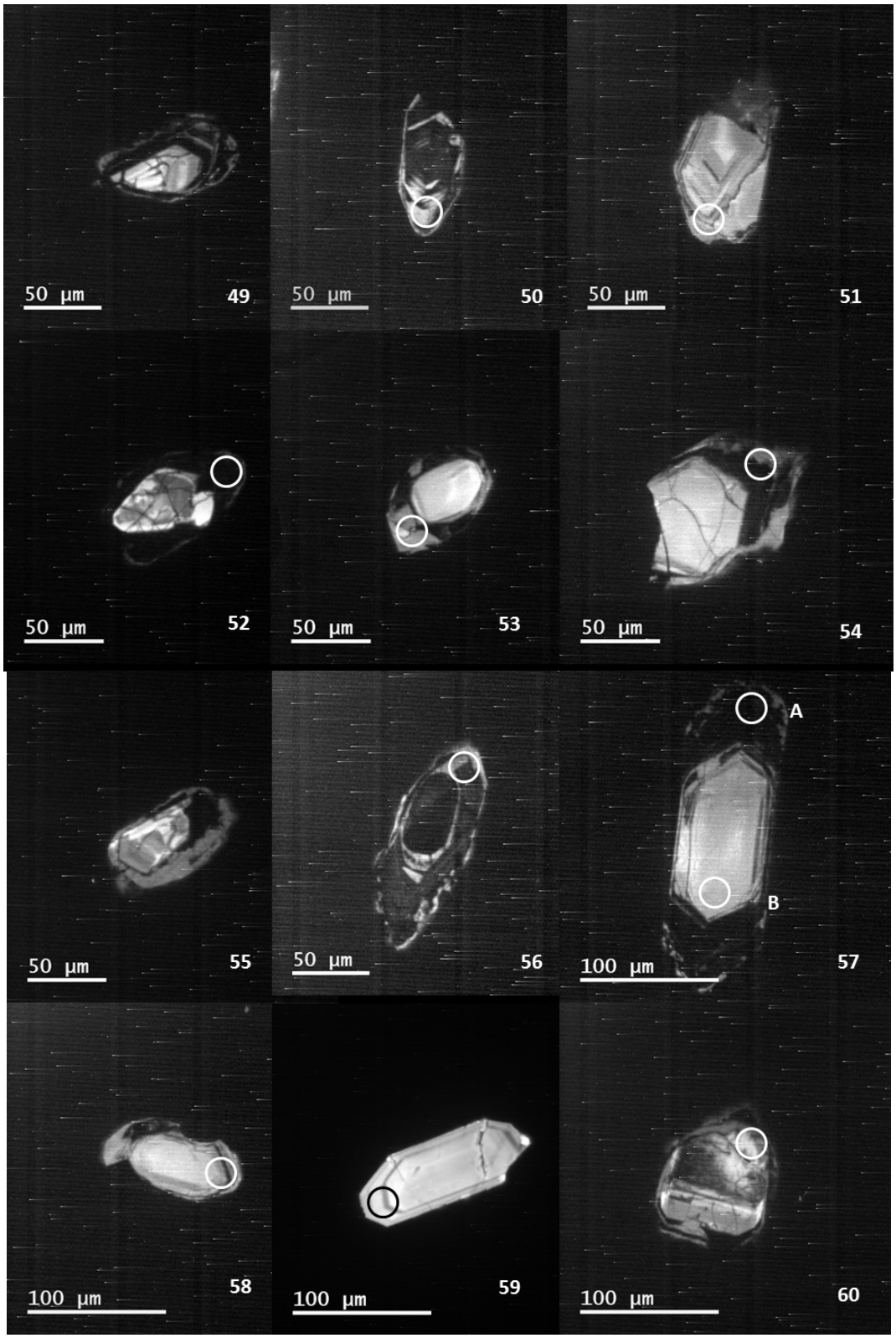
50 µm
49
50 µm
50
50 µm
51
50 µm
52
50 µm
53
50 µm
54
50 µm
55
50 µm
56
A
B
100 µm
57
100 µm
58
100 µm
59
100 µm
60

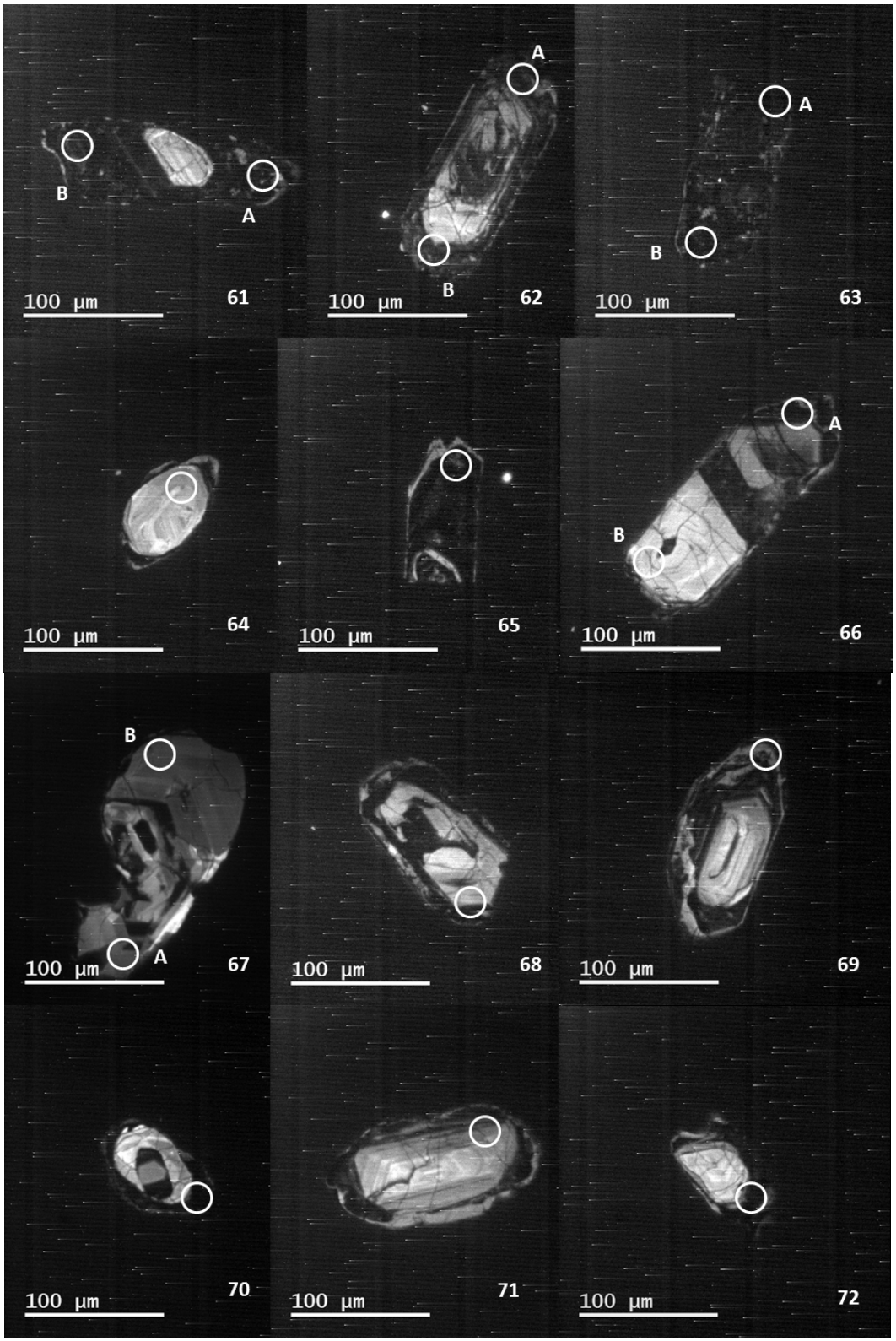
B
A
100 µm
61
A
B
100 µm
62
A
B
100 µm
63
100 µm
64
100 µm
65
A
B
100 µm
66
B
A
100 µm
67
100 µm
68
100 µm
69
100 µm
70
100 µm
71
100 µm
72

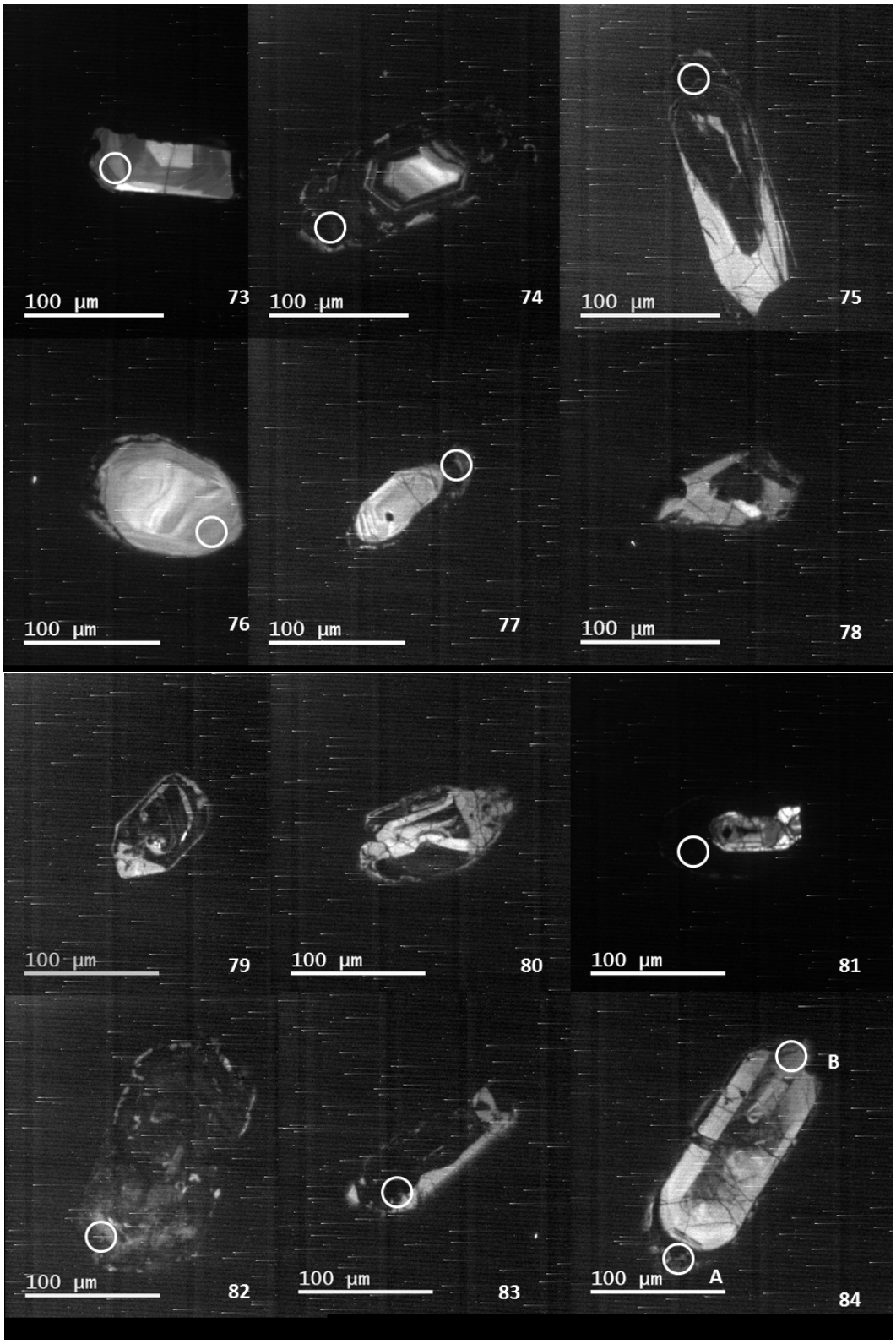
100 µm
73
100 µm
74
100 µm
75
100 µm
76
100 µm
77
100 µm
78
100 µm
79
100 µm
80
100 µm
81
100 µm
82
100 µm
83
B
100 µm
A
84

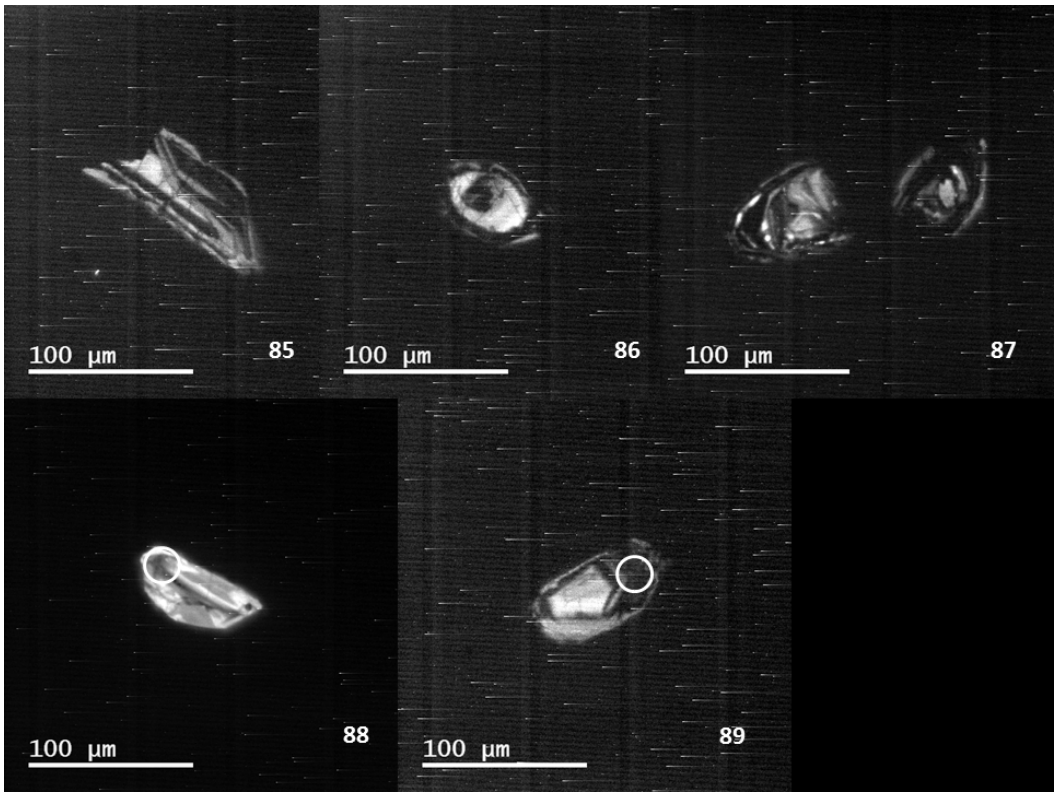
100 µm
85
100 µm
86
100 µm
87
100 µm
88
100 µm
89

C-14. SAG-GM (BR061113-04)

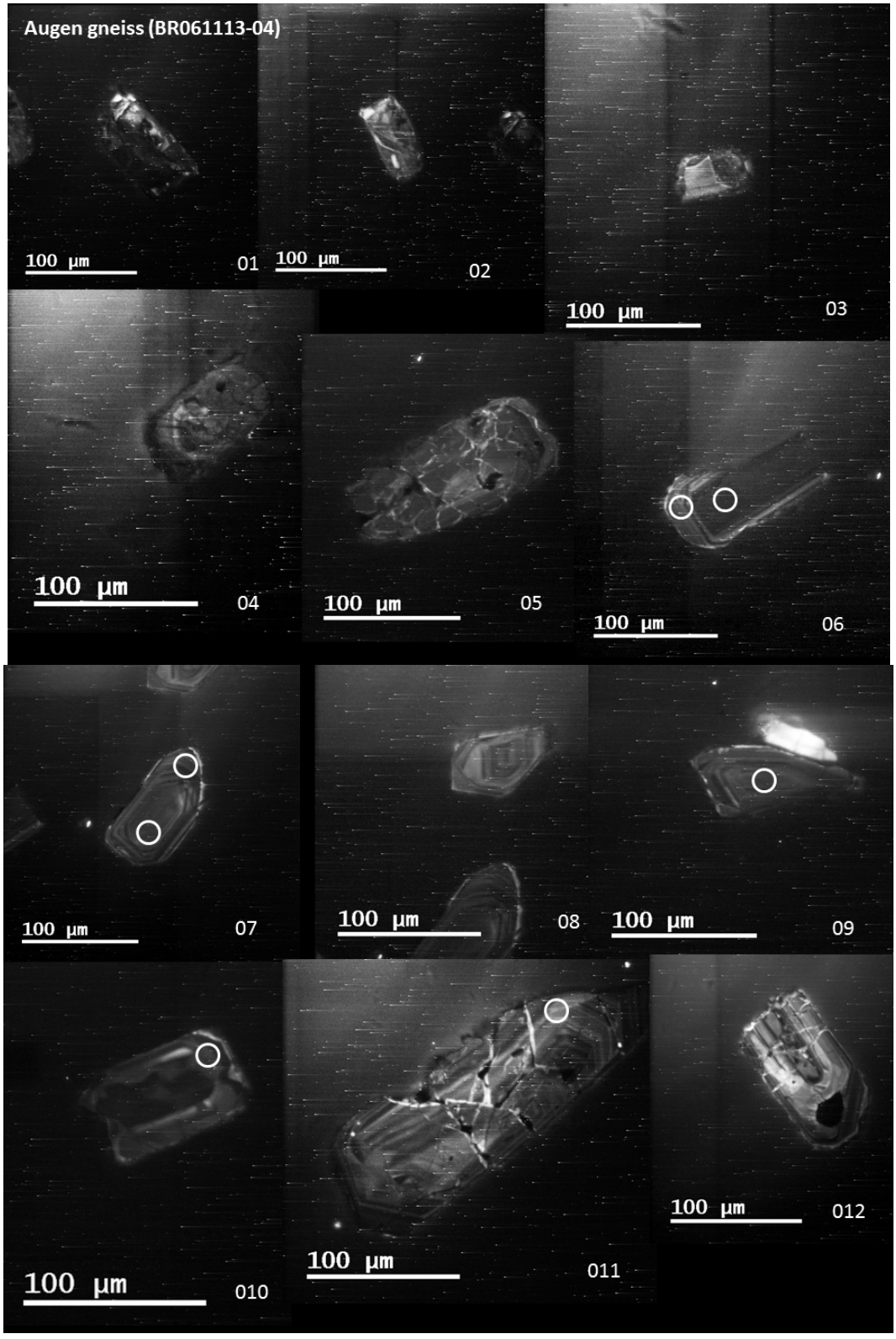

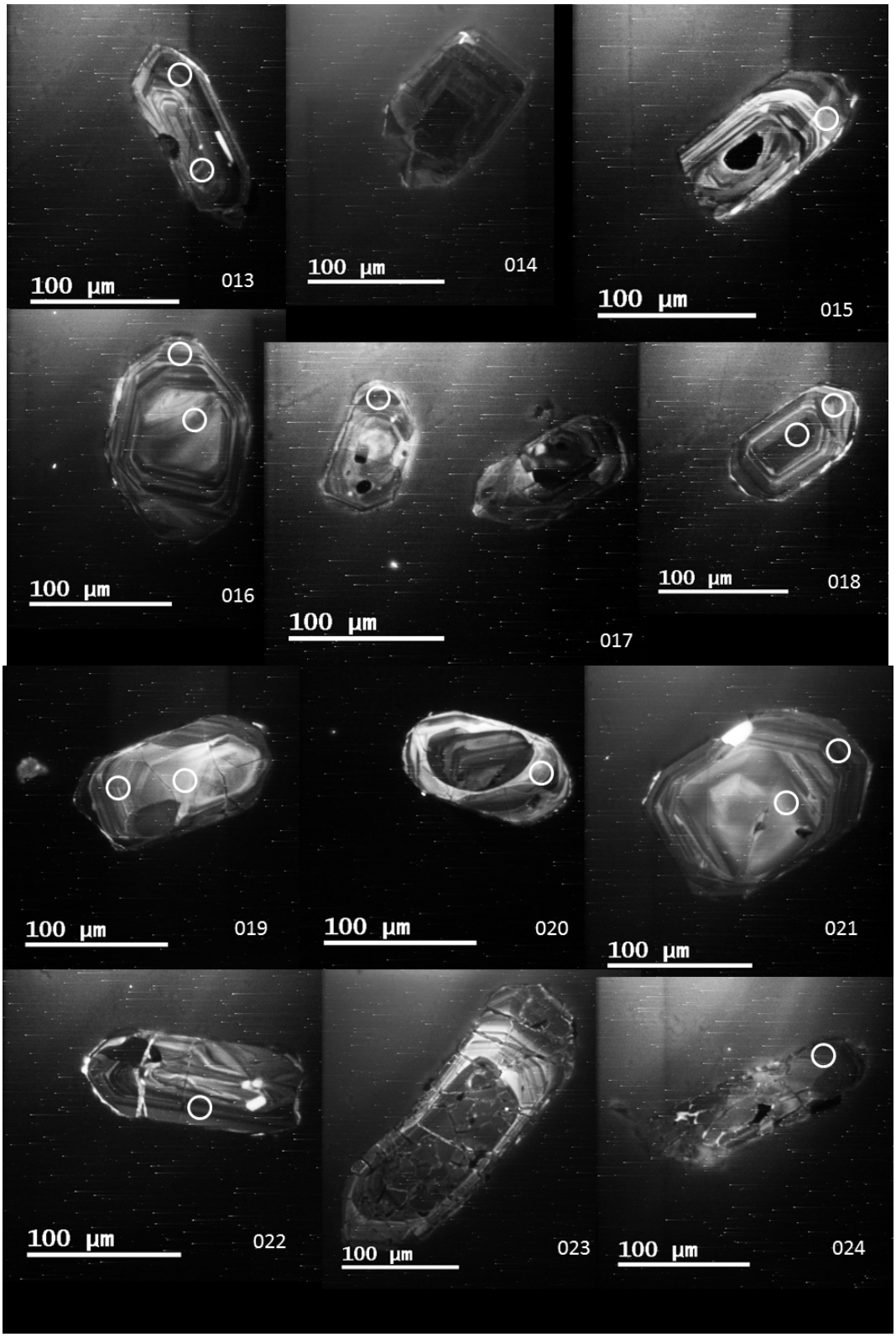
100 µm
013
100 µm
014
100 µm
015
100 µm
016
100 µm
017
100 µm
018
100 µm
019
100 µm
020
100 µm
021
100 µm
022
100 µm
023
100 µm
024

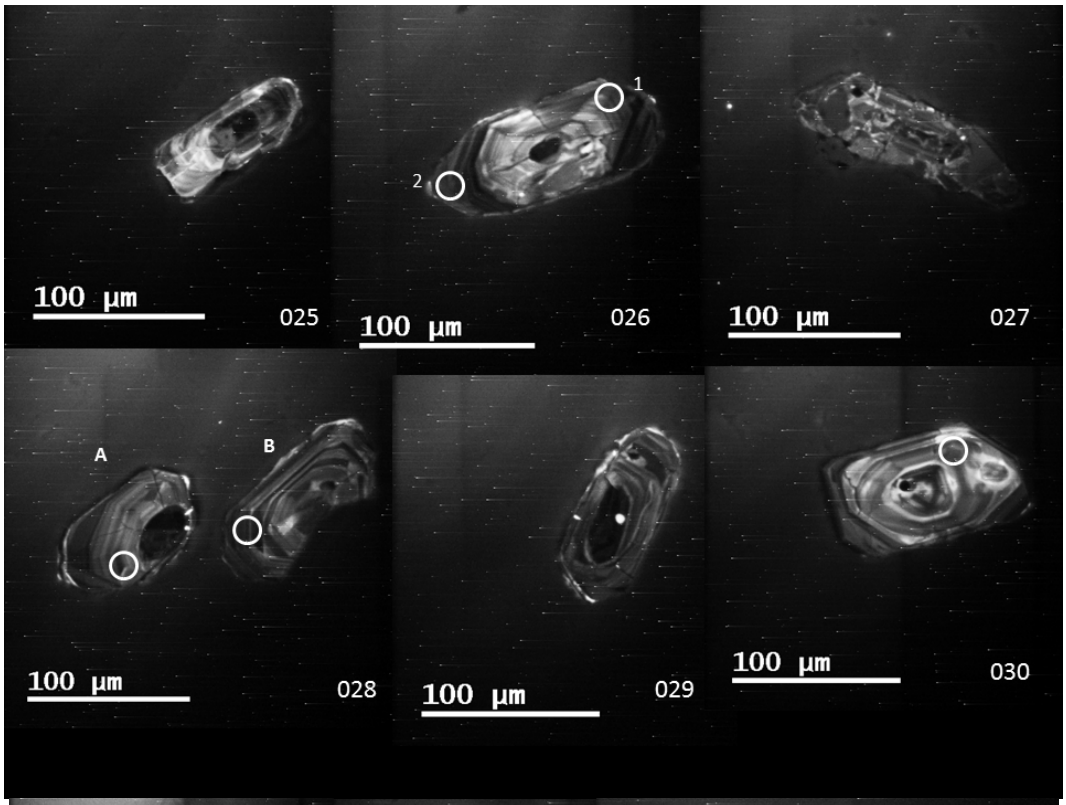
100 µm
025
1
2
100 µm
026
100 µm
027
A
B
100 µm
028
100 µm
029
100 µm
030

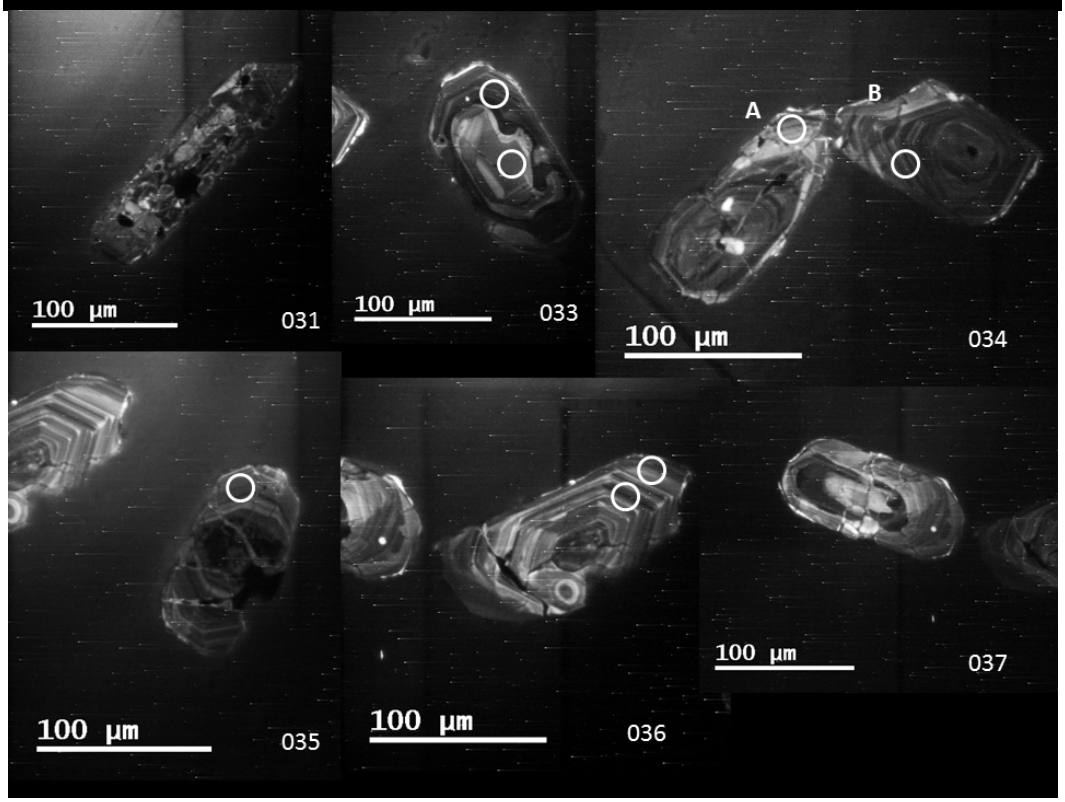
100 µm
031
100 µm
033
A
B
100 µm
034
100 µm
035
100 µm
036
100 µm
037

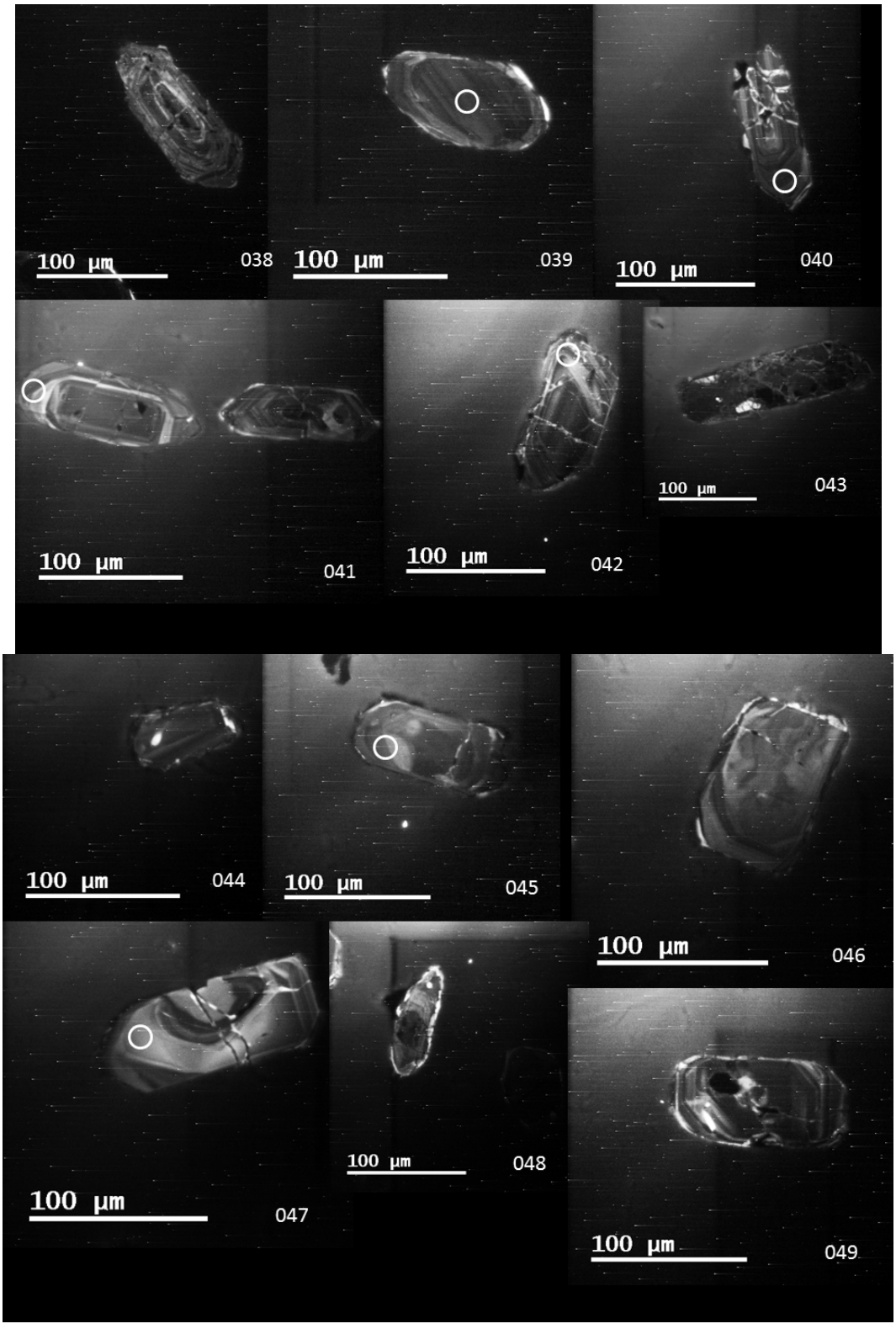
100 µm
038
100 µm
039
100 µm
040
100 µm
041
100 µm
042
100 µm
043
100 µm
044
100 µm
045
100 µm
046
100 µm
047
100 µm
048
100 µm
049

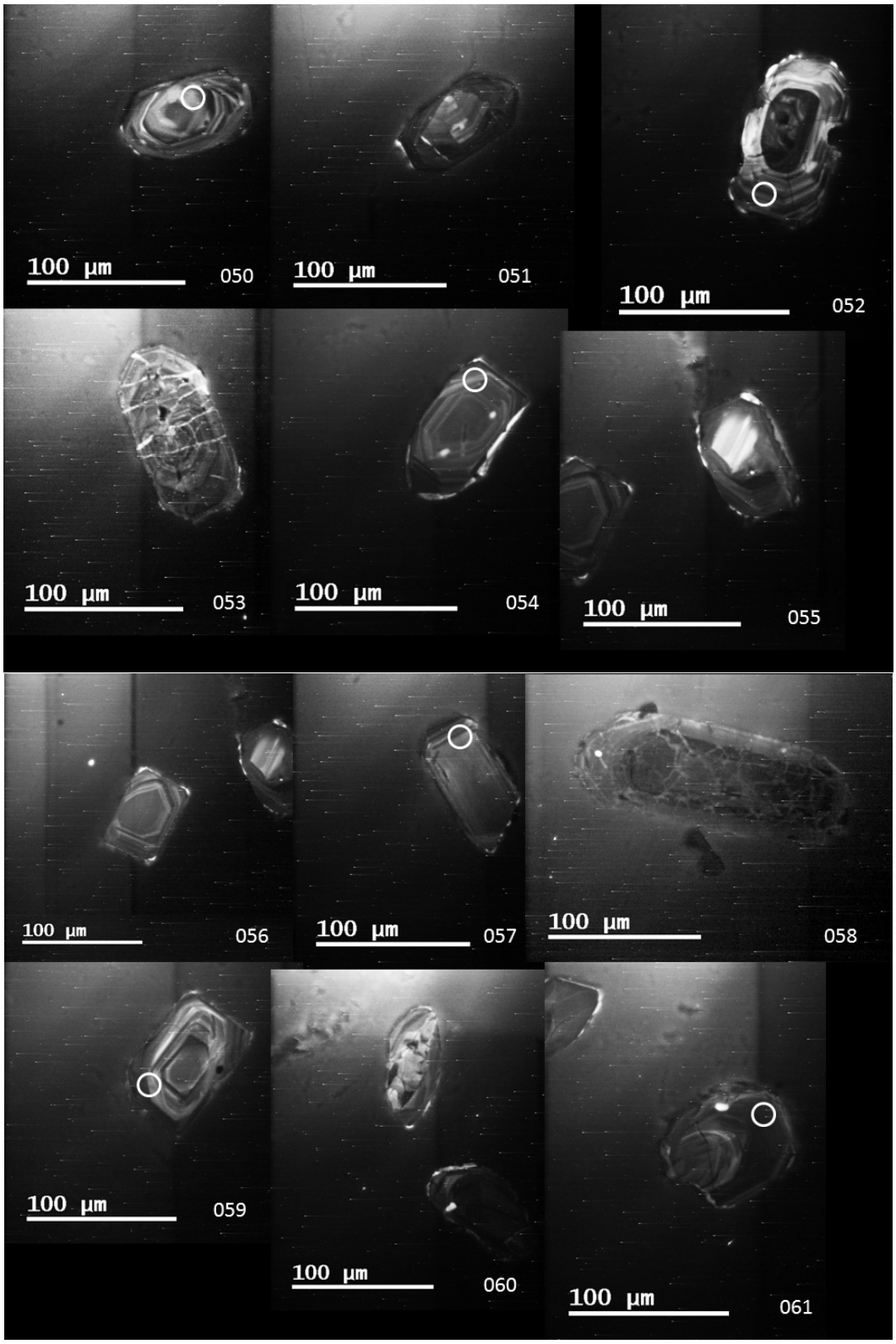
100 µm
050
100 µm
051
100 µm
052
100 µm
053
100 µm
054
100 µm
055
100 µm
056
100 µm
057
100 µm
058
100 µm
059
100 µm
060
100 µm
061

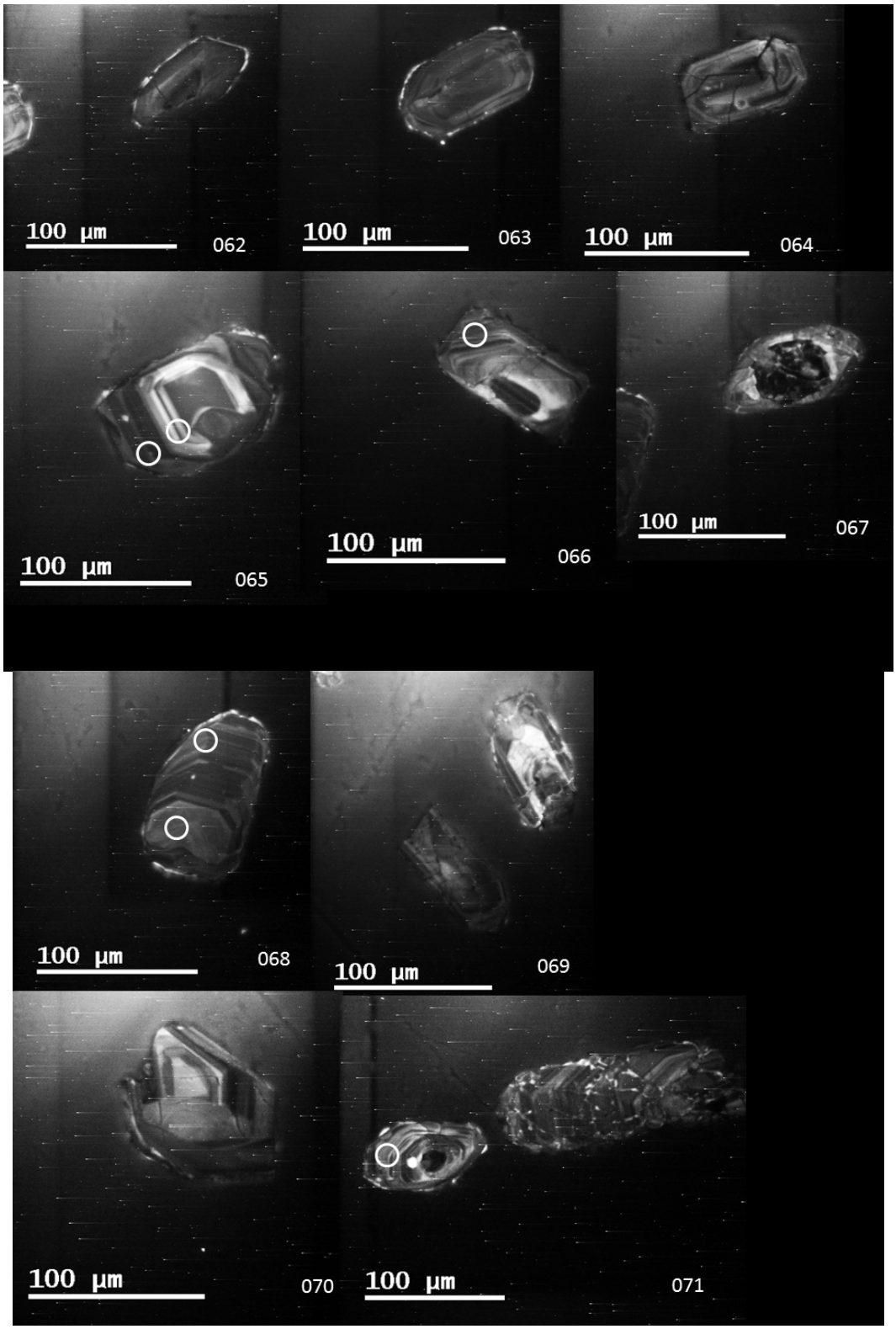
100 µm
062
100 µm
063
100 µm
064
100 µm
065
100 µm
066
100 µm
067
100 µm
068
100 µm
069
100 µm
070
100 µm
071

Appendix D. Sm/Nd Isotopic Data

Sample	Rock Type	Age	(143Nd/144Nd)m	ENd(0)	ENd(T)	T(DM)	Nd-ID (ppm)	Sm-ID (ppm)
BR061113-02	Granodiorite	1710	0.511946658	-13.48597069	1.82931	1913.74	29.12584538	6.114510528
BR060913-04A	Granite	1710	0.511786966	-16.60106633	1.788161	1888.291	34.32803967	6.410988721
BR061113-01	Granite	1710	0.511450479	-23.16490719	3.11646	1765.759	19.45289405	2.476285943
BR060913-01	Amphibole-bearing leucosome	1100	0.511818239	-15.99103891	-2.83484	1679.7	4.124752264	0.70428568
BR060913-04B	Syenite	1710	0.511997896	-12.4864665	2.506128	1855.378	35.34629669	7.507168684
BR060314-01	Diabase	1100	0.512325238	-6.101038894	4.502231	1182.433	63.59746006	12.78096076

Appendix E. Whole Rock and REE data.

Table E-1.

Whole rock XRF data

(wt %)	BR011314-01	BR011314-03	BR011414-03	BR011414-04	BR060913-01	BR060913-04A
SiO_2	60.32	78.94	69.80	74.20	63.42	70.29
TiO_2	0.83	0.52	0.33	0.68	1.05	0.51
Al_2O_3	18.98	11.72	15.30	14.96	15.27	13.90
Fe_2O_3	10.09	5.07	2.26	5.22	5.71	3.14
MnO	0.03	0.01	0.03	0.02	0.08	0.05
MgO	1.86	0.37	0.52	0.26	1.45	0.73
CaO	0.24	0.02	2.00	0.16	4.31	2.35
Na_2O	0.93	0.02	3.89	0.02	4.43	2.44
K_2O	5.72	3.89	3.94	4.05	2.87	3.94
P_2O_5	0.06	0.05	0.10	0.05	0.32	0.11
Sum	99.06	100.60	98.17	99.62	98.91	97.45

(wt %)	BR060913-04B	BR061113-01	BR061113-02	BR061213-01	BR061213-04	BR061213-05
SiO_2	63.55	54.27	63.17	53.78	75.65	54.78
TiO_2	0.77	1.00	1.16	1.07	0.52	1.00
Al_2O_3	16.05	22.12	15.73	21.37	10.88	21.88
Fe_2O_3	4.95	11.29	6.83	14.07	12.85	11.23
MnO	0.10	0.07	0.11	0.12	0.02	0.08
MgO	1.11	2.75	1.69	3.37	0.27	2.81
CaO	0.66	0.20	4.31	0.48	0.16	0.61
Na_2O	0.98	0.22	3.07	0.08	0.04	0.01
K_2O	10.32	6.64	2.47	4.70	1.88	5.79
P_2O_5	0.43	0.22	0.37	0.25	0.03	0.43
Sum	98.91	98.78	98.91	99.29	102.31	98.62

Whole rock XRF data

(wt %)	BR061313-01	BR061313-03	BR061413-02	BR061513-01	BR061513-03	BR061513-06
SiO_2	74.86	74.97	65.33	71.24	67.94	67.03
TiO_2	0.79	0.72	0.89	0.47	0.55	0.71
Al_2O_3	11.88	10.40	14.31	12.18	13.58	17.25
Fe_2O_3	8.15	6.80	13.61	8.87	10.37	5.10
MnO	0.02	0.04	0.08	0.15	0.16	0.09
MgO	0.86	2.49	1.17	1.32	1.31	1.50
CaO	0.02	0.45	0.01	0.67	0.59	0.84
Na_2O	0.09	2.23	0.08	2.94	2.85	1.53
K_2O	4.00	2.13	5.04	2.25	2.67	4.80
P_2O_5	0.07	0.04	0.06	0.06	0.04	0.06
Sum	100.74	100.28	100.58	100.16	100.06	98.92

(wt %)	BR061613-08A	BR061613-08B	BR061713-01	BR6912-2
SiO_2	70.54	69.62	77.05	71.78
TiO_2	0.55	0.57	0.45	0.77
Al_2O_3	15.66	16.16	9.11	12.44
Fe_2O_3	4.56	4.75	9.91	7.89
MnO	0.07	0.07	0.07	0.07
MgO	1.53	1.61	1.54	2.58
CaO	0.20	0.19	0.07	0.53
Na_2O	0.51	0.54	0.39	2.21
K_2O	5.24	5.46	3.43	2.00
P_2O_5	0.07	0.06	0.03	0.04
Sum	98.93	99.04	102.06	100.31

REE data

(ppm)	BR011314-01	BR061413-02A	BR061513-06	BR061613-08A	BR011314-03	BR011414-03
Ga	22.8	18.4	18.2	19.1	15.6	27.5
Rb	209.3	206.7	151.9	188.7	165.0	187.6
Sr	57.1	47.2	46.4	26.1	17.7	28.7
Y	34.4	52.4	45.7	41.1	41.8	57.7
Zr	156.9	214.5	336.0	224.0	320.3	170.5
Nb	19.4	18.1	20.4	20.9	17.0	19.1
Ba	597.7	324.5	601.4	420.5	204.7	504.9
La	43.4	57.5	55.4	52.4	46.3	57.1
Ce	85.9	115.2	96.9	95.6	82.5	105.2
Pr	9.7	13.3	12.4	11.5	9.3	14.0
Nd	39.3	54.6	50.4	45.6	35.1	59.0
Sm	7.8	11.0	9.4	8.7	5.9	13.3
Eu	1.5	2.1	1.8	1.3	1.3	2.5
Gd	7.54	10.74	8.64	7.90	5.72	13.54
Tb	1.04	1.47	1.29	1.14	1.02	1.90
Dy	6.49	9.43	8.44	7.58	7.06	11.68
Er	4.10	5.88	5.21	4.79	4.86	6.53
Yb	3.65	5.42	4.89	4.88	4.66	5.52
Lu	0.55	0.82	0.77	0.77	0.69	0.84
Hf	4.68	6.10	9.19	6.70	8.79	5.36
Ta	1.65	2.25	1.63	1.77	1.39	1.52
Pb	5.61	5.37	3.41	12.11	4.82	7.73
Th	12.84	13.63	18.33	17.36	13.46	14.76
U	3.00	4.44	3.16	3.22	2.28	3.61
Cr	100.00	80.30	24.10	25.30	24.70	132.90
Ni	37.40	23.50	26.00	19.50	10.00	54.20
Sr	70.80	52.10	56.80	35.30	20.10	28.30
V	83.00	87.10	48.90	38.40	32.80	113.40
Zn	90.50	59.80	81.10	82.30	32.30	87.10
Zr	155.50	201.60	281.80	197.50	258.70	150.20

REE data

(ppm)	BR061613-08B	BR061713-01	BR011414-04	BR060913-01	BR060913-04A	BR060913-04B
Ga	18.3	12.4	18.4	18.7	16.8	17.0
Rb	188.1	177.5	116.8	143.7	140.1	344.0
Sr	24.2	11.1	23.3	254.9	129.0	114.9
Y	35.5	19.3	44.0	6.2	31.0	43.9
Zr	209.6	295.8	398.6	233.6	185.3	330.4
Nb	20.1	12.5	19.5	9.2	16.6	44.7
Ba	394.0	238.4	151.5	1020.4	855.4	1645.8
La	47.8	32.7	54.2	42.8	45.0	32.4
Ce	87.4	66.8	94.4	65.7	99.2	61.7
Pr	10.4	8.3	11.0	6.8	10.5	8.1
Nd	40.5	34.2	40.7	23.7	40.8	35.4
Sm	7.7	6.4	6.6	3.7	8.2	8.3
Eu	1.2	1.1	1.5	0.9	1.8	1.9
Gd	6.90	5.54	6.39	2.37	7.47	9.16
Tb	1.01	0.72	1.02	0.26	0.99	1.42
Dy	6.54	4.27	7.48	1.26	6.11	8.92
Er	4.24	2.44	5.48	0.68	3.37	4.74
Yb	4.36	2.25	5.72	0.48	2.99	3.91
Lu	0.63	0.34	0.83	0.09	0.43	0.58
Hf	6.35	7.95	10.90	5.81	5.21	9.31
Ta	1.57	0.86	1.54	2.09	1.15	7.11
Pb	11.36	4.65	8.15	11.87	14.80	29.49
Th	16.07	5.82	16.69	21.08	20.90	12.18
U	3.03	1.66	2.75	3.10	1.77	3.10
Cr	27.50	32.60	33.90	2.10	2.90	0.70
Ni	20.20	8.10	5.00	4.20	14.80	40.80
Sr	35.00	14.20	29.90	462.10	174.20	143.70
V	39.60	40.20	39.50	73.40	26.40	45.40
Zn	83.40	96.30	28.20	70.20	56.70	89.10
Zr	207.50	261.70	349.00	356.50	175.20	266.30

REE data

(ppm)	BR061113-01	BR061113-02	BR061213-05	BR061313-01	BR061513-03	BR6912-2
Ga	22.5	18.8	25.8	16.5	14.849	15.839
Rb	63.9	139.3	143.6	159.1	133.776	70.790
Sr	452.8	447.5	15.1	31.6	58.3	65.5
Y	47.7	46.4	72.3	57.6	35.11	38.27
Zr	511.0	469.8	148.6	392.8	311.9	646.3
Nb	24.1	20.0	17.8	12.5	13.36	16.02
Ba	1593.9	1508.4	523.7	395.3	234.1	338.3
La	60.8	41.8	56.4	61.9	37.694	65.078
Ce	108.2	76.4	107.9	121.0	76.858	132.844
Pr	15.0	10.1	14.8	14.9	9.973	15.831
Nd	63.0	43.5	68.1	65.0	41.474	64.539
Sm	12.2	9.8	17.9	13.2	8.345	10.714
Eu	3.4	2.6	2.5	2.4	1.614	1.817
Gd	11.73	10.12	20.04	12.69	7.334	7.064
Tb	1.62	1.47	2.73	1.68	1.108	1.011
Dy	9.75	9.33	15.64	10.54	7.274	6.906
Er	5.36	5.26	7.62	6.46	4.284	4.818
Yb	4.72	4.36	6.10	5.95	3.972	5.115
Lu	0.69	0.65	0.87	0.92	0.594	0.830
Hf	12.85	11.25	4.47	10.58	8.671	17.160
Ta	1.49	1.06	1.42	1.10	0.911	1.219
Pb	10.78	7.89	4.33	8.21	3.964	4.998
Th	13.30	7.21	14.48	14.15	9.835	15.652
U	6.16	1.97	2.88	3.15	2.213	3.659
Cr	0.00	3.80	133.40	55.90	52.80	59.00
Ni	5.00	12.00	59.30	22.70	7.80	46.70
Sr	359.30	486.30	16.10	39.30	63.70	80.50
V	17.70	84.70	114.20	78.60	55.20	66.90
Zn	50.00	109.80	140.30	48.40	80.40	62.80
Zr	205.40	347.50	133.70	345.40	272.90	592.30

REE data

(ppm)	BR061213-01	BR061213-04	BR061313-03	BR061513-01
Ga	24.875	15.477	11.315	12.757
Rb	157.928	62.609	82.593	127.120
Sr	30.5	12.5	68.2	55.7
Y	53.59	21.71	44.23	22.55
Zr	163.9	268.1	824.1	221.0
Nb	20.42	13.83	16.98	12.50
Ba	388.5	699.1	450.1	183.7
La	49.552	35.198	47.459	30.006
Ce	96.852	69.045	93.015	62.918
Pr	11.777	7.264	10.941	7.920
Nd	48.496	27.453	44.826	33.003
Sm	10.117	5.399	7.826	6.078
Eu	1.945	1.554	1.770	1.283
Gd	10.520	5.932	7.017	5.075
Tb	1.561	0.722	1.067	0.707
Dy	9.919	4.325	7.780	4.392
Er	5.947	2.650	5.563	2.689
Yb	5.552	2.579	6.018	2.573
Lu	0.834	0.397	0.930	0.412
Hf	4.738	7.355	21.403	5.978
Ta	1.570	1.269	1.274	0.845
Pb	5.021	5.167	5.076	4.178
Th	14.636	16.358	18.288	8.474
U	4.606	2.300	3.670	1.824
Cr	151.20	71.90	50.70	37.90
Ni	55.20	2.50	26.10	21.90
Sr	34.50	13.30	78.80	66.50
V	134.40	44.90	50.40	37.80
Zn	103.60	30.30	40.30	77.60
Zr	169.50	248.70	667.90	209.80

Table E-2. Multi-element concentrations normalized to the chondrite values of Sun and McDonough (1989)

(ppm)	Rb	Ba	Th	U	K	Ta	Nb	La	Ce	Sr	Nd	P	Zr	Sm	Ti	Y
BR011314-01	90.22	248.01	442.69	374.49	88.03	117.59	78.95	183.30	140.39	7.86	84.19	0.23	40.54	50.89	11.25	21.93
BR061413-02	89.08	134.64	470.12	555.17	76.29	160.42	73.50	242.75	188.30	6.50	117.01	0.21	55.43	71.97	11.86	33.36
BR061513-06	65.46	249.53	631.91	394.66	73.90	116.64	82.85	233.67	158.29	6.39	107.97	0.23	86.81	61.13	9.72	29.10
BR061613-08	81.34	174.50	598.66	402.23	80.66	126.12	84.88	221.20	156.22	3.59	97.62	0.24	57.89	56.61	7.52	26.15
BR061713-01	76.50	98.93	200.68	207.07	51.15	61.23	50.76	138.11	109.08	1.53	73.18	0.11	76.44	42.05	5.99	12.31
BR011314-03	71.12	84.94	464.16	284.74	58.86	99.50	69.28	195.36	134.84	2.44	75.16	0.18	82.77	38.87	6.93	26.60
BR011414-03	80.88	209.50	508.80	451.36	102.41	108.81	77.48	240.79	171.96	3.96	126.29	0.79	44.07	87.12	13.70	36.77
BR061213-05	61.89	217.32	499.15	359.64	89.50	101.56	72.40	237.87	176.31	2.08	145.73	1.56	38.39	117.19	13.64	46.04
BR061313-01	68.58	164.03	487.82	393.30	60.55	78.35	50.63	261.20	197.77	4.36	139.26	0.25	101.51	86.28	10.51	36.69
BR011414-04	50.33	62.85	575.40	343.39	61.95	110.09	79.26	228.82	154.17	3.21	87.08	0.20	102.99	43.27	9.15	28.05
BR060913-01	61.93	423.41	726.75	387.18	44.14	148.96	37.56	180.53	107.40	35.11	50.70	1.16	60.37	24.09	14.27	3.97
BR060913-04A	60.37	354.96	720.65	221.14	61.53	81.97	67.62	189.79	162.08	17.77	87.47	0.42	47.87	53.47	7.04	19.74
BR060913-04B	148.28	682.90	420.12	386.96	158.84	507.64	181.64	136.56	100.75	15.83	75.75	1.55	85.37	54.37	10.48	27.99
BR061113-01	27.54	661.37	458.76	770.43	61.08	106.63	98.05	256.38	176.73	62.38	134.85	0.36	132.05	79.92	4.51	30.39
BR061113-02	60.05	625.89	248.67	246.73	38.07	75.82	81.46	176.27	124.82	61.63	93.11	1.34	121.40	64.11	15.86	29.53
BR061213-01	68.07	161.22	504.69	575.81	72.05	112.16	83.02	209.08	158.26	4.20	103.84	0.90	42.36	66.12	14.45	34.13
BR061213-04	26.99	290.09	564.08	287.46	28.01	90.62	56.23	148.51	112.82	1.72	58.79	0.11	69.28	35.29	6.89	13.83
BR061313-03	35.60	186.75	630.62	458.81	32.43	90.98	69.04	200.25	151.98	9.39	95.99	0.13	212.94	51.15	9.65	28.17
BR061513-01	54.79	76.24	292.21	227.95	34.24	60.36	50.83	126.61	102.81	7.67	70.67	0.22	57.10	39.73	6.34	14.36
BR061513-03	57.66	97.15	339.14	276.65	40.70	65.06	54.32	159.05	125.58	8.03	88.81	0.15	80.60	54.54	7.45	22.36
BR060912-02	30.51	140.37	539.72	457.42	30.38	87.06	65.14	274.59	217.07	9.02	138.20	0.15	167.01	70.03	10.28	24.38

Table E-3. REE concentrations normalized to the chondrite values of Anders and Grevesse (1989)

(ppm)	La	Ce	Pr	Nd	Sm	Eu	Gd	Tb	Dy	Er	Yb	Lu	Y
BR011314-01	185.10	142.44	109.27	86.90	52.93	26.27	38.34	28.55	26.73	25.82	22.43	22.54	22.07
BR061413-02	245.13	191.04	148.84	120.78	74.85	37.20	54.62	40.37	38.84	37.02	33.35	33.83	33.58
BR061513-06	235.96	160.60	139.01	111.45	63.58	31.35	43.93	35.58	34.78	32.81	30.07	31.58	29.29
BR061613-08	223.36	158.50	129.19	100.77	58.88	22.88	40.16	31.33	31.23	30.17	30.04	31.58	26.32
BR061713-01	139.47	110.67	93.47	75.54	43.73	20.33	28.19	19.75	17.58	15.34	13.83	14.04	12.38
BR011314-03	197.27	136.81	104.84	77.59	40.43	23.28	29.11	28.21	29.07	30.62	28.65	28.56	26.77
BR011414-03	243.15	174.47	156.77	130.37	90.61	44.49	68.85	52.42	48.12	41.07	33.99	34.67	37.01
BR061213-05	240.20	178.89	166.49	150.44	121.89	45.42	101.93	75.33	64.44	47.96	37.55	35.65	46.33
BR061313-01	263.76	200.66	167.07	143.75	89.74	43.51	64.57	46.35	43.43	40.63	36.64	37.80	36.93
BR011414-04	231.06	156.42	123.24	89.89	45.01	26.12	32.50	28.10	30.81	34.49	35.18	34.05	28.23
BR060913-01	182.30	108.96	76.32	52.34	25.05	16.01	12.07	7.17	5.17	4.26	2.93	3.60	3.99
BR060913-04A	191.65	164.44	117.65	90.29	55.62	31.91	37.99	27.23	25.19	21.24	18.39	17.65	19.87
BR060913-04B	137.90	102.22	90.72	78.19	56.55	34.44	46.61	39.22	36.74	29.85	24.04	23.71	28.17
BR061113-01	258.89	179.31	168.65	139.20	83.12	61.10	59.67	44.67	40.16	33.74	29.06	28.36	30.58
BR061113-02	178.00	126.65	113.84	96.11	66.68	47.23	51.48	40.43	38.45	33.11	26.84	26.83	29.72
BR061213-01	211.13	160.56	132.17	107.20	68.77	34.73	53.51	42.99	40.87	37.43	34.16	34.34	34.35
BR061213-04	149.97	114.46	81.53	60.68	36.70	27.74	30.17	19.89	17.82	16.68	15.87	16.33	13.92
BR061313-03	202.21	154.20	122.80	99.08	53.20	31.61	35.69	29.40	32.06	35.01	37.03	38.28	28.36
BR061513-01	127.85	104.31	88.89	72.95	41.32	22.91	25.81	19.47	18.10	16.92	15.84	16.94	14.45
BR061513-03	160.60	127.42	111.94	91.68	56.73	28.82	37.30	30.53	29.97	26.96	24.44	24.45	22.50
BR060912-02	277.28	220.23	177.68	142.66	72.84	32.45	35.93	27.86	28.45	30.32	31.48	34.16	24.53

Table E-4. Molar percent of select oxides used for CIA calculation

$CIA = [Al_2O_3/(Al_2O_3 + CaO + Na_2O + K_2O)]*100$

Molar %	Al2O3	CaO	Na2O	K2O	(CaO+Na_2O)	CIA (%)
BR011314-01	19.159	0.17055953	0.69431	5.77916	1.174548982	73.4
BR011314-03	11.6477	0.01214815	0.01283	3.86421	0.034293314	74.9
BR011414-03	22.3901	0.14260443	0.16582	6.7236	0.423053211	75.8
BR011414-04	15.0171	0.11686322	0.01281	4.06726	0.180778462	77.9
BR061213-01	21.5272	0.34197309	0.0585	4.73046	0.557342642	80.3
BR061213-04	10.634	0.11422055	0.03075	1.83872	0.201260739	83.9
BR061213-05	22.1873	0.44126633	0.00865	5.87583	0.629075581	77.3
BR061313-01	11.7879	0.0175942	0.0676	3.97535	0.115742464	74.2
BR061313-03	10.368	0.32278544	1.64781	2.12895	2.672829442	68.3
BR061413-02	14.2241	0.00561376	0.0568	5.00871	0.084413189	73.6
BR061513-01	12.1586	0.47837665	2.17443	2.24804	3.600393376	67.5
BR061513-03	13.5692	0.42064328	2.11174	2.67195	3.435111071	69.0
BR061513-06	17.4387	0.60763918	1.14581	4.85171	2.394718033	70.6
BR061613-08	15.8313	0.14556567	0.38445	5.29532	0.721904891	72.5
BR061713-01	8.92708	0.05027955	0.28516	3.35782	0.454731174	70.1
BR060912-02	12.405	0.38019634	1.63116	1.99477	2.730713977	72.4

Table E-5. Molar percent of 13 metasedimentary rocks used for P-T calculations using the Theriak-Domino software of Capitani and Petrakakis, (2010)

Molar %	SiO2	TiO2	Al2O3	Fe2O3	MnO	MgO	CaO	Na2O	K2O	P2O5	Sum
BR011314-03	76.65	0.378	13.41	4.12	0.01	0.54	0.018	0.032	4.81	0.042	100.01
BR011414-04	72.04	0.49	17.12	4.238	0.054	0.373	0.207	0.42	5.01	0.045	99.997
BR061213-01	51.94	0.772	24.33	11.36	0.0999	4.86	0.49	0.147	5.79	0.205	99.9939
BR061213-04	73.65	0.384	12.48	10.46	0.016	0.392	0.171	0.08	2.34	0.025	99.998
BR061213-05	52.98	0.724	24.94	9.08	0.062	4.05	0.63	0.02	7.15	0.351	99.987
BR061313-03	71.56	0.516	11.7	5.43	0.035	3.55	0.464	4.12	2.6	0.03	100.005
BR061413-02	63.66	0.648	16.42	11.09	0.065	1.709	0.008	0.146	6.25	0.049	100.045
BR061513-01	67.97	0.339	13.69	7.08	0.123	1.88	0.69	5.43	2.74	0.05	99.992
BR061513-03	64.88	0.397	15.28	8.28	0.129	1.87	0.6	5.28	3.25	0.033	99.999
BR061513-06	64.14	0.514	19.45	4.08	0.07	2.14	0.86	2.83	5.86	0.051	99.995
BR061613-08	68.19	0.401	17.84	3.69	0.058	2.2	0.209	0.96	6.47	0.055	100.073
BR061713-01	74.08	0.328	10.33	7.97	0.058	2.21	0.07	0.73	4.21	0.025	100.011
BR060912-02	68.43	0.547	13.99	6.29	0.05	3.66	0.545	4.08	2.43	0.032	100.054

Appendix F: EPMA Data and Garnet-Biotite Thermometry Data.

Table F-1. Electron probe micronalysis data for garnet in sample BR060912-02 (Cations, Total O = 12)

EPMA Shot

ID#	Al	Ti	Ca	Mg	Mn	Si	Fe	K	Na	Cr	Total
1grt1rim	2.009	0	0.0431	0.322	0.216	3.017	2.371	0	0	0	7.9782
2grt1rim	2.004	0.0057	0.0399	0.349	0.205	2.998	2.391	0	0	0	7.9926
3grt1	2.001	0	0.0326	0.36	0.22	2.985	2.417	0	0	0	8.0156
4grt1	2.018	0	0.0484	0.35	0.199	3.005	2.366	0	0	0	7.9864
5grt1	2.005	0	0.044	0.351	0.203	2.992	2.41	0	0	0	8.005
6grt1core	1.99	0	0.0488	0.367	0.208	2.994	2.402	0	0	0	8.0098
7grt1core	2.007	0.0018	0.0384	0.367	0.214	2.971	2.424	0	0	0	8.0232
8grt1core	1.996	0.0042	0.04	0.353	0.21	2.987	2.422	0	0	0	8.0122
9grt1core	2.01	0	0.0377	0.331	0.203	3.012	2.389	0	0	0	7.9828
10grt1	1.998	0.0029	0.0348	0.336	0.204	2.999	2.426	0	0	0	8.0007
11grt1rim	1.995	0.0072	0.0401	0.314	0.23	2.988	2.433	0	0	0	8.0073
12grt1rim	1.988	0.0008	0.042	0.31	0.226	3.003	2.432	0	0	0	8.0019
13bt1	1.941	0.111	0.0051	1.133	0.0033	2.908	1.4	0.988	0.0272	0	8.5167
14bt1	1.988	0.1025	0.0051	1.154	0.0047	2.863	1.486	0.84	0.0299	0.0021	8.4753
15bt2	1.929	0.13	0.0034	1.105	0.009	2.887	1.451	0.968	0.0317	0.0016	8.5158
16bt2	1.944	0.139	0.0051	1.086	0.0047	2.904	1.404	0.94	0.0509	0.0027	8.4804
17bt3	1.885	0.106	0.0165	1.138	0.0057	2.914	1.482	0.935	0.0366	0.0026	8.5214
18bt3	1.892	0.137	0.0018	1.121	0.0032	2.914	1.431	0.952	0.0434	0.0028	8.4982
19grt2rim	2.007	0	0.0408	0.336	0.214	2.997	2.405	0	0	0	7.9998
20grt2rim	2.005	0	0.0372	0.344	0.205	2.996	2.414	0	0	0	8.0012
21grt2	1.994	0.0006	0.0447	0.359	0.204	3.008	2.385	0	0	0	7.9954
22grt2	2.004	0	0.0529	0.364	0.205	2.99	2.392	0	0	0	8.0079
23grt2	2.004	0.0014	0.0528	0.366	0.203	2.969	2.432	0	0	0	8.0282
24grt2core	2.004	0.0019	0.051	0.371	0.201	2.98	2.408	0	0	0	8.0169
25grt2core	1.987	0.0053	0.0429	0.372	0.208	3.009	2.369	0	0	0	7.9932
26grt2core	2.006	0	0.0465	0.371	0.202	2.985	2.403	0	0	0	8.0135
27grt2core	2	0	0.0486	0.377	0.21	2.986	2.392	0	0	0	8.0136
28grt2	2.004	0.0058	0.0391	0.354	0.201	2.985	2.418	0	0	0	8.0069
29grt2rim	2	0	0.0353	0.348	0.204	3	2.413	0	0	0	8.0003
30grt2rim	2.008	0.0009	0.0352	0.347	0.207	2.995	2.408	0	0	0	8.0011
31grt2rim	1.999	0.0023	0.0389	0.33	0.223	3.007	2.389	0	0	0	7.9892
36bt4	1.939	0.136	0.002	1.09	0.0045	2.922	1.397	0.906	0.046	0.0025	8.445
37bt4	1.933	0.106	0	1.103	0.0079	2.929	1.423	0.937	0.0473	0.0033	8.4895
38bt5	1.944	0.119	0	1.194	0.0073	2.822	1.559	0.86	0.0144	0.0035	8.5232
39bt5	1.921	0.123	0.0102	1.102	0.0057	2.889	1.513	0.908	0.0183	0.0011	8.4913
42grt3rim	2.005	0.0022	0.0408	0.344	0.219	2.989	2.408	0	0	0	8.008
43grt3rim	1.989	0.0064	0.0399	0.356	0.219	2.995	2.398	0	0	0	8.0033
44grt3rim	2.009	0.0037	0.0434	0.36	0.217	2.967	2.425	0	0	0	8.0251

Table F-1 (continued). Electron probe micronalysis data for garnet in sample BR060912-02 (Cations, Total O = 12)

EPMA Shot ID#	Al	Ti	Ca	Mg	Mn	Si	Fe	K	Na	Cr	Total
45grt3	2.004	0	0.0572	0.349	0.211	2.991	2.395	0	0	0	8.0072
46grt3	2.006	0.0051	0.0485	0.356	0.213	2.983	2.397	0	0	0	8.0086
47grt3	1.997	0	0.0445	0.361	0.207	2.995	2.401	0	0	0	8.0055
48grt3core	2.003	0.0028	0.0523	0.369	0.208	2.981	2.401	0	0	0	8.0171
49grt3core	2.009	0	0.055	0.381	0.206	2.991	2.363	0	0	0	8.005
50grt3core	2.009	0.001	0.0543	0.368	0.207	2.987	2.383	0	0	0	8.0093
51grt3core	1.969	0.0037	0.0543	0.393	0.211	2.978	2.425	0	0	0	8.034
52grt3	1.998	0	0.0413	0.378	0.212	2.991	2.389	0	0	0	8.0093
53grt3	1.981	0.004	0.0365	0.378	0.213	2.98	2.434	0	0	0	8.0265
54grt3rim	1.984	0	0.0402	0.359	0.207	3.013	2.391	0	0	0	7.9942
55grt3rim	2.017	0.0025	0.0418	0.343	0.221	2.973	2.418	0	0	0	8.0163
56grt3rim	2.003	0.0028	0.044	0.343	0.226	2.99	2.398	0	0	0	8.0068
57bt6	1.888	0.117	0.0023	1.157	0.0058	2.929	1.415	0.939	0.0473	0.0023	8.5028
58bt6	1.959	0.109	0.0031	1.174	0.0046	2.86	1.492	0.866	0.0232	0.0043	8.4952
59bt7	2.154	0.0542	0.009	1.519	0.0057	2.559	1.831	0.339	0.0081	0.0024	8.4815
60bt7	1.992	0.121	0.0167	1.11	0.0067	2.898	1.39	0.87	0.032	0	8.4364
65grt4rim	2.029	0	0.0406	0.341	0.22	2.995	2.366	0	0	0	7.9917
66grt4rim	2.016	0.0031	0.0372	0.369	0.22	2.979	2.386	0	0	0	8.0103
67grt4	1.997	0	0.0534	0.371	0.211	3.006	2.357	0	0	0	7.9955
68grt4	2.034	0.0015	0.0575	0.349	0.21	2.962	2.407	0	0	0	8.021
69grt4	1.99	0.0076	0.0532	0.354	0.21	2.993	2.398	0	0	0	8.0058
70grt4core	2.01	0	0.052	0.377	0.21	2.982	2.383	0	0	0	8.014
71grt4core	1.977	0.0049	0.0565	0.392	0.199	3.002	2.373	0	0	0	8.0044
72grt4core	2.005	0.001	0.0576	0.39	0.207	3.008	2.32	0	0	0	7.9886
73grt4core	2.006	0	0.0609	0.382	0.203	2.984	2.377	0	0	0	8.0129
74grt4core	2.017	0	0.0587	0.401	0.203	2.972	2.368	0	0	0	8.0197
75grt4core	2.004	0.0052	0.0597	0.376	0.209	2.991	2.358	0	0	0	8.0029
76grt4core	2.078	0.0057	0.0566	0.378	0.21	2.935	2.357	0	0	0	8.0204
77grt4	1.991	0.004	0.0389	0.364	0.223	2.982	2.414	0	0	0	8.017
78grt4	2.016	0	0.0412	0.347	0.22	2.997	2.372	0	0	0	7.9933
79grt4rim	2	0	0.0398	0.347	0.223	2.992	2.406	0	0	0	8.0078
82bt8	1.92	0.0902	0.0036	1.142	0.0038	2.933	1.429	0.964	0.0234	0.0021	8.5111
83bt8	1.906	0.129	0.0166	1.13	0.0053	2.877	1.553	0.826	0.0181	0.0013	8.4623
84bt9	1.907	0.109	0	1.16	0.0064	2.907	1.441	0.966	0.0215	0.0035	8.5214
85bt9	1.913	0.149	0.003	1.105	0.0028	2.921	1.383	0.932	0.0494	0.0038	8.4621

Table F-1 (continued). Electron probe micronalysis data for garnet in sample BR060912-02 (Cations, Total O = 12)

EPMA Shot ID#	Al	Ti	Ca	Mg	Mn	Si	Fe	K	Na	Cr	Total
86grt5rim	1.992	0	0.0393	0.336	0.228	3.007	2.394	0	0	0	7.9963
87grt5rim	1.979	0.0014	0.0378	0.347	0.22	2.995	2.433	0	0	0	8.0133
88grt5	1.993	0.0027	0.0434	0.356	0.211	2.982	2.43	0	0	0	8.0181
89grt5	2.006	0	0.0508	0.359	0.219	2.996	2.37	0	0	0	8.0008
90grt5	1.994	0.008	0.0427	0.379	0.215	2.983	2.39	0	0	0	8.0117
91grt5core	1.986	0	0.054	0.357	0.209	3.001	2.399	0	0	0	8.006
92grt5core	2.052	0.0038	0.0525	0.357	0.208	2.959	2.379	0	0	0	8.0113
93grt5core	1.986	0.0036	0.0476	0.359	0.216	2.999	2.392	0	0	0	8.0033
94grt5core	1.986	0.0035	0.0482	0.367	0.217	2.993	2.396	0	0	0	8.0107
95grt5	2.002	0.0037	0.0411	0.345	0.214	2.993	2.404	0	0	0	8.0028
96grt5	2.005	0.0033	0.0363	0.34	0.22	2.997	2.397	0	0	0	7.9987
97grt5rim	2.007	0.0015	0.037	0.343	0.222	3.004	2.377	0	0	0	7.9915
98grt5rim	2.009	0	0.0423	0.343	0.225	3	2.377	0	0	0	7.9963
99bt10	1.903	0.126	0.02	1.13	0.0084	2.922	1.411	0.917	0.0265	0.0046	8.4685
100bt10	1.926	0.115	0.0181	1.099	0.0051	2.945	1.398	0.901	0.0361	0.0026	8.4459
101bt11	1.928	0.166	0.0095	1.261	0.0083	2.777	1.519	0.805	0.0316	0.0033	8.5087

Table F-2. Calculated garnet fractions from sample BR060912-02

EPMA Shot ID#	Almandine	Pyrope	Spessartine	Grossular	Fe/(Fe + Mg)	Mg / (Fe + Mg)
1grt1rim	0.803157075	0.109074896	0.073168253	0.014599776	0.880430746	0.119569254
2grt1rim	0.80103186	0.11692184	0.068679018	0.013367282	0.872627737	0.127372263
3grt1	0.797795088	0.118827568	0.072616847	0.010760496	0.870363702	0.129636298
4grt1	0.798407235	0.118107579	0.067152595	0.016332591	0.871134021	0.128865979
5grt1	0.801196809	0.11668883	0.067486702	0.01462766	0.872872148	0.127127852
6grt1core	0.793839646	0.121290237	0.068742151	0.016127966	0.867461177	0.132538823
7grt1core	0.796477624	0.120588815	0.070316094	0.012617467	0.868505912	0.131494088
8grt1core	0.800661157	0.116694215	0.069421488	0.01322314	0.872792793	0.127207207
9grt1core	0.806903773	0.111797886	0.068564866	0.012733475	0.878308824	0.121691176
10grt1	0.80845108	0.111970141	0.067981872	0.011596907	0.878349022	0.121650978
11grt1rim	0.8064035	0.104073448	0.076232143	0.013290908	0.885693484	0.114306516
12grt1rim	0.807973422	0.102990033	0.075083056	0.013953488	0.886943837	0.113056163
19grt2rim	0.802790573	0.11215702	0.07143334	0.013619067	0.877417001	0.122582999
20grt2rim	0.804613026	0.114659023	0.068328778	0.012399173	0.875271936	0.124728064
21grt2	0.796939219	0.119958566	0.06816587	0.014936345	0.869169096	0.130830904
22grt2	0.79365606	0.120773748	0.068018182	0.017552009	0.867924528	0.132075472
23grt2	0.796384832	0.119850678	0.066474556	0.017289934	0.86919228	0.13080772
24grt2core	0.794457275	0.122401848	0.066314748	0.01682613	0.866498741	0.133501259
25grt2core	0.791804539	0.124335706	0.06952104	0.014338715	0.864283108	0.135716892
26grt2core	0.795037221	0.122746071	0.066832093	0.015384615	0.866258111	0.133741889
27grt2core	0.790064738	0.124521073	0.069361871	0.016052319	0.863849765	0.136150235
28grt2	0.802762192	0.117525979	0.066730852	0.012980977	0.872294372	0.127705628
29grt2rim	0.804252908	0.115988401	0.067993201	0.01176549	0.873958711	0.126041289
30grt2rim	0.803416522	0.115774723	0.06906446	0.011744295	0.874047187	0.125952813
31grt2rim	0.801435808	0.110704821	0.074809621	0.01304975	0.87863185	0.12136815
42grt3rim	0.799521881	0.114217412	0.072713992	0.013546716	0.875	0.125
43grt3rim	0.795910916	0.118158585	0.072687444	0.013243055	0.870733479	0.129266521
44grt3rim	0.796282919	0.118211072	0.071255008	0.014251002	0.870736086	0.129263914
45grt3	0.795099927	0.115862161	0.07004847	0.018989443	0.872813411	0.127186589
46grt3	0.795156742	0.11809587	0.070658484	0.016088904	0.870686524	0.129313476
47grt3	0.796747967	0.119794259	0.068690891	0.014766882	0.86929761	0.13070239
48grt3core	0.792330792	0.121770122	0.068640069	0.017259017	0.866787004	0.133212996
49grt3core	0.786356073	0.126788686	0.068552413	0.018302829	0.861151603	0.138848397
50grt3core	0.791089865	0.122165787	0.068718255	0.018026093	0.866230462	0.133769538
51grt3core	0.786494989	0.127460837	0.068433172	0.017611001	0.86053939	0.13946061
52grt3	0.790981028	0.12515313	0.070191703	0.013674138	0.863389953	0.136610047
53grt3	0.795035114	0.123468888	0.069573738	0.01192226	0.865576102	0.134423898
54grt3rim	0.797744562	0.11977846	0.06906446	0.013412518	0.869454545	0.130545455

Table F-2 (continued). Calculated garnet fractions from sample BR060912-02

EPMA Shot ID#	Almandine	Pyrope	Spessartine	Grossular	Fe/(Fe + Mg)	Mg / (Fe + Mg)
55grt3rim	0.799656062	0.113433428	0.073086844	0.013823666	0.875769649	0.124230351
56grt3rim	0.796413152	0.113915643	0.07505812	0.014613085	0.874863189	0.125136811
65grt4rim	0.797277261	0.114907669	0.07413398	0.013681089	0.874030292	0.125969708
66grt4rim	0.792112078	0.122501826	0.073036319	0.012349778	0.866061706	0.133938294
67grt4	0.787662077	0.123980751	0.070511964	0.017845208	0.864002933	0.135997067
68grt4	0.796097238	0.115429138	0.069455929	0.019017695	0.873367199	0.126632801
69grt4	0.795303794	0.117405147	0.069647121	0.017643937	0.871366279	0.128633721
70grt4core	0.788550629	0.12475182	0.069490404	0.017207148	0.863405797	0.136594203
71grt4core	0.785631518	0.129779838	0.065883132	0.018705512	0.858227848	0.141772152
72grt4core	0.779936798	0.131110065	0.069589188	0.019363948	0.856088561	0.143911439
73grt4core	0.786331007	0.126368719	0.067154057	0.020146217	0.861544038	0.138455962
74grt4core	0.781337645	0.132312667	0.066981225	0.019368463	0.855182376	0.144817624
75grt4core	0.785293236	0.125220635	0.069604023	0.019882106	0.862472568	0.137527432
76grt4core	0.785247868	0.125932836	0.069962687	0.01885661	0.86179159	0.13820841
77grt4	0.794105069	0.119740781	0.073357676	0.012796474	0.868970482	0.131029518
78grt4	0.795919737	0.116435139	0.073820549	0.013824576	0.872379551	0.127620449
79grt4rim	0.797798262	0.11506068	0.073943895	0.013197162	0.873955685	0.126044315

Table F-3. Calculated garnet core and rim temperatures at 4000, 5000, & 6000 kb for sample BR060912-02.
Calculations based on garnet-biotite thermometer of Perchuk and Lavrent'Eva (1983).

Garnet 1

4000 kb

1grt1rim	2grt1rim	3grt1	4grt1	5grt1	6grt1core	7grt1core	8grt1core	9grt1core	10grt1	11grt1rim	12grt1rim
Bt1-13	Bt1-13	Bt1-13	Bt1-13	Bt1-13	Bt1-13	Bt1-13	Bt1-13	Bt1-13	Bt1-13	Bt1-13	Bt1-13
566.3	579.5	583.3	582.0	579.1	588.1	586.4	579.3	569.9	569.9	557.2	555.0
Bt1-14	Bt1-14	Bt1-14	Bt1-14	Bt1-14	Bt1-14	Bt1-14	Bt1-14	Bt1-14	Bt1-14	Bt1-14	Bt1-14
573.8	587.3	591.1	589.8	586.9	596.0	594.3	587.0	577.5	577.4	564.6	562.3
Bt2-15	Bt2-15	Bt2-15	Bt2-15	Bt2-15	Bt2-15	Bt2-15	Bt2-15	Bt2-15	Bt2-15	Bt2-15	Bt2-15
577.4	591.0	594.9	593.6	590.6	599.8	598.1	590.7	581.2	581.1	568.1	565.9
Bt2-16	Bt2-16	Bt2-16	Bt2-16	Bt2-16	Bt2-16	Bt2-16	Bt2-16	Bt2-16	Bt2-16	Bt2-16	Bt2-16
574.6	588.0	591.9	590.6	587.6	596.8	595.0	587.8	578.3	578.2	565.3	563.1
Bt3-17	Bt3-17	Bt3-17	Bt3-17	Bt3-17	Bt3-17	Bt3-17	Bt3-17	Bt3-17	Bt3-17	Bt3-17	Bt3-17
575.9	589.4	593.3	592.0	589.0	598.2	596.4	589.1	579.6	579.5	566.6	564.4
Bt3-18	Bt3-18	Bt3-18	Bt3-18	Bt3-18	Bt3-18	Bt3-18	Bt3-18	Bt3-18	Bt3-18	Bt3-18	Bt3-18
572.2	585.6	589.5	588.2	585.2	594.4	592.6	585.4	575.9	575.8	563.0	560.8

5000kb

1grt1rim	2grt1rim	3grt1	4grt1	5grt1	6grt1core	7grt1core	8grt1core	9grt1core	10grt1	11grt1rim	12grt1rim
Bt1-13	Bt1-13	Bt1-13	Bt1-13	Bt1-13	Bt1-13	Bt1-13	Bt1-13	Bt1-13	Bt1-13	Bt1-13	Bt1-13
570.8	584.1	587.9	586.6	583.6	592.7	591.0	583.8	574.4	574.3	561.6	559.4
Bt1-14	Bt1-14	Bt1-14	Bt1-14	Bt1-14	Bt1-14	Bt1-14	Bt1-14	Bt1-14	Bt1-14	Bt1-14	Bt1-14
578.3	591.8	595.7	594.4	591.4	600.6	598.9	591.6	582.0	582.0	569.0	566.8
Bt2-15	Bt2-15	Bt2-15	Bt2-15	Bt2-15	Bt2-15	Bt2-15	Bt2-15	Bt2-15	Bt2-15	Bt2-15	Bt2-15
581.9	595.6	599.5	598.2	595.2	604.5	602.7	595.3	585.7	585.6	572.6	570.3
Bt2-16	Bt2-16	Bt2-16	Bt2-16	Bt2-16	Bt2-16	Bt2-16	Bt2-16	Bt2-16	Bt2-16	Bt2-16	Bt2-16
579.1	592.6	596.5	595.2	592.2	601.4	599.6	592.3	582.8	582.7	569.7	567.5
Bt3-17	Bt3-17	Bt3-17	Bt3-17	Bt3-17	Bt3-17	Bt3-17	Bt3-17	Bt3-17	Bt3-17	Bt3-17	Bt3-17
580.4	594.0	597.9	596.6	593.6	602.8	601.1	593.7	584.1	584.1	571.0	568.8
Bt3-18	Bt3-18	Bt3-18	Bt3-18	Bt3-18	Bt3-18	Bt3-18	Bt3-18	Bt3-18	Bt3-18	Bt3-18	Bt3-18
576.7	590.2	594.0	592.7	589.8	599.0	597.2	589.9	580.4	580.3	567.4	565.2

Table F-3 (continued). Calculated garnet core and rim temperatures at 4000, 5000, & 6000 kb for sample BR060912-02. Calculations based on garnet-biotite thermometer of Perchuk and Lavrent'Eva (1983).

Garnet 1

6000kb

1grt1rim	2grt1rim	3grt1	4grt1	5grt1	6grt1core	7grt1core	8grt1core	9grt1core	10grt1	11grt1rim	12grt1rim
Bt1-13	Bt1-13	Bt1-13	Bt1-13	Bt1-13	Bt1-13	Bt1-13	Bt1-13	Bt1-13	Bt1-13	Bt1-13	Bt1-13
575.2	588.6	592.4	591.1	588.2	597.3	595.5	588.3	578.9	578.8	566.0	563.8
Bt1-14	Bt1-14	Bt1-14	Bt1-14	Bt1-14	Bt1-14	Bt1-14	Bt1-14	Bt1-14	Bt1-14	Bt1-14	Bt1-14
582.8	596.4	600.3	599.0	596.0	605.2	603.5	596.1	586.5	586.5	573.5	571.2
Bt2-15	Bt2-15	Bt2-15	Bt2-15	Bt2-15	Bt2-15	Bt2-15	Bt2-15	Bt2-15	Bt2-15	Bt2-15	Bt2-15
586.5	600.2	604.1	602.8	599.7	609.1	607.3	599.9	590.2	590.1	577.0	574.7
Bt2-16	Bt2-16	Bt2-16	Bt2-16	Bt2-16	Bt2-16	Bt2-16	Bt2-16	Bt2-16	Bt2-16	Bt2-16	Bt2-16
583.5	597.2	601.1	599.7	596.7	606.0	604.2	596.9	587.3	587.2	574.2	571.9
Bt3-17	Bt3-17	Bt3-17	Bt3-17	Bt3-17	Bt3-17	Bt3-17	Bt3-17	Bt3-17	Bt3-17	Bt3-17	Bt3-17
584.9	598.6	602.5	601.2	598.1	607.5	605.7	598.3	588.7	588.6	575.5	573.2
Bt3-18	Bt3-18	Bt3-18	Bt3-18	Bt3-18	Bt3-18	Bt3-18	Bt3-18	Bt3-18	Bt3-18	Bt3-18	Bt3-18
581.2	594.7	598.6	597.3	594.3	603.6	601.8	594.5	584.9	584.8	571.9	569.6

Table F-3 (continued). Calculated garnet core and rim temperatures at 4000, 5000, & 6000 kb for sample BR060912-02.
Calculations based on garnet-biotite thermometer of Perchuk and Lavrent'Eva (1983).

Garnet 2

4000 kb												
19grt2rim	20grt2rim	21grt2	22grt2	23grt2	24grt2core	25grt2core	26grt2core	27grt2core	28grt2	29grt2rim	30grt2rim	31grt2rim
36bt4	36bt4	36bt4	36bt4	36bt4	36bt4	36bt4	36bt4	36bt4	36bt4	36bt4	36bt4	36bt4
578.2	581.9	592.2	594.3	592.2	596.7	600.4	597.1	601.2	587.0	584.1	584.0	576.1
37bt4	37bt4	37bt4	37bt4	37bt4	37bt4	37bt4	37bt4	37bt4	37bt4	37bt4	37bt4	37bt4
579.4	583.1	593.5	595.6	593.5	598.0	601.7	598.4	602.4	588.2	585.4	585.2	577.3
38bt5	38bt5	38bt5	38bt5	38bt5	38bt5	38bt5	38bt5	38bt5	38bt5	38bt5	38bt5	38bt5
581.6	585.4	595.8	597.9	595.8	600.4	604.1	600.8	604.8	590.5	587.6	587.5	579.5
39bt5	39bt5	39bt5	39bt5	39bt5	39bt5	39bt5	39bt5	39bt5	39bt5	39bt5	39bt5	39bt5
591.1	595.0	605.6	607.8	605.6	610.3	614.1	610.7	614.8	600.2	597.3	597.1	589.0
5000 kb												
19grt2rim	20grt2rim	21grt2	22grt2	23grt2	24grt2core	25grt2core	26grt2core	27grt2core	28grt2	29grt2rim	30grt2rim	31grt2rim
36bt4	36bt4	36bt4	36bt4	36bt4	36bt4	36bt4	36bt4	36bt4	36bt4	36bt4	36bt4	36bt4
582.7	586.4	596.8	598.9	596.8	601.3	605.1	601.8	605.8	591.5	588.7	588.5	580.6
37bt4	37bt4	37bt4	37bt4	37bt4	37bt4	37bt4	37bt4	37bt4	37bt4	37bt4	37bt4	37bt4
583.9	587.6	598.1	600.2	598.1	602.6	606.4	603.0	607.1	592.8	589.9	589.8	581.8
38bt5	38bt5	38bt5	38bt5	38bt5	38bt5	38bt5	38bt5	38bt5	38bt5	38bt5	38bt5	38bt5
586.2	589.9	600.4	602.6	600.4	605.0	608.7	605.4	609.5	595.1	592.2	592.0	584.1
39bt5	39bt5	39bt5	39bt5	39bt5	39bt5	39bt5	39bt5	39bt5	39bt5	39bt5	39bt5	39bt5
595.7	599.6	610.3	612.5	610.3	615.0	618.8	615.4	619.5	604.8	601.9	601.7	593.6

Table F-3 (continued). Calculated garnet core and rim temperatures at 4000, 5000, & 6000 kb for sample BR060912-02.
Calculations based on garnet-biotite thermometer of Perchuk and Lavrent'Eva (1983).

Garnet 2

6000 kb

19grt2rim	20grt2rim	21grt2	22grt2	23grt2	24grt2core	25grt2core	26grt2core	27grt2core	28grt2	29grt2rim	30grt2rim	31grt2rim
36bt4	36bt4	36bt4	36bt4	36bt4	36bt4	36bt4	36bt4	36bt4	36bt4	36bt4	36bt4	36bt4
587.2	590.9	601.4	603.5	601.4	606.0	609.7	606.4	610.4	596.1	593.2	593.1	585.1
19grt2rim	20grt2rim	21grt2	22grt2	23grt2	24grt2core	25grt2core	26grt2core	27grt2core	28grt2	29grt2rim	30grt2rim	31grt2rim
37bt4	37bt4	37bt4	37bt4	37bt4	37bt4	37bt4	37bt4	37bt4	37bt4	37bt4	37bt4	37bt4
588.4	592.2	602.7	604.8	602.7	607.3	611.0	607.7	611.7	597.3	594.5	594.3	586.3
19grt2rim	20grt2rim	21grt2	22grt2	23grt2	24grt2core	25grt2core	26grt2core	27grt2core	28grt2	29grt2rim	30grt2rim	31grt2rim
38bt5	38bt5	38bt5	38bt5	38bt5	38bt5	38bt5	38bt5	38bt5	38bt5	38bt5	38bt5	38bt5
590.7	594.5	605.0	607.2	605.0	609.6	613.4	610.0	614.1	599.7	596.8	596.6	588.6
19grt2rim	20grt2rim	21grt2	22grt2	23grt2	24grt2core	25grt2core	26grt2core	27grt2core	28grt2	29grt2rim	30grt2rim	31grt2rim
39bt5	39bt5	39bt5	39bt5	39bt5	39bt5	39bt5	39bt5	39bt5	39bt5	39bt5	39bt5	39bt5
600.3	604.2	615.0	617.2	614.9	619.6	623.5	620.1	624.3	609.5	606.5	606.3	598.1

Table F-3 (continued). Calculated garnet core and rim temperatures at 4000, 5000, & 6000 kb for sample BR060912-02.
Calculations based on garnet-biotite thermometer of Perchuk and Lavrent'Eva (1983).

Garnet 3

4000 kb

42grt3rim	43grt3rim	44grt3rim	45grt3	46grt3	47grt3	48grt3core	49grt3core	50grt3core	51grt3core	52grt3	53grt3	54grt3rim	55grt3rim	56grt3rim
82bt8	82bt8	82bt8	82bt8	82bt8	82bt8	82bt8	82bt8	82bt8	82bt8	82bt8	82bt8	82bt8	82bt8	82bt8
577.9	585.1	585.1	581.6	585.1	587.5	591.6	600.9	592.6	601.9	597.3	593.6	587.2	576.6	578.1
83bt8	83bt8	83bt8	83bt8	83bt8	83bt8	83bt8	83bt8	83bt8	83bt8	83bt8	83bt8	83bt8	83bt8	83bt8
595.6	603.1	603.1	599.5	603.2	605.6	610.0	619.7	610.9	620.7	615.8	612.1	605.4	594.3	595.9
84bt9	84bt9	84bt9	84bt9	84bt9	84bt9	84bt9	84bt9	84bt9	84bt9	84bt9	84bt9	84bt9	84bt9	84bt9
576.5	583.7	583.7	580.2	583.8	586.1	590.3	599.5	591.2	600.5	595.8	592.3	585.8	575.2	576.8
85bt9	85bt9	85bt9	85bt9	85bt9	85bt9	85bt9	85bt9	85bt9	85bt9	85bt9	85bt9	85bt9	85bt9	85bt9
577.9	585.1	585.1	581.6	585.2	587.5	591.7	601.0	592.6	602.0	597.3	593.7	587.2	576.6	578.1

5000 kb

42grt3rim	43grt3rim	44grt3rim	45grt3	46grt3	47grt3	48grt3core	49grt3core	50grt3core	51grt3core	52grt3	53grt3	54grt3rim	55grt3rim	56grt3rim
82bt8	82bt8	82bt8	82bt8	82bt8	82bt8	82bt8	82bt8	82bt8	82bt8	82bt8	82bt8	82bt8	82bt8	82bt8
582.4	589.6	589.6	586.1	589.7	592.0	596.2	605.6	597.2	606.6	601.9	598.2	591.8	581.1	582.6
83bt8	83bt8	83bt8	83bt8	83bt8	83bt8	83bt8	83bt8	83bt8	83bt8	83bt8	83bt8	83bt8	83bt8	83bt8
600.2	607.8	607.8	604.1	607.8	610.3	614.7	624.4	615.6	625.4	620.5	616.8	610.0	598.9	600.5
84bt9	84bt9	84bt9	84bt9	84bt9	84bt9	84bt9	84bt9	84bt9	84bt9	84bt9	84bt9	84bt9	84bt9	84bt9
581.0	588.2	588.2	584.7	588.3	590.6	594.8	604.1	595.8	605.1	600.5	596.8	590.4	579.7	581.3
85bt9	85bt9	85bt9	85bt9	85bt9	85bt9	85bt9	85bt9	85bt9	85bt9	85bt9	85bt9	85bt9	85bt9	85bt9
582.4	589.7	589.7	586.1	589.7	592.1	596.3	605.6	597.2	606.6	601.9	598.3	591.8	581.1	582.7

Table F-3 (continued). Calculated garnet core and rim temperatures at 4000, 5000, & 6000 kb for sample BR060912-02.
Calculations based on garnet-biotite thermometer of Perchuk and Lavrent'Eva (1983).

Garnet 3

6000 kb

42grt3rim	43grt3rim	44grt3rim	45grt3	46grt3	47grt3	48grt3core	49grt3core	50grt3core	51grt3core	52grt3	53grt3	54grt3rim	55grt3rim	56grt3rim
82bt8	82bt8	82bt8	82bt8	82bt8	82bt8	82bt8	82bt8	82bt8	82bt8	82bt8	82bt8	82bt8	82bt8	82bt8
586.9	594.2	594.2	590.6	594.2	596.6	600.8	610.2	601.7	611.2	606.5	602.8	596.3	585.6	587.1
83bt8	83bt8	83bt8	83bt8	83bt8	83bt8	83bt8	83bt8	83bt8	83bt8	83bt8	83bt8	83bt8	83bt8	83bt8
604.8	612.4	612.4	608.7	612.5	614.9	619.3	629.1	620.3	630.2	625.3	621.5	614.7	603.5	605.1
84bt9	84bt9	84bt9	84bt9	84bt9	84bt9	84bt9	84bt9	84bt9	84bt9	84bt9	84bt9	84bt9	84bt9	84bt9
585.5	592.8	592.8	589.3	592.9	595.2	599.4	608.8	600.3	609.8	605.1	601.4	594.9	584.2	585.8
85bt9	85bt9	85bt9	85bt9	85bt9	85bt9	85bt9	85bt9	85bt9	85bt9	85bt9	85bt9	85bt9	85bt9	85bt9
586.9	594.2	594.2	590.7	594.3	596.6	600.9	610.2	601.8	611.2	606.5	602.9	596.4	585.6	587.2

Table F-3 (continued). Calculated garnet core and rim temperatures at 4000, 5000, & 6000 kb for sample BR060912-02.
Calculations based on garnet-biotite thermometer of Perchuk and Lavrent'Eva (1983).

Garnet 4

4000 kb														
65grt4rim	66grt4rim	67grt4	68grt4	69grt4	70grt4core	71grt4core	72grt4core	73grt4core	74grt4core	75grt4core	76grt4core	77grt4	78grt4	79grt4rim
82bt8	82bt8	82bt8	82bt8	82bt8	82bt8	82bt8	82bt8	82bt8	82bt8	82bt8	82bt8	82bt8	82bt8	82bt8
579.5	592.8	596.2	580.6	584.0	597.2	605.7	609.2	600.3	610.6	598.8	599.9	588.0	582.3	579.6
83bt8	83bt8	83bt8	83bt8	83bt8	83bt8	83bt8	83bt8	83bt8	83bt8	83bt8	83bt8	83bt8	83bt8	83bt8
597.3	611.2	614.8	598.5	602.0	615.8	624.6	628.3	619.0	629.8	617.4	618.6	606.2	600.2	597.5
84bt9	84bt9	84bt9	84bt9	84bt9	84bt9	84bt9	84bt9	84bt9	84bt9	84bt9	84bt9	84bt9	84bt9	84bt9
578.2	591.4	594.8	579.3	582.6	595.8	604.3	607.7	598.9	609.2	597.3	598.5	586.6	580.9	578.3
85bt9	85bt9	85bt9	85bt9	85bt9	85bt9	85bt9	85bt9	85bt9	85bt9	85bt9	85bt9	85bt9	85bt9	85bt9
579.6	592.9	596.3	580.7	584.0	597.3	605.7	609.2	600.3	610.7	598.8	599.9	588.1	582.3	579.7
5000 kb														
65grt4rim	66grt4rim	67grt4	68grt4	69grt4	70grt4core	71grt4core	72grt4core	73grt4core	74grt4core	75grt4core	76grt4core	77grt4	78grt4	79grt4rim
82bt8	82bt8	82bt8	82bt8	82bt8	82bt8	82bt8	82bt8	82bt8	82bt8	82bt8	82bt8	82bt8	82bt8	82bt8
584.0	597.4	600.9	585.2	588.5	601.8	610.3	613.8	604.9	615.3	603.4	604.5	592.6	586.8	584.2
83bt8	83bt8	83bt8	83bt8	83bt8	83bt8	83bt8	83bt8	83bt8	83bt8	83bt8	83bt8	83bt8	83bt8	83bt8
602.0	615.9	619.5	603.1	606.7	620.5	629.4	633.0	623.7	634.6	622.1	623.3	610.9	604.9	602.1
84bt9	84bt9	84bt9	84bt9	84bt9	84bt9	84bt9	84bt9	84bt9	84bt9	84bt9	84bt9	84bt9	84bt9	84bt9
582.7	596.0	599.4	583.8	587.2	600.4	608.9	612.4	603.5	613.8	602.0	603.1	591.2	585.5	582.8
85bt9	85bt9	85bt9	85bt9	85bt9	85bt9	85bt9	85bt9	85bt9	85bt9	85bt9	85bt9	85bt9	85bt9	85bt9
584.1	597.5	600.9	585.2	588.6	601.9	610.4	613.9	605.0	615.4	603.4	604.5	592.6	586.9	584.2

Table F-3 (continued). Calculated garnet core and rim temperatures at 4000, 5000, & 6000 kb for sample BR060912-02.
Calculations based on garnet-biotite thermometer of Perchuk and Lavrent'Eva (1983).

Garnet 4

6000 kb														
65grt4rim	66grt4rim	67grt4	68grt4	69grt4	70grt4core	71grt4core	72grt4core	73grt4core	74grt4core	75grt4core	76grt4core	77grt4	78grt4	79grt4rim
82bt8	82bt8	82bt8	82bt8	82bt8	82bt8	82bt8	82bt8	82bt8	82bt8	82bt8	82bt8	82bt8	82bt8	82bt8
588.6	602.0	605.5	589.7	593.1	606.5	615.0	618.5	609.5	620.0	608.0	609.1	597.1	591.4	588.7
83bt8	83bt8	83bt8	83bt8	83bt8	83bt8	83bt8	83bt8	83bt8	83bt8	83bt8	83bt8	83bt8	83bt8	83bt8
606.6	620.6	624.2	607.7	611.3	625.2	634.2	637.8	628.4	639.4	626.8	628.0	615.5	609.5	606.7
84bt9	84bt9	84bt9	84bt9	84bt9	84bt9	84bt9	84bt9	84bt9	84bt9	84bt9	84bt9	84bt9	84bt9	84bt9
587.2	600.6	604.0	588.3	591.7	605.0	613.6	617.1	608.1	618.5	606.6	607.7	595.7	590.0	587.3
85bt9	85bt9	85bt9	85bt9	85bt9	85bt9	85bt9	85bt9	85bt9	85bt9	85bt9	85bt9	85bt9	85bt9	85bt9
588.6	602.1	605.5	589.7	593.1	606.5	615.1	618.6	609.6	620.0	608.0	609.2	597.2	591.4	588.7

Appendix G: QEMSCAN® imagery scans, modal abundance tables, and mineral assay diagrams

Imagery scans

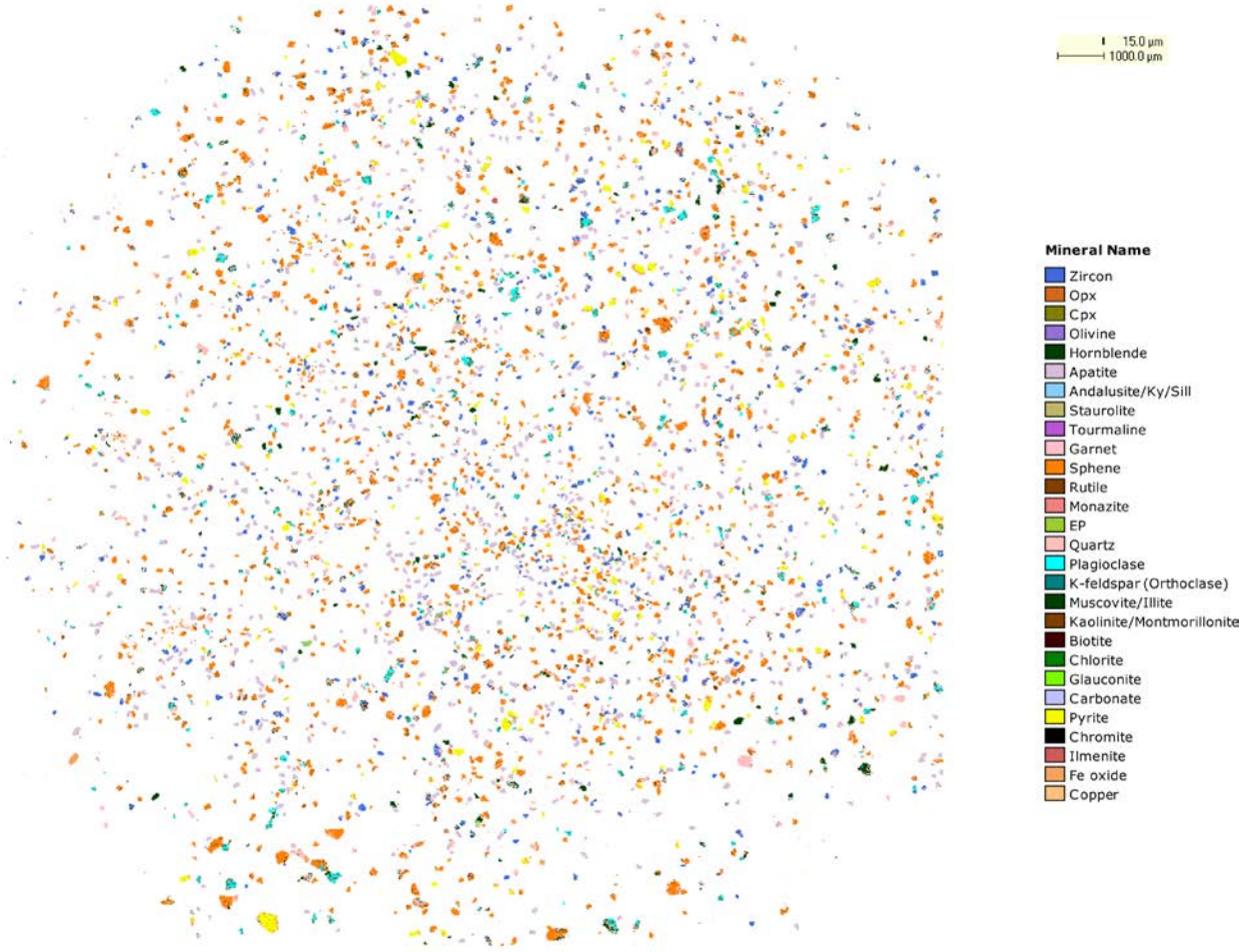

Amphibole-bearing leucosome BR060913-01

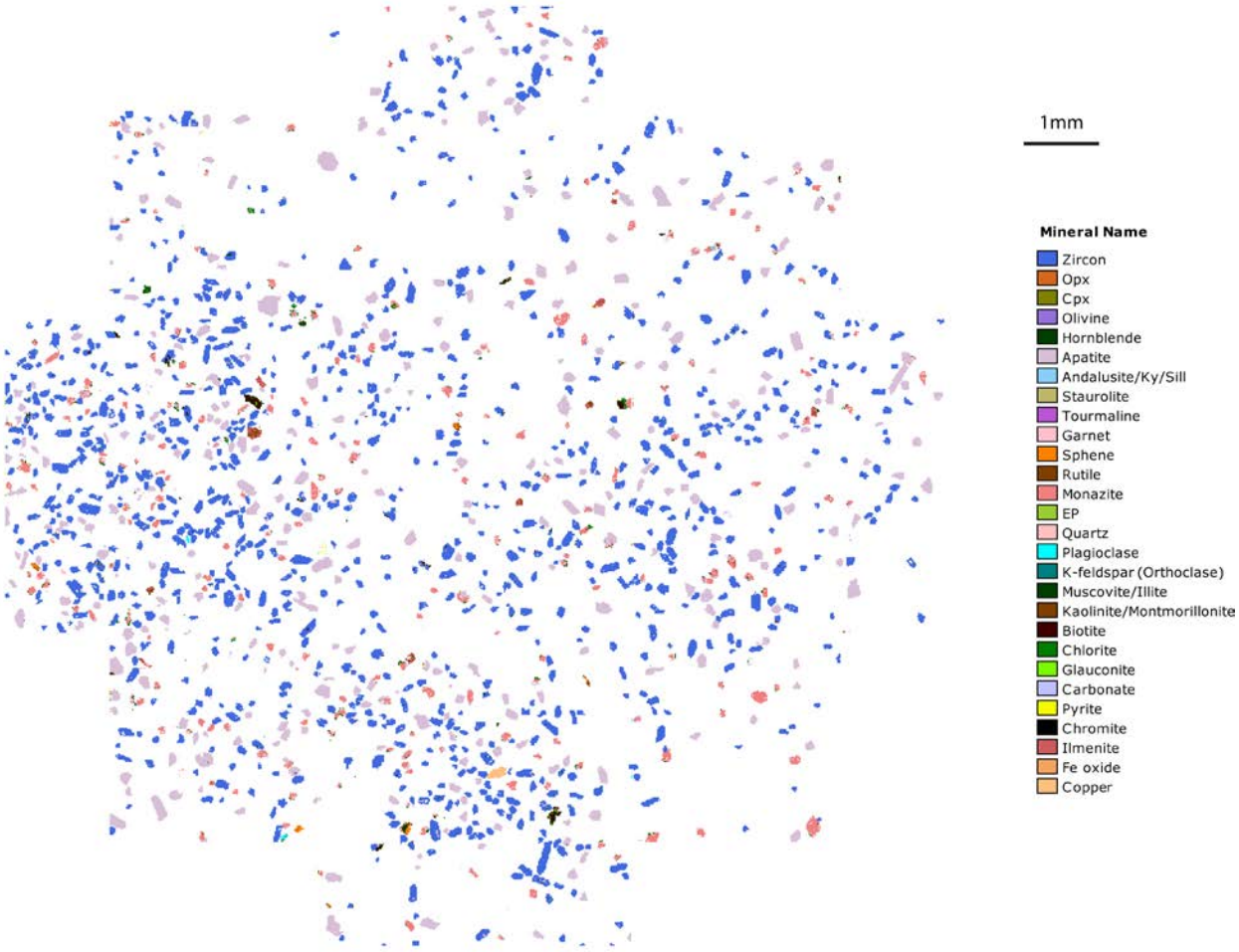

Northern granite BR060913-04A

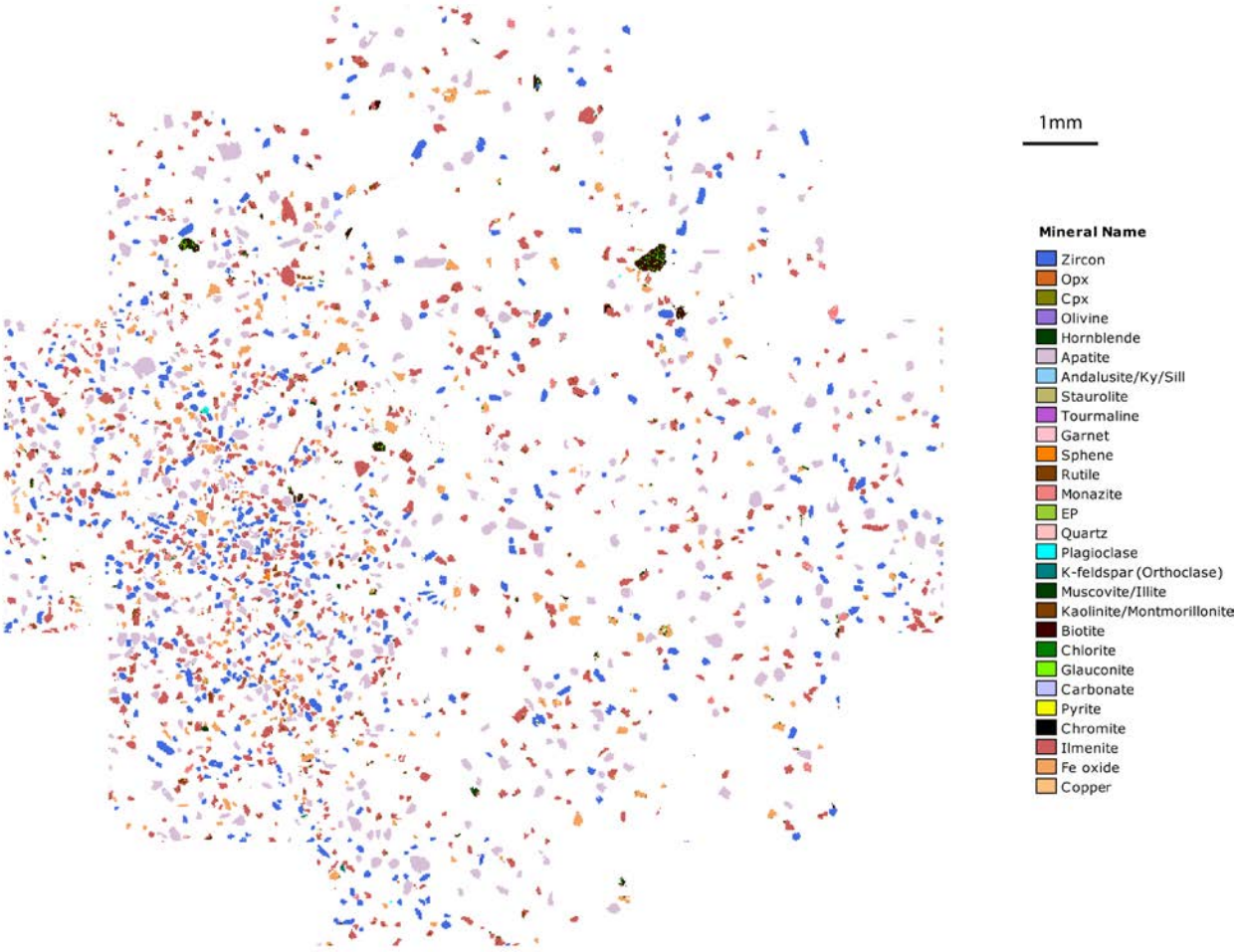

Northern syenite BR060913-04B

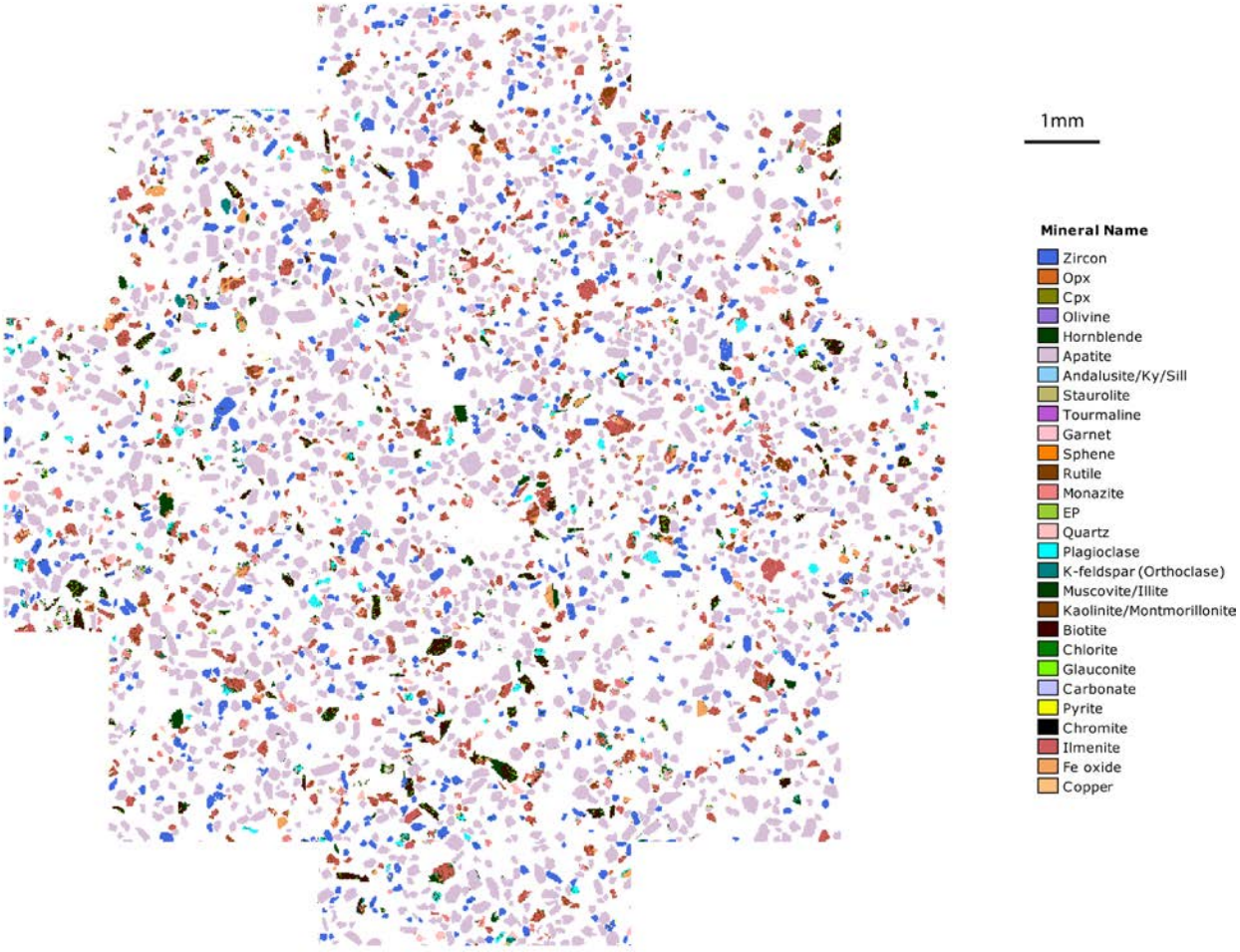

Northern foliated granite BR060913-05

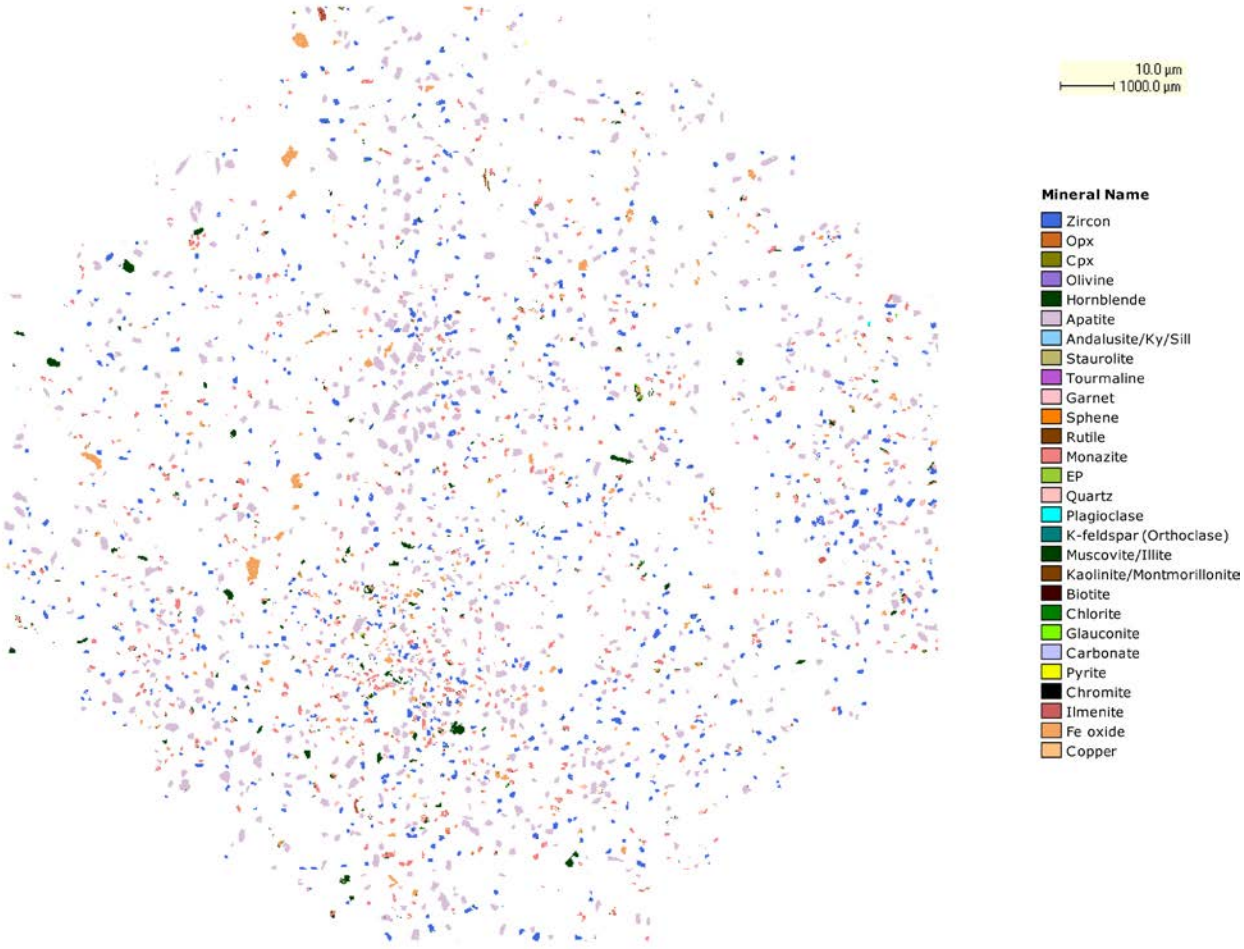

Quartz pebble conglomerate BR060913-07

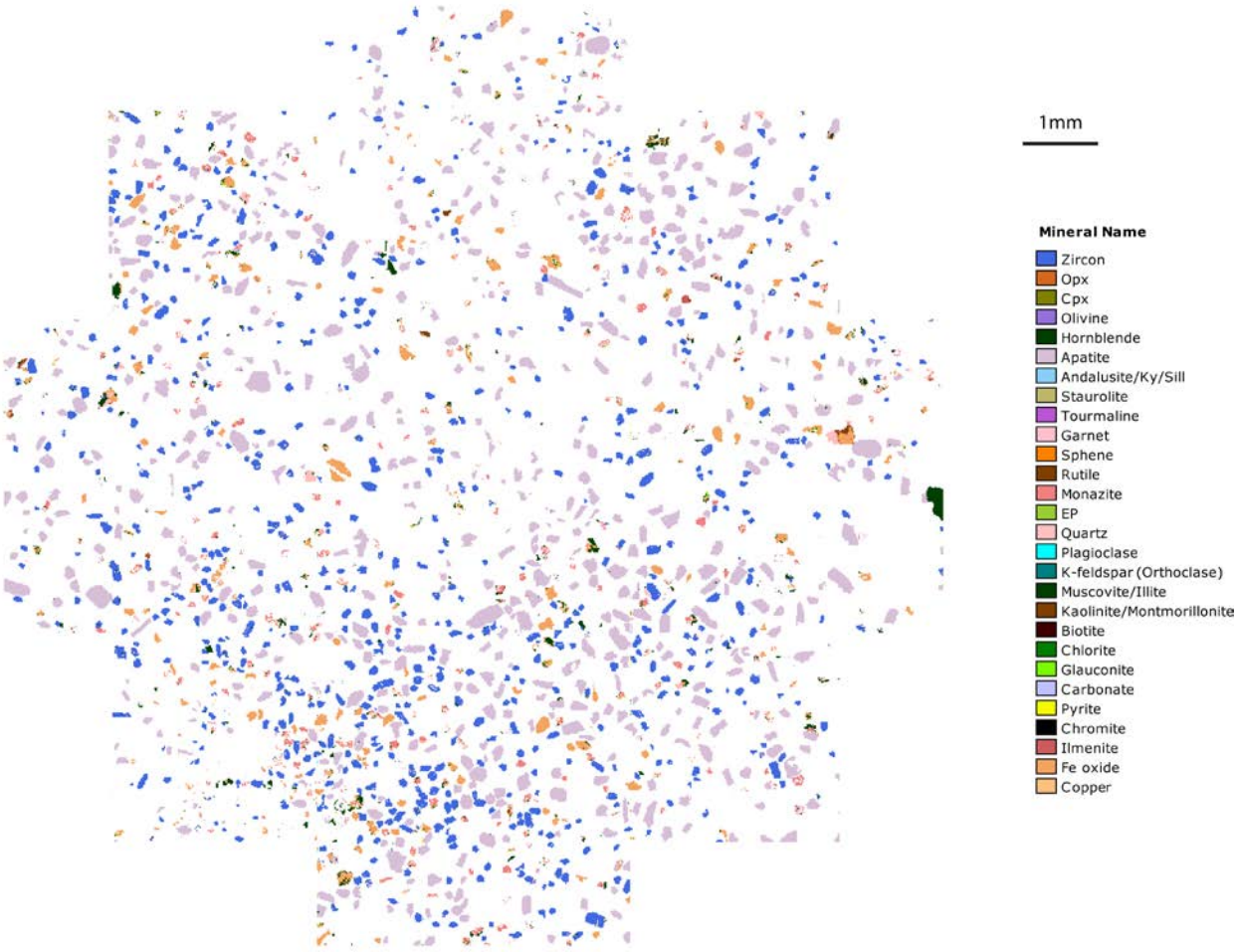

Quartz pebble conglomerate BR060913-08

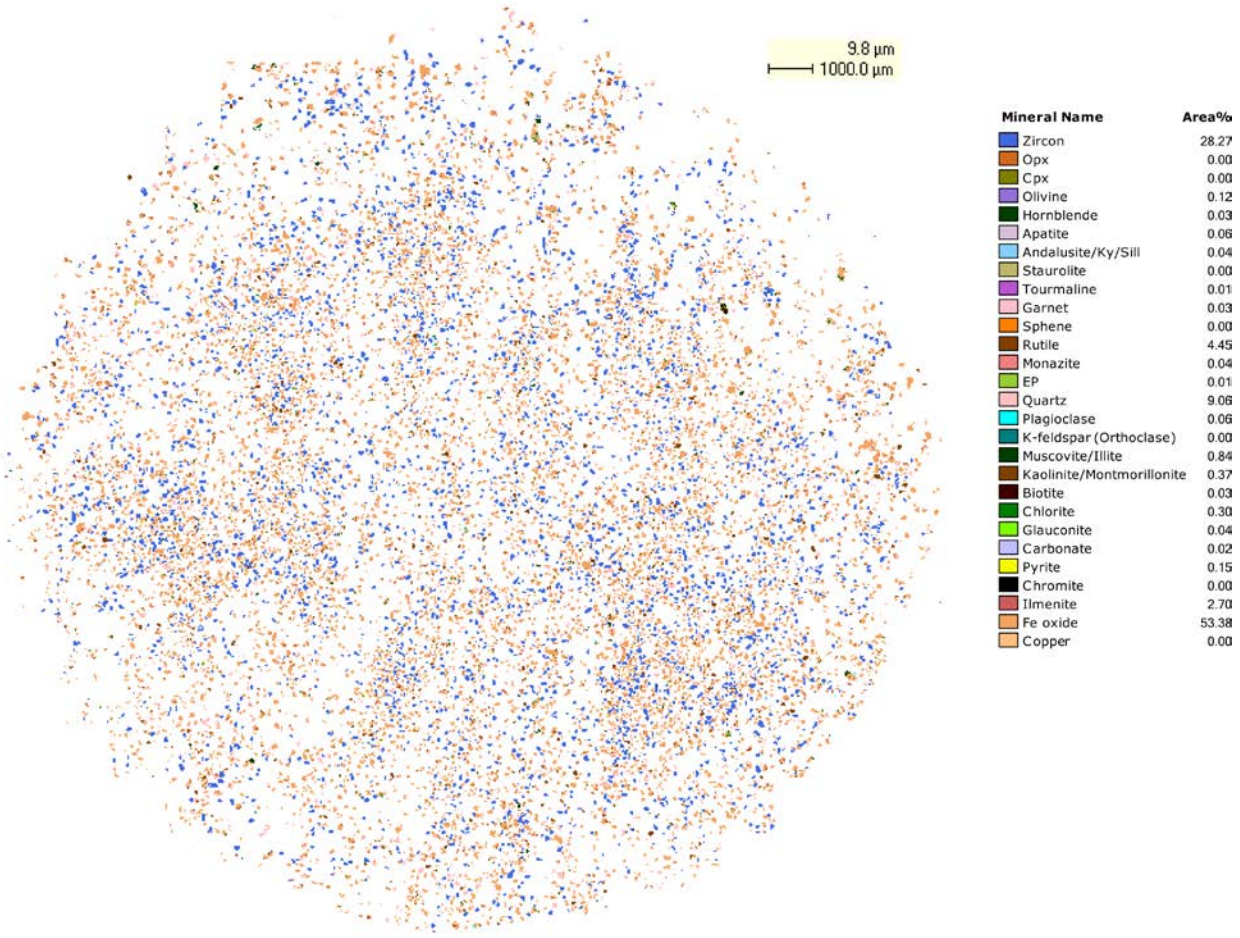

Quartzite BR061013-01

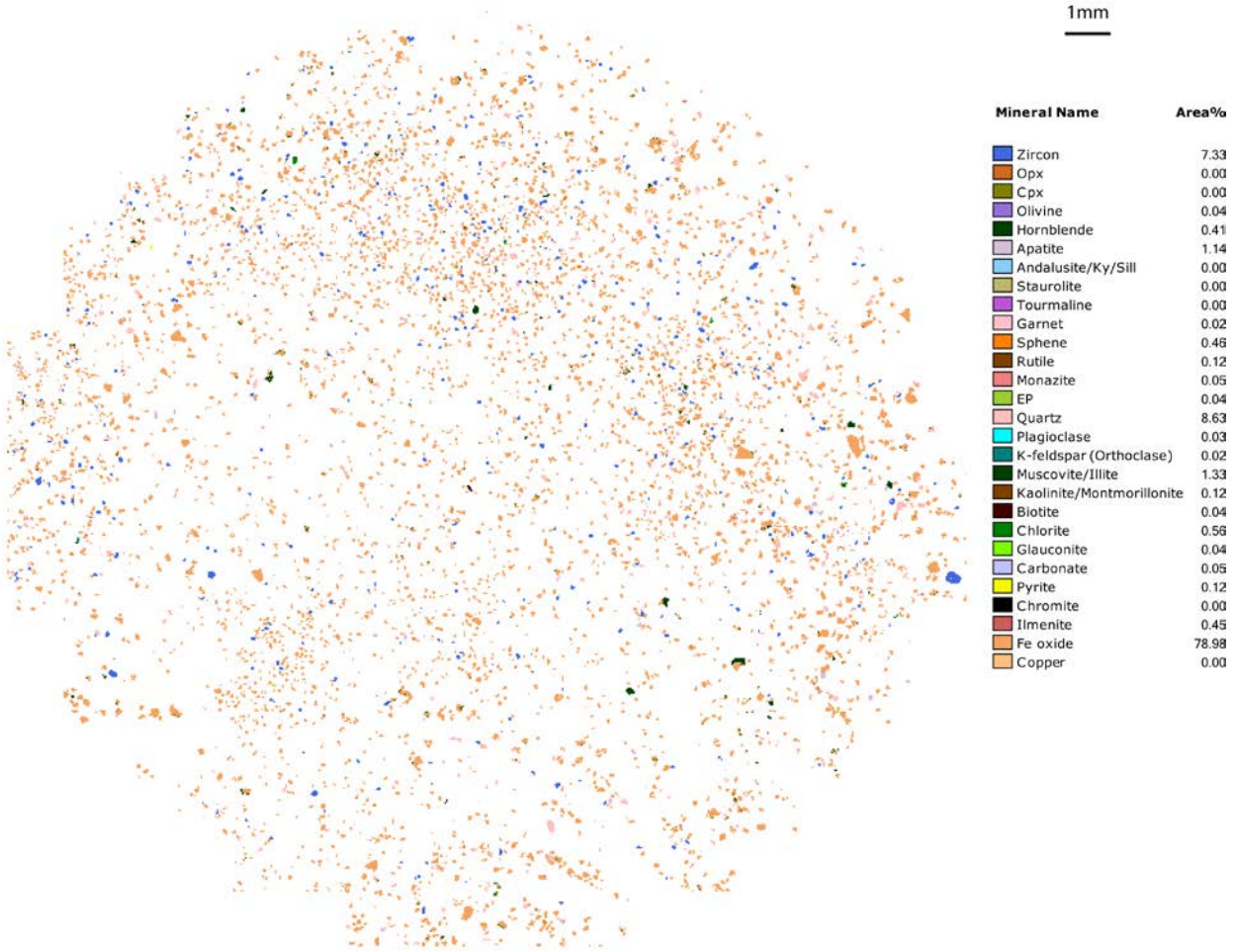

Quartzite BR061013-02

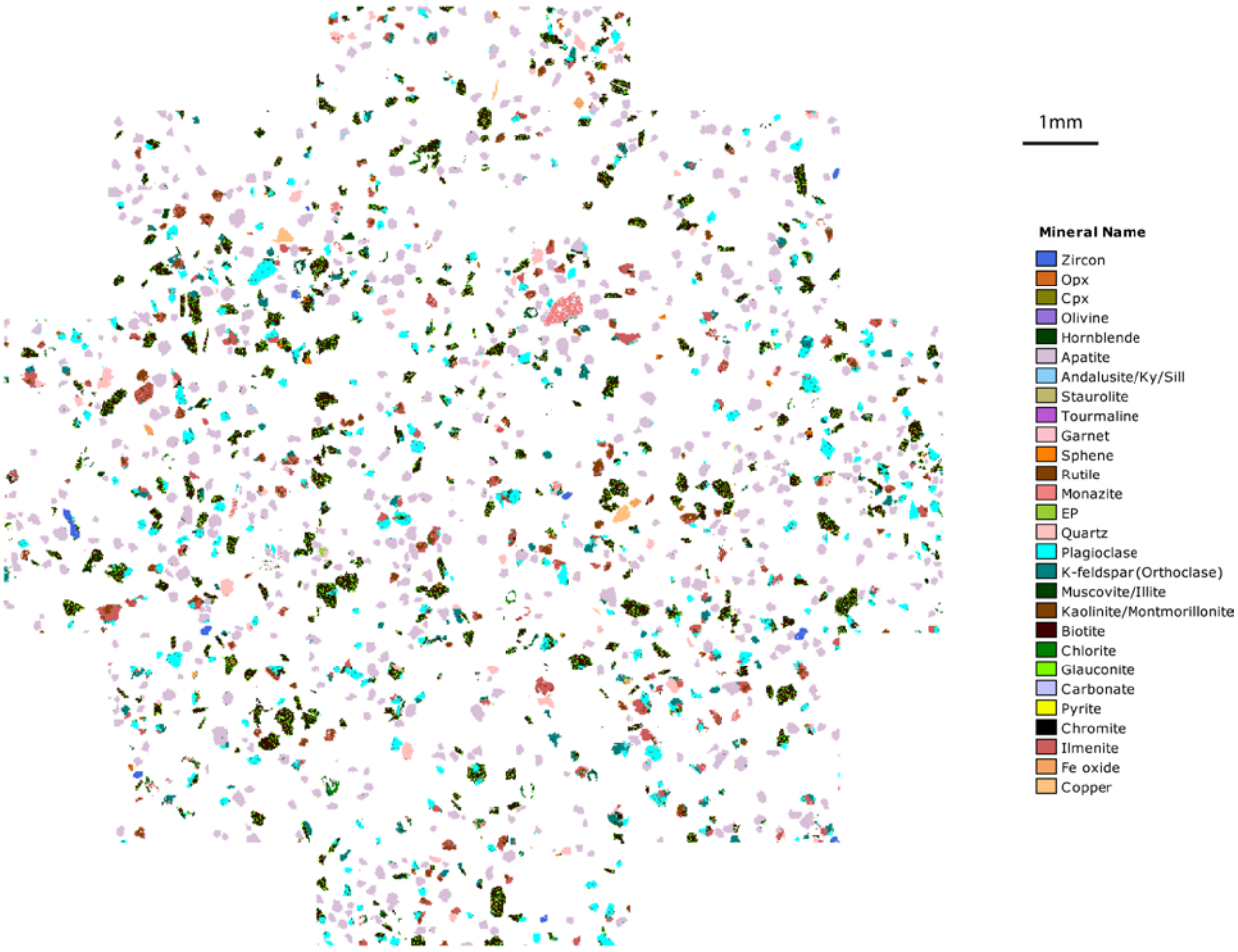

Southern granite BR061113-01

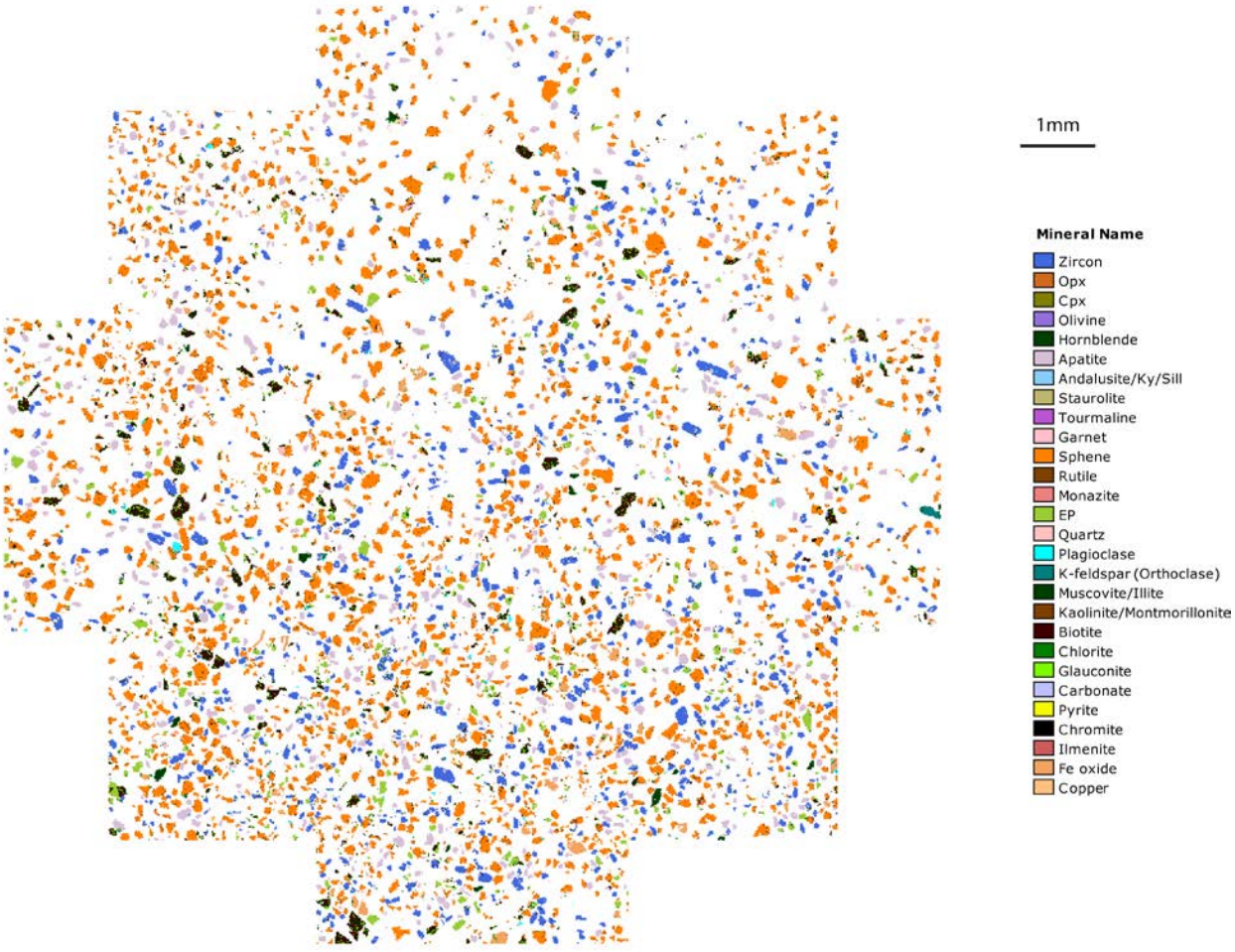

Southern granodiorite split 1 BR061113-02A

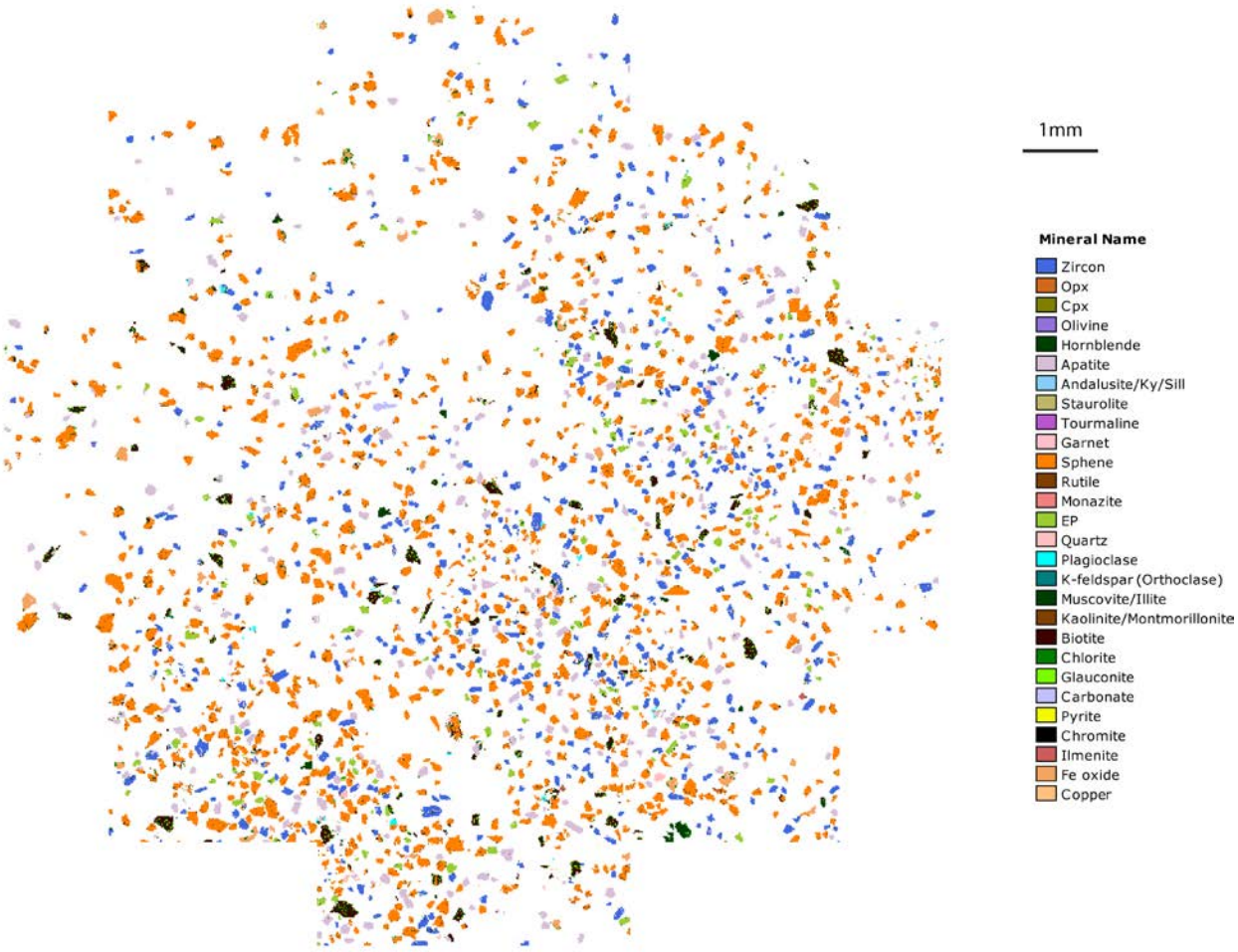

Southern granodiorite split 2 BR061113-02B

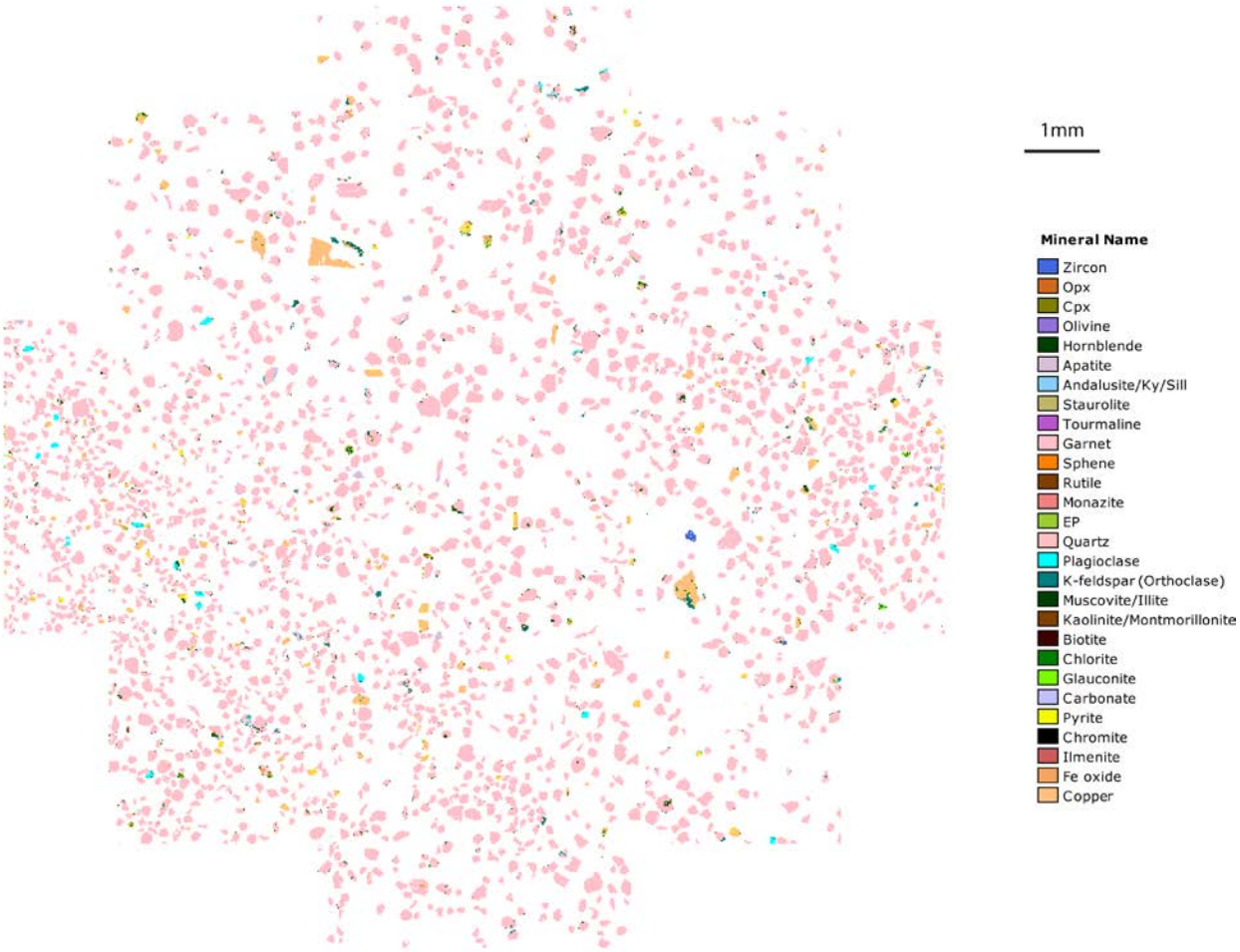

Pegmatite 1 BR061113-05

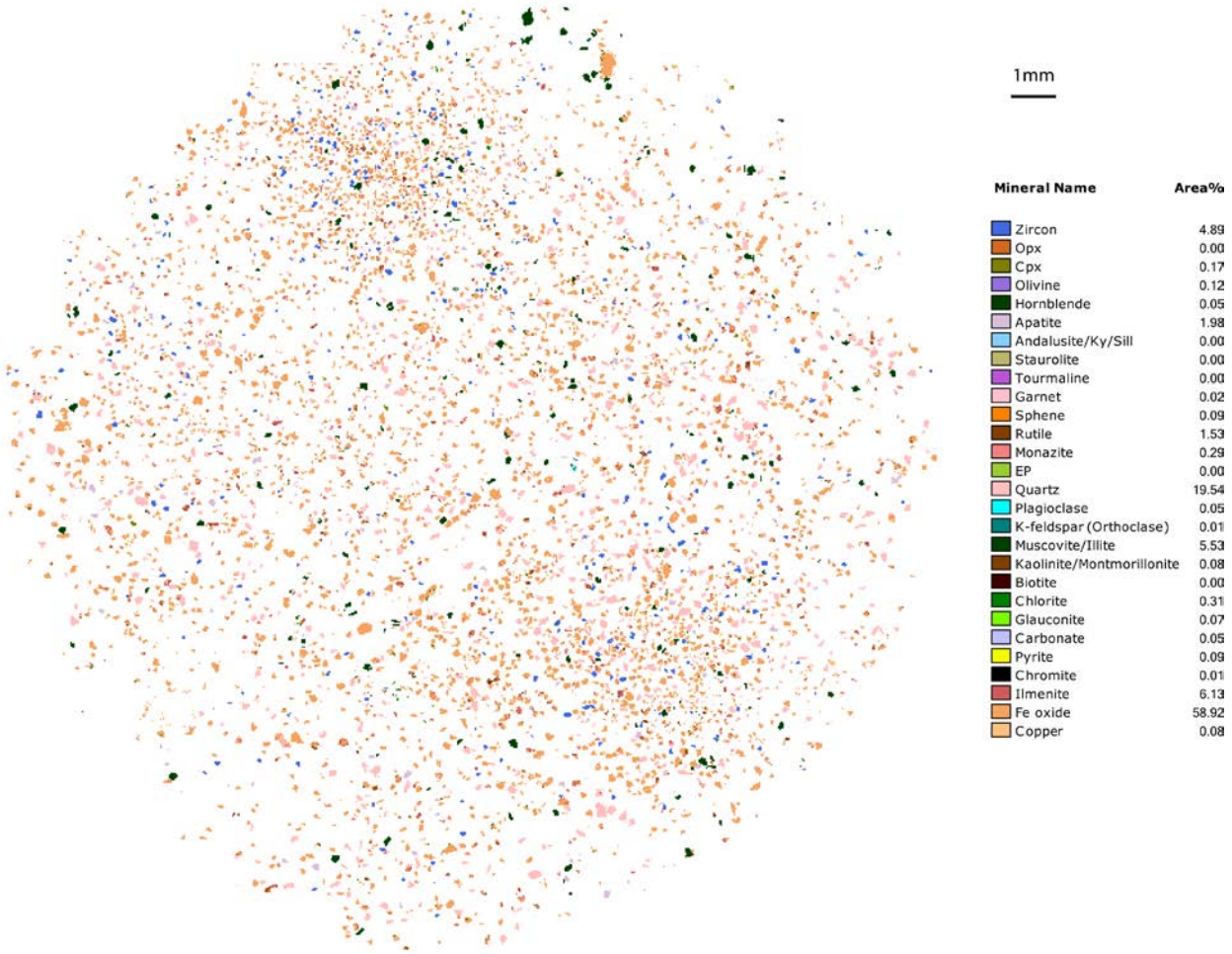

Quartzite BR061113-07

Table G-1: Mineral modal abundance in Vol.%

	BR060913-01	BR060913-04A	BR060913-04B	BR060913-05	BR060913-07	BR060913-08	BR061113-01	BR061113-02A	BR061113-02B
Zircon	9.08	50.50	18.35	12.28	17.52	24.93	0.69	17.61	16.34
Monazite	0.02	8.71	1.70	3.14	12.29	4.32	0.68	0.00	0.00
Apatite	20.68	35.10	35.16	56.88	46.33	51.05	39.26	12.58	12.16
Quartz	9.19	0.45	0.53	1.46	1.34	1.34	3.15	1.41	1.45
Garnet	0.01	0.02	0.02	0.01	0.00	0.00	0.01	0.04	0.03
Plagioclase	7.68	0.17	0.08	1.37	2.98	1.19	11.28	0.44	0.39
K-feldspar (Orthoclase)	2.82	0.05	0.12	0.43	0.02	0.02	3.91	0.10	0.06
Olivine	0.01	0.00	0.01	0.00	0.01	0.01	0.00	0.00	0.00
Orthopyroxene	0.00	0.00	0.00	0.00	0.00	0.00	0.00	0.00	0.00
Clinopyroxene	0.02	0.00	0.00	0.00	0.00	0.00	0.06	0.00	0.00
Hornblende	2.26	0.06	0.06	0.01	0.00	0.00	0.08	0.86	0.84
Muscovite/Illite	2.32	1.36	1.59	3.83	5.74	3.74	15.05	4.11	3.76
Kaolinite/Montmorillonite	1.63	0.15	0.08	0.23	3.34	1.94	0.84	0.14	0.14
Biotite	0.18	0.63	1.25	2.17	0.07	0.00	12.01	4.37	4.50
Chlorite	0.37	0.79	0.23	0.20	0.15	0.13	0.44	0.43	0.35
Epidote	0.11	0.08	0.05	0.02	0.00	0.00	0.06	5.51	4.47
Andalusite/Ky/Sill	0.07	0.03	0.05	0.02	0.12	0.07	0.02	0.01	0.03
Staurolite	0.00	0.00	0.00	0.00	0.00	0.00	0.00	0.00	0.00
Tourmaline	0.00	0.00	0.00	0.00	0.00	0.00	0.00	0.00	0.00
Carbonate	1.03	0.20	0.79	0.52	0.12	0.11	0.54	0.51	0.52
Pyrite	6.99	0.13	0.15	0.08	3.13	1.53	0.12	0.12	0.10
Chromite	0.00	0.00	0.00	0.00	0.00	0.00	0.00	0.00	0.00
Ilmenite	0.48	0.65	27.03	11.63	0.23	0.24	7.10	0.11	0.09
Sphene	27.17	0.24	0.03	0.01	0.00	0.01	0.32	43.03	47.11
Rutile	3.58	0.57	2.26	3.68	0.14	0.16	4.23	5.56	4.80
Fe oxide	4.30	0.11	10.46	2.00	6.45	9.21	0.15	3.05	2.86

Table G-1 (continued): Modal Mineral Abundance in Volume %

	BR061013-01 QEM	BR061013-02 QEM	BR061113-07 QEM
Zircon	28.3	7.33	4.89
Opx	0.00	0.00	0.00
Cpx	0.00	0.00	0.17
Olivine	0.12	0.04	0.12
Hornblende	0.03	0.41	0.05
Apatite	0.06	1.14	1.98
Andalusite/Ky/Sill	0.04	0.00	0.00
Staurolite	0.00	0.00	0.00
Tourmaline	0.01	0.00	0.00
Garnet	0.03	0.02	0.02
Sphene	0.00	0.46	0.09
Rutile	4.45	0.12	1.53
Monazite	0.04	0.05	0.29
EP	0.01	0.04	0.00
Quartz	9.06	8.63	19.54
Plagioclase	0.06	0.03	0.05
K-feldspar (Orthoclase)	0.00	0.02	0.01
Muscovite/Illite	0.84	1.33	5.53
Kaolinite/Montmorillonite	0.37	0.12	0.08
Biotite	0.03	0.04	0.00
Chlorite	0.30	0.56	0.31
Glauconite	0.04	0.04	0.07
Carbonate	0.02	0.05	0.05
Pyrite	0.15	0.12	0.09
Chromite	0.00	0.00	0.01
Ilmenite	2.70	0.45	6.13
Fe oxide	53.4	79.0	58.9
Copper	0.00	0.00	0.08

Table G-2. Normalized mineral modal abundance in Volume %

	Northern granite (BR060913-04A)	Northern syenite (BR060913-04B)	Northern foliated granite (BR060913-05)	Quartz-pebble conglomerate (BR060913-07)	Quartz-pebble conglomerate (BR060913-08)	Quartzite 1 (BR061013-01)	Quartzite 2 (BR061013-02)	Quartzite 3 (BR061113-07)
	BR060913-04A	**BR060913-04B**	**BR060913-05**	**BR060913-07**	**BR060913-08**	**BR061013-01 QEM**	**BR061013-02 QEM**	**BR061113-07 QEM**
Zircon	50.50	18.35	12.28	17.52	24.93	28.3	7.33	4.89
Apatite	35.10	35.16	56.88	46.33	51.05	0.06	1.14	1.98
Rutile	0.57	2.26	3.68	0.14	0.16	4.45	0.12	1.53
Monazite	8.71	1.70	3.14	12.29	4.32	0.04	0.05	0.29
Ilmenite	0.65	27.03	11.63	0.23	0.24	2.70	0.45	6.13
Fe oxide	0.11	10.46	2.00	6.45	9.21	53.4	79.0	58.9
Total	95.64	94.96	89.62	82.97	89.90	88.90	88.08	73.73
Normalized								
Zircon	52.80	19.33	13.71	21.12	27.73	31.79	8.33	6.63
Apatite	36.70	37.03	63.47	55.84	56.78	0.07	1.29	2.68
Rutile	0.59	2.38	4.11	0.17	0.17	5.00	0.14	2.08
Monazite	9.10	1.79	3.51	14.82	4.81	0.05	0.06	0.39
Ilmenite	0.68	28.47	12.98	0.28	0.26	3.04	0.52	8.32
Fe oxide	0.12	11.01	2.23	7.78	10.24	60.05	89.67	79.91
Total	100	100	100	100	100	100	100	100
Heavy Mineral/Zr ratios								
Apatite/Zircon	0.70	1.92	4.63	2.64	2.05	0.00	0.16	0.40
Rutile/Zircon	0.01	0.12	0.30	0.01	0.01	0.16	0.02	0.31
Monazite/Zircon	0.17	0.09	0.26	0.70	0.17	0.00	0.01	0.06
Ilmenite/Zircon	0.01	1.47	0.95	0.01	0.01	0.10	0.06	1.25

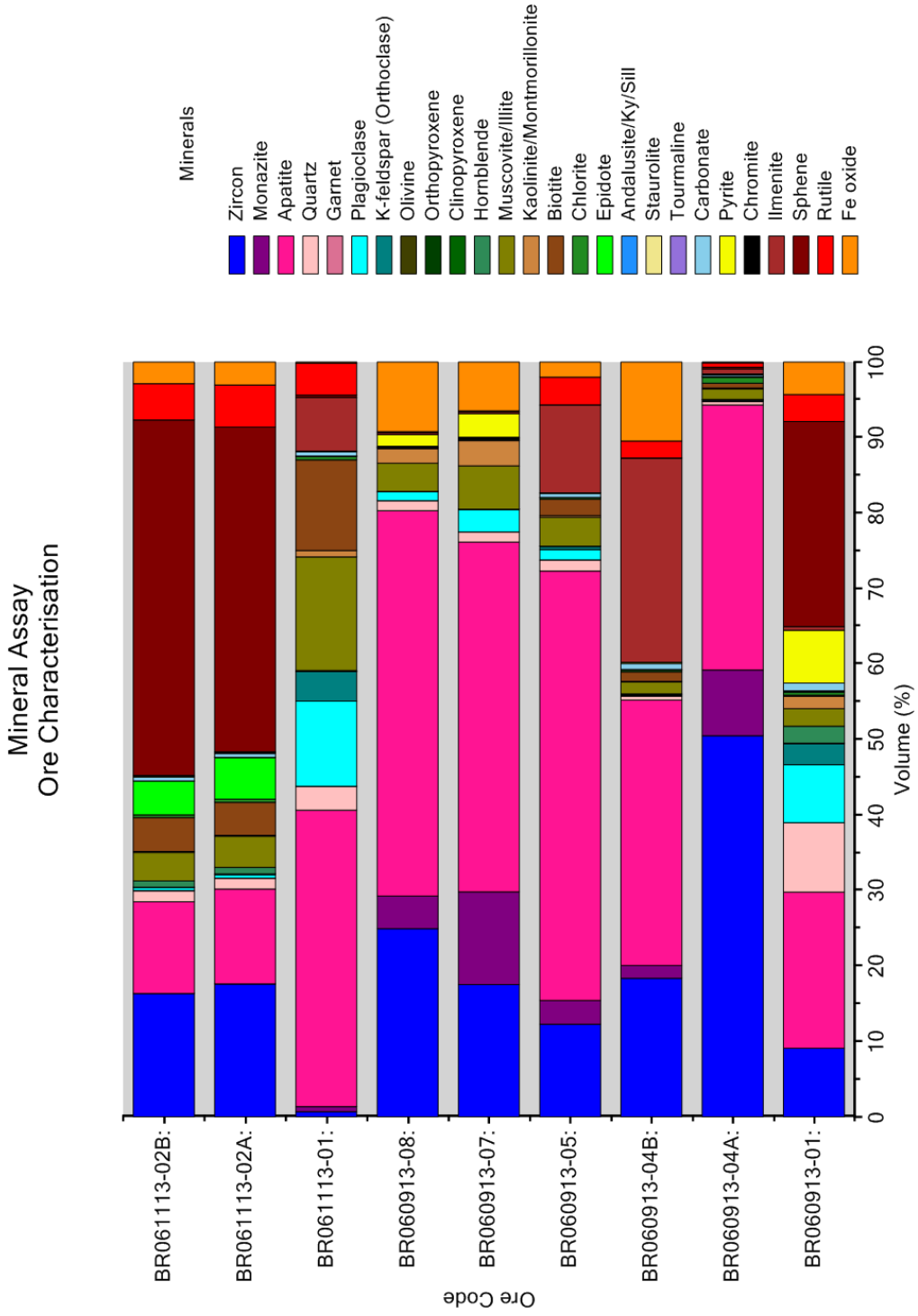
Mineral Assay
Ore Characterisation
Minerals
Zircon
Monazite
Apatite
Quartz
Garnet
Plagioclase
K-feldspar (Orthoclase)
Olivine
Orthopyroxene
Clinopyroxene
Hornblende
Muscovite/Illite
Kaolinite/Montmorillonite
Biotite
Chlorite
Epidote
Andalusite/Ky/Sill
Staurolite
Tourmaline
Carbonate
Pyrite
Chromite
Ilmenite
Sphene
Rutile
Fe oxide
BR061113-02B:
BR061113-02A:
BR061113-01:
BR060913-08:
BR060913-07:
BR060913-05:
BR060913-04B:
BR060913-04A:
BR060913-01:
Ore Code
0
10
20
30
40
50
60
70
80
90
100
Volume (%)

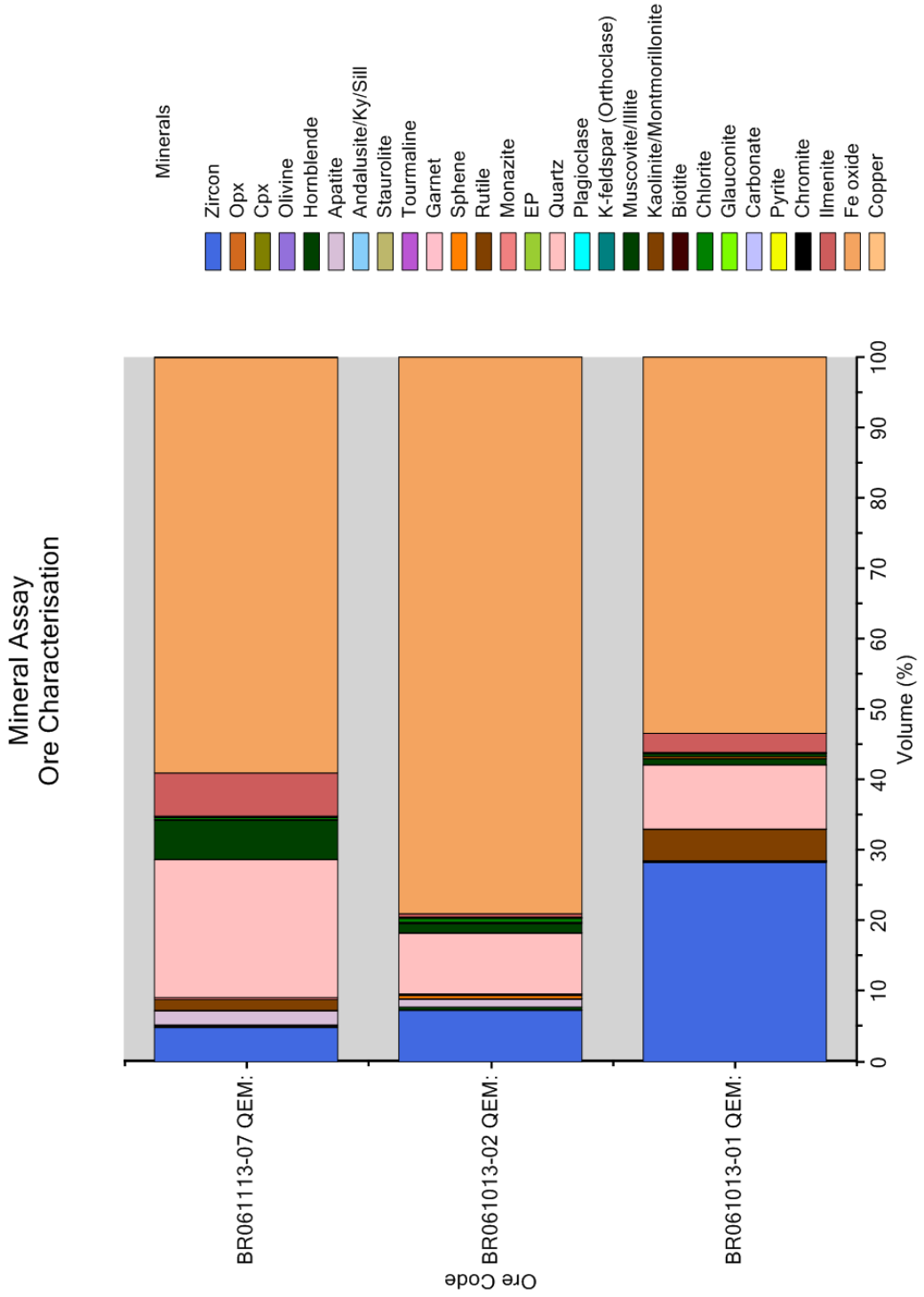
Mineral Assay
Ore Characterisation
Minerals
Zircon
Opx
Cpx
Olivine
Hornblende
Apatite
Andalusite/Ky/Sill
Staurolite
Tourmaline
Garnet
Sphene
Rutile
Monazite
EP
Quartz
Plagioclase
K-feldspar (Orthoclase)
Muscovite/Illite
Kaolinite/Montmorillonite
Biotite
Chlorite
Glauconite
Carbonate
Pyrite
Chromite
Ilmenite
Fe oxide
Copper
0
10
20
30
40
50
60
70
80
90
100
Volume (%)
Ore Code
BR061113-07 QEM:
BR061013-02 QEM:
BR061013-01 QEM: